

**What drove the methane cycle in the past -
evidence from carbon isotopic data of
methane enclosed in polar ice cores**

Dissertation

to achieve
the scientific degree of

Dr. rer. nat.

at the
Department of Geosciences
of the
University of Bremen

submitted by

Lars Möller

on October 18th, 2013;

thesis defense on December 16th, 2013.

Alfred Wegener Institute Helmholtz Centre for Polar and Marine
Research, Bremerhaven

What drove the methane cycle in the past - evidence from carbon isotopic data of methane enclosed in polar ice cores

Dissertation

zur Erlangung des Doktorgrades
der Naturwissenschaften

Dr. rer. nat.,

dem

Fachbereich Geowissenschaften

der

Universität Bremen

vorgelegt von

Lars Möller

am 18.Oktober 2013;

Disputation erfolgte am 16.Dezember 2013.

Alfred-Wegener-Institut Helmholtz-Zentrum für Polar- und
Meeresforschung, Bremerhaven

Supervisors:

Prof. Dr. Heinrich Miller

Alfred Wegener Institute Helmholtz Centre for Polar and Marine Research,
Bremerhaven

Prof. Dr. Hubertus Fischer

Department of Climate and Environmental Physics,
Physics Department, University of Bern

Summary

Atmospheric greenhouse gases play an important role in the energy balance of Earth's climate system. Methane (CH_4) is the third most important radiatively active gas after water vapor and carbon dioxide. Together with carbon dioxide (CO_2) and nitrous oxide (N_2O) methane has seen a steep increase in the last 250 years due to human activity that was unprecedented in the preceding 800,000 years. The anthropogenic contribution on the increase of CH_4 can only be assessed by comparing it with the natural variability in the past. Air enclosed in polar ice and firn cores represent the only direct archive of the atmospheric past. During the last eight glacial cycles CH_4 concentrations varied in a range of ~ 350 ppb during glacial periods, reaching concentrations of up to ~ 800 ppb during interglacial times. Looking at the short-term variability of CH_4 in the last glacial, rapid variations occur in intimate coupling to high-latitude Northern Hemisphere temperatures. In concert with some of these Northern Hemisphere warmings, the CH_4 concentration rose by 100–200 ppb within a few decades. However, thus far the causes for this steep increase are vastly unresolved. This thesis presents the first high resolution $\delta^{13}\text{CH}_4$ data covering both long-term and millennial-scale climatic changes and respective CH_4 variations during the last glacial period. With the help of measurements on ice core material from Vostok, Antarctica at the Pennsylvania State University (PSU), the database of atmospheric $\delta^{13}\text{CH}_4$ could be extended back as far as 160,000 years into the past. In combination with previous methane stable isotope records, this allows a detailed study of methane geochemistry at two late glacial maxima, the subsequent glacial-interglacial transitions and the full sequence of the last glaciation, including rapid Dansgaard-Oeschger (DO) climate fluctuations. At the Marine Isotope Stage (MIS) boundary 5 to 4, characterized by strong drops of sea-level and CO_2 concentration evidencing a severe global cooling, the $\delta^{13}\text{CH}_4$ record is further complemented by novel EDML $\delta\text{D}(\text{CH}_4)$ data obtained at the Climate and Environmental Physics division (KUP), University of Bern. The discussion of results of these measurements are presented in chapter 5 in form of a peer-reviewed publication. In-depth discussion of aspects that could not be covered by this article are presented as 'Extended Supplementary Information' in that same chapter. Moreover, this thesis presents strategies to account for recently discovered instrumental contamination by atmospheric krypton, affecting many stable isotope laboratories involved in $\delta^{13}\text{CH}_4$ analysis. The respective publication is provided in chapter 4.

The $\delta^{13}\text{CH}_4$ time series reveals a series of surprising observations of which the most important is the apparent and unexpected decoupling of $\delta^{13}\text{CH}_4$ variability from variations in CH_4 concentrations. In fact, only one of the various steep CH_4 increases of 100 ppb and more over glacial terminations and DO warmings are found to induce a synchronous shift in $\delta^{13}\text{CH}_4$. In the framework of common paradigms of methane geochemistry, the missing $\delta^{13}\text{CH}_4$ response to the abrupt CH_4 increases at DO events, preclude a predominant role of high-northern latitude (boreal) sources in DO CH_4 variability. Similar to the findings for DO CH_4 rises, both the CH_4 concentration jumps of ~ 200 ppb at the last two glacial-interglacial transitions demonstrate a lack of coherence of CH_4 and $\delta^{13}\text{CH}_4$ variability. Furthermore, while the CH_4 concentrations quickly (i.e. in $\sim 16,000$ years) return to early glacial values of ~ 450 ppb after the steep rise into the penultimate interglacial, $\delta^{13}\text{CH}_4$ values remain at relatively low levels for an additional 40,000 years. By then, the $\delta^{13}\text{CH}_4$ data shifts within a few millennia by several per mil towards higher values, notably a period when CH_4 variations are smaller than 50 ppb.

Over the full sequence of more than 160,000 years, $\delta^{13}\text{CH}_4$ data exhibit an intimate coherence with other climate parameters such as Southern Ocean temperature and, more notably, atmospheric CO_2 , which are both known to vary almost in lock-step. The combined evidence of isotopic data presented in this thesis suggests that tropical wetlands are the most important driver for glacial CH_4 variability and are believed to wax and wane proportionally along with other sources. The manuscript further presents the hypothesis that CO_2 and climate mediated changes occurring in tropical wetlands and seasonally inundated floodplain throughout the glaciation, which had a direct effect on vegetation and the $\delta^{13}\text{C}$ signature of its biomass, represent the key aspects towards the explanation for long-term $\delta^{13}\text{CH}_4$ variability over both glacial-interglacial and millennial time-scales, with a potential minor contribution from geologic sources and individual sink processes. Finally, this thesis demonstrates that there are still considerable gaps in the scientific understanding of methane geochemistry of the past and provide the grounds to inspire future research.

Zusammenfassung

Atmosphärische Treibhausgase spielen eine wichtige Rolle in der Energiebilanz des Klimasystems der Erde. Methan (CH_4) ist das drittwichtigste strahlungsaktive Gas nach Wasserdampf und Kohlendioxid. Gemeinsam mit Kohlendioxid (CO_2) und Distickstoffoxid (N_2O) ist Methan in den letzten 250 Jahren aufgrund von Aktivitäten des Menschen so steil angestiegen wie es in 800.000 Jahren Klimageschichte noch nicht vorgekommen ist. Der menschengemachte Anteil am Anstieg des Methans kann nur durch den Vergleich mit der natürlichen Variabilität erfasst werden. Lufteinschlüsse in polaren Firn- und Eiskernen stellen das einzige direkte Archiv der atmosphärischen Vergangenheit dar. Über die letzten acht Glazialzyklen variierte CH_4 in einem Bereich von etwa 350 ppb während der Kaltperioden bis zu etwa 800 ppb während der Warmzeiten. Im letzten Glazial traten kurzzeitige Variabilität des CH_4 in enger Verknüpfung zum Temperaturverlauf in hohen Breiten der Nordhämispäre auf. Bei einigen dieser nordhämispärischen Erwärmungsereignissen stieg CH_4 innerhalb weniger Dekaden rapide um Werte von 100–200 ppb an. Allerdings sind die Gründe für diesen Anstieg noch immer unbekannt. Diese Dissertation präsentiert die ersten hoch-aufgelösten $\delta^{13}\text{CH}_4$ -Daten die sowohl langfristige als auch wenige Jahrtausende dauernde Klimavariationen und einhergehende Veränderungen in CH_4 des letzten Glazials abdeckt. Mithilfe von Messungen an Eiskernmaterial aus Vostok in der Antarktis der Pennsylvania State University (PSU) konnte der gesamte Datensatz atmosphärischen $\delta^{13}\text{CH}_4$ damit bis 160.000 Jahre in die Vergangenheit verlängert werden. Zusammen mit vorherigen Datensätzen stabiler Isotope des Methans erlaubt dies ein genaues Studium der CH_4 -Geochemie an zwei späten glazialen Maxima, darauf folgenden Glazial-interglazial-Übergängen sowie des gesamten Ablaufs der letzten Vereisung, schnelle Dansgaard-Oeschger (DO) Klimafluktuationen mit eingeschlossen. Beim Übergang vom Marinen Isotopen-Stadium (MIS) 5 zu 4, wo es zu starken Abfällen des Meeresspiegels und der CO_2 -Konzentrationen kommt, die ein starkes globales Abkühlen dokumentieren, wird der $\delta^{13}\text{CH}_4$ -Datensatz des weiteren durch $\delta\text{D}(\text{CH}_4)$ -Daten von EDML ergänzt, die am Institut der Klima- und Umwelphysik der Universität Bern gemessen wurden. Die Diskussion der Ergebnisse aller dieser Datensätze wird in Kapitel 5 in Form einer Veröffentlichung präsentiert. Weiter in die Tiefe gehende Diskussionen bestimmter Aspekte, die in der Veröffentlichung nicht abgehandelt werden konnten, werden im selben Kapitel als "Erweiterte zusätzliche Informationen" angehängt.

Des weiteren beinhaltet diese Arbeit Strategien zur Vermeidung und nachträglichen Korrektur von erst vor kurzem entdeckten Kontaminationen durch atmosphärisches Krypton bei Kohlenstoff-Isotopenmessungen, welches viele Stabile Isotopen-Laboratorien weltweit betrifft. Die entsprechende Publikation befindet sich im Kapitel 4.

Die $\delta^{13}\text{CH}_4$ -Datenserie enthüllt eine ganze Reihe überraschender Beobachtungen. Die wichtigste davon ist die offensichtliche und unerwartete Entkopplung der Veränderungen im $\delta^{13}\text{CH}_4$ von den Variationen in CH_4 . Genauer gibt es nur einen einzigen der vielen CH_4 -Anstiege von mehr als 100 ppb im Zusammenhang mit Dansgaard-Oeschger- und Glazial-Interglazial-Erwärmungen, der einen gleichzeitige Veränderung in $\delta^{13}\text{CH}_4$ hervorruft. Im Rahmen der üblichen Interpretation der Methan-Geochemie, schließt das Fehlen von Veränderungen im $\delta^{13}\text{CH}_4$ im Zusammenhang mit DO CH_4 -Anstiegen eine bedeutende Rolle von (borealen) Quellen aus hohen Breiten an DO CH_4 -Veränderungen weitestgehend aus. Ähnlich verhält es sich bei beiden CH_4 -Sprüngen von etwa 200 ppb bei den zwei letzten Übergängen von Glazialen in Interglaziale. Während sich CH_4 beim vorletzten Übergang nach diesem Anstieg des weiteren relativ schnell wieder glazialen Werten von etwa 450 ppb annähern verbleibt $\delta^{13}\text{CH}_4$ noch für weitere 40.000 Jahre auf einem relativ niedrigem Niveau. Dann aber steigen die Werte innerhalb weniger Jahrtausende um einige Promille an, bemerkenswerterweise zu einer Zeit in der sich CH_4 um weniger als 50 ppb verändert.

Über den gesamten Zeitraum von mehr als 160.000 Jahren zeigt $\delta^{13}\text{CH}_4$ dagegen eine intime Verknüpfung mit anderen Klimafaktoren wie der Temperatur des Südozeans, und, noch bemerkenswerter, den Konzentrationen von atmosphärischen CO_2 welche sich bekanntermaßen beide fast im Gleichschritt verändern. Die gesammelten Beweise aus den Isotopendaten, die in dieser Dissertation präsentiert werden, legen nahe, dass tropische Feuchtgebiete die entscheidende Einflussgröße für glaziale CH_4 -Variabilität darstellt, deren Emissionen zusammen mit geringeren Beiträgen anderer Quellen proportional zu- und abnehmen. In diesem Manuskript wird darüber hinaus die Hypothese präsentiert, dass während des letzten Glazials CO_2 - und klimagesteuerte Veränderungen, die einen direkten Einfluss auf Vegetation in tropischen Feucht- und Überschwemmungsgebieten und die $\delta^{13}\text{C}$ Signaturen seiner Biomasse ausübten, die Schlüsselemente bei der Erklärung der Langzeitvariabilität des $\delta^{13}\text{CH}_4$ sowohl auf Glazial-Interglazialen Zeitskalen als auch für lediglich Jahrtausende andauernde Veränderungen darstellen. Schlussendlich demonstriert diese Arbeit auch, dass weiterhin erhebliche Lücken im wissenschaftlichen Verständnis der Methan-Geochemie vergangener Zeiten bestehen, und sollte die Grundlagen bieten weitere Forschung auf diesem Gebiet anzuregen.

Contents

| | |
|--|-----------|
| 1. Introduction | 1 |
| 2. Methane – an inventory of the present and the past | 4 |
| 2.1. Recent methane budgets | 5 |
| 2.2. The methane record I - early values and a strong rise | 11 |
| 2.3. The methane record II - trapped in ice | 15 |
| 2.4. Stable isotopes and signatures of sources and sinks of atmospheric methane | 21 |
| Stable isotopes, the δ -notation, and reference materials | 21 |
| Present-day atmospheric values of $\delta^{13}\text{C}$ and $\delta\text{D}(\text{CH}_4)$ | 23 |
| 2.4.1. Sources and sinks of CH_4 and their effect on $\delta^{13}\text{C}/\delta\text{D}$ | 23 |
| Formation pathways of biogenic methane | 25 |
| Factors influencing the isotopic signature of biogenic methane | 28 |
| Isotope mass balances and fractionation during methane removal | 30 |
| Geographical distribution of sources and changes in the past | 32 |
| 2.4.2. $\delta^{13}\text{C}/\delta\text{D}(\text{CH}_4)$ records for the past and what they have taught us | 34 |
| 3. Ice cores - Spyglass into the atmospheric history | 43 |
| 3.1. How atmosphere is conserved in the ice | 44 |
| 3.2. Changes during gas enclosure | 46 |
| 4. Experimental | 50 |
| 4.1. Tracing an exemplary ice sample through the system | 50 |
| 4.2. Referencing strategies and their realization | 54 |
| 4.3. Data processing | 56 |
| 4.3.1. Script based raw data processing | 58 |
| 4.3.2. Script-based data post-processing | 59 |
| Internal calibration | 60 |
| External calibration | 63 |

| | |
|--|------------|
| Evaluation of the script-based data processing | 65 |
| 4.4. Methane synchronization of ice core age scales | 67 |
| 4.5. Corrections for Kr interference | 68 |
| 4.5.1. Publication on Kr interference by Schmitt et al., 2013 | 70 |
| 4.5.2. A posteriori correction of EDML and Vostok $\delta^{13}\text{CH}_4$ data | 92 |
| EDML samples measured at AWI | 92 |
| Vostok samples measured at the PSU | 92 |
| 5. Results and Discussion | 95 |
| 5.1. Publication on EDML and Vostok $\delta^{13}\text{CH}_4$ data by Möller et al., 2013 | 96 |
| 5.2. Extended supplementary information and discussion | 114 |
| 5.2.1. The glacial EDML $\delta^{13}\text{CH}_4$ record | 114 |
| 5.2.2. Laboratory inter-calibration between PSU and AWI | 114 |
| 5.2.3. Model results for gravitational settling & diffusional fractionation | 115 |
| 5.2.4. Age scales and ice core CH_4 synchronization | 119 |
| Manual CH_4 synchronization for Vostok $\delta^{13}\text{CH}_4$ and CO_2 records | 119 |
| Manual CH_4 synchronization for the Byrd atmospheric CO_2 record | 119 |
| 5.2.5. Extended discussion of rapid methane variability during the last glacial | 120 |
| Dansgaard-Oeschger cycles | 120 |
| Heinrich events | 131 |
| Role of water table changes | 135 |
| Final thoughts about the interpretation of rapid CH_4 variability | 136 |
| 5.2.6. Extended discussion of long-term variability of $\delta^{13}\text{CH}_4$ | 137 |
| Atmospheric CO_2 - a potential driver for $\delta^{13}\text{CH}_4$ variability? | 138 |
| Did sea-level contribute to $\delta^{13}\text{CH}_4$ variations? | 143 |
| Conclusions | 146 |
| A. Acronyms | 191 |
| B. Supplementary Information for the publication by Möller et al., 2013 | 195 |
| C. Carbon isotope data | 221 |
| D. Python Code | 230 |
| D.1. Raw data processing | 230 |

| | |
|--------------------------------|------------|
| D.2. Post processing | 263 |
| E. Acknowledgements | 299 |

1. Introduction

The main driving force behind the climate on earth is the radiation that the planet receives from the sun. The distribution of land, ocean and cryosphere controls how much of the short-wave solar radiation is reflected or absorbed by the surface. A part of the absorbed thermal energy is radiated back to space at longer wave-lengths. The greenhouse gases in the atmosphere absorb and re-scatter parts of this long-wave radiation and thus contribute significantly to the energy balance of the climate system. After water vapor and carbon dioxide (CO₂), methane (CH₄) is the third most important contributor to the greenhouse effect. The global concentrations of CH₄ have increased by more than 150 % over the last 250 years since the onset of the industrialization from their pre-industrial value of 715 ppb ¹ (*Etheridge et al.*, 1998) to a value of ~1800 ppb in 2008 (*Dlugokencky et al.*, 2009). This increase is proportionately far greater than the parallel increase in atmospheric CO₂ and contributes significantly (0.5 Wm⁻²) to the total direct radiative forcing by long-lived greenhouse gases (*Dlugokencky et al.*, 2011, 2.77, Wm⁻²). This radiative forcing is an expression of the influence of a greenhouse gas on the radiative balance. In addition to the direct absorption of long-wave radiation emitted from the ground, the role of CH₄ in atmospheric chemistry adds another ~0.2 Wm⁻² as indirect forcing (*Dlugokencky et al.*, 2011). The indirect effect is mainly due to the chemical reaction with its major sink, the hydroxyl radical ·OH, which is involved in a series of other break-down reactions of radiatively active gases (*Lelieveld et al.*, 2008). Via the positive feedback of CH₄ on ·OH, higher methane levels reduce the ·OH concentration, leading to longer lifetimes and concentrations of CH₄ in the atmosphere. The atmospheric CH₄ burden thus

¹ The abundance of gases in the atmosphere is usually expressed as a dimensionless ratio of particles of the respective gas species relative to the remaining constituents in a given volume of air, also often referred to as mole fractions. Atmospheric carbon dioxide (CO₂) levels are thus reported in parts per million (ppm), which translate into micro-moles per mole of air. The less abundant methane (CH₄) and nitrous oxide (N₂O), however, are reported in parts per billion (ppb), equivalent to nano-moles per mole of air. Trace gas concentrations also often expressed as the volume fractions parts per million by volume (ppmv) and ppbv, respectively. Note that these units are only equivalent to ppm and ppb when the respective compound is considered an ideal gas which is not strictly true in the case of CO₂, for example.

influences the oxidative capacity of the atmosphere and the removal of other trace gases such as non-methane volatile organic compounds (NMVOCs) by $\cdot\text{OH}$ (Keppler *et al.*, 2006). Methane oxidation in the stratosphere is further responsible for the formation of approximately half of the stratospheric water that is essential for the formation of polar stratospheric clouds in the Arctic and Antarctic winter. After the evaporation of these clouds in spring, elementary chlorine is liberated and is responsible for the massive destruction of ozone that leads to the formation of large ozone holes over the Arctic and Antarctica.

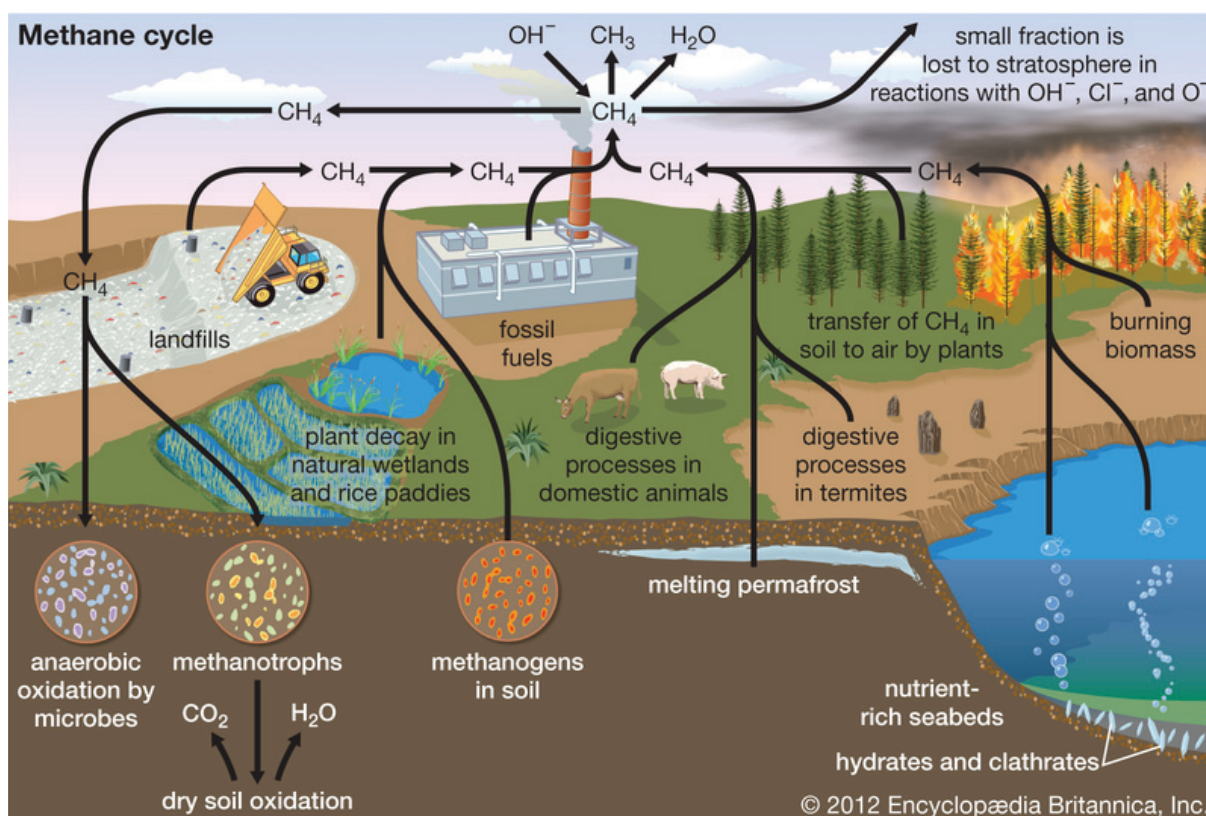


Figure 1.1.: A simplified scheme of factors involved in the present-day methane cycle.
© Encyclopædia Britannica, Inc., 2012

The strong increase of the three greenhouse gases CO_2 , N_2O and CH_4 since ~ 1750 AD has mainly been attributed to human activities such as exploitation and burning of fossil fuels or land use changes (e.g. deforestation in the tropics) (IPCC, 2007). Emissions from rice cultivation, waste treatment, biomass burning and farming of domestic ruminants considerably contribute to atmospheric methane budgets that were previously dominated

by natural processes. The study of CH₄ content in air bubbles of polar ice cores has revealed that the range of natural variability of CH₄ over the last 800,000 years has not significantly exceeded 300–700 ppb (*Loulergue et al.*, 2008), proving that mankind exerts a considerable influence on the contemporary CH₄ cycle. However, not much is known about the consequences and potential feedback mechanisms on natural CH₄ sources that are induced by the recent substantial changes taking place in Earth’s climate system (*IPCC*, 2007). A better understanding of the natural variability of CH₄ and the driving forces behind it may help to assess the extent of the actual human impact and improve predictions of future trends. Stable isotope reconstructions from air enclosed in polar ice cores represent a powerful tool to study the natural processes involved in the methane cycle of the past.

This thesis presents a carbon isotopic record of atmospheric methane ($\delta^{13}\text{CH}_4$) that extends previous $\delta^{13}\text{CH}_4$ time series to as much as 160,000 years into the past, now including the penultimate deglaciation into the Eemian warm period ($\sim 120,000$ years before the present) and the full sequence of the last glaciation. This record thus covers more than a full glacial cycle (i.e. more than 140,000 years), allowing for the study of natural long-term and millennial scale variations of CH₄ observed throughout the last glacial period and ultimate deglaciations with unprecedented coverage and precision.

The $\delta^{13}\text{CH}_4$ data will be presented in chapter 5 of this manuscript. A comprehensive description of the methods used to infer the data, apply corrections to account for post-depositional processes in the ice and to grant comparability with other stable isotope laboratories will be given in chapter 4. This chapter will also include a publication on how to avoid and account for analytical contaminations with atmospheric krypton (*a posteriori* treatment), which has recently been found to affect many isotope ratio monitoring mass spectrometry (IrmMS) systems. The following chapter is dedicated to an introduction into the methane cycle, the theoretical background concerning stable isotopes in methane geochemistry and a brief review of characteristics of the enclosure of air in the climate archive ice cores.

2. Methane – an inventory of the present and the past

The famous Italian scientist Alessandro Volta, inspired by a publication of Benjamin Franklin on natural sources of "flammable air", was the first man in recorded history, to systematically study CH₄. At the shores of *Lago Maggiore* in Italy he sampled what he called "inflammable gas from the marshlands" from bubbles emerging to the surface from the lake's muddy underground and was able to isolate methane from it in 1778 (*Wolfe*, 1996; *Hoffmann et al.*, 2004). Almost 200 years later, in 1948, the Belgian astrophysicist Marcel Migeotte identified absorption bands of methane, the smallest compound from the group of hydrocarbons, in the infrared range of the solar spectrum, proving that it is a natural component of the Earth's atmosphere (*Migeotte*, 1948a). From his infrared absorption measurements, he estimated the atmospheric abundance of CH₄ to be around 2000 ppb.

The pioneering study by *Bates and Witherspoon* (1952) of the geochemical cycles and the photochemistry of CH₄ and carbon monoxide (CO) in the atmosphere established many of the basic features of the processes involving these gases (*Wofsy*, 1976). *Bates and Witherspoon* (1952) concluded that CH₄ must have a sizable natural source and proposed anaerobic fermentation as a likely candidate for it. A conclusion that was in agreement with an earlier finding by *Glückauf* (1951) based on an early stable isotope measurements, suggesting that atmospheric CH₄ was of biogenic rather than of geologic origin.

Early global emission inventories by *Singer* (1971) and *Ehhalt* (1974) later synthesized studies of more than a decade to provide a much more elaborate and concrete description of source and sink processes controlling atmospheric methane. This includes a series of emissions unequivocally caused by human activities that were directly associated with the increase of the atmospheric burden for the first time (*Ehhalt*, 1974). However, this hypothesis was first met with serious skepticism (*Rasmussen and Khalil*, 1981).

2.1. Recent methane budgets

The atmospheric CH₄ budget represents the balance of CH₄ source emissions and removal processes. Precise estimates of individual contributions, however, are difficult to achieve. Three different approaches are commonly used to derive trace gas emission scenarios: 1) extrapolation from direct flux measurements in the field, 2) process based (bottom-up) modeling and 3) inverse or top-down modeling. The first two approaches provide good measures of the multitude of processes involved, their individual contribution and timing, but tend to suffer from large uncertainties concerning spatial extent and temporal variability of observed fluxes (*Cicerone and Oremland, 1988; Walter et al., 2001a,b; Kaplan, 2002; Valdes et al., 2005; Kaplan et al., 2006; Wania et al., 2009a,b; Berrittella and van Huissteden, 2011*). The last approach is based on high accuracy atmospheric measurements direct from flask samples or indirect via satellites (e.g. Scanning Imaging Absorption Spectrometer for Atmospheric Chartography (SCIAMACHY)) (*Dlugokencky et al., 1995; Frankenberg et al., 2005, 2008; Bergamaschi et al., 2009*). They allow a better deconvolution of temporal and spatial CH₄ variability, but rely on a series of assumptions and constraining parameterization to distinguish between sources, take sink processes into consideration, and finally infer global budget calculations (*Hein et al., 1997; Houweling et al., 1999; Mikaloff Fletcher et al., 2004a,b; Chen and Prinn, 2006*). In contrast, one major advantage of inverse modeling, particularly if it is derived from satellite measurements, is that these model calculations allow to complement and evaluate direct flux measurements and process based model results (*Bergamaschi et al., 2009; Spahni et al., 2011*).

Estimates for recent CH₄ emissions and sinks, derived from a series of models mainly following the top-down approach, are summarized in the Fourth Assessment Report (AR4) of the Intergovernmental Panel on Climate Change (IPCC). According to these models, ~503–610 Tg yr⁻¹ (1 Tg = 1 × 10¹² g) are emitted to the atmosphere (*IPCC, 2007, Figure 2.2*). A wide spectrum of sources contribute to this budget, a range of natural processes and emissions that emerge from human activity (so-called anthropogenic sources). Anthropogenic CH₄ emissions make up 54–72% of the modern total global flux, with fossil fuel production, coal mining, livestock, anthropogenic biomass burning, landfills or other waste management, and rice agriculture being the largest CH₄ contributors (*IPCC, 2007*). The remaining 28–46% of atmospheric CH₄ are emitted by natural sources. A predominant share of natural CH₄ emissions stems from the anaerobic degradation of organic material in wet, permanently and seasonally inundated ecosystems (wetlands), and poorly

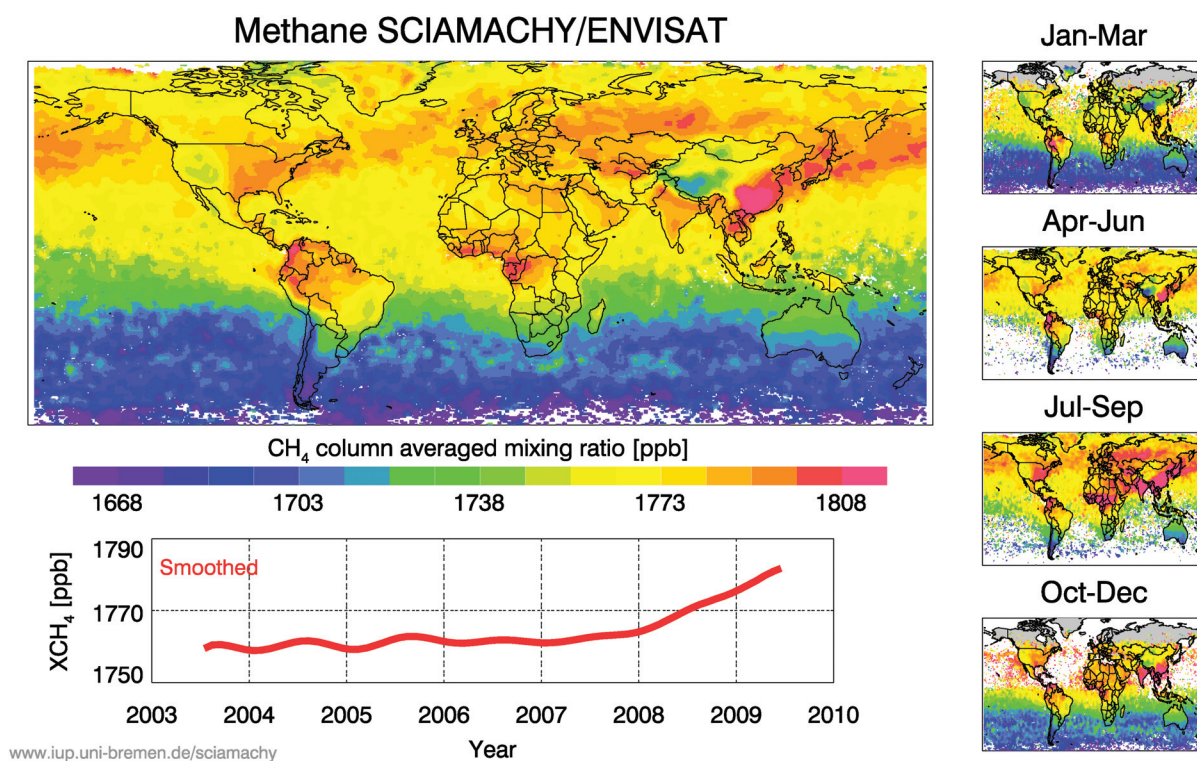


Figure 2.1.: Global map of atmospheric methane inferred from SCIAMACHY measurements on board of ENVISAT.

A global map of atmospheric methane (years 2003–2005) is shown at the top left, seasonal variations on the right, and a smoothed time series confirming the stable CH₄ level at the beginning of this millennium and the start of an increase since 2007 (compare also section 2.2). Methane dry air column-averaged mixing ratios (mole fractions) were retrieved from the near-infrared nadir spectra of reflected and backscattered solar radiation measured by the SCIAMACHY instrument on board the European environmental satellite ENVISAT using the retrieval algorithm WFM-DOAS (Buchwitz *et al.*, 2005). The figure was taken from <http://www.iup.uni-bremen.de/sciamachy>.

constrained contributions are caused by oceans, wildfires, geological sources, wild animals and termites. Budget calculations usually only include net fluxes. The gross production of methane is significantly larger, but substantial quantities of methane are consumed in soils, oxic freshwater, and the ocean before reaching the atmosphere (Reeburgh, 2004, net to gross flux). Due to the respiration CH₄ by methanotrophic bacteria, certain oxic soil types are even net sinks of methane.

Recent discoveries proposed some additional, potentially influential, sources of methane, which were not considered in the budgets presented in the AR4 of the IPCC. Highly elevated CH₄ concentrations over tropical rain forests were indicated by the first global

scale CH₄ air column concentration data retrieved with the SCIAMACHY satellite instrument (*Frankenberg et al.*, 2005). *Keppeler et al.* (2006) associated these emissions with *in situ* CH₄ production in plants under aerobic conditions when these plants were exposed to high levels of ultraviolet (UV) radiation. The authors justified this assumption with findings from experiments in growing chambers, and estimated the source strength of this process, the first aerobic production pathway of biogenic CH₄ ever reported, to account for emissions in the range of 62–236 Tg yr⁻¹, corresponding to 10–45 % of the global methane source output.

This hypothesis, however, created a serious controversy in the scientific community. Some criticism was focused on the formation mechanism itself, as the results of *Keppeler et al.* (2006) could not be validated in other studies (*Dueck et al.*, 2007; *Beerling et al.*, 2008). Others focused on the plausibility of the extrapolations and resulting global emission estimates (*Kirschbaum et al.*, 2006; *Parsons et al.*, 2006). Later, experimental evidence for the aerobic, UV-induced production of CH₄ in plants was found (*Vigano et al.*, 2008; *Kamakura et al.*, 2012, and others), but emission rates and the impact on global budgets were scaled down by order of magnitudes (*Bloom et al.*, 2010). *Nisbet et al.* (2009) argued that although plants do not contain a known biochemical pathway to synthesize methane, there may be spontaneous breakdown of plant material under high UV stress conditions. But plants could contribute to the observed CH₄ emissions by the transport of water containing dissolved methane from the soils to the atmosphere (*Nisbet et al.*, 2009; *Rice et al.*, 2010). Another hypothesis suggests that these emissions might stem from wetland-like micro-environments in tank bromeliads that grow on dead, decomposing leaves on the branches of tropical trees (*Yavitt*, 2010; *Martinson et al.*, 2010). However, the SCIAMACHY results from *Frankenberg et al.* (2005) were revised in a later publication, and the corresponding estimates of tropical rain forest CH₄ emissions were significantly reduced. The erroneously high values were caused by an instrumental retrieval error and were related to inaccuracies in water vapor spectroscopic parameters that led to the overestimations of CH₄ mixing ratios in the air column (*Frankenberg et al.*, 2008).

In the recent years, two more CH₄ sources with potential impact on global CH₄ budgets have attracted increased attention in scientific research. *Shakhova et al.* (2010) report on methane out-gassing from the Arctic continental shelf off northeastern Siberia in the Laptev and East Siberian Seas. The shallow seabed, residing 50 meters and less below the surface, consists of old permafrost soils that formed a frozen arctic coastal plain during glacial periods when sea levels were considerably lower than today. The permafrost layer contains substantial amounts of organic carbon and was long thought to be an

impermeable barrier to methane seeping up from underneath. In colder periods, the methane forms relatively stable methane hydrates, but the recent warming of seawater destabilizes the hydrates, and the permafrost has now found to be perforated and starting to leak large amounts of methane, estimated to as much as 6.3–9.7 Tg yr⁻¹, into the atmosphere (*Shakhova et al.*, 2010).

Another potentially important source of methane was recently reported for sub-glacial environments, that are permanently covered by ice sheets (*Wadham et al.*, 2008; *Boyd et al.*, 2010; *Skidmore*, 2011; *Hamilton et al.*, 2013; *Thor Marteinsson et al.*, 2013). The new studies suggest that organic matter in old sedimentary basins located beneath the ice, including the inland basal zones of the Arctic and Antarctic polar ice sheets (*Christner et al.*, 2012; *Stibal et al.*, 2012; *Wadham et al.*, 2012), may in part be converted to methane by active communities of micro-organisms living under low oxygen conditions. Therefore this sources may have had important implications on the methane cycle on glacial-interglacial timescales, and also in the future when ice sheets further retreat due to the ongoing global warming (*Stibal et al.*, 2012; *Wadham et al.*, 2012).

Although the major CH₄ fluxes are now probably identified, and the source ensemble thus almost complete, the quantification of individual processes still remains largely unconstrained. Particularly the lack of understanding of the geographical distribution and inter-annual variability of emissions from the marine and terrestrial biosphere adds a considerable degree of uncertainty to source estimates. Their contributions are known to vary considerably in time and space (e.g. CH₄ fluxes from wetlands (*Bousquet et al.*, 2006; *Nahlik and Mitsch*, 2011), thermokarst lakes (*Walter et al.*, 2007) or geological sources (*Judd et al.*, 2002)). However, budget calculations suffer additionally from unknowns concerning the removal processes of CH₄ that determine the residence time of CH₄ molecules in the atmosphere.

The mean lifetime of atmospheric CH₄ is estimated to be within the range of 8.5–9.7 yr (*Stevenson et al.*, 2006; *Prather et al.*, 2012; *Naik et al.*, 2013) and is chiefly a consequence of the oxidation reaction with hydroxyl radicals ($\cdot\text{OH}$) in the troposphere. The OH radicals are formed in a photolytic reaction chain involving UV radiation, ozone (O₃) and water vapor (H₂O) (*Cicerone and Oremland*, 1988; *Thompson*, 1992; *Prinn*, 2003), and are thought to be responsible for the removal of ~85–90% of tropospheric methane (*Dlugokencky et al.*, 1994; *Wuebbles and Hayhoe*, 2002; *O'Connor et al.*, 2010):



| References | Indicative ^{13}C , ‰ ^{a,b} | Hein et al., 1997 ^c | Houweling et al., 2000 ^c | Olivier et al., 2005 | Wuebbles and Hayhoe, 2002 | Scheehle et al., 2002 | J. Wang et al., 2004 ^c | Mikaloff Fletcher et al., 2004 ^{a,c} | Chen and Prinn, 2006 ^c | TAR | AR4 |
|------------------------------|---|--------------------------------|-------------------------------------|----------------------|---------------------------|-----------------------|-----------------------------------|---|-----------------------------------|-----------|-----|
| Base year | | 1983–1989 | 2000 | 2000 | 1990 | 1994 | 1999 | 1996–2001 | 1998 | 2000–2004 | |
| Natural sources | | 222 | 145 | 200 | 264 | 307 | 350 | 168 | | | |
| Wetlands | -58 | 231 | 100 | 176 | 231 | 231 | 231 | 145 | | | |
| Termites | -70 | 20 | 20 | 20 | 29 | 29 | 29 | 23 | | | |
| Ocean | -60 | 15 | 4 | 4 | | | | | | | |
| Hydrates | -60 | 4 | 5 | 4 | | | | | | | |
| Geological sources | -40 | 4 | 14 | | | | | | | | |
| Wild animals | -60 | 15 | | | | | | | | | |
| Wildfires | -25 | 5 | 2 | | | | | | | | |
| Anthropogenic sources | | 361 | 320 | 307 | 428 | | | | | | |
| Energy | | | | | 74 | 77 | | | | | |
| Coal mining | -37 | 32 | 34 | 30 | 46 | 48 ^d | | | | | |
| Gas, oil, industry | -44 | 68 | 64 | 52 | 60 | 36 ^e | | | | | |
| Landfills & waste | -55 | 43 | 66 | 35 | 61 | 49 | | | | | |
| Ruminants | -60 | 92 | 80 | 91 | 76 | 83 | | 189 ^f | | | |
| Rice agriculture | -63 | 83 | 39 | 54 | 31 | 57 | | 112 | | | |
| Biomass burning | -25 | 43 | 50 | 88 | 14 | 41 | | 43 ^e | | | |
| C3 vegetation | -25 | | 27 | | | | | | | | |
| C4 vegetation | -12 | | 9 | | | | | | | | |
| Total sources | | 592 | 503 | 507 | 596 | 598 | 610 | 582 | | | |
| Imbalance | | +33 | | | | | | +22 | | +1 | |
| Sinks | | | | | | | | | | | |
| Soils | -18 | 26 | 30 | 34 | 30 | 30 | 30 | 30 ^g | | | |
| Tropospheric OH | -3.9 | 488 | 445 | 428 | 507 | 511 ^g | | | | | |
| Stratospheric loss | | 45 | 40 | 30 | 40 | 40 | | | | | |
| Total sink | | 559 | 515 | 492 | 577 | 576 | 581^g | | | | |

Notes:

^a Table shows the best estimate values.^b Indicative ^{13}C values for sources are taken mainly from Mikaloff Fletcher et al. (2004a). Entries for sinks are the fractionation, $(k_{13}/k_{12}-1)$ where k_{13} is the removal rate of $^{13}\text{CH}_4$; the fractionation for OH is taken from Saueressig et al. (2001) and that for the soil sink from Snover and Quay (2000) as the most recent determinations.^c Estimates from global inverse modelling (top-down method).^d Includes natural gas emissions.^e Biofuel emissions are included under Industry.^f Includes emissions from landfills and wastes.^g Numbers are increased by 1% from the TAR according to recalibration described in Chapter 2.Figure 2.2.: Compilation of atmospheric budgets, sources and sinks of CH_4 .Modeled budgets, sources and sinks of atmospheric CH_4 according to several studies summarized in the AR4 (IPCC, 2007).

The subsequent radical chain reaction leads to formaldehyde (HCHO), which further oxidizes to CO₂, water and ozone. ·OH concentrations are not constant in the atmosphere, and vary diurnally, seasonally, and spatially. The OH abundance and, consequently, the CH₄ lifetime depend on concentrations of CH₄ itself, nitrogen oxides (NO_x), CO, and NMVOCs (*Lelieveld et al.*, 2002, 2004). Highest values are found in the tropical troposphere, where the primary production of OH radicals from ozone photolysis is most efficient because of the combination of strong UV radiation intensity and high humidity (see Figure 2.3). In the stratosphere, CH₄ is destroyed by reactions with ·OH, Cl radicals (·Cl), and oxygen O(¹D) (*Saueressig et al.*, 2001). Another removal process for atmospheric CH₄ is oxidation in aerated soils (*Born et al.*, 1990; *Ridgwell et al.*, 1999; *Dutaur and Verchot*, 2007). Combined, these two processes account for ~40 Tg yr⁻¹ methane loss. Finally, one further CH₄ sink has been proposed by *Allan et al.* (2001b) involving the reaction of CH₄ with Cl radicals in the marine boundary layer (MBL). It was deduced from the observation of anomalously depleted δ¹³C values in methane in the South Pacific region, at Baring Head, New Zealand, and Scott Base, Antarctica (*Allan et al.*, 2001b,a, 2005) and ellipsoidal seasonal variations in the southern hemisphere (*Allan et al.*, 2010; *Lassey et al.*, 2011). Although the global importance of the MBL sink is not clear at present due to the difficulty of in-situ direct measurement of ·Cl, it was estimated to account for 19–25 Tg yr⁻¹ (*Platt et al.*, 2004; *Allan et al.*, 2007), i.e. 3.3–5% of the total CH₄ sink of ~428–511 Tg yr⁻¹ (*IPCC*, 2007).

The ±15% error range in the AR4 global budget (Figure 2.2) largely reflects the uncertainties in sink estimates and the lifetime of CH₄ used in the mass balance calculations. Based on the mean global ·OH concentration derived from the methyl chloroform (CH₃CCl₃) budget, the ·OH sink strength is believed to be quantified with relatively good accuracy (*Prinn et al.*, 1995). Despite the inter-annual variability of OH abundance being high, the downward trend in CH₄ growth rates for the period 1984–2002 for example has been attributed to a small positive global trend in OH concentrations (*Prinn et al.*, 2005) rather than to decreasing source emissions as a primary cause (*Bousquet et al.*, 2006; *Chen and Prinn*, 2006, and others (see also section 2.2)). However, the debate about the importance of inter-annual variability in OH-loss in recent decades remains unresolved (*Monteil et al.*, 2011; *Montzka et al.*, 2011).

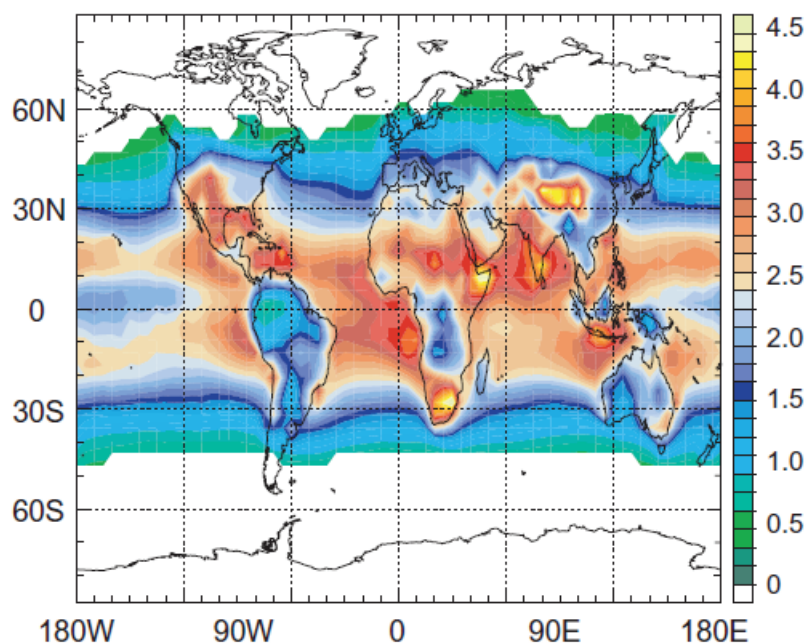


Figure 2.3.: Annual mean OH concentrations near the earth's surface.

Values for $\cdot\text{OH}$ in the boundary layer at low and middle latitudes are calculated with a chemistry-transport model by *Lelieveld et al.* (2002) and given in 1×10^6 radicals cm^{-3} . Figure taken from *Lelieveld et al.* (2004).

2.2. The methane record I - early values and a strong rise

The initial values in the late 1950s from infrared absorption measurements for the atmospheric abundance of CH_4 by *Migeotte* (1948b) of ~ 2000 ppb were subsequently considered an overestimation. Further sporadic measurements in the 60s and 70s using newly developed gas chromatography and flame ionization detector (FID) techniques suggested values rather around 1350 ppb in the early 60s, and an increasing trend towards 1850 ppb over the following two decades (*Khalil et al.*, 1989, and references within). Due to early studies on air enclosures in polar ice cores, which documented that atmospheric abundance of CH_4 had been at less than half the present levels not even 300 years ago (*Robbins et al.*, 1973), this steep trend was publicly perceived as seriously disturbing. Initially, *Robbins et al.* (1973) assumed that partial oxidation of CH_4 to CO occurred during air enclosure in the firn, as they also found elevated CO levels in their ice core material from Greenland and Antarctica (see chapter 3.1 for an extensive description of how air is conserved in ice sheets). Consequently, they believed that the observed low CH_4 levels in the ice were an artifact rather than a realistic reconstruction of past CH_4 atmospheric abundances. But *Rasmussen et al.* (1982) proposed an alternative explanation for the elevated CO values,

i.e. that the enrichment is entirely due to adsorption of CO on the surface of snow before its accumulation in firn. Subsequent measurements from the Greenland Dye 3 core further proved that the measurements by *Robbins et al.* (1973) indeed reflected the atmospheric concentration of CH₄ in ancient air at that time (*Craig and Chou, 1982*).

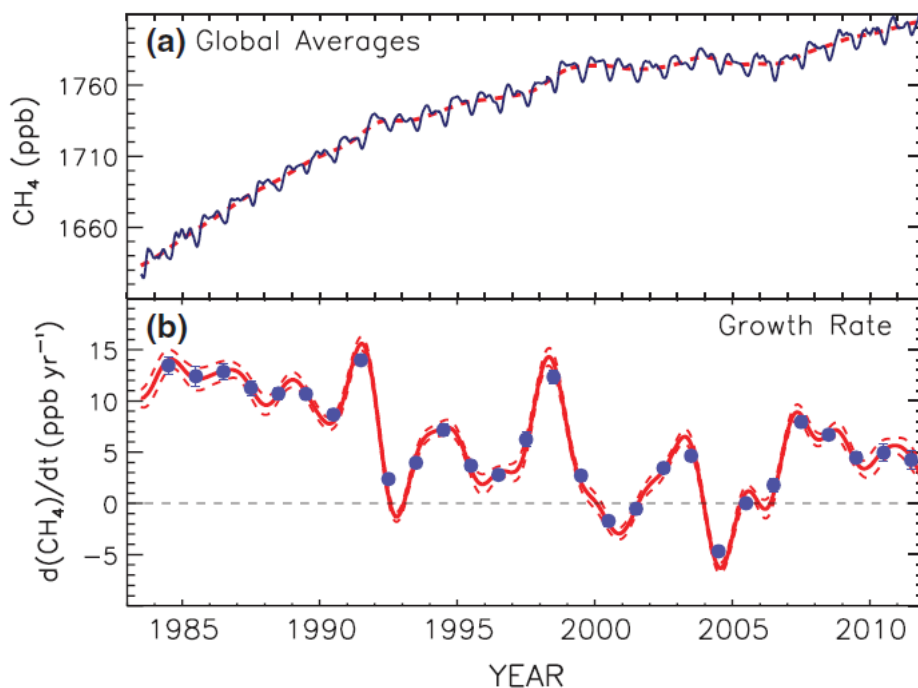


Figure 2.4.: Trends of atmospheric methane over the last three decades.

Subplot (a) shows the globally averaged CH₄ mixing ratios over the last thirty years (dry air mole fractions measured on weekly samples from the NOAA Global Cooperative Air Sampling Network). The deseasonalized increasing trend (as a fit to the global averages) is represented by the red dashed line. The lower sub-figure (b) illustrates the growth rates over the same period calculated from the fitted trend in (a). Uncertainties of 1 σ are shown as dashed lines and circles represent annual increases calculated from the 1st of January of one year to the 1st of January of the next. Content from *Dlugokencky et al.* (2011).

The continuing concentration increase of methane and other atmospheric trace gases, as well as rapid improvements in the field of instrumental analytics, led to the foundation of a world-wide range of networks that emerged among universities and other institutions of atmospheric sciences in the early 1980s that started to continuously monitor the chemical composition of the atmosphere at various locations around the globe. Probably the most comprehensive of them is the Global Cooperative Air Sampling Network initiated by the NOAA Earth System Research Laboratory (ESRL), contributing with frequent measurements from more than 100 sites today. The networks' continuous record of

globally averaged atmospheric CH_4 concentrations (Figure 2.4a) impressively documents the continued global increase of CH_4 mixing ratios until the end of the last millennium (e.g. *Dlugokencky et al.* (1994, 1998)). The smoothed latitudinal distribution of atmospheric CH_4 shown in figure 2.5 further illustrates the existing North-South concentration gradient of approximately 90 ppb for CH_4 over the last decade (also known as the inter-polar difference (IPD)), with an anti-phased seasonality of about 2% in the northern and southern hemisphere, and maxima occurring in local winter (*NOAA*, 2011). The higher concentration levels in the North are mainly attributed to preferential release of methane due to the larger extent of landmasses (e.g. *Dlugokencky et al.* (1994)), potentially combined with smaller CH_4 lifetimes in the southern hemisphere caused by higher OH radical concentrations, the predominant CH_4 oxidation agent (*Mayer et al.*, 1982, and references within).

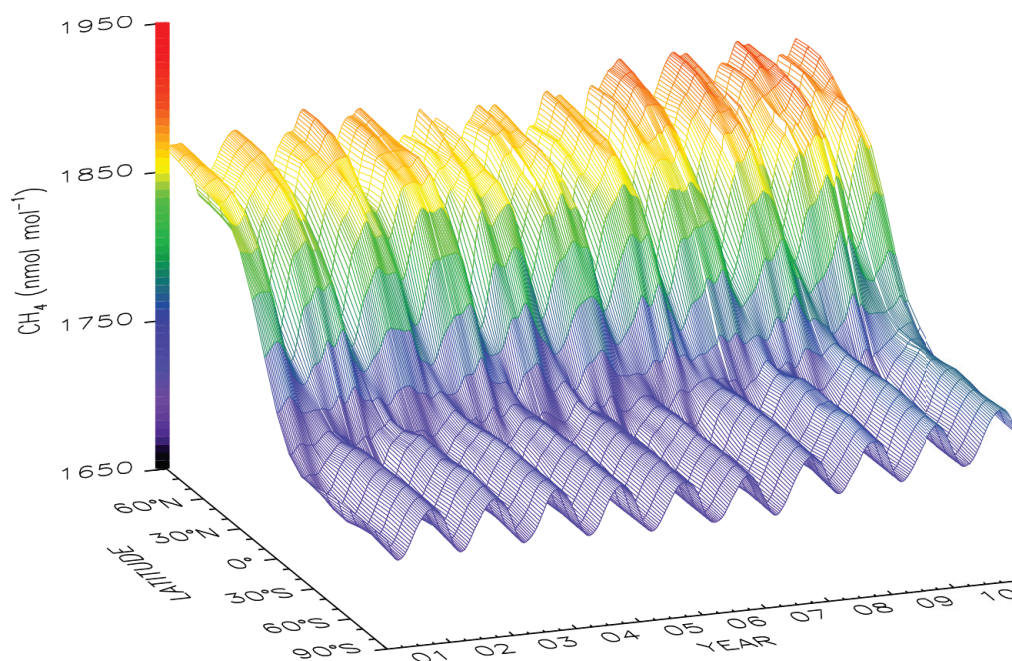


Figure 2.5.: Global distribution of atmospheric methane over the last decade.

Three-dimensional representation of the latitudinal distribution of atmospheric methane in the marine boundary layer. Data from the Carbon Cycle cooperative air sampling network were used. The surface represents data smoothed in time and latitude (*NOAA*, 2011).

In the early 1990s methane growth rates (the imbalance between sources and sinks) started to decline, causing almost stable concentration values of around 1760 ppb for more than a decade (*Steele et al.*, 1992; *Dlugokencky et al.*, 1998, Figure 2.4b). This stabilization

inspired a vital, and occasionally controversial, discussion in the scientific community, whether it is rather a temporary or a persistent phenomenon, what caused the decline and what potential implications it would have (e.g. *Dlugokencky et al.* (2003); *Hansen et al.* (1996); *Bousquet et al.* (2006)). The initial slow-down was tentatively attributed to fundamental changes of common industrial practices in Eastern Europe and the former Soviet Union for the exploitation of fossil energy sources (*Dlugokencky et al.*, 1994). *Hansen et al.* (1996) in turn speculated that a wide-spread cooling in the Northern hemisphere following the eruption of Mount Pinatubo might have been the cause, consistent with model results suggesting reduced CH₄ emissions in the high Northern latitudes (*Dlugokencky et al.*, 2003). This hypothesis was based on the assumption that the major CH₄ sink processes were constant during that time (*Dlugokencky et al.*, 1998). From an inversion model of CH₄ atmospheric transport and chemistry, *Bousquet et al.* (2006) deduced that anthropogenic emissions might have declined throughout the 1990s and started to increase again at the very end of the last millennium, in concert with a coinciding decrease of emissions from wetlands. Based on CH₄ carbon isotopic data, *Monteil et al.* (2011) proposed that a reduced tropospheric lifetime due to elevated OH levels might be the potential explanation for the ceasing CH₄ growth rates observed before 2000 AD, a finding supported by methyl chloroform data and inversion model results (*Prinn et al.*, 2005). Yet another study suggested reductions in agricultural emissions or another microbial source in the Northern Hemisphere to be the primary cause (*Kai et al.*, 2011). However, the re-accelerating growth of CH₄ mixing ratios since 2006 indicates that it was a temporary rather than a permanent phenomenon (*Rigby et al.*, 2008; *Dlugokencky et al.*, 2009, 2011). Whether this second increase is caused by elevated emissions from the tropics due to stronger precipitation in this area (*Dlugokencky et al.*, 2009), by increased contributions from Boreal Eurasia (*Bousquet et al.*, 2011), or rather by enhanced microbial soil respiration due to rises in land temperature and CO₂ levels (*Spahni et al.*, 2011) remains largely unresolved at present. *Frankenberg et al.* (2011) in turn even called in question whether restarting growth is a valid interpretation or rather the actual anomaly. As long as the key players of the global methane cycle remain broadly undetermined, a solid assessment of the present state and, perhaps even more importantly, reliable future projections seem elusive. The wealth of arguments and hypotheses presented in the last paragraph markedly underline the complexity of the methane cycle and the large variety of regulative parameters in the present-day world. The level of complexity was drastically increased by human activities. From the exploitation of fossil energy sources, changes in land use and agricultural practices (e.g. rice cultivation) to post-industrial value creation

chains and the consequences of modern lifestyles (waste management, large scale domestic animal farming etc.). Many of them have direct implications on the global methane budget, others influence it via far-reaching indirect feedback mechanisms (e.g. emissions of pollutants like NO_x , CO, volatile halogenated hydrocarbons and others that change the atmospheric chemistry of $\cdot\text{OH}$ and ozone).

Moreover, direct atmospheric measurements are confined to the last few decades, when CH_4 concentration levels were already drastically elevated and rising. In order to better understand the modern global methane cycle particularly in terms of the footprint by mankind, the study of the underlying, natural "background" processes may provide invaluable information. A look into the atmospheric history has already helped to elucidate the natural variability of these processes (the following chapter 2.3 gives an overview of $[\text{CH}_4]$ reconstructions). The study of the isotopic composition of atmospheric CH_4 may further help to disentangle their individual contributions on CH_4 budgets in the past, and how rapid and long-term climatic changes have influenced them over time (see chapter 2.4 and 5.1).

2.3. The methane record II - trapped in ice

Enclosures of air in polar ice and firn cores are an unique archive of atmospheric compositions of the past. They helped to extend the record of atmospheric CH_4 and other trace gases far beyond anthropogenic influence, and have thus proven to be a genuine tool to shed light on the history of atmospheric trace gases. As of now, the atmospheric CH_4 and CO_2 records reach back as far as 800,000 years into the past and, hence, cover eight glacial cycles (*Petit et al.*, 1999; *Spahni et al.*, 2003; *Loulergue et al.*, 2008; *Lüthi et al.*, 2008, see Figure 2.6). These datasets inferred from the long Antarctic ice cores from EDC (75°06'S 123°21'E, 3233 meter above sea level (masl.)) and from Vostok (78°27'51.92"S 106°50'14.38"E, 3.488 masl.) unequivocally demonstrated that the concentrations of these greenhouse gases for this period almost never exceeded as much as half the levels observed today.

The reliability and robustness of ice core reconstructions is evidenced by the consistency of records from ice cores and firn air from a large number of different locations in Greenland and Antarctica, measured by various independent laboratories world-wide. Some of the CH_4 records nicely document the good agreement of firn air and ice core mixing ratios with direct atmospheric measurements (*Etheridge et al.*, 1998; *MacFarling Meure et al.*,

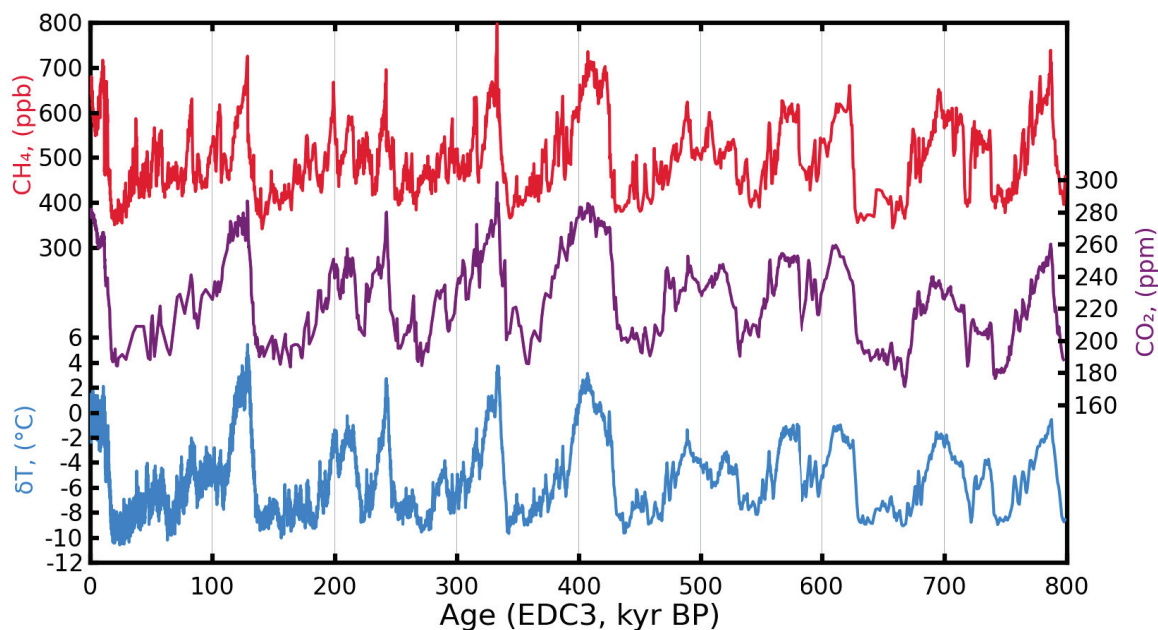


Figure 2.6.: Carbon dioxide and methane records over eight glacial cycles.

From top: a) CH_4 record from EPICA Dome C (EDC) (Loulergue *et al.*, 2008, red), b) composite CO_2 data from Vostok, Taylor Dome and EDC (Lüthi *et al.*, 2008, purple), c) calculated temperature difference (δT) relative to the average of the last 1000 years, inferred from $\delta D(\text{H}_2\text{O})$ (Jouzel *et al.*, 2007, blue). Please note that owing to the age given in thousand years before present (kyr BP), the records read from left to the right further into the past.

2006; Mitchell *et al.*, 2011, Figure 2.7 b)). The compilation of data from Law Dome, Antarctica (66.733°S, 112.833°E, 1390 masl.), shown in Figure 2.7 further illustrates the more than two-fold increase of CH_4 concentrations since the beginning of the industrial revolution at around 1750 AD (Etheridge *et al.*, 1998, Figure 2.7 a)).

Before that increase, CH_4 concentrations were relatively stable at about 650 ppb for a few thousand years in the Holocene period (0–10 kyr BP), and were even more reduced during the Last Glacial Maximum (LGM) (18–22 kyr BP) at roughly 350 ppb (Stauffer *et al.*, 1985, 1988). These pioneering values were confirmed by early measurements on an Antarctic ice core from Vostok, that extended the CH_4 record back to 160,000 years into the past, covering more than a full glacial cycle (Chappellaz *et al.*, 1990). Glacial periods were associated with low CH_4 concentrations, whereas interglacials were correlated with high values, respectively. The large-amplitude CH_4 oscillation during the last deglaciation, when CH_4 values fell back from ~ 650 ppb during the Bølling-Allerød (BA) period (~ 14 – 13 kyr BP) to below 500 ppb was further interpreted as a reaction of methane sources to the cooling during the Younger Dryas (YD) climate event (Chappellaz *et al.*,

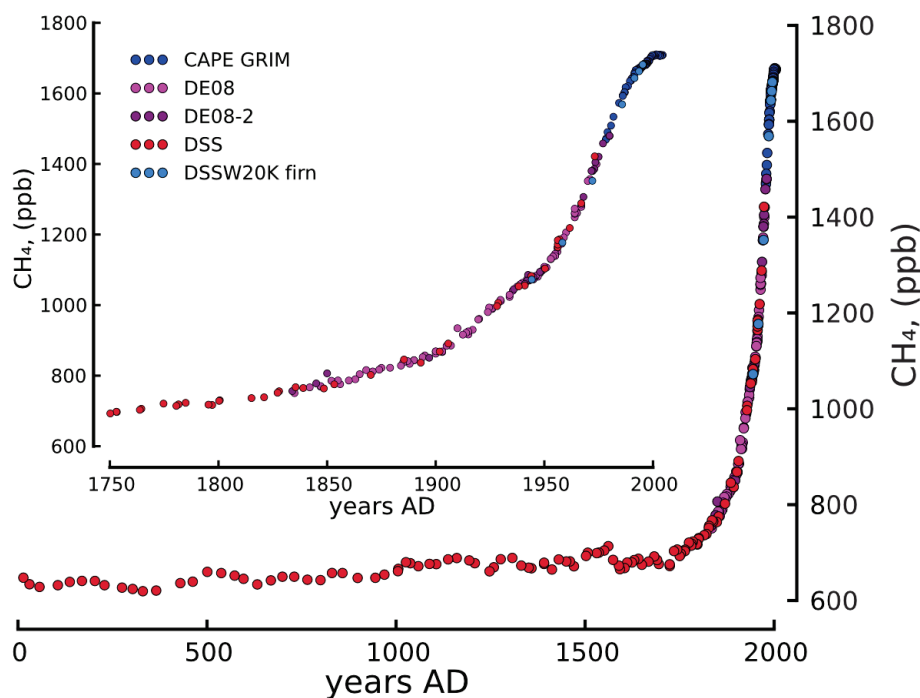


Figure 2.7.: Overlapping Ice core, firn air and ambient air methane records.

Methane records from Law Dome ice cores DE08, DE08-2 and DSS; from firn air samples (DSSW20k) and from ambient air of Cape Grim, Antarctica (*MacFarling Meure et al.*, 2006, and references within). The figure insert shows the anthropogenic CH_4 increase in higher detail, and further illustrates the good data overlap of the three different sample types.

1990, YD \sim 12–11 kyr BP). Consequently, *Chappellaz et al.* (1990) concluded that apart from the long term trends, methane could also respond to abrupt climate change, triggered for example by rapid atmospheric warming in high northern latitudes that led to thawing bogs and tundra peat-lands etc., or by increasing precipitation rates in low latitudes that potentially increased wetland source areas and productivity. *Kaplan* (2002) argued that neither varying emission strengths nor changes in the areal extent of wetlands could explain the observed glacial- interglacial of reduced CH_4 emissions during the LGM. Finally, based on results from a comprehensive Earth system model, *Valdes et al.* (2005) concluded that reduced lifetimes of CH_4 amplified the reduction in the atmospheric loading owing to increased sink activity under glacial conditions. However, the effect was estimated to be too weak to be regarded a principal cause for low CH_4 concentrations during the LGM (*Martinerie et al.*, 1995; *Levine et al.*, 2011a).

Large CH_4 concentration changes were not only observed on glacial-interglacial time scales, but also contemporaneous to short-term climate fluctuations over the glacial period, usually referred to as Dansgaard-Oeschger (DO) events. The $[\text{CH}_4]$ changes roughly

resemble patterns of northern hemisphere summer insolation, and were thus interpreted to be caused primarily by changes in tropical sources (*Chappellaz et al.*, 1990; *Petit-Maire et al.*, 1991; *Chappellaz et al.*, 1993a,b). *Crowley* (1991) argued, however, that the influence of temperature and precipitation patterns on high northern latitude source areas caused the 21 kyr periodicity in the glacial CH₄ record, rather than the impact of solar insolation on the tropical monsoon systems. This view was supported by modeling results that largely attributed the low CH₄ concentration levels under glacial conditions to reduced high northern latitude source emissions (*Valdes et al.*, 2005). Initial studies comparing the CH₄ concentration differences between ice cores from Greenland and Antarctica inferred higher values in northern versus southern polar regions during warm stages (*Brook et al.*, 2000; *Dällenbach et al.*, 2000; *Chappellaz et al.*, 1997), a finding which seemed to underline the importance of these boreal sources for DO CH₄ variability. The North-South concentration gradient, the IPD, is usually interpreted to be caused by additional emissions from sources in the northern hemisphere during warm periods (*Brook et al.*, 2000; *Dällenbach et al.*, 2000; *Chappellaz et al.*, 1997; *Baumgartner et al.*, 2012; *Ringeval et al.*, 2013). However, it was recently shown that stadial IPD values were considerably underestimated by *Dällenbach et al.* (2000). This also reduced the inferred stadial-interstadial difference of the IPD and the contribution of boreal sources to changes of methane mixing ratios over DO events (*Baumgartner et al.*, 2012). Additionally, it remains uncertain whether and to which degree sink processes contribute to the IPD. The principle CH₄ oxidation agent, the hydroxyl (OH) radicals, are formed primarily in tropical regions (*Lelieveld et al.*, 2002, 2008). Due to the smaller extent of land masses in the southern hemisphere, OH is only to a lesser degree consumed by competing substrate molecules such as CO and biogenic volatile organic compounds (VOCs). It is similarly unclear to what extent the tropical CH₄ sources contribute to the respective hemispheres, as the latitudinal position of the meteorological equator, the Inter-Tropical Convergence Zone (ITCZ), is intimately linked to the DO climate variability throughout the glacial period (*Wang et al.*, 2004; *Ivanochko et al.*, 2005; *Peterson and Haug*, 2006; *Leduc et al.*, 2007; *Wang et al.*, 2008a; *Kanner et al.*, 2012, and others).

How tightly CH₄ concentrations were coupled to these climate variations even on millennial timescales was underlined by highly resolved CH₄ records from Greenland and Antarctica (*Brook et al.*, 1996; *Blunier et al.*, 1998; *Baumgartner et al.*, 2013), which indicated CH₄ changes in near lock-step to northern hemisphere temperatures (see Figure 2.8). Large CH₄ concentration jumps in the range of 100–200 ppb within a few decades are observed in MIS 3, an interval from 57–29 kyr BP characterized by an exceptionally

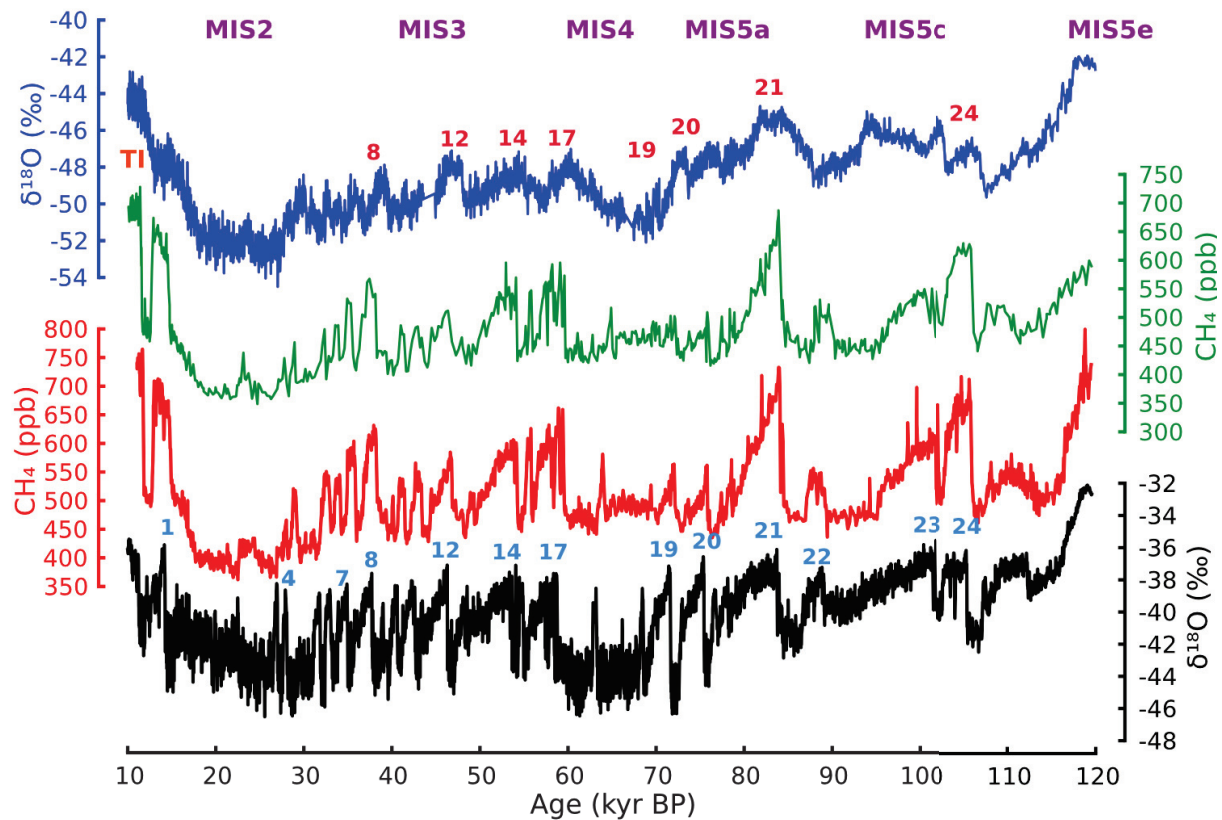


Figure 2.8.: Polar methane and temperature records for the last glacial cycle.

This figure shows the CH_4 and $\delta^{18}\text{O}$ records from the two polar ice caps in Antarctica (upper two) and Greenland (lower two sub-figures). The $\delta^{18}\text{O}$ profiles, a proxy for local temperature, were measured on ice core material from EDML (Antarctica, blue, *EPICA community members* (2006)) and NGRIP (Greenland, black, *North GRIP members* (2004)). The upper CH_4 dataset is from EDML (green, (*Schilt et al.*, 2010)), the lower is a compilation of the Greenland ice cores GRIP, GISP II and NGRIP (red, *Blunier et al.* (2007); *Huber et al.* (2006); *Grachev et al.* (2009); *Capron et al.* (2010)). Sample ages for EDML are given on the EDML1 age scale (*Ruth et al.*, 2007), NGRIP data on the extended GICC05 age model described in *Wolff et al.* (2010). Note that the differences in the timing of major CH_4 rises in the Arctic and Antarctic records, especially in older sections of the cores, are due to increasing dating uncertainties with increasing ice depth. Characteristic climate epochs, used in the discussion of the last glacial cycle, are denoted as Marine isotope stages (MISs, purple), and glacial terminations (TI+TII, orange). Pronounced Dansgaard-Oeschger (DO) events are given in light blue, the corresponding Antarctic isotope maxima (AIMs) in dark red. Data is given with respect to the new AICC chronology (*Veres et al.*, 2013)

high frequency of rapid climate change in the last glacial period, and were attributed to strongly fluctuating CH₄ emissions from boreal and tropical wetlands (*Brook et al.*, 1996; *Flückiger et al.*, 2004). These sources have been assumed to be able to respond quickly enough to changes in the hydrological cycle and the large temperature variability during DO stadials and interstadials (*Chappellaz et al.*, 1993b; *Brook et al.*, 1996; *van Huissteden*, 2004), an assumption that was called into question by another prominent hypothesis. It was based on observations on foraminifera in e.g. Santa Barbara basin sediments, whose shell carbonates showed large $\delta^{13}\text{C}$ depletions during periods of rapid climate change on millennial (e.g. DO events) and glacial-interglacial time-scales (*Kennett et al.*, 2000; *de Garidel-Thoron et al.*, 2004, and others). The theory, also known as "The Clathrate Gun Hypothesis" (*Kennett et al.*, 2003), proposed that rising intermediate water temperatures, i.a. induced by sea-level fall during the glaciation or/and reorganizations in the thermohaline circulation due to climatic changes, may have destabilized large amounts of marine gas hydrates stored on the continental margins (*Nisbet*, 1992; *Kvenvolden*, 1988; *Kennett et al.*, 2000; *de Garidel-Thoron et al.*, 2004; *Millo et al.*, 2005). The $\delta^{13}\text{C}$ excursions were interpreted as indicators for catastrophic outbursts of huge amounts of methane from these so-called clathrates, solid crystalline compounds formed by water and natural gases (mostly methane) under high pressure and low temperature conditions (e.g. *Hester and Brewer* (2009)), and gaseous CH₄ trapped beneath it (*Maslin and Thomas*, 2003, and refs. within). The destabilizations were assumed to be large enough to release considerable amounts of CH₄ to the atmosphere (e.g. *Milkov* (2004)), enough to trigger rapid warming events on a wide range of time scales including glacial-interglacial cycles and DO events in association with climate feedback mechanisms (*Kennett et al.*, 2003).

It was in fact unclear for some time, whether changing CH₄ concentrations were a consequence of or to a certain degree rather responsible for the temperature variability, despite the fact that the greenhouse effect of methane on the applicable order of magnitude is considered to be rather low (*Chappellaz et al.*, 1990). This ambiguity was a result of uncertainties concerning the precise timing of warming events in ice cores relative to the correlated changes of relevant trace gas species in the air enclosures. But the interpretation of an anomaly in the Greenland Ice Sheet Project (GISP) 2 ice core record of $\delta^{15}\text{N}_2$ from Summit Station, Greenland (72°34'44.10"N 38°27'34.56"W, 3.261 masl.) at the end of the YD, an abrupt return to near-glacial temperatures in the high-latitude North Atlantic with an impact on climate beyond hemispheric extent, precluded a causal role for methane in the warming into the Pre-boreal Holocene (PB), as the initial CH₄ increase

began 0–30 years after the warming at Summit (*Severinghaus et al.*, 1998). For DO temperature changes in MIS 3, *Huber et al.* (2006) and *Baumgartner et al.* (2013) inferred analogous lags of 25–70 years for the CH₄ rises relative to the DO temperature increases. The characteristic differences of the ratio of the heavy to light carbon ($\delta^{13}\text{C}$) and hydrogen (δD) isotopes of these processes are excellent tools to better constrain individual contributions of methane sources and sinks. This will be discussed in the next chapter.

2.4. Stable isotopes - and what they teach us about the sources and sinks of atmospheric methane

After a brief introduction into the terminology and theoretical background of stable isotope geochemistry of CH₄ (definitions, δ -notation etc.), this chapter gives an overview of which processes determine the isotopic composition of atmospheric methane. The values for carbon ($\delta^{13}\text{CH}_4$) and hydrogen ($\delta\text{D}(\text{CH}_4)$) depend mostly on the isotopic compositions of the inputs of methane to the atmosphere (sources) and the alterations to the averaged source signature due to fractionation processes associated with methane removal (sinks). The sources are discussed in terms of their principal formation pathways, and how these pathways, the precursor material and post-formation processes influence their respective isotopic signatures. While anthropogenic sources are not entirely omitted, this discussion clearly focuses on the natural background processes from a paleo-atmospheric perspective. Later in that chapter, known sink processes are introduced and discussed in terms of their impact on atmospheric $\delta^{13}\text{CH}_4$ and $\delta\text{D}(\text{CH}_4)$. Finally, previous studies of CH₄ isotopes are presented in form of a short summary, particularly focusing on what is currently known about the methane geochemistry of the past.

Stable isotopes, the δ -notation, and reference materials

Isotopes are variations of atoms from a chemical element that differ only by the number of neutrons in its nucleus. Those variations are chemically indistinguishable, but physically distinct due to their differing nuclear masses. With a few exceptions, all elements on earth are mixtures of two or more isotopes with characteristic natural abundances. Some decay spontaneously in nuclear transformations and are termed unstable or radioactive, but the majority of the naturally occurring atoms are so-called stable isotopes.

The group of possible combinations of isotopes in a molecule with identical chemical composition and properties are called isotopologues. Methane can theoretically consist

Table 2.1.: Globally averaged abundances of stable isotopes relevant to this work

| Element | Isotope & its natural abundance in % | | | | | |
|----------|--------------------------------------|--------|------------------|-------|-----------------|-------|
| Hydrogen | ¹ H | 99.985 | ² H/D | 0.015 | | |
| Carbon | ¹² C | 98.90 | ¹³ C | 1.10 | | |
| Nitrogen | ¹⁴ N | 99.63 | ¹⁵ N | 0.37 | | |
| Oxygen | ¹⁶ O | 99.762 | ¹⁸ O | 0.200 | ¹⁷ O | 0.038 |

of 10 different combinations of the stable isotopes of carbon (¹²C/¹³C) and hydrogen (¹H/²H; ²H is usually referred to as deuterium or D), but only the three single substituted isotopologues ¹²CH₄, ¹³CH₄ and ¹²CH₃D are relevant in earth science owing to the very low abundance of the others.

Isotopic compositions are usually expressed as the ratio R of the rare versus the more abundant isotope. For carbon and hydrogen this reads

$${}^{13}\text{R} = \frac{[{}^{13}\text{C}]}{[{}^{12}\text{C}]}, {}^2\text{R} = \frac{[{}^1\text{H}^2\text{H}]}{[{}^1\text{H}_2]}. \quad (2.2)$$

Most applications of stable isotopes deal with natural variations. Those changes of isotopic ratios are typically very small. For this reason, they are commonly reported in "per mil" (‰, parts per thousand) and quantified with the delta notation (δ) expressed as a relative deviation from a standard (*Craig*, 1953)

$$\delta = \frac{\text{R}_{\text{sample}}}{\text{R}_{\text{standard}}} - 1. \quad (2.3)$$

In order to compare results from different laboratories worldwide, the International Atomic Energy Agency (IAEA) has defined standard materials for each isotope species that define the zero point of the δ -scale. The isotopic ratio ¹²C/¹³C is reported with respect to Vienna Pee Dee Belemnite (VPDB) as

$$\delta^{13}\text{C}(\text{‰}) = \left[\frac{\left(\frac{{}^{12}\text{C}}{{}^{13}\text{C}}\right)_{\text{sample}}}{\left(\frac{{}^{12}\text{C}}{{}^{13}\text{C}}\right)_{\text{VPDB}}} - 1 \right] * 1000 \quad (2.4)$$

The eponymous primary carbon reference material Pee Dee Belemnite, a Cretaceous marine fossil of *Belemnitella americana* found at the Pee Dee Formation in South Carolina (US.), has long been exhausted and was replaced in 1985 by a secondary standard, the limestone NBS-19, a carbonate material whose composition is defined to be $\delta^{13}\text{C} =$

+1.95 ‰ and $\delta^{18}\text{O} = -2.2$ ‰ relative to the replacement scale VPDB (Coplen, 1995). The Vienna Standard Mean Ocean Water (V-SMOW) was established in 1976 as a recalibration of the original reference SMOW, that was created in 1960 as an average value of ocean water sampled at multiple sites around the globe (Craig, 1961). It is the internationally recommended standard to report D/H ratios according to

$$\delta\text{D}(\text{‰}) = \left[\frac{\left(\frac{\text{D}}{\text{H}}\right)_{\text{sample}}}{\left(\frac{\text{D}}{\text{H}}\right)_{\text{VSMOW}}} - 1 \right] * 1000. \quad (2.5)$$

Present-day atmospheric values of $\delta^{13}\text{CH}_4$ and $\delta\text{D}(\text{CH}_4)$

Bromley *et al.* (2012) report recent atmospheric $\delta^{13}\text{CH}_4$ values from a collaborative ship-board project in the western Pacific Ocean on eight voyages from 2004 to 2007 that suggest values of ~ -47.2 ‰, a small mean $\delta^{13}\text{C}$ gradient of 0.21 ‰ between 30°S and 30°N in austral summer and almost no gradient (0.03 ‰) during austral winter. The values are in good agreement with results from a recent project involving measurements on commercial aircrafts and container ships in the same Western Pacific region from 2005–2010, which suggest a similar gradient of 0.2 ‰ for $\delta^{13}\text{CH}_4$, and ~ 10 ‰ for $\delta\text{D}(\text{CH}_4)$, both with more depleted values in the North (Umezawa *et al.*, 2012). For measurements from multiple sites between 1988 and 1995, Quay *et al.* (1999) reported a slightly higher north-south $\delta^{13}\text{C}$ gradient of 0.5 ‰ between 71°N and 41°S and also observed a seasonal variability of 0.4 ‰ at 71°N but only 0.1 ‰ at 14°S, attributed to the CH_4 sources that are predominantly located in the northern hemisphere and an enrichment during the southward transport (e.g. Dlugokencky *et al.* (1994) and Miller *et al.* (2002)). The mean $\delta\text{D}(\text{CH}_4)$ was inferred to be -86 ± 3 ‰ with a north-south gradient of 10 ‰, again with more enriched values in the south.

2.4.1. Sources and sinks of CH_4 and their effect on $\delta^{13}\text{C}/\delta\text{D}$

The atmospheric methane budget is composed of various terrestrial and aquatic sources balanced by a number of sink processes. Emissions of methane are either of biogenic, thermogenic, or pyrogenic origin, with both natural and anthropogenic contributions.

Biogenic methane is formed through microbial activity during the re-mineralization of organic matter under anaerobic conditions in aquatic environments. It is by far the most important class of natural CH_4 sources (in terms of emission strength) and will be discussed in more detail below. Pyrogenic methane, however, has a large influence on

the atmospheric carbon isotopic composition $\delta^{13}\text{C}\text{H}_4$. It is formed as a by-product during the combustion of organic materials in natural wildfires and anthropogenic biomass (or biofuel) burning, along with the major product CO_2 . Very little fractionation is associated with the partial combustion of biomass to CH_4 (Yamada *et al.*, 2006, +6.9 to -8.6 ‰). Pyrogenic CH_4 is thus highly enriched in ^{13}C compared to the atmospheric mean and the other source types. Snover *et al.* (2000) estimated the global average of $\delta^{13}\text{C}\text{H}_4$ emitted from biomass burning sources to be -24 ± 3 ‰, in good agreement with earlier estimates by Stevens and Engelkemeir (1988, -25 ± 3 ‰) and Stevens and Wahlen (2000, -24 ± 3 ‰). However, emission rates and isotopic composition of pyrogenic methane depend on characteristics of the fire (temperature, amount of smoldering etc.) and the biomass (i.a. vegetation type, moisture content), which are difficult to assess on a global scale even at present times (Bowman *et al.*, 2009). Chanton *et al.* (2000) suggested that $\delta^{13}\text{C}$ of CH_4 varies according to $\delta^{13}\text{C}$ of the fuel biomass, and that emissions from combusted C_4 biomass would be enriched in $\delta^{13}\text{C}\text{H}_4$ according to the characteristic $\delta^{13}\text{C}$ difference of C_4 and C_3 plant material (e.g. Ehleringer *et al.* (1997)). Their reported $\delta^{13}\text{C}\text{H}_4$ values were in the range of -26 ‰ to -30 ‰ for C_3 forest fires and -17 ‰ to -26 ‰ for C_4 grass fires, respectively. Similar differences were found by Yamada *et al.* (2006) for biomass burning emissions of maize (C_4 , 20 ‰) and rice (C_3 , 35 ‰) under the same burning conditions. The authors also inferred considerable fractionation of $\delta\text{D}(\text{CH}_4)$ versus δD of the fuel biomass during the combustion (-101 ‰ to -174 ‰), in line with results of Snover *et al.* (2000, -130 ‰ to -180 ‰). The global estimate for $\delta\text{D}(\text{CH}_4)$ of pyrogenic emissions, however, varies from -169 ‰ Yamada *et al.* (2006) to -210 ‰ (Snover *et al.*, 2000) in both studies. From aircraft observations over Alaska, Umezawa *et al.* (2011) derived $\delta^{13}\text{C}\text{H}_4$ and $\delta\text{D}(\text{CH}_4)$ of methane emitted by wildfires to be -27.5 ± 2.0 ‰ and -285 ± 11 ‰, showing that the isotopically depleted fuel biomass of (mostly) C_3 vegetation and the depleted δD of local precipitation in high northern latitudes is transferred into wildfire $\delta^{13}\text{C}\text{H}_4$ and $\delta\text{D}(\text{CH}_4)$ signatures.

Finally, organic matter in detritus-rich soil layers buried deep in the Earth's crust is slowly transformed into reservoirs of fossil fuels. At depths typically larger than 1 km (Schoell, 1988; Whiticar, 1990), thermogenic methane is formed under the influence of high pressures and elevated temperatures during the degradation of complex, long chain organic molecules on geologic time scales. If the methane is not trapped on its way to the surface in natural gas accumulations (e.g. in coal, or crude oil deposits) or by the formation of gas hydrates, it migrates along cracks and tectonic dislocations towards the surface (Judd *et al.*, 2002). There it is either vented in volcanic and geothermal emissions,

marine and terrestrial micro- and macro-seeps, or mud volcanoes (*Etioppe and Klusman, 2002; Etioppe, 2004; Judd, 2004; Kvenvolden and Rogers, 2005; Etioppe et al., 2009; Etioppe and Klusman, 2010*, and references within). The emissions from this group of 'geologic sources' are considerably enriched in ^{13}C because the thermogenic CH_4 formation pathway also discriminates less against the heavier isotope. As a consequence, isotopic signatures of methane from geologic sources, which usually have varying amounts of methane of thermogenic origin, are enriched with respect to (wrt.) $\delta^{13}\text{C}$ relative to biogenic CH_4 emissions (*Schoell, 1980; Whiticar, 1990*). Typical $\delta^{13}\text{CH}_4$ ranges for geologic CH_4 (-30 to -50 ‰, *Reeburgh (2007)*) are intermediate between the relatively $\delta^{13}\text{C}$ enriched pyrogenic methane emissions and depleted biogenic sources, but overlap with this two source classes considerably.

Formation pathways of biogenic methane

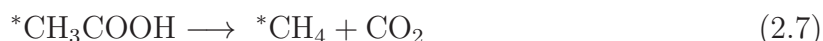
Biogenic methane is almost exclusively produced by a group of micro-organisms classified as Archaea (*Stadtman, 1967; Wolfe, 1971*). These single-celled microbes, which are distinct from bacteria, produce approximately 70 % of today's total global methane (*Schimel, 2004*). They play a major role in the anaerobic bio-degradation chain of organic matter in a wide range of aquatic environments (*Bartlett and Harriss, 1993; Aselmann and Crutzen, 1989; Matthews and Fung, 1987*, and references within). Such environments include anoxic freshwater sediments in floodplains, shallow lakes, bogs, fens, marshes, mires, peat-lands and rice paddy fields, which are commonly subsumed as wetlands (*Mitsch and Gosselink, 2007*). Together with marine sediments, which contain considerable amounts of organic material, these settings develop zones of oxygen (O_2) deficiency due to consumptive respiration of O_2 and restricted diffusion from the atmosphere or an aerated water column. Under these anoxic conditions, a complex community of micro-organisms (i.e. hydrolytic and fermentic, hydrogen-reducing, or homoacetogenic bacteria) participate in the successive breakdown of organic matter. Methanogens are secondary fermenters and, thus, strongly dependent on these communities that provide the relatively few and simple substrate compounds, which are consumed by the methanogenic Archaea during CH_4 formation, and include short-chained fatty acids, acetic and other carboxylated acids, alcohols and CO_2 +hydrogen (H_2) (*Conrad, 1989; Drake et al., 2009*). In saline environments, methylated amines and sulfides are also precursor substrates for methanogenesis (*Oremland, 1988; Zinder, 1993*).

The end-product of methanogenesis is formed via several metabolic pathways, of which the predominant are the so-called acetate fermentation and carbonate reduction. Carbonate reduction can be represented by the general reaction:



The electrons needed for the reduction of CO_2 to CH_4 are provided either by oxidation of H_2 , formate, and occasionally alcohols. The oxidative removal of excess H_2 produced by other members of the microbe consortia during the anoxic fermentation of organic matter is important to maintain suitable conditions for the assembly (*Schimel*, 2001).

Other methanogens catabolize methyl groups of simple molecules like acetate, methanol and to a minor degree also methylated amines and sulfides. The net reaction for the acetate fermentation, the predominant variant of this pathway, is:



where the transferred methyl position into the CH_4 molecule is indicated by the asterisk (*Whiticar*, 1999). Approximately 70% of the CH_4 is estimated to be produced via acetotrophic methanogenesis (*Winfrey et al.*, 1977; *Liu et al.*, 2013). The predominance of acetate fermentation (eqn. 2.7) appears well-correlated with the presence of labile organic substances in freshwater sediments, for example. In the upper layers they are enriched in labile organic carbon (e.g. (*Winfrey and Zeikus*, 1979; *Phelps and Zeikus*, 1984; *Lovley and Klug*, 1982)), but decreasing availability of these substances (i.e. increasing substrate limitation) with increasing depth likely causes a shift towards more CO_2 reduction (*Whiting and Chanton*, 1993; *Hornibrook et al.*, 1997, 2000).

Marine sediments on the other hand are usually depleted in labile organic carbon due to elevated concentrations of sulfate and activation of sulfate microbial reducers, so methanogens are seriously out-competed for available substrate (H_2 , acetate and formate). Sulphate-reducing bacteria form hydrogen sulphide from the sulphate ions while organic carbon is largely oxidized to CO_2 (*Hoehler et al.*, 1998). As a consequence, sulphate reduction is the predominant process in marine sediments until most of the sulphate is consumed. Only then does the consumption of organic carbon become coupled to CH_4 formation, so methanogens are largely restricted to depths below the sulphate reduction zone. Due to the limitation of labile organic matter in these settings, the CH_4 is believed to be produced predominantly via carbonate reduction (*Whiticar et al.*, 1986; *Whiticar*, 1999, eqn. 2.6). The relatively high sulphate concentration in sea water also restricts

substantial CH₄ production in coastal environments like estuaries, salt marshes, coastal mangroves and marine surface sediments.

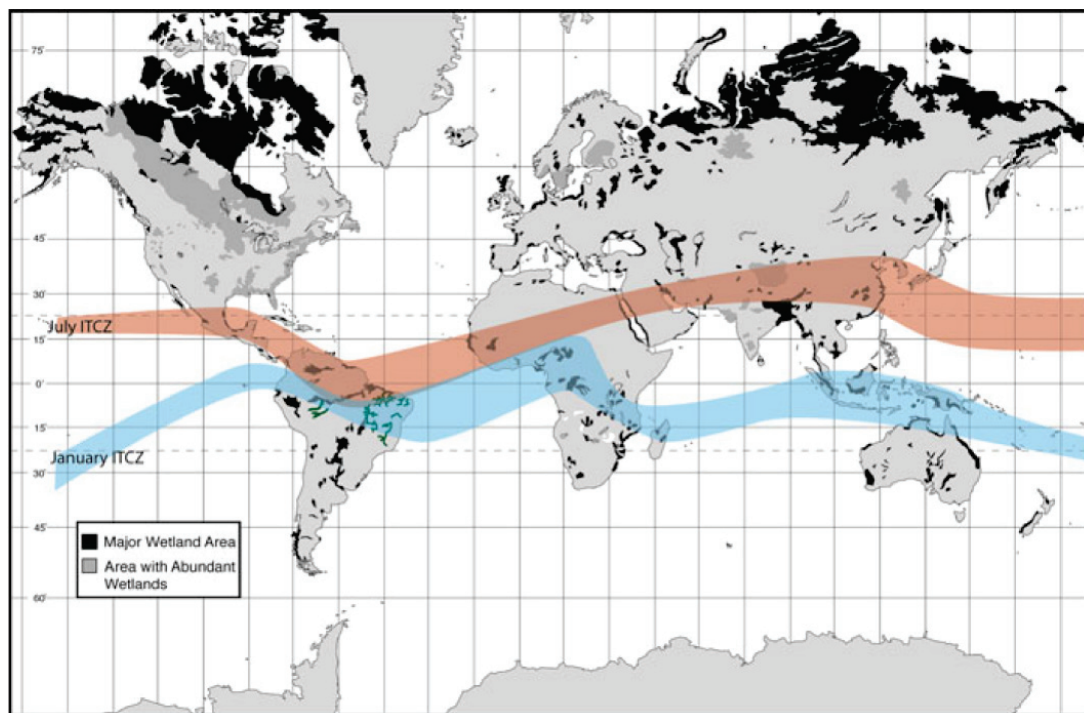


Figure 2.9.: Map of major wetland areas in the world.

The map shows the modern distribution of global wetland areas (*Mitsch and Gosselink, 2007*). It also highlights two (schematic) modes of the earth's "climatic equator" in January and July, the ITCZ, which dominates the tropical and subtropical climate and monsoon intensities (e.g. *Ivanochko et al. (2005)*). Figure from *Mitsch et al. (2010)*.

Apart from wetlands and marine sediments, biogenic methane is produced in a series of anaerobic micro-environments known to be inhabited by methanogenic Archaea (*Rasmussen and Khalil, 1983; Khalil et al., 1990; Hackstein and Stumm, 1994*). It is formed from ingested organic matter in guts of termites and other terrestrial arthropods, by enteric fermentation in stomachs of wild and domesticated ruminants, and in plants referred to as tank bromeliads, living on decomposing dead leaves on branches of tropical forests (*Sanderson, 1996; Brune, 2000; Johnson et al., 2000; Moss et al., 2000; Cottle et al., 2011; Martinson et al., 2010*).

Factors influencing the isotopic signature of biogenic methane

At first order, each of the two simplified CH_4 formation pathways above generates a distinctive shift in the carbon isotopic composition of the CH_4 molecules produced. Since hydrogenotrophic methanogenesis (eqn. 2.6, $\eta = 1.055$ to 1.0090) expresses a larger kinetic isotope effect (KIE or η , i.e. differences in the reaction rates of the light and heavy isotopes) than acetotrophic methane formation (eqn. 2.7, $\eta = 1.040$ to 1.0055), CH_4 formed via the carbonate reduction pathway is estimated to be more depleted in terms of $\delta^{13}\text{C}$ (60–90 ‰) than via acetate fermentation (40–60 ‰) (Whiticar *et al.*, 1986; Whiticar, 1999; Conrad, 2005). However, the two pathways have an opposing effect on $\delta\text{D}(\text{CH}_4)$. Methane produced by the CO_2 reduction pathway is significantly less depleted (170–250 ‰) than during methanogenesis of methylated substrates (250–400 ‰, Whiticar (1999)). The correlation of wetland $\delta\text{D}(\text{CH}_4)$ and the surrounding soil pore water $\delta\text{D}(\text{H}_2\text{O})$ along a latitudinal gradient, however, suggests that emitted CH_4 predominantly reflects the δD of environmental water (Waldron *et al.*, 1999; Chanton *et al.*, 2006). Biochemical studies further suggest that at least three (if not all) of the hydrogen atoms in the CO_2 reduction stem from water and only one from H_2 (Daniels *et al.*, 1980; Schleucher *et al.*, 1994; Klein *et al.*, 1995, see equation 2.6), and H_2 potentially underwent isotopic equilibration before the H atoms are added during CO_2 reduction (Valentine *et al.*, 2004).

Similarly, $\delta^{13}\text{C}\text{CH}_4$ signatures are influenced by the $\delta^{13}\text{C}$ of the decomposing organic matter and simpler precursor molecules that are provided by the microbial community and utilized in methanogenesis, e.g. metabolites such as acetate, which is affected by fractionation processes during homoacetogenesis and syntrophic acetate oxidation (Conrad *et al.*, 2011; Heuer *et al.*, 2010). $\delta^{13}\text{C}$ is known to vary considerably (~ 15 ‰) in the two primary photosynthetic carbon sequestration pathways, i.e. the Calvin-Benson cycle (C_3) and the Hatch-Slack cycle (C_4). About 80–90 % of the present-day plant species follow the C_3 route to incorporate CO_2 during photosynthesis (Farquhar *et al.*, 1982, 1989, and others), although this is obviously not representative of the total amount of biomass, which may also be respired in the form of CH_4 . However, while the C_4 route may be of lesser importance during (warm) interglacial periods with elevated CO_2 levels, it is thought to provide a competitive advantage in some environmental settings during (colder and dryer) glacial conditions with characteristically low CO_2 concentrations (Ehleringer *et al.*, 1997; Cowling and Sykes, 1999; Harrison and Prentice, 2003; Gerhart and Ward, 2010; Bragg *et al.*, 2012, and more). The C_3/C_4 abundance is considered a key aspect in the interpretation

of the $\delta^{13}\text{C}_4$ data presented in this thesis.

In addition to the isotopic signatures of the precursor molecules, the isotopic fractionation is further influenced by the H_2 partial pressure and energetic conditions in hydrogenotrophic methanogenesis (Penning *et al.*, 2005; Valentine *et al.*, 2004), and by (*in-situ*) temperatures (e.g. Games *et al.* (1978); Westermann (1993)). But these factors are considered less important in terms of the overall methane $\delta^{13}\text{C}$ and δD source signatures compared to the factors controlling the composition of active consortia producing methane in a certain environment (Bridgham *et al.*, 2013).

Finally, an estimated 20% – 40% of the methane produced in wetlands is consumed by methanotrophic bacteria during gas transport to the atmosphere (Coleman *et al.*, 1981; Walter and Heimann, 2000). The residual CH_4 is enriched in ^{13}C due to the preferential elimination of $^{12}\text{CH}_4$ (Whiticar *et al.*, 1986; Chanton, 2005). The CH_4 loss due to oxidation in aerated soil layers and the water column is usually treated separately from the sink processes that remove CH_4 from the atmosphere (described in the following section).

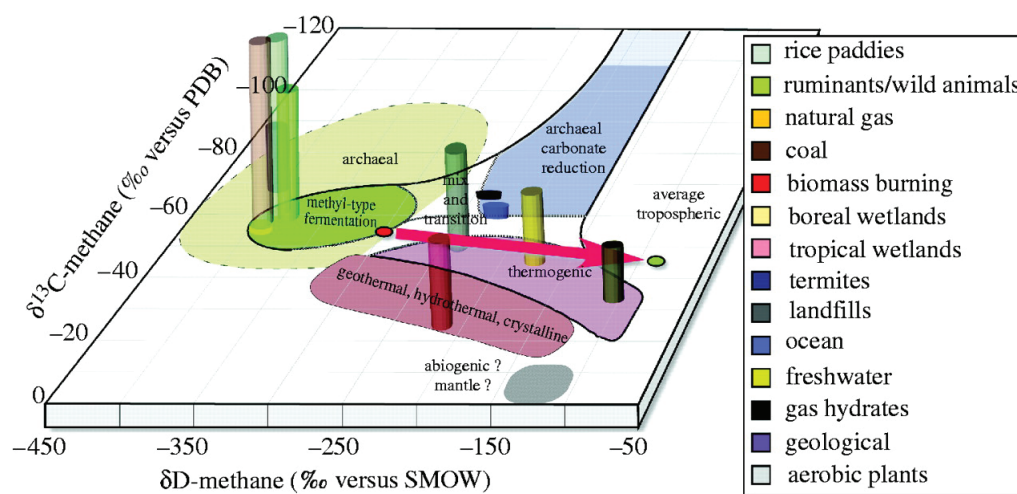


Figure 2.10.: Isotopic signatures of major methane sources - the CD diagram.

This figure shows the combination of typical $\delta^{13}\text{C}_4$ and $\delta\text{D}(\text{CH}_4)$ ranges of the major methane source types (based on Whiticar (1999)), and respective flux strengths of the primary tropospheric methane sources at present day. Also indicated are the integrated isotopic compositions of the sources ($\delta^{13}\text{C}_E/\delta\text{D}_E$ in equation 2.8, red circle) and the offset to the average tropospheric values ($\delta^{13}\text{C}_4$ & $\delta\text{D}(\text{CH}_4)$, green circle) induced by the sink fractionation (ϵ_{WT} in eq. 2.8, red arrow). Figure taken from (Whiticar and Schaefer, 2007).

In summary, the significant natural diversity of wetlands and the individual dependence on a series of environmental parameters affecting methanogenesis leads to relatively large

empirical ranges for CH₄ isotopic compositions in field observations (see e.g. *Bréas et al.* (2001) for a more comprehensive summary). However, the imprint of the predominant CH₄ formation pathways on $\delta^{13}\text{CH}_4$ and $\delta\text{D}(\text{CH}_4)$ still allows a crude allocation of CH₄ emitters to specific classes of sources (Figure 2.10).

Isotope mass balances and fractionation during methane removal

Following the nomenclature introduced by *Schaefer and Whiticar* (2008), the isotopic composition of methane in the atmosphere can be expressed as the sum of the average isotopic signatures of CH₄ sources ($\delta^{13}\text{C}_E$) and the change of this value induced by fractionation (ϵ_{WT}) processes associated with decay of CH₄ (equations are equivalent for $\delta\text{D}(\text{CH}_4)$):

$$\delta^{13}\text{CH}_4 = \delta^{13}\text{C}_E + \epsilon_{\text{WT}}. \quad (2.8)$$

$\delta^{13}\text{C}_E$ can be broken down into the emission strength of individual sources, E_i , and its respective isotopic composition $\delta^{13}\text{C}_{E_i}$:

$$\delta^{13}\text{C}_E = \frac{\sum \delta^{13}\text{C}_{E_i} * E_i}{\sum E_i}. \quad (2.9)$$

The relatively short residence time of less than 10 years for CH₄ molecules in the atmosphere are due to a series of oxidative removal processes, such as the reaction with hydroxyl radicals ($\cdot\text{OH}$) and $\text{O}(^1\text{D})$ in the troposphere, oxidation by chlorine radicals ($\cdot\text{Cl}$) in the stratosphere and in the MBL, and CH₄ uptake and degradation in soils. The sink processes are associated with isotope effects and cause distinct shifts in the isotope ratios of atmospheric CH₄. The average isotopic fractionation caused by the sum of CH₄ decay processes thus determines the offset (ϵ_{WT}) between the average isotopic composition of all CH₄ source emissions ($\delta^{13}\text{C}_E$) and the carbon ($\delta^{13}\text{C}$) and deuterium (δD) isotopic signature of methane in the atmosphere (see eqn. 2.8 and figure 2.10). The isotopic discrimination is a result of differing turnover rates in the reaction of the oxidant with the light (^{12}C or ^1H) versus the heavy (^{13}C or $^2\text{H}/\text{D}$) isotope species of CH₄. ^{12}C reacts faster and is, thus, removed preferentially, leaving atmospheric methane enriched in ^{13}C . The kinetic isotope effect (KIE) (or η) is defined by the ratio of the reaction rate constants k_i of the "light" versus the "heavy" isotope (*Rust and Stevens*, 1980). However, to describe

fractionation processes in atmospheric chemistry, the reciprocal fractionation factor α_i is often used instead (*Cantrell et al.*, 1990):

$$\alpha_{C/H} = \frac{k_{13C/D}}{k_{12C/1H}} = \frac{1}{\eta}. \quad (2.10)$$

Using the following equation, α can be converted to the fractionation ϵ (*Craig et al.*, 1988), which translates to the offset that a given sink process causes to the atmospheric isotopic signature in per mil:

$$\epsilon = (\alpha - 1) \times 1000. \quad (2.11)$$

For the reaction of CH₄ with the hydroxyl radical hydroxyl radical ($\cdot\text{OH}$), the primary tropospheric oxidation reactant, α_C was determined experimentally to 0.9946 ± 0.0009 for carbon (*Cantrell et al.*, 1990). This would correspond to a fractionation ϵ_{OH} of -5.4‰ (*Quay et al.*, 1999).

The total sink fractionation (ϵ_{WT}) is calculated using the proportions of methane removed by each sink (F_R), multiplied with its fractionation factor α_R :

$$\alpha = F_{Ri} \times \alpha_{Ri} + \dots + F_{Rn} \times \alpha_{Rn}. \quad (2.12)$$

Or, following equations 2.8 and 2.11:

$$\epsilon_{\text{WT}} = \sum ((\alpha_{Ri} - 1) \times 1000.) \times F_{Ri}. \quad (2.13)$$

The sink fractions F_R are usually not well constrained. A widely accepted estimate was 0.87, 0.05, 0.07 for oxidation by tropospheric $\cdot\text{OH}$, for soil respiration, and for the stratospheric sink (*Hein et al.*, 1997; *Quay et al.*, 1999). Note that the removal of CH₄ in the MBL by chlorine radicals is not considered in these calculations. Depending on the size of ϵ assumed for $\cdot\text{OH}$ oxidation, the scenario of *Quay et al.* (1999) suggests that the mean isotopic composition of all sources is $8.8 \pm 2\text{‰}$ and $218 \pm 50\text{‰}$ more depleted than the atmospheric values for $\delta^{13}\text{CH}_4$ and $\delta\text{D}(\text{CH}_4)$, respectively. The relatively large upper bound of total fractionation ϵ_{WT} of up to 10.8‰ for $\delta^{13}\text{CH}_4$ is derived from a theoretical value by *Gupta et al.* (1997), who estimated the KIE for tropospheric removal by $\cdot\text{OH}$ to be 1.010 ($\epsilon_{\text{OH}} = -10\text{‰}$). That estimate, however, would imply unrealistically high fractionation between source and atmospheric reservoir. The latest experimental determination by *Saueressig et al.* (2001, $\epsilon_{\text{OH}} = -3.9\text{‰}$ ($\alpha_{\text{OH}} = 0.9961 \pm 0.0004$)), inferred with a higher analytical precision than *Cantrell et al.* (1990), suggests that the fractionation

effect caused by $\cdot\text{OH}$ radicals contributes less to the overall sink. Table 2.2 summarizes the major sink processes of atmospheric CH_4 , and estimates of the respective fractionation associated with them in the literature. Assuming that 3-4% of CH_4 is removed in the MBL (*Platt et al.*, 2004; *Allan et al.*, 2007; *Levine et al.*, 2011a), would increase the estimates for ϵ_{WT} by $\sim 2\text{‰}$ and $\sim 13\text{‰}$ in $\delta^{13}\text{CH}_4$ and $\delta\text{D}(\text{CH}_4)$, respectively, due to the large KIE determined for the CH_4 oxidation by chlorine radicals (*Saueressig et al.*, 2001).

Table 2.2.: Sink fractionation factors for the main sink processes and both stable isotopes of CH_4 . The following fractions were used for the estimate of the overall sink fractionation not including chlorine radical oxidation in the marine boundary layer: 87% of CH_4 lost via reaction with tropospheric $\cdot\text{OH}$, 5% lost to soil uptake and 8% lost in the stratosphere (*Hein et al.*, 1997). For the scenario with 4% CH_4 removal in the MBL (*Allan et al.*, 2007; *Levine et al.*, 2011a) the remaining fractions were adjusted in equal proportions to yield 100%.

| sink process | $\delta^{13}\text{CH}_4$ ϵ [‰] | $\delta\text{D}(\text{CH}_4)$ ϵ [‰] |
|--|--|---|
| tropospheric $\cdot\text{OH}$ | $-3.9\pm 0.4 - -5.4\pm 0.9^{\text{a}}$ | $-230\pm 45^{\text{b}}$ |
| soil uptake | $-17 - -25^{\text{c}}$ | $-81\pm 24^{\text{d}}$ |
| $\cdot\text{Cl}$ in stratosphere & MBL | $-60 - -66^{\text{e}}$ | $-474 - -522^{\text{f}}$ |
| stratospheric loss | $-12 - -17^{\text{g}}$ | $-160\pm 20^{\text{h}}$ |
| overall (no MBL) | $-5.2 - -7.3$ | -217 ± 42 |
| overall (4% MBL) ⁱ | $-7.2 - -9.3$ | -230 ± 42 |

^a values from *Saueressig et al.* (2001) and *Cantrell et al.* (1990)

^b *Gierczak et al.* (1997)

^c *King et al.* (1989); *Tyler et al.* (1994); *Snover and Quay* (2000); *Reeburgh et al.* (1997)

^d *Snover and Quay* (2000)

^e *Saueressig et al.* (1995); *Lassey et al.* (2007)

^f *Tyler et al.* (2000), calculated for 20°C from *Saueressig et al.* (2001)

^g *Brenninkmeijer et al.* (1995); *Röckmann et al.* (2011)

^h *Irion et al.* (1996); *Röckmann et al.* (2011)

ⁱ fraction estimate from *Allan et al.* (2007)

Geographical distribution of sources and changes in the past

The global extent of wetlands is estimated to be 8.3–10.2 million square kilometers, or about 5-8% of the land surface (*Lehner and Döll*, 2004). The largest portion is situated in boreal regions around 60° North (see figure 2.11 and 2.9). A second latitudinal belt representing $\sim 30\%$ of the total wetland area is found in the tropics. Wetlands are by far the largest natural source of methane today. Owing to large differences in the productivity and biomass turnover in boreal and tropical wetlands, low latitude wetlands

emit larger quantities of methane despite smaller areal extent. Estimates for tropical CH_4 emissions range from 60% (Bartlett and Harriss, 1993) to more recent determinations of up to 76% of the total emissions from natural wetlands based on satellite remote sensing (Bergamaschi et al., 2007). Generally, the isotopic signature of a methane source is determined by typical physical and chemical parameters, such as local temperature and substrate availability affecting reaction rates, CH_4 loss during the transport to the atmosphere, or by biological characteristics of the ecosystem. Certain differences in the mean carbon isotopic signature were reported for tropical and boreal methane sources (Quay et al., 1988; Stevens and Engelkemeir, 1988, and others). These differences are likely the result of combined effects due to the occurrence of ^{13}C -enriched organic matter in C_4 plants in tropical regions, temperature sensitivity of the isotopic fractionation (KIE) during methanogenesis and methanotrophy (e.g. Botz et al. (1996); Fey et al. (2004)), and factors such as substrate availability or microbial community structure (Schaefer and Whiticar, 2008; Bridgham et al., 2013).

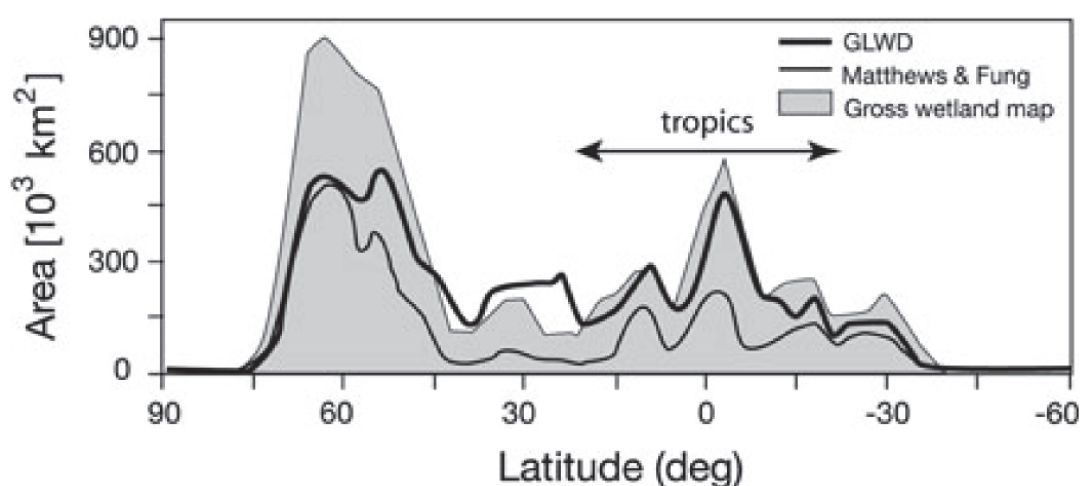


Figure 2.11.: Latitudinal wetland distribution.

Recent latitudinal distribution of wetlands based on data from *Matthews and Fung* (1987), the global lakes and wetlands database (GLWD), and a gross wetland map (redrawn from *Lehner and Döll* (2004)). Figure taken from *Mitsch et al.* (2010).

Studies focused on the reconstruction of pre-anthropogenic methane budgets have to consider that similar factors controlling latitudinal differences in wetland isotopic source signatures today may have also been at play during past periods of different climatic conditions (*Whiticar and Schaefer*, 2007). *Schaefer and Whiticar* (2008) have provided a reasonable set of assumptions of how and to what degree individual CH_4 source and sink processes were presumably affected by the different climatic conditions during the

pre-industrial Holocene (PIH), the LGM, and the transitional stage of the last glacial termination, the YD. The assessment of *Schaefer and Whiticar* (2008) suggests that isotopic source signatures have changed over glacial cycles and relative to today. They further postulate that differences of atmospheric CO₂ induced changes in the isotopic signatures of sources, which were affected by shifts in the abundance of C₃/C₄ vegetation in past times. The contribution of glacial-interglacial changes of CO₂ and C₃/C₄ ratios, however, was considered of minor importance regarding shifts in atmospheric δ¹³CH₄ (*Schaefer and Whiticar*, 2008). The low estimates of ~0.4 to ~0.7 ‰ for changes of δ¹³C_E between the LGM and the PIH are mainly due to model calculations by *Collatz et al.* (1998), who provided the estimates for the C₃–C₄ distribution for these time intervals based on a crossover function of monthly temperature and precipitation. This study suggested that PIH environments hosted 4% more C₄ vegetation than during the LGM and attributed the largest share of the C₃ contribution increase of 17% to the transition from the PIH into present times. Moreover, the calculations of *Collatz et al.* (1998) did not consider potential changes of the areal extent of grasslands and other vegetation types in the course of the glacial-interglacial transition. However, such shifts are derived by the majority of subsequent and more comprehensive vegetation model studies (*Harrison and Prentice*, 2003; *Prentice and Harrison*, 2009; *Prentice et al.*, 2011; *Woillez et al.*, 2011; *Bragg et al.*, 2012).

2.4.2. δ¹³CH₄/δD(CH₄) records for the past and what they have taught us

The first measurements of the stable carbon isotopes of methane from ice cores were provided by the pioneering study of *Craig et al.* (1988). Due to the technology available at that time, however, the measurements required relatively large quantities of air to resolve variations in δ¹³CH₄ in the range of 0.2 ‰. Unfortunately, the large sample sizes of ~25 kg ice from 4 – 6 m large sections of the Dye 3 ice core, Greenland, caused the temporal resolution to be too low to record dynamic variations of δ¹³CH₄ (*Craig et al.*, 1988). Moreover, such large sample sizes are prohibitive for the use of this technique in modern multi-component ice core studies, where sample sizes are strongly limited by the large demand of ice. But their results suggested that atmospheric δ¹³CH₄ was more depleted by approximately 2 ‰ not more than 100 years ago and the 2-3 centuries prior. *Craig et al.* (1988) attributed the trend towards the enriched value of -47.7 ‰ in the 1980s, which accompanied the doubling of atmospheric CH₄ mixing ratios, to an increase

in isotopically heavy (i.e. rich in ^{13}C) anthropogenic emissions. They postulated that a considerable share of these emissions must have originated from anthropogenic biomass burning, as the $\delta^{13}\text{CH}_4$ signature of this source is the most ^{13}C -enriched of all sources, and far from the mean 1980s source signature of -55.4‰ (*Craig et al.*, 1988).

It took some 20 more years of improvements in the field of instrumental analytics for the

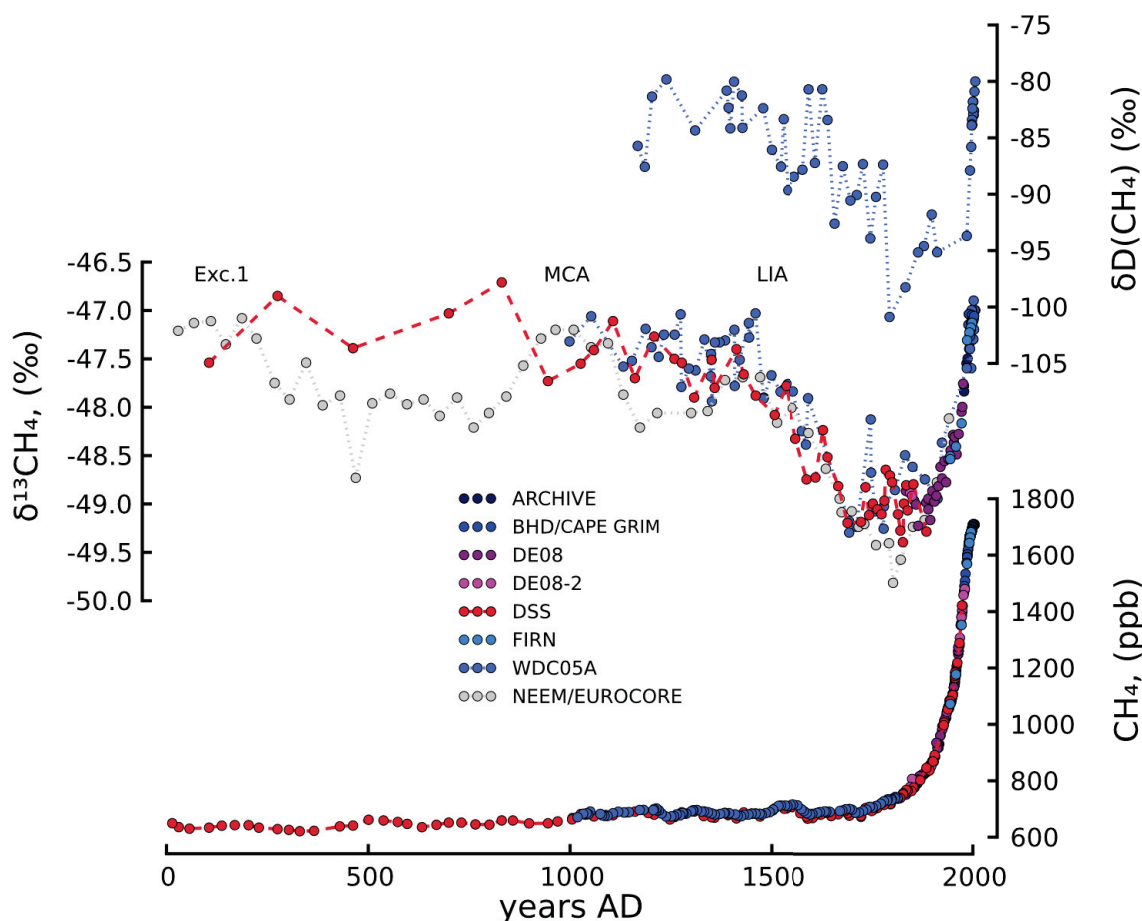


Figure 2.12.: Records of methane and its stable isotopes over the last two millennia.

bottom: Methane concentration data from Law Dome ice cores DE08, DE08-2 and DSS; from firn air samples (DSSW20k) and from ambient air of Cape Grim, Antarctica (*MacFarling Meure et al.*, 2006, and references within). In between 1000 to 1800 AD, CH_4 data from the WAIS ice core WDC05A illustrates relatively stable CH_4 concentrations over the LPIH (data from *Mitchell et al.* (2011)), and the good overlap of the two Antarctic ice cores. center: Composite atmospheric $\delta^{13}\text{CH}_4$ record from ambient air ("BHD", "Archive"), firn air (DSSW20k), and ice core air bubble enclosures from Law Dome (*Ferretti et al.*, 2005, same sample description as in 'bottom:'). Furthermore, $\delta^{13}\text{CH}_4$ data is shown from the WAIS divide ice core WDC05A over the last millennium (*Mischler et al.*, 2009), and from the ice cores NEEM and EUROCORE (*Sapart et al.*, 2012). The $\delta^{13}\text{CH}_4$ excursions relevant for the discussion are annotated as Exc. 1, Medieval Climate Anomaly (MCA) and Little Ice Age (LIA). top: WAIS WDC05A ice core $\delta\text{D}(\text{CH}_4)$ data over the last millennium (*Mischler et al.*, 2009).

first continuous record of ice core $\delta^{13}\text{CH}_4$ to be published by *Ferretti et al.* (2005, see figure 2.12). The data covers the last 2000 years in high resolution, an era they called the late pre-industrial Holocene (LPIH). The record is a composite of Southern Hemisphere ambient air, Antarctic firn air, and Antarctic ice core air samples from three cores drilled at Law Dome, East Antarctica (see section 2.3). The $\delta^{13}\text{CH}_4$ measurements were based on a gas chromatography mass spectrometry method developed by (*Miller et al.*, 2002), which reduced the requirements for ice core material to only ~ 700 g. Based on inverse source partitioning using the LPIH CH_4 atmospheric concentration data, assumptions of a constant CH_4 lifetime of 7.6 yr and a total sink fractionation of 7.4‰ (ϵ_{WT} , compare section 2.4.1) and constraints from $\delta^{13}\text{CH}_4$, *Ferretti et al.* (2005) inferred surprisingly high contributions from pyrogenic methane sources between 0 and 1000 AD. Over the next 700 years, however, these contributions decreased by almost 40% leaving the atmospheric $\delta^{13}\text{CH}_4$ depleted by ~ 2 ‰ in 1700 AD, before the fossil fuel emissions of industrialization started the exponential rise towards the modern, highly enriched $\delta^{13}\text{CH}_4$ values. *Ferretti et al.* (2005) attributed the depletion from 1000 to 1700 AD to both natural climate changes and human activities, an interpretation that was questioned by *Houweling et al.* (2006), who concluded that early anthropogenic CH_4 emissions from isotopically depleted sources such as rice-cultivation, domestic ruminants and waste treatment might have increasingly influenced atmospheric $\delta^{13}\text{CH}_4$. The features of the $\delta^{13}\text{CH}_4$ record of *Ferretti et al.* (2005) were later confirmed by a dual CH_4 isotope study covering the last millennium (*Mischler et al.*, 2009, figure 2.12). The additional constraint provided by $\delta\text{D}(\text{CH}_4)$ supported the assumption of a human influence on atmospheric methane at that time, as $\delta\text{D}(\text{CH}_4)$ indicated an increase of emissions from agricultural activities after 1000 AD, while biomass burning began to decrease. Just recently, a new high-resolution $\delta^{13}\text{CH}_4$ record, measured on the two Greenland ice cores NEEM (North Greenland Eemian Ice Drilling program) and EUROCORE, revealed three centennial-scale excursions between 100 BC and 1600 AD that have not been previously resolved (*Sapart et al.*, 2012). With the help of a two-box model, the authors attributed the first $\delta^{13}\text{CH}_4$ excursion between 100 BC and 200 AD ("Excursion 1" in figure 2.12) to early industrial activity (e.g. metal production) in the Roman empire and the Han dynasty and the sudden population decline associated with the downfall of both high cultures. The other two $\delta^{13}\text{CH}_4$ maxima, however, were attributed to climatic changes associated with the MCA at ~ 1000 AD and the LIA at around 1500 AD. For the MCA the model suggested a decrease in isotopically depleted biogenic emissions and increasing pyrogenic emissions, potentially due to extended droughts in Northern Europe and accelerated deforestation as a result of population expansion in

Europe and Asia, both accompanied by natural and anthropogenic fire activity (*Sapart et al.*, 2012). The third maximum in the $\delta^{13}\text{CH}_4$ data, just before the $\sim 2\text{‰}$ depletion towards 1700 AD, which is present in all three records (*Ferretti et al.*, 2005; *Mischler et al.*, 2009; *Sapart et al.*, 2012), coincides with the LIA which is associated with decreases in Northern hemisphere temperatures and precipitation (*Sapart et al.*, 2012, and references within). The authors concluded, that this climatic change might have reduced biogenic CH_4 emissions at that time, and ^{13}C -enriched emissions from natural wildfires and ongoing human land clearance affected $\delta^{13}\text{CH}_4$, while keeping the overall CH_4 budget nearly unchanged. It is important to bear in mind, however, that the $\delta^{13}\text{CH}_4$ datasets introduced thus far, are likely all, at least to some degree, affected by the analytical interference with atmospheric krypton (Kr), that has been discovered recently (*Schmitt et al.*, 2013, presented in chapter 4.5.1 of this thesis). The data by *Sapart et al.* (2012), for example, was found to be 0.15 to 0.88 ‰ too high owing to this effect, with the highest deviations for samples covering the industrial period (*Sperlich et al.*, 2013). Moreover, *Sperlich et al.* (2013) found some considerable, and yet unresolved, disagreement between their and the corresponding $\delta^{13}\text{CH}_4$ data of *Sapart et al.* (2012) for the period of the second data excursion (MCA), that could not be explained by Kr contamination.

Further back in time, $\delta^{13}\text{CH}_4$ values become progressively lighter throughout the Holocene, the current warm period that has started approximately 11000 years ago (11 thousand years before present (kyr BP), figure 2.13). Irrespective of the "bowl shaped" CH_4 record between the early Pre-boreal Holocene (PB) and the LPIH, a ~ 150 ppb excursion with its minimum at ~ 5 kyr BP, $\delta^{13}\text{CH}_4$ values decrease by $\sim 3\text{‰}$ from $\sim -46.5\text{‰}$ in the PB to late pre-industrial levels (*Sowers*, 2010).

The renewed CH_4 increase after 5 kyr BP gave rise to a prominent hypothesis by William F. Ruddiman, who assumed that early human civilizations reversed the natural trend towards lower CH_4 concentration levels by excessive flooding and rice agriculture (*Ruddiman*, 2003, 2007), although the world population was extremely low at that time. However, alternative hypotheses proposed that the CH_4 increase was rather caused by hydrological changes affecting low latitude wetlands, the largest natural source of CH_4 (*Chappellaz et al.*, 1997), or were a result of changes in the sink term. Latest findings, inferred from a model-based reconstruction of climate and vegetation suggest that the Holocene increase results from natural changes in the Earth's orbital configuration causing increasing emissions in the Southern Hemisphere tropics, and that early agricultural emissions are not required to account for the CH_4 concentration increase in the 5000 years

before the industrial era (*Singarayer et al.*, 2011).

The complementary Holocene $\delta\text{D}(\text{CH}_4)$ data shows a slightly decreasing trend from the early to the mid Holocene, and a $\sim 20\%$ increase in a period between 4 and 1 kyr BP (*Sowers*, 2010). The author attributes the decreasing early to mid Holocene trends in both CH_4 isotope datasets to growing emissions from Arctic lake ecosystems, which are known for their highly depleted $\delta^{13}\text{CH}_4$ and $\delta\text{D}(\text{CH}_4)$ source signatures (*Walter et al.*, 2006, 2007). As a result of increasing atmospheric CO_2 levels throughout the Holocene, $\delta^{13}\text{CH}_4$ is assumed to be further affected by an increase in the C_3/C_4 plant ratio induced by growing C_3 plant contributions (*Sowers*, 2010). This increase is partly due to the higher efficiency of the C_3 photosynthetic pathway under high CO_2 conditions and the predominance of C_3 plant species in high northern latitude ecosystems, which successively became ice-free and more active as a source of CH_4 after the retreat of the Fennoscandian and Laurentide ice sheets. The explanation for the $\sim 20\%$ $\delta\text{D}(\text{CH}_4)$ increase between 4 and 1 kyr BP, however, during which $\delta^{13}\text{CH}_4$ values remained basically constant, seems far less straight-forward. *Sowers* (2010) speculates, that an increase in the ratio of tropical to Arctic wetland sources might have the potential to explain the temporal $\delta\text{D}(\text{CH}_4)$ rise after 4 kyr BP. It is remarkable, however, that these dramatic shifts in CH_4 emissions from higher latitudes to the tropics should not have a corresponding response in $\delta^{13}\text{CH}_4$. Also a gradual release of CH_4 from marine clathrates during this period, usually with enriched $\delta\text{D}(\text{CH}_4)$ values and nearly neutral wrt. $\delta^{13}\text{CH}_4$, would be in line with the observations in both CH_4 isotope records (*Sowers*, 2010).

The transition from the last glacial period to the current warm phase, also called the (glacial) termination 1, was accompanied by two major CH_4 concentration increases, one during the warming from the late glacial Oldest Dryas (OD) interval into the intermittent warm stage Bølling-Allerød (BA) at ~ 14.7 kyr BP, and the second associated with the Younger Dryas (YD) – Pre-boreal Holocene (PB) transition at around 11.6 kyr BP. Various hypotheses had been put forward to explain these steep increases, "The Clathrate Gun Hypothesis" being the one that possibly received the greatest attention due to its potential implications for future climate projections (*Kennett et al.*, 2003, see the last paragraph of section 2.3 for further reference). $\delta\text{D}(\text{CH}_4)$ data inferred from GISP II ice core suggested, however, that large releases of CH_4 from marine clathrates, typically with very enriched values with respect to $\delta\text{D}(\text{CH}_4)$, did not contribute substantially to the OD–BA or the YD–PB methane rises (*Sowers*, 2006), and each transition led to slightly lower $\delta\text{D}(\text{CH}_4)$ values in the PB and the BA, respectively (approx. 10 to 15 ‰). A $\delta^{13}\text{CH}_4$ record measured on outcropping ice at Pákitsoq (Western Greenland) by *Schaefer et al.*

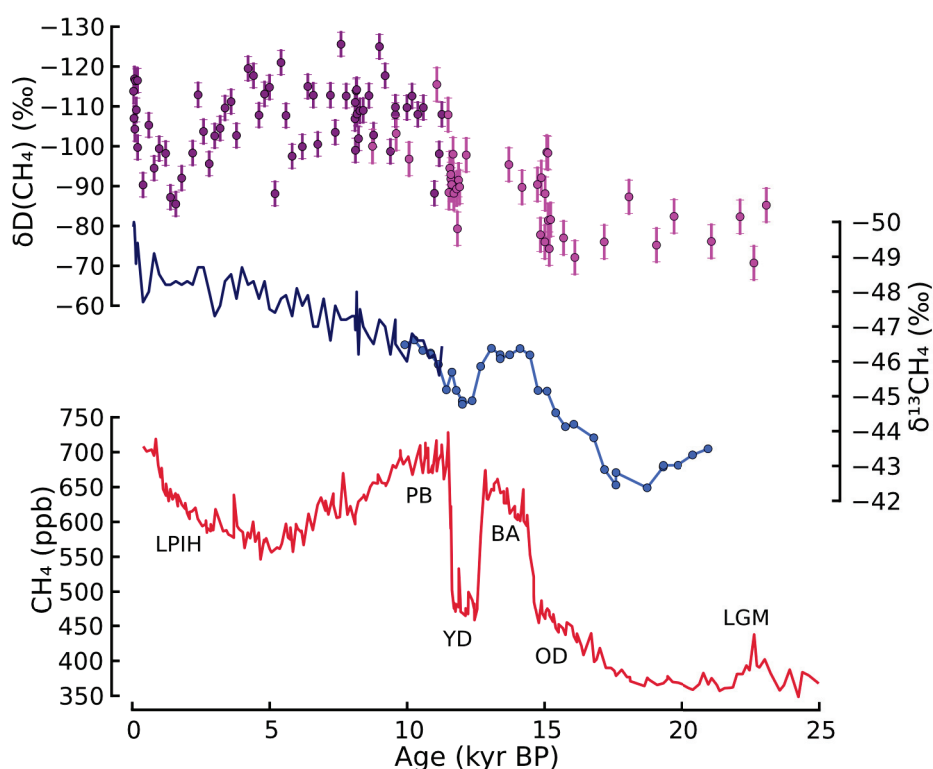


Figure 2.13.: Records of methane and its stable isotopes over the last 25000 years.

Bottom: Methane concentration data from EDML, Antarctica (*Schilt et al.*, 2010). The various climatic stages used for the discussion of the last glacial-interglacial transition (termination 1) and the Holocene period are given as references. Center: Atmospheric $\delta^{13}\text{CH}_4$ records from the GISP II ice core over the Holocene (dark blue, *Sowers* (2010)) and from EDML over termination 1 (T1, light blue, *Fischer et al.* (2008)), both as published (no correction for analytical interference with krypton applied - please see section 4.5 for further details). Top: $\delta\text{D}(\text{CH}_4)$ data for the Holocene (dark magenta, *Sowers* (2010)) and T1 (magenta, *Sowers* (2006), both GISP II). Note that the axes for $\delta^{13}\text{CH}_4$, $\delta\text{D}(\text{CH}_4)$ and the age scale are inverted by convention. EDML $\delta^{13}\text{CH}_4$ and CH_4 records are plotted wrt. the 'unified' ice core age scale by *Lemieux-Dudon et al.* (2010).

(2006) provided further evidence that neither gradual nor catastrophic release of CH_4 from marine clathrates was the essential driver for the CH_4 concentration rise of ~ 250 ppb during the YD–PB transition. Surprisingly, *Schaefer et al.* (2006) observed no significant difference in $\delta^{13}\text{CH}_4$ between the two climatic intervals, nor an isotopic shift during the steep CH_4 concentration increase. No less surprising was the observation that $\delta^{13}\text{CH}_4$ values during the YD (~ -46 ‰) were more enriched than the levels inferred for the LPIH (~ -49 ‰) and in the modern atmosphere (~ -47 ‰, e.g. *Ferretti et al.* (2005); *Mischler et al.* (2009)), although pre-anthropogenic $\delta^{13}\text{CH}_4$ was expected to be more depleted in ^{13}C due to the absence of fossil fuel combustion, land clearance by fire, landfills and other

^{13}C -enriched anthropogenic emissions. *Schaefer et al.* (2006) propose five possible scenarios to explain the YD–PB $\delta^{13}\text{CH}_4$ record. (1) Literature estimates for late glacial and YD fire emissions may be too low. (2) Geologic sources probably constituted a larger fraction to the CH_4 budget than today, as the overall emissions in the YD were lower, and emissions of geologic CH_4 were potentially enhanced due to lower sea-levels (*Luyendyk et al.*, 2005). (3) Tropical wetlands with their slightly more enriched $\delta^{13}\text{CH}_4$ signatures could have been more important during the YD than earlier anticipated (e.g. in *Hein et al.* (1997)). (4) Aerobic methane production from plant material (enriched $\delta^{13}\text{C}$ signature of $\sim -50\text{‰}$) might have contributed substantially in earlier budgets and caused higher $\delta^{13}\text{CH}_4$ values. And (5), the large isotope effect of the MBL $\cdot\text{Cl}$ sink led to enriched $\delta^{13}\text{CH}_4$ due to a potentially higher fraction of methane removed by this sink.

Melton et al. (2012) later remeasured the same interval again on Pākitoq outcrop ice with a refined analytical setup and enhanced resolution (*Melton et al.*, 2011). Based on a $\sim 1\text{‰}$ reversal of the general $\delta^{13}\text{CH}_4$ depletion trend from the YD into the PB (see the discussion of results from *Fischer et al.* (2008) below) corresponding to the ~ 250 ppb CH_4 increase, they concluded that ^{13}C -enriched sources played an important role in the CH_4 rise. With the help of triple isotope mass-balance calculations including $\delta^{13}\text{CH}_4$, $\delta\text{D}(\text{CH}_4)$ (*Sowers*, 2006, 2010), and radiocarbon data (^{14}C of CH_4 , *Petrenko et al.* (2009)), they attempted to quantify the various source and sink contributions during the YD–PB transition. The results suggest biomass burning (42–66 %) and thermokarst lakes (27–59 %) as the dominant contributing sources to the total methane flux increase, and in contrast to earlier interpretations of the YD–PB increase (*Chappellaz et al.*, 1990; *Brook et al.*, 2000; *Singarayer et al.*, 2011) attributed only a minor role to tropical wetlands. Marine gas hydrates were also unlikely to have played a dominant role (*Melton et al.*, 2012).

The $\delta^{13}\text{CH}_4$ record from EDML, Antarctica, covering the entire glacial termination, shows a near continuous trend towards depleted values from the start of the YD that persists far into the PB without an inversion towards enriched $\delta^{13}\text{CH}_4$ values (*Fischer et al.*, 2008, see figure 2.13). *Melton et al.* (2012) argue that this record does not resolve the fast, 150 year YD–PB transition in detail. On the other hand, Pākitoq ice was reported to be subject to *in-situ* production of methane, prevalent especially in ice from warmer periods (*Petrenko et al.*, 2006; *Schaefer et al.*, 2009). A systematic effect of this excess CH_4 on $\delta^{13}\text{CH}_4$ in Pākitoq ice, however, was considered unlikely (*Schaefer et al.*, 2006; *Melton et al.*, 2012).

Still, the $\delta^{13}\text{CH}_4$ data of *Fischer et al.* (2008) confirmed the high values of the YD period, and the depletion trend of $\sim 1.4\text{‰}$ throughout the PB is in good agreement with

the $\delta^{13}\text{CH}_4$ dataset of *Sowers* (2010). Further back in time, the EDML $\delta^{13}\text{CH}_4$ values indicate a $\sim 1.1\text{‰}$ excursion over the OD–BA–YD climate oscillation, following a $\sim 2.5\text{‰}$ depletion trend from $\sim -42.5\text{‰}$ at the end the coldest stage of the glacial period, the Last Glacial Maximum (LGM), dated at around 25 to 20 kyr BP (*Clark et al.*, 2009). In this period, large amounts of water were bound in glaciers and ice sheets, while sea-level was reduced by more than 100 m (*Bintanja et al.*, 2005; *Lisiecki and Raymo*, 2005). For the interpretation of the EDML $\delta^{13}\text{CH}_4$ record, *Fischer et al.* (2008) defined four steady state periods throughout the termination (LGM, BA, YD and PB, plus one recent state "1990" for model validation) and estimated the individual contributions of major source processes to the respective transitions with a 4-box model (North and South hemispheric box, each with a box for the troposphere and stratosphere) assuming the isotopic signatures of individual sources to remain temporally constant. The inter-polar difference (IPD) in atmospheric methane concentrations (*Chappellaz et al.*, 1997; *Dällenbach et al.*, 2000; *EPICA community members*, 2006), GISP II $\delta\text{D}(\text{CH}_4)$ data (*Sowers*, 2006), reasonable assumptions for CH_4 atmospheric lifetime, and the new EDML $\delta^{13}\text{CH}_4$ data were used as boundary conditions in the model runs using a Monte Carlo approach. The model suggests a predominant role of boreal wetland emissions driving the 3.5–4‰ depletion during warm periods and the $\sim 1.1\text{‰}$ BA–YD reversal, and a near shut-down of this CH_4 source during the LGM. The latter is mainly controlled by the CH_4 IPD observations available at that time (*Dällenbach et al.*, 2000), which had to be significantly revised in the meantime (*Baumgartner et al.*, 2012). Moreover, emissions from biomass burning were found to remain roughly constant over the glacial termination, that turned out to be a direct consequence of the assumption of constant source signatures. The secondary trends in the PB were attributed to expanding boreal sources, e.g. by activation of thermokarst lakes, and the $\sim 1\text{‰}$ enrichment during the LGM to a change of the $\delta^{13}\text{C}$ signature of wildfire emissions due to shifts from C_3 to C_4 dominated grasslands.

Again with the help of $\delta\text{D}(\text{CH}_4)$ data measured on North Greenland ice core project (NGRIP) ice core material, *Bock et al.* (2010b, see figure 5.4) demonstrated that marine clathrate emissions likely also have not dominated CH_4 budgets during millennial scale climate fluctuations in MIS 3 (compare figure 2.8). The results from an adaptation of the box model used in *Fischer et al.* (2008) suggest that the ~ 15 to 20‰ $\delta\text{D}(\text{CH}_4)$ dynamics during DO interstadials 7 and 8 is largely due to isotopically depleted boreal wetland emissions. According to the model, high-latitude wetland emissions increased by a factor of 6 from ~ 5 to $\sim 32\text{ Tg yr}^{-1}$ CH_4 from stadial to interstadial conditions, while tropical wetland emissions increased only moderately from ~ 84 to $\sim 118\text{ Tg yr}^{-1}$. Marine clathrate

emissions were supposedly rather constant at stadial-interstadial transitions and biomass burning emissions slightly elevated during the two DO interstadials (*Bock et al.*, 2010b). In agreement with the set of 7 MIS 3 $\delta\text{D}(\text{CH}_4)$ data points of *Sowers* (2006), *Bock et al.* (2010b) observed a pronounced 16 ‰ drop in $\delta\text{D}(\text{CH}_4)$ that precedes the DO 8 CH_4 rise by ~ 500 years, likely induced by the slow restart of the Atlantic Meridional Overturning Circulation (AMOC) after the decline from a period of peak ice rafting debris counts associated with the Heinrich event 4 (*Hemming*, 2004, H4 in figure 5.4). Transient runs of the Monte Carlo Box model could reconcile the $\delta\text{D}(\text{CH}_4)$ changes with constraints from the CH_4 IPD, $\delta^{13}\text{CH}_4$ and CH_4 atmospheric lifetime only if not a single source but boreal and tropical wetland sources together were forced to increase (300 ‰ and 10 ‰). And only if the typical $\delta\text{D}(\text{CH}_4)$ source signatures were reduced by 30 ‰ and 5 ‰, respectively (*Bock et al.*, 2010b), in line with expected stadial/interstadial changes in the water isotopic composition in both regions.

3. Ice cores - Spyglass into the atmospheric history

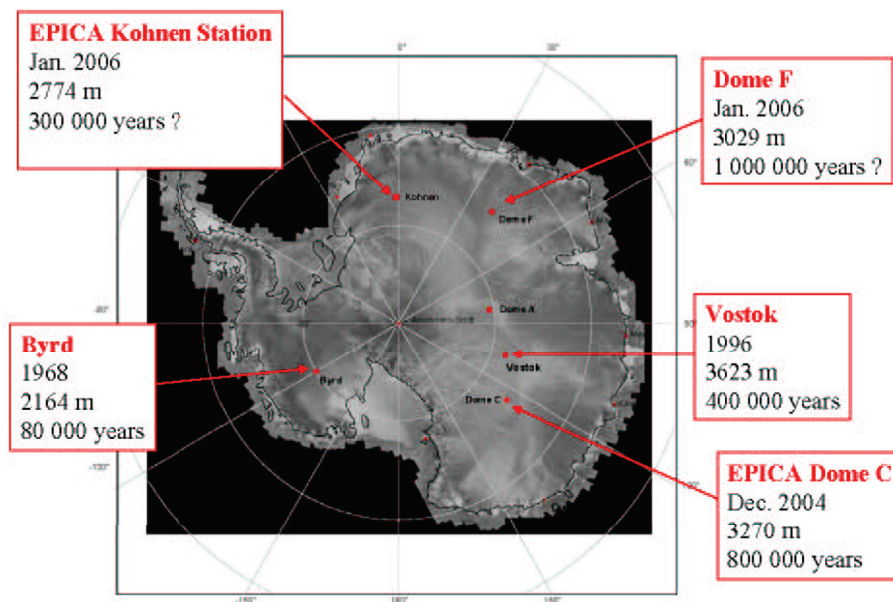


Figure 3.1.: Sites of deep ice core drilling projects in Antarctica.

A map showing the positions of Antarctic deep ice core drilling sites. The boxes indicate the respective name of the drilling, the year of its completion, the final depth and the estimated maximum age of the recovered climate and environmental records. Figure is from *Masson-Delmotte et al. (2006)*.

For roughly 50 years now, beginning with the first deep ice core retrieved at Camp Century in north-west Greenland, polar ice cores have provided a wealth of information from the environmental past. In favorable positions on the polar ice caps, an image of the respective current climate state is filed in almost perfect chronological order together with the precipitation deposited at that sites. The continuous long-term prehistorical records of physical and chemical parameters of climate history have had impacts on a wide spectrum of scientific disciplines such as geophysics, oceanography, geology, meteorology and climatology. The water isotope signatures in the ice ($\delta^{18}\text{O}$), for example, inherit

information about the precipitation at the deposition site and the moisture source areas (*Dansgaard et al.*, 1969; *Johnsen et al.*, 1972; *Lorius et al.*, 1985, and many more) in addition to the global ice volume and sea level (*Bintanja et al.*, 2005). Particulate ice inclusions of chemical compounds, dust and aerosols give insight into past volcanic events, meteorological trajectories, reorganization of wind regimes and aridity of remote source areas (*Fischer et al.*, 2007; *Kaufmann et al.*, 2008; *Bigler et al.*, 2010).

But the most outstanding and unique feature of ice cores from the polar ice sheets are air enclosures that provide the only direct historical record of the atmospheric composition. Various ice cores from Greenland and Antarctica have helped to extend the time series of modern direct and continuous measurements of the greenhouse gases CO₂ and CH₄ far into the past (*Berner et al.*, 1980; *Barnola et al.*, 1987; *Chappellaz et al.*, 1990; *Etheridge et al.*, 1998, and many others). A great achievement that proved that climate change and greenhouse gas evolution are considerably linked, and that modern concentration levels exceed the range of their respective natural variability during the past 800,000 years, i.e. the last 8 glacial cycles, by far (*Loulergue et al.*, 2008; *Lüthi et al.*, 2008, see figure 2.6). While the ice core results of atmospheric CH₄ have been already discussed in chapter 2.3, the following sections introduce the specific glaciological features of the ice core gas archive.

3.1. How atmosphere is conserved in the ice

On the areas of the two polar ice sheets in Antarctica and Greenland where the mean annual temperatures are mostly below the freezing point throughout the year, snowfall is accumulated layer by layer and compacted by subsequent precipitation. In the uppermost 50–150 m below the surface, the compacting snow, referred to as "firn" once it reaches a certain density, is successively transformed into ice. This process usually takes several decades to millennia, depending on local conditions such as snow accumulation rate, annual mean temperature and surface wind speeds inducing snow drifts.

The firn column is schematically divided into three zones according to the different modes of air movement in the pore space (*Sowers et al.*, 1992). In the "convective zone" close to the surface, air is freely mixed with the atmosphere by convection and by venting processes like surface winds and seasonal temperature variations. Below that layer, free air exchange is increasingly restricted. The open pore space of firn in that depth retains air in a quasi-

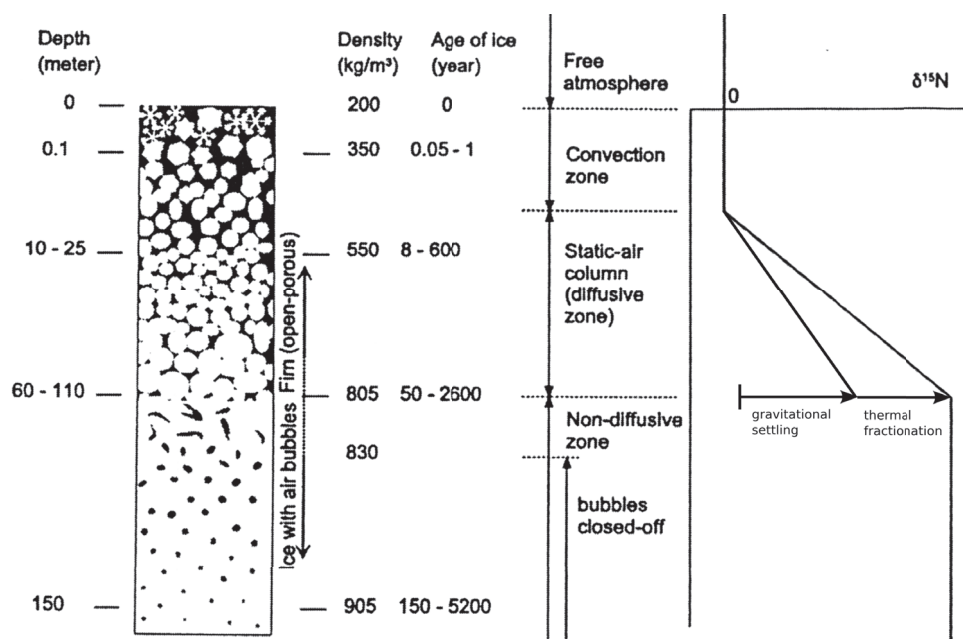


Figure 3.2.: Scheme of the firn to ice transition and characteristics of air enclosure.

This figure provides an overview of typical ranges of depth, density and ages for firn columns of polar ice sheets on the left, and the theoretical subdivision into zones characterized by the modes of vertical gas movement according to (Sowers *et al.*, 1992) on the right. The $\delta^{15}\text{N}_2$ profile is a schematic representation of the sum of expected fractionation processes induced by gravitational settling and thermal diffusion along a negative temperature gradient from the top to the bottom of the diffusive zone of the firn column. Figure from Schwander (1996), with modifications by Bock (2010).

static gas column in diffusive equilibrium (Schwander *et al.*, 1988). The diffusive gas transport in that column, which is still tied to conditions at the surface, causes a series of specific alterations to the chemical and isotopic composition that are discussed later in this section (compare also (cf.) subsection 3.2). At the bottom of this diffusive zone, more and more of the pore space becomes isolated, and the effective gas exchange in the open pores ceases. Below, the fraction of closed pore space exponentially increases in this so-called "non-diffusive zone" until no open connections to the layers above exist. The air is finally trapped within the ice matrix at the "bubble close-off depth", which is better characterized as a transition zone rather than a concrete depth. As a consequence, the air enclosed in a bubble has an age distribution rather than a distinct age (Schwander, 1989; Spahni *et al.*, 2003). Furthermore, the occluded air is always younger than the surrounding ice. The difference between the gas age and the ice age is called Δage (Sowers *et al.*, 1992) and reflects the age of the firn at the bottom of the diffusive firn column minus

the age of the air at that depth. The Δ age has proven difficult to estimate with sufficient accuracy so far and is connected to a considerable degree of uncertainty (*Severinghaus et al.*, 2010). For the Greenland Ice Core Project (GRIP) core from central Greenland, values inferred from dynamic firn densification model (*Schwander et al.*, 1997) range from approximately 200 years for modern snow accumulation and temperature to 400 and 1000 years for MIS 3 interstadial and stadial conditions, respectively. For the Antarctic counterpart core EPICA Dronning Maud Land (EDML), however, Δ ages range from approximately 800 ± 200 years for recent to around 1800 ± 400 years for glacial conditions in MIS 2 (*Siegenthaler et al.*, 2005; *Blunier et al.*, 2007).

Even deeper in the ice sheet, typically at a depth of around 1000 m, when the pressure of the overlying ice column at low temperatures reaches critical values, the gas molecules are forced into the ice matrix to form so-called gas hydrates or clathrates. Gradually, more and more bubbles disappear and the ice becomes clear. The changes imposed on the crystal structure of ice in this transitional zone are known to make it a very brittle material when it is brought to the surface.

3.2. Changes to the gas composition induced by the enclosure in the ice matrix

Atmospheric compositions of the past inferred from air enclosed in the firn and in an ice core can only be reconstructed truthfully if the physical processes that alter the composition of air in the firn column before it is finally occluded in bubbles are properly understood. The air in the uppermost layer of snow and firn, known as the "convective zone" (*Sowers et al.*, 1992), is homogenized with the atmosphere by turbulent and convective air movement that is largely induced by surface winds and atmospheric pressure variations, but may also partly be driven by seasonal temperature gradients and thermal buoyancy (*Albert et al.*, 2004). The convective layer thickness is mainly influenced by firn permeability, atmospheric pressure gradients, surface wind speeds and topography (*Colbeck*, 1989, 1997). Below this zone of vigorous mixing, the air composition in the static porous firn column are subject to alterations due to (i) gravitational settling (*Schwander et al.*, 1988; *Craig et al.*, 1988) and molecular diffusion along (ii) concentration (*Schwan-*

der, 1989; Trudinger et al., 1997) and (iii) thermal gradients (Severinghaus et al., 2001). The diffusion processes can be described by the one dimensional diffusion equation:

$$\frac{\partial C}{\partial t} = \frac{\partial}{\partial z} \left(D_{\text{eff}}(z, T) \left(\frac{\partial C}{\partial z} - \frac{\Delta m g}{RT} + \Omega \frac{dT}{dz} \right) \right) \quad (3.1)$$

with

C = concentration of a certain gas species in a mixture or the isotopic composition of a pair of isotopes of a gas species, e.g. $^{12}\text{C}/^{13}\text{C}$ of methane,

t = time (s),

z = depth (m),

D_{eff} = effective molecular diffusivity ($\text{m}^2 \text{s}^{-1}$) in porous snow and firn,

T = temperature (K),

Δm = mass difference of the gas species relative to the mass of the mixture or the mass difference of the two isotopic species (g mol^{-1}),

g = gravitational acceleration (m s^{-2}),

R = ideal gas constant ($\text{J mol}^{-1} \text{K}^{-1}$) and

Ω = thermal diffusion sensitivity (‰ K^{-1}).

In the presence of thermal gradients, a gas mixture encounters thermal fractionation that drives the heavier species toward the cold side and the lighter species to the warm (Grachev and Severinghaus, 2003). Thermal gradients may for example be generated by seasonal temperature variations or rapid warmings during the last glacial period or at glacial-interglacial transitions. However, the occurrence and magnitude of thermal gradients in the firn are highly dependent on how fast temperature changes are propagated into the ice sheet. At sites with high snow accumulation, typically associated with higher annual temperature variability, thermal gradients in firn and ice are far more prevalent and significantly steeper than those at low-accumulation sites, where temporary deviations from thermal equilibrium are smoothed over long time periods.

In a porous static air column like the "diffusive zone" in firn (Figure 3.2), the heavier species or isotopologues of a gas mixture progressively accumulate at the bottom. This phenomenon, also known as gravitational settling, separates gases according to the mass difference Δm as given by the barometric equation (Severinghaus et al., 1998, eqn. 3.2).

$$\delta = \left(\frac{R}{R_0} - 1 \right) \times 10^3 = \left(\exp \frac{\Delta m g z}{R_G T} - 1 \right) \times 10^3 \quad (3.2)$$

with

δ = isotopic composition in per mil (‰)

R = isotopic ratio at the specific depth z ,

R_0 = isotopic ratio of air at the surface,

Δm = mass difference of the two isotopic species (g mol^{-1}),

g = gravitational acceleration (m s^{-2}),

z = depth (m),

R_G = ideal gas constant ($\text{J mol}^{-1} \text{K}^{-1}$) and

T = temperature (K).

Measurements of the slight deviations from the quasi-static ratios of $^{15}\text{N}/^{14}\text{N}$ ($\delta^{15}\text{N}_2$) of atmospheric nitrogen or $^{40}\text{Ar}/^{36}\text{Ar}$ ($\delta^{40}\text{Ar}$) of argon allow a quantification of thermal diffusion and gravitational settling of air components in the firn column (*Sowers et al.*, 1992; *Severinghaus et al.*, 2003).

The ordinary diffusion according to Fick's law creates a stream of matter from a site of higher toward a site of lower molecular concentration. Diffusion acts as a compensatory process against concentration differences and balances the previous two effects to form an equilibrium state. As mentioned earlier, the transition from the open pore system with free gas exchange to a closed pore space does not occur at a defined depth but rather in a zone of several meters. That causes the age distribution of those gas molecules, which are trapped in a certain layer of the ice, to be even wider. As a consequence, fast variations of any of the atmospheric trace gases at the surface are recorded in the ice as an dampened signal (*Spahni et al.*, 2003). At sites with low temperatures and very low accumulation rates, where the trapping of air is very slow and the gas may diffuse for a long time, the attenuation effect is strongest. As the whole sequence of air bubble enclosure in an ice sheet usually takes several decades to millennia, but the ordinary gas diffusion is significantly faster, concentration changes at the surface are propagated down to the close-off depth relatively quickly. However, if the concentration changes at the surface are fast enough, the diffusive equilibrium is temporarily disturbed (*Schwander et al.*, 1988), and a measurable delay of the heavier isotope of a gas species is created on its way down the diffusive firn column due to differing diffusion speeds (*Trudinger et al.*, 1997). Accordingly, a shift in the isotopic ratio is recorded in the ice until the equilibrium state is regained. An estimate of the size of this effect for glacial conditions at the EDML

core site based on a model to assess fractionation processes in firn (*Schwander et al.*, 1997) is presented in section 5.2.3.

4. Experimental

The methane carbon isotope ($\delta^{13}\text{CH}_4$) data of air extracted from ice cores and of atmospheric samples presented in this work have been measured on a gas chromatography combustion isotope ratio monitoring mass spectrometry (GC/C/irmMS) system developed by *Behrens et al.* (2008). To briefly summarize its mode of operation, air is extracted from an ice core sample in a wet-extraction line, methane is separated from the main air components on a pre-concentration unit and isolated on a gas chromatography (GC) column. Then it is combusted to CO_2 in a high temperature micro-oxidation furnace, and the carbon isotopic signature of these CO_2 molecules is determined by the (isotope ratio monitoring) mass spectrometer (MS). The setup of the AWI instrument is illustrated as a flow scheme in figure 4.1. It can virtually be divided into three parts: a high helium (He) flow extraction part (I), a low-flow gas separation and combustion part (II) and the part for the final CO_2 isotope measurement (III).

The following chapters outline the sequence of an exemplary ice sample measurement including a detailed description of the instrument and the reference strategy. After a brief summary of the corresponding reference standard measurements, it is discussed how these time series are integrated into novel script-based data processing procedures and finally what corrections are applied to secure internal calibration and the standardization to the international VPDB scale.

Later work by *Schmitt et al.* (2013) showed that krypton (Kr) interferes with the CH_4 mass spectrometric analysis. How this comes about and how the $\delta^{13}\text{CH}_4$ data can be corrected for this "Kr effect" is discussed in the publication by *Schmitt et al.* (2013) and in the following paragraphs of section 4.5.

4.1. Tracing an exemplary ice sample through the system

Initially, the outer 2 mm at the surface of an ice sample with the mass of 150 g to 200 g are scraped off with a microtome knife to prevent surface contamination. The ice is then

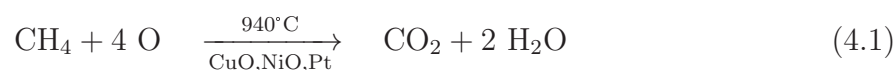
weighed and transferred to a pre-chilled ultra-high-vacuum stainless steel-to-glass sample vessel with a DN 63 CF-flange (SEG-250; Caburn-MDC Europe Ltd., UK) and an approximate inner volume of 350 ml. After sealing the vessel with a copper gasket, the manual valves are closed (SS-DSVCR4, Swagelok, USA), the vessel transferred from the cold lab, its inlet attached to the extraction line of the system and the outlet to a ultra-high vacuum turbo molecular pump (Turbovac 50, Oerlikon Leybold GmbH, Germany). Ambient air and potentially adsorbed gaseous compounds on the sample surface are then removed by evacuation for 60 to 90 min at 2×10^{-6} to 4×10^{-6} mbar. Meanwhile, vessel temperatures are kept below -10°C in a metal dewar. The subsequent extraction is started only when the pressure behind the water trap (KF16 corrugated tube, Pfeiffer, Switzerland) reaches at least 4×10^{-6} mbar to ensure that the vessel is leak-tight.

After the evacuation is finished, the vessel outlet is also attached to the extraction line via $1/4$ " Ultra-Torr connectors (Swagelok, Solon, OH, USA), and the sample is melted in a 30°C to 40°C warm water bath within 25 min. Beginning with the melting of the ice sample, a custom programmed Visual Basic script, implemented in the MS software Masslynx (Elementar Analysensysteme, Germany), controls all the subsequent measurement operations. Except for the two manual valves attached to the sample vessel, all valves are toggled by the scripts. During the melting procedure, the manual valves of the sample vessel are purged with a $15 \text{ ml}/\text{min}$ He stream. To equilibrate the water phase temperature in the vessel for extraction and to reduce the risk of overloading the Nafion dryer, the warm water bath is then replaced with a crushed ice/water cold bath to lower water vapor pressure and to adjust the temperature close to a constant 0°C . To prevent water droplets from entering the extraction line, the vessel outlet is protected by a metal frit ($10 \mu\text{m}$, Thomachrom 83341, Reichelt, Germany). The vessel is then brought to operating pressure for methane extraction in about two minutes by switching V2 and opening the vessel inlet valve to let helium fill the vessel. At around 2.1 bar overpressure, monitored by a diaphragm pressure gauge (UHP flow-through-gauge, WIKA Alexander Wiegand SE & Co. KG, Germany), the manual inlet valve is closed again and V2 toggled in order to cool the CO_2 and CH_4 traps under steady helium flow. After 3 min, V2 is switched again, the two manual vessel valves are opened simultaneously and the sample air is stripped out of the head-space and the melt water by He purged through a $1/16$ " stainless steel inflow capillary that reaches down to the bottom of the vessel. The extraction procedure continues for 90 min, equivalent to the vessel head-space being flushed about 15 times at continuous $150 \text{ ml}/\text{min}$ helium carrier gas stream. The bulk of water vapor is removed from the He stream by a 60 cm Nafion membrane (0.07 " inner diameter (i.d.); Perma Pure

LLC, USA) chilled to $-15\text{ }^{\circ}\text{C}$. Residual water and the easily condensable gases N_2O and CO_2 are trapped in a $1/8\text{''}$ stainless steel tubing cooled to $-196\text{ }^{\circ}\text{C}$ (Liquid Nitrogen (LN_2)) filled with Nickel (Ni) wires to increase its adsorption capacity.

Further downstream, methane from the sample air is pre-concentrated in a $50\text{ cm } 1/8\text{''}$ stainless steel tube filled with a hydrocarbon retaining polymer (Hayesep D 80/100 mesh) at $-140\text{ }^{\circ}\text{C}$. Temperature control of the CH_4 trap is maintained by a PID-heat controller (West 6400; West Instruments, UK) with a thermocouple attached to the center of the tubing, and deviations are held below $1\text{ }^{\circ}\text{C}$. The bulk of non-methane air constituents from the sample are removed from the carrier gas stream through the vent at V3 during the extraction and pre-concentration procedure. Once the 90 min extraction period has ended, V3 is switched, the CH_4 pre-concentration trap detached from the high-flow extraction line and looped into the low-flow part ($1.1\text{ ml}/\text{min}$) for further gas separation and CH_4 combustion. The manual valves of the sample vessel are closed in order to check extraction efficiency in a following synthetic air measurement (cf. section 4.2 below). Residual nitrogen (N_2) and oxygen (O_2) on the CH_4 trap is allowed to leave for 5.5 min when it is lifted out of the LN_2 and successively warmed by the ambient air before CH_4 is trapped and "cryofocused" for 10 min on a $1\text{ m } 0.32\text{ mm i.d. CP-Porabond Q}$ column (Varian, Germany) in LN_2 .

Afterwards, the CH_4 and remaining air components are separated chromatographically at $30\text{ }^{\circ}\text{C}$ on a subsequent 30 m GC column ($0.32\text{ mm i.d. CarbonPLOT GC}$ column, Agilent, Germany). The eluents are then combusted at $940\text{ }^{\circ}\text{C}$ in an aluminium oxide (Al_2O_3) micro-oxidation tube filled with CuO, NiO and Pt wires (ThermoFinnigan). Water formed in the oxidation reaction of CH_4 (equation 4.1) is removed by a second Nafion membrane downstream of the oven, while the CO_2 is admitted into the mass spectrometer via a movable open split. An exemplary chromatogram of the MS mass beam recordings for a ice core sample is presented in figure 4.2.



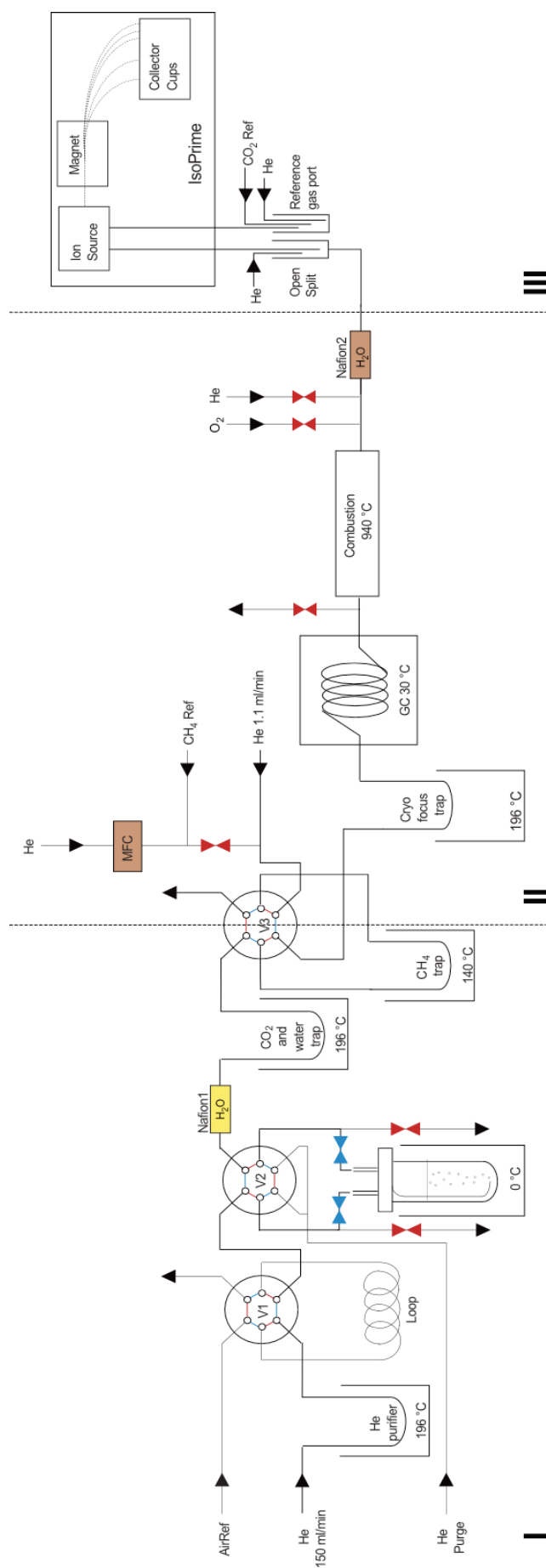


Figure 4.1.: Flow scheme representation of the AWI instrument. The measurements are performed on an IsoPrime mass spectrometer (Elementar Analysensysteme, Germany) equipped with three Faraday collectors for the masses m/z 44, 45 and 46 as well as two additional collectors to monitor m/z 28 (N₂ and CO) and 32 (O₂) simultaneously. It is coupled to a custom-built extraction and pre-concentration system. All tubing is stainless steel (SST) or fused silica. Valves V1 to V4 are pneumatic six-port two-position valves (first/second position; 1/16" fittings, 0.4 mm port diameter, Valcon M rotor; Valco, VICI AG, Switzerland). The other automated valves are pneumatic on/off needle valves (symbol \bowtie , valve *open/closed*; MOVPT; Vespel seat and ferrules; SGE, Germany). The helium carrier gas (99.999 vol.-% purity; Air Liquide, Germany) is pre-cleaned by a high-capacity gas purifier and an OMI™ Indicating Purifier (both Supelco, USA; not shown in here) that remove H₂O, O₂, CO₂ and CO. A supplemental He purifier trap filled with Hayesep D 80/100 mesh (Supelco) cooled to -196 °C with LN₂ additionally prevents a potential contamination from CH₄ and higher hydrocarbons - the figure is an adaption to the scheme shown in Behrens *et al.* (2008).

4.2. Referencing strategies and their realization

Methane from ice or air samples may encounter a series of contamination, mass loss and fractionation processes on its way through the different parts of the instrument. This includes potential sample loss during the extraction or the primary trapping of water and CO₂, incomplete absorption of CH₄ on the Haysep D polymer trap, partial CH₄ losses during the release of bulk air components from the trap and incomplete transfer of sample CH₄ on the pre-concentration cryofocus capillary. Isotopic fractionation may occur during the chromatographic separation of residual air components in the GC column caused by mass discriminations either due to the chromatographic isotope effect or chromatographic distortion, fractionation effects imposed by the combustion in the micro-oxidation furnace or the flow conditions at the open-split. Therefore it is crucial to be able to independently check the different parts of the system for the aforementioned processes and potential blank contributions in order to maintain long-term system stability and reproducibility. These requirements were satisfied with a series of reference measurements based on the strategies proposed by *Behrens et al.* (2008):

- i) The correction for potential effects occurring in the source of the mass spectrometer is achieved with injections of a reference CO₂ working standard (cf. Table 4.1) admitted via the reference gas port in each individual acquisition.
- ii) Potential fractionation processes occurring in the low-flow part of the system (sector I in figure 4.1) are monitored by injections of a CH₄/He-mixture directly into the GC flow upstream of the cryofocus trap. CH₄ standard peaks are generated both in separate daily acquisition runs used to observe the state and long-term stability of the oxidation furnace (three acquisitions with six consecutive CH₄ peaks, hereafter called 'methane monitoring' acquisitions) and during each ice sample and air standard acquisition, i.e. before and after the sample peak, to check the stability during the acquisition runs. The diluted laboratory standard CH₄ reference gas (99.9995 vol-% purity; Air Liquide, Düsseldorf, Germany), a mixture of approximately 1500 ppm CH₄ in He, is injected into the GC carrier gas stream via a pneumatic on/off valve to generate peaks similar in size and shape to one from atmospheric CH₄ extracted from an ice sample. 'Methane monitoring' measurements are further used to analyze and evaluate systematic long-term drifts of the instrument, caused for instance by aging of the combustion oven (see also subsection ??).
- iii) Acquisitions of air samples injected either directly through the loop at valve V1 (see figure 4.1) or through the sample vessel (empty or filled with degassed melt-water) are

performed on a regular basis, ensuring the highest possible degree of similarity to ice sample measurements in agreement with the Identical Treatment principle (IT principle) (*Werner and Brand, 2001*). Measurements of typically two consecutive 10 mL injections of our laboratory synthetic air standard (at standard temperature and pressure (STP)), cf. Table 4.1), help to trace potential mass loss effects and other long-term systematic errors induced by the extraction and methane/air separation. Apart from that, those acquisitions termed 'reference loops' are used to check the system state directly before every ice sample measurement and comprise an essential part of the internal calibration routine (cf. subsection 4.3.2).

- iv) Every individual ice sample measurement is further directly followed by the acquisition of a 20 mL sample of the same air standard, this time injected directly into the melt-water of the previous ice sample. Those measurements, also referred to as 'loop after', help to evaluate extraction efficiency and provide indications whether sample fractions were retarded somewhere else in the system.
- v) The systems' signal dependency of $\delta^{13}\text{CH}_4$ versus CH_4 load (i.a. controlling the peak sizes) is tested regularly by consecutive measurements of 1 to 4 times 10 mL (STP) injections of the laboratory air standard.
- vi) Finally, the overall accuracy of the system is determined by measurements of a conventionally calibrated sample of modern air ('Neumayer loops'), following the same procedure as for synthetic air acquisitions. The recent air sample was taken at the German Antarctic station Neumayer and its $\delta^{13}\text{CH}_4$ value wrt. VPDB (-46.97‰ , $1\sigma=0.04\text{‰}$ ($n=7$)) was determined by off-line sample preparation and dual-inlet IrmMS on a MAT 252 mass spectrometer (Thermo Finnigan) at the Institut für Umweltphysik, Heidelberg (*Poß, 2003*). Calibration of the Heidelberg $\delta^{13}\text{CH}_4$ measurements was performed using pure CO_2 IAEA Standard Reference Materials (RM 8562: $\delta^{13}\text{C}_{\text{VPDB}} = -3.72\text{‰}$, RM 8564: $\delta^{13}\text{C}_{\text{VPDB}} = -10.45\text{‰}$, RM 8563: $\delta^{13}\text{C}_{\text{VPDB}} = -41.59\text{‰}$ (*Coplen et al., 2006*). The absolute agreement of the Heidelberg $\delta^{13}\text{CH}_4$ measurements on the VPDB scale is estimated to be better than $\pm 0.1\text{‰}$ (1σ). An inter-comparison with three air samples from the southern hemisphere between Heidelberg and the National Institute of Water and Atmospheric Research, Wellington (NIWA) yielded a $\delta^{13}\text{CH}_4$ difference NIWA-Heidelberg of $0.04 \pm 0.04\text{‰}$ wrt. VPDB (*Poß, 2003*).

Table 4.1.: Gases and gas mixtures used for the internal calibration of the AWI system. Isotopic signatures are reported wrt. VPDB for $\delta^{13}\text{C}$ and $\delta^{18}\text{O}$.

| Synthetic Air Standards | | | | |
|---|-----------|-----------------------------|-------------------------------|-------------------------------------|
| Name | Installed | Components | Fraction*, (ppb) ^a | Notes |
| "Synth. Air" ^b | 2005/09 | CO ₂ | 250 × 10 ³ | ISOTOP-CO ₂ |
| | | CH ₄ | 1000 | 99.995 vol.-% purity |
| | | N ₂ O | 250 | 99.999 vol.-% purity |
| "Crystal-Air" ^b | 2010/01 | CO ₂ | 249.9 × 10 ³ | ISOTOP-CO ₂ |
| | | CH ₄ | 1081 ± 22 | 99.995 vol.-% purity |
| | | N ₂ O | 259 ± 26 | |
| Carbon dioxide working standards | | | | |
| | | $\delta^{13}\text{C}$, (‰) | $\delta^{18}\text{O}$, (‰) | |
| Btl-NR.:9154E | 2005/09 | -49.35 | -22.59 | ISOTOP-CO ₂ ^b |
| Btl-NR.:56216 | 08/06/11 | -24.4 | -17.7 | ^c |
| Btl-NR.:11952 | 09/03/17 | -49.2 | -19.4 | ISOTOP-CO ₂ ^b |

* error ranges are given where supplier specifications were available

^a mixed in synthetic air

^b Air Liquide, Germany

^c Messer Group GmbH, Germany

4.3. Data processing

The software Masslynx 4.0 (GV Instruments, Manchester, UK) provided by the MS manufacturer was used for the instrument control and automated operational sequences during acquisition. Typically, the results of individual measurements are processed automatically and each presented on a single spreadsheet. However, the MS software lacks the desired degree of transparency e.g. in terms of the determination of sample peak boundaries. Moreover, its flexibility is limited, as a cascade of subsequent manual spreadsheet operations is required to converge individual acquisition results to the corresponding time series according to the referencing strategies as outlined in section 4.2. Nevertheless, this approach was successfully applied in *Behrens et al.* (2008) and for the less extensive EDML $\delta^{13}\text{CH}_4$ ice core record published by *Fischer et al.* (2008). In this work, two custom made scripts written in Python are introduced (a platform independent open-source programming language, <http://www.python.org/>), aimed to improve the handling and processing of larger datasets and further adapt the method to our specific needs.

The first script in the sequence performs the complete raw MS data processing of each

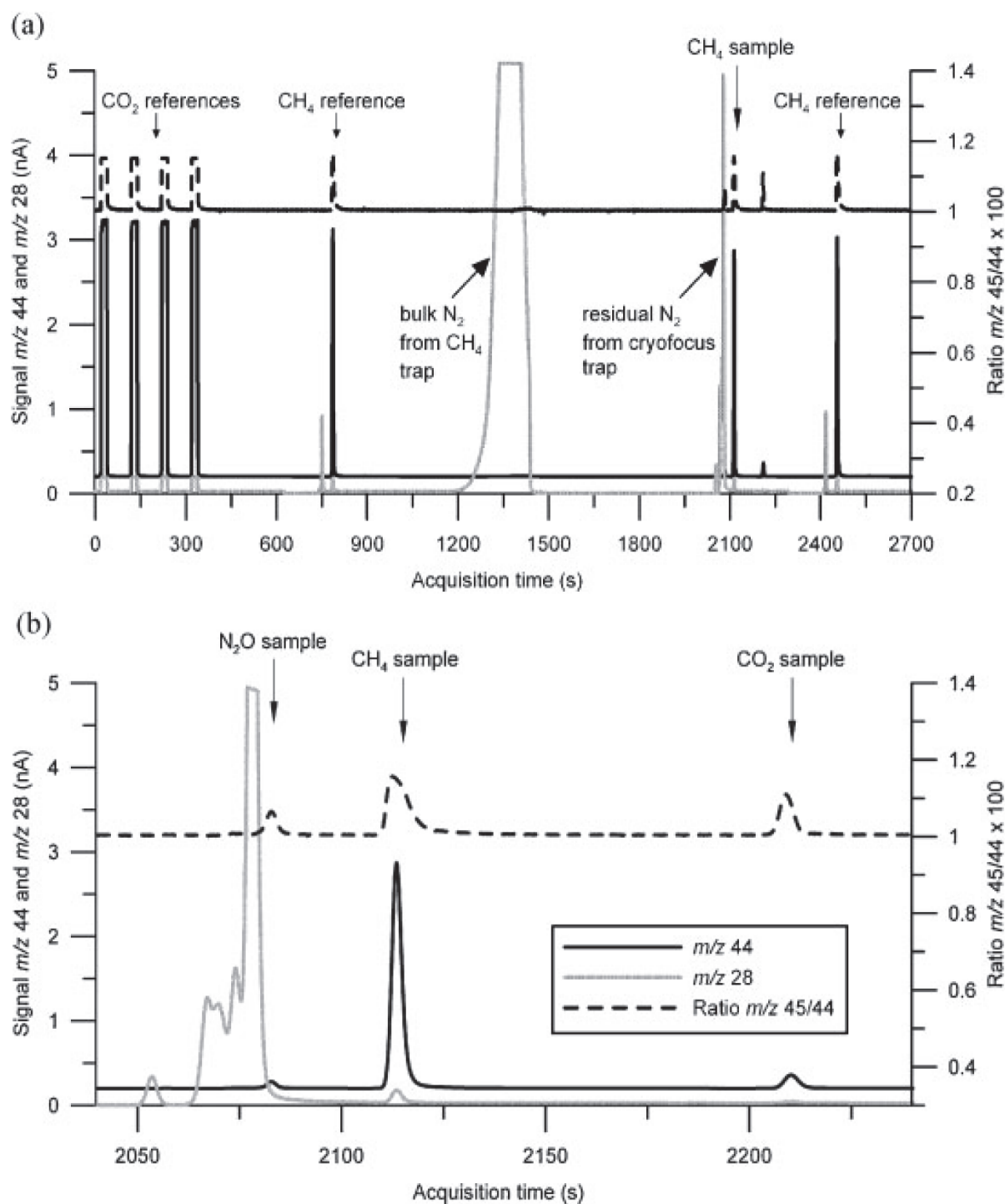


Figure 4.2.: Exemplary chromatogram of an ice core sample This figure shows the mass beam recordings of m/z 44 and 28 and the ratio of m/z 44 and 45 for a pre-industrial ice core sample as acquired by the MS instrument. The general features of this chromatogram are representative for all types of air sample acquisitions, including standard and reference air measurements. In the m/z 44 beam recording (solid black lines) of the complete acquisition run (a), there are four 'rectangular' (on/off) peaks of reference CO_2 directly injected into the MS, followed by the first of two CH_4 reference peaks, the CH_4 sample peak, a separated small peak of residual sample CO_2 , and the second of CH_4 reference peaks passing only the low-flow part of the system. In the m/z 28 recording (gray lines) there is a huge excursion caused by the bulk of sample N_2 , interrupted by the cooling of the cryofocus trap. The enlarged section shown in (b) illustrates that some of the N_2 remained on the cryofocus trap and eluated shortly before the N_2O peak, but more than 30s before the CH_4 sample peak. The figure is adopted from *Behrens et al.* (2008).

individual acquisition in a standardized, efficient and transparent fashion and directly allocates the results to the respective time series. This way, all potential errors introduced by the manual spreadsheet operations are categorically omitted and complete control over any aspect of raw acquisition data processing is secured. Furthermore, the quick and fully automated computation of each individual acquisition offers almost real-time access to all relevant information needed to observe the overall system performance and helps to evaluate the quality of the day's sample measurement results. For a detailed description of the scripts *modus operandi*, the reader is referred to subsection 4.3.1.

The second script is used to extract all required information from the respective datasets and to perform the post-processing routines in accordance with our reference strategies. This is extensively described in subsection 4.3.2. Later in this section, the results of EDML ice samples generated by our script-based approach are compared with those from the original publications (*Fischer et al.*, 2008; *Behrens et al.*, 2008, subsection 4.3.2).

4.3.1. Script based raw data processing

The required MS raw data are exported from the operation software Masslynx 4.0 to an ASCII text file. The mass beam readings m/z 44, 45 and 46 of each measurement are recorded in three columns with time steps of 0.1 s. The data processing script reads this raw file and performs a floating window peak detection routine applying the Offset Centre of Gravity Retracker (OCO_G) (*Wingham et al.*, 1986). The three entities peak 'width', 'amplitude' and 'position' are continuously calculated for a 30 s floating time window with the following equations:

$$width = \frac{(\sum y^2(t))^2}{\sum y^4(t)} \quad (4.2)$$

$$amplitude = \sqrt{\frac{\sum y^4(t)}{\sum y^2(t)}} \quad (4.3)$$

$$position = \frac{\sum ty^2(t)}{\sum y^2(t)} \quad (4.4)$$

with the beam reading y in [fA] and the time in the data series t in [ms]. Peaks are localized by 'position' and further classified with respect to their shape, defined by their 'width' and 'amplitude', similar to the proceedings in *Bock et al.* (2010a).

The terms "Gaussian" and "Rectangular" peaks are used in the following for GC eluted and the internal on/off CO₂ working standard gas peaks introduced via open-split (cf.

chapter 4.2, i)), respectively, even though peak shapes in continuous flow measurements are neither strictly Gaussian nor rectangular. Peaks of a width less than 16 s and with an amplitude exceeding 1 nA are identified by the script as Gaussian, those wider than 16 s and with an amplitude greater than 1 nA as Rectangular reference peaks. Finally, all detections exceeding the width of 16 s and amplitudes below 1 nA are classified as "blank-like" peaks. Only then are the exact integration limits of each detected peak from the first two categories determined by individual routines basically following the steps described in *Ricci et al.* (1994). Accordingly, the peak start and peak end are specified using prescribed thresholds of changes in the slope of the first derivative of m/z 44, thereby marking the integration limits for Gaussian peaks. The small temporal discrepancies between the chromatographical elution of the three isotopes of interest (the "time shift") is considered negligible for this analytical setup, as the differences are smaller than the minimal instrumental acquisition step of 100 ms. Comparison of the cubic spline covering the sample peak maxima, which is used to determine the peak position (10 ms steps) in the mass beam readings m/z 44, 45 and 46, yields maximum deviations of 60 ms (median 30 ms) between the two most distant peak maxima (m/z 45 and 46) in reference loop and sample acquisitions.

The integration of rectangular peak areas is, in contrast, confined to a 12 s window centered on the peak plateau. Signal background levels for all three masses are averaged over a 5 s window preceding the detected peak start and accounted for in the numerical integration of peak areas with the composite Simpson's rule method (*Dragomir et al.*, 2000). The Gaussian peak isotope ratios are referenced to the averaged ratio of the CO₂ working standard rectangular peaks. The m/z (45/44) ratios are corrected for ¹⁷O using the Craig algorithm (*Craig*, 1957) and converted to the standard δ -notation. The δ -values, position of the maxima, amplitude, area and isotope ratios of all detected peaks are stored in the appropriate database file according to the acquisition type 'ice sample', 'air sample' and the reference measurements 'methane monitoring', 'reference loops' and 'loop after' (detailed description in subsection 4.2).

4.3.2. Script-based data post-processing

The data post-processing routines are performed by another custom-made script, also written in Python, and basically comprise the following functionality:

- i) quickly gather and visualize comprehensive information about the actual system state,

- ii) calculate the internal calibration of the instrument based on the standard synthetic air measurements ('reference loops'),
- iii) standardize to the international VPDB scale by means of conventionally calibrated air samples (e.g. 'Neumayer loops'),
- iv) correct all ice and air samples in the database according to these calibrations,
- v) apply corrections for gravitational settling in the firn column,
- vi) export the calibrated and corrected ice core data-set to a comma separated values (csv) text file.

Internal calibration

The measurements of our synthetic air standard ('reference loops') are intended to have the highest possible degree of similarity to the conditions during ice core sample acquisitions. After 'methane monitoring' measurements, which document the state of the low-flow part of the system, 'reference loops' are the most frequent type of acquisitions and the most reliable recorder of the overall system performance. Drifts observed in the long-term sequence of this time series reflect the sum of all potential fractionation contributions induced in the different parts of the instrument, i.e. the extraction line, the separation of CH₄ from the remaining air constituents, the combustion of CH₄ to CO₂ and the final measurement in the MS. Moreover, they document the actual system state directly before each (non-standard) ice and ambient air sample acquisition and are thus considered the best suited instrument to correct for systematic deviations from an hypothetical "ideal", stable system status.

However, every individual reference value is further affected by a stochastic measurement error, introducing another degree of uncertainty to attempts to correct the systematic error alone. In order to omit the stochastic error contribution, our internal calibration procedure is based on a cubic spline smoothing through the standard air measurements. The spline is calculated from the point in time when the 'reference loops' methane sample peak maximum is recorded versus the respective $\delta^{13}\text{CH}_4$ value of the peak. The spline thus represents a temporally smoothed measure of the actual system accuracy, which is caused by the long-term machine drift. Each spline evaluation, or rather its numerical difference to a defined point of reference, represents the deviation of the system accuracy at the specific point in time, for example when a CH₄ sample peak (e.g. from an ice sample) is recorded by the MS. Accordingly, each individual non-standard sample mea-

surement is calibrated wrt. an interpolated value of the standard air at the CH₄ sample peak recording time evaluating the spline properties.

. Our laboratory air standard "Synth. Air" was exhausted in early 2010. For convenience, the time period is henceforth denoted as "Ref. Period I". It was replaced by another synthetic air ("Crystal Air") in "Ref. Period II". One spline fit was applied to the data series of each of the two reference air standards (cf. Table 4.1). Their smoothing parameter were varied independently in order to obtain minimized deviation of the data vs. spline evaluation values over the respective time series. As a result, non-standard acquisitions during both periods are calibrated against two different points of reference. Both of their "true" $\delta^{13}\text{CH}_4$ values are unknown, so the mean $\delta^{13}\text{CH}_4$ value of all acquisitions of the respective synthetic air was assigned. To align the two basically independent calibrations, measurements acquired during the shorter "Ref. Period II" are corrected for an offset inferred from cross-referencing the standard air cylinders from both periods. The final link to the international scale, the absolute standardization, is established with the external calibration wrt. VPDB described in subsection 4.3.2.

Figure 4.3 illustrates the system drifts observed throughout the time of the EDML ice sample acquisitions presented in chapter 5.1. Most of the changes seem to occur in the low-flow part of the instrument, as $\delta^{13}\text{CH}_4$ trends in the time series of the separate daily 'methane monitoring' measurements as well as the two methane standard peaks admitted in any of the other acquisition types (both complying to item **ii** in section 4.2) almost perfectly reconcile the trends in $\delta^{13}\text{CH}_4$ also observed for CH₄ extracted from the laboratory air standards, that additionally pass the high-flow part of the instrument. The insert **a** of figure 4.3 demonstrates the close resemblance of the machine drift depicted by the cubic spline representation of the 'reference loops' (magenta line) in a zoomed section of the acquisitions with corresponding splines through the daily 'methane monitoring' measurements (purple line) and the two synthetic methane peaks of 'reference loops' (light blue line), ice sample and subsequent 'loop after' acquisitions (white and gray circles). The two most pronounced positive excursions in April and September 2008 directly coincide with an exchange of the oxidation furnace tubes. The subsequent successive drift towards more isotopically depleted $\delta^{13}\text{CH}_4$ values are likely related to an aging process of the tubes. Both observations provide evidence that much of the systems' long-term $\delta^{13}\text{CH}_4$ variability traces back to processes in the oxidation furnace. After major maintenance measures of the instrument and a furnace exchange in late 2009, however, conditions in the oven and the low-flow part proved to be much more stable (see insert **b** of figure 4.3). When the initial step of the internal calibration routine, the long-term trend correction

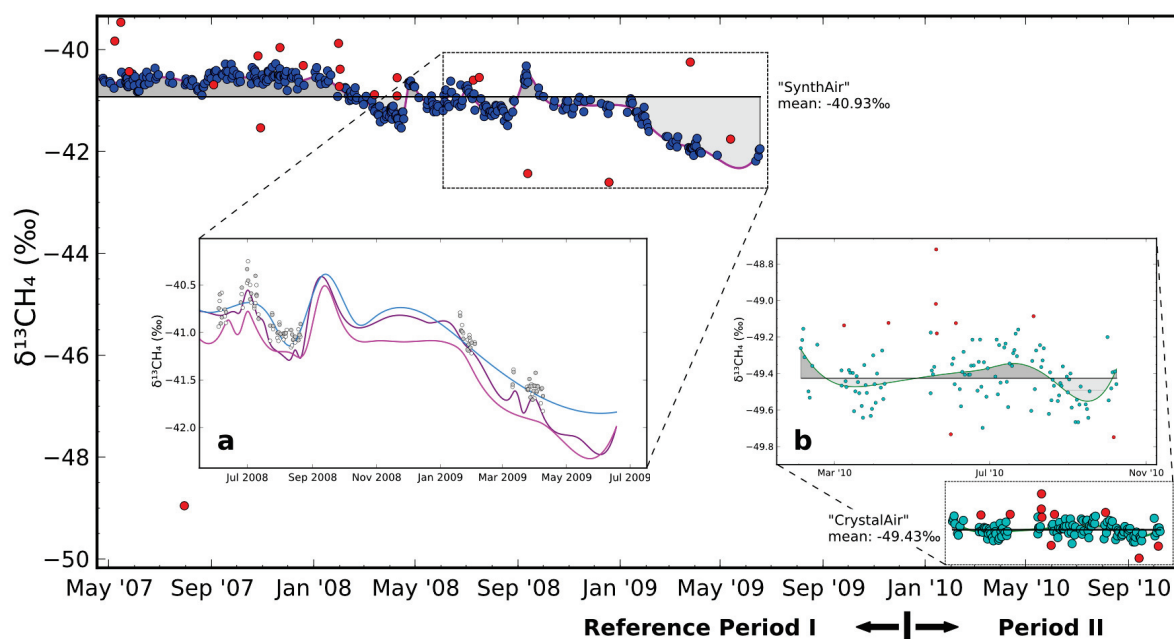


Figure 4.3.: Time series of 'reference loops' and calibration splines. The compilation of standard air measurements used for the internal calibration procedure are shown in this figure. Results for acquisitions of the synthetic air standard "Synth. Air", in use before 2010 ("Ref. Period I"), are marked as blue circles. Results for "Crystal Air", also shown in the zoomed figure insert **b**, in cyan. Data points in red indicate outliers that were disregarded in the calculation of the cubic spline fits (depicted as colored lines for the "Synth. Air" (magenta) and "Crystal Air" (green)). The gray shaded areas represent the offset from the point of reference (here the arithmetic mean of all acquisitions of the respective synthetic air standard) at a given instance of time, which are later accounted for in the long-term trend correction. The figure insert **a** shows one of the most pronounced $\delta^{13}\text{CH}_4$ drifts in the record. The systematic trend, here represented by the cubic spline curve of our air standard (magenta line), closely resembles the analogous cubic splines of the 'methane monitoring' acquisitions (purple line) as well as the two methane standard peaks in 'reference loop' measurements (light blue line). Equivalent methane standard peak $\delta^{13}\text{CH}_4$ values in ice sample (white circles) and subsequent "loop after" (gray circles) acquisitions drift at the same rate toward lower values. As methane standard peaks only pass through the low-flow part of the instrument, the variability is obviously mainly caused by the low-flow part of the instrument (sector II in figure 4.1).

based on the cubic spline smoothing of 'reference loops', is applied to the synthetic air standards themselves (illustrated in figure 4.4), the statistical variance of the acquisitions (σ^2) wrt. $\delta^{13}\text{CH}_4$ is reduced from 0.146 to 0.010 ($n=442$) for "Ref. Period I", and from 0.016 to 0.011 ($n=115$) for "Ref. Period II", resulting in a good overall agreement with the methodical uncertainty range of 0.10‰ (1σ) inferred for the laboratory air standard by *Behrens et al.* (2008).

Cross-referencing "Synth. Air" measurements of "Ref. Period II" ($\delta^{13}\text{C}$ -40.69‰,

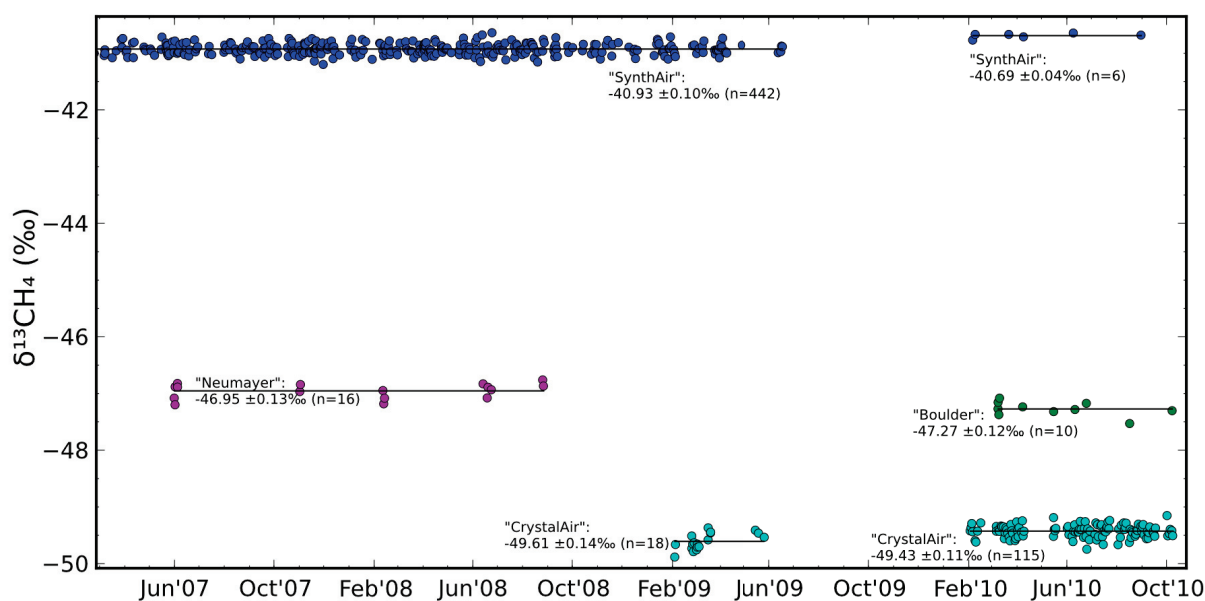


Figure 4.4.: Reference results after removal of the long-term trend. Intermediary results for the standard air 'reference loops' (again "Synth. Air" in blue, "Crystal Air" in cyan), the external standard "Neumayer" (purple) and another independent external synthetic air standard ("Boulder", green, see also Table 4.2) after the removal of the long-term instrument drift. The offset between "Synth. Air" measurements of Ref. Periods I & II is used to align all acquisitions performed in "Ref. Period II". Finally, the marginal offset of the mean value of "Neumayer loops" to its designated value of -46.97‰ (*PoB*, 2003) is applied to all non-standard measurements to establish the link to the VPDB scale.

$1\sigma=0.04\text{‰}$ ($n=6$)) to "Ref. Period I" ($\delta^{13}\text{C} -40.93\text{‰}$, $1\sigma=0.10\text{‰}$ ($n=442$)) yielded an offset of 0.24‰ . This amount is applied to measurements performed during "Ref. Period II" to align their calibration relative to the point of reference of "Ref. Period I". The correction also causes the "Crystal Air" mean values of "Ref. Period I" ($\delta^{13}\text{C} -49.61\text{‰}$, $1\sigma=0.14\text{‰}$ ($n=18$)) to be in better agreement with the adjusted mean level of "Ref. Period II" ($\delta^{13}\text{C} -49.67\text{‰}$, $1\sigma=0.11\text{‰}$ ($n=115$)).

External calibration

The AWI system accuracy is determined by frequent measurements of a calibrated sample of recent air from the German Antarctic station Neumayer ('Neumayer loops', see section 4.2, vi for details). Those acquisitions are evaluated as non-standard samples and treated according to the procedure outlined in subsection 4.3.2. The resulting $\delta^{13}\text{CH}_4$ mean value of -46.95‰ ($1\sigma=0.13\text{‰}$ ($n=16$)), cf. figure 4.4) deviates from the reference value by an amount of 0.02‰ (*PoB*, 2003, $\delta^{13}\text{C}_{\text{VPDB}} = -46.97\text{‰}$). Consequently, reported $\delta^{13}\text{CH}_4$

Table 4.2.: Compilation of results for reference air standards and ice measurements performed on the AWI system (ice samples not corrected for gravitational settling). Values are reported with respect to the VPDB scale.

| Synthetic, ambient and firn air measurements | | | | | | | | |
|--|---------------------------|-------------------|----------------------------|-------------------|----------------------------|------------|----|--------------------------------------|
| Sample Name | Reference values | | | | Internal results | | | Sources |
| | [CH ₄] ppb | 1 σ ppb | $\delta^{13}\text{C}$ ‰ | 1 σ ‰ | $\delta^{13}\text{C}$ ‰ | \pm ‰ | n | |
| "Boulder" (CA08463) | 1512.49 ^a | 0.24 | -47.32 | 0.03 | -47.53 | 0.12 | 10 | NOAA ^b |
| Alert (2002/11) | 1831 ^a | 2 | -47.44 ^c | 0.03 | -47.59 | 0.05 | 2 | Alert Station ^d |
| CA01179 ^e | 372.17 ^a | 0.19 | -46.16 ^f | — | -46.48 | 0.08 | 3 | IPY ^e , NOAA ^b |
| CC71560 ^e | 904.23 ^a | 0.17 | -47.34 ^f | — | -47.34 | 0.02 | 3 | IPY ^e , NOAA ^b |
| CA03560 ^e | 1830.59 ^a | 0.20 | -47.08 ^f | — | -47.37 | 0.04 | 3 | IPY ^e , NOAA ^b |
| Dome13 ^g | 1476 ^h | — | -49.99 ^h | — | -49.62 | 0.05 | 2 | Firn Air ^g |
| Dome6 ^g | 1718 ^h | — | -46.99 ^h | — | -46.96 | 0.17 | 2 | Firn Air ^g |
| Schauinsland ⁱ | 1899.5 ^{j,a} | 2.60 | -48.00 ^k | 0.03 | -47.74 | 0.06 | 2 | Black Forest ⁱ |
| Ice sample measurements | | | | | | | | |
| B34 ^m , 197.2mbs. | — | — | -46.46 ⁿ | 0.21 | -46.52 | 0.05 | 3 | ~250 AD ⁿ |
| ShGISP2 ^o , ~142mbs. | 703 ^p | 43 ^p | -49.37 ^p | 0.58 ^p | -48.63 | 0.03 | 2 | ~1720 AD ^p |
| WDC05 ^q , 164.96mbs. | 707 ^r | — | -47.94 ^s | — | — | — | — | 1571 AD ^r |
| WDC05 ^q , 166.78mbs. | 714 ^r | — | — | — | -47.68 | 0.03 | 2 | 1564 AD ^r |
| WDC05 ^q , 169.8mbs. | 714 ^r | — | -47.53 ^s | — | — | — | — | 1551 AD ^r |

^a on NOAA04 scale (*Dlugokencky et al.*, 2005)

^b NOAA, Boulder, CO., US.

^c *Poß* (2003)

^d Canadian Forces Station Alert, Nunavut, Canada

^e part of the IPY Inter-calibration exercise, compare subsection 4.3.2

^f Todd Sowers, Pennsylvania State University (PSU), personal communication

^g from EDC station

^h *Bräunlich et al.* (2001)

ⁱ Schauinsland station in the Black Forest, Germany

^j *Levin et al.* (1999)

^k *Brass and Röckmann* (2010)

^m shallow core drilled at Kohlen Station, Antarctica in 2003/04

ⁿ *Sapart* (2012)

^o GISPII shallow core #139, Central Greenland

^p *Melton* (2009)

^q West Antarctic ice sheet divide ice core WDC05 A, West Antarctica

^r values interpolated from data of *Mitchell et al.* (2011)

^s *Mischler et al.* (2009)

values in this work were further corrected for this offset in order to link them to the international VPDB scale. However, the results for a second definite $\delta^{13}\text{CH}_4$ external standard ("Boulder"/"CA08463") obtained from NOAA ($\delta^{13}\text{CH}_4$ -47.53 ‰, $1\sigma=0.12$ ‰ (n=10)) have a slight discrepancy to the reference value determined at the Institute of Arctic and Alpine Research, University of Colorado, Boulder (INSTAAR) (*Vaughn et al.*, 2004; *Miller et al.*, 2002, $\delta^{13}\text{C}_{\text{VPDB}} = -47.32$ ‰, $1\sigma=0.03$ ‰ (n=18)) potentially indicating that the results acquired in 2010 might be slightly too low. Nevertheless, the calibration versus VPDB is valid within the reported uncertainty levels.

A series of additional ambient air ("Alert", "Schauinsland") and firn air samples ("Dome6", "Dome13") were measured in order to evaluate our system accuracy. The results are summarized in Table 4.2. Furthermore, the AWI methane stable isotope laboratory participated in a worldwide inter-comparison effort known as the "2007 - International Polar Year (IPY) International Ice Core Gas Inter-calibration Exercise" launched by Todd Sowers (Penn State University) and Ed Brook (Oregon State University) with the aim of addressing the calibration differences in the different labs and establishing a unified scale among them. The three recent ambient air samples were retrieved at Niwot Ridge preserve, Colorado, US in 2007, and were diluted with ultra-pure air (free of CH_4) in order to simulate the full spectrum of atmospheric methane concentrations typical for present day (sample "CA03560"), pre-industrial ("CC71560") and glacial ("CA01179") atmospheric conditions. The corresponding AWI system results are also given in table 4.2. Furthermore, ice samples from the WAIS divide ice core WDC05 A drilled in West Antarctica (79°27.70S 112°7.510W; 1,759 masl.) in 2005/2006 were measured by means of the IPY inter-comparison exercise. The results were also used to test the alignment of the systems in operation at AWI and the Pennsylvania State University (PSU) stable isotope laboratory and were applied to the joint $\delta^{13}\text{CH}_4$ dataset presented in chapter 5.1. All of the test measurements agreed within the stated analytical uncertainties, demonstrating both the high accuracy and precision of the AWI system.

Evaluation of the script-based data processing

As a final test of the reliability of script-based raw data processing, we applied our procedure to the raw data of the $\delta^{13}\text{CH}_4$ measurements of the last glacial-interglacial transition (EDML depth interval 654-1009 meter below the surface (mbs.)) published in *Fischer et al.* (2008), which were treated according to the method described in (*Behrens et al.*, 2008).

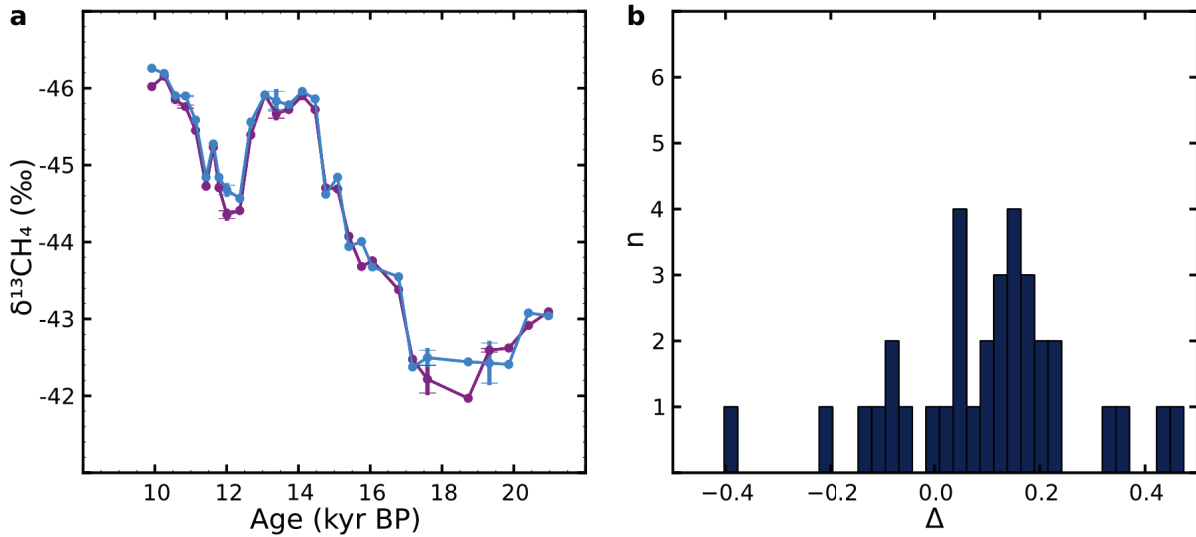


Figure 4.5.: Comparison of results for EDML ice covering the last deglaciation. a) Time series as published in *Fischer et al.* (2008, purple line) and according to the novel processing approach introduced here (light blue line). Both datasets have been internally and externally calibrated following their respective routine and are dated according to the EPICA "unified" age scale (*Lemieux-Dudon et al.*, 2010, cf. chapter 4.4 and B). Error bars indicate replicate measurements and their standard deviation. b) A histogram depicting the deviations Δ between the individual data points of the two time series. The mean of the values is slightly more enriched relative to the original routine but indistinguishable within the given uncertainty range (*Behrens et al.*, 2008).

Using our new approach, the mean deviation of the 34 measurements including 5 replicates was 0.10‰ ($1\sigma=0.17\text{‰}$, figure 4.5) compared to the results presented in the original publication. This is well within the uncertainty limits of 0.30‰ reported for both methods (*Behrens et al.*, 2008, cf. chapter B)). Note that the correction for gravitational settling in the firn that was based on EDML $\delta^{15}\text{N}_2$ proxy data (*Landais et al.*, 2006) had been removed from the data in *Fischer et al.* (2008) before the comparison. It is further important to keep in mind that the $\delta^{13}\text{CH}_4$ ice core data in *Fischer et al.* (2008) were internally corrected for long-term machine drifts on the basis of the 'methane monitoring' acquisitions rather than 'reference loops' (*Behrens et al.*, 2008).

The slightly higher but almost identical values of the novel processing approach relative to the original values give strong evidence that our new routine is robust and its results are reliable. However, the differences of both time series, especially in the age range 17-20 kyr BP (see figure 4.5, a), suggest a somewhat differing visual impression of the $\delta^{13}\text{CH}_4$ trend before the step rise into the BA warm period.

4.4. Methane synchronization of ice core age scales

The creation of precise age scales for ice cores is a complex endeavor. Various techniques are combined to construct an ice core chronology, including manual layer counting where accumulation rates are sufficient, cross-correlations with characteristic time markers in proxies of other ice cores and climate archives (for example $\delta^{18}\text{O}$ and δD of precipitation, concentrations of chemical compounds and dust particles), which have an existing chronology, and finally, numerical modeling of horizontal ice flow and vertical thinning rates with glaciological models in deeper sections of the core. Poorly constrained changes of site temperature and accumulation rates, for instance with changing climate boundary conditions on glacial-interglacial and millennial time scales, and post-depositional processes affecting glaciological parameters may lead to large uncertainties in the dating of ice (e.g. *Parrenin et al.* (2007)). Although specific time markers like ash layers, chemical tracers and tephra layers from e.g. volcanic eruptions help to tune the chronologies, dating uncertainties in the range of several centuries to millennia are not uncommon and usually increase with depth. Accordingly, when proxy information from different ice cores are compared, the individual dating uncertainties may add up to large age discrepancies among the cores. Due to the short lifetimes of CH_4 molecules in the atmosphere, this parameter is used to synchronize age models from different ice core locations as it has been done for example for NGRIP/GRIP in Greenland and the Byrd core, Antarctica (*Blunier and Brook*, 2001), or for the same high-resolution Arctic cores and another Antarctic counterpart, EDML (*EPICA community members*, 2006). While this method may simplify the comparison of highly resolved trace gas records and the age models of ice cores from different locations, especially at times of rapid CH_4 changes recorded in the core, differences in the specific gas enclosure characteristics and unknowns in the determination of age differences of the enclosed air parcels and the surrounding ice (the Δage , see also section 3.1) likewise induce considerable uncertainties for the respective ice core records (*Blunier et al.*, 2007). In order to minimize the age discrepancies among the various Arctic and Antarctic deep ice core age models, new studies have focused on the construction of unified chronologies, which are based on multi-factor Bayesian inverse modeling (*Lemieux-Dudon et al.*, 2010; *Veres et al.*, 2013; *Bazin et al.*, 2013).

For the comparison of climate proxies in the study presented in this work (section 5.1), ice core data has been reported with respect to the "unified" age scale by *Lemieux-Dudon et al.* (2010). However, for the cores (or sections of cores) that were not yet covered by the unified chronology, some manual, first-order age scale synchronizations

were performed with the help of the respective CH_4 datasets over the last glacial cycle. For each synchronization, one CH_4 record with a known depth-to-(unified) age relationship (A) was plotted against a record with an unknown dating (B). A custom-made python script was applied to manually pick pairs of tie-points at specific visual features of last glacial CH_4 variability, preferentially at strong CH_4 concentration rises and decreases, occurring in both records. The respective ice core depth of the tie-point from core B was thus linked to a corresponding depth of core A, and could accordingly be directly translated to a certain unified age. Based on this set of dated tie-points, the individual depths of all samples of core B were then associated with respective unified ages by linear interpolation. The results of two of these manual CH_4 tie-point synchronizations are presented in section 5.2.4.

4.5. Corrections for Kr interference

The chromatographic separation of CH_4 and the noble gas krypton (Kr) imposes special demands on a setup used to separate air components, owing to the very similar physico-chemical properties of these compounds. Kr has previously not been accounted for in $\delta^{13}\text{CH}_4$ studies, as none of the multiple stable isotopes of Kr are close to the mass to charge ratio (m/z) 44, 45 and 46 considered in CO_2 -based $\delta^{13}\text{CH}_4$ measurements. In the publication presented in the following section it is demonstrated that the doubly charged isotope $^{86}\text{Kr}^{2+}$ can in fact interfere with the $\delta^{13}\text{C}$ measurement of CH_4 , if Kr enters the ion source of the IrmMS.

During a thorough review of the raw data for the ice core $\delta^{13}\text{CH}_4$ time series presented in this work, irregularities in the raw chromatograms at the peak flanks of the CH_4 -derived CO_2 were identified in the measurements performed with the AWI instrument. The Kr peak causes anomalies in the ratio of $m/z = 45$ to $m/z = 44$ and the $m/z = 46$ to $m/z = 44$ ratio, which generate higher $\delta^{13}\text{CH}_4$ values the more Kr contributes to the total peak areas (hereafter referred to as Kr effect). While the symptoms are distinct due to instrumental differences of the two analytical setups used for the $\delta^{13}\text{CH}_4$ datasets presented in section 5.1, we also found the Pennsylvania State University (PSU) system to be affected by Kr interference.

Because polar ice core samples are not easily replaced, it was not possible to repeat the measurements of the EDML and Vostok $\delta^{13}\text{CH}_4$ time series with enhanced instrumental setups. Instead, the $\delta^{13}\text{CH}_4$ values are corrected for the Kr interference as briefly summa-

rized in the subsection (4.5.2) below. This section also gives an overview as to how these Kr-corrected results compare to the uncorrected values.

For a detailed description of the Kr interference phenomenon, appropriate strategies to avoid it in future $\delta^{13}\text{CH}_4$ measurements, and measures to account for its effects after the actual sample measurement (*a posteriori* treatment), the reader is referred to the following publication (subsection 4.5.1).

4.5.1. On the interference of Kr during carbon isotope analysis of methane using continuous-flow combustion–isotope ratio mass spectrometry

J. Schmitt, B. Seth, M. Bock, C. van der Veen, L. Möller, C. J. Sapart, M. Prokopiou, T. Sowers, T. Röckmann, and H. Fischer

Published in *Atmospheric Measurement Techniques*, Volume 6, pp. 1425–1445, 2013

Abstract

Stable carbon isotope analysis of methane ($\delta^{13}\text{C}$ of CH_4) on atmospheric samples is one key method to constrain the current and past atmospheric CH_4 budget. A frequently applied measurement technique is gas chromatography (GC) isotope ratio mass spectrometry (IRMS) coupled to a combustion-preconcentration unit. This report shows that the atmospheric trace gas krypton (Kr) can severely interfere during the mass spectrometric measurement, leading to significant biases in $\delta^{13}\text{C}$ of CH_4 , if krypton is not sufficiently separated during the analysis. According to our experiments, the krypton interference is likely composed of two individual effects, with the lateral tailing of the doubly charged ^{86}Kr peak affecting the neighboring m/z 44 and partially the m/z 45 Faraday cups. Additionally, a broad signal affecting m/z 45 and especially m/z 46 is assumed to result from scattered ions of singly charged krypton. The introduced bias in the measured isotope ratios is dependent on the chromatographic separation, the krypton-to- CH_4 mixing ratio in the sample, the focusing of the mass spectrometer as well as the detector configuration and can amount to up to several per mil in $\delta^{13}\text{C}$. Apart from technical solutions to avoid this interference, we present correction routines to a posteriori remove the bias.



On the interference of Kr during carbon isotope analysis of methane using continuous-flow combustion–isotope ratio mass spectrometry

J. Schmitt¹, B. Seth¹, M. Bock¹, C. van der Veen³, L. Möller², C. J. Sapart³, M. Prokopiou³, T. Sowers⁴, T. Röckmann³, and H. Fischer¹

¹Climate and Environmental Physics, Physics Institute, & Oeschger Centre for Climate Change Research, University of Bern, Sidlerstrasse 5, 3012 Bern, Switzerland

²Alfred Wegener Institute Helmholtz Centre for Polar and Marine Research, Bremerhaven, Germany

³Institute for Marine and Atmospheric research Utrecht, Utrecht University, Princetonplein 5, 3584CC Utrecht, The Netherlands

⁴Earth and Environment Systems Institute, Penn State University, University Park, PA, USA

Correspondence to: J. Schmitt (schmitt@climate.unibe.ch)

Received: 12 January 2013 – Published in Atmos. Meas. Tech. Discuss.: 7 February 2013

Revised: 30 April 2013 – Accepted: 2 May 2013 – Published: 27 May 2013

Abstract. Stable carbon isotope analysis of methane ($\delta^{13}\text{C}$ of CH_4) on atmospheric samples is one key method to constrain the current and past atmospheric CH_4 budget. A frequently applied measurement technique is gas chromatography (GC) isotope ratio mass spectrometry (IRMS) coupled to a combustion-preconcentration unit. This report shows that the atmospheric trace gas krypton (Kr) can severely interfere during the mass spectrometric measurement, leading to significant biases in $\delta^{13}\text{C}$ of CH_4 , if krypton is not sufficiently separated during the analysis. According to our experiments, the krypton interference is likely composed of two individual effects, with the lateral tailing of the doubly charged ^{86}Kr peak affecting the neighbouring m/z 44 and partially the m/z 45 Faraday cups. Additionally, a broad signal affecting m/z 45 and especially m/z 46 is assumed to result from scattered ions of singly charged krypton. The introduced bias in the measured isotope ratios is dependent on the chromatographic separation, the krypton-to- CH_4 mixing ratio in the sample, the focusing of the mass spectrometer as well as the detector configuration and can amount to up to several per mil in $\delta^{13}\text{C}$. Apart from technical solutions to avoid this interference, we present correction routines to a posteriori remove the bias.

1 Introduction

Methane is the third most important greenhouse gas besides water vapour and CO_2 . The isotopic composition of atmospheric methane (CH_4) provides important constraints on globally integrated CH_4 sources and sinks (Kai et al., 2011; Levin et al., 2011). Both the concentration and the isotopic composition of atmospheric CH_4 in the past have been reconstructed from trapped bubbles in ice cores as well as from the interstitial air in snow pack (firn) on polar glaciers (Miller et al., 2002; Schaefer et al., 2006; Fischer et al., 2008; Sowers, 2011; Sapart et al., 2012). Originally, the dual-inlet technique coupled to an isotope ratio mass spectrometer (IRMS) was used (Stevens and Rust, 1982; Lowe et al., 1991). With the advent of the continuous-flow (CF) technique (Matthews and Hayes, 1978), a growing number of groups have developed systems that allow smaller quantities of CH_4 to be analysed, permitting routine analyses on ice core samples (Merritt et al., 1995; Rice et al., 2001; Miller et al., 2002; Ferretti et al., 2005; Sowers et al., 2005; Schaefer and Whiticar, 2007; Behrens et al., 2008; Umezawa et al., 2009; Melton et al., 2011; Sapart et al., 2011). An overview of these techniques is provided in Table 1. The general procedure for $\delta^{13}\text{C}$ - CH_4 analysis on air samples using the CF-IRMS technique usually involves several steps to separate a large number of major and trace atmospheric components (see general scheme in Fig. 1). For ice core samples, an additional extraction step

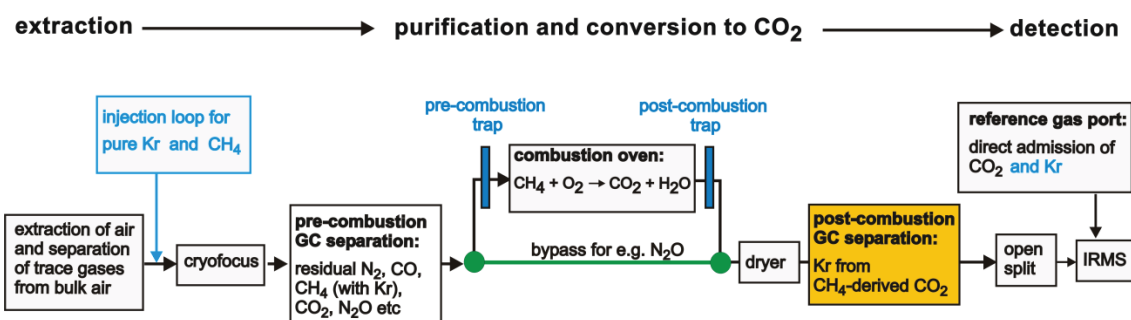


Fig. 1. Simplified flow scheme used for $\delta^{13}\text{C}$ analysis of CH_4 on air samples applying the continuous-flow IRMS technique. The scheme provides an overview of basic components and specific add-ons of the systems used in this study. The analysis comprises three main steps (from left to right: extraction, purification and combustion of CH_4 to CO_2 , and finally the detection in the isotope ratio mass spectrometer). The grey boxes represent the basic components used by all laboratories and date back to the milestone publications in this field (Merritt et al., 1995; Rice et al., 2001). An exception is the IMAU system described by Sapart et al. (2011), where no pre-combustion GC is used and the separation of the gases is achieved solely by a preconcentration step. Coloured symbols denote additional devices, which are specific for the certain laboratory. Blue and green colours denote features of the Bern system, while the yellow box is specific for the updated IMAU system. The injection loop (blue box) allows injecting pure CH_4 and Kr into the GC flow to monitor the system and allow special experiments. The pre-combustion trap and the post-combustion trap were included later on into the updated Bern system to remove the Kr interference. The yellow box represents the post-combustion GC, which was included in the updated IMAU system to remove the Kr interference.

either by dry or melt extraction has to be performed first. The purified CH_4 is then admitted to a combustion interface where CH_4 is converted to CO_2 , which is subsequently measured in the IRMS. Here, the most abundant isotopologues of CO_2 are measured using Faraday cups for the mass-to-charge ratios (m/z) 44, 45 and 46. From these ion beam intensities, the $\delta^{13}\text{C}$ of CH_4 is then calculated applying a correction for the isobaric contribution at m/z 45 due to the presence of $^{12}\text{C}^{17}\text{O}^{16}\text{O}$ (Craig, 1957).

The separation of CH_4 from the bulk air components (N_2 , O_2 and Ar) and also from minor components like CO is a delicate task. Usually, gas chromatography (GC) is used to separate CH_4 from CO, N_2 , and CO_2 , which would otherwise interfere with the mass spectrometric detection. In this respect, an interference with the atmospheric trace gas krypton (Kr) has not yet been considered during the method development. The noble gas krypton has a natural atmospheric abundance of 1099 ± 9 ppb (Aoki and Makide, 2005) and consists of many stable isotopes, with the most abundant being ^{84}Kr with 57% and ^{86}Kr with 17%. Although Kr is a trace gas, for several types of samples Kr levels are comparable or even higher than the corresponding CH_4 , e.g. for stratospheric samples (Rice et al., 2003; Röckmann et al., 2011) and air extracted from deep ice cores.

Since none of the Kr isotopes produces an ion that has exactly the same mass as the target ions with m/z 44, m/z 45 and m/z 46, Kr has not been regarded as an issue during $\delta^{13}\text{C}$ analysis of CH_4 until now. The physico-chemical properties of CH_4 and Kr are very similar, making them hard to separate from one another. Similar boiling points (Kr = 119 K and CH_4 = 111 K) make cryo-separation impossible, and gas chromatographic separation has proven to be very difficult. To ensure a sufficient separation of CH_4 from Kr, the GC

has to be operated at sub-ambient temperatures (Schüpbach et al., 2009) or at high flow rates ($50 \text{ mL STP min}^{-1}$) with a packed column at 25°C (Burford and Bremner, 1972).

Here we show that Kr actually does interfere with the measurement of $\delta^{13}\text{C}$ of CH_4 if Kr reaches the ion source together with the CO_2 peak derived from CH_4 combustion. The magnitude of the Kr interference depends on the preconcentration and GC separation of the Kr/ CH_4 mixture, the mass spectrometer and its source settings. We will show that the bias introduced by this interference can be as large as 2‰ when dealing with atmospheric samples with low CH_4 concentrations (< 400 ppb). More generally, for other types of samples, like water samples, these CH_4 concentrations correspond to CH_4/Kr ratios of < 0.5 . For atmospheric samples, the Kr interference scales with the atmospheric CH_4 mixing ratio since Kr is a well-mixed, inert constituent with an atmospheric mixing ratio that is assumed to vary by only $< 1\%$ between glacial and interglacial climate (Headly and Severinghaus, 2007; Ritz et al., 2011).

We demonstrate how this interference comes about and how this issue can be resolved. Initially, we discuss ways to identify Kr anomalies in chromatograms from $\delta^{13}\text{C}$ CH_4 analyses. In the second part of the manuscript we highlight techniques to correct for the Kr interference and compare these techniques. This paper focuses only on the aspect of Kr interference during $\delta^{13}\text{C}$ analysis of CH_4 . However, based on the underlying mechanism of this interference we note that other IRMS applications might also be affected. This effect occurs in situations where a target species and a second species producing singly, doubly or triply charged ions with m/z close to the target masses are simultaneously present in the ion source due to co-elution or measurement of gas mixtures in dual inlet. For example Xe, which elutes in the vicinity of volatile

Table 1. Collection of publications dealing with $\delta^{13}\text{C}$ - CH_4 measurements in view of possible Kr interferences. The collection is not exhaustive and lists only some of the publications in the field of ice core and atmospheric measurements. To allow a faster orientation of which data set is produced by which method, we used the following scheme: technical paper (data paper).

| Publication | Pre-combustion GC | Technical details and remarks |
|---|---|---|
| <i>dual-inlet techniques:</i> Stevens and Rust (1982) (Quay et al., 1999), Lowe et al. (1991) (Francey et al., 1999), Tyler et al. (1999) (Tyler et al., 2007) Bergamaschi et al. (2000) | No GC, only CO is removed prior to combustion. Therefore, all other organic compounds are combusted as well. However, ethane and other NMHC have low conc. compared to CH_4 , so the effect is small. | Prior to the conversion of CH_4 to CO_2 , atmospheric CO_2 is removed from the air stream. After the combustion unit, the produced CO_2 is trapped at LN_2 , thus separating it from Kr. |
| <i>continuous-flow techniques:</i> Merritt et al. (1995) | PoraPLOT Q, 25 m, 0.32 mm i.d., 20–25 °C, 1 mL min ⁻¹ | no special measures to separate Kr from CH_4 |
| Rice et al. (2001) (Rice et al., 2003) | PoraPLOT Q, 25 m, 0.32 mm i.d., GC temperature ramped from -50 °C to 30 °C, 2.6 mL min ⁻¹ | GC with cryogenic unit to allow separation of CH_4 from an “unknown contaminant peak that otherwise interferes with masses 45 and 46” |
| Bräunlich et al. (2001) | MPI: Bergamaschi et al. (2000); LGGE: GS-Q, 30 m, 0.32 mm i.d. | The MPI data set is measured with dual inlet. For LGGE, Kr might co-elute with CH_4 . |
| Behrens et al. (2008) (Fischer et al., 2008) | CarbonPLOT, 30 m, 0.32 mm i.d., 30 °C, 1.1 mL min ⁻¹ | no special measures to separate Kr from CH_4 |
| Miller et al. (2002) (Ferretti et al., 2005; Bousquet et al., 2006) | Molecular Sieve 5A, 80 °C, 2.0 mL min ⁻¹ | Separation of CH_4 and Kr on this column is unknown |
| Sowers et al. (2005) (Mischler et al., 2009) | PoraPLOT Q, 30 m, 0.32 mm i.d. | no special measures to separate Kr from CH_4 |
| Schaefer and Whiticar (2007) (Schaefer et al., 2006) | GSQ PLOT, 30 m, 0.53 mm i.d., 0 °C, 1 mL min ⁻¹ | Kr is separated from CO_2 by the post-combustion GC |
| Umezawa et al. (2009) | PoraPLOT Q, 25 m, 0.32 mm i.d., -30 °C, 3.0 mL min ⁻¹ | GC with cryogenic unit to separate CH_4 from an unknown contaminant peak |
| Melton et al. (2011) (Melton et al., 2012) | GSQ PLOT, 30 m, 0.53 mm i.d., 25 °C, 1 mL min ⁻¹ | post-combustion trap followed by an additional GC (GSQ PoraPLOT, 30 m, 0.53 mm i.d., 25 °C) separates Kr from CH_4 -derived CO_2 |
| Brass and Röckmann (2010); Sapart et al. (2011) (Keppler et al., 2006; Vigano et al., 2009; Röckmann et al., 2011; Sapart et al., 2012) | No pre-combustion GC | Purification relies on preconcentration and cryofocus, as a replacement of the omitted pre-combustion GC |

organic compounds, produces several triply charged ions in the m/z 44 to m/z 45 range, thus potentially interfering during carbon isotope analysis of trace gases that are measured as CO_2 .

Section 2 provides a brief overview on the setup of the four analytical systems where we identified the Kr interference. In Sect. 3, $\delta^{13}\text{C}$ chromatograms from the four analytical systems illustrate the common features and differences of the Kr interference. In Sect. 4, we describe tests that can be performed to determine if and to what degree Kr interferes in the chromatogram. Experiments were performed to assess the Kr impact on $\delta^{13}\text{C}$ analyses involving direct Kr injections

into the CF-IRMS and dual-inlet systems. It will be shown that the Kr interference affect all three Faraday cups. We then discuss the experimental results to illustrate just how the Kr interference works. Finally, Sect. 5 presents a suite of possible solutions to either separate Kr from CH_4 or CH_4 -derived CO_2 , or correct for this effect in existing data sets. While the paper is structured in these consecutive steps, the reader might profit from a first quick look at Figs. 3 and 7. Note that for practical reasons we use the term CH_4 peak, which corresponds to the CO_2 peak from the original CH_4 peak. Additionally, $\delta^{13}\text{C}$ denotes $\delta^{13}\text{C}$ of a CH_4 sample without specifying it.

2 Experimental setup and air samples

For the measurements and experiments described in this paper, we used four different analytical systems; they are named after the institutes or cities in which they were developed: AWI (Alfred Wegener Institute for Polar and Marine Research), Bern (University of Bern), IMAU (Institute for Marine and Atmospheric research Utrecht), and PSU (Penn State University).

2.1 AWI system

The AWI system is described in detail by Behrens et al. (2008) and was used to generate a $\delta^{13}\text{C}$ data set covering the last deglaciation (Fischer et al., 2008) as well as a new data set covering the last glacial period (Möller et al., 2013). In short, the pre-purified CH_4 sample (together with Kr) is injected onto a 30 m CarbonPLOT column at 30 °C with a flow rate of ca. 1.1 mL min^{-1} . The detector is an Isoprime IRMS equipped with five Faraday cups: a universal triple collector for m/z 44, 45 and 46 to calculate $\delta^{13}\text{C}$ of CH_4 and two additional cups for m/z 28 and m/z 32 for monitoring the efficiency of the O_2 and N_2 separation of the trapping system. The five Faraday cups are connected to the following feedback resistors: $5 \times 10^8 \Omega$ (“ N_2 cup”, m/z 28), $1 \times 10^9 \Omega$ (“ O_2 cup”, m/z 32), $5 \times 10^8 \Omega$ (major m/z 44), $5 \times 10^{10} \Omega$ (minor1, m/z 45), and $1 \times 10^{11} \Omega$ (minor2, m/z 46).

2.2 Bern system

The Bern system is an updated and more versatile follow-up device compared to the AWI system, and its description is currently in preparation. While the AWI system is constructed to measure only $\delta^{13}\text{C}$ of CH_4 , the Bern system can analyse a larger suite of trace gases (CH_4 , N_2O and its stable isotopologues, xenon, ethane, propane, methyl chloride, CF_4). For that reason the Bern system is equipped with additional technical features allowing special experiments to be performed, e.g. a bypass valve for the combustion oven, and additional valves to inject CH_4 and Kr mixtures in helium (He) onto the GC system (Fig. 1). Like the AWI system, the Bern system uses a 30 m CarbonPLOT column, at 30 °C with a flow rate of ca. 1.0 mL min^{-1} . The Bern system uses an identical Isoprime IRMS to AWI, equipped with five Faraday cups: the raw data from the mass spectrometer measurements was processed using our in-house isotope software (Bock et al., 2010; Schmitt et al., 2011). After the identification of the Kr interference, two additional traps (pre-combustion trap and post-combustion trap) were installed to get rid of the Kr interference (Sect. 5.3). This new system is referred to as the updated Bern system.

2.3 IMAU system

A detailed description of the IMAU system is provided elsewhere (Brass and Röckmann, 2010; Sapart et al., 2011).

A special feature of this system is that it lacks the pre-combustion GC common in other systems (Fig. 1). The IMAU system uses a Thermo Finnigan Delta plus XL as detector. After the Kr interference was identified, the system was modified to remove the interference (Sect. 5.2). As shown in Fig. 1, a GC was added after the conversion of CH_4 to CO_2 (post-combustion GC), and this modified system is referred to as updated IMAU system.

2.4 PSU system

The measurements done at PSU use the system described earlier in Sowers et al. (2005). The mass spectrometer is a Finnigan MAT 252. Modifications to remove the Kr interference are in process.

2.5 Air samples

All four labs measured a set of three cylinders, which were part of an international round-robin study. These cylinders were filled at Niwot Ridge, Colorado, in 2007 to varying CH_4 concentrations with a balance of ultra-high-purity air (no CH_4) to mimic the pre-industrial period (PI, ~ 900 ppb), the last glacial period (GLA, ~ 380 ppb) and the present day (PD, 1870 ppb). The cylinders were then measured at NOAA to confirm the CH_4 values (GLA, cylinder no. CA01179 = 372 ppb; PI, cylinder no. CC71560 = 904 ppb; and PD, cylinder no. CA03560 = 1831 ppb). While the CH_4 concentration is different, the Kr concentrations of all cylinders should be at natural abundance (1099 ppb), as the GLA and PI cylinders were produced by diluting atmospheric air with CH_4 -free air. The three cylinders have the following CH_4 /Kr mixing ratios: 0.33 (GLA), 0.82 (PI) and 1.69 (PD), thus yielding CH_4 /Kr mixing ratios that vary by a factor of 5. Additionally, cylinder CA08289 (NOAA, Boulder) is used at Bern as a working standard containing 1508.2 ppb CH_4 , and IMAU used a natural whole-air working standard of Groningen (“GRO”) air with 1981.2 ppb CH_4 for the experiments where pure Kr is added.

3 First hints and visual inspection of chromatograms

The possible existence of an interfering compound during the IRMS analysis of $\delta^{13}\text{C}$ of CH_4 on air samples was first described in 2001 when Rice et al. (2001) described “an unknown contaminant peak”. As the contaminant could not be identified, it remained unclear if this was only a problem of their specific setup or if it is a general feature of air samples. We believe that this unknown contaminant peak was Kr. In hindsight, it is unfortunate that this interference was not resolved as subsequent groups that developed new systems for $\delta^{13}\text{C}$ analysis on CH_4 for air and ice core samples did not account for the Kr interference. This led to the current situation where many systems do not properly separate this “contaminant peak” from CH_4 , while others managed

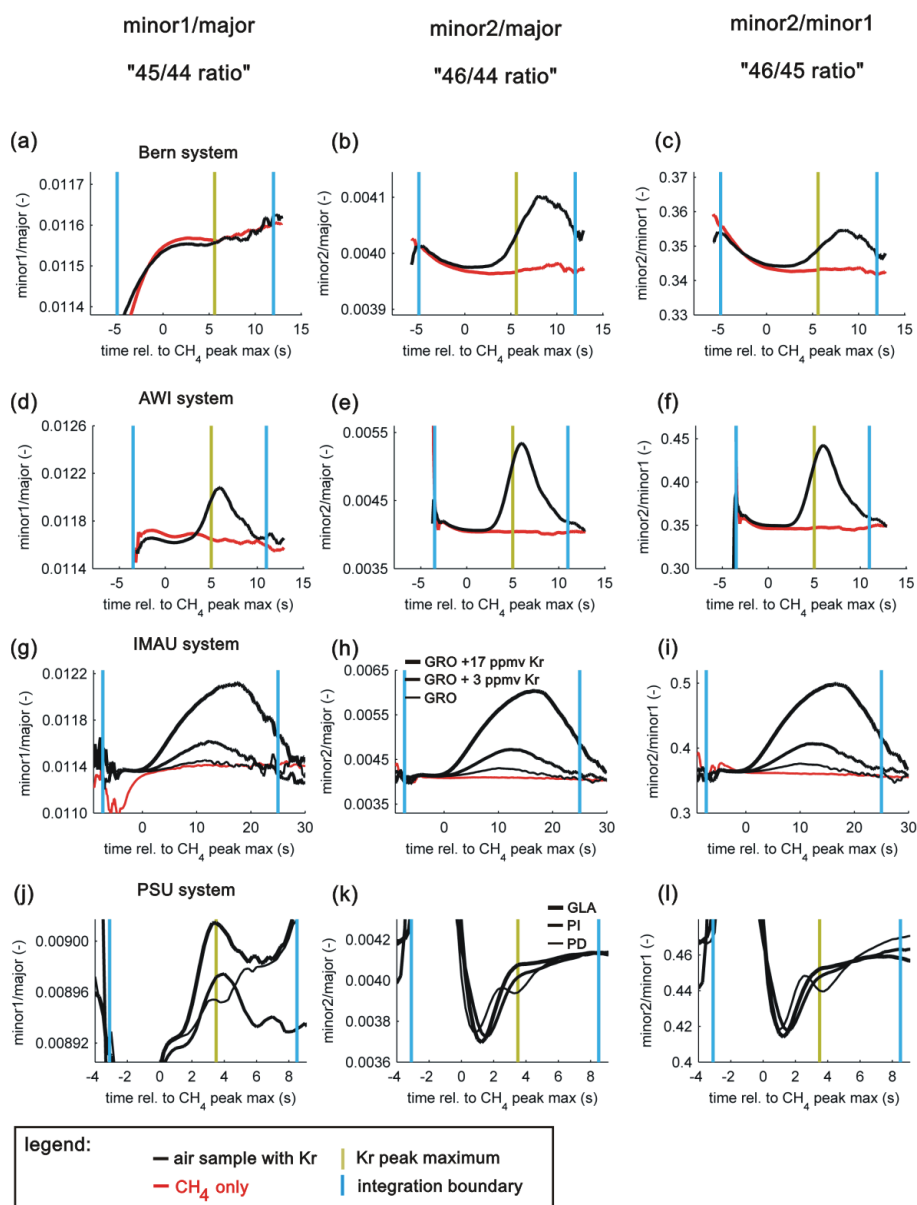


Fig. 2. Comparison of the ion current ratios of the four systems (from top to bottom: Bern, AWI, IMAU, PSU). The left column shows the minor1 / major ratio (“45/44 ratio”); the middle column shows minor2 / major (“46/44 ratio”), the right column minor2 / minor1 (“46/45 ratio”). Natural-air samples and air samples with added Kr are plotted as black lines, and injections of pure CH₄ are shown as red lines, illustrating the anomalies seen in the Kr containing samples. Blue vertical lines mark the left and right integration limits. Green vertical lines mark the maximum position of the Kr peak where we could determine its precise position. The Kr interference in the AWI system is visually more pronounced compared to the Bern system due to the differences in peak separation and focusing of the IRMS.

to separate this interfering substance (Schaefer and Whiticar, 2007; Umezawa et al., 2009; Melton et al., 2011).

The search for an interfering substance during $\delta^{13}\text{C}$ analysis of air samples was started during the interlaboratory calibration exercise involving both air cylinders and glacial ice samples (see results in Table 2). The observed $\delta^{13}\text{C}$ differences scaled with CH₄ mixing ratios and were as large as 2 ‰ for low CH₄ samples (e.g. CH₄ < 400 ppb). While the co-

elution of CH₄ and Kr and the generation of a m/z 43 peak due to $^{86}\text{Kr}^{2+}$ was recognised during the development phase of the Bern system, it was the addition of Kr to a natural-air sample (GRO) at IMAU that confirmed the Kr interference on $\delta^{13}\text{C}$. The effects on the measured $\delta^{13}\text{C}$ and $\delta^{18}\text{O}$ values were significant and scaled linearly with the Kr amount added. For each 1 ppm Kr addition, the $\delta^{13}\text{C}$ values and $\delta^{18}\text{O}$ values of the spiked air sample shifted by 0.79 ‰ and by

Table 2. Collection of $\delta^{13}\text{C}\text{-CH}_4$ results from the interlaboratory calibration round robin. As described in Sect. 2.5 these three cylinders with contrasting CH_4 mixing ratios are referred as GLA, PI, and PD. For some results Kr correction was applied using the following methods: ^a using the approach described in Sect. 5.4, and ^b according to Sect. 5.6. Besides the NIWA (National Institute of Water & Atmospheric Research) lab, which measured the cylinders with dual-inlet IRMS measurement and CF-IRMS, all results were obtained using CF-IRMS. The NIWA dual-inlet data were measured according to Lowe et al. (1999), and Kr would have been pumped away once CO_2 (from CH_4) was recovered from the combustion step. These values should be regarded as close to the true values. The NIWA CF-IRMS data were obtained using the method described in Miller et al. (2002) but used a CP-PoraBOND Q column ($50 \times 0.32 \text{ mm} \times 5 \mu\text{m}$ at 40°C) instead of the Molecular Sieve 5A column at 80°C used in the original publication. Ideally, the NIWA dual-inlet results and the values after Kr correction should be the same within their common error. Deviations among the results are the sum of differences due to referencing standards, amount effects, and imperfect Kr correction.

| Cylinder name [CH_4] | GLA 372 ppb | | PI 904 ppb | | PD 1831 ppb | |
|---|-------------|-----------|------------|-----------|-------------|-----------|
| | mean | 1σ | mean | 1σ | mean | 1σ |
| $\delta^{13}\text{C}\text{-CH}_4$ (‰ VPDB) | | | | | | |
| PSU as measured | -46.86 | 0.06 | -47.15 | 0.10 | -47.08 | 0.16 |
| PSU Kr-corrected ^a | -47.52 | 0.06 | -47.41 | 0.10 | -47.20 | 0.16 |
| Bern as measured | -47.31 | 0.11 | -47.37 | 0.07 | -47.41 | 0.09 |
| AWI as measured | -46.25 | 0.11 | -47.07 | 0.09 | -47.14 | 0.05 |
| AWI Kr-corrected ^a | -47.06 | 0.13 | -47.40 | 0.12 | -47.32 | 0.06 |
| NIWA dual inlet | -47.43 | 0.02 | -47.44 | 0.02 | -47.23 | 0.02 |
| NIWA CF as measured | -46.52 | 0.08 | -47.78 | 0.20 | -47.02 | 0.15 |
| IMAU old method | -44.82 | 0.33 | -46.64 | 0.13 | -47.22 | 0.11 |
| IMAU Kr-corrected ^b | -47.18 | 0.24 | -47.43 | 0.11 | -47.26 | 0.05 |
| IMAU updated method | -47.20 | 0.20 | -47.52 | 0.11 | -47.27 | 0.07 |

7.2 ‰ towards heavier values, respectively. This experiment clearly showed that Kr did interfere and could explain a large part of the discrepancies between the labs. However, it was unclear whether the observed effect was specific for this system or if other systems were affected as well. Additionally, the nature of this interference had to be elucidated in order to come up with technical solutions and correction routines for older data sets.

Since the ion current intensities of this interference are difficult to visualise in the chromatograms themselves, we chose to use the ratio of ion currents to identify the position of the Kr peak relative to the CH_4 peak. Commercial IRMS software packages usually provide graphs of the ion current ratios only for the measured total ion current ratios, i.e. the combined intensities for the sample peak and the background. When the interference in one of the ion current ratios is very pronounced, it is possible to identify it in the total ion current ratios (Rice et al., 2001; Schaefer and Whiticar, 2007). This is the case when the CH_4 and the interference peak are chromatographically well separated. However, when the two peaks strongly overlap, the influence is less visible. A more sensitive way to identify such interferences in chromatograms is to inspect ion current ratio plots where the background signal has been subtracted from the measured signal to yield the signal of the sample peak only. The plots of this paper show ion current ratios which were corrected for the background signal. Figure 2 shows the three ion current ratios for the time interval around the CH_4 peak.

The retention time of the CH_4 peak maximum is defined as 0 s. Throughout the paper we label the three ion current ratios according to the involved Faraday cups and the m/z of the ions which are commonly detected in this cup at CO_2 focusing: minor1 / major (“45 / 44”), minor2 / major (“46 / 44”), and minor2 / minor1 (“46 / 45”). Note the m/z pairs are put in parenthesis (e.g. “45 / 44”) to indicate that only the target ions produced by CO_2 strictly adhere to this rule. It will be shown in this paper that a small fraction of the m/z 43 beam ($^{86}\text{Kr}^{2+}$) tails all the way into all three cups (major, minor1 and minor2). For the Bern, AWI and IMAU systems, air samples containing Kr (Fig. 2 black lines) are compared with pure- CH_4 samples (Fig. 2 red lines). For the systems where it was explicitly determined (see below and Figs. 3 and 4), the position of the Kr peak relative to the CH_4 peak is marked for orientation. As can be seen for all four systems, most ion current ratios of samples containing Kr deviate from the ratios of pure CH_4 . While these anomalies are well pronounced in all three ratios for the AWI system and resemble a Gaussian shape, the Bern system exhibits no visible anomaly for the “45 / 44 ratio”, which will be discussed later. In the IMAU case, where Kr was added to natural air in increasing amounts, one sees that the anomalies become larger with more Kr added. Note that the large anomalies are only the result of large amounts of Kr to an air sample (3 times or 17 times the Kr amount of a natural sample (GRO)). The anomalies of the natural-air sample (GRO) are small and hard to detect without prior knowledge. In the

case of the PSU system, an anomaly is only barely visible for the “45/44 ratio” and obscured by the internal fractionation within the peak (time shift due to mismatch of the resistor-capacitor pair). In conclusion, the visual inspection of the ion current ratios of all four systems points to an interfering substance present in natural-air samples. The appearance of this anomaly is specific for each of the four systems and depends on chromatographic separation and properties of the IRMS itself. These anomalies in the ion current ratios can be hidden especially when the background is not subtracted. It requires a careful comparison of the ratios from the natural-air sample with those from pure CH₄ to recognise this matrix effect.

4 Experiments and results

4.1 Simple experiment to identify Kr in the chromatogram

The visual inspection of the chromatograms described above revealed that an interfering compound that we believe is Kr produces anomalies in the ion current ratios. Here we go one step further and provide a test to identify whether the retention time of Kr overlaps with the CH₄ peak. As mentioned above, the behaviour of Kr and CH₄ on GC columns is similar and can result in overlapping peaks with Kr eluting only a few seconds after CH₄. The following experiment uses the fact that, for the electron energies used in the ion source of the IRMS (e.g. 80 eV for the Bern system), ions with two (and sometimes three) electrons removed are also produced (Denifl et al., 2002; King and Price, 2008). Since the optical system of the IRMS separates ions according to their mass-to-charge ratio (m/z), heavy isotopes like ⁸⁶Kr can be readily transformed into m/z 43 ⁸⁶Kr²⁺ ions that strike the imaging plane close to the major ion Faraday cups. Therefore, ⁸⁶Kr²⁺ ions can be easily monitored by shifting the accelerating voltage (AV) to higher values, e.g. 4030 V instead of 3975 V for the CO₂ focusing for the Bern Isoprime, so that the m/z 43 ⁸⁶Kr²⁺ ions are detected in the m/z 44 cup. The m/z 43 beam (⁸⁶Kr²⁺) falls into the major cup, while the m/z 45 beam (mostly ¹³C¹⁶O¹⁶O) falls into minor2, monitoring the position of the CH₄ peak. This focusing test has the advantage that it can be run on any system with any natural-air sample without modifications to the CH₄ separation system. The results of these focusing experiments are shown in Fig. 3. As can be seen in Fig. 3a, the chromatographic separation of CH₄ from Kr is about 6 s for the Bern system. Since the peak width (FWHM) for both CH₄ and Kr is also 5–6 s, both peaks do overlap considerably (Fig. 3a), but the overlap is system dependent. From this experiment we can derive the following conclusions. First, a considerable amount of doubly charged Kr ions are produced within the source of the IRMS. Second, ⁸⁶Kr²⁺ ions allow identifying the retention time of Kr and illustrate that the GC conditions of the Bern and PSU systems are insufficient to separate Kr from CH₄. Third, the position

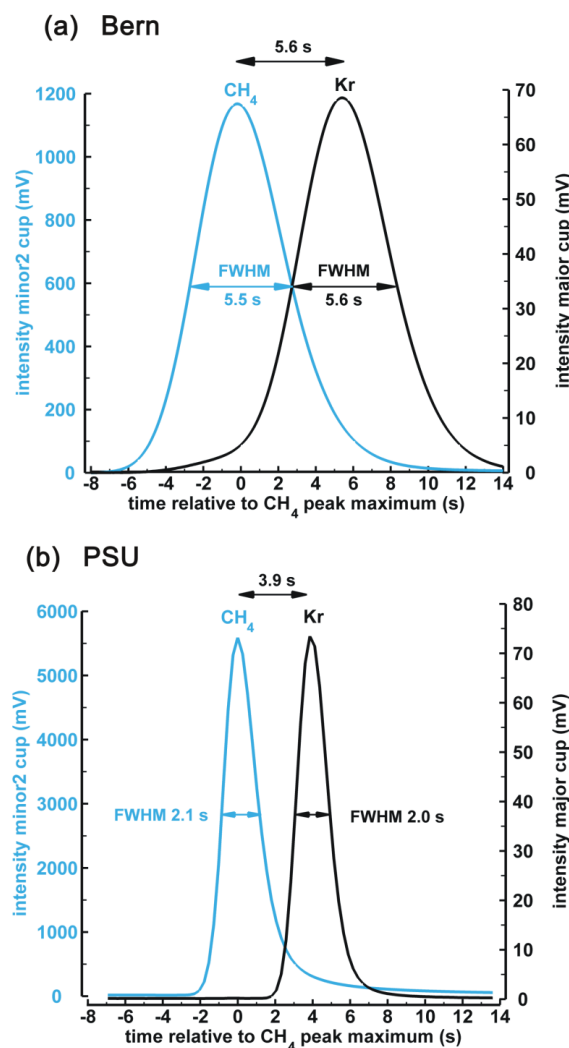


Fig. 3. Chromatogram of an atmospheric air sample showing the separation of CH₄ from Kr for the Bern system (a) and the PSU system (b). The ion source of the IRMS was focused such that the m/z 43 beam of ⁸⁶Kr²⁺ falls into the major cup (black line, right axis). The isotopologues of CO₂ with m/z 45 fall into the minor2 cup and mark the position of the CH₄ peak (blue line, left axis).

of the Kr peak and the observed anomalies seen in the ion current ratios (Fig. 2) are similar and suggest that Kr causes these anomalies.

4.2 Injections of pure Kr into GC flow

The visual peak inspection and the overlap of CH₄ and Kr from the focusing exercise point to Kr as the source of the interference. However, at this stage it remains unclear how Kr might interfere with the $\delta^{13}\text{C}$ measurement since a direct isobaric effect seems unlikely as none of the Kr isotopes are expected to fall into the given Faraday cups at their nominal m/z as singly or doubly charged ions. Several studies report on non-isobaric interferences during stable isotope analysis

of gas mixtures without a clear hint of the mechanisms behind them (Mariotti, 1984; Sarma et al., 2003). One possible mechanism generating our anomalies could be that the presence of Kr in the ion source changes the relative ionisation efficiency of the CO₂ isotopologues in the sense of “ionisation quench” coined by Meier-Augenstein et al. (2009). In dual-inlet applications such matrix interactions of gases in the ion source are commonly termed “chemical slope” (Severinghaus et al., 2003) and refer to differences in the composition of sample and standard gas mixture. While correcting for this effect is common practice, the underlying processes in the ion source are poorly understood.

Alternatively, Kr itself without any interaction with CO₂ produces the observed signals. A simple test to distinguish between these two possibilities is the injection of pure Kr. If the pure Kr does not produce a positive signal by itself, then the interference relies on the interaction of CO₂ and Kr in the ion source. In contrast, if Kr alone generates these signals, then some of the Kr ions are deflected from their expected flight path to fall into Faraday cups with m/z values up to 3 units higher.

To perform this experiment a mixture of pure Kr in He was injected via the injection loop into the GC flow of the Bern system (see Fig. 1). The amount of injected Kr roughly equals the amount of Kr of ca. 10 mL STP natural air; thus, a similar amount as is used in our routine ice core measurements. The injected Kr is cryofocused first and then sent to the pre-combustion GC (Fig. 1). After the Kr peak left the GC, the flow passes a dryer before admitting it to the ion source of the IRMS (operated at CO₂ configuration). Note that the combustion oven is bypassed in this experiment to prevent the generation of a small CO₂ peak from trace amounts of residual CH₄ present in the He flow. The results of this experiment are shown in Fig. 4, together with the measurement of a natural-air sample. Kr itself produces signals in all Faraday cups at a retention time of ca. 6 s after the usual CH₄ peak maximum (Fig. 4c). This result supports the idea that Kr alone produces the signals detected in the three cups. A comparison with the signal intensities of the air sample (Fig. 4a) shows that the Kr intensities are clearly too small to be directly seen in the air sample itself; e.g. for the minor2 cup, the Kr signal is 4 mV at its maximum while for the air sample, the minor2 signal at the same time is ten times higher. Besides these two basic features, the experiment with pure Kr affords us the opportunity to investigate the general features observed in the ion current ratios of the air sample. A combusted CH₄ sample produces signal intensities (mV) in the three Faraday cups reflecting the natural abundance of the CO₂ isotopologues. For example, the signal of the major cup is a bit higher than the minor2 signal (Fig. 4a). In contrast, Kr produces a 4-times-higher minor2 signal compared to the signal on the major cup (Fig. 4c). In other words, the signals produced by Kr have a very different isotopic fingerprint compared to the CO₂ signals. In this example dealing with minor2 vs. major cup (“46/44 ratio”),

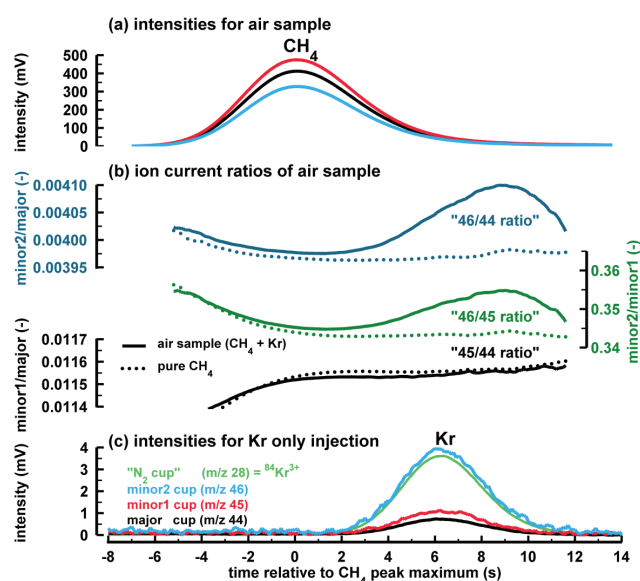


Fig. 4. Comparison of a CH₄ peak of an air sample with the signals gained from an injection of pure Kr measured with the Bern system at CO₂ focusing. **(a)** Beam intensities in mV for the CH₄ sample peak (369 ppb CH₄ with natural abundance of Kr) with the retention time centred to the CH₄ peak maximum. **(b)** Background-corrected ion current ratios (“46/44 ratio” in blue, “46/45 ratio” in green and “45/44 ratio” in black) of the atmospheric air sample (solid line) and pure CH₄ (dotted line), illustrating the anomalies seen in “46/44” and “46/45” but with no visible effect on “45/44”. Panel **(c)** shows the beam intensities for a measurement where Kr was injected into the GC flow. Due to the chromatographic effect of the GC column, the retention time of the Kr peak is ca. 6 s longer than the CH₄ peak, yet there is a considerable overlap. Note the signal measured at m/z 28 (“N₂ cup”) can be directly related to ⁸⁴Kr³⁺, which has the exact value of m/z = 28.

the Kr signals translate into a very heavy apparent $\delta^{18}\text{O}$ signature since the $\delta^{18}\text{O}$ is mainly determined by the “46/44 ratio”. When such an anomaly is added to the signals from combusted CH₄, the observed “46/44 ratio” will increase as it is the case for the air sample (Fig. 4b, “46/44 ratio”). In contrast, the minor1/major ratio of both the air sample and Kr are comparable, with the signal on minor1 being slightly higher than on major (Fig. 4a and b). Consequently, the signals created by Kr do not produce a visible anomaly in the minor1/major ratio as the “45/44 ratio” of the air sample closely follows the ratio of pure CH₄ (Fig. 4b “45/44 ratio”). Note that this close match of the “45/44” signature of Kr and CO₂ is just a coincidence and only observed for the Bern system. The other three systems show anomalies in the “45/44 ratio” (Fig. 2), which translate into too-heavy $\delta^{13}\text{C}$ values for natural-air samples as well. In addition to the more direct influence of the “45/44” anomaly on $\delta^{13}\text{C}$, the “46/44” anomaly also alters $\delta^{13}\text{C}$ of CH₄ samples. This is due to the fact that the ¹⁷O correction algorithm (Craig, 1957; Santrock et al., 1985) relies on assumptions regarding

the natural proportions of the stable oxygen isotopes, i.e. the relative contribution of ^{17}O ($^{12}\text{C}^{17}\text{O}^{16}\text{O}$ with m/z 45) and ^{18}O ($^{12}\text{C}^{18}\text{O}^{16}\text{O}$ with m/z 46), which are violated by the Kr signals.

4.3 Injection of pure Kr at varied accelerating voltage

The previous experiments clearly showed that Kr is responsible for the observed effects; yet, the underlying mechanism cannot be unambiguously derived from these experiments. Because the m/z 43 beam produced by $^{86}\text{Kr}^{2+}$ is only a few m/z units away from the target signals at m/z 44, m/z 45 and m/z 46, we propose two hypotheses. The first hypothesis assumes that the observed signals detected in the three Faraday cups are caused by ions with a mass-per-charge ratio corresponding to the nominal m/z of the cups, i.e. m/z 44, m/z 45 and m/z 46. Since ions with m/z 43 are available in the source, one might assume that light gases or their ions (e.g. He, H_2 or H) might react with $^{86}\text{Kr}^{2+}$ ions to form molecules or adducts (Leckrone and Hayes, 1998; Sessions et al., 2001), which then could provide the necessary m/z 44, m/z 45 and m/z 46 signals. The other hypothesis assumes scattering processes lead to broader m/z distributions, e.g. that the lateral tail of the m/z 43 beam ($^{86}\text{Kr}^{2+}$) extends all the way to m/z 46, thus covering 3 m/z units. The fact that the major ion beam contributes some intensity to the neighbouring minor was already observed during the early days of dual-inlet IRMS and termed “pressure effect” or “pressure broadening” and has been treated with abundance sensitivity corrections (Deines, 1970; Mook and Grootes, 1973; Fallick and Baxter, 1977). Peak-tailing effects are also of concern during clumped-isotope analysis of CO_2 where far reaching tails of the major beam on the distant minor beams have been investigated (He et al., 2012). A peak-tailing effect was also observed during stable-sulphur analysis using SF_6 , giving rise to an abundance sensitivity correction to prevent scale compression and accuracy problems (Ono et al., 2006). However, in these cases it is the regular major beam which contributes intensity to the minor beam and not a contaminant species like Kr as assumed in our case. Figuring out the actual process leading to this interference is not only helpful in understanding the different phenomena seen in the four investigated systems, but also in making assumptions about the stability of this interference over time and its sensitivity to changes in focusing parameters, etc. These characteristics are important for developing robust correction routines on existing data sets.

To explore the nature of the interference in more detail we conducted two different experiments where the ion current intensities are monitored as a function of the AV. In the first experiment, Kr was repeatedly injected into the GC flow, while the AV was slightly changed after each injection. In a second experiment, Kr was continuously admitted to the ion source through a capillary, while the AV was changed over a wide range.

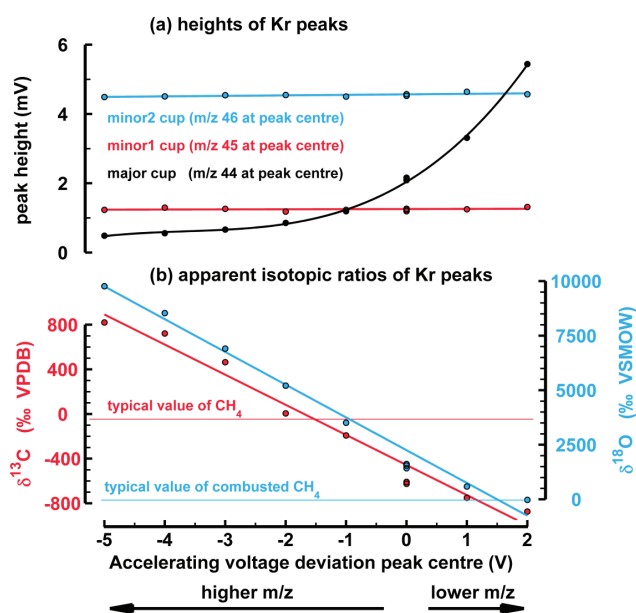


Fig. 5. Influence of slight changes in the accelerating voltage on the peak heights and apparent isotopic signatures of Kr peaks. Results of Kr injection into GC flow carried out with the Bern system with the source focused to CO_2 . (a) The upper panel shows the measured peak heights for the three Faraday cups (major, minor1, minor2) of the Kr peak as a function of the accelerating voltage; dots represent measurements and lines a linear fit for minor1 and minor2, and a cubic fit for the major cup. (b) The lower panel shows the apparent isotopic composition ($\delta^{13}\text{C}$ in red and $\delta^{18}\text{O}$ in blue) of the Kr interference calculated from the peak area of the Kr peaks; dots represent measurements and lines the linear fits.

4.3.1 Kr injections onto GC flow at varied accelerating voltage

In the following experiment pure Kr was repeatedly (10 times) injected into the GC flow of the Bern system and cryofocused prior to GC separation. The amount of injected Kr roughly matches the Kr amount of a 10 mL air sample to provide realistic measurement conditions. Measurements were conducted using the CO_2 configuration, but after each Kr peak the AV of the ion source was slightly changed to cover a range from -5 V to $+2$ V relative to the peak centre (PC) value of the CO_2 focusing. Each Kr peak is preceded by a rectangular CO_2 peak from the reference port (“standard on-off type”) and measured at the same AV to monitor the effect on the $\delta^{13}\text{C}$ and $\delta^{18}\text{O}$ values of CO_2 . Since the applied AV variations cover less than 0.1 m/z unit, the ion beams still fall into their respective Faraday cups. As a consequence, the $\delta^{13}\text{C}$ and $\delta^{18}\text{O}$ values of the rectangular CO_2 peaks are only slightly affected by these AV shifts (ca. 2‰ for both $\delta^{13}\text{C}$ and $\delta^{18}\text{O}$, data not shown). In contrast, the maxima of the Kr peaks in the major cup (m/z 44 at PC) increase from ca. 0.5 mV to almost 6 mV, i.e. a factor of 12 as the AV is increased from -5 V to $+2$ V (Fig. 5a). Since the peak heights

and areas for minor1 (m/z 45 at PC) and minor2 (m/z 46 at PC) remain fairly constant, the apparent isotopic ratios $\delta^{13}\text{C}$ and $\delta^{18}\text{O}$ of the Kr peaks show huge changes, reflecting these drastic changes in the beam ratios (Fig. 5b). We calculated these apparent $\delta^{13}\text{C}$ and $\delta^{18}\text{O}$ values by integrating the peak areas of the tiny Kr peaks for the three cups and applied the same algorithm as if they were CO_2 peaks. Our interpretation is that by increasing AV, the amount of $^{86}\text{Kr}^{2+}$ falling into the major cup quickly increases since the steep tail of this m/z 43 beam is moved closer to the edge of the major cup. The observation of this strong intensity increase on the major cup thus rules out the notion of an ion with m/z 44 producing this interference. However, for the rather constant intensities measured on minor1 and minor2 this experiment cannot rule out the existence of an ion at m/z 45 or m/z 46 since the AV changes were too small to move the centred beam out of the Faraday cup, as can be inferred from the rather constant $\delta^{13}\text{C}$ and $\delta^{18}\text{O}$ values of the CO_2 rectangular peaks (data not shown) and illustrated in Figs. 6 and 7.

Apart from identifying the nature of this interference, this experiment provides valuable information regarding the effects of the Kr interference during sample measurements. From Fig. 5 it is obvious that the apparent $\delta^{13}\text{C}$ or $\delta^{18}\text{O}$ signatures of the Kr interference are not constant but depend on the peak centre setting. Consequently, the influence of Kr on the calculated $\delta^{13}\text{C}$ values of CH_4 samples is not a constant property for any instrument, but both the sign and the magnitude of this effect are sensitive to the setting and stability of the source. As an example, at an AV offset of -1.5 V with respect to the peak centre, the apparent $\delta^{13}\text{C}$ value of the Kr interference intersects with the range of $\delta^{13}\text{C}$ values typical for natural CH_4 samples (around -40 to -70 ‰, red horizontal line in Fig. 5b). If samples are measured at this AV setting, then the Kr effect on $\delta^{13}\text{C}$ of CH_4 will be relatively small and hard to detect. However, for AV offsets < -1.5 V the measured $\delta^{13}\text{C}$ values will be heavier, and for AV offsets > -1.5 V $\delta^{13}\text{C}$ will become progressively lighter. For $\delta^{18}\text{O}$, the Kr bias will always push towards higher values. Note that these values are specific for a certain focusing of a specific instrument. How subtle differences can produce very different effects can be seen in the results of the AWI and Bern instruments, which have identical IRMS. The AWI system shows a pronounced effect in “45/44” (i.e. $\delta^{13}\text{C}$), while the effect on “45/44” for the Bern instrument is small (compare Fig. 2a and d). Usually, the AV at peak centre is determined automatically during the peak centre procedure; thus the bias could be relatively constant for a certain focusing. However, after performing a peak centre its actual position can move by up to 1 V over the course of hours, thus generating a time-dependent bias on the $\delta^{13}\text{C}$ values during a measurement, which will add noise to the data set. On the other hand, the close relationship between apparent $\delta^{13}\text{C}$ and $\delta^{18}\text{O}$ values provides a means to correct biased $\delta^{13}\text{C}$ measurements if the expected $\delta^{18}\text{O}$ value of a sample can be predicted or assumed with good precision. This situation often holds for $\delta^{13}\text{C}$ since

the $\delta^{18}\text{O}$ value of the CH_4 -derived CO_2 is not dependent on the CH_4 sample but set by the O_2 used during the combustion process. Therefore, the tight $\delta^{18}\text{O}$ – $\delta^{13}\text{C}$ correlation seen in Fig. 5b can be used to correct samples which are affected by the Kr interference (see Sect. 5.6).

4.3.2 Admission of Kr into the ion source at varied accelerating voltage

The aim of the following experiments is to better characterise the Kr interference using a wider m/z range.

To better understand an AV scan with pure Kr, we first present an AV scan for CO_2 (Fig. 6a). For practical reasons, the cups of the triple collector unit (universal collector) of most manufacturers have different widths (resolving slit width) to accommodate multipurpose usage, e.g. $\delta^{15}\text{N}$ of N_2 , $\delta^{18}\text{O}$ of O_2 . For the Bern IRMS, an AV change of 85 V is roughly equivalent to 1 m/z difference in this mass range. Figure 6b shows the ion current intensities for the three cups in fA for the same AV scan, but with Kr being admitted to the ion source. The $^{86}\text{Kr}^{2+}$ ion beam with nominally m/z 43.0 starts to fall into the major cup at around $+5$ V and reaches plateau intensity at $+20$ V (“transition zone”) with around 600 000 fA (Fig. 6b bottom panel). Zooming into the major signal reveals that after the initial steep drop to the left of the transition zone (towards higher m/z), the intensity only gradually decays when moving to -90 V, i.e. corresponding to ions with a nominal m/z of already 45 (see Fig. 6a with 85 V corresponding to about 1 m/z unit). The continuation to even-higher m/z is visible in the signal of minor1, where the intensity decreases from ca. 80 fA at $+60$ V (corresponding to ca. m/z 44.7) to ca. 30 fA at -90 V (corresponding to ca. m/z 46.0). Similarly, the continuation is visible in minor2, where the Kr signal becomes almost flat at around 80 fA, covering a range of m/z 45.7 to m/z 47.0. The fact that Kr produces higher intensities for minor2 compared to minor1 reflects the contrasting widths of the two cups: the wider minor2 cup collects Kr ions from a larger m/z range than the smaller minor1 cup (see also scheme of Fig. 7). Again, it is obvious that very small changes in the choice of the peak centre position can have a large effect on the apparent $\delta^{13}\text{C}$ and $\delta^{18}\text{O}$ signature of the Kr interference as already seen in Fig. 5b. Further, the flatness of the Kr signal in the region of m/z 45 and m/z 46 explains the strong linear correlation of $\delta^{13}\text{C}$ and $\delta^{18}\text{O}$ seen in the other experiments and measured air samples and is the basis for one of the correction methods explained below which rely on a linear relation of the m/z 45 and m/z 46 biases.

4.4 Summary of experiments and concept of Kr interference

Figure 7 shows a schematic drawing which illustrates the involved Faraday cups and the positions of the respective ion beams for CO_2 and $^{86}\text{Kr}^{2+}$ as well as the two effects which

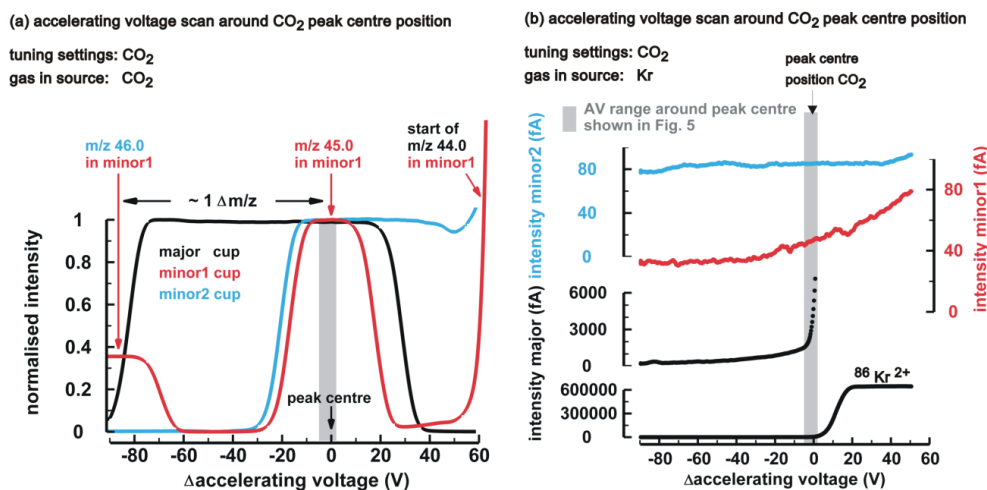


Fig. 6. Accelerating voltage (AV) scans around the peak centre position of CO₂ measured with the Bern system. The plots show beam intensities as a function of ΔAV , i.e. the differences to the AV at peak centre position at 3975 V. **(a)** AV scan with CO₂ from the reference port with normalised beam intensities for the three Faraday cups. The different peak widths reflect the geometric widths of the cups from small (minor1) to intermediate (minor2) to wide (major). **(b)** AV scan with Kr admittance by an additional valve at the Isoprime ref gas box showing the evolution of the Kr interference over a wide m/z range covering all three Faraday cups. The intensities are plotted in fA, thus, proportional to the number of ions collected in the cup. For the major cup, the full range is shown in the bottom panel covering the plateau (600 000 fA at $\Delta AV > 20$ V). The zoomed version of the major cup allows a better inspection of this signal decay to values < 1000 fA. The intensity of the Kr signal decays further in the m/z 45 region, as monitored by the minor1 cup and becomes almost flat at around m/z 46 (minor2 cup). Note the intensities measured with the minor2 cup are ca. factor 2 higher than for minor1 mirroring the different widths of the two cups.

might contribute individually to the observed Kr signals. For the construction of the Kr signals shown in the lower panels (Fig. 7b and c) we used the measured data of Figs. 5 and 6 and the interpretation we derive from these experiments. It is clear from Fig. 6b that most ions are well focused into a sharp beam with steep flanks as intensity rapidly drops to $< 1/1000$ of the plateau level for a 15 V shift in the accelerating voltage, corresponding to about 0.2 m/z units. Only the close-by major cup is strongly affected by this broadening effect. This rapidly dropping signal close to the beam centre can be attributed to the abundance sensitivity effect (Deines, 1970). We refer this contribution of the total Kr signal as the $^{86}\text{Kr}_{\text{tail}}^{2+}$ since it corresponds to the lateral tail of the proper $^{86}\text{Kr}^{2+}$ beam (light green curve Fig. 7b). However, the remarkable feature of the measured Kr signal is that this drop does not continue its rapid drop but decays only very slowly and finally becomes flat when its intensity reaches about $1/10,000$ of the plateau signal at the 20 V distance from the plateau edge (Fig. 6b). This observation is not predicted by abundance sensitivity because in that case the signal far out of the beam centre (the region of minor1 and especially minor2 cup) should drop more rapidly. One option to produce such an elevated background for higher masses far from the beam centre is that ions must have experienced a higher accelerating energy in the ion source. The other option would be interaction or scattering of $^{86}\text{Kr}^{2+}$ ions with He, thus energy loss, after the ions passed the magnetic field. It is also

conceivable that this flat contribution might be unrelated to the $^{86}\text{Kr}^{2+}$ beam, but originate rather from unspecific, broad scattering of the more abundant singly charged Kr ions. For example, filament or ion source processes could produce a broad distribution of low-energy Kr^+ ions which then lead to a broad field of ions with apparent m/z in the range the CO₂ target masses. Likewise, Kr^+ ions could hit the flight tube and produce a field of secondary ions which reach the Faraday cups indirectly. We name this flat contribution $\text{Kr}_{\text{scatter}}$ (brown line in Fig. 7b).

Figure 7c shows the sum of both contributions ($^{86}\text{Kr}_{\text{tail}}^{2+}$ and $\text{Kr}_{\text{scatter}}$) resembling the general features of our experiments and illustrates the Kr interference. While the ion density of the total Kr signal gradually declines further away from the peak maximum at m/z 43, the transformation from the ion current (apparent fA unit) to the voltage unit (apparent mV unit) overcompensates this drop (Fig. 7c). As a consequence, the signals (on an apparent mV unit) gained from minor1 and minor2 are higher compared to the major signal. The signal intensities are spatially integrated according to the width of the Faraday cups: the wider the cup, the more ions from the tail are collected. Accordingly, the integrated signal from minor2 is higher than the integrated minor1 signal. In summary, the Kr interference signal of a certain Faraday cup is not only a function of the ion flux at this position along the optical plane, but also depends on the width of the Faraday cup.

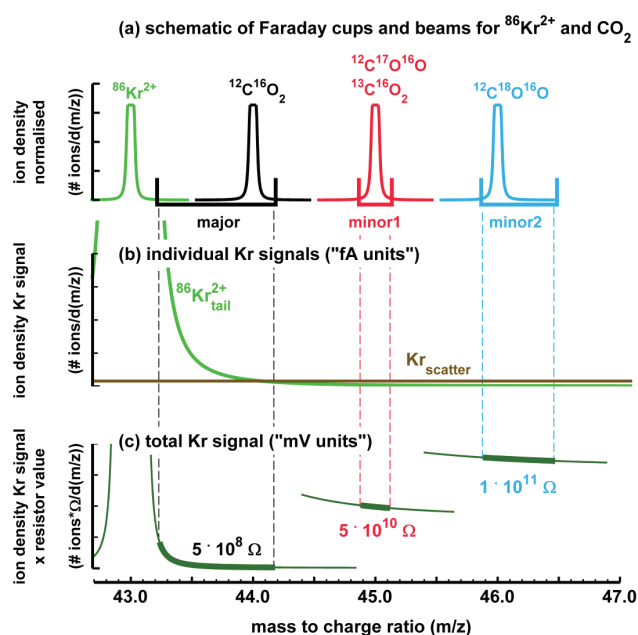


Fig. 7. Schematic showing the Faraday cups and the involved ion beams of CO_2 and the contribution from Kr to help visualise the observed Kr interference during $\delta^{13}\text{C}$ analysis as observed with the Bern IRMS. **(a)** Estimated positioning and width of the Faraday cups and the position of the respective ion beams (m/z) of the CO_2 isotopologues and $^{86}\text{Kr}^{2+}$. **(b)** Individual contributions from Kr. To illustrate the tailing of the m/z 43 $^{86}\text{Kr}^{2+}$ beam ($^{86}\text{Kr}^{2+}_{\text{tail}}$, light green) into the major cup, an artificial density distribution is used to provide a reasonable lateral distribution. The broad, unspecific part of the Kr interference, $\text{Kr}_{\text{scatter}}$, is illustrated by a brown horizontal line. **(c)** The sum of the two Kr contributions is plotted in dark green, but ion densities were converted to a mV unit using the respective values of the feedback resistors of the Bern Isoprime machine; the thick line represents that part of the continuous beam which becomes finally collected in the respective Faraday cups (vertical dashed lines mark the geometric limits of the Faraday cups as a visualisation of the spatial integration of the Faraday cup).

Using this concept of two individual contributions to the total Kr signal, one can explain the following observations:

- pure Kr produces signals at nominal m/z 44 and higher
- the magnitude of the Kr interference depends on the mass spectrometer
- the focusing parameters of the ion source can alter the interferences
- at stable focusing conditions, the effects on $\delta^{13}\text{C}$ and $\delta^{18}\text{O}$ are closely correlated

We want to point out that these observations refer to IRMS measurements in continuous-flow mode where He is admitted continuously to the ion source, leading to a typical pressure of 2×10^{-6} mbar. In dual-inlet mode the source pressure

is about a factor of 10 lower. We have indications from additional tests with dual-inlet IRMS measurements (IMAU), where we admitted Kr without He background, that here the Kr interference is less pronounced. Based on these results we speculate that the m/z 43 ion beam is better focused at dual-inlet conditions, but in continuous-flow mode it is broadened by collisions with He ions in the source or He atoms in the flight tube. A peak broadening during continuous-flow IRMS compared to dual inlet was also observed during stable sulphur isotope analysis using SF_6 (Ono et al., 2006).

5 Solutions for the Kr interference

The observations and experiments discussed above show that Kr can severely interfere with $\delta^{13}\text{C}$ measurements of CH_4 samples if the Kr peak is within the integration boundaries of the CH_4 peak. Given the fact that the Kr interference can produce systematic offsets exceeding the analytical precision, we propose the following strategies to account for or eliminate this effect.

1. GC separation of Kr from CH_4 prior to conversion to CO_2
2. GC separation of Kr from CO_2 after the CH_4 -to- CO_2 conversion
3. Cryogenic separation of Kr from CO_2 after the CH_4 -to- CO_2 conversion
4. Raw beam time series correction using anomalies in the ion current ratios
5. Early peak cut-off at the right integration boundary
6. Correction using relations between $\delta 45$ and $\delta 46$

It is beyond the scope of this paper to discuss all strategies in great detail. Separate technical papers will deal with the individual solutions applied to a particular system. Instead, we want to provide an overview of possible solutions to let the reader make a first selection on the preferred strategy. The six strategies fall into two classes. Strategies 1 to 3 are technical solutions, which prevent the peak overlap in the ion source and thus avoid the Kr interference for new measurements. Strategies 4 to 6 allow correcting existing data sets. These correction strategies were specifically developed for the existing data sets of our respective systems. As the four systems show different characteristics of the Kr interference, these correction strategies cannot be applied interchangeably. Consequently, we could not compare the performance of the three correction approaches, but discuss their strengths and limitations individually.

5.1 GC separation of Kr from CH_4

Of all the proposed solutions in this section, the chromatographic separation of CH_4 from Kr seems to be the most

elegant and straightforward way since no additional device is needed besides the basic setup described by Merritt et al. (1995). The only requirement is that the chromatographic separation is good enough to allow a sufficient separation of CH₄ and Kr. Without knowing that Kr was the “unknown contaminant peak”, Rice et al. (2001) were the first to master this problem with a cryo-GC at -50°C . To maintain narrow peak width, they used high flow rates of 2.6 mL min^{-1} , thus a factor 2.5 higher than typically used for ice core analyses. This approach is also applied by others (Umezawa et al., 2009). Schaefer and Whiticar (2007) followed the same route and used a sub-ambient GC at 0°C to separate what they call N₂O. However, they concluded that separation at 0°C was insufficient, and a second GC column was introduced after the combustion oven.

With the Bern system, we tested the option to better separate CH₄ from Kr using lower GC temperatures. For the experiments we used a 30 m PoraPLOT column at a flow rate of ca. 1 mL min^{-1} and measured the chromatographic separation between CH₄ and Kr for three temperatures: 5, 18, and 30°C . A Kr–He mixture was injected onto the GC flow and cryofocused (Fig. 1). Measurements were made under CO₂ focusing conditions. We did not inject CH₄ but used the small amount of CH₄ cryofocused as blank contribution. This small CH₄ amount turned out to be ideal for these experiments as an amount of CH₄ comparable to samples would otherwise overwhelm the Kr peak. The results are shown in Fig. 8. For 30°C (Fig. 8a) the separation is only 8 s – thus, insufficient – and results in comparable retention time differences to the CarbonPLOT column (ca. 6 s). A reduction to 5°C (Fig. 8c) shows that the separation of CH₄ from Kr is much better and amounts to 16 s, allowing Kr-free $\delta^{13}\text{C}$ analysis of CH₄. However, this low GC temperature had the disadvantage that N₂O eluted very late and showed a very broad peak shape, which is not suitable for isotope analysis on N₂O. Since in our ice core analysis we measure $\delta^{13}\text{C}$ and N₂O isotopes in the same run, we did not choose this route but decided to follow the route described in Sect. 5.3.

5.2 Chromatographic separation after the CH₄-CO₂ conversion

The following section describes the separation of Kr from the combusted CH₄ peak using a post-combustion GC column. As shown above and from other studies (Rice et al., 2001), a sufficient separation of CH₄ from Kr requires low GC temperatures due to similar physico-chemical properties of CH₄ and Kr on the GC column. However, after the combustion oven the resulting CO₂ is relatively easy to separate from Kr since already at ambient temperatures (e.g. 30°C) Kr elutes much earlier than CO₂ on regular GC columns.

The usage of a post-combustion GC column for $\delta^{13}\text{C}$ of CH₄ was first described in Schaefer and Whiticar (2007), who included this device to separate what they interpreted as N₂O. In the following, we show results from the updated

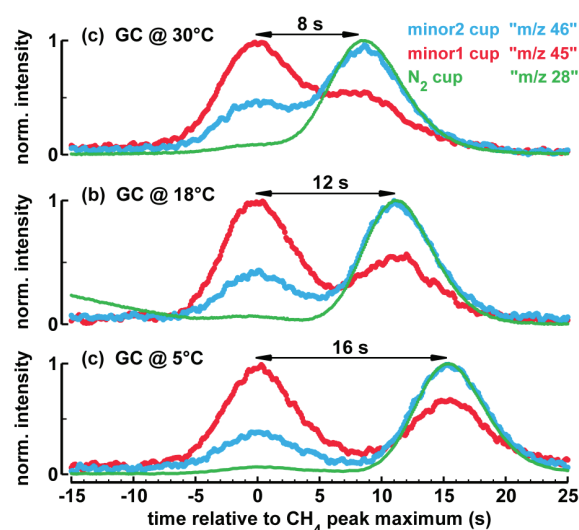


Fig. 8. Chromatograms showing the separation between CH₄ (left peak) and Kr (right peak) on a PoraPLOT column for 30°C , 18°C and 5°C measured with the Bern system. The Kr interference is visible in all Faraday cups, either as a direct signal of $^{84}\text{Kr}^{3+}$ in the m/z 28 cup (thin green line) or from the broad Kr interference for the minor1 and minor2 (thick red and blue, respectively).

IMAU $\delta^{13}\text{C}$ system, where also a post-conversion GC column is used to avoid the Kr interference (Fig. 1). The additional component consists of a 12.5 m piece of PoraPlotQ column in a GC which is operated at 24°C . This GC column was inserted between the Nafion dryer and the open split (see Fig. 1 in Sapart et al., 2011) and provides a separation of Kr from CO₂ (CH₄) of about 30 s (Fig. 9b). The figure also nicely shows the response of the IMAU mass spectrometer to pure Kr resulting in a very pronounced peak on the minor2 cup collecting the nominal m/z 46 ions. A much smaller peak can be seen on minor1 cup (nominal m/z 45). This observation fits with the experiments where pure Kr was added to an air sample and a strong enrichment for $\delta^{18}\text{O}$ was observed while the enrichment for $\delta^{13}\text{C}$ was smaller (7.2 ‰ for $\delta^{18}\text{O}$, and 0.79 ‰ for $\delta^{13}\text{C}$ per 1 ppm Kr added). In contrast to the Bern system, here the Kr signal on the major cup $< 0.1\text{ mV}$ is too small to be visible; thus, the intensities on minor1 and minor2 become fully expressed as anomalies, leading to the strong biases in $\delta^{13}\text{C}$ and $\delta^{18}\text{O}$ observed for the original IMAU system (compare with the Bern system, Figs. 4, 5 and 10).

To assess the overall performance of the updated IMAU system, the three intercomparison cylinders which were measured with the original IMAU system were remeasured with the updated system as well. A comparison between the original and updated IMAU systems shows that the Kr interference at IMAU amounted to ca. 2.38 ‰ for the GL cylinder, ca. 0.88 ‰ for the PI cylinder and ca. 0.05 ‰ for the PD cylinder (Table 2). The results from the updated IMAU method are also comparable with the measurements

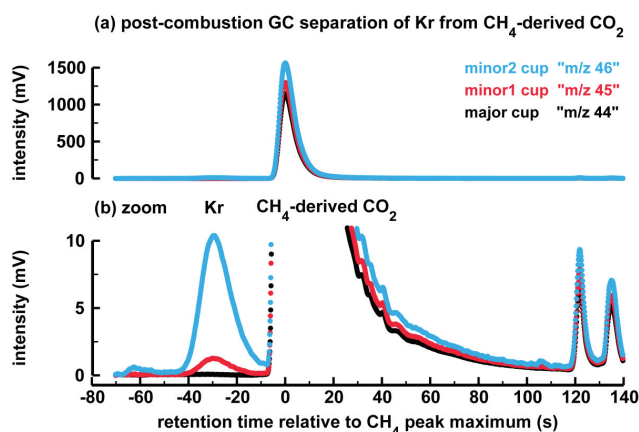


Fig. 9. Chromatogram showing the separation of Kr from CH_4 -derived CO_2 achieved with the improved IMAU system, which includes a GC column after the combustion oven. Due to the additional GC, Kr elutes before instead of after the CH_4 -derived CO_2 peak as shown in the chromatograms of Fig. 3.

obtained at NIWA using dual inlet IRMS, which is free of Kr interference, and with the Kr-corrected results obtained from other labs.

5.3 Cryogenic separation of Kr from CO_2 after the CH_4 - CO_2 conversion

In this section we describe an alternative procedure to separate CO_2 and Kr after the combustion oven, based on the fact that CO_2 can be trapped on a capillary at liquid nitrogen (LN_2) temperature (-196°C) while Kr passes this trap. In the updated Bern system, such a trap is inserted after the combustion oven (post-combustion trap, Fig. 1). Such a trap not only separates CO_2 from Kr but also acts as a cryofocus yielding narrow, high-intensity CO_2 peaks after the capillary is lifted out of the LN_2 (Melton et al., 2011). A second movable trap is inserted before the combustion oven to trap any residual CO_2 from the GC flow (pre-combustion trap, Fig. 1). With the addition of these two traps, Kr now elutes sufficiently earlier (we found 25 s to be a good value) before the sharp CH_4 -derived CO_2 peak, thus providing baseline separation between the two species (Fig. 10). The timing of the post-combustion trap is a critical parameter of this strategy to avoid trapping traces of combusted sample CO. While most of the CO is removed during the first purification step, a small fraction of CO remains and elutes before the CH_4 peak and becomes combusted to CO_2 as well (Fig. 10b). As can be seen in the example chromatogram, the post-combustion trap (trap down arrow in Fig. 10b) is lowered only after the CO-derived CO_2 peak has passed the trap. After a trapping time of 50 s, the capillary is lifted and produces the sharp CO_2 peak. Because Kr is not collected on this capillary, its retention time is basically the same as without the trap. Note that the length of the trapping time should not be unnecessary

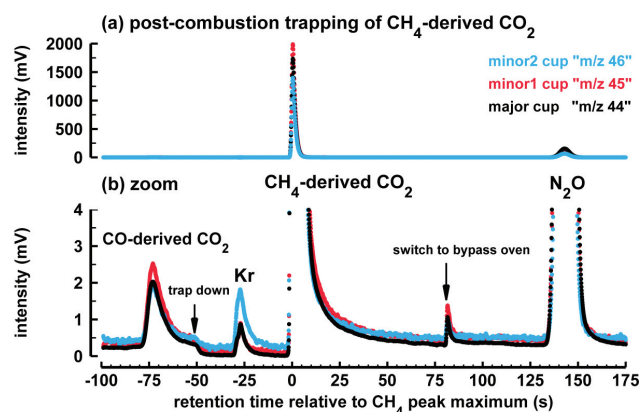


Fig. 10. Sample chromatogram showing the separation of Kr from CH_4 -derived CO_2 for the improved Bern system. **(a)** Full-range plot of the narrow, cryofocused, CH_4 -derived CO_2 peak and the broader N_2O peak without the cryofocusing step. **(b)** Zoomed plot to see the separation of Kr from CH_4 -derived CO_2 . The arrow “trap down” marks the time when the capillary is lowered into LN_2 to trap the CO_2 from the combustion oven. While CO_2 becomes trapped at LN_2 temperature, Kr passes the capillary without delay and shows the typical Kr interference signal.

long since CO_2 bleeding from the combustion oven adds up to blank contribution, which has to be minimised. After the CO_2 peak is measured by the IRMS, a valve is switched to allow the N_2O peak to bypass the combustion oven (Fig. 1, green circles). Note the different peak shape characteristics of the CH_4 -derived CO_2 peak and the N_2O peak due to the cryofocusing step.

5.4 Subtracting the Kr interference peak from raw data

The above hardware solutions all eliminate the Kr interference. However, extant data sets require an algorithm for correcting for the Kr interference. One method for making the correction relies on the anomalies seen in the ion current ratios, which are particularly pronounced in the data set measured with the AWI system (Fig. 11a). This approach requires the time series of the IRMS acquisition file (raw beam data file) and software to read and process this data (Bock et al., 2010; Schmitt et al., 2011). With a set of equations the signal intensity of the Kr peak is calculated which produced these anomalies in the first place. The time series of these reconstructed Kr interferences are then subtracted from the measured time series to yield the corrected time series. The latter one is then used to calculate the $\delta^{13}\text{C}$ values.

In detail, the correction is based on the following equations, with i representing the time series of an ion current and R the ratio of a pair of ion currents. In the case of the AWI measurements, the time series covers the interval beginning at the CH_4 peak start and extends to 10 s after the maximum of the CH_4 peak (see Fig. 11b). Note that the following equations and explanation only show the correction

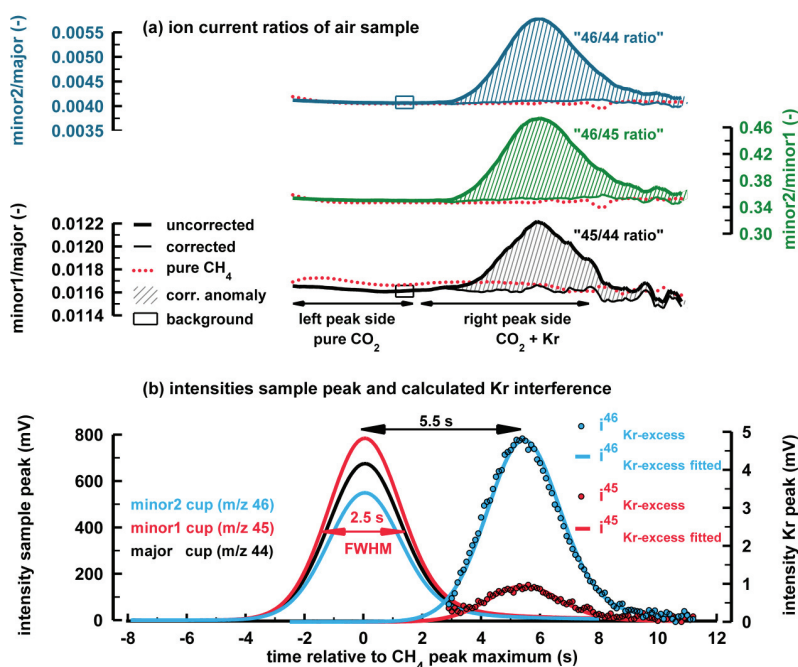


Fig. 11. Compilation showing the principle of the Kr correction for an air sample measured with the AWI system. **(a)** Ion current ratios in bold lines are the uncorrected ratios; the rectangle indicates the time interval that is used to determine the background to calculate the Kr interference shown in the panel below. The thin line and the hatched area show the ratio after the Kr correction, i.e. after the subtraction of the fitted Kr peak from the measured ion current. The red dotted line is the ratio of pure CH₄ without Kr interference. The “46/45 ratio” serves as an independent visual check of whether the correction was successful since the anomaly of this ratio is not used for the correction method. **(b)** Intensities for the three Faraday cups of the CH₄ sample (left axis). The interference calculated from the anomalies plotted in the ratios above (right axis) with the dots representing the calculated raw anomaly for *m/z* 45 and *m/z* 46, the lines are a fit to the respective data used for correction.

of the Kr interference on i^{45} and $R^{45/44}$, the correction for i^{46} is analogous to the i^{45} example. We start by assuming that the CO₂ peak is pure CO₂ in the ion source, i.e. without Kr interference, and the major cup exclusively collects ions, with *m/z* 44 generating the time series of i^{44} , minor1 only *m/z* (i^{45}), and minor2 only *m/z* 46 (i^{46}). In this case, the ion current ratio $R_{\text{measured}}^{45/44}$ is the ratio of the two measured ion currents originating exclusively from CO₂ since i_{measured}^{45} equals $i_{\text{CO}_2}^{45}$ and i_{measured}^{44} equals $i_{\text{CO}_2}^{44}$, given by

$$R_{\text{measured}}^{45/44} = R_{(\text{pure CO}_2)}^{45/44} = i_{\text{CO}_2}^{45} / i_{\text{CO}_2}^{44} = i_{\text{measured}}^{45} / i_{\text{measured}}^{44} \quad (1)$$

However, for a real sample with Kr interference, Eq. (1) is not valid for the entire peak. Instead, the entire CO₂ peak region must be divided into two parts. The left part is dominated by the CO₂ signal and covers the region from ca. 4 s before the CH₄ peak maximum to ca. 2 s after the CH₄ peak maximum (Fig. 11). Equation (1) is only valid for this part. In contrast, the right part is contaminated by Kr. Here, the ion current i_{measured}^{45} is the sum of $i_{\text{CO}_2}^{45}$ and the Kr interference. To generate an anomaly in the ion current ratio of the CO₂ sample, the ion current ratio of the Kr peak must be different from the ion current ratio of the sample. If the ion current ratios of the interfering signals exactly match those of the sample

peak, the $\delta^{13}\text{C}$ and $\delta^{18}\text{O}$ values will be unchanged. For that reason, only the $R^{45/44}$ anomaly to pure CO₂ is calculated in the following equations, with the part of the total i_{Kr}^{45} signal causing this anomaly called $i_{\text{Kr-excess}}^{45}$. The sign of $i_{\text{Kr-excess}}^{45}$ is positive when the minor1/major ratio of the Kr peak is greater than the minor1/major ratio of the pure-CO₂ interval. This case is comparable to the situation of Fig. 5b, left side, with AV < -2 V. Conversely, $i_{\text{Kr-excess}}^{45}$ can be negative for cases resembling the situation in Fig. 5b, right side, with AV > -1 V. Therefore, for the right side of the peak, Eq. (1) is not valid, since $R_{\text{measured}}^{45/44}$ is the sum of $i_{\text{CO}_2}^{45}$ and $i_{\text{Kr-excess}}^{45}$ divided by i_{measured}^{44} :

$$R_{\text{measured}}^{45/44} = R_{(\text{CO}_2+\text{Kr})}^{45/44} = (i_{\text{CO}_2}^{45} + i_{\text{Kr-excess}}^{45}) / i_{\text{measured}}^{44} \quad (2)$$

The next step relies on the observation gleaned from the AWI data that all three ion current ratios of pure-CH₄-derived CO₂ peaks are essentially flat. In contrast, the ratios of the affected sample peaks show large Kr bumps after the flat plateaus due to Kr signals (Figs. 11a and 2d–f). To calculate a quantitative measure of the Kr interference on the ion current ratio, the absolute anomaly of these Kr bumps, $\Delta R^{45/44}$, is defined as follows:

$$\Delta R^{45/44} = R_{(\text{CO}_2+\text{Kr})}^{45/44} - R_{(\text{pure CO}_2)}^{45/44} \quad (3)$$

In practice, $\Delta R^{45/44}$ is calculated by subtracting the “background ratio” defined as $i_{\text{CO}_2}^{45}/i_{\text{measured}}^{44}$, from the ratio of the affected right peak side with the contaminated ratio, $R^{45/44}_{(\text{CO}_2+\text{Kr})}$. The peak section from which the “background ratio” is calculated is indicated by boxes in Fig. 11a. At this step we make the assumption that without any Kr interference the ratio in the background box would continue all the way to the right side, to the right integration boundary (8 to 10 s after CH_4 peak maximum). This assumption is reasonable at this step for defining the “background ratio” since pure- CH_4 peaks show an almost flat ratio over the whole CH_4 peak (see Figs. 2d–f and 11a).

Equation (3) can be transformed into Eq. (4), into Eq. (5) and finally into Eq. (6) where the ion current of the excess Kr, $i_{\text{Kr-excess}}^{45}$, is isolated.

$$\Delta R^{45/44} = (i_{\text{CO}_2}^{45} + i_{\text{Kr-excess}}^{45})/i_{\text{measured}}^{44} - i_{\text{CO}_2}^{45}/i_{\text{measured}}^{44} \quad (4)$$

$$\Delta R^{45/44} = i_{\text{Kr-excess}}^{45}/i_{\text{measured}}^{44} \quad (5)$$

$$i_{\text{Kr-excess}}^{45} = \Delta R^{45/44} \cdot i_{\text{measured}}^{44} \quad (6)$$

The $i_{\text{Kr-excess}}^{45}$ time series resembles a Gaussian peak shape with its maximum at the retention time of the Kr peak (Fig. 11b, blue dots), which indicates that the method allows extracting the Kr interference. Before continuing the calculation, we want to point out the counterintuitive temporal offset between the maximum of the Kr peak and the anomaly maximum of ion current ratio visible in Figs. 2, 4 and 11. Typically, the maximum of the Kr peak occurs a few seconds earlier than the maximum in the ion current ratio. Theoretically, if both the CH_4 -derived CO_2 peak and the Kr peak were ideally Gaussian, the background-corrected ion current ratio on the right side of the Kr peak should asymptotically approach the respective ion current ratio of the Kr peak itself. However, the ion current ratio usually shows a local maximum a few seconds after the maximum of the Kr peak and then declines towards the value of the CO_2 . Our interpretation is that both peaks are non-Gaussian and CO_2 has a longer residence time in the ion source and in the capillaries due to adsorption effects compared to the noble gas krypton. For that reason the measured ion current ratio in the region of the declining flank of the Kr peak becomes progressively dominated by CO_2 . The $i_{\text{Kr-excess}}^{45}$ is not directly used for the correction but a fit to this time series. This fit is called $i_{\text{Kr-excess}}^{45 \text{ fitted}}$. The fit is more accurate and more robust to the selected “background ratio” used in Eq. (3) than the raw $i_{\text{Kr-excess}}^{45}$ time series, and the entire Kr peak can be subtracted (see Fig. 11b). The fit is obtained by scaling the CH_4 -derived CO_2 peak with the height of the $i_{\text{Kr-excess}}^{45}$ peak using the observation that a Kr peak and a CH_4 -derived CO_2 peak are of almost congruent peak shape. Accordingly, the fitting step aims to extract only the part of the $\Delta R^{45/44}$ anomaly that can be related to a Kr peak (Fig. 11b); for details see the corrected minor1 / major ratio (thin line, Fig. 11a) which is not a flat line as would be

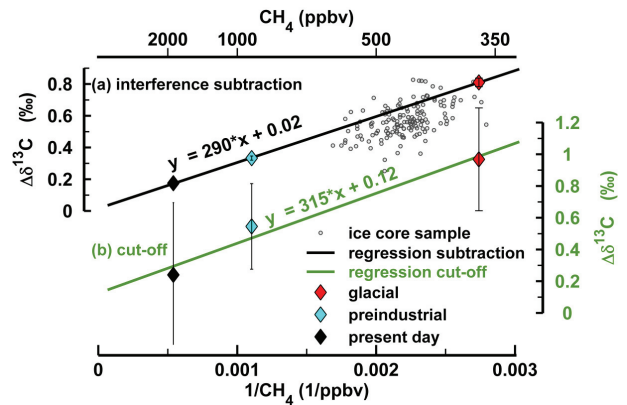


Fig. 12. Comparison of two methods to account for the Kr interference based on measurements with the AWI system using the three intercomparison cylinders with contrasting CH_4/Kr mixing ratios. Plotted are the $\Delta\delta^{13}\text{C}$ numbers, i.e. the differences between the original results and the results obtained after removing the Kr effect. Both methods reveal that with decreasing CH_4 concentrations (hence, CH_4/Kr mixing ratios) $\Delta\delta^{13}\text{C}$ becomes larger. **(a)** Results for the method of Sect. 5.4, where the Kr interference is subtracted from the raw data time series. Coloured diamonds with error bars mark the cylinder measurements; grey circles show a data set of 152 ice core measurements. **(b)** Results for the relatively simple method, where the right integration boundary is shifted from 10 to 3 s after the CH_4 peak maximum to cut off a large fraction of the Kr peak. This method is more vulnerable to peak shape variations leading to more noise in the results.

the case if the full $\Delta R^{45/44}$ (raw anomaly) had been removed (Fig. 11a). Using $i_{\text{Kr-excess}}^{45 \text{ fitted}}$ the measured time series can be corrected as follows:

$$i_{\text{corrected}}^{45} = i_{\text{measured}}^{45} - i_{\text{Kr-excess}}^{45 \text{ fitted}} \quad (7)$$

These equations provide a quantitative way to correct for the Kr interference measured on the minor1 cup. To correct the interference on the minor2 cup, equivalent equations for i^{46} have to be solved. The corrected time series are then fed into our peak integration software to determine the peak areas within the integration limits of the CH_4 -derived CO_2 peak and finally the $\delta^{13}\text{C}$ value. We have applied this correction to results from the intercalibration cylinders with contrasting CH_4 mixing ratios (CH_4/Kr ratios) to demonstrate how the interference scales with CH_4 mixing ratio and to estimate the precision of this correction (Fig. 12a). We see a close linear relationship between the absolute correction, $\Delta\delta^{13}\text{C}$, and the inverse CH_4 mixing ratio ($1/\text{CH}_4$) with $\Delta\delta^{13}\text{C}$ values of only 0.18 ‰ for the “present day” cylinder, 0.33 ‰ for the “pre-industrial” cylinder and 0.81 ‰ for the “glacial” cylinder of the round-robin exercise. The standard deviation of the absolute correction, $\Delta\delta^{13}\text{C}$ values, averaged over the three cylinders is 0.02 ‰; thus, the correction algorithm adds only little noise to the measurement noise of the results.

In principle, this close linear relationship seen in Fig. 12a can be exploited to correct samples with known CH_4 mixing

ratio in the sense of applying a calibration curve to samples. This approach could be valuable, if samples cannot be corrected individually with the above-described algorithm. To evaluate this route, Fig. 12a additionally shows the results from a large data set of ice core samples which were measured with the AWI system. Here we see that the individually corrected samples show a similar CH₄ dependency to the results from the cylinder measurements, yet the correlation is much weaker. The weaker correlation and the scatter around the regression line of the cylinder results do not reflect the correction method itself; the scatter is rather due to the temporal variability of the Kr effect. While the cylinder measurements were obtained within a few weeks, the ice core data set was measured over a period of two years with some changes in the source focusing parameters. From this we can conclude that if the relation of $\Delta\delta^{13}\text{C}$ vs. $1/\text{CH}_4$ is used for correcting affected samples, this can be done very precisely when the calibration measurements are done in close proximity to the sample measurements. On the contrary, additional noise is added to the data when measurement and calibration are not performed at the same instrument conditions, as the relation of $\Delta\delta^{13}\text{C}$ vs. $1/\text{CH}_4$ is subject to changes over time.

5.5 Early peak cut-off

Another method for correcting extant data for Kr may be employed when there is sufficient separation between the Kr and CH₄ peaks. The relative position of the Kr and CH₄ peaks must first be determined as discussed in Sect. 4.1. Once the position of the Kr peak has been established, one can determine when to cut off the CH₄ peak in order to minimise the Kr interference. There is a trade-off involved in removing larger portions of the Kr interference as that requires larger portions of the sample peak to be removed as well. If we assume that the total Kr effect on $\delta^{13}\text{C}$ for a sample amounts to 0.8‰, a 90% cut-off of the Kr peak brings the remaining interference to 0.08‰, i.e. already below the usual measurement precision of ca. 0.1 to 0.2‰. With this approach most of the Kr peak is removed, while only about 10% of the CH₄ peak is lost. In the case of the AWI measurements this translates to a right integration boundary position of 3 s after CH₄ peak maximum. Clearly, this approach violates the rule that the entire peak must be used for isotope analysis, but this can be accommodated by the identical treatment principle (Werner and Brand, 2001). The consequences can be seen in Fig. 12b. The price for this cut is a higher noise level of ca. 0.35‰ and a systematic bias of ca. 0.2‰ which results from systematic differences of the isotopic ratio along the peak. The results of this simple cutting approach could be improved when a certain peak fraction, i.e. 10%, is cut off instead of a fixed time as used here to accommodate for peak shape changes in different chromatograms.

The simplicity of this approach allows for a first check of whether and to what extent the $\delta^{13}\text{C}$ data might be influenced by the Kr interference. It also provides confidence

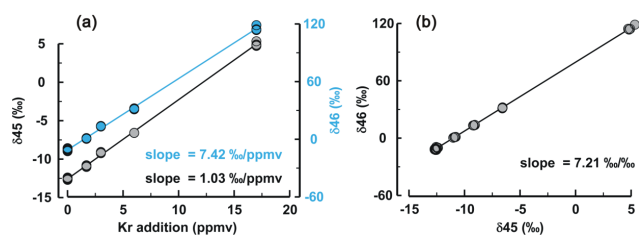


Fig. 13. Results of artificially adding pure Kr to a CH₄ sample. **(a)** Both isotope ratios show a linear relation of the δ values with the amount of Kr added. **(b)** The isotope ratios are closely correlated ($r^2 = 1.00$) and this relation can be used to correct for the Kr interference without knowing the exact CH₄-Kr mixing ratio of a sample. Note that here the $\delta 46/\delta 45$ slope is shown, i.e. the inverse value used in Eq. (9).

in the more sophisticated correction algorithm presented in Sect. 5.4 as it yields a correction of similar magnitude. We applied both the cut-off technique and the subtraction technique on the large ice core data set measured at AWI and conclude that both correction techniques provide similar $\delta^{13}\text{C}$ -corrected values (data not shown).

5.6 Correction using relations between $\delta 45$ and $\delta 46$

The following section describes a correction routine applied by IMAU. The basis for this correction approach is the fact that the Kr interference affects both the minor1 and the minor2 cup, thus $\delta 45$ ($\delta^{45/44}$) and $\delta 46$ ($\delta^{46/44}$) as shown in Fig. 13. This leads to biases for both $\delta^{13}\text{C}$ and $\delta^{18}\text{O}$, which show a tight linear relation (e.g. Fig. 5).

A necessary prerequisite to using the $\delta 45/\delta 46$ relation for correction is the fact that the $\delta^{18}\text{O}$ of the combustion product CO₂ is very similar for sample and reference air peaks. This is usually the case because all oxygen atoms of CO₂ are derived from O₂ during the combustion process. Consequently, the $\delta^{18}\text{O}$ deviation of a Kr-affected sample from a pure-CH₄ sample can be ascribed to the influence of the Kr interference on $\delta^{13}\text{C}$. Note that this assumption is only valid if sample and the pure CH₄ are measured closely together, at least on the same day; otherwise the $\delta^{18}\text{O}$ values are subject to long-term drift caused by the redox state of the combustion furnace. To apply this correction, the relation of $\delta 45/\delta 46$ for the Kr interference has to be acquired. For this, we used the results from the experiments where increasing amounts of Kr were added to a CH₄ sample (Sect. 3). For the correction, the following equation is used:

$$\delta^{13}\text{C}_{\text{corrected}} = \delta^{13}\text{C}_{\text{measured}} - (\delta^{18}\text{O}_{\text{sample}} - \delta^{18}\text{O}_{\text{reference}}) \cdot \text{slope}_{\delta 45/\delta 46}, \quad (8)$$

where $\delta^{13}\text{C}_{\text{corrected}}$ is the $\delta^{13}\text{C}$ value after correction, $\delta^{13}\text{C}_{\text{measured}}$ is the raw measured value, $\delta^{18}\text{O}_{\text{sample}}$ and $\delta^{18}\text{O}_{\text{reference}}$ are the $\delta^{18}\text{O}$ values of the sample and a bracketing reference measurement of pure CH₄, and $\text{slope}_{\delta 45/\delta 46}$ is the slope of the experiments from Sect. 3 (see Fig. 13).

The value used for the slope is $\delta^{45}/\delta^{46} = 0.1388 \pm 0.0008 \text{‰}$, or approximately 0.14 ‰ in $\delta^{13}\text{C}$ for 1 ‰ in $\delta^{18}\text{O}$. Note that for samples the introduced error stemming from the uncertainty of the slope is small and scales with the CH_4/Kr mixing ratio. As an example, for a sample which is corrected by 1.39 ‰, a typical value for glacial ice samples, the error due to the slope amounts to only 0.008 ‰ and, thus, is small compared to the analytical uncertainty of ca. 0.1 to 0.2 ‰. A second type of error results from the measurement uncertainty of $\delta^{18}\text{O}$ for both the sample and the reference. Ideally, the measured $\delta^{18}\text{O}$ values for samples and references should only deviate due to the Kr interference and should be equal for Kr-free CH_4 samples. However, the $\delta^{18}\text{O}$ values might vary over time since the conditions of the combustion furnace can change with time. Depending on how and in which intervals the furnace is reoxidised with O_2 , the variability of $\delta^{18}\text{O}$ is dependent on the system used and should be checked before this correction technique is used to correct a measured data set of $\delta^{13}\text{C}$. Moreover, changes in the IRMS source focusing may change the slope over time. The advantage of this method is that it does not involve special software to do the raw data correction as described in Sect. 5.4. To calibrate this correction, it would suffice to have two gases with known and different CH_4/Kr ratio.

Again, the results from the three intercomparison cylinders provide the means to assess the Kr correction. The comparison of Kr-corrected $\delta^{13}\text{C}$ values measured with the original IMAU method and measurements with the updated IMAU system shows that the Kr-corrected values are very close to the results from the updated IMAU system and the dual-inlet measurement of NIWA (Table 2).

6 Summary and conclusions

This paper identified for the first time that Kr can severely interfere with the measurement of $\delta^{13}\text{C}$ of CH_4 during CF-IRMS analysis. The interference for $\delta^{13}\text{C}$ can be as large as 2 ‰ if samples are measured which have high Kr-to- CH_4 ratios, e.g. air extracted from ice core samples or stratospheric samples, relative to modern atmospheric air as reference gas. In the ion source of the mass spectrometer the krypton isotope ^{86}Kr produces doubly charged ions with a m/z of 43. We demonstrate that the lateral tail of this beam extends into the major and partly also into the minor1 cup, compromising the measured m/z 44 and m/z 45 signal. We speculate that the rather flat Kr interference observed in the minor2 cup (m/z 46) either results from a further extension of this $^{86}\text{Kr}^{2+}$ tail or is due to reflections of the more abundant singly charged Kr ions. As a result, all three Faraday cups used for $\delta^{13}\text{C}$ analysis are affected by the Kr interference. The sign and magnitude of this bias is specific for the used instrument and is dependent on the focusing; thus, the bias can change over time. In this sense, the Kr interference can

lead to incorrect values, concentration effects (scale effects), and drifts over time and can simply increase the measurement noise. At constant instrument conditions, the $\delta^{13}\text{C}$ bias of atmospheric CH_4 samples inversely scales with the CH_4 mixing ratio since the Kr mixing ratio can be regarded as constant. For example, air samples with lower CH_4 mixing ratios will yield higher (heavier) apparent $\delta^{13}\text{C}$ values compared to samples with higher CH_4 mixing ratios. In the second part of the paper we presented several strategies to tackle the Kr problem. Existing methods can be adapted to separate Kr from CH_4 either before the combustion process or after conversion to CO_2 . For existing data sets we propose several correction methods to account for the Kr interference.

Regarding the implications of this effect, we identified the following fields of research using $\delta^{13}\text{C}$ of CH_4 where the Kr interference could be relevant if it is not taken into account. The Kr interference is relevant if high accuracy in $\delta^{13}\text{C}$ is needed and/or samples with low CH_4/Kr ratio mixing ratios are analysed. Note that round-robin intercomparison studies aimed to identify offsets between laboratories cannot solve this issue if pure- CH_4 standards, synthetic-air mixtures (N_2 , O_2) or real samples with only one CH_4/Kr ratio are distributed. Examples for such studies are as follows:

- Palaeo-atmospheric studies on air with low CH_4/Kr mixing ratios (atmospheric CH_4 mixing ratios as low as 360 ppb), e.g. during the glacial period.
- Current atmospheric studies in settings where the atmospheric CH_4/Kr mixing ratio is considerably lowered due to a loss process (e.g. high-stratospheric air samples, microbial oxidation in aerobic soil layers).
- High-precision and -accuracy studies of recent atmospheric $\delta^{13}\text{C}\text{CH}_4$. Note that since the late 1990s when many $\delta^{13}\text{C}\text{CH}_4$ long-term measurements started, by coincidence the atmospheric CH_4 mixing ratio has remained unusually stable.
- Studies analysing the interhemispheric gradient of $\delta^{13}\text{C}$ which rely on measurements from different measurement systems.
- Fresh or sea water samples which had atmospheric contact having low CH_4/Kr mixing ratios due to higher solubility of Kr compared to CH_4 .

The compilation shows that the Kr interference is most relevant for the atmospheric community since the demand on accuracy is often high. However, $\delta^{13}\text{C}$ analyses on CH_4 in other sample matrices could be biased by this effect as well. In the case of natural-water samples which equilibrated with the atmosphere, the higher solubility of Kr relative to CH_4 (about a factor of 1.8) leads to a lower CH_4/Kr ratio for the dissolved gases in the water phase. In settings where CH_4 is consumed by methane oxidising bacteria (e.g. deep-water samples), CH_4/Kr mixing ratios can approach values as low

as 0.1 (nmol nmol⁻¹) (Heeschen et al., 2004). Like for other types of studies where the fractionation factor of a sink process is analysed (e.g. stratospheric samples), any covariation between the CH₄ concentration and an erroneously measured $\delta^{13}\text{C}$ finally translates into an erroneous assessment of the fractionation factor α .

The described effect in this paper could also be relevant for other precise measurements using IRMS, where the gas matrix of sample and standard are different and a variable component produces a large beam with a m/z close to a target mass of the analysed species.

Acknowledgements. The work at Bern was supported by the University of Bern, the Swiss National Science Foundation, and the ERC advanced grant project “MATRICS”. The work at Utrecht University was funded by the Dutch Science Foundation (NWO) (Projects: 851.30.020 & 865.07.001). TAS support for this research came from NSF 0944584. We would like to thank Hinrich Schaefer for generously sharing the NIWA measurements of the round-robin cylinder intercomparison shown in Table 2. We also thank Jeff Severinghaus, Willi Brand and Hinrich Schaefer for their constructive and very helpful comments on the discussion version of this paper, which improved this paper considerably.

Edited by: P. Herckes

References

- Aoki, N. and Makide, Y.: The concentration of krypton in the atmosphere – Its revision after half a century, *Chem. Lett.*, 34, 1396–1397, doi:10.1246/cl.2005.1396, 2005.
- Behrens, M., Schmitt, J., Richter, K.-U., Bock, M., Richter, U., Levin, I., and Fischer, H.: A gas chromatography/combustion/isotope ratio mass spectrometry system for high-precision $\delta^{13}\text{C}$ measurements of atmospheric methane extracted from ice core samples, *Rapid Commun. Mass Sp.*, 22, 3261–3269, doi:10.1002/rcm.3720, 2008.
- Bergamaschi, P., Bräunlich, M., Marik, T., and Brenninkmeijer, C. A. M.: Measurements of the carbon and hydrogen isotopes of atmospheric methane at Izana, Tenerife: Seasonal cycles and synoptic-scale variations, *J. Geophys. Res.-Atmos.*, 105, 14531–14546, doi:10.1029/1999JD901176, 2000.
- Bock, M., Schmitt, J., Behrens, M., Möller, L., Schneider, R., Sapart, C., and Fischer, H.: A gas chromatography/pyrolysis/isotope ratio mass spectrometry system for high-precision δD measurements of atmospheric methane extracted from ice cores, *Rapid Commun. Mass Sp.*, 24, 621–633, doi:10.1002/rcm.4429, 2010.
- Bousquet, P., Ciais, P., Miller, J. B., Dlugokencky, E. J., Hauglustaine, D. A., Prigent, C., Van der Werf, G. R., Peylin, P., Brunke, E. G., Carouge, C., Langenfelds, R. L., Lathiere, J., Papa, F., Ramonet, M., Schmidt, M., Steele, L. P., Tyler, S. C., and White, J.: Contribution of anthropogenic and natural sources to atmospheric methane variability, *Nature*, 443, 439–443, doi:10.1038/nature05132, 2006.
- Brass, M. and Röckmann, T.: Continuous-flow isotope ratio mass spectrometry method for carbon and hydrogen isotope measurements on atmospheric methane, *Atmos. Meas. Tech.*, 3, 1707–1721, doi:10.5194/amt-3-1707-2010, 2010.
- Bräunlich, M., Aballanin, O., Marik, T., Jockel, P., Brenninkmeijer, C. A. M., Chappellaz, J., Barnola, J. M., Mulvaney, R., and Sturges, W. T.: Changes in the global atmospheric methane budget over the last decades inferred from ^{13}C and D isotopic analysis of Antarctic firn air, *J. Geophys. Res.-Atmos.*, 106, 20465–20481, doi:10.1029/2001JD900190, 2001.
- Burford, J. R. and Bremner, J. M.: Gas chromatographic determination of carbon dioxide evolved from soils in closed systems, *Soil Biol. Biochem.*, 4, 191–197, 1972.
- Craig, H.: Isotopic standards for carbon and oxygen and correction factors for mass-spectrometric analysis of carbon dioxide, *Geochim. Cosmochim. Acta*, 12, 133–149, 1957.
- Deines, P.: Mass spectrometer correction factors for the determination of small isotopic composition variations of carbon and oxygen, *Int. J. Mass Spectro. Ion Phys.*, 4, 283–295, 1970.
- Denifl, S., Gstir, B., Hanel, G., Feketeova, L., Matejcik, S., Becker, K., Stamatovic, A., Scheier, P., and Mark, T. D.: Multiple ionization of helium and krypton by electron impact close to threshold: appearance energies and Wannier exponents, *J. Phys. B.*, 35, 4685–4694, doi:10.1088/0953-4075/35/22/310, 2002.
- Fallick, A. E. and Baxter, M. S.: Pressure Effect and Peak Broadening in Gas Source Stable Isotope Mass-Spectrometry, *Int. J. Mass Spectro. Ion Process.*, 25, 155–165, doi:10.1016/0020-7381(77)80046-6, 1977.
- Ferretti, D. F., Miller, J. B., White, J. W. C., Etheridge, D. M., Lassey, K. R., Lowe, D. C., Meure, C. M. M., Dreier, M. F., Trudinger, C. M., van Ommen, T. D., and Langenfelds, R. L.: Unexpected changes to the global methane budget over the past 2000 years, *Science*, 309, 1714–1717, doi:10.1126/science.1115193, 2005.
- Fischer, H., Behrens, M., Bock, M., Richter, U., Schmitt, J., Loulergue, L., Chappellaz, J., Spahni, R., Blunier, T., Leuenberger, M., and Stocker, T. F.: Changing boreal methane sources and constant biomass burning during the last termination, *Nature*, 452, 864–867, doi:10.1038/nature06825, 2008.
- Francey, R. J., Manning, M. R., Allison, C. E., Coram, S. A., Etheridge, D. M., Langenfelds, R. L., Lowe, D. C., and Steele, L. P.: A history of delta $\delta^{13}\text{C}$ in atmospheric CH₄ from the Cape Grim Air Archive and Antarctic firn air, *J. Geophys. Res.-Atmos.*, 104, 23631–23643, doi:10.1029/1999JD900357, 1999.
- He, B., Olack, G. A., and Colman, A. S.: Pressure baseline correction and high-precision CO₂ clumped-isotope (Δ_{47}) measurements in bellows and micro-volume modes, *Rapid Commun. Mass Spectrom.*, 26, 2837–2853, doi:10.1002/rcm.6436, 2012.
- Headly, M. A. and Severinghaus, J. P.: A method to measure Kr/N₂ ratios in air bubbles trapped in ice cores and its application in reconstructing past mean ocean temperature, *J. Geophys. Res.-Atmos.*, 112, D19105, doi:10.1029/2006JD008317, 2007.
- Heeschen, K. U., Keir, R. S., Rehder, G., Klatt, O., and Suess, E.: Methane dynamics in the Weddell Sea determined via stable isotope ratios and CFC-11, *Global Biogeochem. Cy.*, 18, GB2012, doi:10.1029/2003GB002151, 2004.
- Kai, F. M., Tyler, S. C., Randerson, J. T., and Blake, D. R.: Reduced methane growth rate explained by decreased Northern Hemisphere microbial sources, *Nature*, 476, 194–197,

- doi:10.1038/nature10259, 2011.
- Keppler, F., Hamilton, J. T. G., Brass, M., and Röckmann, T.: Methane emissions from terrestrial plants under aerobic conditions, *Nature*, 439, 187–191, doi:10.1038/nature04420, 2006.
- King, S. J. and Price, S. D.: Electron ionization of CO₂, *Int. J. Mass Spectrom.*, 272, 154–164, doi:10.1016/j.ijms.2008.02.008, 2008.
- Leckrone, K. J. and Hayes, J. M.: Water-Induced Errors in Continuous-Flow Carbon Isotope Ratio Mass Spectrometry, *Anal. Chem.*, 70, 2737–2744, doi:10.1021/ac9803434, 1998.
- Levin, I., Veidt, C., Vaughn, B. H., Brailsford, G., Bromley, T., Heinz, R., Lowe, D., Miller, J. B., Poss, C., and White, J. W. C.: No inter-hemispheric $\delta^{13}\text{C}_{\text{CH}_4}$ trend observed, *Nature*, 486, E3–E4, doi:10.1038/nature11175, 2011.
- Lowe, D. C., Brenninkmeijer, C. A. M., Tyler, S. C., and Dlugokencky, E. J.: Determination of the Isotopic Composition of Atmospheric Methane and its Application in the Antarctic, *J. Geophys. Res.-Atmos.*, 96, 15455–15467, doi:10.1029/91JD01119, 1991.
- Lowe, D. C., Allan, W., Manning, M. R., Bromley, T., Brailsford, G., Ferretti, D., Gomez, A., Knobben, R., Martin, R., Mei, Z., Moss, R., Koshy, K., and Maata, M.: Shipboard determinations of the distribution of C-13 in atmospheric methane in the Pacific, *J. Geophys. Res.-Atmos.* 104, 26125–26135, doi:10.1029/1999jd900452, 1999.
- Mariotti, A.: Natural N-15 abundance measurements and atmospheric nitrogen standard calibration, *Nature*, 311, 251–252, doi:10.1038/311251a0, 1984.
- Matthews, D. E. and Hayes, J. M.: Isotope-Ratio-Monitoring Gas Chromatography-Mass Spectrometry, *Anal. Chem.*, 50, 1465–1473, doi:10.1021/ac50033a022, 1978.
- Meier-Augenstein, W., Kemp, H. F., and Lock, C. M.: N₂: a potential pitfall for bulk ²H isotope analysis of explosives and other nitrogen-rich compounds by continuous-flow isotope-ratio mass spectrometry, *Rapid Commun. Mass Spectrom.*, 23, 2011–2016, doi:10.1002/rcm.4112, 2009.
- Melton, J. R., Whiticar, M. J., and Eby, P.: Stable carbon isotope ratio analyses on trace methane from ice samples, *Chem. Geol.*, 288, 88–96, doi:10.1016/j.chemgeo.2011.03.003, 2011.
- Melton, J. R., Schaefer, H., and Whiticar, M. J.: Enrichment in ¹³C of atmospheric CH₄ during the Younger Dryas termination, *Clim. Past*, 8, 1177–1197, doi:10.5194/cp-8-1177-2012, 2012.
- Merritt, D. A., Hayes, J. M., and Des Marais, D. J.: Carbon Isotopic Analysis of Atmospheric Methane by Isotope-Ratio-Monitoring Gas-Chromatography Mass-Spectrometry, *J. Geophys. Res.-Atmos.*, 100, 1317–1326, doi:10.1029/94JD02689, 1995.
- Miller, J. B., Mack, K. A., Dissly, R., White, J. W. C., Dlugokencky, E. J., and Tans, P. P.: Development of analytical methods and measurements of ¹³C/¹²C in atmospheric CH₄ from the NOAA Climate Monitoring and Diagnostics Laboratory global air sampling network, *J. Geophys. Res.-Atmos.*, 107, 4178, doi:10.1029/2001JD000630, 2002.
- Mischler, J. A., Sowers, T. A., Alley, R. B., Battle, M., McConnell, J. R., Mitchell, L., Popp, T., Sofen, E., and Spencer, M. K.: Carbon and hydrogen isotopic composition of methane over the last 1000 years, *Global Biogeochem. Cy.*, 23, GB4024, doi:10.1029/2009GB003460, 2009.
- Möller, L., Sowers, T., Bock, M., Spahni, R., Behrens, M., Schmitt, J., Miller, H., and Fischer, H.: Independent control of methane emissions and isotopic composition over the last 160,000 years, *Nat. Geosci.*, under review, 2013.
- Mook, W. G. and Grootes, P. M.: The Measuring Procedure and corrections for the High-Precision mass-spectrometric analysis of isotopic abundance ratios, especially referring to carbon, oxygen and nitrogen, *Int. J. Mass Spectrom. Ion Phys.*, 12, 273–298, 1973.
- Ono, S., Wing, B., Rumble, D., and Farquhar, J.: High precision analysis of all four stable isotopes of sulfur (³²S, ³³S, ³⁴S and ³⁶S) at nanomole levels using a laser fluorination isotope-ratio-monitoring gas chromatography-mass spectrometry, *Chem. Geol.*, 225, 30–39, doi:10.1016/j.gca.2006.06.1271, 2006.
- Quay, P., Stutsman, J., Wilbur, D., Snover, A., Dlugokencky, E., and Brown, T.: The isotopic composition of atmospheric methane, *Global Biogeochem. Cy.*, 13, 445–461, doi:10.1029/1998GB900006, 1999.
- Rice, A. L., Gotoh, A. A., Ajie, H. O., and Tyler, S. C.: High-Precision Continuous-Flow Measurement of $\delta^{13}\text{C}$ and δD of Atmospheric CH₄, *Anal. Chem.*, 73, 4104–4110, doi:10.1021/ac0155106, 2001.
- Rice, A. L., Tyler, S. C., McCarthy, M. C., Boering, K. A., and Atlas, E.: Carbon and hydrogen isotopic compositions of stratospheric methane: 1. High-precision observations from the NASA ER-2 aircraft, *J. Geophys. Res.-Atmos.*, 108, 4460, doi:10.1029/2002JD003042, 2003.
- Ritz, S. P., Stocker, T. F., and Severinghaus, J. P.: Noble gases as proxies of mean ocean temperature: sensitivity studies using a climate model of reduced complexity, *Quaternary Sci. Rev.*, 30, 3728–3741, doi:10.1016/j.quascirev.2011.09.021, 2011.
- Röckmann, T., Brass, M., Borchers, R., and Engel, A.: The isotopic composition of methane in the stratosphere: high-altitude balloon sample measurements, *Atmos. Chem. Phys.*, 11, 13287–13304, doi:10.5194/acp-11-13287-2011, 2011.
- Santrock, J., Studley, S. A., and Hayes, J. M.: Isotopic analyses based on the mass spectrum of carbon dioxide, *Anal. Chem.*, 57, 1444–1448, 1985.
- Sapart, C. J., van der Veen, C., Vigano, I., Brass, M., van de Wal, R. S. W., Bock, M., Fischer, H., Sowers, T., Buizert, C., Sperlich, P., Blunier, T., Behrens, M., Schmitt, J., Seth, B., and Röckmann, T.: Simultaneous stable isotope analysis of methane and nitrous oxide on ice core samples, *Atmos. Meas. Tech.*, 4, 2607–2618, doi:10.5194/amt-4-2607-2011, 2011.
- Sapart, C. J., Monteil, G., Prokopiou, M., van de Wal, R. S. W., Kaplan, J. O., Sperlich, P., Krumhardt, K. M., van der Veen, C., Houweling, S., Krol, M. C., Blunier, T., Sowers, T., Martinerie, P., Witrant, E., Dahl-Jensen, D., and Röckmann, T.: Natural and anthropogenic variations in methane sources during the past two millennia, *Nature*, 490, 85–88, doi:10.1038/nature11461, 2012.
- Sarma, V., Abe, O., and Saino, T.: Chromatographic separation of nitrogen, argon, and oxygen in dissolved air for determination of triple oxygen isotopes by dual-inlet mass spectrometry, *Anal. Chem.*, 75, 4913–4917, doi:10.1021/ac034314r, 2003.
- Schaefer, H. and Whiticar, M. J.: Measurement of stable carbon isotope ratios of methane in ice samples, *Org. Geochem.*, 38, 216–226, doi:10.1016/j.orggeochem.2006.10.006, 2007.
- Schaefer, H., Whiticar, M. J., Brook, E. J., Petrenko, V. V., Ferretti, D. F., and Severinghaus, J. P.: Ice record of $\delta^{13}\text{C}$ for atmospheric CH₄ across the Younger Dryas-Preboreal transition, *Science*, 313, 1109–1112, doi:10.1126/science.1126562, 2006.

- Schmitt, J., Schneider, R., and Fischer, H.: A sublimation technique for high-precision measurements of $\delta^{13}\text{C}\text{O}_2$ and mixing ratios of CO_2 and N_2O from air trapped in ice cores, *Atmos. Meas. Tech.*, 4, 1445–1461, doi:10.5194/amt-4-1445-2011, 2011.
- Schüpbach, S., Federer, U., Kaufmann, P. R., Hutterli, M. A., Buirion, D., Blunier, T., Fischer, H., and Stocker, T. F.: A New Method for High-Resolution Methane Measurements on Polar Ice Cores Using Continuous Flow Analysis, *Environ. Sci. Technol.*, 43, 5371–5376, doi:10.1021/es9003137, 2009.
- Sessions, A. L., Burgoyne, T. W., and Hayes, J. M.: Correction of H^3+ contributions in hydrogen isotope ratio monitoring mass spectrometry, *Anal. Chem.*, 73, 192–199, doi:10.1088/0953-4075/35/22/310, 2001.
- Severinghaus, J. P., Grachev, A., Luz, B., and Cailion, N.: A method for precise measurement of argon 40/36 and krypton/argon ratios in trapped air in polar ice with applications to past firn thickness and abrupt climate change in Greenland and at Siple Dome, Antarctica, *Geochim. Cosmochim. Acta*, 67, 325–343, doi:10.1016/S0016-7037(02)00965-1, 2003.
- Sowers, T.: Atmospheric methane isotope records covering the Holocene period, *Quaternary Sci. Rev.*, 29, 213–221, doi:10.1016/j.quascirev.2009.05.023, 2011.
- Sowers, T., Bernard, S., Aballain, O., Chappellaz, J., Barnola, J. M., and Marik, T.: Records of the $\delta^{13}\text{C}$ of atmospheric CH_4 over the last 2 centuries as recorded in Antarctic snow and ice, *Global Biogeochem. Cy.*, 19, GB2002, doi:10.1029/2004GB002408, 2005.
- Stevens, C. M. and Rust, F. E.: The Carbon Isotopic Composition of Atmospheric Methane, *J. Geophys. Res.-Ocean. Atmos.*, 87, 4879–4882, doi:10.1029/JC087iC07p04879, 1982.
- Tyler, S. C., Ajie, H. O., Gupta, M. L., Cicerone, R. J., Blake, D. R., and Dlugokencky, E. J.: Stable carbon isotopic composition of atmospheric methane: A comparison of surface level and free tropospheric air, *J. Geophys. Res.-Atmos.*, 104, 13895–13910, doi:10.1029/1999JD900029, 1999.
- Tyler, S. C., Rice, A. L., and Ajie, H. O.: Stable isotope ratios in atmospheric CH_4 : Implications for seasonal sources and sinks, *J. Geophys. Res.-Atmos.*, 112, D03303, doi:10.1029/2006JD007231, 2007.
- Umezawa, T., Aoki, S., Nakazawa, T., and Morimoto, S.: A High-precision Measurement System for Carbon and Hydrogen Isotopic Ratios of Atmospheric Methane and Its Application to Air Samples Collected in the Western Pacific Region, *J. Meteorol. Soc. Jpn.*, 87, 365–379, doi:10.2151/jmsj.87.365, 2009.
- Vigano, I., Röckmann, T., Holzinger, R., van Dijk, A., Keppler, F., Greule, M., Brand, W. A., Geilmann, H., and van Weelden, H.: The stable isotope signature of methane emitted from plant material under UV irradiation, *Atmos. Environ.*, 43, 5637–5646, doi:10.1016/j.atmosenv.2009.07.046, 2009.
- Werner, R. A. and Brand, W. A.: Referencing strategies and techniques in stable isotope ratio analysis, *Rapid Commun. Mass Spectrom.*, 15, 501–519, doi:10.1002/rcm.258, 2001.

4.5.2. A posteriori correction of EDML and Vostok $\delta^{13}\text{CH}_4$ data

The following strategies were applied to correct the PSU and AWI $\delta^{13}\text{CH}_4$ measurements for the Kr effect and account for relative laboratory offsets with respect to the VPDB scale. The results are presented in table 5.1 of section 5.2.2.

EDML samples measured at AWI

AWI EDML measurements are corrected for Kr individually by a method applied to the respective raw data chromatograms. The method uses the visible anomalies seen in the m/z ratios 45/44 and m/z 46/44 and subtracts the modeled Kr peak area contributions (Kr interference) from the raw data time series as described in 4.5.1. Afterwards, the respective chromatograms are reprocessed with the modified raw data time series, and the isotopic composition of the CH_4 sample peak is calculated according to the standard procedure described in section 4.3. Henceforth, these values are referred to as the 'Kr-corrected' $\delta^{13}\text{CH}_4$ values. In contrast, $\delta^{13}\text{CH}_4$ values obtained without the subtraction algorithm are referred to as 'original' $\delta^{13}\text{CH}_4$ values. The difference between original and corrected values are termed 'Kr correction values' or ' $\Delta\delta^{13}\text{C}_{\text{Kr}}$ '. For the EDML time series, $\Delta\delta^{13}\text{C}_{\text{Kr}}$ range between 0.4 ‰ for interstadial (medium CH_4 mixing ratios) to 0.8 ‰ during glacial (MIS 2) and stadial conditions (lower CH_4 levels, compare also figure 4.6). The results are further calibrated internally and are tied to the VPDB scale as outlined in section 4.3.2 and 4.3.2.

Vostok samples measured at the PSU

Unfortunately, an analogous direct approach could not be applied to the Vostok ice core $\delta^{13}\text{CH}_4$ acquisitions performed at the PSU, as the raw chromatograms were not stored after processing the $\delta^{13}\text{C}$ data. Instead, it was necessary to find an indirect way to correct for the Kr effect in the Vostok $\delta^{13}\text{CH}_4$ time series. For the purpose of this correction, the atmospheric krypton mixing ratio can safely be considered constant over time (*Schmitt et al.*, 2013; *Headly and Severinghaus*, 2007). If instrumental conditions are uniform, the Kr effect scales only with the atmospheric concentration of methane and is thus directly proportional to the Kr/ CH_4 ratio (*Schmitt et al.*, 2013). We inferred the linear relationship between the Kr effect and $1/\text{CH}_4$ from the laboratory inter-calibration samples of "IPY" air samples (a detailed description is given in section 4.3.2) with differing methane mixing ratios but similar Kr levels (Note that the dilution of the "IPY" samples with CH_4 free air did not affect the noble gas concentration in the respective cylinders).

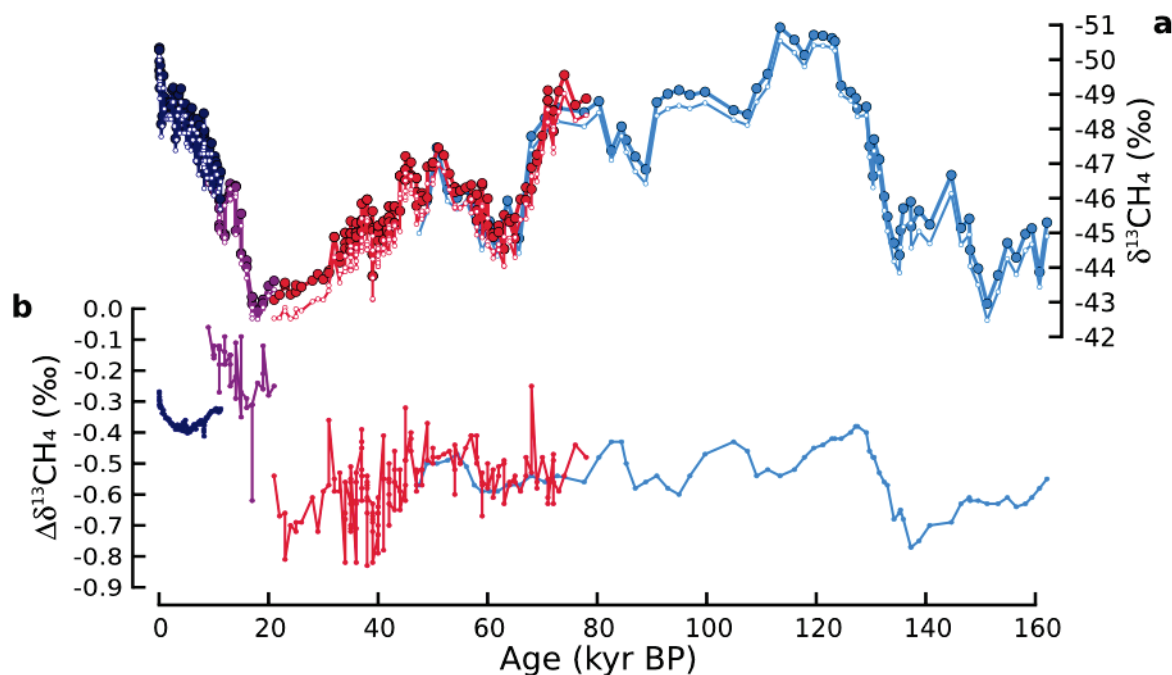


Figure 4.6.: Magnitude of the Kr effect $\Delta\delta^{13}\text{C}_{\text{Kr}}$ derived from two distinct methods for the AWI and PSU instrument.

a) The new $\delta^{13}\text{CH}_4$ time series of Vostok (light blue) and EDML (red), the Holocene GISP II record (Sowers (2010), dark blue, on its original time scale), and the published EDML record over termination I (Fischer *et al.*, 2008) that was re-processed according to the procedures in this publication (purple). The 'Kr-corrected' time series are illustrated with thicker lines and large circles. The 'original' records before the correction are shown as thin lines with open circles.

b) The range of $\Delta\delta^{13}\text{C}_{\text{Kr}}$ values applied as individual correction to the respective datasets to account for the Kr-bias on $\delta^{13}\text{CH}_4$. The color coding is the same as in a). Note that $\Delta\delta^{13}\text{C}_{\text{Kr}}$ of both Vostok and GISP II data measured at the PSU were inferred indirectly from CH_4 mixing ratios, while the correction for the two EDML records is based on the Kr-induced anomaly derived from the ion-current ratios (see section 4.5.1 for a detailed description of both approaches).

The raw data chromatograms of “IPY” air samples performed with the PSU instrument were treated in the same way as the EDML ice core samples, with the routine adapted to the specific characteristics of the PSU setup. Based on these PSU measurements, Kr correction values of 0.12‰, 0.26‰ and 0.66‰ for cylinders “CA03560”, “CC71560” and “CA01179” were obtained, respectively. To a first approximation, $\Delta\delta^{13}\text{C}_{\text{Kr}}$ scales with the inverse of the CH_4 mixing ratios of 1852 ppb, 906 ppb and 365 ppb (illustrated in figure 4.7), yielding a dependence of $\Delta\delta^{13}\text{C}_{\text{Kr}}$ to CH_4 for the PSU measurements. Table 5.1 in section 5.2.2 provides a detailed compilation of results for the “IPY” air samples for both the PSU and the AWI instruments.

When the linear $\Delta\delta^{13}\text{C}_{\text{Kr}} - 1/\text{CH}_4$ relationship was applied to the CH_4 mixing ratios of the

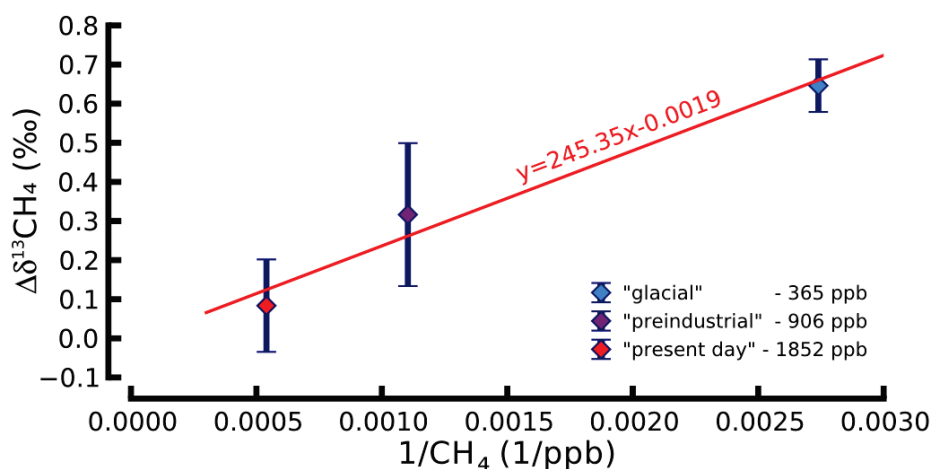


Figure 4.7.: Linear scaling of the size of interference on carbon isotope measurements caused by Kr ($\Delta\delta^{13}\text{C}_{\text{Kr}}$) relative to variations in CH_4 mixing ratios for the PSU instrument Atmospheric krypton mixing ratios are considered constant over time (*Headly and Severinghaus, 2007*). The size of the interference (Kr effect or $\Delta\delta^{13}\text{C}_{\text{Kr}}$) thus scales inversely with CH_4 concentrations. Measurements of three ambient air samples were used to infer a linear relationship between $\Delta\delta^{13}\text{C}_{\text{Kr}}$ and the inverted CH_4 mixing ratio for the PSU instrument, which was used to account for the Kr effect of ice core (Vostok, WDC05) and laboratory inter-calibration measurements (see section 4.3.2 for further details). Results for the IPY cylinder with a mixing ratio representative of glacial conditions ("glacial", 365 ppb) is shown as a light blue diamond, the one with "preindustrial" values (906 ppb) in purple, and the one representative for modern concentrations ("present-day", 1852 ppb) in red, all illustrated with their corresponding 1σ error range. The linear relationship indicated as red line allowed a first-order estimate of $\Delta\delta^{13}\text{C}_{\text{Kr}}$ for ice core samples measured at the PSU laboratory based on interpolated CH_4 mixing ratios of the respective samples inferred from data by *Petit et al. (1997)*.

Vostok ice core (*Petit et al., 1997*), the procedure yielded $\Delta\delta^{13}\text{C}_{\text{Kr}}$ values in the range of 0.4‰ for interglacial conditions (e.g. MIS 5.e) to 0.7‰ and 0.8‰ for the glacial stages MIS 2 and MIS 6, respectively (see figure 4.6). Note that while these corrections on the PSU and AWI data of several tenths of a permille are significant, they are still small compared to the atmospheric changes of several permille observed in the ice core data on glacial/interglacial time scales and do not influence the interpretations.

5. Results and Discussion

The following sections present novel datasets of atmospheric $\delta^{13}\text{CH}_4$ and $\delta\text{D}(\text{CH}_4)$ from EDML and from Vostok and their respective interpretation. An extended discussion of a series of aspects that could not be covered in the publication (section 5.1) are provided in the subsequent section 5.2 in form of "Extended Supplementary Information" to indicate that a part of its contents were already included in the official "Supplementary Information" manuscript that accompanied the publication. For details about the instrumental setups of the cooperating laboratories at the PSU and the Climate and Environmental Physics division (KUP, University of Bern), the reader is therefore referred to appendix D.2 where the official supplemental materials are attached. Note however, that the remaining content was merged into the respective chapters of this manuscript.

5.1. Independent control of CH₄ emissions and isotopic composition over the last 160,000 years.

Lars Möller, Todd Sowers, Michael Bock, Renato Spahni, Melanie Behrens, Jochen Schmitt, Heinrich Miller and Hubertus Fischer

Due to licensing restrictions, the following pages include the final, accepted draft of the article published in *Nature Geoscience*, Volume **6**, pp. 885–890, **2013**, DOI: 10.1038/n-geo1922

Abstract

During the last glacial cycle, greenhouse gas concentrations fluctuated on decadal and longer timescales. Concentrations of methane, as measured in polar ice cores, show a close connection with Northern Hemisphere temperature variability, but the contribution of the various methane sources and sinks to changes in concentration is still a matter of debate. Here we assess changes in methane cycling over the past 160,000 years by measurements of the carbon isotopic composition $\delta^{13}\text{C}$ of methane in Antarctic ice cores from Dronning Maud Land and Vostok. We find that variations in the $\delta^{13}\text{C}$ of methane are not generally correlated with changes in atmospheric methane concentration, but instead more closely correlated to atmospheric CO₂ concentrations. We interpret this to reflect a climatic and CO₂-related control on the isotopic signature of methane source material, such as ecosystem shifts in the seasonally inundated tropical wetlands that produce methane. In contrast, relatively stable $\delta^{13}\text{C}$ values occurred during intervals of large changes in the atmospheric loading of methane. We suggest that most methane sources—most notably tropical wetlands—must have responded simultaneously to climate changes across these periods.

Independent variations of CH₄ emissions and isotopic composition over the past 160,000 years

Authors:

5 Lars Möller (moeller@climate.unibe.ch)^{1,2}, Todd Sowers (sowers@geosc.psu.edu)³, Michael Bock (bock@climate.unibe.ch)², Renato Spahni (spahni@climate.unibe.ch)², Melanie Behrens (melanie.behrens@awi.de)¹, Jochen Schmitt (schmitt@climate.unibe.ch)², Heinrich Miller (heinrich.miller@awi.de)¹, Hubertus Fischer (hubertus.fischer@climate.unibe.ch)^{2*,1}

¹ Alfred Wegener Institute, Helmholtz Centre for Polar and Marine Research, Am Alten Hafen 26, 27568 Bremerhaven, Germany

10 ² Climate and Environmental Physics, Physics Institute & Oeschger Centre for Climate Change Research, University of Bern, Sidlerstrasse 5, 3012 Bern, Switzerland

³ Pennsylvania State University, University Park, PA 16802, USA

* corresponding address

15 **The response of natural CH₄ sources to climate changes will be an important factor to consider as concentrations of this potent greenhouse gas continue to increase. Polar ice cores provide the means to assess this sensitivity in the past and have shown a close connection between CH₄ levels and northern hemisphere temperature variability over the last glacial cycle. However, the contribution of the various CH₄ sources and sinks to these changes is still**

20 **a matter of debate. Contemporaneous stable CH₄ isotope records in ice cores provide additional boundary conditions for assessing changes in the CH₄ sources and sinks. Here we present new ice core CH₄ isotope data covering the last 160,000 years, showing a clear decoupling between CH₄ loading and carbon isotopic variations over most of the record. We suggest that $\delta^{13}\text{CH}_4$ variations were not dominated by a change in the source mix but rather**

25 **by climate- and CO₂-related ecosystem control on the isotopic composition of the methane precursor material, especially in seasonally inundated wetlands in the tropics. In contrast, relatively stable $\delta^{13}\text{CH}_4$ intervals occurred during large CH₄ loading changes concurrently with past climate changes implying that most CH₄ sources (most notably tropical wetlands) responded simultaneously.**

30 Climate variations over the last glacial cycle are characterized by global temperature changes^{1,2}, sea level fluctuations^{3,4}, and substantial changes in atmospheric greenhouse gas concentrations⁵. Abrupt climate shifts, e.g. Dansgaard/Oeschger (DO) events, characterize much of the glacial records in the northern hemisphere and are mirrored in the ice core CH₄ record^{6,7}. The nature of the CH₄/climate coupling on glacial-interglacial and millennial time scales is still a matter of debate^{7,8}. Studies of the inter-polar CH₄ concentration difference using ice cores from both polar regions are interpreted as a constraint of the latitudinal distribution of CH₄ emission sources^{9,10}. In addition, most CH₄ sources/sinks have characteristic isotope signatures. Accordingly, atmospheric CH₄ isotope records provide refined boundary conditions to constrain changes in individual sources or sinks over time¹¹⁻¹³.

40 Here we present CH₄ isotope data from ice cores covering the last 160,000 years (Figure 1), thereby extending the atmospheric $\delta^{13}\text{CH}_4$ record to a full glacial/interglacial cycle.

Generally, our record confirms elevated $\delta^{13}\text{CH}_4$ values under full glacial conditions¹¹, decreasing $\delta^{13}\text{CH}_4$ during terminations (except during the unique Younger Dryas (YD) cold reversal) and the continuation of this declining trend over the following interglacial¹³, irrespective of the CH₄ evolution.

While an unambiguous alignment of termination I and II is not possible due to the YD event, $\delta^{13}\text{CH}_4$ values of the two deglaciations seem to be offset by ~ 2 ‰ (Figure 2). Minimum $\delta^{13}\text{CH}_4$ values are found during MIS 5d-e. $\delta^{13}\text{CH}_4$ increases over the last glaciation, superimposed by variability largely in parallel to millennial CO₂ changes. Most importantly, this new $\delta^{13}\text{CH}_4$ record does not share common features with the CH₄ record over the same interval. The most striking of these dissimilarities is found during the MIS 5/4 transition (between 70 and 64 kyr before present (BP, where present is defined as 1950), when $\delta^{13}\text{CH}_4$ rises by ~ 4 ‰, while CH₄ fluctuations are smaller than 50 ppb (Figure 3). In stark contrast to the MIS 5/4 transition, rapid CH₄ changes during DO events are not imprinted in the $\delta^{13}\text{CH}_4$ record.

Comparing the full $\delta^{13}\text{CH}_4$ record with other global climate records provides some surprising insights into the CH₄/ $\delta^{13}\text{CH}_4$ system (Figure 1): correlations of our $\delta^{13}\text{CH}_4$ record with CH₄, sea level and CO₂ data leads to correlation coefficients (R^2) of 0.29, 0.47 and 0.74, respectively.

60 Moreover, $\delta^{13}\text{CH}_4$ and CO₂ are not only correlated on the glacial-interglacial time scale, but also

over millennial scale variations associated with the Antarctic Isotope Maxima (AIM)^{2,14}.

In summary, the decoupling of CH₄ loading and $\delta^{13}\text{CH}_4$ can be separated into two general phenomena: 1) times when CH₄ source/sink variations change the atmospheric loading with little or no imprint in $\delta^{13}\text{CH}_4$ and, 2) times when $\delta^{13}\text{CH}_4$ varies substantially but the balance of sources and sinks, thus CH₄ concentration, appears to be constant. We will discuss the $\delta^{13}\text{CH}_4$ record in two parts, based on these two surprising observations.

Rapid CH₄ changes during DO events and glacial-interglacial terminations

The mean carbon isotopic signature of atmospheric CH₄ represents a flux weighted mean of all source emissions shifted by the isotopic fractionation induced by its sinks¹⁵. We can think of several explanations for periods where CH₄ loading changed, but $\delta^{13}\text{CH}_4$ remained effectively constant. Given that the primary sink for atmospheric CH₄ is OH oxidation (>85 %), changes in the paleo OH reaction rates would influence the loading through changes in lifetime, but leave $\delta^{13}\text{CH}_4$ unchanged. We discount this possibility based on atmospheric chemical modeling studies that show only subtle changes (<20 %) in OH sink strength during glacial periods^{16,17}. We note however, that the lifetime estimate is somewhat uncertain due to the lack of accurate reconstructions for glacial NO_x and volatile organic carbon (VOC) concentrations, which influence tropospheric OH levels.

Alternatively, rapid DO CH₄ variability without a corresponding imprint in $\delta^{13}\text{CH}_4$ could imply an almost proportional scaling of the major sources, causing the atmospheric $\delta^{13}\text{CH}_4$ signature to remain relatively stable. The latitudinal position of the Inter-Tropical Convergence Zone (ITCZ) and the associated major monsoon systems are intimately coupled to DO climate variability^{6,18-21}. Hydrological changes in low latitudes and their primary control on waxing and waning of tropical wetland emissions is arguably the most important factor driving glacial CH₄ emissions^{6,18}. As the isotopic signature of tropical wetland emissions is closest to the mean $\delta^{13}\text{CH}_4$ signature of all sources, changes in their emissions have only little impact on atmospheric $\delta^{13}\text{CH}_4$.

Paleofire reconstructions inferred from charcoal records suggest increasing wildfire activity during interstadial periods²², although they do not allow for a quantitative estimate of wildfire CH₄ emissions. Wildfire emissions have the strongest leverage on the atmospheric $\delta^{13}\text{CH}_4$ value, as its carbon isotopic signature is strongly enriched. Accordingly, the lack of considerable $\delta^{13}\text{CH}_4$ shifts

during DO events implies that increased wildfire emissions had to be compensated by another, isotopically light source. Combinations including additional ^{13}C -enriched wildfire emissions during interstadials²² and ^{13}C -depleted boreal permafrost emissions^{12,23,24} could explain the observations, although it seems fortuitous that such relative changes would perfectly balance each other in all investigated events.

Enhanced emissions from high-latitude northern hemisphere CH_4 wetland sources (such as thermokarst lakes²⁴, peatlands and permafrost thaw²³, further denoted as boreal wetlands) have been suggested to explain increased inter-polar CH_4 gradients (IPG) during interstadial periods^{9,10}. Elevated northern hemisphere CH_4 levels during interstadials however, could also be caused by increased emissions from mid-to-low latitude wetland sources, e.g. seasonally inundated floodplains in the Chinese lowlands, which are affected by expansive Asian summer monsoon rainfall²¹.

Finally, while geological CH_4 sources are thought to be slightly elevated during glacial times due to lowered sea levels^{25,26}, they should be unaffected by DO events. In addition, large emissions from marine hydrates²⁷ during abrupt CH_4 episodes have been ruled out based on our recent $\delta\text{D}(\text{CH}_4)$ ice core studies^{12,28}.

Possible sink configuration changes that could induce an equivalent enrichment in $\delta^{13}\text{CH}_4$ to compensate for potential boreal CH_4 emissions would have to reduce the relative importance of the OH sink in the troposphere. However, due to the expected reduction of VOCs during the glacial^{29,30} and the feedback of lower CH_4 concentrations on the atmospheric OH concentration itself, the OH sink was likely even more important during cold conditions. In summary, a strong feedback of the major monsoon systems on tropical wetland emissions, fostered by a proportional scaling of emissions from the remaining non-geological CH_4 sources (mainly boreal wetlands and biomass burning), combined with a slight change in CH_4 lifetime during rapid climate change, represent the most likely explanation for strong CH_4 variability that is not accompanied by synchronous $\delta^{13}\text{CH}_4$ changes.

120

Climate and CO_2 -induced changes in wetland ecosystems

The time interval between 71 and 65 kyr BP in our $\delta^{13}\text{CH}_4$ record (the MIS 5/4 transition), in particular demonstrates the decoupling of changes in $\delta^{13}\text{CH}_4$ from atmospheric CH_4 mixing ratios,

which were stable at that time (~450 ppb). CH₄ variations did not exceed 50 ppb, while δ¹³CH₄ shifted strongly (~4 ‰) towards higher values. At the same time sea level dropped by 30-40 m and CO₂ levels decreased by 35 ppm leading to boundary conditions comparable to glacial maxima.

We can think of two plausible explanations that would account for δ¹³CH₄ variations during periods of relatively constant CH₄ concentrations. First, there could be periods when one or more sources with low δ¹³CH₄ were replaced by an equivalent increase in a source with an elevated δ¹³CH₄ signature, causing a net shift in the mean isotopic composition, while keeping the overall CH₄ loading constant. For example, the progressive glaciation of high-latitude northern hemisphere land masses was likely accompanied by a significant reduction of ¹³C-depleted boreal methane sources^{6,18,31}. The CH₄ load could be maintained by the increase of tropical emissions, e.g. related to the expansion of tropical wetland sources on newly exposed shelf areas such as the sunda shelf³¹. Assuming a 10 ‰ difference in their δ¹³CH₄ signature, shifting 30 Tg CH₄/yr from boreal to tropical wetland emissions could explain an atmospheric increase of 2 ‰ in δ¹³CH₄. Note that this would also imply a near shutdown of all boreal sources.

To investigate whether such a shift occurred during the MIS 5/4 transition, we also measured δD(CH₄) over this interval (Figure 3b). At first order, δD(CH₄) is a function of the hydrogen isotopic signature of the precipitation in wetland areas^{12,28}. Accordingly, we would expect a general increase in δD(CH₄) values to accompany the observed δ¹³CH₄ shift, if boreal CH₄ sources were exchanged with tropical sources which are more enriched in deuterium. However, our complementary δD(CH₄) data do not show such a co-variation, indicating that a simple “exchange” of one source for another cannot satisfactorily explain the observed δ¹³CH₄ enrichment. Note that a large change in the hydrogen isotopic signature of boreal wetlands expected for cold conditions³² would not have had a strong influence on the atmospheric composition if boreal wetland emissions were already low before the MIS 5/4 transition³¹. This hypothesis would lend support to the idea that δ¹³CH₄ is governed mainly by processes taking place in the tropics at that time.

Another, more likely explanation for the δ¹³CH₄ shift during the MIS 5/4 transition involves changes in the characteristic isotope values of individual sources themselves³³, controlled by climate and CO₂-induced changes in ecosystem composition. As the primary process of CH₄ production is the anaerobic decomposition of plant material, atmospheric CO₂ affects δ¹³CH₄ in multiple ways.

Changes in the carbon isotopic signature of CO₂ ($\delta^{13}\text{CO}_2$) are directly imprinted in $\delta^{13}\text{CH}_4$ via incorporation into the plant precursor material during photosynthesis. However, the $\delta^{13}\text{CO}_2$ variations over glacial-interglacial cycles (0.2-0.5 ‰) are small³⁴ compared to those in $\delta^{13}\text{CH}_4$. More importantly, the CO₂ concentration itself may have an impact on $\delta^{13}\text{CH}_4$ in two ways.

160

Firstly, CO₂ influences the C3/C4 plant ratio, with the relatively ¹³C-enriched C4 plants being favored under glacial, low CO₂ conditions³⁵⁻³⁷. The effect of this C3/C4 plant shift on $\delta^{13}\text{CH}_4$ has been estimated to be about 0.7 ‰³³. This estimate, however is a lower limit as it was based on the direct competition of C3 and C4 grasses for prescribed grassland areas derived from a modern
165 vegetation map³⁸. Taking an extension of grasslands under glacial conditions into account^{36,37,39}, we expect a significantly stronger effect. The weight of CO₂ variability for the isotopic signature of plant precursor material is also indicated by the striking correlation between CO₂ and $\delta^{13}\text{CH}_4$ over the entire 160 kyr period. Pronounced deviations in this correlation occur immediately after some abrupt increase in CH₄ (i.e. DO events 17, 21, 24 and the onsets of both interglacials, Figure 1).
170 Note that each of these intervals is preceded by a significant increase in sea level^{3,4}, which would have flooded low-lying coastal regions. This implies that changes in the source signature do not follow a simple one-to-one relationship with CO₂, but that $\delta^{13}\text{CH}_4$ is most likely a convoluted signal of wetland area and ecosystem response.

Secondly, a further effect on $\delta^{13}\text{CH}_4$ is caused by the change of the isotopic signature of C3
175 vegetation, linked to a change in isotopic fractionation during CO₂ uptake³⁹. Differences in the range of 3-4 ‰ are reported within C3 plant materials in equatorial Africa between rainforest habitats on the one extreme and open savanna type habitats on the other⁴⁰. Accordingly, a shift from forest- and rainforest-type ecosystems during interglacial conditions to seasonally inundated savanna-type ecosystems during the glacial would also lead to CH₄ emissions increasingly enriched
180 in ¹³C during the MIS 5/4 transition.

Indicative evidence for such ecosystem changes may be found in coastal marine sediment records. For example, $\delta^{13}\text{C}$ of plant biomarkers in sediment cores off the East Atlantic coast close to the river mouths of the Congo and Angola basin indicate 3-4 ‰ higher values during glacial times⁴¹,
185 similar to evidence from the Guinea Plateau margin recording Sahara/Sahel vegetation⁴². A comparable marine geological study from the Cariaco Basin in the tropical West Atlantic, reported a 4-5 ‰ $\delta^{13}\text{C}$ decrease in leaf waxes from the LGM to the preboreal Holocene⁴³. We acknowledge

that such signature changes may only reflect vegetation shifts in river catchment areas. Furthermore, it remains unclear whether changes in atmospheric CO₂ exert a similar influence on $\delta^{13}\text{C}$ of plant material in permanent wetlands. However, we assume that during generally drier glacial conditions an even larger part of tropical CH₄ emissions are caused by seasonally inundated flood plains⁴⁴ whose vegetation is controlled by the postulated influence of climate and CO₂ on the carbon isotope composition of the plant precursor material. Moreover, shifts in the isotopic signature of such seasonal wetland ecosystems would also be documented in coastal marine sediment records through riverine transport.

Considering the still insufficient understanding of the factors controlling ecosystem composition and CH₄ emissions, a definitive quantification of the combined effects of shifts in the C3/C4 plant ratio and changes in the C3 plant isotopic signature on low-latitude $\delta^{13}\text{CH}_4$ appears to be premature. Our estimates show that none of the proposed processes discussed above is likely to explain the full range of observed $\delta^{13}\text{CH}_4$ changes over the MIS 5/4 transition (~4 ‰) or even over the full glacial sequence (~8 ‰). However, the sum of the individual processes together with changes in the ratio of net to gross production of CH₄ in wetlands²⁸ lie well within the range of the observed $\delta^{13}\text{CH}_4$ changes. We stress that, except for a change in net to gross production of CH₄, all these effects are neutral with respect to $\delta\text{D}(\text{CH}_4)$, in line with our results. In essence, a change in the carbon isotopic signature of CH₄ from tropical, seasonally inundated floodplains controlled by changing climate and CO₂ conditions, appears to be an essential ingredient to explain the large changes in $\delta^{13}\text{CH}_4$ at times when CH₄ concentrations remained rather constant.

210 **Implications for glacial/interglacial CH₄ changes**

The conclusions above encourage a reinterpretation of the changes over the last glacial/interglacial transition. In previous work¹¹, we proposed changes in the source mix to explain CH₄ changes over termination I, where we kept the isotopic signatures of individual sources essentially constant. A close look at the evolution of CH₄ and $\delta^{13}\text{CH}_4$ during the transition indicates that only the 1.1 ‰ depletion of $\delta^{13}\text{CH}_4$ into the BA is synchronous with a concurrent steep CH₄ rise of about 150 ppb (Figure 2), while the rapid YD – Preboreal Holocene transition exhibits a more gradual change in $\delta^{13}\text{CH}_4$. A decoupling of $\delta^{13}\text{CH}_4$ and CH₄ thus also applies for the rapid CH₄ changes during termination I. Similar to the strong increase in $\delta^{13}\text{CH}_4$ during the MIS 5/4 transition, at least part of the deglacial $\delta^{13}\text{CH}_4$ decrease during termination I could alternatively be attributed to a progressive

220 depletion of the isotopic signature of CH₄ sources. Such a depletion in δ¹³CH₄ source signatures
from the LGM to the Holocene would also have a pronounced effect on the change in the source
mix required to explain the CH₄ changes. For example, our previous box model approach assumed
temporally constant wetland isotopic signatures over the last 25,000 years leading to comparable
wildfire CH₄ emission for the LGM and the Holocene. However, if we increase the glacial δ¹³CH₄
225 signature of tropical floodplains and biomass burning emissions due to isotopic changes in the plant
precursor material, much smaller wildfire emissions are required for the LGM to close the methane
isotope budget. Accordingly, such a tropical source signature change would bring wildfire activity
reconstructions from charcoal records^{22,45} and δ¹³CH₄ into closer agreement.

230 The expanded database of δ¹³CH₄ variations over the last glacial cycle presented here provides
unique information on unexpected changes in the CH₄ source regions. Fast methane concentration
rises at DO warmings and during the deglaciations do not appear to be driven by large relative
source or sink mix changes, or by activation of northern high-latitude sources alone. Rather, the
new isotopic data constraints suggest that glacial changes in atmospheric CH₄ and δ¹³CH₄ are
235 related to a predominant tropical wetland source, which responded quickly to DO climate variability
and associated changes in the hydrological cycles. Scaling of other non-geological sources, as well
as emission feedbacks on atmospheric CH₄ lifetimes, likely contributed to major CH₄ changes, but
were in most cases either neutral with regard to δ¹³CH₄ or of lesser importance.

240 Our new data provides strong evidence that shifts in the isotopic signature of tropical floodplain
emissions could be the main driver of δ¹³CH₄ variability, especially in glacial periods. δ¹³CH₄
changes are likely modulated by feedbacks of climate and atmospheric CO₂ on the composition of
wetland ecosystems in the low latitudes. Quantifying individual source and sink contributions to the
glacial δ¹³CH₄ changes will remain elusive until the uncertainties in source and sink variability are
245 reduced. Further high-resolution studies of δD(CH₄) could complement the data presented here, but
a deeper understanding of wetland dynamics and vegetation shifts is also required and should be
implemented in CH₄ emission schemes in dynamic vegetation models.

Methods Summary

250 We reconstructed atmospheric δ¹³CH₄ records using wet extraction techniques and continuous flow

gas chromatography combustion isotope ratio mass spectrometry (GC/C/IRMS) measurements performed on ice core material from both the European Project for Ice Coring in Antarctica (EPICA) core from Dronning Maud Land (EDML) and the Vostok cores. At the Alfred Wegener Institute (AWI) we analyzed 151 samples from the EDML core (including 32 replicates, 255 reproducibility of 0.2 ‰, 1 σ) to construct a high resolution record between 20 kyr and 75 kyr BP with an average temporal resolution of better than one sample every 500 years. The period covering the two most pronounced climatic excursions in the Greenland temperature record during MIS 3 (DO events 7 and 8) were sampled with a resolution of ~200 years. A complementary record of 79 samples of Vostok ice core material covering a time period from 50 kyr to 160 kyr BP was 260 measured at the Pennsylvania State University (PSU) with an analytical uncertainty of 0.3 ‰ (1 σ), equivalent to an average temporal resolution of 1660 years. Both datasets overlap well between 50 and 75 kyr, suggesting the spliced record is likely to be a good representation of the true atmospheric record between 20 and 160 kyr. The two records were corrected for instrumental interference from atmospheric krypton, for gravitational settling in the firn, and for a minor 265 inter-laboratory offset of 0.14 ‰. Owing to the uncertainties concerning firn transport characteristics at the core sites under glacial conditions and the exact timings of the onsets of relevant rapid CH₄ increases, we did not apply a general correction for diffusive fractionation. The largest CH₄ rises are estimated to cause $\delta^{13}\text{C}$ shifts in the range of 0.6-1.0 ‰. We marked those 7 $\delta^{13}\text{CH}_4$ samples that are potentially affected by diffusive fractionation in the respective figures to 270 illustrate their limited reliability. All $\delta^{13}\text{C}$ values are reported versus Vienna PeeDee Belemnite (VPDB).

We further analyzed 20 samples of EDML ice for $\delta\text{D}(\text{CH}_4)$ with an external precision of about 2.5 ‰ (1 σ). The measurements were performed at the University of Bern using a purge and trap extraction coupled to a gas chromatography pyrolysis isotope ratio mass spectrometer 275 (GC/P/IRMS) and cover the MIS 5/4 transition with an average resolution of 1.5 kyr in between 54 and 85 kyr BP. The $\delta\text{D}(\text{CH}_4)$ values are reported with respect to the international Vienna Standard Mean Ocean Water (VSMOW) scale.

The $\delta^{13}\text{CH}_4$ and $\delta\text{D}(\text{CH}_4)$ records are dated according to the unified Antarctic ice core chronology⁴⁶. For additional details on the chronology, analytical methods, correction procedures and 280 corresponding references, please refer to the Supplementary Information.

Correspondence and requests for materials should be addressed to H.F.

Acknowledgements

285 This work is a contribution to the “European Project for Ice Coring in Antarctica” (EPICA), a joint
ESF/EC scientific program, funded by the EC and by national contributions from Belgium,
Denmark, France, Germany, Italy, The Netherlands, Norway, Sweden, Switzerland and the United
Kingdom.

This is EPICA publication no. 293.

290 Funding of this work has been provided in part by the European Research Council (ERC) Advanced
Grant MATRICs, Schweizerischer Nationalfonds and Deutsche Forschungsgemeinschaft, and is
also a contribution to the European Union’s Seventh Framework programme (FP7/2007-2013,
grant no. 243908), "Past4Future. Climate Change: Learning from the past climate". This is
Past4Future contribution no. 55. Funding for T.A.S. was derived from NSF grants 09-44584 and
09-68391.

295 All data are available at www.pangaea.de (<http://doi.pangaea.de/10.1594/PANGAEA.812116>) and
in the NOAA/World Data Center for Paleoclimatology archive ([http://hurricane.ncdc.noaa.gov
/pls/paleox/f?p=519:1:::P1_STUDY_ID:14651](http://hurricane.ncdc.noaa.gov/pls/paleox/f?p=519:1:::P1_STUDY_ID:14651)).

Author Contributions

300 L.M., T.A.S., M.Bo. and M.Be. performed the measurements. R.S. modeled the diffusion
fractionation in the firn column. L.M. and H.F. wrote the manuscript. All authors worked on the
scientific interpretation, contributed to the discussion with ideas and comments or helped to review
the manuscript.

Competing Financial Interests Statement

305 The authors declare no competing financial interests.

References

1. North GRIP members, High-resolution record of Northern Hemisphere climate extending into the last interglacial period. *Nature*, **431**, 147-151 (2004).
- 310 2. EPICA community members, One-to-one coupling of glacial climate variability in Greenland and Antarctica. *Nature*, **444**, 195-198 (2006).
3. Rohling, E. J.; Grant, K.; Bolshaw, M.; Roberts, A. P.; Siddall, M.; Hemleben, C. & Kucera, M. Antarctic temperature and global sea level closely coupled over the past five glacial cycles. *Nature Geosci*, **2**, 500-504 (2009).
- 315 4. Grant, K. M.; Rohling, E. J.; Bar-Matthews, M.; Ayalon, A.; Medina-Elizalde, M.; Ramsey, C. B.; Satow, C. & Roberts, A. P. Rapid coupling between ice volume and polar temperature over the past 150,000 years. *Nature*, **491**, 744-747 (2012).
5. Schilt, A.; Baumgartner, M.; Schwander, J.; Buiron, D.; Capron, E.; Chappellaz, J.; Loulergue, L.; Schüpbach, S.; Spahni, R.; Fischer, H. & Stocker, T. F. Atmospheric nitrous oxide during the last 140,000 years. *Earth and Planetary Science Letters*, **300**, 33-43 (2010).
- 320 6. Chappellaz, J.; Blunier, T.; Raynaud, D.; Barnola, J. M.; Schwander, J. & Stauffer, B. Synchronous changes in atmospheric CH₄ and Greenland climate between 40 and 8 kyr BP. *Nature*, **366**, 443-445 (1993).
7. Loulergue, L.; Schilt, A.; Spahni, R.; Masson-Delmotte, V.; Blunier, T.; Lemieux, B.; Barnola, J.-M.; Raynaud, D.; Stocker, T. F. & Chappellaz, J. Orbital and millennial-scale features of atmospheric CH₄ over the past 800,000 years.. *Nature*, **453**, 383-386 (2008).
- 325 8. Brook, E. J.; Harder, S.; Severinghaus, J.; Steig, E. J. & Sucher, C. M. On the Origin and Timing of Rapid Changes in Atmospheric Methane During the Last Glacial Period. *Global Biogeochem. Cycles*, **14**, (2000).
- 330 9. Dällenbach, A.; Blunier, T.; Flückiger, J.; Stauffer, B.; Chappellaz, J. & Raynaud, D. Changes in the Atmospheric CH₄ Gradient Between Greenland and Antarctica During the Last Glacial and the Transition to the Holocene. *Geophys. Res. Lett.*, **27**, 1005–1008 (2000).
10. Baumgartner, M.; Schilt, A.; Eicher, O.; Schmitt, J.; Schwander, J.; Spahni, R.; Fischer, H. & Stocker, T. F. High-resolution inter-polar difference of atmospheric methane around the Last Glacial Maximum. *Biogeosciences Discuss.*, **9**, 5471-5508 (2012).
- 335 11. Fischer, H.; Behrens, M.; Bock, M.; Richter, U.; Schmitt, J.; Loulergue, L.; Chappellaz, J.; Spahni, R.; Blunier, T.; Leuenberger, M. & Stocker, T. F. Changing boreal methane sources and constant biomass burning during the last termination.. *Nature*, **452**, 864-867 (2008).
12. Bock, M.; Schmitt, J.; Möller, L.; Spahni, R.; Blunier, T. & Fischer, H. Hydrogen Isotopes Preclude Marine Hydrate CH₄ Emissions at the Onset of Dansgaard-Oeschger Events. *Science*, **328**, 1686-1689 (2010).
- 340 13. Sowers, T. Atmospheric methane isotope records covering the Holocene period. *Quaternary Science Reviews*, **29**, 213-221 (2010).
14. Ahn, J. & Brook, E. J. Atmospheric CO₂ and Climate on Millennial Time Scales During the Last Glacial Period. *Science*, **322**, 83-85 (2008).
- 345 15. Whiticar, M. & Schaefer, H. Constraining past global tropospheric methane budgets with carbon and hydrogen isotope ratios in ice. *Philosophical Transactions of the Royal Society A: Mathematical, Physical and Engineering Sciences*, **365**, 1793-1828 (2007).
16. Hopcroft, P. O.; Valdes, P. J. & Beerling, D. J. Simulating idealized Dansgaard-Oeschger events and their potential impacts on the global methane cycle. *Quaternary Science Reviews*, **30**, 3258-3268 (2011).
- 350 17. Levine, J. G.; Wolff, E. W.; Jones, A. E.; Sime, L. C.; Valdes, P. J.; Archibald, A. T.; Carver, G. D.; Warwick, N. J. & Pyle, J. A. Reconciling the changes in atmospheric methane sources and sinks between the Last Glacial Maximum and the pre-industrial era. *Geophys. Res. Lett.*,

- 355 **38**, L23804- (2011).
18. Brook, E. J.; Sowers, T. & Orchardo, J. Rapid Variations in Atmospheric Methane Concentration During the Past 110,000 Years. *Science*, **273**, 1087-1091 (1996).
 19. Wang, X.; Auler, A. S.; Edwards, R. L.; Cheng, H.; Cristalli, P. S.; Smart, P. L.; Richards, D. A. & Shen, C.-C. Wet periods in northeastern Brazil over the past 210 kyr linked to distant
360 climate anomalies. *Nature*, **432**, 740-743 (2004).
 20. Peterson, L. C. & Haug, G. H. Variability in the mean latitude of the Atlantic Intertropical Convergence Zone as recorded by riverine input of sediments to the Cariaco Basin (Venezuela). *Palaeogeography, Palaeoclimatology, Palaeoecology*, **234**, 97-113 (2006).
 21. Wang, Y.; Cheng, H.; Edwards, R. L.; Kong, X.; Shao, X.; Chen, S.; Wu, J.; Jiang, X.; Wang, X. & An, Z. Millennial- and orbital-scale changes in the East Asian monsoon over the past
365 224,000 years. *Nature*, **451**, 1090-1093 (2008).
 22. Daniau, A.-L.; Harrison, S. & Bartlein, P. Fire regimes during the Last Glacial. *Quaternary Science Reviews*, **29**, 2918-2930 (2010).
 23. Zimov, S. A.; Voropaev, Y. V.; Semiletov, I. P.; Davidov, S. P.; Prosiannikov, S. F.; Chapin, F. S.; Chapin, M. C.; Trumbore, S. & Tyler, S. North Siberian Lakes: A Methane Source Fueled
370 by Pleistocene Carbon. *Science*, **277**, 800-802 (1997).
 24. Walter, K. M.; Edwards, M. E.; Grosse, G.; Zimov, S. A. & Chapin, F. S., I. Thermokarst Lakes as a Source of Atmospheric CH₄ During the Last Deglaciation. *Science*, **318**, 633-636 (2007).
 - 375 25. Judd, A. G.; Hovland, M.; Dimitrov, L. I.; García Gil, S. & Jukes, V. The geological methane budget at Continental Margins and its influence on climate change. *Geofluids*, **2**, 109-126 (2002).
 26. Luyendyk, B.; Kennett, J. & Clark, J. F. Hypothesis for increased atmospheric methane input from hydrocarbon seeps on exposed continental shelves during glacial low sea level. *Marine and Petroleum Geology*, **22**, 591-596 (2005).
 - 380 27. Kennett, J. P.; Cannariato, K. G.; Hendy, I. L. & Behl, R. J. Carbon Isotopic Evidence for Methane Hydrate Instability During Quaternary Interstadials. *Science*, **288**, 128-133 (2000).
 28. Sowers, T. Late Quaternary Atmospheric CH₄ Isotope Record Suggests Marine Clathrates Are Stable. *Science*, **311**, 838-840 (2006).
 - 385 29. Valdes, P. J.; Beerling, D. J. & Johnson, C. E. The ice age methane budget. *Geophys. Res. Lett.*, **32**, (2005).
 30. Kaplan, J. O.; Folberth, G. & Hauglustaine, D. A. Role of methane and biogenic volatile organic compound sources in late glacial and Holocene fluctuations of atmospheric methane concentrations. *Global Biogeochem. Cycles*, **20**, (2006).
 - 390 31. Weber, S. L.; Drury, A. J.; Toonen, W. H. J. & van Weele, M. Wetland methane emissions during the Last Glacial Maximum estimated from PMIP2 simulations: Climate, vegetation, and geographic controls. *J. Geophys. Res.*, **115**, (2010).
 32. Jouzel, J.; Hoffmann, G.; Koster, R. & Masson, V. Water isotopes in precipitation: data/model comparison for present-day and past climates. *Quaternary Science Reviews*, **19**, 363-379
395 (2000).
 33. Schaefer, H. & Whiticar, M. J. Potential glacial-interglacial changes in stable carbon isotope ratios of methane sources and sink fractionation. *Global Biogeochem. Cycles*, **22**, (2008).
 34. Schmitt, J.; Schneider, R.; Elsig, J.; Leuenberger, D.; Lourantou, A.; Chappellaz, J.; Köhler, P.; Joos, F.; Stocker, T. F.; Leuenberger, M. & Fischer, H. Carbon Isotope Constraints on the
400 Deglacial CO₂ Rise from Ice Cores. *Science*, **336**, 711-714 (2012).
 35. Ehleringer, J. R.; Cerling, T. E. & Helliker, B. R. C₄ photosynthesis, atmospheric CO₂, and climate. *Oecologia*, **112**, 285-299-299 (1997).

- 405 36. Harrison, S. P. & Prentice, C. I. Climate and CO₂ controls on global vegetation distribution at the last glacial maximum: analysis based on palaeovegetation data, biome modelling and palaeoclimate simulations. *Global Change Biology*, **9**, 983-1004 (2003).
37. Bragg, F. J.; Prentice, I. C.; Harrison, S. P.; Eglinton, G.; Foster, P. N.; Rommerskirchen, F. & Rullkötter, J. Stable isotope and modelling evidence for CO₂ as a driver of glacial–interglacial vegetation shifts in southern Africa. *Biogeosciences*, **10**, 2001-2010 (2013).
- 410 38. Collatz, G. J.; Berry, J. A. & Clark, J. S. Effects of climate and atmospheric CO₂ partial pressure on the global distribution of C4 grasses: present, past, and future. *Oecologia*, **114**, 441-454 (1998).
39. Kaplan, J. O.; Prentice, I. C.; Knorr, W. & Valdes, P. J. Modeling the dynamics of terrestrial carbon storage since the Last Glacial Maximum. *Geophys. Res. Lett.*, **29**, 2074 (2002).
- 415 40. Vogts, A.; Moossen, H.; Rommerskirchen, F. & Rullkötter, J. Distribution patterns and stable carbon isotopic composition of alkanes and alkan-1-ols from plant waxes of African rain forest and savanna C3 species. *Organic Geochemistry*, **40**, 1037-1054 (2009).
41. Rommerskirchen, F.; Eglinton, G.; Dupont, L. & Rullkötter, J. Glacial/interglacial changes in southern Africa: Compound-specific δ¹³C land plant biomarker and pollen records from southeast Atlantic continental margin sediments. *Geochem. Geophys. Geosyst.*, **7**, (2006).
- 420 42. Castañeda, I. S.; Mülitz, S.; Schefuß, E.; Lopes dos Santos, R. A.; Sinninghe Damsté, J. S. & Schouten, S. Wet phases in the Sahara/Sahel region and human migration patterns in North Africa. *Proceedings of the National Academy of Sciences*, **106**, 20159-20163 (2009).
43. Hughen, K. A.; Eglinton, T. I.; Xu, L. & Makou, M. Abrupt Tropical Vegetation Response to Rapid Climate Changes. *Science*, **304**, 1955-1959 (2004).
- 425 44. Mitsch, W.; Nahlik, A.; Wolski, P.; Bernal, B.; Zhang, L. & Ramberg, L. Tropical wetlands: seasonal hydrologic pulsing, carbon sequestration, and methane emissions. *Wetlands Ecology and Management*, **18**, 573-586 (2010).
45. Marlon, J. R.; Bartlein, P. J.; Walsh, M. K.; Harrison, S. P.; Brown, K. J.; Edwards, M. E.; Higuera, P. E.; Power, M. J.; Anderson, R. S.; Briles, C.; Brunelle, A.; Carcaillet, C.; Daniels, M.; Hu, F. S.; Lavoie, M.; Long, C.; Minckley, T.; Richard, P. J. H.; Scott, A. C.; Shafer, D. S.; Tinner, W.; Umbanhowar, C. E. & Whitlock, C. Wildfire responses to abrupt climate change in North America. *Proceedings of the National Academy of Sciences*, **106**, 2519-2524 (2009).
- 430 46. Lemieux-Dudon, B.; Blayo, E.; Petit, J.-R.; Waelbroeck, C.; Svensson, A.; Ritz, C.; Barnola, J.-M.; Narcisi, B. M. & Parrenin, F. Consistent dating for Antarctic and Greenland ice cores. *Quaternary Science Reviews*, **29**, 8-20 (2010).
47. Petit, J. R.; Jouzel, J.; Raynaud, D.; Barkov, N. I.; Barnola, J.-M.; Basile, I.; Bender, M.; Chappellaz, J.; Davis, M.; Delaygue, G.; Delmotte, M.; Kotlyakov, V. M.; Legrand, M.; Lipenkov, V. Y.; Lorius, C.; Pepin, L.; Ritz, C.; Saltzman, E. & Stievenard, M. Climate and atmospheric history of the past 420,000 years from the Vostok ice core, Antarctica. *Nature*, **399**, 429-436 (1999).
- 440 48. Bereiter, B.; Lüthi, D.; Siegrist, M.; Schüpbach, S.; Stocker, T. F. & Fischer, H. Mode change of millennial CO₂ variability during the last glacial cycle associated with a bipolar marine carbon seesaw. *Proceedings of the National Academy of Sciences*, (2012).
- 445 49. Monnin, E.; Indermühle, A.; Dällenbach, A.; Flückiger, J.; Stauffer, B.; Stocker, T. F.; Raynaud, D. & Barnola, J.-M. Atmospheric CO₂ Concentrations over the Last Glacial Termination. *Science*, **291**, 112-114 (2001).
50. EPICA community members, Eight glacial cycles from an Antarctic ice core. *Nature*, **429**, 623-628 (2004).
- 450

Figure legends

Figure 1 | Methane carbon isotope and other climate records

From top: Relative sea-level (Rsl.) reconstruction^{3,4}. Atmospheric CO₂ from Vostok⁴⁷ (brown),
455 EDML and Talos Dome⁴⁸ (orange), Byrd¹⁴ (turquoise) and EDC⁴⁹ (yellow). $\delta^{13}\text{CH}_4$ from Vostok
(light blue) and EDML (dark red). Records for termination I¹¹ (EDML, purple) and the Holocene¹³
(GISP2, dark blue), all with inverted y-axes. Samples potentially affected by diffusive fractionation
are marked by white circle fillings. Atmospheric CH₄ from EDC⁷ (light green) and EDML⁵ (dark
green). δD in precipitation from the EDC⁵⁰ (red). All records, except GISP II $\delta^{13}\text{CH}_4$ and Rsl., are
460 given on the unified ice core chronology⁴⁶. Vertical bars indicate periods when the correlation
between CO₂ and CH₄ breaks down.

Figure 2 | Climate conditions during the ultimate and penultimate glacial terminations

a) CO₂ from Vostok⁴⁷ (TII, brown) and EDC⁴⁹ (TI, yellow), b) $\delta^{13}\text{CH}_4$ from Vostok (TII, light blue),
465 EDML¹¹ (TI, purple, re-processed and corrected for Kr effect) and GISP2¹³ (TI, dark blue, original
time scale, corrected for Kr effect), all with inverted y-axes. c) CH₄ from EDC⁷ (TII, light green)
and EDML⁵ (TI, dark green). Except for GISP2 $\delta^{13}\text{CH}_4$, all records are given on the unified ice core
chronology⁴⁶. Upper x-axis refers to TI (0-25 kyr BP), lower x-axis to TII (118-143 kyr BP), aligned
at the major CH₄ rises (gray dotted line).

470

Figure 3 | Zoom into MIS 3 and the MIS 5 – MIS 4 boundary

a) CO₂ from EDML and Talos Dome⁴⁸ (purple), after 38.5 kyr BP from Byrd¹⁴ (closed circles).
 $\delta^{13}\text{CH}_4$ from EDML (blue) and CH₄ from EDML⁵ (green). b) CO₂ from EDML and Talos Dome⁴⁸
(purple). Composite $\delta^{13}\text{CH}_4$ (blue) (80-90 kyr BP from Vostok (filled circles), all others from
475 EDML (open circles), y-axes inverted). Samples potentially subject to diffusive fractionation
marked by red circle fillings. $\delta\text{D}(\text{CH}_4)$ from EDML (orange), CH₄ from EDML⁵ (green). All data
sets are reported on the unified ice core chronology⁴⁶. Standard deviations of replicate
measurements illustrated by error bars.

480 **Figure 1**

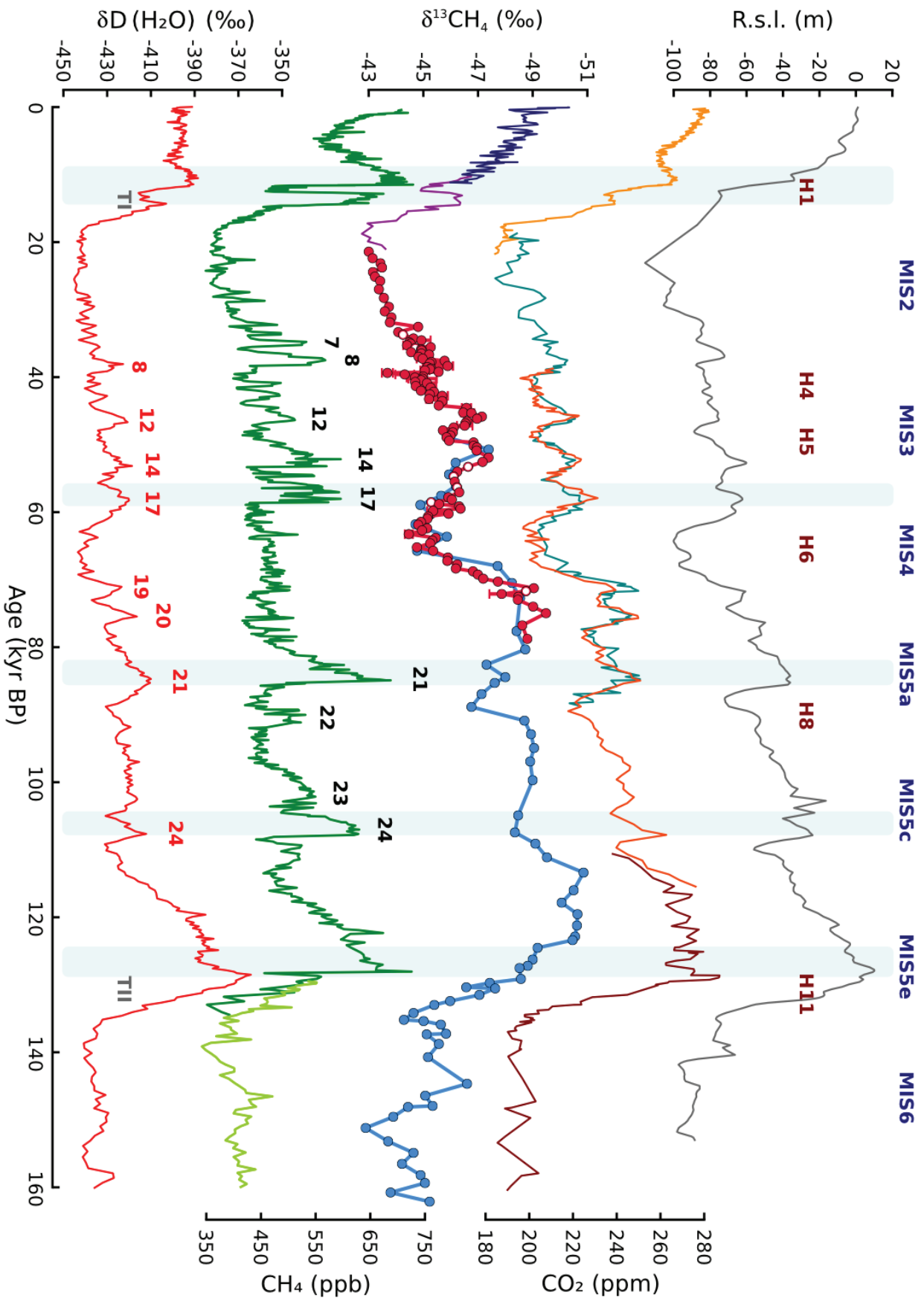


Figure 2

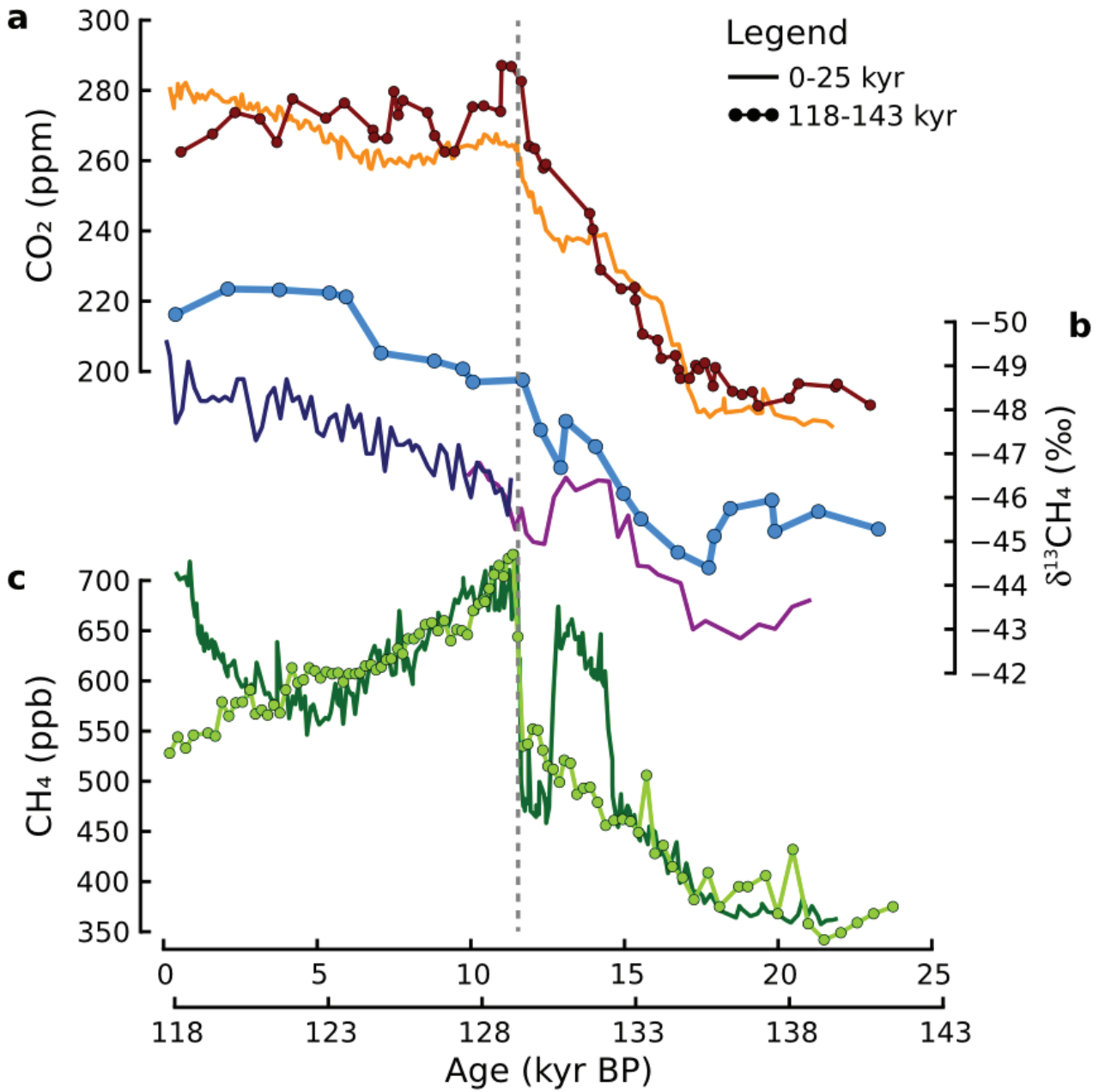
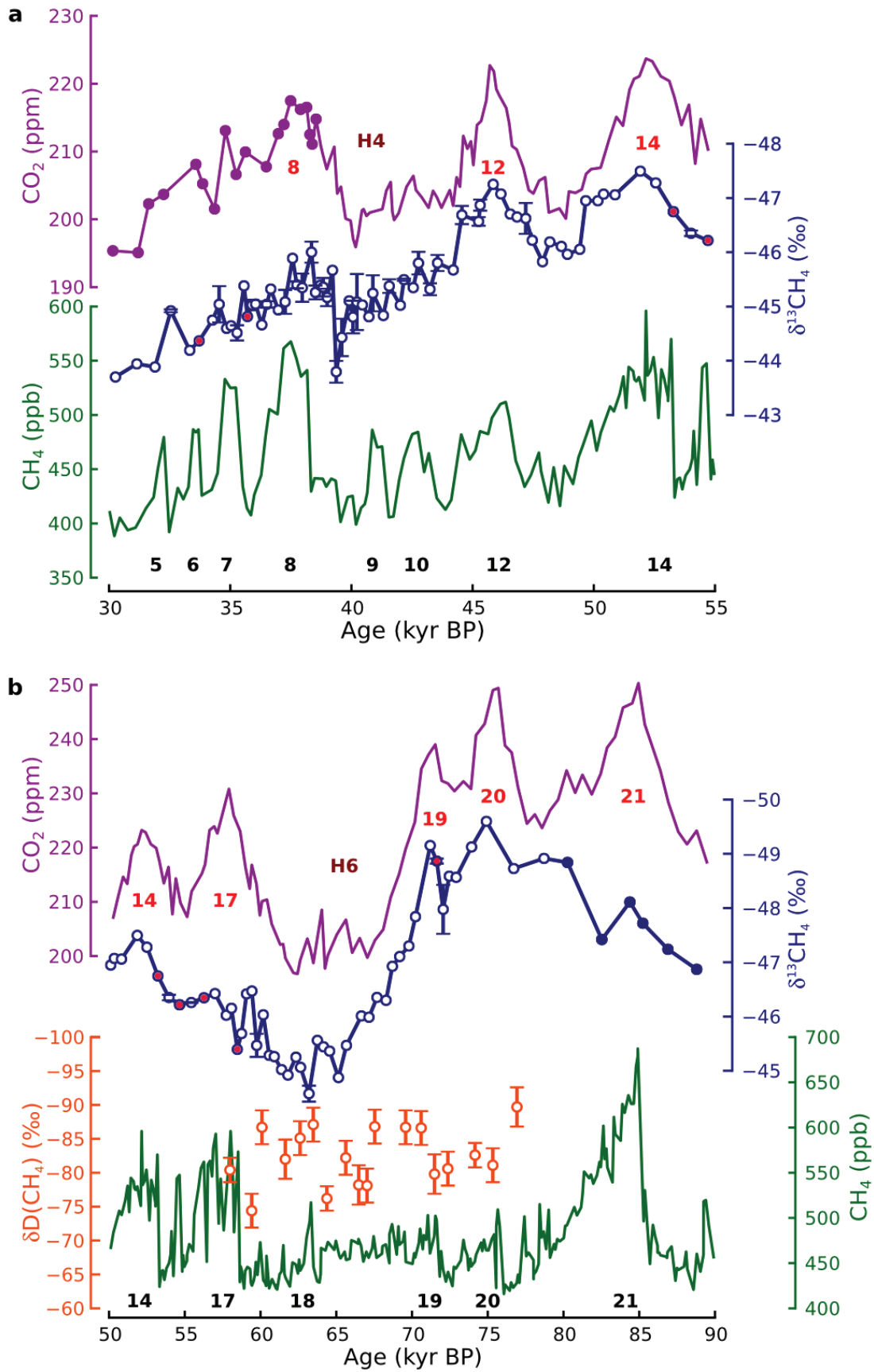


Figure 3



5.2. Extended supplementary information and discussion

5.2.1. The glacial EDML $\delta^{13}\text{CH}_4$ record

The EDML $\delta^{13}\text{CH}_4$ time series includes 129 data points and 32 replicates from different depth intervals with a mean reproducibility of the replicates of $\pm 0.18\text{‰}$. A total of 19 outliers, either caused by machine instabilities or other experimental problems, were excluded from the dataset and remeasured. Processing of the chromatogram for each measurement was performed using a self developed, fully automated peak detection, integration and referencing script written in the Python programming language (see section 4.3). This script allows uniform and comprehensible background and peak detection, genuine automation for post-processing (e.g. long term trend corrections) and data archiving. Using this script it was possible to reproduce published $\delta^{13}\text{CH}_4$ data for termination I (*Fischer et al.*, 2008), which were obtained with the software provided with the MS (Isoprime, Elementar, Germany) with an offset of 0.10‰ (1σ : 0.17‰ , $n=34$) without and 0.17‰ (1σ : 0.15‰) with correction for Kr interference (see chapter 4.5). Note that both offsets are smaller than the measurement uncertainty of this data set (*Fischer et al.*, 2008, 0.3‰ , 1σ). This re-evaluated record for termination I was used in Figures 1 and 2 in the main text (cf. section 5.1) and is further shown in figure 4.6 for comparison with the unmodified, uncorrected data of *Fischer et al.* (2008). The data are presented in Appendix C.

5.2.2. Laboratory inter-calibration between PSU and AWI

In order to minimize offsets between the absolute standardization of both laboratory setups at the AWI and the PSU, inter-calibration measurements were performed on three IPY air samples (cf. chapter 4.3.2) and on ice core samples from the WAIS Divide ice core WDC05 A ($79^\circ 27.70\text{S}$ $112^\circ 7.510\text{W}$; 1.759 masl.). Therefore, the dependence of $\Delta\delta^{13}\text{C}_{\text{Kr}}$ from CH_4 was used to account for the Kr effect encountered in the ice core and air sample measurements using the PSU instrument. The results were compared with those for the IPY air and WDC05 A measurements performed with the AWI setup that were corrected according to procedure described for the EDML ice samples in section 4.5.2. The results for both systems yield an AWI-PSU laboratory offset of 0.14‰ with respect to $\delta^{13}\text{CH}_4$ and are presented in tables 5.1 and 5.2. As a final adjustment, the Vostok $\delta^{13}\text{CH}_4$ time series was thus shifted by 0.14‰ towards lower values to account for the differences in the absolute standardizations of both laboratories. Note that this inter-laboratory offset

is significantly smaller than the measurement uncertainty of 0.3 ‰, showing that the AWI and PSU data sets are fully compatible after correction of the Kr effect.

Table 5.1.: Comparison of $\delta^{13}\text{CH}_4$ results for the measurements of air samples performed at the AWI and PSU that were part of the "2007 - IPY International Ice Core Gas Inter-calibration Exercise".

Ambient air was diluted with CH_4 free air to resemble atmospheric methane mixing ratios typical for present day (1852 ppb), pre-industrial (906 ppb) and glacial (365 ppb) conditions. $\delta^{13}\text{CH}_4$ values are reported with respect to VPDB. The first two columns report original measurements, the following two columns the respective values after the correction for Kr interference. Deviations in the carbon isotopic signature caused by the ionized Kr ($\Delta\delta^{13}\text{C}_{\text{Kr}}$) and its dependency on CH_4 levels are summarized in the final column. The results are further used to infer the absolute standardization offset between both laboratories.

| Sample ID | epoch | $\delta^{13}\text{CH}_4$ | 1σ | $\delta^{13}\text{CH}_4$ | 1σ | $\Delta\delta^{13}\text{C}_{\text{Kr}}$ |
|--|---------------|--------------------------|------------------|--------------------------|-----------|---|
| | | (‰) | (‰) | (‰) | (‰) | |
| | | Original | Corrected for Kr | | | |
| AWI analyses (5/2010) | | | | | | |
| CA03560 | present day | -47.14 | 0.05 | -47.33 | 0.06 | 0.19 |
| CC71560 | preindustrial | -47.07 | 0.09 | -47.40 | 0.12 | 0.33 |
| CA01179 | glacial | -46.25 | 0.11 | -46.97 | 0.13 | 0.72 |
| PSU analyses (7/2007) | | | | | | |
| CA03560 | present day | -47.08 | 0.16 | -47.20 | 0.16 | 0.12 |
| CC71560 | preindustrial | -47.15 | 0.10 | -47.41 | 0.10 | 0.26 |
| CA01179 | glacial | -46.86 | 0.06 | -47.52 | 0.06 | 0.66 |
| Difference (AWI - PSU) | | | | | | |
| CA03560 | present day | -0.06 | | -0.13 | | |
| CC71560 | preindustrial | 0.08 | | 0.01 | | |
| CA01179 | glacial | 0.61 | | 0.55 | | |
| Average laboratory offset | | 0.21 | | 0.14 | | |
| Standard deviation (1σ) | | 0.35 | | 0.36 | | |

5.2.3. Model results for gravitational settling and diffusional fractionation in the EDML ice core

During the enclosure of air bubbles in the polar ice sheets, the methane molecules like other air components are subject to diffusion processes in the open pore space of the firn column, which also affect their isotopic composition archived after bubble close-off (*Schwander et al.*, 1988). In the diffusive firn zone methane is subject to gravitational settling, which enriches the heavier isotope at the bottom of the firn column (e.g. *Sowers*

Table 5.2.: $\delta^{13}\text{CH}_4$ values of WDC05 A ice core material.

Samples were measured with the AWI and PSU instruments to further test the alignment of both systems. No adjustments have been applied to correct for gravitational settling. Values denoted as “original” are inferred according to the standard routines in the respective laboratories, before the correction for Krypton interference. Acquisitions with the AWI instrument were treated similarly with respect to EDML ice and IPY air samples in the Kr interference corrections based on raw data, PSU measurements using the CH_4 dependent $\Delta\delta^{13}\text{C}_{\text{Kr}}$ to account for Kr. WDC05A CH_4 values and approximate age of the samples (hash sign) were interpolated from data of *Mitchell et al.* (2011). Note, that the two PSU measurements (marked by asterisks) are not from the same depth as the AWI sample, but $\delta^{13}\text{CH}_4$ variability (1σ) is less than 0.3‰ over the depth interval 161.5 m (1593 AD) to 173.4 m (1540 AD) and thus on the the order of the analytical uncertainty (*Mischler et al.*, 2009).

| Sample ID | Lab | Depth (m) | Age [#] AD | $\delta^{13}\text{CH}_4$ | 1σ | $\delta^{13}\text{CH}_4$ | 1σ | $\Delta\delta^{13}\text{C}_{\text{Kr}}$ | n |
|-----------|-----|--------------|------------------------|--------------------------|------------------|--------------------------|-----------|---|---|
| | | | | (‰) | (‰) | (‰) | (‰) | (‰) | |
| | | | | Original | Corrected for Kr | | | | |
| WDC05A* | PSU | 164.96 | 1571 | -47.94 | - | -48.28 | - | 0.34 | - |
| WDC05A | AWI | 166.78 | 1564 | -47.53 | 0.03 | -47.85 | 0.04 | 0.32 | 2 |
| WDC05A* | PSU | 169.80 | 1551 | -47.53 | - | -47.87 | - | 0.34 | - |

[#] interpolated values derived from WDC05A CH_4 data by *Mitchell et al.* (2011)

* PSU values from *Mischler et al.* (2009)

et al. (1992)). In addition, strong concentration gradients caused by rapid atmospheric methane concentration changes induce diffusive fluxes that lead to isotopic fractionation (*Trudinger et al.*, 1997). Finally, thermal diffusion corrections are required when large temperature gradients exist in the firn layer (*Severinghaus et al.*, 2001). Temperature variations at Vostok and at the EDML core site (Kohnen Station) were relatively small and slow during the last glacial cycle. Hence, the firn column down to the close-off depth was essentially in thermal equilibrium, and thermal diffusion effects are thus negligible for the datasets presented here.

In order to quantify the impact of gravitational settling and diffusion processes (DF) on the carbon isotopic composition of CH_4 for the EDML ice core, a modeling experiment with a sudden and rapid increase of CH_4 was carried out with the diffusion and enclosure model by *Schwander et al.* (1993) adapted to glacial conditions at the EDML core site. A methane pulse of 200 ppb with an initial increase rate of 4 ppb per year and the respective decline of 0.25 ppb/yr (black line in figure 5.1, upper sub-figure) was prescribed to the model as a peak value representation of the most vigorous natural methane rises occurring during the last glacial cycle (e.g. at the strongest of the DO events (*Johnsen*

et al., 1992) or the last two deglaciations). The colored model output curves in the same sub-figure illustrate the respective methane concentration changes in isolated air parcels at the modeled "bubble" lock-in depth for three differing glacial temperature and snow accumulation scenarios at the core site. This three parameter sets include a "minimal" (-52.14 °C, 2.978 cm water equivalent per year (w.e./yr)), a "maximal" (-46.64 °C, 5.075 cm w.e./yr), and a "best guess" scenario (-49.52 °C, 3.859 cm w.e./yr), and are derived from estimates by *Siegenthaler et al.* (2005) for a realistic representation of glacial conditions at the EDML core location.

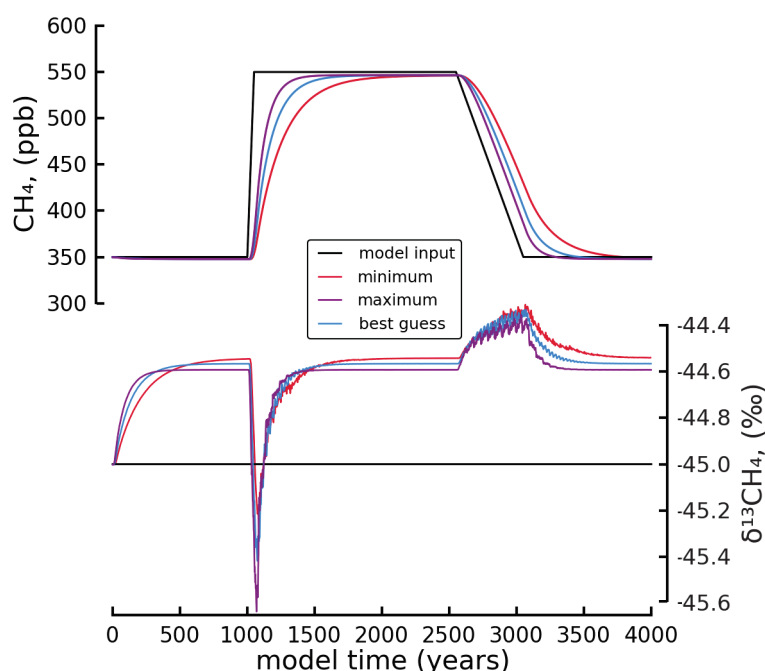


Figure 5.1.: Model results of fractionation processes in firn of EDML altering the isotopic composition of CH₄ for three prescribed local site temperature scenarios under glacial conditions (*Siegenthaler et al.*, 2005). In black the model input of CH₄ mixing ratios (upper sub-figure) at the model "surface" with a base level typical for glacial conditions and a strong 200 ppm pulse resembling the largest of CH₄ increases observed at DO warmings and glacial-interglacial transitions. The excursions in $\delta^{13}\text{CH}_4$ values induced by the "surface" CH₄ concentration changes come about due to by the separation of the two stable isotopologues of CH₄ caused by diffusion processes.

Corresponding changes in $\delta^{13}\text{CH}_4$ values of the air parcels are depicted in the lower sub-figure. The initial drift of $\delta^{13}\text{CH}_4$ towards values around -44.6‰ represent the (specific) model approximation to equilibrium conditions. Still, the offset to the value prescribed for surface $\delta^{13}\text{CH}_4$ is in good agreement with proxy results for gravitational separation inferred from $\delta^{15}\text{N}_2$ data for EDML (*Landais et al.*, 2006). Surface $\delta^{13}\text{CH}_4$ values are held constant at -45‰ for an isolated consideration of processes occurring in the mod-

eled firn pore space. Modeled peak deviations in $\delta^{13}\text{CH}_4$ in response to the CH_4 rise are in the range of roughly -0.7‰ for the minimum (red line in Figure 5.1) to -1.0‰ for the maximum site temperature scenario (purple line), respectively. However, this effect is relatively short-lived and decreases to levels below the experimental uncertainty limit of 0.3‰ in less than 150 years after the initial methane increase, indicating that only the $\delta^{13}\text{CH}_4$ samples that closely follow strong atmospheric CH_4 increases are considerably affected by the DF effect in the EDML ice core. In the best guess scenario (blue line), for example, values exceed half of the maximal excursion of -0.85‰ for only about 80 model years, and exceed the instrumental uncertainty for less than 120 years. After about 500 years the $\delta^{13}\text{CH}_4$ value is essentially back at its value from before the CH_4 increase. During the slower decline of methane concentration back to the base level of 350 ppb, the highest observed diffusional fractionation of 0.24‰ does not even exceed the measurement uncertainty. In conclusion, only those data points of the EDML $\delta^{13}\text{CH}_4$ record may be affected that fall within the relatively short time window during major methane concentration increases. Seven samples have been identified to fulfill this criterion (see the "Method Summary" in section 5.1). In view of the small amount of affected samples, and the fact that the EDML CH_4 record does not have the necessary resolution to infer reliable estimates about the size of the DF effect and the exact timing of the individual onsets of the large glacial CH_4 increases, no general correction for diffusion effects were applied to the datasets. However, one has to keep in mind that individual samples that coincide with the rapid CH_4 changes may be biased by a few tenth of a per mil towards lower (more negative) $\delta^{13}\text{CH}_4$ values.

Accordingly, all $\delta^{13}\text{CH}_4$ data are solely corrected for gravitational fractionation. Vostok samples have been corrected with interpolated $\delta^{15}\text{N}_2$ data according to published procedures (*Sowers et al.*, 1992). For the EDML ice core no $\delta^{15}\text{N}_2$ record is available to date that covers the whole time interval of the presented $\delta^{13}\text{CH}_4$ data. However, $\delta^{15}\text{N}_2$ data over the last glacial-interglacial transition vary only between 0.4 to 0.45‰ . Thus, EDML values were shifted by a constant offset of 0.41‰ to higher values. This 0.41‰ shift reflects expected values for glacial conditions very well (*Landais et al.*, 2006, 2010) and is also in line with model results for EDML (*EPICA community members*, 2006). The error introduced by this constant correction is at most 0.05‰ and thus negligible compared to the overall analytical uncertainty of 0.3‰ .

5.2.4. Age scales and ice core CH₄ synchronization

If not stated otherwise, all records shown in the publication in section 5.1 are reported with respect to the chronology by *Lemieux-Dudon et al.* (2010), hereafter denoted as “unified” age scale. The chronology was developed by inverse modeling of multiple glaciological and gas/ice stratigraphic constraints of EPICA and various other ice cores, in order to implement a consistent chronology (see section 4.4 for more detail). Where applicable, a direct age calculation was performed by linear interpolation of the depth-age relationship provided by *Lemieux-Dudon et al.* (2010). Other records required additional conversion steps according to the procedures described below.

Manual CH₄ synchronization for Vostok $\delta^{13}\text{CH}_4$ and CO₂ records

The published Vostok depth to EDC3 gas age relationship for the Vostok CO₂ record provided by *Lüthi et al.* (2008) was adopted to infer corresponding interpolated EDC3 ages for the Vostok $\delta^{13}\text{CH}_4$ data. However, an evident misalignment of the fast methane concentration rises at Dansgaard-Oeschger (DO) event 24 compared to EDC CH₄ data was found (*Loulergue et al.*, 2008). Because relative timings of $\delta^{13}\text{CH}_4$ and CH₄ rises is a special focus of this thesis, this offset was accounted for by manual methane synchronization, described in more detail in section 4.4. In this case, five tie-points between DO event 21 and Termination 2 were selected at peak flanks of the respective CH₄ rises (table 5.3) and the included data points were linearly interpolated to the EDC3 age scale (*Parrenin et al.*, 2007). The EDC3 ages including the adjusted section between 83.6 kyr BP and 128.9 kyr BP were then converted to the target “unified” age model. The adjustments were applied to the Vostok CO₂ record (*Lüthi et al.*, 2008) and Vostok $\delta^{13}\text{CH}_4$ presented in section 5.1.

Manual CH₄ synchronization for the Byrd atmospheric CO₂ record

No official age conversion to the “unified” age scale exists for the Byrd ice core. Hence, another methane synchronization between the Byrd (*Blunier and Brook*, 2001) and EDML CH₄ records (*Schilt et al.*, 2010) was performed in order to obtain corresponding EDML depths, which were then converted to “unified” ages. The limitations of the methane synchronization approach is acknowledged, especially if the resolution differences of the compared CH₄ datasets are large, or at times where CH₄ variations are low and, thus, tie-points are scarce (*Blunier et al.*, 2007). However, the very good temporal agreement of the Byrd (*Ahn and Brook*, 2008) and the EDML CO₂ data (*Bereiter et al.*, 2012)

Table 5.3.: Manual CH₄ tie-points used for the correction of the Vostok dating.

The synchronization of the misaligned Vostok section between 129-84 kyr BP (*Lüthi et al.*, 2008) was performed with EDC (*Loulergue et al.*, 2008) and Vostok atmospheric methane records (*Chappellaz et al.*, 1990). The EDC3 ages of the five listed Vostok sample depths were adjusted according to the corresponding EDC tie points. All Vostok records presented in this study are dated according to this adjustments.

| tie-point | EDC depth (m) | EDC3 age years BP | EDC CH ₄ (ppb) | Vostok depth (m) | Vostok CH ₄ (ppb) |
|-----------|------------------|----------------------|------------------------------|---------------------|---------------------------------|
| 1 | 1241.67 | 83627 | 500.7 | 1266.83 | 500.1 |
| 2 | 1367.89 | 95866 | 470.2 | 1440.34 | 470.0 |
| 3 | 1473.40 | 106781 | 510.1 | 1536.00 | 510.8 |
| 4 | 1543.59 | 115081 | 480.2 | 1635.97 | 480.4 |
| 5 | 1723.46 | 128871 | 559.9 | 1881.99 | 560.1 |

show that the relative CH₄ synchronization error is likely small and does not affect the conclusions in the publication. The list of manual tie-points applied in the Byrd–EDML CH₄ synchronization are presented in table 5.4.

No direct age conversion to the "unified" target chronology could be applied to the relative sea-level (rsl.) data, used for example in figure 1 of section 5.1, without invoking an ad-hoc phase relationship between the sea level and the ice core records. Therefore, the sea level record of *Rohling et al.* (2009) was given without any modifications, i.e. with respect to the speleothem synchronized age-scale provided by *Grant et al.* (2012).

5.2.5. Extended discussion of rapid methane variability during the last glacial

Dansgaard-Oeschger cycles

One of the main phenomena observed in the glacial $\delta^{13}\text{CH}_4$ data is the lack of a direct imprint of the rapid atmospheric methane concentration changes in conjunction with millennial-scale climate variability on the carbon isotopic signature of methane. Figure 5.2 illustrates this missing coherence on the basis of six of the strongest Dansgaard/Oeschger (DO) warmings of the last glacial period, but the observation similarly applies to the remaining DO events (cf. e.g. figure 5.3). Also shown are the two major methane increases of terminations I and II in the right pair of panels of the figure for completeness, indicating a similar lack of $\delta^{13}\text{CH}_4$ response to the corresponding CH₄ rises. Corresponding segments of CH₄ (subplot 5.2 a) and $\delta^{13}\text{CH}_4$ data (subplot 5.2 b), centered around the respective

Table 5.4.: Methane synchronization tie-points used for dating the Byrd ice core. The age conversion to the “unified” age scale (*Lemieux-Dudon et al.*, 2010) is based on EDML (*Schilt et al.*, 2010) and Byrd (*Blunier and Brook*, 2001) atmospheric methane records.

| tie-point | EDML depth (m) | “unified” age years BP | EDML CH ₄ (ppb) | Byrd depth (m) | Byrd CH ₄ (ppb) |
|-----------|-------------------|---------------------------|-------------------------------|-------------------|-------------------------------|
| 1 | 717.02 | 11599 | 609.35 | 1071.76 | 574.28 |
| 2 | 829.64 | 14543 | 529.66 | 1195.84 | 543.30 |
| 3 | 1070.95 | 23231 | 383.60 | 1446.29 | 361.95 |
| 4 | 1154.20 | 27748 | 392.50 | 1498.37 | 392.42 |
| 5 | 1173.61 | 28810 | 419.31 | 1526.10 | 417.05 |
| 6 | 1233.17 | 32339 | 435.59 | 1595.76 | 443.86 |
| 7 | 1260.48 | 33728 | 456.60 | 1617.35 | 417.67 |
| 8 | 1286.47 | 35417 | 467.63 | 1654.37 | 449.47 |
| 9 | 1337.80 | 38258 | 488.11 | 1716.45 | 490.03 |
| 10 | 1365.07 | 39433 | 423.15 | 1744.35 | 415.49 |
| 11 | 1403.97 | 41378 | 443.35 | 1780.49 | 422.27 |
| 12 | 1436.97 | 43074 | 452.35 | 1806.94 | 441.63 |
| 13 | 1489.88 | 46719 | 469.20 | 1863.57 | 461.97 |
| 14 | 1601.65 | 53264 | 491.10 | 1960.44 | 488.11 |
| 15 | 1627.36 | 54732 | 493.91 | 1973.59 | 491.04 |
| 16 | 1666.48 | 57333 | 532.10 | 2000.30 | 523.93 |
| 17 | 1680.64 | 58176 | 538.28 | 2011.48 | 533.62 |
| 18 | 1688.09 | 58586 | 497.84 | 2017.44 | 463.90 |
| 19 | 1760.37 | 63448 | 468.08 | 2062.90 | 476.49 |
| 20 | 1860.22 | 71706 | 470.32 | 2082.65 | 460.38 |
| 21 | 1914.24 | 75872 | 460.21 | 2100.52 | 455.18 |
| 22 | 1949.26 | 78706 | 480.43 | 2111.69 | 494.55 |
| 23 | 2023.03 | 85207 | 550.63 | 2133.58 | 546.72 |
| 24 | 2065.88 | 89241 | 493.35 | 2139.75 | 489.08 |

methane rise, have been aligned in order to illustrate the phasing and individual timings of the concentration changes and the corresponding changes in $\delta^{13}\text{CH}_4$. Note that the data points in $\delta^{13}\text{CH}_4$ closest to the most vigorous methane increases are possibly biased by diffusional fractionation (DF) in the firn column. The DF may lead to biased $\delta^{13}\text{CH}_4$ data close to major CH_4 changes by up to -1‰ (see the discussion in ?? for further details). The two negative $\delta^{13}\text{CH}_4$ excursions at DO 8 and termination I, for example, are located so close to the corresponding methane increase that they are presumably affected by the DF effect. It is crucial to know the exact onset of concentration changes at the surface in order to constrain which samples are definitively affected, and the EDML data by *Schilt et al.* (2010) does not provide such highly resolved CH_4 reconstructions. Nevertheless, a

150 yr box was introduced in figure 5.2 (gray bar) to visually mark the range where $\delta^{13}\text{CH}_4$ values are potentially biased by DF. The choice of 150 yrs is derived from the firnification model exercise presented in section 5.2.3 and corresponds to the period where the modeled effect of diffusional fractionation exceeded the experimental uncertainty range of 0.3‰ in the maximum surface temperature/accumulation rate scenario. Note, however, that the 150 yr box likely represents an overestimation, as it is aligned with the visual center of the increase and not to its (unfortunately unconstrained) onset.

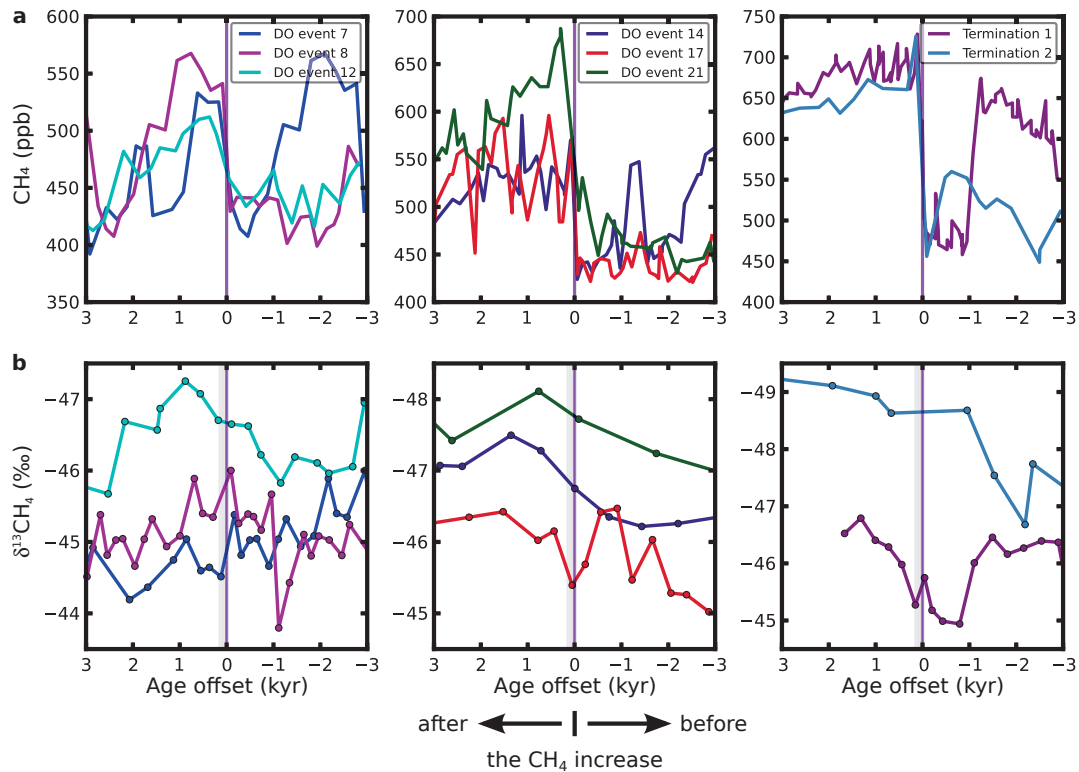


Figure 5.2.: $\delta^{13}\text{CH}_4$ response to DO climate variability. The panels show a selection of major DO methane increases during the last glacial period and the respective imprint on the CH₄ carbon isotope signature. **a** Six strong methane rises (color coding in the figure legends) coeval to major DO events (left and middle figure column) and the two ultimate terminations (right column) in a 6,000 year time window aligned and centered around the major methane rise (illustrated by the vertical gray line). CH₄ data from the EDML ice core (*Schilt et al., 2010*). **b** Time windows of the respective $\delta^{13}\text{CH}_4$ data sections from Vostok and EDML (this study, color coding and alignment according to **a**). The shaded bar represents the 150 year time window, in which data points might potentially be biased by diffusional fractionation beyond the measurement uncertainty.

The predominant sink for atmospheric CH₄ is the oxidative removal by $\cdot\text{OH}$ radicals within the troposphere. Atmospheric chemistry models suggest that changes in the sink account only for a small proportion of the atmospheric CH₄ concentration variability

over the last glacial-interglacial transition and Quaternary changes of the $\cdot\text{OH}$ induced tropospheric oxidation varied by less than 17% (*Crutzen and Brühl, 1993; Thompson et al., 1993; Martinerie et al., 1995; Levine et al., 2011b*). As a consequence, the main reason for DO CH_4 variability should be found in variations of the sources. Some possible explanations for the observation of a systematically missing response in the $\delta^{13}\text{CH}_4$ record to DO methane variability are discussed in the publication in section 5.1. In the following paragraphs, the focus will lie on some aspects of source changes that would have exceeded the scope of the discussion in the publication. A more detailed review of sink changes and how they may have affected the carbon isotopic signature of methane will also be included later in this chapter.

Source changes | The lack of net effects on the $\delta^{13}\text{CH}_4$ record at all rapid concentration changes during the last glacial period and during the last and penultimate glacial termination illustrated in figure 5.2 implies that climate-related changes of the source mix composition do not exert primary control on short-term $\delta^{13}\text{CH}_4$ variability. A considerable role of isotopically depleted high-northern latitude sources to DO CH_4 increases (*Brook et al., 1996; Dällenbach et al., 2000*), for example, is similarly precluded by the $\delta^{13}\text{CH}_4$ data as a possible systematic increase of highly ^{13}C enriched emissions from wildfires or from geologic sources. The influence of geologic sources is presumably more important for long-term climatic changes with implications for sea-level and global ice volume. Reduced sea-levels are assumed to have consequences for hydrostatic pressures and water column heights over marine CH_4 seeps or the exposure of subaerial sea-floor seeps on continental margins, and terrestrial gas seeps may respond to crustal deformations induced by glacial advances and retreats (*Judd et al., 2002; Luyendyk et al., 2005; Etiope et al., 2008b*). Methane emitted by sub-glacial environments (*Wadham et al., 2008; Boyd et al., 2010; Wadham et al., 2012*) and from Arctic continental shelves are similarly bound to the advance and retreat of the large Laurentide and Fennoscandian ice sheets and may thus contribute to long-term CH_4 variations but are not expected to be of importance on millennial time-scales. Therefore, these groups of sources will be discussed in section 5.2.6, which covers long-term changes of $\delta^{13}\text{CH}_4$.

The frequency and severity of wildfires is assumed to be elevated during DO interstadials compared to stadials (*Power et al., 2008; Daniaou et al., 2010*). Based on reconstructions of charcoal records from various sites world-wide, the authors attribute the enhanced fire activity during interstadials to elevated net primary productivity (NPP), expansion of woody and shrub-like vegetation and, thus, above-ground biomass and fuel availability.

Moreover, due to differences in flame temperatures and smoldering, increasing proportions of woody vegetation associated with DO interstadials (*Harrison and Sanchez Goñi, 2010*) are believed to emit higher amounts of reduced trace gases in comparison to stadial conditions with more open vegetation and a presumably higher abundance of grassy and herbaceous plant types (*Randerson et al., 2005*). Savanna grass pastures and dry open canopy ecosystems more prevalent in stadials are expected to burn with higher temperatures and oxygen supply and, thus, were not likely to produce considerable amounts of methane (*Bowman et al., 2009*). However, the wildfire frequency can not be used as an unambiguous measure for the size of CH₄ emissions associated with it. The rapidly decreasing amount of charcoal sample sites with increasing ages in *Daniau et al. (2010)* further raise the question as to if and to what degree the inferred z-scores are representative for a global assessment of wildfire activity in earlier phases of the last glacial period. Nevertheless, the $\delta^{13}\text{CH}_4$ data do not provide any indication for considerable, systematic increases of wildfire CH₄ emissions during DO interstadials.

It is further not very plausible to assume that large proportions of the rapid DO CH₄ increases were induced by combinations of emissions from two sources, whose net effect on $\delta^{13}\text{CH}_4$ have mutually canceled each other out. Not considering the unknowns associated with the question of how quickly boreal sources such as thermokarst lakes are likely to respond to DO interstadial warming, it is similarly unclear whether potential compensatory emissions from wildfires could contribute substantially to initial phases of the respective CH₄ increases, because the changes in NPP and vegetation shifts are assumed to cause a delay in the range of centuries (*Harrison and Sanchez Goñi, 2010*). Therefore, this is highly unlikely to have been an influential factor in early phases of DO CH₄ rises. And in light of presumably differing climate boundary conditions at each of the DO events, the requirement of a quasi-synchronous activation of both source contributions without any net effect on $\delta^{13}\text{CH}_4$ casts doubt on the influence of this mechanism on DO CH₄ variability in general.

Unfortunately, $\delta^{13}\text{CH}_4$ data cannot resolve whether and to what degree aerobic CH₄ production by terrestrial plants may have played a role in DO CH₄ variability. Median $\delta^{13}\text{C}$ values for CH₄ emissions from recent plant material range from -58.2 ‰ to -67.0 ‰ for C₃ and from -49.5 ‰ to -52.3 ‰ for C₄ plant biomass in estimates from *Keppler et al. (2006)* and *Vigano et al. (2009)*, respectively. Assuming that the signatures were tendentially more enriched during glacial climate conditions, e.g. due to the effects imposed by lowered CO₂ concentrations on C₃–C₄ plant abundance and C₃ biomass carbon isotope signatures (see the respective paragraphs in section 5.2.6 for more details), the range would still

considerably overlap with biogenic sources such as tropical wetlands. Accordingly, the $\delta^{13}\text{C}$ signatures of CH_4 emissions induced by aerobic production in plants were presumably too close to the expected mean CH_4 source signature to even qualitatively discuss potential stadial-interstadial changes with respect to this source and its consequence for the $\delta^{13}\text{CH}_4$ record. However, larger emissions of plants could be expected for periods of increased global ecosystem NPP, especially in combination with elevated levels of solar insolation during summer. The mean insolation of the summer months June, July and August are usually considered the important period for CH_4 production (e.g. *Christensen et al.* (2003), here especially in northern latitudes). Regardless of the latitudinal band the emphasis is exactly placed on in the consideration (except maybe for latitudes beyond 60° North), MIS 3 is associated with elevated mean summer insolation maxima (*Berger and Loutre*, 1991), and DO interstadials are periods of increased NPP (*Harrison and Sanchez Goñi*, 2010; *Severinghaus*, 2009). Therefore, aerobic plant emissions presumably contributed greater amounts of CH_4 during interstadials than during stadials, and likely also more in MIS 3 than in MIS 4 and 2.

The "Clathrate Gun Hypothesis" by *Kennett et al.* (2003) invokes significant and sudden emissions from gas hydrates in shallow sediments on the ocean floor that were decomposed in response to oscillations of intermediate water temperatures. The methane released from these gas hydrate deposits would have contributed to temperature rises, which would in turn further destabilize clathrate deposits in a kind of positive feedback mechanism. Given the long durations of some of the DO events (e.g. 10-12, 14, 20 and 21), the global gas hydrate inventory may simply not be large enough to have supplied the amount of methane needed to initiate and maintain the increases in atmospheric concentrations (*Etioppe et al.*, 2008b), especially in view of the relatively quick succession of events observed during the last glacial period. Moreover, highly resolved CH_4 concentration records, notably those from Greenland, should be able to detect short-lived (and thus catastrophic) releases of clathrate derived methane during periods of DO CH_4 variability, these records do not provide any indication for such events (*Brook et al.*, 2000; *Flückiger et al.*, 2004; *Huber et al.*, 2006; *Grachev et al.*, 2009; *Bock et al.*, 2012; *Baumgartner et al.*, 2013). The contributions of marine clathrate emissions cannot be unambiguously resolved by $\delta^{13}\text{CH}_4$ data, as the empirical range of source signatures covers almost the full spectrum of natural $\delta^{13}\text{C}$ variability from isotopically enriched thermogenic CH_4 of geologic origin ($\sim -40\text{‰}$) to strongly depleted signatures for biogenic methane produced in ocean sediments (*Milkov*, 2005, $\sim -75\text{‰}$). However, *Milkov* (2005) argue that the total mass of hydrate bound methane of geologic origin is significantly smaller globally than that of microbial origin. As a result,

the global average $\delta^{13}\text{C}$ signature of methane in marine gas hydrates is estimated to values below -60‰ . Taking this estimate at face value, large episodic releases of clathrate bound methane would be detectable in $\delta^{13}\text{CH}_4$ records, especially during MIS 4 and 2 when $\delta^{13}\text{CH}_4$ base levels were relatively enriched, but also during the globally slightly warmer MIS 3. None of the DO CH_4 increases between MIS 4 and 2 provide indication of corresponding excursions in $\delta^{13}\text{CH}_4$. In view of the relatively depleted typical $\delta^{13}\text{C}$ signatures of CH_4 from clathrates postulated in *Milkov* (2005), large contributions to DO CH_4 increases are considered unlikely. Finally, marine hydrate emissions represent the source with the most enriched signature wrt. $\delta\text{D}(\text{CH}_4)$, with an estimated 100 to 150‰ difference to the mean signature of all sources. Accordingly, significant CH_4 emissions from marine hydrates would induce significant excursions towards enriched values in $\delta\text{D}(\text{CH}_4)$, which are observed neither for the last glacial-interglacial termination (*Sowers*, 2006) nor for two pronounced DO events 7 and 8 (*Bock et al.*, 2010b), also in line with ^{14}C data for the YD–PB transition by *Petrenko et al.* (2009).

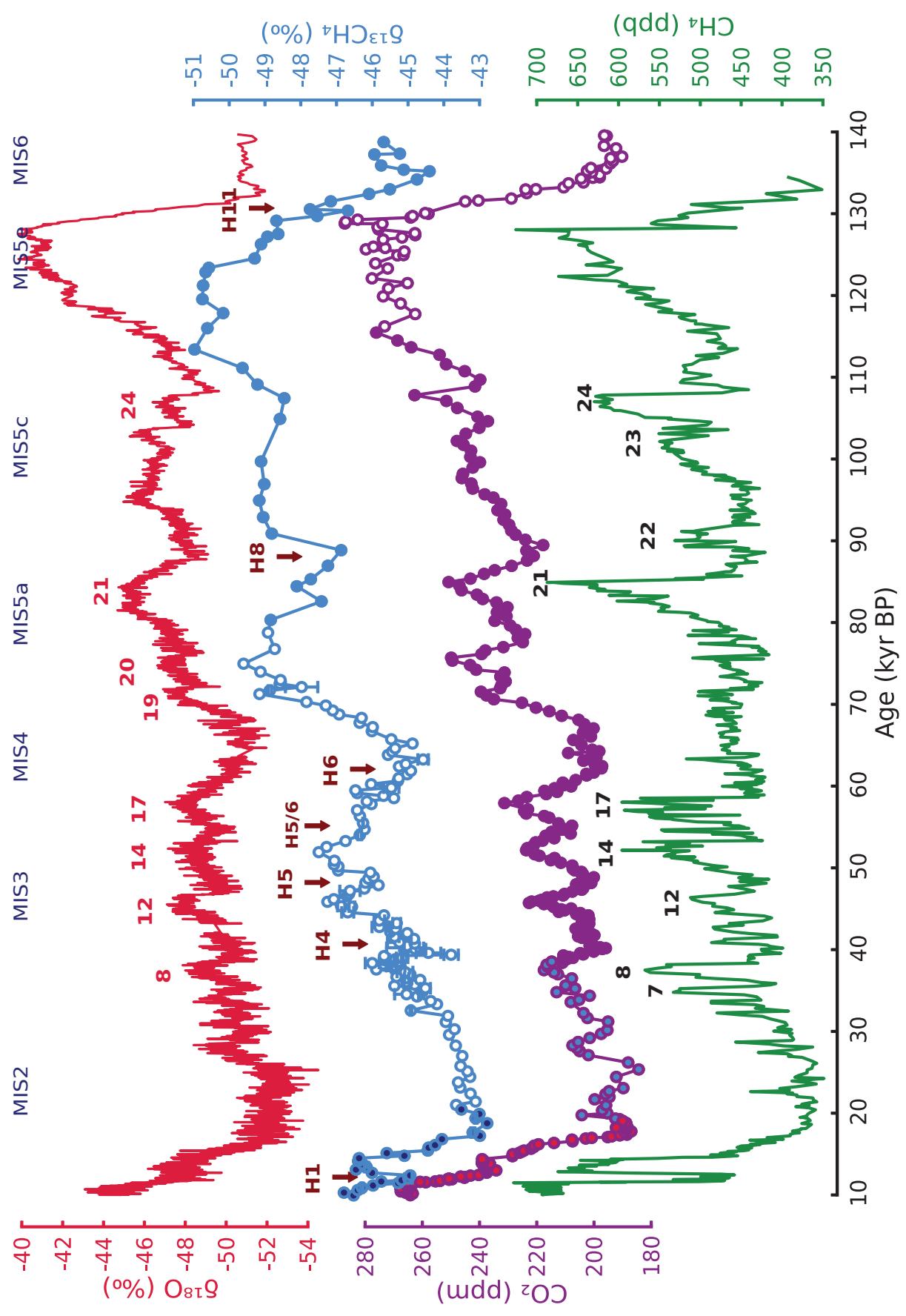


Figure 5.3.: Variability in two atmospheric trace gases over more than a full glacial cycle. From top: $\delta^{18}\text{O}$ of precipitation (*EPICA community members*, 2006, EDML), composite record of $\delta^{13}\text{C}$ of CH_4 (open blue circles from EDML, closed light blue circles from Vostok, this study, closed dark blue circles from EDML (*Fischer et al.*, 2008)), composite record of CO_2 (closed red circles from EDC (*Monnin et al.*, 2001), closed blue circles from Byrd (*Ahn and Brook*, 2008), closed unicolored circles from Talos Dome/EDML (*Bereiter et al.*, 2012) and open circles from Vostok (*Petit et al.*, 1999), more details in section 5.2.6), atmospheric methane concentration (*Schilt et al.*, 2010, green line, EDML). The estimated onsets of Heinrich events (H) are indicated by dark red arrows, DO interstadials as black, corresponding AIMs as red numbers. The records are given wrt. the 'unified' chronology (*Lemieux-Dudon et al.*, 2010).

Sink changes | Considering sink processes, significant changes to $\delta^{13}\text{CH}_4$ would require either considerable changes to the typical fractionation α associated with one or more of the influential individual sinks, or large relative shifts in the contribution of individual sinks to the overall sink term. Proportional scaling of the general oxidative capacity of atmospheric and terrestrial sinks would affect the atmospheric residence time of CH_4 (τ_{CH_4}) but would remain entirely neutral wrt. the isotopic signature of methane under steady state conditions (*Tans*, 1997). As indicated earlier in this chapter, the tropospheric oxidation by $\cdot\text{OH}$ radicals is believed to vary in the range of up to 17% on glacial-interglacial time-scales (*Crutzen and Brühl*, 1993; *Thompson et al.*, 1993). Subsequent model studies suggest that the variation may be even larger (25% and 22%), due to substantial changes in the concentration of NMVOCs over the course of the glacial termination that were not included in the previous studies (*Valdes et al.*, 2005; *Kaplan et al.*, 2006). NMVOCs are short-lived compounds such as isoprene, terpenes, acetone, methanol and various others emitted mainly by terrestrial vegetation and are known to compete with CH_4 for their common primary sink, the tropospheric $\cdot\text{OH}$ radicals. The changes in $\cdot\text{OH}$ concentration between the LGM and the PIH were calculated to induce a lifetime increase of 17–29% during termination I (*Valdes et al.*, 2005; *Kaplan et al.*, 2006). However, *Levine et al.* (2011b) inferred from a chemistry-transport model that the increase in τ_{CH_4} caused by NMVOCs would largely be compensated by increasing air temperatures over the same period that would have induced elevated humidity and thus increased both $\cdot\text{OH}$ formation and reactivity towards CH_4 due to altered kinetics, reducing the expected overall changes of τ_{CH_4} to only 2–3%. In a follow-up study, *Levine et al.* (2012) demonstrated that the two physical effects of changes in air temperature similarly negate elevated NMVOC concentrations (by $\sim 10\%$) during idealized DO interstadials in comparison to the respective stadials (*Hopcroft et al.*, 2011). Accordingly, one direct implication of this findings for

DO CH_4 variability would be that the CH_4 concentration changes are almost entirely source-driven. Another is, that a relative reduction of the $\cdot\text{OH}$ fraction with a relatively low fractionation factor α in favor of sink processes that induce higher fractionations could be considered rather unlikely, implying that no major changes to the overall sink fractionation occurred during DO stadial-interstadial transitions. Whether the changes of the kinetics of the removal reaction of CH_4 through $\cdot\text{OH}$ due to air temperature changes during DO climate variability would have a consequence for α_{OH} has not been determined yet. However, α_{OH} was postulated to be independent of temperature variability between 0° and 80°C (Cantrell *et al.*, 1990; Saueressig *et al.*, 2001). Moreover, despite the relatively large temperature differences of several degrees inferred for high-northern latitudes over DO stadial-interstadial transitions (e.g. Huber *et al.* (2006)), temperature variability in tropical regions was presumably much lower and in the range of $0.4\text{--}1.0^\circ\text{C}$ (Hopcroft *et al.*, 2011). Given that only an estimated 25 % of the CH_4 is oxidized outside of the tropics (Levine *et al.*, 2011b, and references within), the fractionation induced by the KIE of $\cdot\text{OH}$ should not be affected significantly.

Glacial-interglacial changes of the stratospheric sink, a combination of CH_4 removal by $\cdot\text{OH}$, O^1D and $\text{Cl}\cdot$, was estimated to be negligible due to the minimal total effect on $\delta^{13}\text{CH}_4$ induced by this source (Schaefer and Whiticar, 2008, and references within), in line with results by Martinerie *et al.* (1995). Similar assumptions can be made for DO climate variability. Another sink, however, is considered variable on glacial-interglacial time-scales. CH_4 oxidation in soils is controlled by diffusion, soil moisture and microbial oxidation rates (Schaefer and Whiticar, 2008, and references within). Schaefer and Whiticar (2008) suggest that the soil sink would almost be absent during the LGM. That would be due to lowered glacial temperatures, the generally drier glacial conditions, changes in the ice-free surface area available for CH_4 uptake, and finally, lowered atmospheric CH_4 concentrations, which is expected to cause most soil microbial communities to starve. These assumptions were in line with a process-based model which proposed a near shut-down of the soil sink during the LGM (Kaplan, 2002, $\sim 0.6\text{ Tg yr}^{-1}$). Due to the temperature dependency of the microbial soil oxidation reaction, the fractionation α_{Soil} induced by this sink was presumably increased during the glacial period. The combined effects of reduced contributions of the soil sink and changes to α_{Soil} inferred for the LGM led to a glacial-interglacial difference of the total sink fractionation ϵ_{WT} of $\sim 2.3\text{‰}$ wrt. $\delta^{13}\text{CH}_4$ in the first-order approximation by Schaefer and Whiticar (2008). This value is based on two assumptions that presumably make the total effect of the soil sink an upper-limit estimate for the glacial period. First, the LGM-PIH global temperature difference of

7° C that was chosen for consistency with the study by *Collatz et al.* (1998) is significantly higher than estimates from other, more comprehensive climate models (*Joos et al.*, 2004; *Braconnot et al.*, 2007; *Claussen*, 2009; *Woillez et al.*, 2011), which center around values of 4° C for the respective change. Second, the main cause for the postulated near shut-down of the soil sink during the LGM was the proximity of the glacial CH₄ concentration minimum to the linearity threshold for microbial kinetics, presumably causing most of the methanotrophs to starve under those conditions (*Schaefer and Whiticar*, 2008). However, stadial CH₄ base levels were elevated by ~100 ppm over much of the glacial period in comparison to the LGM. The microbial starvation should thus be less pronounced during MIS 5–3 stadials and less influential during DO climate variability. Moreover, elevated summer solar insolation in mid-northern latitudes during MIS 3 should have maintained suitable conditions for methanotrophic soil respiration also in the extra-tropical, not permanently ice-covered Northern hemisphere. Finally, (except for peak glacial conditions in the LGM) there is no apparent reason to assume that the soil sink was drastically reduced in tropical regions, especially in view of the shift of ice-free land area from higher latitudes to tropical regions due to lowered sea-levels and the exposure of continental shelves (*Kaplan*, 2002; *Prentice et al.*, 2011). Performing a first-order approximation for an ideal stadial-interstadial change of 100 ppb with the assumptions of an unchanged stratospheric sink, a stadial-interstadial difference of global annual mean temperature of 2°–3° C, and an upper-bound estimate of a doubling of the soil sink fraction of 3% (~5 Tg yr⁻¹ of a 170 Tg yr⁻¹ total sink flux) during stadials to 6% for interstadials (~12 Tg yr⁻¹ out of 207 Tg yr⁻¹) would in both cases lead to a change of the total sink fractionation $\Delta\epsilon_{\text{WT}}$ of ~+0.55‰, i.e. almost twice the analytical uncertainty of the $\delta^{13}\text{CH}_4$ measurements. Note that the sink fraction increase of 3% in this example was prescribed to be entirely at the cost of the ·OH sink (with very low α_{OH}) in order to maintain a total sink of 100%. Including the stratospheric sink in a proportional reduction in favor of the soil sink only slightly reduces $\Delta\epsilon$ to values around 0.5‰, which should still be detectable in $\delta^{13}\text{CH}_4$ as enriched values during interstadials. Except for stadial-interstadial shifts in ice-free surface area, the response to increased temperatures and diffusive CH₄ flux should have a rather instantaneous effect on the soil sink. However, there is no apparent systematic increase in DO interstadial $\delta^{13}\text{CH}_4$ in the data, suggesting that the assumptions about the soil sink activation during DO warmings or the stadial base activity likely represent an upper limit.

The first-order estimates mentioned thus far disregarded an influence by the chlorine radical sink in the MBL, which was postulated based on the observations of anomalously

depleted values of atmospheric $\delta^{13}\text{CH}_4$ and an exceptionally high seasonal variability in the southern Pacific (*Allan et al.*, 2001a,b; *Platt et al.*, 2004; *Allan et al.*, 2005, 2007, 2010; *Lassey et al.*, 2011). Similar to the soil sink, the MBL Cl sink (Cl_{MBL}) is considered very influential wrt. $\delta^{13}\text{CH}_4$ owing to the relatively high fractionation associated with the CH_4 removal via Cl radicals (*Saueressig et al.*, 1995, $\alpha_{\text{Cl}} > 1.06$). Accordingly, an assumed 3-4% contribution of Cl_{MBL} would cause a 2.6‰ higher total sink fractionation ϵ_{WT} than estimates disregarding this sink. *Levine et al.* (2011a) have used a variety of general circulation models to calculate Cl_{MBL} concentration changes as a function of temperature and ocean surface wind speeds for the last glacial-interglacial termination and found Cl_{MBL} variations that would induce changes to $\delta^{13}\text{CH}_4$ in the range of 10% of the 3.5‰ difference between the LGM and the early Holocene (*Fischer et al.*, 2008). Respective changes of Cl_{MBL} for DO variability are not easy to quantify, as these rapid, short-term changes of global climate parameters are profoundly different to those of a deglaciation. Changes in the sea-salt aerosol (SSA) concentration over DO cycles recorded in polar ice cores (e.g. *Fischer et al.* (2007)), which is assumed to be associated with the formation of Cl_{MBL} (*Levine et al.*, 2011a, and references within), suggest that there is the potential for DO variations in Cl_{MBL} formation. However, the model simulations by *Levine et al.* (2011a) inferred a reduction of Cl_{MBL} abundance for the LGM, which is interpreted as the primary cause for the associated modeled depletion in $\delta^{13}\text{CH}_4$, although ice core records indicate an LGM increase in sea salt by a factor of 15 and 3 for the Arctic and Antarctic, respectively (*Fischer et al.*, 2007; *Levine et al.*, 2011a). Accordingly, the correlation of global Cl_{MBL} abundance and SSA concentrations does not seem to be a reliable indicator for potential DO changes in $\delta^{13}\text{CH}_4$ induced by the Cl_{MBL} sink. Simple scaling of the estimated Cl_{MBL} sink effect to DO temperature variability (i.e. $\sim 50\%$ of 0.35‰), supposedly justified by its influence on the kinetic reaction rates of Cl_{MBL} with CH_4 , would yield a DO interstadial enrichment below the analytical uncertainty threshold of the $\delta^{13}\text{CH}_4$ acquisitions. However, in combination with the estimates for changes in the soil sink, stadial-interstadial changes in ϵ_{WT} should lead to $\delta^{13}\text{CH}_4$ variability in the range of 0.35‰ to 0.65‰.

Heinrich events

While $\delta^{13}\text{CH}_4$ variability appears to be fundamentally decoupled from DO CH_4 changes, there are indications of an influence of the climatic perturbations caused by the strongest Heinrich events (H) on the methane isotopic signature. Heinrich events are periods of

500 ± 250 years characterized by massive discharges of icebergs calving from the Laurentide and (to a lesser degree) Fenno-Scandian ice sheets evidenced by layers of ice-rafted debris (IRD) recorded in marine mid-latitude sediment cores in the North-Atlantic region (Heinrich, 1988; Bond *et al.*, 1993; Hemming, 2004). These events are associated with pronounced northern-hemispheric cooling and a strong global precipitation feedback (Wang *et al.*, 2001, 2004, 2008b; Fleitmann *et al.*, 2009; Kanner *et al.*, 2012). The cooling is thought to be due to a strong reduction in or even stagnation of North Atlantic Deep Water formation induced by the massive freshwater input and corresponding reduction of sea surface salinity (Bond *et al.*, 1993; Shackleton *et al.*, 2000; McManus *et al.*, 2004) that is essential for the latitudinal heat transport from the tropics to the North Atlantic via the AMOC. Consequently, the cooling in North-Atlantic regions is accompanied by significant warming in the southern hemisphere that is documented i.a. by a sea-level rise in the order of 10-30 m (Siddall *et al.*, 2003; Arz *et al.*, 2007; Rohling *et al.*, 2009; Grant *et al.*, 2012) and by increasing temperature over Antarctica (Blunier and Brook, 2001; EPICA community members, 2006; Jouzel *et al.*, 2007).

The $\delta^{13}\text{CH}_4$ data indicate a short term enrichment of more than 1‰ in response to the arguably strongest glacial H event 4 at ~40 kyr BP, as well as pronounced maxima in the $\delta^{13}\text{CH}_4$ record at H5, H6, H8 and even H11 (see figure 5.3), which interrupts termination II (de Abreu *et al.*, 2003). The same H event 4 similarly caused a dip in δD of methane measured on NGRIP ice by Bock *et al.* (2010b), both the $\delta^{13}\text{C}$ and δD response in CH_4 roughly coinciding with the H4 induced Southern Ocean warming, indicated by the corresponding Antarctic temperature increase (EPICA community members, 2006, see figure 5.4). While the ~500 year enrichment trend in $\delta^{13}\text{CH}_4$ is suddenly inversed within < 150 years at around 39.4 kyr BP following the Southern Ocean temperature and CO_2 increase (discussed in the following sub-section), $\delta\text{D}(\text{CH}_4)$ data show a plateau for additional ~700 years at around -82‰ before the steep $\delta\text{D}(\text{CH}_4)$ drop of 16‰ occurred a few centuries before the major CH_4 increase at DO event 8. The strong drop in $\delta\text{D}(\text{CH}_4)$ could only be explained by strongly δD depleted northern high-latitude CH_4 emissions due to a strongly depleted water source. Assuming a significant difference in $\delta^{13}\text{C}$ signatures of boreal vs. tropical sources this seems not to agree with our new observations of $\delta^{13}\text{CH}_4$, which are stable in that time. $\delta\text{D}(\text{CH}_4)$ is assumed to predominantly reflect the δD signature of environmental water (Waldron *et al.*, 1999; Chanton *et al.*, 2006; Sowers, 2006; Bock *et al.*, 2010b). Thus, the 16‰ shift in $\delta\text{D}(\text{CH}_4)$ would suggest an increasing contribution of boreal CH_4 sources due to relatively depleted precipitation in high northern latitudes. CH_4 data from NGRIP suggest only minor CH_4 concentration

increases (< 30 ppb) (*Baumgartner et al.*, 2013) coeval to the $\delta D(\text{CH}_4)$ shift, while EDML merely indicates a plateau (the difference may arise from the different gas enclosure characteristics at both sites). Contemporary $\delta^{13}\text{CH}_4$ levels do not show a clear trend. From the perspective of assumed considerable differences for the $\delta^{13}\text{CH}_4$ signatures of boreal and tropical wetlands, the new $\delta^{13}\text{CH}_4$ observations cannot support the assumption that the 16‰ drift in $\delta D(\text{CH}_4)$ is due to elevated boreal wetland CH_4 emissions. Note that the difference of the source isotopic signature of boreal and tropical wetlands is hardly constrained and that a smaller difference of the latter would bring both interpretations to closer agreement: CH_4 concentration and $\delta^{13}\text{CH}_4$ are mainly determined by tropical processes while $\delta D(\text{CH}_4)$ indicates boreal imprints superimposed.

Classically, the $\delta^{13}\text{C}$ trend during H event 4 towards higher values would call for emissions of CH_4 from an enriched source like biomass burning or thermogenic CH_4 from geologic sources, or alternatively, a corresponding sink effect. Geologic emissions are not expected to change on such short time-scales (*Judd et al.*, 2002). In fact, they are not assumed to change considerably even over glacial-interglacial time scales (*Luyendyk et al.*, 2005; *Etioppe et al.*, 2008b, discussed in more details in section 5.2.6 below). Findings from stadial-interstadial paleo-fire reconstructions (*Daniau et al.*, 2010) suggest lower wildfire activity during stadials rather than higher, in line with the contemporary negative excursion in $\delta D(\text{CH}_4)$. Relative shifts in the sink mix, e.g. an increasing importance of the Cl_{MBL} sink during Heinrich events due to major changes of ocean surface wind velocities as a consequence of increasing latitudinal temperature gradients, or variations of the soil sink due to the changes in global precipitation patterns and soil temperatures, would both induce changes in the same direction wrt. δD and $\delta^{13}\text{C}$ of methane and can thus be ruled out as valid explanations. Similar to what is observed for the MIS 5–4 transition, the $\delta^{13}\text{CH}_4$ and $\delta D(\text{CH}_4)$ evolution over H4 and the subsequent DO events 7 and 8 appear entirely independent of each other.

The lack of covariation of $\delta^{13}\text{CH}_4$ and $\delta D(\text{CH}_4)$ during these periods supports the idea that both CH_4 isotopic species are dominated by entirely independent parameters, i.e. the carbon isotopic signature of decomposing plant biomass on the one hand and hydrological variations reflected in $\delta D(\text{CH}_4)$ on the other. A relatively precise picture of the global extent (*Voelker*, 2002) and the local implications of reduced AMOC and Heinrich stadial climate can be drawn from the increasing wealth of terrestrial and marine proxy evidence (see e.g. *Clark et al.* (2007) for a comprehensive review). The hydrological implications of Heinrich events on low-latitudes and tropical wetlands, however, are neither uniform nor unequivocal. For example, while the hydrological cycle during Heinrich events was

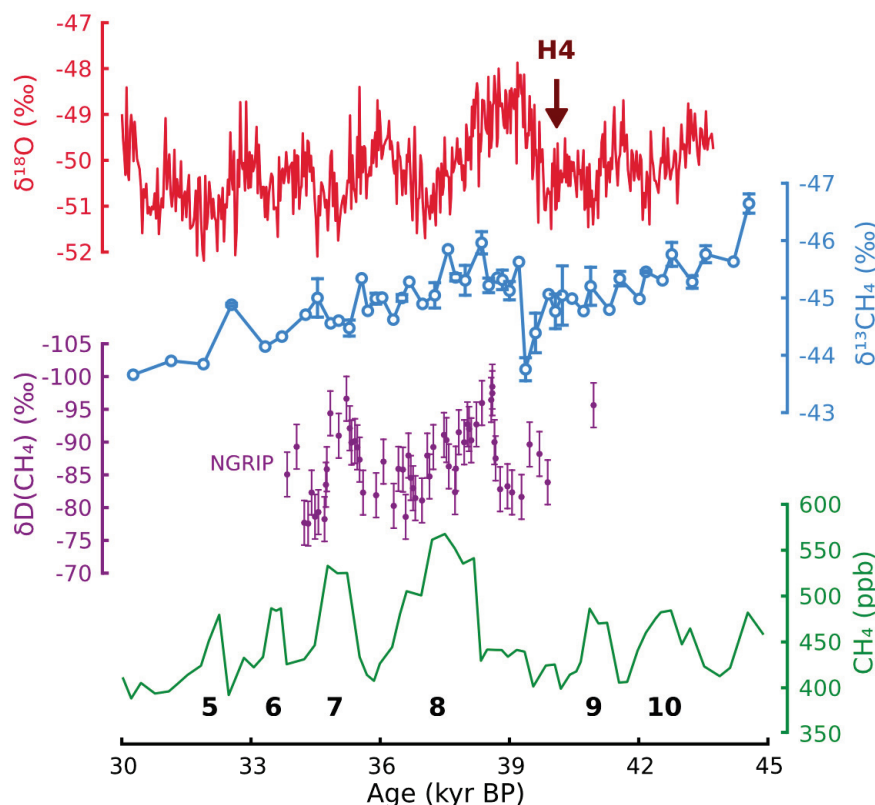


Figure 5.4.: $\delta^{13}\text{CH}_4$ & $\delta\text{D}(\text{CH}_4)$ response to Heinrich event 4. This figure illustrates the variations of (from the bottom) atmospheric methane concentration (*Schilt et al.*, 2010, EDML), both δD (*Bock et al.*, 2010b, NGRIP) and $\delta^{13}\text{C}$ of CH_4 (EDML, this study), and $\delta^{18}\text{O}$ of precipitation (*EPICA community members*, 2006, EDML) over a period of five DO events (black numbers) and Heinrich event 4 (H4, the potential onset indicated by a dark red arrow) during MIS3 as recorded in ice cores. The records are given wrt. the 'unified' chronology (*Lemieux-Dudon et al.*, 2010).

enhanced over northeastern Brazil (*Wang et al.*, 2004) and in the Peruvian Altiplano (*Baker*, 2001) and Andes (*Kanner et al.*, 2012), northeastern Africa and large parts of Asia were presumably drier (*Ivanochko et al.*, 2005), which led to a suppression of Arabian and East Asian monsoons (*Wang et al.*, 2001; *Cai et al.*, 2006; *Lewis et al.*, 2010). These changes are associated with a latitudinal displacement of the mean position of the ITCZ that is associated with major changes in the distribution patterns of global precipitation (*Lea et al.*, 2003; *Burns et al.*, 2003; *Wang et al.*, 2004; *Cruz et al.*, 2005; *Peterson and Haug*, 2006; *Leduc et al.*, 2007; *Wang et al.*, 2008b). However, the local consequences on the hydrology, areal extent, the productivity and seasonality of tropical wetlands are not known, and so are the global implications for $\delta^{13}\text{CH}_4$ and $\delta\text{D}(\text{CH}_4)$ of tropical wetland emissions. Vegetation shifts during Heinrich events occur on a global scale (reviewed for example in *Hessler et al.* (2010)), such as shifts from open to closed canopy vegetation

with potential implications for C₃/C₄ plant ratios presumably affecting $\delta^{13}\text{CH}_4$, but a coherent picture of the consequences of vegetation and hydrological changes especially wrt. wetland vegetation remains elusive. Accordingly, one can only speculate that the Heinrich $\delta^{13}\text{CH}_4$ changes were a consequence of a net increase of contributions from C₄ vegetation decomposed in tropical wetlands, that may have been induced by corresponding reductions of atmospheric CO₂, mean annual air temperatures and global (wetland) net effects of reduced precipitation intensity. Reduced river run-off in northern South America at Heinrich events could be interpreted as such (*Peterson et al.*, 2000). Weakened East Asian monsoon strengths indicate similarly reduced Asian Summer Monsoons for India and South-East Asia (*Wang et al.*, 2001; *Cai et al.*, 2006). The $\delta^{18}\text{O}$ reconstructions from calcite of speleothems at that sites indicate shifts in the range of 1-2 ‰ for the stronger Heinrich stadials H4 and H5. This would translate into corresponding shifts $\sim 8\text{--}16$ ‰ in δD of precipitation according to the slope of the meteoric line in the relationship of δD and $\delta^{18}\text{O}$ of precipitation¹. Consequently, large proportions of the relatively low glacial variability of $\delta\text{D}(\text{CH}_4)$ in the range of 10–15 ‰ may go back on the δD variations of meteoric water in mid- to low-latitudes, but these could only be assessed properly if shifts in the locations and individual emission rates of wetland source regions could be constrained better. Unfortunately, this is not possible right now. Significant changes to low latitude monsoon rainfall, however, have been documented in various cave speleothem records (*Wang et al.*, 2001, 2004; *Cruz et al.*, 2005; *Wang et al.*, 2008b; *Fleitmann et al.*, 2009; *Kanner et al.*, 2012), and in $\delta^{18}\text{O}$ of O₂ for the stadial-interstadial cycles (*Severinghaus*, 2009). Further indications for the proposed mid- to low-latitudes shifts of δD of precipitation may arise from further research concerning δD of leaf waxes from ocean and lake sediments that have been shown to vary considerably (*Tierney et al.*, 2008, 2010; *Collins et al.*, 2013). However, their interpretative value may similarly be limited due to their regional character and the fact that these locations are potentially not representative of major tropical methane sources.

Role of water table changes

The hydrological changes discussed in the last paragraphs also have direct implications on water table heights in wetlands. The soil oxidative layer thickness directly affects the net/gross primary productivity and thus CH₄ emission strength of a given wetland system. But an increased/decreased oxidative layer thickness would also induce an enrichment/de-

¹ $\delta\text{D} = 8 \times \delta^{18}\text{O} + 10$

pletion in the mean $\delta^{13}\text{CH}_4$ signature of emitted methane, as a higher/lower proportion of methane is oxidized on its way to the surface. This parameter is highly dependent on the local hydrology, topography and soil characteristics and poorly constrained spatially and temporally. The new $\delta^{13}\text{CH}_4$ record suggests that it is of minor importance for the millennial scale variability of methane over DO cycles or is compensated on a global scale as there is no remarkable imprint of DO climate variability on $\delta^{13}\text{CH}_4$. A general contribution to the glacial-interglacial difference in $\delta^{13}\text{CH}_4$ due to enhanced global aridity in the course of the glaciation, however, cannot be ruled out.

Final thoughts about the interpretation of rapid CH_4 variability

The systematic lack of response of $\delta^{13}\text{CH}_4$ to rapid DO variability is probably the most surprising and controversial finding of the whole 160 kyr $\delta^{13}\text{CH}_4$ sequence. However, much of the interpretation of DO $\delta^{13}\text{CH}_4$ data is centered around a series of assumptions inferred from contemporary observations, which self-evidently define the boundaries of the understanding and horizon of expectations of the processes in the past. That is plainly a natural consequence of the lack of direct observations and experience. One of these contemporary observations is the systematic difference of $\delta^{13}\text{CH}_4$ source signatures from wetlands in low and high latitudes. The paradigm of 'highly depleted' signatures for boreal wetlands is the main reason, why their contribution to DO CH_4 rises is more or less precluded categorically. The evidence from recent observations of boreal sources is unequivocal. Thermokarst lakes for example emit CH_4 with very depleted signatures today (*Walter et al.*, 2007). However, thus far it is impossible to proof, how much these lakes have contributed to the 'boreal' source during the glacial period or the DO climate fluctuations. It is possibly even hard to proof, though a likely assumption, that the $\delta^{13}\text{CH}_4$ signatures of thermokarst lakes at that time were similarly depleted. Model studies (*Kaplan*, 2002) and $\delta\text{D}(\text{CH}_4)$ data over DO 7 and 8 (*Bock et al.*, 2010b) suggest a contribution from northern latitude wetlands. Reconstructions of the IPD similarly indicate elevated CH_4 emissions into the northern hemisphere (*Baumgartner et al.*, 2012), even though the interpretation of the IPD is not unambiguous wrt. to the allocation of these emissions to the high North. However, $\delta^{13}\text{CH}_4$ precludes a contribution that would significantly change the source mix. Considering the observations of $\delta^{13}\text{CH}_4$ over longer time-scales, that are presented in the publication in 5.1 and in the following section, it is maybe also possible, that there is something fundamentally wrong in the present-day understanding of the under-laying processes, that there is a piece missing in the puzzle

of past CH₄ variability. The contemporary distribution of wetland area (e.g. *Lehner and Döll* (2004)) with two maxima in the low and high northern latitudes suggests a classification as 'boreal' and 'tropical' wetlands. Climate reconstructions suggest increasingly steep low to high latitude temperature gradients and latitudinal compressions of the major meteorologic features distributing atmospheric energy and moisture due to the growing ice masses on the poles (e.g. *Prentice et al.* (2011)). This contraction is estimated to force former high-latitude sources to migrate pole-wards (*Kaplan*, 2002). However, no reliable estimate exists what consequences this migration had on the latitudinal distribution of wetland area, and further, if the most northern (from a modern perspective still mid-latitude) wetlands would still bear a similarly distinctive $\delta^{13}\text{CH}_4$ signature. Assuming that the glacial global wetland distribution would form a continuous latitudinal band with a more or less uniform source signature rather than two distinctive maxima with differing $\delta^{13}\text{CH}_4$ signatures, the observations in $\delta^{13}\text{CH}_4$ and previous inferences could be brought to much higher agreement.

5.2.6. Extended discussion of long-term variability of $\delta^{13}\text{CH}_4$

The discussion in the previous section focused mainly on the very low coherence of $\delta^{13}\text{CH}_4$ and CH₄ concentration, which is documented in numbers by the very low correlation coefficient of only 0.29 (r^2 , see figure 5.5). The following section will reflect on the general, long-term climatic evolution over the last glacial period and two glacial terminations, and how the globally integrated $\delta^{13}\text{CH}_4$ signal recorded in the Antarctic ice cores EDML and Vostok was influenced by this variability. In the publication in section 5.1 the main observations and concepts for their explanation were already introduced. The following chapters, however, will provide a more detailed discussion of these concepts, and will introduce some additional aspects that may help to shed some more light on the observations in $\delta^{13}\text{CH}_4$ and processes that influence its long-term variability.

Figure 5.3 illustrates the remarkable resemblance of $\delta^{13}\text{CH}_4$ variations to atmospheric CO₂ and southern hemisphere temperature that is documented by the high coherence of $\delta^{13}\text{CH}_4$ to CO₂ ($r^2=0.74$) and to the temperature proxy $\delta^{18}\text{O}$ ($r^2=0.63$). A smaller coherence is inferred to sea level variations and hence to continental ice volume ($r^2=0.47$, see the notes in figure 5.5).

The southern hemisphere temperatures recorded in Antarctic ice cores reflect the southern mode of the energy balance between both hemispheres and the latitudinal heat transfer from the great Southern Ocean reservoir and warm tropical regions into northern Atlantic

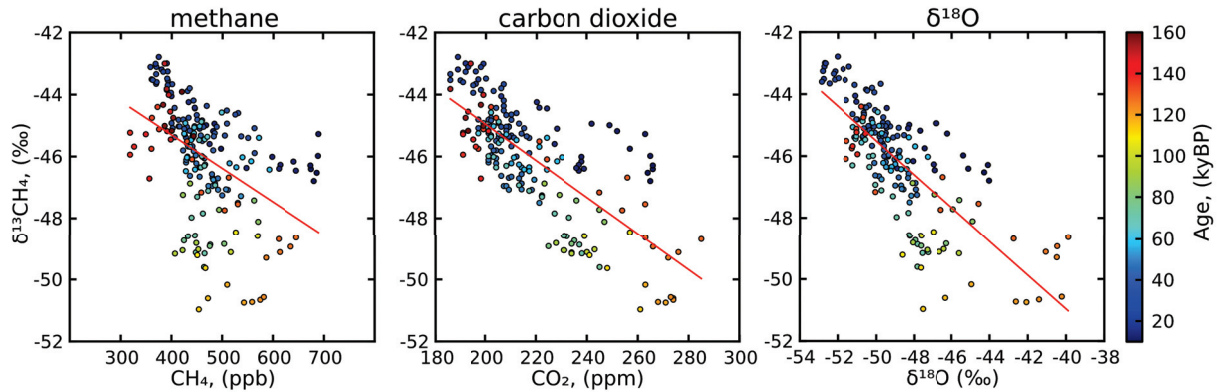


Figure 5.5.: Coherence of $\delta^{13}\text{CH}_4$ with other parameters of global climate.

The correlation of $\delta^{13}\text{CH}_4$ with atmospheric CH_4 (Schilt *et al.*, 2010, EDML), with atmospheric carbon dioxide and $\delta^{18}\text{O}$ data of precipitation at EDML (EPICA community members, 2006) have been calculated using a combined dataset for $\delta^{13}\text{CH}_4$ (this study, Vostok: 80–160 kyr BP 1190–2250 m and EDML: 21–79 kyr BP, 1018–1950 m) and a composite dataset for CO_2 (Byrd: 19–39, Ahn and Brook (2008); Talos Dome and EDML: 39–115 kyr BP, Bereiter *et al.* (2012); Vostok: 116–160 kyr BP, Petit *et al.* (1999)). Ages are given wrt. to the 'unified' chronology (Lemieux-Dudon *et al.*, 2010). Note that the original EDC3 dating of relative sea-level data by Rohling *et al.* (2009, 3-pt moving average, not shown) was based on visual links to EDC δD of precipitation (Jouzel *et al.*, 2007). The correlation coefficient given in the text should thus be interpreted with care.

and Pacific regions via large oceanic "conveyor belts" (EPICA community members, 2006; Jouzel *et al.*, 2007). The consequences of this large-scale energy transfer controls much of the global sea-surface temperature (SST) patterns, which in turn have direct consequences on regional air temperatures and precipitation (e.g. Braconnot *et al.* (2007); MARGO members (2009); Braconnot *et al.* (2012)). Accordingly, it is not surprising that Antarctic $\delta^{18}\text{O}$ variability, a proxy for Southern Ocean temperatures, will also to some degree feedback on CH_4 source regions. However, why $\delta^{18}\text{O}$ should only have an impact on $\delta^{13}\text{CH}_4$ variability, while atmospheric methane concentrations are apparently intimately coupled to processes that have similarly high expressions in the northern-most regions of the Atlantic, for example in Greenland stadial-interstadial climate variability (Johnsen *et al.*, 1992; North GRIP members, 2004), is an open question. There is no existing mechanism that directly links southern hemisphere temperature to the isotopic signature of methane without similarly affecting the emissivity of the respective CH_4 source.

Atmospheric CO_2 - a potential driver for $\delta^{13}\text{CH}_4$ variability?

However, there is a robust link between Antarctic temperatures and atmospheric CO_2 concentrations (see for example Schmittner and Galbraith (2008) and many more). And

the remarkable coherence of $\delta^{13}\text{CH}_4$ and CO_2 is not only apparent on glacial-interglacial time-scales but with a few exceptions also with respect to millennial scale variations of CO_2 in conjunction with Antarctic isotope maximum (AIM) (*EPICA community members*, 2006). Changes in CO_2 presumably affect $\delta^{13}\text{CH}_4$ in multiple ways, on the one hand via direct effects such as $\delta^{13}\text{C}$ of CO_2 that is reflected in the $\delta^{13}\text{C}$ signature of the global biomass, and the potential $\delta^{13}\text{C}$ changes of C_3 plant biomass induced by reduced CO_2 concentrations, and on the other hand via indirect processes such as a shift of the global abundance of $\delta^{13}\text{C}$ enriched C_4 vegetation versus more depleted C_3 plant species. These concepts have been discussed in the Nature Geoscience publication (see section 5.1). In the following two paragraphs, however, both hypotheses will be set on a more profound basis with respect to supportive evidence found in recent literature.

Proxy evidence for C_4 plant expansion | Methane production under natural conditions involves the decomposition of organic precursor material that has previously been accumulated by plants through photosynthetic sequestration of CO_2 . Owing to fundamental physiological differences of the two major photosynthetic pathways, which characteristically discriminate the heavy isotope ^{13}C during carbon assimilation, the typical ranges of isotopic signatures imposed on the plant material differ considerably (*O'Leary*, 1981; *Farquhar et al.*, 1989). 85–90% of terrestrial plant species today, covering the whole spectrum of vegetation from grasses and herbs to shrubs and trees, follow the C_3 photosynthetic pathway (*Gerhart and Ward*, 2010). C_3 plant biomass is characterized by a depleted $\delta^{13}\text{C}$ signature ($\sim -32\text{‰}$ to $\sim -22\text{‰}$), caused by the lower reactivity of $^{13}\text{CO}_2$ with the primary carboxylating enzyme RUBISCO (*Farquhar et al.*, 1982). C_4 vegetation on the other hand, mostly grasses and sedges, are able to pre-concentrate CO_2 internally at the cost of reduced quantum yield (*Ehleringer*, 1978). As a consequence, C_4 plant carbon fixation fractionates less against ^{13}C ($\sim -16\text{‰}$ to $\sim -9\text{‰}$). The isotopic composition of the terrestrial biosphere, i.e. the pre-cursor biomass for methanogenesis, is controlled by the primary productivity of an assemblage of plants under local growth conditions, the individual adaptation of its members to this conditions, as well as its tolerance against limitation factors. Plants of both photosynthetic pathways are unequally tolerant to limitations in CO_2 , light intensity, local temperature, and to moisture and nutrient availability (*Farquhar et al.*, 1989; *Cowling and Sykes*, 1999; *Ehleringer*, 2005). Seasonality of precipitation has an equally significant impact on the local balance between C_3 and C_4 vegetation (*Ehleringer*, 2005). However, the relative importance of any of the limitations, especially in terms of a competitive advantage of plant families against others

in the struggle for habitats, remains a vastly unresolved and vitally discussed question (*Sankaran et al.*, 2005; *Gerhart and Ward*, 2010; *Edwards et al.*, 2010; *Prentice et al.*, 2011; *Bragg et al.*, 2012; *Claussen et al.*, 2012). Accordingly, it is neither physiologically well constrained how strong a C₃ to C₄ plant shift might have been in tropical regions under generally colder, drier conditions with low CO₂ levels that were characteristic for the glacial period, nor is it extensively documented by the scarce terrestrial proxy evidence from these areas. Such a shift, however, is one of the relevant processes for the given hypothesis to explain the observed, very pronounced $\delta^{13}\text{CH}_4$ changes. Some of the available ecosystem evidence with relevance for this hypothesis will be discussed in the following paragraphs.

In temperate regions in Northern- and Meso-America (*Huang et al.*, 2001) and the Chinese loess plateau (*Zhang et al.*, 2003; *Vidic and Montañez*, April, 2004; *Wang et al.*, 2008a), growing season temperature and the local climatic constellation seems to out-compete the physiological effect of low CO₂ level as predominant control upon the C₃/C₄ ratio. With warm growing seasons in the tropics, however, water insufficiency and low CO₂ possess an increased influence as plant-growth limitation factors and pose high adaptive pressure on prevalent ecosystems (*Ehleringer et al.*, 1997; *Street-Perrott et al.*, 1997; *Sage et al.*, 1999; *Sage*, 2004). A study by *Collatz et al.* (1998) quantified the glacial-interglacial reduction of C₄ abundance in grasslands to be in the order of only 4% between the LGM (74%) and the PIH (70%). Based on this assumption, budget calculations to estimate the effect of C₃/C₄ plant ratios on $\delta^{13}\text{C}$ of methane yield a depletion of 1.5‰ integrated over all sources (and 2.1‰ in wetlands only) for this particular shift (*Schaefer and Whiticar*, 2008). However, this assessment just focused on the competition of C₃/C₄ grasses in an otherwise unmodified ecosystem of a prescribed size. Therefore, variability of spatial extension/contraction of C₃ or C₄ dominated ecosystems have not been taken into account. Recent vegetation model experiments indicate high vegetation sensitivity to low atmospheric CO₂ levels during glacial periods (*Harrison and Prentice*, 2003; *Prentice and Harrison*, 2009; *Bragg et al.*, 2012; *Claussen et al.*, 2012). Globally, simulations for glacial climate conditions and typical CO₂ concentrations lead to significant retractions of closed canopy forest habitats in favor of open vegetation types (*Jolly and Haxeltine*, 1997; *Prentice et al.*, 2011; *Woillez et al.*, 2011). Tropical rainforests seem especially affected by the combined effects of increased aridity and low CO₂, and large arboreal areas were encroached on or replaced by open savanna- and shrub-like vegetation.

Analogue findings are well documented by terrestrial proxy data from tropical regions in Africa (*Elenga et al.*, 2000; *Wooller et al.*, 2003; *Rommerskirchen et al.*, 2006; *Castañeda*

et al., 2009; *Hessler et al.*, 2010), Meso- and South America (*Behling*, 2002; *Hughen et al.*, 2004; *Punyasena et al.*, 2008; *Hessler et al.*, 2010; *Lane et al.*, 2011). These studies also report large proportions of C₄ vegetation contributing to the widespread grasslands in equatorial Africa and South America in the LGM. Glacial-Interglacial differences in $\delta^{13}\text{C}$ of vascular plant waxes from sediment cores off the East Atlantic coast close to the river mouths of the Congo and Angola basin, indicate 3-4‰ shifts towards higher $\delta^{13}\text{C}$ values and thus, relative increases of C₄ abundance in the range of 20-40% (*Rommerskirchen et al.*, 2006). Increased C₄ contribution has also been inferred from another marine core retrieved at the Guinea Plateau margin recording Sahara/Sahel vegetation (*Castañeda et al.*, 2009). It also indicates raised aridity, falling temperatures and exceptionally high C₄ predominance for the period between 71 and 65 kyr BP, i.e. the MIS 5/4 transition, which is also characterized by a strong increase (+4‰) in the EDML $\delta^{13}\text{CH}_4$ record (figure 5.3). A comparable study from the Cariaco Basin in the tropical west Atlantic, reported a 4-5‰ $\delta^{13}\text{C}$ decrease in leaf waxes from the LGM to the Preboreal Holocene (*Hughen et al.*, 2004). This probably documents a reoccupation of forest vegetation in the peripheral Amazonian lowlands, that potentially retracted under glacial conditions (*Mayle et al.*, 2000; *Turcq et al.*, 2002; *Mayle et al.*, 2004; *Mayle and Beerling*, 2004; *Anhuf et al.*, 2006). Moreover, huge land masses the size of Europe from Southern Thailand to Sumatra, Borneo and Java became exposed in South-East Asia, when sea-level fell in glacial periods. This territory, known as Sundaland, was also vastly covered by savanna type vegetation with considerable C₄ contribution (*Bird et al.*, 2005; *Wurster et al.*, 2010).

A global shift of C₃ to C₄ plants may not be representative for the conditions encountered in permanent (tropical) wetlands. Intuitively, one may expect that the missing water limitation in such a wetland would reduce the adaptive pressure on plants in that ecosystem and hence level competitive advantages of one species against another. C₃ plants, for example, are not forced into the natural trade-off between necessary stomatal opening for carbon sequestration and excessive water loss. In this light it is yet not fully understood, why large modern wetland ecosystems in tropical East Africa (*Jones and Muthuri*, 1997), South Africa (*Kotze and O'Connor*, 2000; *Saunders et al.*, 2007), or areas of the Amazon floodplain (*Piedade et al.*, 1991) exhibit clear C₄ plant predominance (mostly papyrus), a phenomenon that is not uncommon in permanent and seasonally waterlogged environments where tree maintenance and establishment is presumably not possible (*Piedade et al.*, 1994; *Mantlana et al.*, 2008). Moreover, there is evidence that C₄ dominance in east-equatorial Africa (at least near lake Challa) persisted during both wet and dry phases

under glacial conditions (*Sinninghe Damsté et al.*, 2011). The cumulated observations of $\delta^{13}\text{CH}_4$ changes in the record strongly suggest that seasonally inundated wetlands must have played an increasing role for CH_4 emissions during cold climate conditions. These tropical non-permanent wetlands are assumed to foster the shift to open grasslands with high C_4 contribution, as the higher water use efficiency and productivity of the C_4 plants under low CO_2 levels in glacial periods should prove advantageous in this environment of seasonally contrasting, very dry to very wet conditions.

Impact of location and habitat on the isotopic signature of C_3 plants | Environmental factors as humidity, light availability, CO_2 concentration and use of recycled CO_2 differ largely between C_3 plant habitats like rain forest and savanna (*Vogts et al.*, 2009). Dense closed canopy rain forest habitats provide a higher degree of natural protection from wind movement and hence reduced water loss and air mass exchange, but on the other hand increase the competition for light intensity. The low photon flux caused by the light deficit for example diminishes carbon fixation rates, especially in the undergrowth vegetation. Due to decreased wind penetration into lower vegetation layers of thick, closed canopy habitats and the hampered exchange of air masses, a larger proportion of CO_2 molecules in these air masses are likely to have their origin in CO_2 recycling processes and soil respiration. Consequently, this CO_2 fraction already underwent previous discrimination processes and will be isotopically lighter relative to atmospheric CO_2 when it is assimilated to plant biomass (*Medina and Minchin*, 1980; *Buchmann et al.*, 1997). Furthermore, rainforest habitats have much higher water supply and air moisture levels compared to open vegetation types. Reduced evapo-transpirative water loss in closed canopies allows longer periods of opened leaf stomata and, thus, increased CO_2 levels in the leaves. Light deficit and high intracellular CO_2 levels enhance the discrimination of the heavier ^{13}C isotope during photosynthesis (*Ehleringer et al.*, 1986). In contrast, open shrub, herb and grassy C_3 vegetation is, especially in low latitudes, exposed to high levels of direct sunlight and high leaf temperatures. To avoid extensive water loss, the stomatal conductance of these plants is usually highly restricted (*Farquhar et al.*, 1982), and carbon dioxide limitation in the leaf cells reduces the relative discrimination of the heavier isotope by the enzymes involved in photosynthesis. As a consequence of these effects, C_3 rain forest plant material is found to be 3-4‰ more depleted than C_3 plant material from open savanna (*Vogts et al.*, 2009). Although large reductions in forest cover are also reported for subtropical, temperate or even boreal regions (*Allen*, 1999; *Elenka et al.*, 2000; *Williams*, 2003; *Müller et al.*, 2009; *Prentice et al.*, 2011; *Wolfe et al.*, 2011)

the proposed glacial enrichment of C₃ plant biomass was supposedly most pronounced in the tropics, where the gradients in soil and air moisture, light intensity and leaf temperatures between open and closed canopy habitats are expected to be higher compared to the extra-tropics.

Did sea-level contribute to $\delta^{13}\text{CH}_4$ variations?

The sea-level varied considerably on glacial-interglacial as well as on sub-millennial timescales. The combined effects of water accumulation in global ice masses and thermal contraction have led to glacial sea-levels that were approximately 120 m lower compared to today (*Siddall et al.*, 2003; *Lisiecki and Raymo*, 2005; *Bintanja et al.*, 2005; *Arz et al.*, 2007). Sea-level may have affected CH₄ sources in many ways. Coastal and fluvial wetlands, for example, likely encountered increased drainage due to elevated land–ocean height gradients with consequences on local hydrology and water table heights, an effect that is presumably compensated by wetland dislocations towards the coasts and into regions with more favorable topography. The model simulations by *Kaplan* (2002) predict a 15 % glacial increase of global wetland area, largely owing to the low relief of increasingly exposed continental shelves that promoted wetland formation, e.g. on the Atlantic coast of North and South America, New Guinea and Sundaland. This mid- to low-latitude wetland expansion, thus, over-compensated the loss of wetland area in higher latitudes due to the advances of ice-sheets that buried vast regions in Siberia, the Hudson Bay and Europe (*Kaplan*, 2002). As a consequence of this north-south displacement of wetland area, reduced CH₄ emissions are expected from the high-latitude boreal regions and, assuming a systematic difference in the mean carbon isotopic signature of boreal and tropical sources, should be reflected in an enriched atmospheric $\delta^{13}\text{CH}_4$ in glacial periods.

Contributions from geologic sources Lowered sea-levels are expected to cause exposure of hydrocarbon seeps in shallow continental shelf regions in hydrocarbon basins such as the Persian Gulf, Sundaland and the Gulf of Mexico (*Luyendyk et al.*, 2005; *Judd et al.*, 2002). Under high sea-level conditions, much of the CH₄ emitted by these seeps is oxidized on its way to the surface (*Luyendyk et al.*, 2005). Hydrocarbon seeps belong to the group of geologic sources that are still one of the greatest unknowns in CH₄ budget calculations. While the evidence for the existence of marine gas seeps, mud volcanoes, micro-seepage and other geothermal sources is large and well documented, the total atmospheric flux is still vastly unresolved (*Hovland and Judd*, 1992; *Lacroix*, 1993; *Judd et al.*, 1997; *Etiopie*

and Klusman, 2002; MacDonald *et al.*, 2002; Etiope, 2004; Kvenvolden and Rogers, 2005; Leifer *et al.*, 2006; Etiope *et al.*, 2008a, 2009) Methane emissions from off-shore sources are believed to be dissolved and oxidized on its way through the water column to the surface. Model studies and empirical observations suggest that continuous marine CH₄ emissions reach the surface only at very shallow locations with water table heights below $\sim 100\text{m}$ and that just a very small fraction of CH₄ would escape to the atmosphere (Leifer and Patro, 2002; Schmale *et al.*, 2005; McGinnis *et al.*, 2006). Nevertheless, the median of bottom-up estimates for shallow seabed gas seep emissions suggests a global contribution of $\sim 20 \text{ Tg yr}^{-1}$, but the range of estimates is extremely large (0.4–48 Tg yr⁻¹) due to varying assumptions concerning extrapolation (Judd, 2004). Etiope *et al.* (2008b) argues, that the amount of methane emitted from contemporary onshore geologic sources is likely even greater than that released from offshore sources, and that these emissions could potentially explain the relatively high $\delta^{13}\text{C}_{\text{CH}_4}$ values in the PB, that were $\sim 1\text{‰}$ higher than modern values and unexpected for budgets without considerable ¹³C-rich anthropogenic emissions (Schaefer *et al.*, 2006). The cumulated estimates for the total modern contributions of geologic sources including marine seeps, mud volcanoes, micro-seepage and geothermal sources span the wide range of 14.5–94 Tg yr⁻¹ (Etiope *et al.*, 2008b). While onshore seepage were presumably more widespread due to the exposure of continental shelves in the glacial that may have doubled the amount of CH₄ from shallow hydrocarbon seeps reaching the atmosphere (Luyendyk *et al.*, 2005), these contributors are mainly unaffected by earths climate and should thus not vary considerably on glacial-interglacial, or even less under stadial-interstadial time scales.

Assuming that the global wetland productivity was decreased during the LGM owing to reduced global annual mean temperatures, the glaciation in higher northern latitudes and decreased global NPP of ecosystems due to CO₂ limitation and generally drier conditions (Prentice *et al.*, 2000; Kaplan, 2002; Severinghaus, 2009; Prentice *et al.*, 2011; Bragg *et al.*, 2012) leading to the low CH₄ concentration levels during the LGM, the sum of geologic emissions should exert a considerable control on the glacial CH₄ budget. The following first order estimate calculations may help to constrain a reasonable range for these contributions.

If the glacial CH₄ lifetime τ_{CH_4} is assumed similar to the interglacial value of 8.6 years (Stevenson *et al.*, 2006; Levine *et al.*, 2011b), the LGM CH₄ concentration corresponds to steady state source emissions of $\sim 132 \text{ Tg yr}^{-1}$ (calculated from equations (eqn.) provided in Etheridge *et al.* (1998); Lassey *et al.* (2007)). If the total sink fractionation ϵ_{WT} is then calculated to -4.5‰ (2‰ soil sink, α_{soil} adjusted to 4 °C lower global annual temperature

during the LGM, a stratospheric sink of 5.5‰ (*Schaefer and Whiticar, 2008*), no Cl_{MBL} sink, the rest is removed by $\cdot\text{OH}$) with equation 2.13, the LGM atmospheric $\delta^{13}\text{CH}_4$ value ($\sim -43\text{‰}$) would yield a total source signature $\delta^{13}\text{C}_E$ of $\sim -47.5\text{‰}$ ($\sim -47.85\text{‰}$ including Cl_{MBL} (*Levine et al., 2011a*), eqn. 2.8). With the help of equation 2.9 the mean source signature $\delta^{13}\text{C}_R$ of all non-geologic sources can be calculated at first order for the range of estimates of emissions from geologic sources provided in table 1 (*Etiopie et al., 2008b*, $\sim 14.5\text{--}94\text{ Tg yr}^{-1}$ without hydrates). This is achieved by taking the mean of the typical $\delta^{13}\text{C}_{E_i}$ signature values for each sources provided in the same table (i.e. -40‰ for marine seeps, -48‰ for mud volcanoes, -35‰ for micro-seeps, -18‰ for geothermal source) and assuming that the sum of geologic (E_G) and non-geologic emissions (E_R) match the total source strength of $\sim 132\text{ Tg yr}^{-1}$. The maximum estimate (94 Tg yr^{-1} E_G) would imply an extremely depleted $\delta^{13}\text{C}_R$ of $\sim -73\text{‰}$ that is an unlikely scenario considering that E_R will likely also include highly enriched wildfire emissions ($\sim -25\text{‰}$) and a great proportion of CH_4 from tropical wetland sources ($\sim -55\pm 5\text{‰}$). The minimal estimate (14.4 Tg yr^{-1}) yields a $\delta^{13}\text{C}_R$ of $\sim -49\text{‰}$ that would call for an almost complete shut-down of contributions from highly depleted CH_4 sources such as boreal wetlands ($> -65\text{‰}$) and a relatively high contribution from wildfire emissions ($\sim 21\%$ of E_R , if boreal emissions are entirely absent). Proposing a final (best guess) estimate of 30 Tg yr^{-1} for the total of geologic emissions during the LGM (14 Tg yr^{-1} marine seeps, 6 Tg yr^{-1} mud volcanoes, 7 Tg yr^{-1} by micro-seepage and 3 Tg yr^{-1} geothermal CH_4), the calculations would yield $\delta^{13}\text{C}_R$ of $\sim -50\text{‰}$. This scenario demonstrates, that under the given assumptions $\delta^{13}\text{C}_R$ is relatively insensitive to a glacial increase of continental shelf seeps according to the hypothesis by *Lwyendyk et al. (2005)*. Further interpretation of the best guess $\delta^{13}\text{C}_R$ would attribute a minimum of 16% of E_R to wildfire CH_4 emissions, if boreal wetland emissions are assumed to be shut off. If an amount of boreal wetland emissions would be allowed, it would require an additional isotopically heavy source to close the $\delta^{13}\text{CH}_4$ budget (approximately twice the amount of wildfire CH_4 for example). Charcoal reconstructions suggest rather moderate wildfire emissions for the LGM (*Power et al., 2008; Marlon et al., 2009*). Accordingly, the best guess estimate likely still represents a lower limit of $\delta^{13}\text{C}_R$ under all these assumptions as it suggests a virtual shut-down of boreal sources at $\sim 16\%$ wildfire emissions, even when the typical $\delta^{13}\text{C}$ signature of CH_4 emitted by tropical wetlands was already prescribed in the calculations to be enriched by 5‰ (e.g. by the CO_2 mediated processes described earlier) compared to contemporary values (e.g. *Quay et al. (1999)*). These calculations did not consider other CH_4 sources, for example emissions by termites, ruminants, aerobic plant production and methane hydrates, because their contributions

are either considered negligible on a global scale or their typical $\delta^{13}\text{CH}_4$ signature too close to $\delta^{13}\text{C}_R$. Accordingly, these scenarios cannot serve as a realistic assessment of the contribution of geologic emissions to the glacial CH_4 budget. But they illustrate the large handle (up to 24 ‰) that variations of geologic sources possess on atmospheric $\delta^{13}\text{CH}_4$. Moreover, if wildfire CH_4 emissions were reduced during the LGM, these first-order calculations suggest a considerable role of geologic sources for the LGM methane budget in order to explain the observed high $\delta^{13}\text{CH}_4$ levels at that time. And that would be the case, even if wetland source signatures would already be shifted by 3–6 ‰ towards enriched values following the earlier considerations of CO_2 feedbacks on $\delta^{13}\text{C}$ of respired biomass.

Conclusions

The competition of C_3/C_4 vegetation for the dominance in tropical ecosystems is well-documented phenomenon, which is not unlikely to feedback on glacial-interglacial changes in $\delta^{13}\text{CH}_4$. The effect of low CO_2 levels and changes to overall air moisture during glacial conditions supported the expansion of grassy, open canopy vegetation in tropical Africa, South America and Asia, with increasing contribution from plants of the C_4 type. While this expansion of C_4 plants may not be fully reflected in permanently inundated wetlands, methane emissions from seasonally waterlogged regions should capture the full extent of the $\delta^{13}\text{C}$ enrichment of plant biomass that is presumably associated with increased C_4 abundance. However, taking the regional estimates of an overall C_3/C_4 shift in the range of 20 % to maximally 50 % at face value (*Hughen et al.*, 2004; *Rommerskirchen et al.*, 2006; *Wurster et al.*, 2010), a 15 ‰ difference of C_3/C_4 plant biomass $\delta^{13}\text{C}$ would translate into only 2.25–4.5 ‰ $\delta^{13}\text{CH}_4$ signature changes of tropical wetland emissions. Accordingly, the C_3/C_4 effect alone may explain ~25 % to ~50 % of the observed ~8 ‰ $\delta^{13}\text{CH}_4$ enrichment from peak negative values in MIS 5.e to the maximum glacial $\delta^{13}\text{CH}_4$ in MIS 2, but only under the assumption that boreal CH_4 emissions were negligible at peak glacial conditions. Similar to C_3/C_4 vegetation shifts, it remains vastly unresolved whether the effect of globally more enriched C_3 plant biomass (wrt. $\delta^{13}\text{C}$) under glacial CO_2 conditions would apply to the full extent for the specific conditions found in wetland ecosystems. The trade-off of plant individuals between stomatal conductance and water use efficiency as a driver for the C_3 $\delta^{13}\text{C}$ shift, for example, does not appear plausible for permanent wetland conditions. The observed 3–4 ‰ difference further only applies for the largest contrast of very thick rainforest vegetation to vastly open savanna ecosystems (*Vogts et al.*, 2009).

Assuming an increased proportion of seasonally inundated wetlands during glacial conditions (*Kaplan, 2002*), the influence of enriched glacial C₃ vegetation on $\delta^{13}\text{CH}_4$ may account for 1–2 ‰ of the MIS 5–MIS 2 $\delta^{13}\text{CH}_4$ difference, again omitting considerable boreal contributions. However, a recent study by *Diefendorf et al. (2010)* suggests relatively large systematic differences of $\delta^{13}\text{C}$ values of C₃ plant biomass between members of differing plant types and biomes. Accordingly, the atmospheric $\delta^{13}\text{CH}_4$ signature may also reflect globally integrated $\delta^{13}\text{C}$ precursor biomass changes of wetland vegetation due to climate-driven changes of biomes and predominant plant types that are independent of C₃/C₄ abundance or geographical constraints. In summary, the combined effects of both concepts potentially account for 3–6 ‰ of the $\delta^{13}\text{CH}_4$ changes observed from the last interglacial to the LGM. The correlation of $\delta^{13}\text{CH}_4$ to CO₂ is considerably weaker at elevated CO₂ concentrations during both interglacial periods, presumably due to decreased CO₂ sensitivity of vegetation above a certain threshold (*Ehleringer, 1978; Edwards et al., 2010*). Increased interglacial contributions from extra-tropical CH₄ sources to the global budget are further expected to replace CO₂ mediated effects wrt. to the control of $\delta^{13}\text{CH}_4$ variations (*MacDonald et al., 2006; Sowers, 2010*).

Large uncertainties exist concerning the role of geologic emissions in methane budgets of the last glacial period. The comparably high $\delta^{13}\text{C}$ signatures of thermogenic CH₄ predominant in these geologic sources may represent an important ingredient to explain elevated $\delta^{13}\text{CH}_4$ values during MIS 2. Accordingly, they represent potential candidates to take the load from wildfire CH₄ emissions that are usually invoked to explain this observation. The majority of geologic CH₄ emitters are independent from climate and not likely to change to great extents over glacial-interglacial time-scales. However, their relative importance for global CH₄ budgets is expected to be increasing with decreasing biogenic CH₄ production due to reduced ecosystem NPP and lower temperatures and may thus have contributed to the 8 ‰ enrichment in $\delta^{13}\text{CH}_4$ observed between MIS 5 to MIS 2. With increasing global ice-volumes and the exposure of continental shelves, geologic emissions may have also slightly increased in total size. However, recent atmospheric modeling studies suggest that glacial sink fluxes of CH₄ and consequently the mean residence time of CH₄ molecules in the atmosphere may have been less variable than anticipated earlier (*Levine et al., 2011b, 2012*). Therefore, almost the whole extent of glacial-interglacial and millennial-scale CH₄ concentration changes is necessarily on behalf of processes in the sources. It has been disputed for years whether wetlands may react quick enough to account for the rapid concentration increases. Assuming that a considerable 'background' contribution comes from steady geologic emitters, the remaining sources were required to

exhibit even higher changes of emission rates to explain the glacial changes in atmospheric methane.

Bibliography

- Ahn, J., and E. J. Brook, Atmospheric CO₂ and climate on millennial time scales during the last glacial period, *Science*, 322(5898), printed "CO₂", 2008.
- Albert, M., C. Shuman, Z. Courville, R. Bauer, M. Fahnestock, and T. Scambos, Extreme firn metamorphism: impact of decades of vapor transport on near-surface firn at a low-accumulation glazed site on the east antarctic plateau, *Annals of Glaciology*, 39(1), 73–78, doi:10.3189/172756404781814041, 2004.
- Allan, W., D. C. Lowe, and J. M. Caine, Active chlorine in the remote marine boundary layer: Modeling anomalous measurements of $\delta^{13}\text{C}$ in methane, *Geophys. Res. Lett.*, 28(17), 3239–3242, 2001a.
- Allan, W., M. R. Manning, K. R. Lassey, D. C. Lowe, and A. J. Gomez, Modeling the variation of $\delta^{13}\text{C}$ in atmospheric methane: Phase ellipses and the kinetic isotope effect, *Global Biogeochem. Cycles*, 15(2), 467–481, 2001b.
- Allan, W., D. C. Lowe, A. J. Gomez, H. Struthers, and G. W. Brailsford, Interannual variation of ^{13}C in tropospheric methane: Implications for a possible atomic chlorine sink in the marine boundary layer, *J. Geophys. Res.*, 110, 2005.
- Allan, W., H. Struthers, and D. C. Lowe, Methane carbon isotope effects caused by atomic chlorine in the marine boundary layer: Global model results compared with southern hemisphere measurements, *J. Geophys. Res.*, 112, D04,306, 2007.
- Allan, W., H. Struthers, D. C. Lowe, and S. E. Mikaloff Fletcher, Modeling the effects of methane source changes on the seasonal cycles of methane mixing ratio and $\delta^{13}\text{C}$ in southern hemisphere midlatitudes, *J. Geophys. Res.*, 115(D7), D07,301–, 2010.
- Allen, J. R. M., Rapid environmental changes in southern Europe during the last glacial period, *Nature*, 400, 740–743, 1999.

- Anhuf, D., et al., Paleo-environmental change in amazonian and african rainforest during the lgm, *Palaeogeography, Palaeoclimatology, Palaeoecology*, 239(3-4), 510–527, 2006.
- Arz, H. W., F. Lamy, A. Ganopolski, N. Nowaczyk, and J. Pätzold, Dominant northern hemisphere climate control over millennial-scale glacial sea-level variability, *Quaternary Science Reviews*, 26(3-4), 312–321, 2007.
- Aselmann, I., and P. J. Crutzen, Global distribution of natural freshwater wetlands and rice paddies, their net primary productivity, seasonality and possible methane emissions, *Journal of Atmospheric Chemistry*, 8(4), 307–358, 1989.
- Baker, P. A., The history of south american tropical precipitation for the past 25,000 years, *Science*, 291, 640–643, 2001.
- Barnola, J. M., D. Raynaud, Y. S. Korotkevich, and C. Lorius, Vostok ice core provides 160,000-year record of atmospheric co₂, *Nature*, 329(6138), 408–414, doi: 10.1038/329408a0, 1987.
- Bartlett, K. B., and R. C. Harriss, Review and assessment of methane emissions from wetlands, *Chemosphere*, 26(1-4), 261–320, 1993.
- Bates, D. R., and A. E. Witherspoon, The photochemistry of some minor constituents of the earth's atmosphere (co₂, co, ch₄, n₂o)., *Mon. Not. R. Astron. Soc.*, 112, 101–124, 1952.
- Baumgartner, M., A. Schilt, O. Eicher, J. Schmitt, J. Schwander, R. Spahni, H. Fischer, and T. F. Stocker, High-resolution inter-polar difference of atmospheric methane around the last glacial maximum, *Biogeosciences*, 9(10), 3961–3977, doi:10.5194/bg-9-3961-2012, 2012.
- Baumgartner, M., et al., NgrIP CH₄ concentration from 120 to 10 kyr before present and its relation to a $\delta^{15}\text{N}$ temperature reconstruction from the same ice core, *Climate of the Past Discussions*, 9(4), 4655–4704, doi:10.5194/cpd-9-4655-2013, 2013.
- Bazin, L., et al., An optimized multi-proxy, multi-site antarctic ice and gas orbital chronology (aicc2012): 120–800 ka, *Climate of the Past*, 9(4), 1715–1731, doi: 10.5194/cp-9-1715-2013, 2013.

- Beerling, D. J., T. Gardiner, G. Leggett, A. Mcleod, and W. P. Quick, Missing methane emissions from leaves of terrestrial plants, *Global Change Biology*, *14*(8), 1821–1826, 2008.
- Behling, H., South and southeast brazilian grasslands during late quaternary times: a synthesis, *Palaeogeogr. Palaeoclim. Palaeoecol.*, *177*, 19–27, 2002.
- Behrens, M., J. Schmitt, K.-U. Richter, M. Bock, U. C. Richter, I. Levin, and H. Fischer, A gas chromatography/combustion/isotope ratio mass spectrometry system for high-precision delta13c measurements of atmospheric methane extracted from ice core samples., *Rapid Commun Mass Spectrom.*, *22*(20), 3261–3269, doi:10.1002/rcm.3720, 2008.
- Bereiter, B., D. Lüthi, M. Siegrist, S. Schüpbach, T. F. Stocker, and H. Fischer, Mode change of millennial co2 variability during the last glacial cycle associated with a bipolar marine carbon seesaw, *Proceedings of the National Academy of Sciences*, *109*(25), 9755–9760, 2012.
- Bergamaschi, P., et al., Satellite cartography of atmospheric methane from sciamachy on board envisat: 2. evaluation based on inverse model simulations, *J. Geophys. Res.*, *112*(D2), D02,304–, 2007.
- Bergamaschi, P., et al., Inverse modeling of global and regional CH₄ emissions using SCIAMACHY satellite retrievals, *J. Geophys. Res.*, *114*, D22,301, 2009.
- Berger, A., and M. F. Loutre, Insolation values for the climate of the last 10 million years, *Quat. Sci. Rev.*, *10*, 297–317, 1991.
- Berner, W., H. Oeschger, and B. Stauffer, Information on the co2 cycle from ice core studies, *Radiocarbon*, *22*(2), 227–235, 1980.
- Berrittella, C., and J. van Huissteden, Uncertainties in modelling ch4 emissions from northern wetlands in glacial climates: the role of vegetation parameters, *Clim. Past*, *7*(4), 1075–1087, doi:10.5194/cp-7-1075-2011, 2011.
- Bigler, M., R. Röthlisberger, F. Lambert, E. W. Wolff, E. Castellano, R. Udisti, T. F. Stocker, and H. Fischer, Atmospheric decadal variability from high-resolution dome c ice core records of aerosol constituents beyond the last interglacial, *Quaternary Science Reviews*, *29*(1-2), 324–337, 2010.

- Bintanja, R., R. S. van de Wal, and J. Oerlemans, Modelled atmospheric temperatures and global sea levels over the past million years, *Nature*, *437*(7055), 125–128, 2005.
- Bird, M. I., D. Taylor, and C. Hunt, Palaeoenvironments of insular southeast asia during the last glacial period: a savanna corridor in sundaland?, *Quaternary Science Reviews*, *24*(20-21), 2228–2242, 2005.
- Bloom, A. A., J. Lee-Taylor, S. Madronich, D. J. Messenger, P. I. Palmer, D. S. Reay, and A. R. McLeod, Global methane emission estimates from ultraviolet irradiation of terrestrial plant foliage, *New Phytologist*, *187*(2), 417–425, 2010.
- Blunier, T., and E. J. Brook, Timing of millennial-scale climate change in antarctica and greenland during the last glacial period, *Science*, *291*(5501), 109–112, doi:10.1126/science.291.5501.109, 2001.
- Blunier, T., R. Spahni, J.-M. Barnola, J. Chappellaz, L. Loulergue, and J. Schwander, Synchronization of ice core records via atmospheric gases, *Clim. Past*, *3*(2), 325–330, 2007.
- Blunier, T., et al., Asynchrony of antarctic and greenland climate change during the last glacial period, *Nature*, *394*(6695), 739–743, 1998.
- Bock, J., P. Martinerie, E. Witrant, and J. Chappellaz, Atmospheric impacts and ice core imprints of a methane pulse from clathrates, *Earth and Planetary Science Letters*, *349–350*(0), 98–108, 2012.
- Bock, M., Measuring the isotopic composition of methane as archived in polar ice cores: a tool to constrain paleoclimatic changes, Ph.D. thesis, 2010.
- Bock, M., J. Schmitt, M. Behrens, L. Möller, R. Schneider, C. Sapart, and H. Fischer, A gas chromatography/pyrolysis/isotope ratio mass spectrometry system for high-precision δd measurements of atmospheric methane extracted from ice cores, *Rapid Commun. Mass Spectrom.*, *24*(5), 621–633, 2010a.
- Bock, M., J. Schmitt, L. Möller, R. Spahni, T. Blunier, and H. Fischer, Hydrogen isotopes preclude marine hydrate ch₄ emissions at the onset of dansgaard-oeschger events, *Science*, *328*(5986), 1686–1689, 2010b.

- Bond, G., W. Broecker, S. Johnsen, J. McManus, L. Labeyrie, J. Jouzel, and G. Bonani, Correlations between climate records from north atlantic sediments and greenland ice, *Nature*, *365*(6442), 143–147, 1993.
- Born, M., H. Dürr, and I. Levin, Methane consumption in aerated soils of the temperate zone, *Tellus B*, *42*(1), 2–8, 1990.
- Botz, R., H.-D. Pokojski, M. Schmitt, and M. Thomm, Carbon isotope fractionation during bacterial methanogenesis by co₂ reduction, *Organic Geochemistry*, *25*(3–4), 255–262, 1996.
- Bousquet, P., et al., Contribution of anthropogenic and natural sources to atmospheric methane variability, *Nature*, *443*(7110), 439–443, 2006.
- Bousquet, P., et al., Source attribution of the changes in atmospheric methane for 2006–2008, *Atmos. Chem. Phys.*, *11*(8), 3689–3700, 2011.
- Bowman, D. M. J. S., et al., Fire in the earth system, *Science*, *324*(5926), 481–484, 2009.
- Boyd, E. S., M. Skidmore, A. C. Mitchell, C. Bakermans, and J. W. Peters, Methanogenesis in subglacial sediments, *Environmental Microbiology Reports*, *2*(5), 685–692, 2010.
- Braconnot, P., S. P. Harrison, M. Kageyama, P. J. Bartlein, V. Masson-Delmotte, A. Abe-Ouchi, B. Otto-Bliesner, and Y. Zhao, Evaluation of climate models using palaeoclimatic data, *Nature Clim. Change*, *2*(6), 417–424, 2012.
- Braconnot, P., et al., Results of pmip2 coupled simulations of the mid-holocene and last glacial maximum – part 1: experiments and large-scale features, *Clim. Past*, *3*(2), 261–277, 2007.
- Bragg, F. J., I. C. Prentice, S. P. Harrison, G. Eglinton, P. N. Foster, F. Rommerskirchen, and J. Rullkötter, Stable isotope and modelling evidence that co₂ drives vegetation changes in the tropics, *Biogeosciences Discuss.*, *9*(11), 15,699–15,722, doi:10.5194/bgd-9-15699-2012, 2012.
- Brass, M., and T. Röckmann, Continuous-flow isotope ratio mass spectrometry method for carbon and hydrogen isotope measurements on atmospheric methane, *Atmospheric Measurement Techniques*, *3*(6), 1707–1721, doi:10.5194/amt-3-1707-2010, 2010.

- Brenninkmeijer, C. A. M., D. C. Lowe, M. R. Manning, R. J. Sparks, and P. F. J. van Velthoven, The ^{13}C , ^{14}C , and ^{18}O isotopic composition of CO , CH_4 , and CO_2 in the higher southern latitudes lower stratosphere, *J. Geophys. Res.*, *100*(D12), 26,163–26,172, 1995.
- Bridgham, S. D., H. Cadillo-Quiroz, J. K. Keller, and Q. Zhuang, Methane emissions from wetlands: biogeochemical, microbial, and modeling perspectives from local to global scales, *Glob Change Biol*, *19*(5), 1325–1346, 2013.
- Bromley, T., W. Allan, R. Martin, S. E. Mikaloff Fletcher, D. C. Lowe, H. Struthers, and R. Moss, Shipboard measurements and modeling of the distribution of CH_4 and $^{13}\text{CH}_4$ in the western pacific, *J. Geophys. Res.*, *117*(D4), D04,307–, 2012.
- Brook, E. J., T. Sowers, and J. Orchardo, Rapid variations in atmospheric methane concentration during the past 110,000 years, *Science*, *273*(5278), 1087–1091, 1996.
- Brook, E. J., S. Harder, J. Severinghaus, E. J. Steig, and C. M. Sucher, On the origin and timing of rapid changes in atmospheric methane during the last glacial period, *Global Biogeochem. Cycles*, *14*, 559–572, 2000.
- Brune, W., OH and HO_2 : Sources, interactions with nitrogen oxides, and ozone production, 2000.
- Bräunlich, M., O. Aballain, T. Marik, P. Jöckel, C. A. M. Brenninkmeijer, J. Chappellaz, J.-M. Barnola, R. Mulvaney, and W. T. Sturges, Changes in the global atmospheric methane budget over the last decades inferred from ^{13}C and d isotopic analysis of antarctic firn air, *J. Geophys. Res.*, *106*, –, 2001.
- Bréas, O., C. Guillou, F. Reniero, and E. Wada, The global methane cycle: Isotopes and mixing ratios, sources and sinks, *Isotopes in Environmental and Health Studies*, *37*(4), 257–379, 2001.
- Buchmann, N., J.-M. Guehl, T. S. Barigah, and J. R. Ehleringer, Interseasonal comparison of CO_2 concentrations, isotopic composition, and carbon dynamics in an amazonian rainforest (french guiana), *Oecologia*, *110*(1), 120–131, 1997.
- Buchwitz, M., et al., Atmospheric methane and carbon dioxide from sciamachy satellite data: initial comparison with chemistry and transport models, *Atmos. Chem. Phys.*, *5*(4), 941–962, 2005.

- Burns, S. J., D. Fleitmann, A. Matter, J. Kramers, and A. A. Al-Subbary, Indian ocean climate during the last glacial period and an absolute chronology over dansgaard/oeschger events 9 to 13, *Science*, *301*(5638), 1365–1367, 2003.
- Cai, Y., Z. An, H. Cheng, R. L. Edwards, M. J. Kelly, W. Liu, X. Wang, and C.-C. Shen, High-resolution absolute-dated indian monsoon record between 53 and 36 ka from xiaobailong cave, southwestern china, *Geology*, *34*(8), 621–624, doi:10.1130/G22567.1, 2006.
- Cantrell, C. A., R. E. Shetter, A. H. Mcdaniel, J. G. Calvert, J. A. Davidson, D. C. Lowe, S. C. Tyler, R. J. Cicerone, and J. P. Greenberg, Carbon kinetic isotope effect in the oxidation of methane by the hydroxyl radical, *J. Geophys. Res.*, *95*(D13), 22,455–22,462, doi:10.1029/JD095iD13p22455, 1990.
- Capron, E., et al., Synchronising edml and northgrip ice cores using $[\delta]18\text{o}$ of atmospheric oxygen ($[\delta]18\text{oatm}$) and ch_4 measurements over mis5 (80–123 kyr), *Quaternary Science Reviews*, *29*(1–2), 222–234, 2010.
- Castañeda, I. S., S. Mulitza, E. Schefuß, R. A. Lopes dos Santos, J. S. Sinninghe Damsté, and S. Schouten, Wet phases in the sahara/sahel region and human migration patterns in north africa, *Proceedings of the National Academy of Sciences*, *106*(48), 20,159–20,163, 2009.
- Chanton, J. P., The effect of gas transport on the isotope signature of methane in wetlands, *Organic Geochemistry*, *36*(5), 753–768, 2005.
- Chanton, J. P., C. M. Rutkowski, C. C. Schwartz, D. E. Ward, and L. Boring, Factors influencing the stable carbon isotopic signature of methane from combustion and biomass burning, *J. Geophys. Res.*, *105*(D2), 1867–1877, 2000.
- Chanton, J. P., D. Fields, and M. E. Hines, Controls on the hydrogen isotopic composition of biogenic methane from high-latitude terrestrial wetlands, *J. Geophys. Res.*, *111*(G4), G04,004–, 2006.
- Chappellaz, J., J. M. Barnola, D. Raynaud, Y. S. Korotkevich, and C. Lorius, Ice-core record of atmospheric methane over the past 160,000 years, *Nature*, *345*(6271), 127–131, 1990.

- Chappellaz, J., T. Blunier, D. Raynaud, J. M. Barnola, J. Schwander, and B. Stauffer, Synchronous changes in atmospheric ch4 and greenland climate between 40 and 8 kyr bp, *Nature*, *366*(6454), 443–445, 1993a.
- Chappellaz, J., I. Y. Fung, and A. M. Thompson, The atmospheric ch4 increase since the last glacial maximum, *Tellus B*, *45*(3), 228–241, 1993b.
- Chappellaz, J., T. Blunier, S. Kints, A. Dällenbach, J.-M. Barnola, J. Schwander, D. Raynaud, and B. Stauffer, Changes in the atmospheric ch4 gradient between greenland and antarctica during the holocene, *J. Geophys. Res.*, *102*, 15,987–15,997, 1997.
- Chen, Y.-H., and R. G. Prinn, Estimation of atmospheric methane emissions between 1996 and 2001 using a three-dimensional global chemical transport model, *J. Geophys. Res.*, *111*(D10), D10,307–, 2006.
- Christensen, T. R., et al., Factors controlling large scale variations in methane emissions from wetlands, *Geophysical Research Letters*, *30*(7), n/a–n/a, doi:10.1029/2002GL016848, 2003.
- Christner, B. C., G. G. Montross, and J. C. Priscu, Dissolved gases in frozen basal water from the ngrip borehole: implications for biogeochemical processes beneath the greenland ice sheet, *Polar Biology*, *35*(11), 1735–1741, 2012.
- Cicerone, R. J., and R. S. Oremland, Biogeochemical aspects of atmospheric methane, *Global Biogeochem. Cycles*, *2*(4), 299–327, 1988.
- Clark, P., S. W. Hostetler, N. G. Piasias, A. Schmittner, and K. J. Meissner, *Mechanisms for an 7-kyr Climate and Sea-Level Oscillation During Marine Isotope Stage 3*, *AGU Geophysical Monograph Series*, vol. 173, ocean circulation: mechanisms and impacts ed., 209-246 pp., American Geophysical Union, doi:10.1029/173GM15, 2007.
- Clark, P. U., A. S. Dyke, J. D. Shakun, A. E. Carlson, J. Clark, B. Wohlfarth, J. X. Mitrovica, S. W. Hostetler, and A. M. McCabe, The last glacial maximum, *Science*, *325*(5941), 710–714, 2009.
- Claussen, M., Late quaternary vegetation-climate feedbacks, *Climate of the Past*, *5*(2), 203–216, doi:10.5194/cp-5-203-2009, 2009.

- Claussen, M., K. Selent, V. Brovkin, T. Raddatz, and V. Gayler, Impact of co₂ and climate on last glacial maximum vegetation – a factor separation, *Biogeosciences Discuss.*, *9*(11), 15,823–15,852, 2012.
- Colbeck, S. C., Air movement in snow due to windpumping, *Journal of Glaciology*, *35*(120), 209–213, 1989.
- Colbeck, S. C., Model of wind pumping for layered snow, *Journal of Glaciology*, *43*(143), 60–65, 1997.
- Coleman, D. D., J. Risatti, and M. Schoell, Fractionation of carbon and hydrogen isotopes by methane-oxidizing bacteria, *Geochimica et Cosmochimica Acta*, *45*(7), 1033–1037, 1981.
- Collatz, G. J., J. A. Berry, and J. S. Clark, Effects of climate and atmospheric co₂ partial pressure on the global distribution of c₄ grasses: present, past, and future, *Oecologia*, *114*(4), 441–454, 1998.
- Collins, J. A., E. Schefuß, S. Mulitza, M. Prange, M. Werner, T. Tharammal, A. Paul, and G. Wefer, Estimating the hydrogen isotopic composition of past precipitation using leaf-waxes from western africa, *Quaternary Science Reviews*, *65*(0), 88 – 101, doi:<http://dx.doi.org/10.1016/j.quascirev.2013.01.007>, 2013.
- Conrad, R., *Exchange of Trace Gases between Terrestrial Ecosystems and the Atmosphere*, chap. Control of methane production in terrestrial ecosystems, p. 39–58, Dahlem Workshop Reports, Wiley, Chichester, 1989.
- Conrad, R., Quantification of methanogenic pathways using stable carbon isotopic signatures: a review and a proposal, *Organic Geochemistry*, *36*(5), 739–752, 2005.
- Conrad, R., M. Noll, P. Claus, M. Klose, W. R. Bastos, and A. Enrich-Prast, Stable carbon isotope discrimination and microbiology of methane formation in tropical anoxic lake sediments, *Biogeosciences*, *8*(3), 795–814, 2011.
- Coplen, T. B., Discontinuance of snow and p_{db}, *Nature*, *375*(6529), 285–285, 1995.
- Coplen, T. B., W. A. Brand, M. Gehre, M. Gröning, H. A. J. Meijer, B. Toman, and R. M. Verkouteren, New guidelines for $\delta^{13}\text{C}$ measurements, *Analytical Chemistry*, *78*(7), 2439–2441, doi:[10.1021/ac052027c](https://doi.org/10.1021/ac052027c), PMID: 16579631, 2006.

- Cottle, D. J., J. V. Nolan, and S. G. Wiedemann, Ruminant enteric methane mitigation: a review, *Anim. Prod. Sci.*, 51(6), 491–514, 2011.
- Cowling, S. A., and M. T. Sykes, Physiological significance of low atmospheric CO₂ for plant/climate interactions, *Quaternary Research*, 52(2), 237–242, 1999.
- Craig, H., The geochemistry of the stable carbon isotopes, *Geochimica et Cosmochimica Acta*, 3(2–3), 53–92, 1953.
- Craig, H., Isotopic standards for carbon and oxygen and correction factors for mass-spectrometric analysis of carbon dioxide, *Geochimica et Cosmochimica Acta*, 12(12), 133–149, doi:10.1016/0016-7037(57)90024-8, 1957.
- Craig, H., Isotopic variations in meteoric waters, *Science*, 133, 1702–1703, 1961.
- Craig, H., and C. C. Chou, Methane: The record in polar ice cores, *Geophys. Res. Lett.*, 9(11), 1221–1224, 1982.
- Craig, H., C. C. Chou, J. A. Welhan, C. M. Stevens, and A. Engelkemeir, The isotopic composition of methane in polar ice cores, *Science*, 242(4885), 1535–1539, 1988.
- Crowley, T. J., Ice-age methane variations, *Nature*, 353(6340), 122–123, 1991.
- Crutzen, P. J., and C. Brühl, A model study of atmospheric temperatures and the concentrations of ozone, hydroxyl, and some other photochemically active gases during the glacial, the pre-industrial holocene and the present, *Geophysical Research Letters*, 20(11), 1047–1050, doi:10.1029/93GL01423, 1993.
- Cruz, F. W., S. J. Burns, I. Karmann, W. D. Sharp, M. Vuille, A. O. Cardoso, J. A. Ferrari, P. L. Silva Dias, and O. Viana, Insolation-driven changes in atmospheric circulation over the past 116,000 years in subtropical Brazil, *Nature*, 434(7029), 63–66, 2005.
- Daniau, A.-L., S. Harrison, and P. Bartlein, Fire regimes during the last glacial, *Quaternary Science Reviews*, 29(21–22), 2918–2930, 2010.
- Daniels, L., G. Fulton, R. W. Spencer, and W. H. Orme-Johnson, Origin of hydrogen in methane produced by methanobacterium thermoautotrophicum., *Journal of Bacteriology*, 141(2), 694–698, 1980.

- Dansgaard, W., S. J. Johnsen, J. M \ddot{a} ller, and C. C. Langway, One thousand centuries of climatic record from camp century on the greenland ice sheet, *Science*, *166*(3903), 377–380, 1969.
- de Abreu, L., N. J. Shackleton, J. Schönfeld, M. Hall, and M. Chapman, Millennial-scale oceanic climate variability off the western iberian margin during the last two glacial periods, *Marine Geology*, *196*(1-2), 1–20, 2003.
- de Garidel-Thoron, T., L. Beaufort, F. Bassinot, and P. Henry, Evidence for large methane releases to the atmosphere from deep-sea gas-hydrate dissociation during the last glacial episode, *Proceedings of the National Academy of Sciences of the United States of America*, *101*(25), 9187–9192, 2004.
- Diefendorf, A. F., K. E. Mueller, S. L. Wing, P. L. Koch, and K. H. Freeman, Global patterns in leaf $\delta^{13}C$ discrimination and implications for studies of past and future climate, *Proceedings of the National Academy of Sciences*, *107*(13), 5738–5743, doi: 10.1073/pnas.0910513107, 2010.
- Dlugokencky, E. J., K. A. Masarie, P. M. Lang, P. P. Tans, L. P. Steele, and E. G. Nisbet, A dramatic decrease in the growth rate of atmospheric methane in the northern hemisphere during 1992, *Geophys. Res. Lett.*, *21*, 1994.
- Dlugokencky, E. J., L. P. Steele, P. M. Lang, and K. A. Masarie, Atmospheric methane at mauna loa and barrow observatories: Presentation and analysis of in situ measurements, *J. Geophys. Res.*, *100*(D11), 23,103–23,113, 1995.
- Dlugokencky, E. J., K. A. Masarie, P. M. Lang, and P. P. Tans, Continuing decline in the growth rate of the atmospheric methane burden, *Nature*, *393*(6684), 447–450, 1998.
- Dlugokencky, E. J., S. Houweling, L. Bruhwiler, K. A. Masarie, P. M. Lang, J. B. Miller, and P. P. Tans, Atmospheric methane levels off: Temporary pause or a new steady-state?, *Geophys. Res. Lett.*, *30*, 1992, 2003.
- Dlugokencky, E. J., R. C. Myers, P. M. Lang, K. A. Masarie, A. M. Croswell, K. W. Thoning, B. D. Hall, J. W. Elkins, and L. P. Steele, Conversion of noaa atmospheric dry air CH_4 mole fractions to a gravimetrically prepared standard scale, *J. Geophys. Res.*, *110*(D18), D18,306–, 2005.

- Dlugokencky, E. J., E. G. Nisbet, R. Fisher, and D. Lowry, Global atmospheric methane: budget, changes and dangers, *Philosophical Transactions of the Royal Society A: Mathematical, Physical and Engineering Sciences*, 369(1943), 2058–2072, 2011.
- Dlugokencky, E. J., et al., Observational constraints on recent increases in the atmospheric CH₄ burden, *Geophys. Res. Lett.*, 36, L18,803, 2009.
- Dragomir, S. S., R. P. Agarwal, and P. Cerone, On simpson's inequality and applications, *Journal of Inequalities and Applications*, 5(6), 533–579, doi:10.1155/S102558340000031X, 2000.
- Drake, H. L., M. A. Horn, and P. K. W¹/₄st, Intermediary ecosystem metabolism as a main driver of methanogenesis in acidic wetland soil, *Environmental Microbiology Reports*, 1(5), 307–318, 2009.
- Dueck, T. A., et al., No evidence for substantial aerobic methane emission by terrestrial plants: a c-13-labelling approach, *New Phytologist*, 175(1), 29–35, doi:10.1111/j.1469-8137.2007.02103.x, 2007.
- Dutaur, L., and L. V. Verchot, A global inventory of the soil ch₄ sink, *Global Biogeochem. Cycles*, 21(4), GB4013–, 2007.
- Dällenbach, A., T. Blunier, J. Flückiger, B. Stauffer, J. Chappellaz, and D. Raynaud, Changes in the atmospheric ch₄ gradient between greenland and antarctica during the last glacial and the transition to the holocene, *Geophys. Res. Lett.*, 27, 1005–1008, 2000.
- Edwards, E. J., C. P. Osborne, C. A. E. Strömberg, S. A. Smith, and C. . G. Consortium, The origins of c₄ grasslands: Integrating evolutionary and ecosystem science, *Science*, 328(5978), 587–591, 2010.
- Ehhalt, D. H., The atmospheric cycle of methane., *Tellus*, 26, 58–70, 1974.
- Ehleringer, J., The influence of atmospheric co₂, temperature, and water on the abundance of c₃/c₄ taxa, in *Ecological Studies*, vol. 177, edited by I. Baldwin, M. Caldwell, G. Heldmaier, R. Jackson, O. Lange, H. Mooney, E.-D. Schulze, U. Sommer, J. Ehleringer, M. Denise Dearing, and T. Cerling, pp. 214–231–, Springer New York, 2005.

- Ehleringer, J. R., Implications of quantum yield differences on the distributions of $\delta^{13}\text{C}$ and $\delta^{14}\text{C}$ grasses, *Oecologia*, 31(3), 255–267, 1978.
- Ehleringer, J. R., C. B. Field, Z.-f. Lin, and C.-y. Kuo, Leaf carbon isotope and mineral composition in subtropical plants along an irradiance cline, *Oecologia*, 70(4), 520–526, 1986.
- Ehleringer, J. R., T. E. Cerling, and B. R. Helliker, C4 photosynthesis, atmospheric CO₂, and climate, *Oecologia*, 112(3), 285–299, 1997.
- Elenga, H., et al., Pollen-based biome reconstruction for southern Europe and Africa 18,000 years BP, *Journal of Biogeography*, 27(3), 621–634, 2000.
- EPICA community members, One-to-one coupling of glacial climate variability in Greenland and Antarctica, *Nature*, 444(7116), 195–198, 2006.
- Etheridge, D. M., L. P. Steele, R. J. Francey, and R. L. Langenfelds, Atmospheric methane between 1000 A.D. and present: Evidence of anthropogenic emissions and climatic variability, *J. Geophys. Res.*, 103, –, 1998.
- Etioppe, G., New directions: Geologic emissions of methane, the missing source in the atmospheric methane budget, *Atmospheric Environment*, 38(19), 3099–3100, 2004.
- Etioppe, G., and R. W. Klusman, Geologic emissions of methane to the atmosphere, *Chemosphere*, 49(8), 777–789, 2002.
- Etioppe, G., and R. W. Klusman, Microseepage in drylands: Flux and implications in the global atmospheric source/sink budget of methane, *Global and Planetary Change*, 72(4), 265–274, 2010.
- Etioppe, G., K. R. Lassey, R. W. Klusman, and E. Boschi, Reappraisal of the fossil methane budget and related emission from geologic sources, *Geophys. Res. Lett.*, 35(9), L09307–, 2008a.
- Etioppe, G., A. V. Milkov, and E. Derbyshire, Did geologic emissions of methane play any role in quaternary climate change?, *Global and Planetary Change*, 61(1–2), 79–88, 2008b.

- Etioppe, G., A. Feyzullayev, and C. L. Baciu, Terrestrial methane seeps and mud volcanoes: A global perspective of gas origin, *Marine and Petroleum Geology*, *26*(3), 333–344, 2009.
- Farquhar, G. D., M. H. O'Leary, and J. A. Berry, On the relationship between carbon isotope discrimination and the inter-cellular carbon-dioxide concentration in leaves, *Australian Journal of Plant Physiology*, *9*(2), 121–137, 1982.
- Farquhar, G. D., J. R. Ehleringer, and K. T. Hubick, Carbon isotope discrimination and photosynthesis, *Annual Review of Plant Physiology and Plant Molecular Biology*, *40*, 503–537, doi:10.1146/annurev.pp.40.060189.002443, 1989.
- Ferretti, D. F., et al., Unexpected changes to the global methane budget over the past 2000 years, *Science*, *309*(5741), 1714–1717, 2005.
- Fey, A., P. Claus, and R. Conrad, Temporal change of ^{13}C -isotope signatures and methanogenic pathways in rice field soil incubated anoxically at different temperatures, *Geochimica et Cosmochimica Acta*, *68*(2), 293–306, 2004.
- Fischer, H., M. L. Siggaard-Andersen, U. Ruth, R. Rothlisberger, and E. Wolff, Glacial/interglacial changes in mineral dust and sea-salt records in polar ice cores: Sources, transport, and deposition, *Reviews of Geophysics*, *45*(1), RG1002, doi: 10.1029/2005RG000192, 2007.
- Fischer, H., et al., Changing boreal methane sources and constant biomass burning during the last termination., *Nature*, *452*(7189), 864–867, doi:10.1038/nature06825, 2008.
- Fleitmann, D., et al., Timing and climatic impact of greenland interstadials recorded in stalagmites from northern turkey, *Geophys. Res. Lett.*, *36*, –, 2009.
- Flückiger, J., T. Blunier, B. Stauffer, J. Chappellaz, R. Spahni, K. Kawamura, J. Schwander, T. F. Stocker, and D. Dahl-Jensen, N_2O and CH_4 variations during the last glacial epoch: Insight into global processes, *Global Biogeochem. Cycles*, *18*, –, 2004.
- Frankenberg, C., J. F. Meirink, M. van Weele, U. Platt, and T. Wagner, Assessing methane emissions from global space-borne observations, *Science*, *308*(5724), 1010–1014, 2005.
- Frankenberg, C., I. Aben, P. Bergamaschi, E. J. Dlugokencky, R. van Hees, S. Houweling, P. van der Meer, R. Snel, and P. Tol, Global column-averaged methane mixing ratios

- from 2003 to 2009 as derived from sciamachy: Trends and variability, *J. Geophys. Res.*, *116*(D4), D04,302–, 2011.
- Frankenberg, C., et al., Tropical methane emissions: A revised view from sciamachy onboard envisat, *Geophys. Res. Lett.*, *35*, –, 2008.
- Games, L. M., J. HayesRobert, and P. Gunsalus, Methane-producing bacteria: natural fractionations of the stable carbon isotopes, *Geochimica et Cosmochimica Acta*, *42*(8), 1295–1297, 1978.
- Gerhart, L. M., and J. K. Ward, Plant responses to low [co₂] of the past, *New Phytologist*, *188*(3), 674–695, 2010.
- Gierczak, T., R. K. Talukdar, S. C. Herndon, G. L. Vaghjiani, and A. R. Ravishankara, Rate coefficients for the reactions of hydroxyl radicals with methane and deuterated methanes, *J. Phys. Chem. A*, *101*(17), 3125–3134, doi:10.1021/jp963892r, 1997.
- Glückauf, E., The composition of atmospheric air, in *Compendium of meteorology*, edited by T. F. Malone, pp. 3–11, American Meteorological Society, Boston, 1951.
- Grachev, A. M., and J. P. Severinghaus, Determining the thermal diffusion factor for ⁴⁰Ar/³⁶Ar in air to aid paleoreconstruction of abrupt climate change, *J. Phys. Chem. A*, *107*(23), 4636–4642, doi:10.1021/jp027817u, 2003.
- Grachev, A. M., E. J. Brook, J. P. Severinghaus, and N. G. Pisias, Relative timing and variability of atmospheric methane and gisp2 oxygen isotopes between 68 and 86 ka, *Global Biogeochem. Cycles*, *23*, –, 2009.
- Grant, K. M., E. J. Rohling, M. Bar-Matthews, A. Ayalon, M. Medina-Elizalde, C. B. Ramsey, C. Satow, and A. P. Roberts, Rapid coupling between ice volume and polar temperature over the past 150,000[thinsp]years, *Nature*, *491*(7426), 744–747, 2012.
- Gupta, M. L., M. P. McGrath, R. J. Cicerone, F. S. Rowland, and M. Wolfsberg, ¹²C/¹³C kinetic isotope effects in the reactions of CH₄ with OH and Cl, *Geophys. Res. Lett.*, *24*(22), 2761–2764, 1997.
- Hackstein, J., and C. Stumm, Methane production in terrestrial arthropods., *Proceedings of the National Academy of Sciences of the United States of America*, *91*(12), 5441–, 1994.

- Hamilton, T. L., J. W. Peters, M. L. Skidmore, and E. S. Boyd, Molecular evidence for an active endogenous microbiome beneath glacial ice, *ISME J*, pp. –, 2013.
- Hansen, J., R. Ruedy, M. Sato, and R. Reynolds, Global surface air temperature in 1995: Return to pre-pinatubo level, *Geophys. Res. Lett.*, *23*(13), 1665–1668, 1996.
- Harrison, S., and M. Sanchez Goñi, Global patterns of vegetation response to millennial-scale variability and rapid climate change during the last glacial period, *Quaternary Science Reviews*, *29*(21-22), 2957–2980, doi:10.1016/j.quascirev.2010.07.016, 2010.
- Harrison, S. P., and C. I. Prentice, Climate and co2 controls on global vegetation distribution at the last glacial maximum: analysis based on palaeovegetation data, biome modelling and palaeoclimate simulations, *Global Change Biology*, *9*(7), 983–1004, doi:10.1046/j.1365-2486.2003.00640.x, 2003.
- Headly, M. A., and J. P. Severinghaus, A method to measure kr/n2 ratios in air bubbles trapped in ice cores and its application in reconstructing past mean ocean temperature, *J. Geophys. Res.*, *112*(D19), D19,105–, 2007.
- Hein, R., P. J. Crutzen, and M. Heimann, An inverse modeling approach to investigate the global atmospheric methane cycle, *Global Biogeochem. Cycles*, *11*(1), 43–76, 1997.
- Heinrich, H., Origin and consequences of cyclic ice rafting in the northeast atlantic ocean during the past 130,000 years, *Quaternary Research*, *29*(2), 142–152, 1988.
- Hemming, S. R., Heinrich events: Massive late pleistocene detritus layers of the north atlantic and their global climate imprint, *Rev. Geophys.*, *42*, –, 2004.
- Hessler, I., et al., Millennial-scale changes in vegetation records from tropical africa and south america during the last glacial, *Quaternary Science Reviews*, *29*(21-22), 2882–2899, doi:10.1016/j.quascirev.2009.11.029, 2010.
- Hester, K. C., and P. G. Brewer, Clathrate hydrates in nature, *Annu. Rev. Marine. Sci.*, *1*(1), 303–327, 2009.
- Heuer, V. B., M. Krüger, M. Elvert, and K.-U. Hinrichs, Experimental studies on the stable carbon isotope biogeochemistry of acetate in lake sediments, *Organic Geochemistry*, *41*(1), 22–30, 2010.

- Hoehler, T. M., M. J. Alperin, D. B. Albert, and C. S. Martens, Thermodynamic control on hydrogen concentrations in anoxic sediments, *Geochimica et Cosmochimica Acta*, 62(10), 1745–1756, 1998.
- Hoffmann, D., H. Laitko, and S. Müller-Wille, *Lexikon der bedeutenden Wissenschaftler*, Spektrum Akademischer Verlag, 2004.
- Hopcroft, P. O., P. J. Valdes, and D. J. Beerling, Simulating idealized dansgaard-oeschger events and their potential impacts on the global methane cycle, *Quaternary Science Reviews*, 30(23–24), 3258–3268, 2011.
- Hornibrook, E. R., F. J. Longstaffe, and W. S. Fyfe, Spatial distribution of microbial methane production pathways in temperate zone wetland soils: Stable carbon and hydrogen isotope evidence, *Geochimica et Cosmochimica Acta*, 61(4), 745–753, 1997.
- Hornibrook, E. R., F. J. Longstaffe, and W. S. Fyfe, Evolution of stable carbon isotope compositions for methane and carbon dioxide in freshwater wetlands and other anaerobic environments, *Geochimica et Cosmochimica Acta*, 64(6), 1013–1027, 2000.
- Houweling, S., T. Kaminski, F. Dentener, J. Lelieveld, and M. Heimann, Inverse modeling of methane sources and sinks using the adjoint of a global transport model, *J. Geophys. Res.*, 104(D21), 26,137–26,160, 1999.
- Houweling, S., T. Rockmann, I. Aben, F. Keppler, M. Krol, J. F. Meirink, E. J. Dlugokencky, and C. Frankenberg, Atmospheric constraints on global emissions of methane from plants, *Geophysical Research Letters*, 33(15), L15,821, 2006.
- Hovland, M., and A. G. Judd, The global production of methane from shallow submarine sources, *Continental Shelf Research*, 12(10), 1231 – 1238, doi:http://dx.doi.org/10.1016/0278-4343(92)90082-U, jce:titlejMethane in Marine Sedimentsj/ce:titlej, 1992.
- Huang, Y., F. A. Street-Perrott, S. E. Metcalfe, M. Brenner, M. Moreland, and K. H. Freeman, Climate change as the dominant control on glacial-interglacial variations in c3 and c4 plant abundance, *Science*, 293(5535), 1647–1651, 2001.
- Huber, C., M. Leuenberger, R. Spahni, J. Flückiger, J. Schwander, T. F. Stocker, S. Johnsen, A. Landais, and J. Jouzel, Isotope calibrated greenland temperature record over marine isotope stage 3 and its relation to ch4, *Earth and Planetary Science Letters*, 243(3-4), 504 – 519, doi:DOI:10.1016/j.epsl.2006.01.002, 2006.

- Hughen, K. A., T. I. Eglinton, L. Xu, and M. Makou, Abrupt tropical vegetation response to rapid climate changes, *Science*, 304(5679), 1955–1959, 2004.
- IPCC, *Climate Change 2007 - The Physical Science Basis: Working Group I Contribution to the Fourth Assessment Report of the Intergovernmental panel on climate change*, IPCC, Cambridge University Press, 2007.
- Irion, F. W., et al., Stratospheric observations of ch₃d and hdo from atmos infrared solar spectra: Enrichments of deuterium in methane and implications for hd, *Geophys. Res. Lett.*, 23(17), 2381–2384, 1996.
- Ivanochko, T. S., R. S. Ganeshram, G.-J. A. Brummer, G. Ganssen, S. J. Jung, S. G. Moreton, and D. Kroon, Variations in tropical convection as an amplifier of global climate change at the millennial scale, *Earth and Planetary Science Letters*, 235(1-2), 302–314, 2005.
- Johnsen, S. J., H. B. Clausen, Dansgaard, W., and C. C. Langway, Oxygen isotope profiles through antarctic and greenland ice sheets, *Nature*, 235(5339), 429–434, doi:10.1038/235429a0, 1972.
- Johnsen, S. J., et al., Irregular glacial interstadials recorded in a new greenland ice core, *Nature*, 359(6393), 311–313, 1992.
- Johnson, D., K. Johnson, G. Ward, and M. Branine, Ruminants and other animals, in *Atmospheric Methane*, edited by M. Khalil, pp. 112–133–, Springer Berlin Heidelberg, 2000.
- Jolly, D., and A. Haxeltine, Effect of low glacial atmospheric co₂ on tropical african montane vegetation, *Science*, 276(5313), 786–788, 1997.
- Jones, M. B., and F. M. Muthuri, Standing biomass and carbon distribution in a papyrus (*Cyperus papyrus* L.) swamp on lake naivasha, kenya, *Journal of Tropical Ecology*, 13(03), 347–356 M3 – 10.1017/S0266467400010,555, 1997.
- Joos, F., S. Gerber, I. C. Prentice, B. L. Otto-Bliesner, and P. J. Valdes, Transient simulations of holocene atmospheric carbon dioxide and terrestrial carbon since the last glacial maximum, *Global Biogeochem. Cycles*, 18(2), GB2002–, 2004.
- Jouzel, J., et al., Orbital and millennial antarctic climate variability over the past 800,000 years, *Science*, 317(5839), 793–796, 2007.

- Judd, A., Natural seabed gas seeps as sources of atmospheric methane, *Environmental Geology*, 46(8), 988–996, doi:10.1007/s00254-004-1083-3, 2004.
- Judd, A., G. Davies, J. Wilson, R. Holmes, G. Baron, and I. Bryden, Contributions to atmospheric methane by natural seepages on the {UK} continental shelf, *Marine Geology*, 137(1–2), 165 – 189, doi:http://dx.doi.org/10.1016/S0025-3227(96)00087-4, Gas in Marine Sediments, *Geology/Geochemistry/Microbiology*, 1997.
- Judd, A. G., M. Hovland, L. I. Dimitrov, S. García Gil, and V. Jukes, The geological methane budget at continental margins and its influence on climate change, *Geofluids*, 2(2), 109–126, 2002.
- Kai, F. M., S. C. Tyler, J. T. Randerson, and D. R. Blake, Reduced methane growth rate explained by decreased northern hemisphere microbial sources, *Nature*, 476(7359), 194–197, 2011.
- Kamakura, M., Y. Kosugi, R. Nakagawa, and M. Itoh, Methane flux of leaves in a tropical rainforest and a temperate conifer forest:, *Journal of Agricultural Meteorology*, 68(1), 25–33, 2012.
- Kanner, L. C., S. J. Burns, H. Cheng, and R. L. Edwards, High-latitude forcing of the south american summer monsoon during the last glacial, *Science*, 335(6068), 570–573, 2012.
- Kaplan, J. O., Wetlands at the last glacial maximum: Distribution and methane emissions, *Geophys. Res. Lett.*, 29, –, 2002.
- Kaplan, J. O., G. Folberth, and D. A. Hauglustaine, Role of methane and biogenic volatile organic compound sources in late glacial and holocene fluctuations of atmospheric methane concentrations, *Global Biogeochem. Cycles*, 20, GB2016, 2006.
- Kaufmann, P. R., U. Federer, M. A. Hutterli, M. Bigler, S. Schüpbach, U. Ruth, J. Schmitt, and T. F. Stocker, An improved continuous flow analysis system for high-resolution field measurements on ice cores, *Environ. Sci. Technol.*, 42(21), 8044–8050, doi:10.1021/es8007722, 2008.
- Kennett, J. P., K. G. Cannariato, I. L. Hendy, and R. J. Behl, Carbon isotopic evidence for methane hydrate instability during quaternary interstadials, *Science*, 288(5463), 128–133, 2000.

- Kennett, J. P., K. G. Cannariato, I. L. Hendy, and R. J. Behl, *Methane Hydrates in Quaternary Climate Change: The Clathrate Gun Hypothesis*, vol. 54, –216 pp., AGU, Washington, DC, 2003.
- Keppler, F., J. T. G. Hamilton, M. Brass, and T. Roeckmann, Methane emissions from terrestrial plants under aerobic conditions, *Nature*, 439(7073), 187–191, 2006.
- Khalil, M. A. K., R. A. Rasmussen, and M. J. Shearer, Trends of atmospheric methane during the 1960s and 1970s, *J. Geophys. Res.*, 94(D15), 18,279–18,288, 1989.
- Khalil, M. A. K., R. A. Rasmussen, J. R. J. French, and J. A. Holt, The influence of termites on atmospheric trace gases: CH_4 , CO_2 , CHCl_3 , N_2O , CO , H_2 , and light hydrocarbons, *J. Geophys. Res.*, 95(D4), 3619–3634, 1990.
- King, S. L., P. D. Quay, and J. M. Lansdown, The $^{13}\text{C}/^{12}\text{C}$ kinetic isotope effect for soil oxidation of methane at ambient atmospheric concentrations, *J. Geophys. Res.*, 94(D15), 18,273–18,277, 1989.
- Kirschbaum, M., D. Bruhn, D. Etheridge, J. Evans, G. Farquhar, R. Gifford, K. Paul, and A. Winters, A comment on the quantitative significance of aerobic methane release by plants, *Funct. Plant Biol.*, 33(6), 521–530, 2006.
- Klein, A. R., V. M. Fernández, and R. K. Thauer, H_2 -forming $\text{N}_5, \text{N}_{10}$ -methylene-tetrahydromethanopterin dehydrogenase: mechanism of H_2 formation analyzed using hydrogen isotopes, *FEBS Letters*, 368(2), 203–206, 1995.
- Kotze, D. C., and T. G. O'Connor, Vegetation variation within and among palustrine wetlands along an altitudinal gradient in kwazulu-natal, south africa, *Plant Ecology*, 146(1), 77–96, 2000.
- Kvenvolden, K. A., Methane hydrate - a major reservoir of carbon in the shallow geosphere?, *Chemical Geology*, 71(1-3), 41–51, 1988.
- Kvenvolden, K. A., and B. W. Rogers, Gaia's breath— global methane exhalations, *Marine and Petroleum Geology*, 22(4), 579–590, 2005.
- Lacroix, A. V., Unaccounted-for sources of fossil and isotopically-enriched methane and their contribution to the emissions inventory: A review and synthesis, *Chemosphere*, 26(1–4), 507–557, 1993.

- Landais, A., et al., Firn-air $\delta^{15}\text{N}$ in modern polar sites and glacial-interglacial ice: a model-data mismatch during glacial periods in Antarctica?, *Quaternary Science Reviews*, 25(1-2), 49–62, 2006.
- Landais, A., et al., What drives the millennial and orbital variations of $[\delta^{18}\text{O}_{\text{atm}}]$?, *Quaternary Science Reviews*, 29(1-2), 235–246, 2010.
- Lane, C., S. Horn, C. Mora, K. Orvis, and D. Finkelstein, Sedimentary stable carbon isotope evidence of late quaternary vegetation and climate change in highland costa rica, *Journal of Paleolimnology*, 45(3), 323–338–338, 2011.
- Lassey, K. R., D. M. Etheridge, D. C. Lowe, A. M. Smith, and D. F. Ferretti, Centennial evolution of the atmospheric methane budget: what do the carbon isotopes tell us?, *Atmos. Chem. Phys.*, 7(8), 2119–2139, 2007.
- Lassey, K. R., W. Allan, and S. E. M. Fletcher, Seasonal inter-relationships in atmospheric methane and companion $\delta^{13}\text{C}$ values: effects of sinks and sources, *Tellus B*, 63(3), 287–301, 2011.
- Lea, D., D. K. Pak, L. C. Peterson, and K. A. Hughen, Synchronicity of tropical and high latitude temperature over the last glacial termination, *Science*, 301, 1361–1364, 2003.
- Leduc, G., L. Vidal, K. Tachikawa, F. Rostek, C. Sonzogni, L. Beaufort, and E. Bard, Moisture transport across central america as a positive feedback on abrupt climatic changes, *Nature*, 445(7130), 908–911, 2007.
- Lehner, B., and P. Döll, Development and validation of a global database of lakes, reservoirs and wetlands, *Journal of Hydrology*, 296(1–4), 1–22, 2004.
- Leifer, I., and R. K. Patro, The bubble mechanism for methane transport from the shallow sea bed to the surface: A review and sensitivity study, *Continental Shelf Research*, 22(16), 2409–2428, 2002.
- Leifer, I., B. P. Luyendyk, J. Boles, and J. F. Clark, Natural marine seepage blowout: Contribution to atmospheric methane, *Global Biogeochem. Cycles*, 20(3), GB3008–, 2006.
- Lelieveld, J., W. Peters, F. J. Dentener, and M. C. Krol, Stability of tropospheric hydroxyl chemistry, *J. Geophys. Res.*, 107(D23), 4715–, 2002.

- Lelieveld, J., F. J. Dentener, W. Peters, and M. C. Krol, On the role of hydroxyl radicals in the self-cleansing capacity of the troposphere, *Atmos. Chem. Phys.*, *4*(9/10), 2337–2344, 2004.
- Lelieveld, J., et al., Atmospheric oxidation capacity sustained by a tropical forest, *Nature*, *452*(7188), 737–740, 2008.
- Lemieux-Dudon, B., E. Blayo, J.-R. Petit, C. Waelbroeck, A. Svensson, C. Ritz, J.-M. Barnola, B. M. Narcisi, and F. Parrenin, Consistent dating for antarctic and greenland ice cores, *Quaternary Science Reviews*, *29*(1-2), 8–20, 2010.
- Levin, I., H. Glatzel-Mattheier, T. Marik, M. Cuntz, M. Schmidt, and D. E. Worthy, Verification of german methane emission inventories and their recent changes based on atmospheric observations, *Journal of Geophysical Research-atmospheres*, *104*(D3), 3447–3456, doi:10.1029/1998JD100064, 1999.
- Levine, J. G., E. W. Wolff, A. E. Jones, and L. C. Sime, The role of atomic chlorine in glacial-interglacial changes in the carbon-13 content of atmospheric methane, *Geophys. Res. Lett.*, *38*(4), L04,801–, 2011a.
- Levine, J. G., E. W. Wolff, A. E. Jones, L. C. Sime, P. J. Valdes, A. T. Archibald, G. D. Carver, N. J. Warwick, and J. A. Pyle, Reconciling the changes in atmospheric methane sources and sinks between the last glacial maximum and the pre-industrial era, *Geophys. Res. Lett.*, *38*(23), L23,804–, 2011b.
- Levine, J. G., E. W. Wolff, P. O. Hopcroft, and P. J. Valdes, Controls on the tropospheric oxidizing capacity during an idealized dansgaard-oeschger event, and their implications for the rapid rises in atmospheric methane during the last glacial period, *Geophysical Research Letters*, *39*(12), n/a–n/a, doi:10.1029/2012GL051866, 2012.
- Lewis, S. C., A. N. LeGrande, M. Kelley, and G. A. Schmidt, Water vapour source impacts on oxygen isotope variability in tropical precipitation during heinrich events, *Clim. Past*, *6*(3), 325–343, doi:10.5194/cp-6-325-2010, 2010.
- Lisiecki, L. E., and M. E. Raymo, A pliocene-pleistocene stack of 57 globally distributed benthic $\delta^{18}\text{O}$ records, *Paleoceanography*, *20*(1), PA1003, 2005.
- Liu, Y., T. Yao, G. Gleixner, P. Claus, and R. Conrad, Methanogenic pathways, ^{13}C isotope fractionation, and archaeal community composition in lake sediments and wetland soils on the tibetan plateau, *J. Geophys. Res. Biogeosci.*, 2013.

- Lorius, C., J. Jouzel, C. Ritz, L. Merlivat, N. I. Barkov, Y. S. Korotkevich, and V. M. Kotlyakov, A 150,000-year climatic record from antarctic ice, *Nature*, *316*(6029), 591–596, doi:10.1038/316591a0, 1985.
- Loulergue, L., et al., Orbital and millennial-scale features of atmospheric ch₄ over the past 800,000 years., *Nature*, *453*(7193), 383–386, doi:10.1038/nature06950, 2008.
- Lovley, D. R., and M. J. Klug, Intermediary metabolism of organic matter in the sediments of a eutrophic lake, *Applied and Environmental Microbiology*, *43*(3), 552–560, 1982.
- Luyendyk, B., J. Kennett, and J. F. Clark, Hypothesis for increased atmospheric methane input from hydrocarbon seeps on exposed continental shelves during glacial low sea level, *Marine and Petroleum Geology*, *22*(4), 591–596, 2005.
- Lüthi, D., et al., High-resolution carbon dioxide concentration record 650,000-800,000 years before present., *Nature*, *453*(7193), 379–382, doi:10.1038/nature06949, 2008.
- MacDonald, G. M., D. W. Beilman, K. V. Kremenetski, Y. Sheng, L. C. Smith, and A. A. Velichko, Rapid early development of circumarctic peatlands and atmospheric ch₄ and co₂ variations, *Science*, *314*(5797), 285–288, 2006.
- MacDonald, I. R., I. Leifer, R. Sassen, P. Stine, R. Mitchell, and N. Guinasso, Transfer of hydrocarbons from natural seeps to the water column and atmosphere, *Geofluids*, *2*(2), 95–107, 2002.
- MacFarling Meure, C., D. Etheridge, C. Trudinger, P. Steele, R. Langenfelds, T. van Ommen, A. Smith, and J. Elkins, Law dome co₂, ch₄ and n₂o ice core records extended to 2000 years bp, *Geophys. Res. Lett.*, *33*(14), L14,810–, 2006.
- Mantlana, K. B., A. Arneth, E. M. Veenendaal, P. Wohland, P. Wolski, O. Kolle, M. Wagner, and J. Lloyd, Photosynthetic properties of c₄ plants growing in an african savanna/wetland mosaic, *Journal of Experimental Botany*, *59*(14), 3941–3952, 2008.
- MARGO members, ., Constraints on the magnitude and patterns of ocean cooling at the last glacial maximum, *Nature Geoscience*, *2*(2), 127–132, 2009.
- Marlon, J. R., et al., Wildfire responses to abrupt climate change in north america, *Proceedings of the National Academy of Sciences*, *106*(8), 2519–2524, 2009.

- Martinerie, P., G. P. Brasseur, and C. Granier, The chemical composition of ancient atmospheres: A model study constrained by ice core data, *J. Geophys. Res.*, *100*(D7), 14,291–14,304, 1995.
- Martinson, G. O., et al., Methane emissions from tank bromeliads in neotropical forests, *Nature Geosci*, *3*(11), 766–769, 2010.
- Maslin, M. A., and E. Thomas, Balancing the deglacial global carbon budget: the hydrate factor, *Quaternary Science Reviews*, *22*(15–17), 1729–1736, 2003.
- Masson-Delmotte, V., et al., Past temperature reconstructions from deep ice cores: relevance for future climate change, *Climate of the Past*, *2*(2), 145–165, 2006.
- Matthews, E., and I. Fung, Methane emission from natural wetlands: Global distribution, area, and environmental characteristics of sources, *Global Biogeochem. Cycles*, *1*, –, 1987.
- Mayer, E. W., D. R. Blake, S. C. Tyler, Y. Makide, D. C. Montague, and F. S. Rowland, Methane: Interhemispheric concentration gradient and atmospheric residence time, *Proc. Natl. Acad. Sci. USA*, *79*(4), 1366–1370, 1982.
- Mayle, F. E., and D. J. Beerling, Late quaternary changes in amazonian ecosystems and their implications for global carbon cycling, *Palaeogeography, Palaeoclimatology, Palaeoecology*, *214*(1-2), 11–25, 2004.
- Mayle, F. E., R. Burbridge, and T. J. Killeen, Millennial-scale dynamics of southern amazonian rain forests, *Science*, *290*, 2291–2294, 2000.
- Mayle, F. E., D. J. Beerling, W. D. Gosling, and M. B. Bush, Responses of amazonian ecosystems to climatic and atmospheric carbon dioxide changes since the last glacial maximum, *Philosophical Transactions of the Royal Society of London. Series B: Biological Sciences*, *359*(1443), 499–514, 2004.
- McGinnis, D. F., J. Greinert, Y. Artemov, S. E. Beaubien, and A. Wüest, Fate of rising methane bubbles in stratified waters: How much methane reaches the atmosphere?, *J. Geophys. Res.*, *111*(C9), C09,007–, 2006.
- McManus, J. F., R. Francois, J.-M. Gherardi, L. D. Keigwin, and S. Brown-Leger, Collapse and rapid resumption of atlantic meridional circulation linked to deglacial climate changes, *Nature*, *428*(6985), 834–837, 2004.

- Medina, E., and P. Minchin, Stratification of $\delta^{13}\text{C}$ values of leaves in amazonian rain forests, *Oecologia*, 45(3), 377–378, 1980.
- Melton, J., Methane stable carbon isotope dynamics spanning the last deglaciation, Ph.D. thesis, School of Earth and Ocean Sciences, University of Victoria, 2009.
- Melton, J. R., M. J. Whiticar, and P. Eby, Stable carbon isotope ratio analyses on trace methane from ice samples, *Chemical Geology*, 288(3–4), 88–96, 2011.
- Melton, J. R., H. Schaefer, and M. J. Whiticar, Enrichment in ^{13}C of atmospheric CH_4 during the younger dryas termination, *Clim. Past*, 8(4), 1177–1197, 2012.
- Migeotte, M. V., Spectroscopic evidence of methane in the earth's atmosphere, *Phys. Rev.*, 73(5), 519–520, 1948a.
- Migeotte, M. V., Methane in the earth's atmosphere, *Astrophysical Journal*, 107(3), 400–403, 1948b.
- Mikaloff Fletcher, S. E., P. P. Tans, L. M. Bruhwiler, J. B. Miller, and M. Heimann, CH_4 sources estimated from atmospheric observations of CH_4 and its $^{13}\text{C}/^{12}\text{C}$ isotopic ratios: 1. inverse modeling of source processes, *Global Biogeochem. Cycles*, 18(4), GB4004–, 2004a.
- Mikaloff Fletcher, S. E., P. P. Tans, L. M. Bruhwiler, J. B. Miller, and M. Heimann, CH_4 sources estimated from atmospheric observations of CH_4 and its $^{13}\text{C}/^{12}\text{C}$ isotopic ratios: 2. inverse modeling of CH_4 fluxes from geographical regions, *Global Biogeochem. Cycles*, 18(4), GB4005–, 2004b.
- Milkov, A. V., Global estimates of hydrate-bound gas in marine sediments: how much is really out there?, *Earth-Science Reviews*, 66(3–4), 183–197, 2004.
- Milkov, A. V., Molecular and stable isotope compositions of natural gas hydrates: A revised global dataset and basic interpretations in the context of geological settings, *Organic Geochemistry*, 36(5), 681 – 702, doi:<http://dx.doi.org/10.1016/j.orggeochem.2005.01.010>, *Stable isotope applications in methane cycle studies*, 2005.
- Miller, J. B., K. A. Mack, R. Dissly, J. W. C. White, E. J. Dlugokencky, and P. P. Tans, Development of analytical methods and measurements of $^{13}\text{C}/^{12}\text{C}$ in atmospheric

- ch4 from the noaa climate monitoring and diagnostics laboratory global air sampling network, *J. Geophys. Res.*, *107*(D13), 4178–, 2002.
- Millo, C., M. Sarnthein, H. Erlenkeuser, and T. Frederichs, Methane-driven late pleistocene delta13c minima and overflow reversals in the southwestern greenland sea, *Geology*, *33*(11), 873–876, doi:10.1130/G21790.1, 2005.
- Mischler, J. A., T. A. Sowers, R. B. Alley, M. Battle, J. R. McConnell, L. Mitchell, T. Popp, E. Sofen, and M. K. Spencer, Carbon and hydrogen isotopic composition of methane over the last 1000 years, *Global Biogeochem. Cycles*, *23*(4), GB4024–, 2009.
- Mitchell, L. E., E. J. Brook, T. Sowers, J. R. McConnell, and K. Taylor, Multidecadal variability of atmospheric methane, 1000-1800 c.e., *J. Geophys. Res.*, *116*(G2), G02,007–, 2011.
- Mitsch, W., A. Nahlik, P. Wolski, B. Bernal, L. Zhang, and L. Ramberg, Tropical wetlands: seasonal hydrologic pulsing, carbon sequestration, and methane emissions, *Wetlands Ecology and Management*, *18*(5), 573–586, 2010.
- Mitsch, W. J., and J. G. Gosselink, *Wetlands*, 4th edition ed., John Wiley & Sons Inc., New York, 2007.
- Monnin, E., A. Indermühle, A. Dällenbach, J. Flückiger, B. Stauffer, T. F. Stocker, D. Raynaud, and J.-M. Barnola, Atmospheric co2 concentrations over the last glacial termination, *Science*, *291*(5501), 112–114, doi:10.1126/science.291.5501.112, 2001.
- Monteil, G., S. Houweling, E. J. Dlugokenky, G. Maenhout, B. H. Vaughn, J. W. C. White, and T. Rockmann, Interpreting methane variations in the past two decades using measurements of ch4 mixing ratio and isotopic composition, *Atmos. Chem. Phys.*, *11*(17), 9141–9153, 2011.
- Montzka, S. A., E. J. Dlugokenky, and J. H. Butler, Non-co2 greenhouse gases and climate change, *Nature*, *476*(7358), 43–50, 2011.
- Moss, A. R., J.-P. Jouany, and J. Newbold, Methane production by ruminants: its contribution to global warming, *Ann. Zootech.*, *49*(3), 231–253, 2000.
- Müller, S., P. E. Tarasov, A. A. Andreev, and B. Diekmann, Late glacial to holocene environments in the present-day coldest region of the northern hemisphere inferred

- from a pollen record of lake Billyakh, Verkhoyansk mts, NE Siberia, *Clim. Past*, 5(1), 73–84, 2009.
- Nahlik, A. M., and W. J. Mitsch, Methane emissions from tropical freshwater wetlands located in different climatic zones of Costa Rica, *Global Change Biology*, 17(3), 1321–1334, 2011.
- Naik, V., et al., Preindustrial to present-day changes in tropospheric hydroxyl radical and methane lifetime from the atmospheric chemistry and climate model intercomparison project (accmip), *Atmos. Chem. Phys.*, 13(10), 5277–5298, 2013.
- Nisbet, E. G., Sources of atmospheric CH₄ in early postglacial time, *J. Geophys. Res.*, 97, –, 1992.
- Nisbet, R., et al., Emission of methane from plants, *Proceedings of the Royal Society B: Biological Sciences*, 276(1660), 1347–1354, doi:10.1098/rspb.2008.1731, 2009.
- NOAA, Global monitoring division, earth system research laboratory (national oceanic and atmospheric administration, NOAA), <http://www.esrl.noaa.gov/gmd/ccgg/>, 2011.
- North GRIP members, ., High-resolution record of northern hemisphere climate extending into the last interglacial period, *Nature*, 431(7005), 147–151, 2004.
- O'Connor, F. M., et al., Possible role of wetlands, permafrost, and methane hydrates in the methane cycle under future climate change: A review, *Rev. Geophys.*, 48(4), RG4005–, 2010.
- O'Leary, M. H., Carbon isotope fractionation in plants, *Phytochemistry*, 20(4), 553–567, doi:10.1016/0031-9422(81)85134-5, 1981.
- Oremland, R. S., *Biology of anaerobic bacteria*, chap. Biogeochemistry of methanogenic bacteria, pp. 641–705, John Wiley & Sons, New York, N.Y., Oremland, R. S. 1988. Biogeochemistry of methanogenic bacteria, p. 641–705. In A. J. B. Zehnder (ed.), *Biology of anaerobic bacteria*. John Wiley & Sons, New York, N.Y., 1988.
- Parrenin, F., et al., The ED3 chronology for the EPICA Dome C ice core, *Clim. Past*, 3(3), 485–497, 2007.
- Parsons, A. J., P. C. Newton, H. Clark, and F. M. Kelliher, Scaling methane emissions from vegetation, *Trends in Ecology & Evolution*, 21(8), 423–424, 2006.

- Penning, H., C. M. Plugge, P. E. Galand, and R. Conrad, Variation of carbon isotope fractionation in hydrogenotrophic methanogenic microbial cultures and environmental samples at different energy status, *Global Change Biology*, 11(12), 2103–2113, 2005.
- Peterson, L. C., and G. H. Haug, Variability in the mean latitude of the atlantic intertropical convergence zone as recorded by riverine input of sediments to the cariaco basin (venezuela), *Palaeogeography, Palaeoclimatology, Palaeoecology*, 234(1), 97–113, 2006.
- Peterson, L. C., G. H. Haug, K. A. Hughen, and U. Rohl, Rapid changes in the hydrologic cycle of the tropical atlantic during the last glacial, *Science*, 290(5498), 1947–1951, 2000.
- Petit, J. R., et al., Four climate cycles in vostok ice core, *Nature*, 387(6631), 359–360, 1997.
- Petit, J. R., et al., Climate and atmospheric history of the past 420,000 years from the vostok ice core, antarctica, *Nature*, 399(6735), 429–436, 1999.
- Petit-Maire, N., M. Fontugne, and C. Rouland, Atmospheric methane ratio and environmental change in the sahara an sahel during the last 130 kyrs, *Palaeogeography, Palaeoclimatology, Palaeoecology*, 86(1-2), 197–206, 1991.
- Petrenko, V. V., J. P. Severinghaus, E. J. Brook, N. Reeh, and H. Schaefer, Gas records from the west greenland ice margin covering the last glacial termination: a horizontal ice core, *Quaternary Science Reviews*, 25(9–10), 865–875, 2006.
- Petrenko, V. V., et al., 14ch4 measurements in greenland ice: Investigating last glacial termination ch4 sources, *Science*, 324(5926), 506–508, 2009.
- Phelps, T. J., and J. G. Zeikus, Influence of ph on terminal carbon metabolism in anoxic sediments from a mildly acidic lake, *Applied and Environmental Microbiology*, 48(6), 1088–1095, 1984.
- Piedade, M., S. Long, and W. Junk, Leaf and canopy photosynthetic co2 uptake of a stand of echinocloa polystachya on the central amazon floodplain, *Oecologia*, 97(2), 193–201, 1994.
- Piedade, M. T. F., W. J. Junk, and S. P. Long, The productivity of the c4 grass echinocloa-polystachya on the amazon floodplain rid a-2488-2008, *Ecology*, 72(4), 1456–1463, doi:10.2307/1941118, 1991.

- Platt, U., W. Allan, and D. Lowe, Hemispheric average cl atom concentration from 13c/12c ratios in atmospheric methane, *Atmos. Chem. Phys.*, 4(9/10), 2393–2399, 2004.
- Power, M., et al., Changes in fire regimes since the last glacial maximum: an assessment based on a global synthesis and analysis of charcoal data, *Climate Dynamics*, 30, 887–907, 10.1007/s00382-007-0334-x, 2008.
- Poß, C., Analysis of the variability of the atmospheric methane budget in high polar regions with a regional trajectory model and using measurements of stable isotopes, Phd thesis, University of Heidelberg, Germany, 2003.
- Prather, M. J., C. D. Holmes, and J. Hsu, Reactive greenhouse gas scenarios: Systematic exploration of uncertainties and the role of atmospheric chemistry, *Geophys. Res. Lett.*, 39(9), L09,803–, 2012.
- Prentice, I. C., and S. P. Harrison, Ecosystem effects of co2 concentration: evidence from past climates, *Clim. Past*, 5(3), 297–307, doi:10.5194/cp-5-297-2009, 2009.
- Prentice, I. C., D. Jolly, and B. . Participants, Mid-holocene and glacial-maximum vegetation geography of the northern continents and africa, *Journal of Biogeography*, 27(3), pp. 507–519, 2000.
- Prentice, I. C., S. P. Harrison, and P. J. Bartlein, Global vegetation and terrestrial carbon cycle changes after the last ice age, *New Phytologist*, 189(4), 988–998, doi:10.1111/j.1469-8137.2010.03620.x, 2011.
- Prinn, R. G., The cleansing capacity of the atmosphere, *Annu. Rev. Environ. Resourc.*, 28(1), 29–57, doi:10.1146/annurev.energy.28.011503.163425, 2003.
- Prinn, R. G., R. F. Weiss, B. R. Miller, J. Huang, F. N. Alyea, D. M. Cunnold, P. J. Fraser, D. E. Hartley, and P. G. Simmonds, Atmospheric trends and lifetime of ch3cci3 and global oh concentrations, *Science*, 269(5221), 187–192, doi:10.1126/science.269.5221.187, 1995.
- Prinn, R. G., et al., Evidence for variability of atmospheric hydroxyl radicals over the past quarter century, *Geophys. Res. Lett.*, 32(7), L07,809–, 2005.
- Punyasena, S. W., F. E. Mayle, and J. C. McElwain, Quantitative estimates of glacial and holocene temperature and precipitation change in lowland amazonian bolivia, *Geology*, 36(8), 667–670, 2008.

- Quay, P., J. Stutsman, D. Wilbur, A. Snover, E. Dlugokencky, and T. Brown, The isotopic composition of atmospheric methane, *Global Biogeochem. Cycles*, *13*(2), 445–461, 1999.
- Quay, P. D., S. L. King, J. M. Lansdown, and D. O. Wilbur, Isotopic composition of methane released from wetlands: Implications for the increase in atmospheric methane, *Global Biogeochem. Cycles*, *2*(4), 385–397, 1988.
- Randerson, J. T., et al., Fire emissions from c3 and c4 vegetation and their influence on interannual variability of atmospheric co2 and $\delta^{13}\text{C}$, *Global Biogeochem. Cycles*, *19*(2), GB2019–, 2005.
- Rasmussen, R. A., and M. A. K. Khalil, Atmospheric methane (ch4): Trends and seasonal cycles, *J. Geophys. Res.*, *86*(C10), 9826–9832, doi:10.1029/JC086iC10p09826, 1981.
- Rasmussen, R. A., and M. A. K. Khalil, Global production of methane by termites, *Nature*, *301*(5902), 700–702, 1983.
- Rasmussen, R. A., M. A. K. Khalil, and S. D. Hoyt, Methane and carbon monoxide in snow, *Journal of the Air Pollution Control Association*, *32*(2), 176–178, doi:10.1080/00022470.1982.10465388, 1982.
- Reeburgh, W., *Treatise on Geochemistry. The Atmosphere.*, vol. 4, chap. Global methane biogeochemistry, pp. 65–89, Elsevier, Amsterdam, 2004.
- Reeburgh, W., Global methane biogeochemistry, in *Treatise on Geochemistry*, edited by H. D. Holland and K. K. Turekian, pp. 1–32, Pergamon, Oxford, 2007.
- Reeburgh, W., A. Hirsch, F. Sansone, B. Popp, and T. Rust, Carbon kinetic isotope effect accompanying microbial oxidation of methane in boreal forest soils, *Geochimica et Cosmochimica Acta*, *61*(22), 4761–4767, 1997.
- Ricci, M. P., D. A. Merritt, K. H. Freeman, and J. Hayes, Acquisition and processing of data for isotope-ratio-monitoring mass spectrometry, *Organic Geochemistry*, *21*(6-7), 561–571, 1994.
- Rice, A. L., C. L. Butenhoff, M. J. Shearer, D. Teama, T. N. Rosenstiel, and M. A. K. Khalil, Emissions of anaerobically produced methane by trees, *Geophys. Res. Lett.*, *37*(3), L03,807–, 2010.

- Ridgwell, A. J., S. J. Marshall, and K. Gregson, Consumption of atmospheric methane by soils: A process-based model, *Global Biogeochem. Cycles*, 13(1), 59–70, 1999.
- Rigby, M., et al., Renewed growth of atmospheric methane, *Geophys. Res. Lett.*, 35(22), L22,805–, 2008.
- Ringeval, B., P. O. Hopcroft, P. J. Valdes, P. Ciais, G. Ramstein, A. J. Dolman, and M. Kageyama, Response of methane emissions from wetlands to the last glacial maximum and an idealized dansgaard-oeschger climate event: insights from two models of different complexity, *Climate of the Past*, 9(1), 149–171, doi:10.5194/cp-9-149-2013, 2013.
- Robbins, R. C., L. A. Cavanagh, L. J. Salas, and E. Robinson, Analysis of ancient atmospheres, *J. Geophys. Res.*, 78(24), 5341–5344, 1973.
- Rohling, E. J., K. Grant, M. Bolshaw, A. P. Roberts, M. Siddall, C. Hemleben, and M. Kucera, Antarctic temperature and global sea level closely coupled over the past five glacial cycles, *Nature Geosci*, 2(7), 500–504, 2009.
- Rommerskirchen, F., G. Eglinton, L. Dupont, and J. Rullkötter, Glacial/interglacial changes in southern africa: Compound-specific $\delta^{13}C$ land plant biomarker and pollen records from southeast atlantic continental margin sediments, *Geochem. Geophys. Geosyst.*, 7, –, 2006.
- Ruddiman, W. F., The anthropogenic greenhouse era began thousands of years ago, *Climatic Change*, 61(3), 261–293, doi:10.1023/B:CLIM.0000004577.17928.fa, 2003.
- Ruddiman, W. F., The early anthropogenic hypothesis: Challenges and responses, *Rev. Geophys.*, 45(4), RG4001, 2007.
- Rust, F., and C. M. Stevens, Carbon kinetic isotope effect in the oxidation of methane by hydroxyl, *Int. J. Chem. Kinet.*, 12(6), 371–377, 1980.
- Ruth, U., et al., "edml1": a chronology for the epica deep ice core from dronning maud land, antarctica, over the last 150 000 years, *Climate of the Past*, 3(3), 475–484, 2007.
- Röckmann, T., M. Brass, R. Borchers, and A. Engel, The isotopic composition of methane in the stratosphere: high-altitude balloon sample measurements, *Atmos. Chem. Phys.*, 11(24), 13,287–13,304, 2011.

- Sage, R. F., The evolution of c4 photosynthesis, *New Phytologist*, 161(2), 341–370, 2004.
- Sage, R. F., D. A. Wedin, and M. Li, 10 - the biogeography of c4 photosynthesis: Patterns and controlling factors, in *C4 Plant Biology*, edited by R. F. Sage and R. K. Monson, pp. 313–I, Academic Press, San Diego, 1999.
- Sanderson, M. G., Biomass of termites and their emissions of methane and carbon dioxide: A global database, *Global Biogeochem. Cycles*, 10(4), 543–557, 1996.
- Sankaran, M., et al., Determinants of woody cover in african savannas, *Nature*, 438(7069), 846–849, doi:10.1038/nature04070, 2005.
- Sapart, C. J., Variations in the methane budget over the last two millenia, Ph.D. thesis, Institute for Marine and Atmospheric research, Utrecht, The Netherlands, 2012.
- Sapart, C. J., et al., Natural and anthropogenic variations in methane sources during the past two millennia, *Nature*, 490(7418), 85–88, doi:10.1038/nature11461, 2012.
- Saueressig, G., P. Bergamaschi, F. Crowley, J., and G. H., Harris, Carbon kinetic isotope effect of the reaction of ch4 with cl atoms, *JOURNAL OF GEOPHYSICAL RESEARCH*, 22, 1225–1228, 1995.
- Saueressig, G., J. N. Crowley, P. Bergamaschi, C. Brühl, C. A. M. Brenninkmeijer, and H. Fischer, Carbon 13 and d kinetic isotope effects in the reactions of ch4 with o(1 d) and oh: New laboratory measurements and their implications for the isotopic composition of stratospheric methane, *J. Geophys. Res.*, 106, –, 2001.
- Saunders, M., M. Jones, and F. Kansime, Carbon and water cycles in tropical papyrus wetlands, *Wetlands Ecology and Management*, 15(6), 489–498, 2007.
- Schaefer, H., and M. J. Whiticar, Potential glacial-interglacial changes in stable carbon isotope ratios of methane sources and sink fractionation, *Global Biogeochem. Cycles*, 22, GB1001, 2008.
- Schaefer, H., M. J. Whiticar, E. J. Brook, V. V. Petrenko, D. F. Ferretti, and J. P. Severinghaus, Ice record of delta13c for atmospheric ch4 across the younger dryas-preboreal transition, *Science*, 313(5790), 1109–1112, doi:10.1126/science.1126562, 2006.
- Schaefer, H., et al., Ice stratigraphy at the pakitsoq ice margin, west greenland, derived from gas records, *Journal of Glaciology*, 55(191), 411–421, 2009.

- Schilt, A., et al., Atmospheric nitrous oxide during the last 140,000 years, *Earth and Planetary Science Letters*, 300(1-2), 33–43, 2010.
- Schimmel, J., 1.13-biogeochemical models: Implicit versus explicit microbiology., in *Global Biogeochemical Cycles in the Climate System*, edited by E.-D. Schulze, M. Heimann, S. Harrison, E. Holland, J. Lloyd, I. Prentice, and D. Schimmel, p. 177–183, Academic, San Diego, 2001.
- Schimmel, J., Playing scales in the methane cycle: From microbial ecology to the globe, *Proceedings of the National Academy of Sciences of the United States of America*, 101(34), 12,400–12,401, 2004.
- Schleucher, J., C. Griesinger, B. Schwoerer, and R. K. Thauer, H₂-forming n₅,n₁₀-methylene-tetrahydromethanopterin dehydrogenase from methanobacterium thermoautotrophicum catalyzes a stereoselective hydride transfer as determined by two-dimensional nmr spectroscopy, *Biochemistry*, 33(13), 3986–3993, doi:10.1021/bi00179a027, 1994.
- Schmale, O., J. Greinert, and G. Rehder, Methane emission from high-intensity marine gas seeps in the black sea into the atmosphere, *Geophysical Research Letters*, 32(7), n/a–n/a, doi:10.1029/2004GL021138, 2005.
- Schmitt, J., et al., On the interference of kr during carbon isotope analysis of methane using continuous-flow combustion–isotope ratio mass spectrometry, *Atmos. Meas. Tech.*, 6(5), 1425–1445, 2013.
- Schmittner, A., and E. D. Galbraith, Glacial greenhouse-gas fluctuations controlled by ocean circulation changes, *Nature*, 456(7220), 373–376, 2008.
- Schoell, M., The hydrogen and carbon isotopic composition of methane from natural gases of various origins, *Geochimica et Cosmochimica Acta*, 44(5), 649–661, 1980.
- Schoell, M., Multiple origins of methane in the earth, *Chemical Geology*, 71(1–3), 1–10, 1988.
- Schwander, J., The transformation of snow to ice and the occlusion of gases, in *The environmental record in glaciers and ice sheets, Physical, Chemical, and Earth Science Research Report*, vol. 8, edited by H. Oeschger and C. Langway Jr., pp. 53–67, John Wiley & Sons, Ltd., New York, 1989.

- Schwander, J., *Chemical exchange between the atmosphere and polar snow*, chap. Gas diffusion in firn, pp. 527–540, Springer-Verlag, Berlin, 1996.
- Schwander, J., B. Stauffer, and A. Sigg, Air mixing in firn and the age of the air at pore close-off, *Annals of Glaciology*, *10*, 141–145, 1988.
- Schwander, J., J.-M. Barnola, C. Andrie, M. Leuenberger, A. Ludin, D. Raynaud, and B. Stauffer, The age of the air in the firn and the ice at summit, greenland, *J. Geophys. Res.*, *98*, 2831–2838, 1993.
- Schwander, J., T. Sowers, J.-M. Barnola, T. Blunier, A. Fuchs, and B. Malaize, Age scale of the air in the summit ice: Implication for glacial-interglacial temperature change, *J. Geophys. Res.*, *102*, 19,483–19,493, 1997.
- Severinghaus, J. P., Monsoons and meltdowns, *Science*, *326*(5950), 240–241, doi:10.1126/science.1179941, printed, 2009.
- Severinghaus, J. P., T. Sowers, E. J. Brook, R. B. Alley, and M. L. Bender, Timing of abrupt climate change at the end of the younger dryas interval from thermally fractionated gases in polar ice, *Nature*, *391*(6663), 141–146, 1998.
- Severinghaus, J. P., A. Grachev, and M. Battle, Thermal fractionation of air in polar firn by seasonal temperature gradients, *Geochem. Geophys. Geosyst.*, *2*(7), –, 2001.
- Severinghaus, J. P., A. Grachev, B. Luz, and N. Caillon, A method for precise measurement of argon 40/36 and krypton/argon ratios in trapped air in polar ice with applications to past firn thickness and abrupt climate change in greenland and at siple dome, antarctica, *Geochimica et Cosmochimica Acta*, *67*(3), 325–343, doi: 10.1016/S0016-7037(02)00965-1, 2003.
- Severinghaus, J. P., et al., Deep air convection in the firn at a zero-accumulation site, central antarctica, *Earth and Planetary Science Letters*, *293*(3-4), 359–367, doi:10.1016/j.epsl.2010.03.003, 2010.
- Shackleton, N. J., M. A. Hall, and E. Vincent, Phase relationships between millennial-scale events 64,000–24,000 years ago, *Paleoceanography*, *15*(6), 565–569, doi:10.1029/2000PA000513, 2000.

- Shakhova, N., I. Semiletov, A. Salyuk, V. Yusupov, D. Kosmach, and O. Gustafsson, Extensive methane venting to the atmosphere from sediments of the east siberian arctic shelf, *Science*, *327*(5970), 1246–1250, 2010.
- Siddall, M., E. J. Rohling, A. Almogi-Labin, C. Hemleben, D. Meischner, I. Schmelzer, and D. A. Smeed, Sea-level fluctuations during the last glacial cycle, *Nature*, *423*(6942), 853–858, 2003.
- Siegenthaler, U., et al., Stable carbon cycle-climate relationship during the late pleistocene., *Science*, *310*(5752), 1313–1317, doi:10.1126/science.1120130, 2005.
- Singarayer, J. S., P. J. Valdes, P. Friedlingstein, S. Nelson, and D. J. Beerling, Late holocene methane rise caused by orbitally controlled increase in tropical sources, *Nature*, *470*(7332), 82–85, 2011.
- Singer, S., Stratospheric water vapour increase due to human activities., *Nature*, *233*(5321), 543–, 1971.
- Sinninghe Damsté, J. S., D. Verschuren, J. Ossebaar, J. Blokker, R. van Houten, M. T. van der Meer, B. Plessen, and S. Schouten, A 25,000-year record of climate-induced changes in lowland vegetation of eastern equatorial africa revealed by the stable carbon-isotopic composition of fossil plant leaf waxes, *Earth and Planetary Science Letters*, *302*(1-2), 236–246, 2011.
- Skidmore, M., Microbial communities in antarctic subglacial aquatic environments, in *Geophys. Monogr. Ser.*, vol. 192, pp. 61–81, AGU, Washington, DC, 2011.
- Snover, A. K., and P. D. Quay, Hydrogen and carbon kinetic isotope effects during soil uptake of atmospheric methane, *Global Biogeochem. Cycles*, *14*, –, 2000.
- Snover, A. K., P. D. Quay, and W. M. Hao, The d/h content of methane emitted from biomass burning, *Global Biogeochem. Cycles*, *14*, –, 2000.
- Sowers, T., Late quaternary atmospheric ch₄ isotope record suggests marine clathrates are stable, *Science*, *311*(5762), 838–840, doi:10.1126/science.1121235, 2006.
- Sowers, T., Atmospheric methane isotope records covering the holocene period, *Quaternary Science Reviews*, *29*(1-2), 213–221, doi:10.1016/j.quascirev.2009.05.023, 2010.

- Sowers, T., M. Bender, D. Raynaud, and Y. S. Korotkevich, ^{15}N of N_2 in air trapped in polar ice: a tracer of gas transport in the firn and a possible constraint on ice age-gas age differences, *J. Geophys. Res.*, *97*, 15,683–15,697, 1992.
- Spahni, R., J. Schwander, J. Flückiger, B. Stauffer, J. Chappellaz, and D. Raynaud, The attenuation of fast atmospheric CH_4 variations recorded in polar ice cores, *Geophys. Res. Lett.*, *30*, 1571, 2003.
- Spahni, R., et al., Constraining global methane emissions and uptake by ecosystems, *Biogeosciences Discuss.*, *8*(1), 221–272, 2011.
- Sperlich, P., C. Buizert, T. M. Jenk, C. J. Sapart, M. Prokopiou, T. Röckmann, and T. Blunier, An automated gc-c-gc-irms setup to measure palaeoatmospheric $d^{13}\text{c-ch}_4$, $d^{15}\text{n-n}_2\text{o}$ and $d^{18}\text{o-n}_2\text{o}$ in one ice core sample, *Atmospheric Measurement Techniques*, *6*(8), 2027–2041, doi:10.5194/amt-6-2027-2013, 2013.
- Stadtman, T. C., Methane fermentation, *Annual review of microbiology*, *21*, 121–, 1967.
- Stauffer, B., G. Fischer, A. Neftel, and H. Oeschger, Increase of atmospheric methane recorded in antarctic ice core, *Science*, *229*(4720), 1386–1388, 1985.
- Stauffer, B., E. Lochbronner, H. Oeschger, and J. Schwander, Methane concentration in the glacial atmosphere was only half that of the preindustrial holocene, *Nature*, *332*(6167), 812–814, 1988.
- Steele, L. P., E. J. Dlugokencky, P. M. Lang, P. P. Tans, R. C. Martin, and K. A. Masarie, Slowing down of the global accumulation of atmospheric methane during the 1980s, *Nature*, *358*(6384), 313–316, 1992.
- Stevens, C., and M. Wahlen, The isotopic composition of atmospheric methane and its sources, in *Atmospheric Methane*, edited by M. Khalil, pp. 25–41–, Springer Berlin Heidelberg, 2000.
- Stevens, C. M., and A. Engelkemeir, Stable carbon isotopic composition of methane from some natural and anthropogenic sources, *J. Geophys. Res.*, *93*(D1), 725–733, 1988.
- Stevenson, D. S., et al., Multimodel ensemble simulations of present-day and near-future tropospheric ozone, *J. Geophys. Res.*, *111*(D8), D08,301–, 2006.

- Stibal, M., et al., Methanogenic potential of arctic and antarctic subglacial environments with contrasting organic carbon sources, *Glob Change Biol*, 18(11), 3332–3345, 2012.
- Street-Perrott, F. A., Y. Huang, R. A. Perrott, G. Eglinton, P. Barker, L. B. Khelifa, D. D. Harkness, and D. O. Olago, Impact of lower atmospheric carbon dioxide on tropical mountain ecosystems, *Science*, 278(5342), 1422–1426, 1997.
- Tans, P. P., A note on isotopic ratios and the global atmospheric methane budget, *Global Biogeochemical Cycles*, 11(1), 77–81, doi:10.1029/96GB03940, 1997.
- Thompson, A. M., The oxidizing capacity of the earth's atmosphere: Probable past and future changes, *Science*, 256(5060), 1157–1165, 1992.
- Thompson, A. M., J. A. Chappellaz, I. Y. Fung, and T. L. Kucsera, The atmospheric ch₄ increase since the last glacial maximum (2). interactions with oxidants, *Tellus B*, 45(3), 242–257, 1993.
- Thor Marteinsson, V., et al., Microbial communities in the subglacial waters of the vatnajökull ice cap, iceland, *ISME J*, 7(2), 427–437, 2013.
- Tierney, J. E., J. M. Russell, Y. Huang, J. S. S. Damste, E. C. Hopmans, and A. S. Cohen, Northern hemisphere controls on tropical southeast african climate during the past 60,000 years, *Science*, 322(5899), 252–255, 2008.
- Tierney, J. E., J. M. Russell, and Y. Huang, A molecular perspective on late quaternary climate and vegetation change in the lake tanganyika basin, east africa, *Quaternary Science Reviews*, 29(5-6), 787–800, 2010.
- Trudinger, C. M., L. G. Enting, D. M. Etheridge, R. J. Francey, V. A. Levchenko, L. P. Steele, D. Raynaud, and L. Arnaud, Modeling air movement and bubble trapping in firn, *J. Geophys. Res.*, 102, –, 1997.
- Turcq, B., R. C. Cordeiro, A. Sifeddine, F. F. Simões Filho, A. L. S. Albuquerque, and J. J. Abrão, Carbon storage in amazonia during the last glacial maximum: secondary data and uncertainties, *Chemosphere*, 49(8), 821–835, 2002.
- Tyler, S. C., P. M. Crill, and G. W. Brailsford, Fractionation of methane during oxidation in a temperate forested soil, *Geochimica et Cosmochimica Acta*, 58(6), 1625 – 1633, doi:DOI:10.1016/0016-7037(94)90564-9, 1994.

- Tyler, S. C., H. O. Ajie, A. L. Rice, R. J. Cicerone, and E. C. Tuazon, Experimentally determined kinetic isotope effects in the reaction of CH_4 with Cl : Implications for atmospheric CH_4 , *Geophys. Res. Lett.*, *27*(12), 1715–1718, 2000.
- Umezawa, T., S. Aoki, Y. Kim, S. Morimoto, and T. Nakazawa, Carbon and hydrogen stable isotopic ratios of methane emitted from wetlands and wildfires in Alaska: Aircraft observations and bonfire experiments, *J. Geophys. Res.*, *116*(D15), D15,305–, 2011.
- Umezawa, T., T. Machida, K. Ishijima, H. Matsueda, Y. Sawa, P. K. Patra, S. Aoki, and T. Nakazawa, Carbon and hydrogen isotopic ratios of atmospheric methane in the upper troposphere over the western Pacific, *Atmos. Chem. Phys.*, *12*(17), 8095–8113, 2012.
- Valdes, P. J., D. J. Beerling, and C. E. Johnson, The ice age methane budget, *Geophys. Res. Lett.*, *32*(2), L02,704, 2005.
- Valentine, D. L., A. Chidthaisong, A. Rice, W. S. Reeburgh, and S. C. Tyler, Carbon and hydrogen isotope fractionation by moderately thermophilic methanogens, *Geochimica et Cosmochimica Acta*, *68*(7), 1571–1590, 2004.
- van Huissteden, J., Methane emission from northern wetlands in Europe during oxygen isotope stage 3, *Quaternary Science Reviews*, *23*(18-19), 1989 – 2005, doi:DOI:10.1016/j.quascirev.2004.02.015, 2004.
- Vaughn, B., J. Miller, D. Ferretti, and J. White, *Handbook of Stable Isotope Analytical Techniques*, chap. Stable isotope measurements of atmospheric CO_2 and CH_4 , pp. 272–304, Elsevier B.V., 2004.
- Veres, D., et al., The Antarctic ice core chronology (aicc2012): an optimized multi-parameter and multi-site dating approach for the last 120 thousand years, *Climate of the Past*, *9*(4), 1733–1748, doi:10.5194/cp-9-1733-2013, 2013.
- Vidic, N. J., and I. P. Montañez, Climatically driven glacial-interglacial variations in C_3 and C_4 plant proportions on the Chinese loess plateau, *Geology*, *32*(4), 337–340, April, 2004.
- Vigano, I., H. van Weelden, R. Holzinger, F. Keppler, and T. Röckmann, Effect of UV radiation and temperature on the emission of methane from plant biomass and structural components, *Biogeosciences Discuss.*, *5*(1), 243–270, 2008.

- Vigano, I., T. Röckmann, R. Holzinger, A. van Dijk, F. Keppler, M. Greule, W. Brand, H. Geilmann, and H. van Weelden, The stable isotope signature of methane emitted from plant material under uv irradiation, *Atmospheric Environment*, *43*(35), 5637–5646, 2009.
- Voelker, A. H. L., Global distribution of centennial-scale records for marine isotope stage (mis) 3: a database, *Quaternary Science Reviews*, *21*(10), 1185–1212, 2002.
- Vogts, A., H. Moossen, F. Rommerskirchen, and J. Rullkötter, Distribution patterns and stable carbon isotopic composition of alkanes and alkan-1-ols from plant waxes of african rain forest and savanna c3 species, *Organic Geochemistry*, *40*(10), 1037–1054, 2009.
- Wadham, J. L., M. Tranter, S. Tulaczyk, and M. Sharp, Subglacial methanogenesis: A potential climatic amplifier?, *Global Biogeochem. Cycles*, *22*(2), GB2021–, 2008.
- Wadham, J. L., et al., Potential methane reservoirs beneath antarctica, *Nature*, *488*(7413), 633–637, 2012.
- Waldron, S., J. Lansdown, E. Scott, A. Fallick, and A. Hall, The global influence of the hydrogen iostope composition of water on that of bacteriogenic methane from shallow freshwater environments - co2 reduction vs. acetate fermentation-isotope evidence, *Geochimica et Cosmochimica Acta*, *63*(15), 2237–2245, doi:10.1016/S0016-7037(99)00192-1, 1999.
- Walter, B. P., and M. Heimann, A process-based, climate-sensitive model to derive methane emissions from natural wetlands: Application to five wetland sites, sensitivity to model parameters, and climate, *Global Biogeochem. Cycles*, *14*(3), 745–765, 2000.
- Walter, B. P., M. Heimann, and E. Matthews, Modeling modern methane emissions from natural wetlands: 1. model description and results, *J. Geophys. Res.*, *106*(D24), 34,189–34,206, 2001a.
- Walter, B. P., M. Heimann, and E. Matthews, Modeling modern methane emissions from natural wetlands: 2. interannual variations 1982–1993, *J. Geophys. Res.*, *106*(D24), 34,207–34,219, 2001b.
- Walter, K. M., S. A. Zimov, J. P. Chanton, D. Verbyla, and F. S. Chapin, Methane bubbling from siberian thaw lakes as a positive feedback to climate warming, *Nature*, *443*(7107), 71–75, 2006.

- Walter, K. M., M. E. Edwards, G. Grosse, S. A. Zimov, and I. Chapin, F. S., Thermokarst lakes as a source of atmospheric ch₄ during the last deglaciation, *Science*, *318*(5850), 633–636, 2007.
- Wang, G., X. Feng, J. Han, L. Zhou, W. Tan, and F. Su, Paleovegetation reconstruction using $\delta^{13}\text{C}$ of soil organic matter, *Biogeosciences*, *5*(5), 1325–1337, 2008a.
- Wang, X., A. S. Auler, R. L. Edwards, H. Cheng, P. S. Cristalli, P. L. Smart, D. A. Richards, and C.-C. Shen, Wet periods in northeastern Brazil over the past 210 kyr linked to distant climate anomalies, *Nature*, *432*(7018), 740–743, 2004.
- Wang, Y., et al., Millennial- and orbital-scale changes in the East Asian monsoon over the past 224,000 years, *Nature*, *451*(7182), 1090–1093, doi:10.1038/nature06692, 2008b.
- Wang, Y. J., H. Cheng, R. L. Edwards, Z. S. An, J. Y. Wu, C.-C. Shen, and J. A. Dorale, A high-resolution absolute-dated late Pleistocene monsoon record from Hulu Cave, China, *Science*, *294*(5550), 2345–2348, doi:10.1126/science.1064618, printed, 2001.
- Wania, R., I. Ross, and I. C. Prentice, Integrating peatlands and permafrost into a dynamic global vegetation model: 1. evaluation and sensitivity of physical land surface processes, *Global Biogeochem. Cycles*, *23*(3), GB3014–, 2009a.
- Wania, R., I. Ross, and I. C. Prentice, Integrating peatlands and permafrost into a dynamic global vegetation model: 2. evaluation and sensitivity of vegetation and carbon cycle processes, *Global Biogeochem. Cycles*, *23*(3), GB3015–, 2009b.
- Werner, R. A., and W. A. Brand, Referencing strategies and techniques in stable isotope ratio analysis, *Rapid Communications in Mass Spectrometry*, *15*(7), 501–519, 2001.
- Westermann, P., Temperature regulation of methanogenesis in wetlands, *Chemosphere*, *26*(1–4), 321–328, 1993.
- Whiticar, M., and H. Schaefer, Constraining past global tropospheric methane budgets with carbon and hydrogen isotope ratios in ice, *Philosophical Transactions of the Royal Society A: Mathematical, Physical and Engineering Sciences*, *365*(1856), 1793–1828, doi:10.1098/rsta.2007.2048, 2007.
- Whiticar, M., E. Faber, and M. Schoell, Biogenic methane formation in marine and freshwater environments: CO₂ reduction vs. acetate fermentation— isotope evidence, *Geochimica et Cosmochimica Acta*, *50*(5), 693–709, 1986.

- Whiticar, M. J., A geochemical perspective of natural gas and atmospheric methane, *Organic Geochemistry*, 16(1–3), 531–547, 1990.
- Whiticar, M. J., Carbon and hydrogen isotope systematics of bacterial formation and oxidation of methane, *Chemical Geology*, 161(1-3), 291–314, doi:10.1016/S0009-2541(99)00092-3, 1999.
- Whiting, G. J., and J. P. Chanton, Primary production control of methane emission from wetlands, *Nature*, 364(6440), 794–795, 1993.
- Williams, J. W., Variations in tree cover in north america since the last glacial maximum, *Global and Planetary Change*, 35(1-2), 1–23, 2003.
- Winfrey, M. R., and J. G. Zeikus, Anaerobic metabolism of immediate methane precursors in lake mendota., *Applied and Environmental Microbiology*, 37(2), 244–253, 1979.
- Winfrey, M. R., D. R. Nelson, S. C. Klevickis, and J. G. Zeikus, Association of hydrogen metabolism with methanogenesis in lake mendota sediments., *Applied and Environmental Microbiology*, 33(2), 312–318, 1977.
- Wingham, D. J., C. G. Rapley, and H. Griffiths, New techniques in satellite altimeter tracking systems, in *Proceedings of the IGARSS Symposium*, vol. SP-254, pp. 1339–1344, Guyenne, T.D. and Hunt, J.J. (European Space Agency), Zurich, 1986.
- Wofsy, S. C., Interactions of ch₄ and co in the earth's atmosphere, *Annual Review of Earth and Planetary Sciences*, 4, 441–469, doi:10.1146/annurev.ea.04.050176.002301, 1976.
- Wuillez, M.-N., M. Kageyama, G. Krinner, N. de Noblet-Ducoudré, N. Viovy, and M. Mancip, Impact of co₂ and climate on the last glacial maximum vegetation: results from the orchidee/ipsl models, *Clim. Past*, 7(2), 557–577, doi:10.5194/cp-7-557-2011, 2011.
- Wolfe, R., Microbial formation of methane, *Adv In Microbial Physiology Vol 6 Apl*, 6, 107, 1971.
- Wolfe, R. S., 1776–1996: Alessandro volta's combustible air., *ASM News*, 62(10), 529–534, 1996.
- Wolff, E., et al., Changes in environment over the last 800,000 years from chemical analysis of the epica dome c ice core, *Quaternary Science Reviews*, 29(1-2), 285–295, 2010.

- Wooller, M. J., D. L. Swain, K. J. Ficken, A. D. Q. Agnew, F. A. Street-Perrott, and G. Eglinton, Late quaternary vegetation changes around lake rutundu, mount kenya, east africa: evidence from grass cuticles, pollen and stable carbon isotopes, *J. Quaternary Sci.*, 18(1), 3–15, 2003.
- Wuebbles, D. J., and K. Hayhoe, Atmospheric methane and global change, *Earth-Science Reviews*, 57(3-4), 177–210, 2002.
- Wurster, C. M., M. I. Bird, I. D. Bull, F. Creed, C. Bryant, J. A. J. Dungait, and V. Paz, Forest contraction in north equatorial southeast asia during the last glacial period, *Proceedings of the National Academy of Sciences*, 107(35), 15,508–15,511, 2010.
- Yamada, K., Y. Ozaki, F. Nakagawa, S. Sudo, H. Tsuruta, and N. Yoshida, Hydrogen and carbon isotopic measurements of methane from agricultural combustion: Implications for isotopic signatures of global biomass burning sources, *J. Geophys. Res.*, 111(D16), D16,306, 2006.
- Yavitt, J. B., Biogeochemistry: Cryptic wetlands, *Nature Geosci*, 3(11), 749–750, doi: 10.1038/ngeo999, 2010.
- Zhang, Z., M. Zhao, H. Lu, and A. M. Faiia, Lower temperature as the main cause of $\delta^{13}C$ plant declines during the glacial periods on the chinese loess plateau, *Earth and Planetary Science Letters*, 214(3-4), 467–481, 2003.
- Zinder, S. H., Physiological ecology of methanogens, in *Chapman & Hall Microbiology Series*, edited by J. Ferry, pp. 128–206–, Springer US, 1993.

A. Acronyms

| | |
|------------------------------------|---|
| Al₂O₃ | aluminium oxide (α -alumina) |
| AIM | Antarctic isotope maximum |
| AMOC | Atlantic Meridional Overturning Circulation |
| AR4 | Fourth Assessment Report of the IPCC, 2007 |
| BA | Bølling-Allerød warm period (~14–13 kyr BP) |
| CH₄ | methane |
| cf. | compare also |
| CO | carbon monoxide |
| CO₂ | carbon dioxide |
| csv | comma separated values |
| Cu | copper |
| DO | Dansgaard-Oeschger climate event |
| EDC | EPICA Dome C |
| EDML | EPICA Dronning Maud Land |
| EPICA | European Project for Ice-Coring in Antarctica |
| ESRL | Earth System Research Laboratory (NOAA), Boulder, Colorado, (US.) |
| FID | flame ionization detector |
| FS | fused silica |

| | |
|-----------------------|---|
| GC | gas chromatography |
| GC/C/irmMS | gas chromatography combustion isotope ratio monitoring mass spectrometry |
| GISP | Greenland Ice Sheet Project |
| GRIP | Greenland Ice Core Project |
| He | helium |
| H₂ | hydrogen |
| H₂O | dihydrogen monoxide (water) |
| IAEA | International Atomic Energy Agency |
| i.e. | id est (that is) |
| INSTAAR | Institute of Arctic and Alpine Research, University of Colorado, Boulder, Colorado, (US.) |
| IPD | inter-polar (CH ₄ concentration) difference |
| IPCC | Intergovernmental Panel on Climate Change |
| IPY | International Polar Year collaborative |
| IrmMS | isotope ratio monitoring mass spectrometry |
| IT principle | Identical Treatment principle |
| ITCZ | Inter-Tropical Convergence Zone |
| KIE | kinetic isotope effect |
| Kr | krypton |
| kyr BP | thousand years before present ('present' defined as 1950) |
| LGM | Last Glacial Maximum (~25–20 kyr BP.) |
| LIA | Little Ice Age (~1500 AD) |
| LN₂ | Liquid Nitrogen |

| | |
|-----------------------|---|
| LPIH | late pre-industrial Holocene |
| masl. | meter above sea level |
| MBL | marine boundary layer |
| mbs. | meter below the surface |
| MCA | Medieval Climate Anomaly (~1000 AD) |
| MIS | Marine Isotope Stage (Paleoclimate time markers) |
| MS | mass spectrometer |
| i.d. | inner diameter |
| Ni | Nickel |
| NEEM | North Greenland Eemian Ice Drilling programme |
| NGRIP | North Greenland ice core project |
| NIWA | National Institute of Water and Atmospheric Research, Wellington (New Zealand) |
| NMVOC | non-methane volatile organic compound |
| N₂ | nitrogen |
| N₂O | nitrous oxide |
| NO_x | mono-nitrogen oxides (e.g. nitric oxide and nitrogen dioxide) |
| NOAA | National Oceanic and Atmospheric Administration, Boulder, Colorado, (US.) |
| OD | Oldest Dryas climate interval (~18–15 kyr BP.) |
| PB | Pre-boreal Holocene (~10 kyr BP.) |
| OCOG | Offset Centre of Gravity Retracker algorithm |
| PIH | pre-industrial Holocene |
| O₂ | oxygen |

| | |
|------------------|---|
| ·OH | hydroxyl radical |
| ppm | parts per million mole fraction, micro-moles per mole |
| ppb | parts per billion mole fraction, nano-moles per mole |
| PSU | Pennsylvania State University |
| Pt | platinum |
| SCIAMACHY | Scanning Imaging Absorption Spectrometer for Atmospheric Chartography |
| SST | sea-surface temperature |
| STP | standard temperature and pressure; 273.15 K (0° C), 101325 Pa (1 atm) |
| UV | ultraviolet radiation (part of the electromagnetic spectrum) |
| VOC | volatile organic compound |
| VPDB | Vienna Pee Dee Belemnite standard |
| V-SMOW | Vienna Standard Mean Ocean Water standard |
| WAIS | West Antarctic ice sheet |
| wrt. | with respect to |
| YD | Younger Dryas climate event (~12-11 kyr BP.) |

**B. Supplementary Information for
"Independent control of CH₄
emissions and isotopic composition
over the last 160,000 years."
(Accepted final draft)**

Independent variations of CH₄ emissions and isotopic composition over the past 160,000 years

Authors:

Lars Möller, Todd Sowers, Michael Bock, Renato Spahni, Melanie Behrens, Jochen Schmitt,
5 Heinrich Miller, Hubertus Fischer*

*Correspondence and requests for materials should be addressed to H.F.

Supplementary Methods and technical descriptions

1.1 $\delta^{13}\text{CH}_4$ measurements performed at Alfred Wegener Institute (AWI)

EDML $\delta^{13}\text{CH}_4$ measurements were performed using a continuous flow gas chromatography
10 combustion isotope ratio mass spectrometry system (GC/C/IRMS) with a preceding purge and trap
extraction and pre-concentration setup. A few modifications have been made compared to the
published experimental and data processing procedure^{1,2}. Sample sizes between 150-200 g of ice,
equivalent to 15-20 ml of air at standard temperature and pressure (STP) were used after scraping
off 1-2 mm at the surface with a microtome knife to minimize the risk of contamination e.g. by drill
15 fluid. Sealed with a copper gasket in an ultra-high-vacuum stainless steel to glass sample vessel
with an inner volume of 350 ml, the samples were melted after evacuation and the air stripped out
of the water and vessel head space with a helium carrier gas stream (150 mL/min) for 90 minutes.
The bulk of the entrained water vapor was removed by a cooled Nafion membrane and most of the
easily condensable gases like CO₂ and N₂O are trapped in a 1/8 inch steel trap at -196 °C (liquid
20 nitrogen, LN₂). While methane from the sample air was subsequently pre-concentrated on a 1/8" steel
tubing filled with an adsorbent (Hayesep D 80/100 mesh, Supelco), bulk components of the air were
vented at -140 °C. The retained sample methane and residual air components were focussed on a
cryofocus trap and separated on a 30 m GC column (30 °C, CarbonPLOT, Agilent, Böblingen,
Germany). The methane was then quantitatively combusted to CO₂ in a 940 °C oxidation furnace
25 (Ni/CU/Pt wires in Al₂O₃ tubing, ThermoFinnigan, Bremen, Germany) and admitted to the IRMS
(Isoprime, Elementar, Germany) using an open split.

A pure CO₂ working standard (ISO-TOP, Air Liquide, Germany) was admitted to the IRMS during
each acquisition. Moreover, a pure methane standard (99.995 vol.-% purity; AirLiquide, Germany)
30 admitted to the GC stream was used to monitor fractionation in the GC or the combustion oven.

20 ml STP synthetic atmospheric air standard injections from two different standard bottles (“SynthAir” with 1000 ppb CH₄ (99.995 vol.-% purity), 250 ppm ISOTOP CO₂ and 250 ppb N₂O (99.999 vol.-% purity); “Crystal-Mix” with 1081 ± 22 ppb CH₄ 4.5, 249.9 ± 5.0 ppm CO₂ and 259 ± 26 ppb; both AirLiquide, Germany) were used to correct for long-term systematic shifts and internal calibration. The mean δ¹³CH₄ value for “SynthAir” was -40.93 ± 0.10 ‰ (n=448) and -49.66 ± 0.11 ‰ (n=136) for “Crystal-Mix” after drift correction. The absolute accuracy of the system was determined by 16 measurements of a modern air sample from Neumayer Station, Antarctica. The target value (δ¹³CH₄: -46.97 ± 0.04 ‰ versus V-PDB (n=7)) was determined by off-line sample preparation and dual-inlet IRMS on a MAT252 mass spectrometer (ThermoFinnigan) at the Institut für Umweltphysik, Heidelberg³. A calculated machine offset of 0.02 ‰ of our GC/C/IRMS determined values after correction for Kr interference (see below) relative to the Heidelberg reference value was used to correct the EDML δ¹³CH₄ data of this study. Accordingly, our data are reported relative to the V-PDB scale as defined by the Heidelberg measurements⁴.

The EDML δ¹³CH₄ time series includes 129 data points and 32 replicates from different depth intervals with a mean reproducibility of the replicates of ± 0.18 ‰. A total of 19 outliers, either caused by machine instabilities or other experimental problems, were excluded from the dataset and remeasured. Processing of the chromatogram for each measurement has been performed using a self developed, fully automated peak detection, integration and referencing script written in the Python programming language (www.python.org). This script allows uniform and comprehensible background and peak detection, genuine automation for post-processing (like e.g. long term trend corrections) and data archiving. Using this script we were able to reproduce published δ¹³CH₄ data for termination I², which were obtained with the software provided with the MS (Isoprime, Elementar, Germany) with an offset of 0.10 ‰ (1σ: 0.17 ‰, n=34) without and 0.17 ‰ (1σ: 0.15 ‰) with correction for Kr interference (see below). Note that both offsets are smaller than the measurement uncertainty of this earlier data set (0.3 ‰, 1σ). This re-evaluated record for termination I was used in Figure 1 and 2 in the main text, and is also shown in supplementary Figure S1 for the comparison with the unmodified, uncorrected data of our previous publication.

1.2 δ¹³CH₄ measurements performed at Pennsylvania State University (PSU)

For the Vostok ice core sample measurements at Penn State University, two different extraction methods were employed. A dry extraction system⁵ was used to liberate gas from ice samples where N₂O measurements were needed^{6,7}. Trapped gases were liberated from 1-1.5 kg ice samples using a “cheese grater” oscillator with immediate cryogenic freezing of liberated air into a 35 ml stainless

65 steel sample tube immersed in liquid Helium. Once the air was transferred, the sample tube was isolated, removed from the Helium Dewar and equilibrated at room temperature before CH₄ and N₂O analyses were performed using standard GC techniques. The sample tube was then attached to the PreCon device where the isotopic composition of N₂O and CH₄ were determined^{8,9}. For those samples where we did not need N₂O data, a wet extraction technique was used to liberate the occluded air. Ice samples weighing 500-700 g were placed into a stainless steel extraction cylinder and sealed with a copper gasket. After evacuation, the ice was allowed to melt for 40 min in 50 °C water before being placed into a liquid nitrogen Dewar for 40 min to refreeze the meltwater. The headspace was then flushed with He (40 ml/min) through a H₂O trap (-110 °C) with the CH₄ ultimately trapped on a Hayesep D trap at -130 °C. After 40 min of flushing, the Hayesep D trap was isolated and attached to the PreCon for CH₄ isotopic analyses¹⁰. Both extraction systems were routinely checked for contamination/fractionation using standard air samples of varying sizes to mimic the amount of CH₄ we extract from the ice core samples (1-3 nmol of CH₄). The air standards were introduced over the residual crushed ice or degassed refrozen meltwater and processed as if they were a real ice sample. For the dry extraction runs, the average of eight separate standard runs was -47.30 ± 0.31 ‰ (1 σ). The average value is 0.17 ‰ lower than the assigned $\delta^{13}\text{CH}_4$ value for the air tank (-47.13 ‰ VPDB) but within the uncertainty associated with the method itself. For the wet extraction system, we processed 15 standard air samples through degassed water samples. The average $\delta^{13}\text{CH}_4$ value for these runs was -47.10 ± 0.34 ‰. These results are close to the assigned value for the standard (-47.13 ‰) and 0.2 ‰ higher than the results from the dry extraction system. To account for the $\delta^{13}\text{CH}_4$ difference between the two extraction systems, we add 0.2 ‰ to all the dry extraction data to be consistent with the wet extraction data and the assigned value for the air standard. We estimate the overall uncertainty based on the replicate analyses of the standard air samples to be 0.3 ‰ (1 σ).

1.3 Correction of $\delta^{13}\text{CH}_4$ data due to Kr interference during IRMS measurements

90 The chromatographic separation of CH₄ and the noble gas krypton (Kr) imposes special demands on a setup used to separate air components, owing to the very similar physico-chemical properties of these compounds. Kr has previously not been accounted for in $\delta^{13}\text{CH}_4$ studies, as none of the multiple stable isotopes of Kr are close to the mass to charge ratio (m/z) 44, 45 and 46 considered in CO₂ based $\delta^{13}\text{CH}_4$ measurements. Recently Schmitt et al. (2013) demonstrated¹¹, that the doubly charged isotope $^{86}\text{Kr}^{2+}$ does in fact interfere with the $\delta^{13}\text{C}$ measurement of CH₄, if Kr enters the ion source of the IRMS.

After a thorough review of the raw data for the ice core $\delta^{13}\text{CH}_4$ time series, we were able to identify irregularities in the raw chromatograms at the peak flanks of the CH_4 -derived CO_2 for the measurements performed with the AWI instrument. The Kr peak causes anomalies in the ratio of $m/z = 45$ to $m/z = 44$ and the $m/z = 46$ to $m/z = 44$ ratio which generates higher $\delta^{13}\text{CH}_4$ values the more Kr contributes to the total peak areas (hereafter referred to as Kr effect). While the symptoms are distinct due to instrumental differences of the two setups, we also found the PSU system to be affected by the Kr interference.

Because polar ice core samples are not easily replaced, we were unable to repeat the measurements of the EDML and Vostok $\delta^{13}\text{CH}_4$ time series with enhanced instrumental setups. Instead we corrected the $\delta^{13}\text{CH}_4$ values for this Kr effect as described in detail in Schmitt et al. (2013)¹¹, which we briefly summarize below.

A posteriori correction of the Kr effect

We applied the following strategies to correct PSU and AWI $\delta^{13}\text{CH}_4$ measurements for the Kr effect and account for relative laboratory offsets with respect to the VPDB scale. AWI EDML measurements are corrected for Kr individually by a method applied to the respective raw data chromatograms. The method uses the visible anomalies seen in the m/z ratios 45/44 and m/z 46/44 and subtracts the derived interference from the raw data time series¹¹. Afterwards, the chromatograms are reprocessed and the isotopic composition of the CH_4 peak calculated. We refer to these values as the Kr-corrected $\delta^{13}\text{CH}_4$ values. In contrast, $\delta^{13}\text{CH}_4$ values obtained without the subtraction algorithm are referred to as original $\delta^{13}\text{CH}_4$ values. The difference between original and corrected values are termed Kr correction values or $\Delta\delta^{13}\text{C}_{\text{Kr}}$. For the EDML time series $\Delta\delta^{13}\text{C}_{\text{Kr}}$ range between 0.4 ‰ for interstadial (medium CH_4 mixing ratios) to 0.8 ‰ during glacial (MIS 2) and stadial conditions (lower CH_4 levels) (compare also Supplementary Figure S1). The results are further calibrated internally and are tied to the VPDB scale as outlined in section 1.1.

Unfortunately, an analogous direct approach could not be applied to the Vostok ice core $\delta^{13}\text{CH}_4$ acquisitions performed at the PSU, as the raw chromatograms were not stored after processing the $\delta^{13}\text{C}$ data. Instead, we had to choose an indirect way to correct for the Kr effect in the Vostok $\delta^{13}\text{CH}_4$ time series.

For the purpose of this correction the atmospheric krypton mixing ratio can safely be considered constant over time^{11,12}. If instrumental conditions are uniform, the Kr effect scales only with the atmospheric concentration of methane, it is thus directly proportional to the Kr/ CH_4 ratio¹¹. We inferred the linear relationship between Kr effect and $1/\text{CH}_4$ from a series of air samples with differing methane mixing ratios but similar Kr levels. The three ambient air samples were retrieved

at Niwot Ridge preserve, Colorado, US in 2007, and were part of the „2007 - IPY International Ice Core Gas Intercalibration Exercise“ launched by Todd Sowers (Penn State University) and Ed Brook (Oregon State University). The samples of recent ambient air were diluted with ultra pure air (free of CH₄) in order to simulate the full spectrum of atmospheric variability from present day, pre-industrial to glacial conditions. Note, that the dilution did not affect the noble gas concentration in the cylinders.

The raw data chromatograms of “IPY” air samples performed with the PSU instrument were treated in the same manner as the EDML ice core samples, with the routine adapted to the specific characteristics of the PSU setup. Based on these PSU measurements we obtained Kr correction values of 0.12 ‰, 0.26 ‰ and 0.66 ‰ for cylinder “CA03560”, ”CC71560” and “CA01179”, respectively. To a first approximation, $\Delta\delta^{13}\text{C}_{\text{Kr}}$ scales with the inverse of the CH₄ mixing ratios of 1852 ppb, 906 ppb and 365 ppb (illustrated in Figure S2), yielding a dependence of $\Delta\delta^{13}\text{C}_{\text{Kr}}$ to CH₄ for the PSU measurements. Supplementary table 1 provides a detailed compilation of results for the “IPY” air samples for both the PSU and the AWI instruments.

When the linear $\Delta\delta^{13}\text{C}_{\text{Kr}} - 1/\text{CH}_4$ relationship was applied to the CH₄ mixing ratios¹³ of the Vostok ice core, we derived $\Delta\delta^{13}\text{C}_{\text{Kr}}$ values in the range of 0.4 ‰ for interglacial conditions (e.g. MIS 5.5) to 0.7 ‰ and 0.8 ‰ for the glacial stages MIS 2 and MIS 6, respectively (see Figure S1). Note that while these corrections on the PSU and AWI data of several tenth of a permille are significant, they are still small compared to the atmospheric changes of several permille observed in our ice core data on glacial/interglacial time scales, and do not influence our interpretations.

1.4 AWI and PSU laboratory inter-calibration

In order to minimize offsets between the absolute standardization of both laboratory setups at the AWI and the PSU, we performed inter-calibration measurements on three IPY air samples and on ice core samples from the WAIS Divide ice core WDC05 A (79°27.70S 112°7.510W; 1.759 masl.).

We applied the CH₄ dependence of $\Delta\delta^{13}\text{C}_{\text{Kr}}$ to account for the Kr effect encountered in the ice core and air sample measurements using the PSU instrument, and the raw data correction procedure described for the EDML ice samples in section 1.3 for the IPY air and WDC05 A measurements performed with the AWI setup. The results for both systems, presented in more detail in Supplementary table 1 and 2, lead to an AWI-PSU laboratory offset of 0.09 ‰ with respect to $\delta^{13}\text{CH}_4$. As a final adjustment, the Vostok $\delta^{13}\text{CH}_4$ time series is hence shifted by 0.09 ‰ towards lower values to account for the differences in the absolute standardization of both laboratories. Note that this inter-laboratory offset is significantly smaller than the measurement uncertainty of 0.3 ‰,

showing that the AWI and PSU data sets are fully compatible after correction of the Kr effect.

165 **1.5 Firn column corrections applied to the $\delta^{13}\text{CH}_4$ ice core records**

During the enclosure of air bubbles in the Antarctic ice sheet, the methane molecules like other air components encounter diffusion processes in the open pore space of the firn column, which also affect their isotopic composition archived after bubble close-off. In the diffusive firn zone¹⁴ methane is subject to gravitational settling, that enriches the heavier isotope at the bottom of the firn column¹⁵. In addition, strong concentration gradients caused by rapid atmospheric methane concentration changes, induce diffusive fluxes that lead to isotopic fractionation¹⁶. Finally, thermal diffusion corrections are required when large temperature gradients exist in the firn layer¹⁷.

170 Temperature variations at Kohnen Station (EDML core site) and Vostok have been slow during the last glacial cycle. Hence, the firn column down to the close-off depth was essentially in thermal equilibrium and thermal diffusion effects are negligible for the datasets presented here.

In order to quantify the order of magnitude of the respective diffusion effects, we used a firn diffusion model¹⁸ with a parameter set adapted to the glacial EDML core characteristics to calculate the combined effects of diffusive fractionation due to gravitation and concentration changes at the surface (see Figure S3). A methane pulse of 200 ppb with an initial rate of increase of 4 ppb/yr and a respective decline of 0.25 ppb/yr (grey line, subfigure **a**)) was prescribed to mimic the most vigorous natural methane rises throughout the glacial cycle (e.g. at the end of terminations or into DO 21). The $\delta^{13}\text{CH}_4$ signature of methane at the surface is prescribed at -45 ‰. Accordingly, all changes to this value recorded at the model bubble close-off on the bottom of the firn column (blue line, subfigure **b**)) are solely due to the two diffusion processes. To account for uncertainties concerning the two most important physical parameters of firnification, site temperature and accumulation rate, we illustrate the range of model results for the fractionation of $\delta^{13}\text{CH}_4$ with a minimal (-52.14 °C, 2.978 cm water equivalent per year (w.e./yr)), maximal (-46.64 °C, 5.075 cm w.e./yr) and a best guess scenario (-49.52 °C, 3.859 cm w.e./yr). This range of site temperatures and snow accumulation rates is a realistic representation of possible glacial conditions at the core site.

185 The initial $\delta^{13}\text{CH}_4$ value, after steady state is reached in the model, is -44.57 ‰. This offset of 0.43 ‰ relative to the atmospheric value is due to the gravitational settling that is established in the firn column. It is also on very good agreement with measured $\delta^{15}\text{N}_2$ for the EDML core for glacial conditions¹⁹. The consecutive prescribed methane rise at the surface causes an additional shift in $\delta^{13}\text{CH}_4$ after bubble close-off in the range of -0.73 ‰ for coldest temperatures and lowest snow

accumulation and up to -1.05 ‰ for maximal temperature and accumulation rate, while the best guess scenario amounts to -0.85 ‰. However, the effect is short-lived and decreases to levels below our experimental uncertainty in less than 150 years after the initial methane increase. After about 200 500 years the $\delta^{13}\text{CH}_4$ value is essentially back at its starting value before the CH_4 increase. During the slower decline of methane concentration back to the base level of 350 ppb, the highest observed diffusional fractionation of -0.24 ‰ does not even exceed the measurement uncertainty. In conclusion, only those data points of our record may be affected that fall within the relatively short time window during major methane concentration increases. Accordingly, we did not correct our 205 data for these diffusion effects, but have to keep in mind that individual samples that coincide with the rapid CH_4 changes may be biased by a few tenth of a permille towards lower (more negative) $\delta^{13}\text{CH}_4$ values.

Accordingly, all our $\delta^{13}\text{CH}_4$ data are solely corrected for gravitational fractionation. Vostok samples 210 have been corrected with interpolated $\delta^{15}\text{N}_2$ data according to published procedures¹⁴. No $\delta^{15}\text{N}_2$ record covering the whole time interval of our $\delta^{13}\text{CH}_4$ data is available for the EDML ice core to date. However, $\delta^{15}\text{N}_2$ data over the last glacial/interglacial transition vary only between 0.4 to 0.45 ‰. Thus, we shifted EDML values by a constant offset of 0.41 ‰ to higher values. This 0.41 ‰ shift does reflect expected values for glacial conditions very well^{19,20}, and is also in line with 215 model studies²¹. The error introduced by this constant correction is 0.05 ‰ at the most, and thus negligible compared to our overall analytical uncertainty of 0.3 ‰.

1.6 $dD(\text{CH}_4)$ measurements performed at University of Bern

$\delta D(\text{CH}_4)$ measurements were performed using a purge and trap extraction coupled to a gas chromatography pyrolysis isotope ratio mass spectrometer (GC/P/IRMS) system as described in 220 detail in Bock et al. (2010)²² with some improvements which will be published elsewhere. External precision of the presented data is about 2.5 ‰ (1σ) based on standard air measurements of corresponding size. In Figure 3 of the main text the error bars represent the standard deviation of standard air measurements (1σ : 1.8 ‰ to 2.9 ‰) used to calibrate the corresponding samples. All $\delta D(\text{CH}_4)$ values are given with respect to the international Vienna Standard Mean Ocean Water (VSMOW) scale. No corrections (e.g. gravitational enrichment) have been applied, as these 225 corrections would only be of minor importance regarding the analytical uncertainty, and do not affect our conclusions. Note, that no Kr interference occurs for our $\delta D(\text{CH}_4)$ system.

1.7 Age scales

Ice core records

230 If not stated otherwise, all gas ages in this document are reported according to a chronology based on the new synchronization effort for EPICA and various other ice core chronologies by Lemieux-Dudon et al. (2010)²³, hereafter denoted as “Unified” age scale. Where applicable, a direct age calculation was performed by linear interpolation of the depth-age relationship provided by Lemieux-Dudon et al. (2010)²³. Other records required additional conversion steps according to the
235 procedures described below.

Vostok $\delta^{13}\text{CH}_4$ and CO_2 records

For Vostok we adopted the published Vostok depth to EDC3 gas age relationship of the Vostok CO_2 record and interpolated corresponding EDC3 ages for the Vostok $\delta^{13}\text{CH}_4$ data. However, we
240 observed an evident misalignment of the fast methane concentration rises at Dansgaard/Oeschger (DO) event 24 compared to EDC CH_4 data²⁶. As part of the focus of our work is directed at relative timings of $\delta^{13}\text{CH}_4$ and CH_4 rises, we performed a manual methane synchronization to account for this offset. Therefore, we picked five tie-points in between DO event 21 and the Termination 2 methane rise at peak flanks (Supplementary table 3) and interpolated the included data points
245 linearly to the EDC3 age scale²⁷. The EDC3 ages including the adjusted section between 83.6 kyr BP and 128.9 kyr BP were then converted to the target “Unified” age model. The adjustments were also applied to the Vostok CO_2 record used in this work^{26,28}. Note that the applied adjustments do not affect the conclusions in this publication on the decoupling of CH_4 and $\delta^{13}\text{CH}_4$ or on the coupling of $\delta^{13}\text{CH}_4$ and atmospheric CO_2 .

250

Byrd atmospheric CO_2

No official age conversion to the “Unified” age scale exists for the Byrd ice core. Hence, we performed another methane synchronization between the Byrd²⁹ and EDML³⁰ CH_4 records in order to obtain corresponding EDML depths. Those were then converted to “Unified” ages. We are aware
255 of the limitations of the methane synchronization approach³¹, especially if the resolution differences of the compared CH_4 datasets are large, or at times where CH_4 variations are low and, thus, tie-points are scarce. However, the very good temporal agreement of the Byrd³² and the EDML CO_2 data³³ show that the relative CH_4 synchronization error is small and does not affect the conclusions in our paper. The list of manual tie-points applied in the synchronization are presented in Supplementary
260 table 4.

Relative sea-level

No direct age conversion to the “Unified” target age scale could be applied to the relative sea-level (rsl.) data without invoking an ad-hoc phase relationship between the sea level and the ice core records. Therefore, we used the sea level record of Rohling et al. (2009)²⁴ on the speleothem
265 synchronized age-scale provided by Grant et al. (2012)²⁵ without any modifications.

2. Complementary information on past $\delta^{13}\text{CH}_4$ changes

2.1 DO methane variability and its missing responses in $\delta^{13}\text{CH}_4$

Figure S4 illustrates the missing imprint of the rapid atmospheric methane concentration variability
270 on the carbon isotopic signature of methane in conjunction with the six strongest DO warmings throughout the last glacial. Segments of the CH_4 ³⁰ and $\delta^{13}\text{CH}_4$ data sets, centered around the respective methane rise, have been aligned (Figure S4 a)) in order to study the phasing and individual timing of the concentration changes and its counterpart in $\delta^{13}\text{CH}_4$ (Figure S4 b)). Note that the data points in $\delta^{13}\text{CH}_4$ closest to the most vigorous methane increases are likely biased by
275 diffusional fractionation in the firn column (see discussion above). This may lead to offsets of $\delta^{13}\text{CH}_4$ data points close to major CH_4 changes. For example, the two negative excursions in $\delta^{13}\text{CH}_4$ of less than 1 ‰ at DO 8 and termination I are located so close to the corresponding methane increase, that they can be attributed to the diffusional fractionation effect. We mark the range of possibly affected values in Figure S4 with a box of the width of 150 yr (gray bar), according to the
280 maximum duration in our firnification model exercise, where the effect of the diffusional fractionation exceeded our experimental uncertainty range of 0.3 ‰. We also show the two major methane increases of termination I and II (right pair of panels in Figure S4). There is no apparent imprint of rapid methane variability on its carbon isotopic signature over the respective DO events and deglaciations.

285 2.2 Proxy evidence for C4 plant expansion

Methane production under natural conditions involves the decomposition of organic precursor material that has previously been accumulated by plants through photosynthetic sequestration of CO_2 . Owing to fundamental physiological differences of the two major photosynthetic pathways, which characteristically discriminate the heavy isotope ^{13}C during carbon assimilation, the typical
290 ranges of isotopic signatures imposed on the plant material differ considerably^{34,35}. 85–90 % of terrestrial plant species today, covering the whole spectrum of vegetation from grasses and herbs to shrubs and trees, follow the C3 photosynthetic pathway³⁶. C3 plant biomass is characterized by a

depleted $\delta^{13}\text{C}$ signature (-32 ‰ - -22 ‰), caused by the lower reactivity of $^{13}\text{CO}_2$ with the primary carboxylating enzyme RUBISCO³⁷. C4 vegetation on the other hand, mostly grasses and sedges, are able to pre-concentrate CO_2 internally at the cost of reduced quantum yield³⁸. As a consequence, C4 plant carbon fixation fractionates less against ^{13}C (~-16 ‰ - -9 ‰). The isotopic composition of the terrestrial biosphere, i.a. the pre-cursor biomass for methanogenesis, is controlled by the primary productivity of an assemblage of plants under local growth conditions, the individual adaptation of its members to this conditions, as well as its tolerance against limitation factors. Plants of both photosynthetic pathways are unequally tolerant to limitations in CO_2 , light intensity, local temperature, and to moisture and nutrient availability^{35,39,40}. Seasonality of precipitation has an equally significant impact on the local balance between C3 and C4 vegetation⁴⁰. However, the relative importance of any of the limitations, especially in terms of a competitive advantage of plant families against others in the struggle for habitats, remains an unresolved and vitally discussed question^{36,41-45}.

Accordingly, it is neither physiologically well constrained how strong a C3 to C4 plant shift might have been in tropical regions under generally colder, drier conditions, and low CO_2 levels that were characteristic for the glacial period, nor is it extensively documented by the scarce terrestrial proxy evidence from these areas. Such a shift, however, is one of the relevant processes of our hypothesis to explain the observed, very pronounced $\delta^{13}\text{CH}_4$ changes. Therefore, we will now discuss some of the ecosystem evidence that is available and relevant for our hypothesis.

In temperate regions in Northern- and Meso-America⁴⁶ and the Chinese loess plateau⁴⁷⁻⁴⁹, growing season temperature and the local climatic constellation seems to out-compete the physiological effect of low CO_2 level as predominant control upon the C3/C4 ratio. With warm growing seasons in the tropics, however, water insufficiency and low CO_2 possess an increased influence as plant-growth limitation factors and pose high adaptive pressure on prevalent ecosystems⁵⁰⁻⁵³.

Recent vegetation model experiments indicate high vegetation sensitivity to low atmospheric CO_2 levels during glacial periods^{44,45,54,55}. Globally, simulations for glacial climate conditions and typical CO_2 concentrations lead to significant retractions of closed canopy forest habitats in favor of open vegetation types^{43,56,57}. Tropical rainforests seem especially affected by the combined effects of increased aridity and low CO_2 , and large arboreal areas are replaced by open savanna- and shrub-like vegetation.

Analogue findings are well documented by terrestrial proxy data from tropical regions in Africa⁵⁸⁻⁶¹, Meso- and South America⁶¹⁻⁶⁴. These studies also report large proportions of C4 vegetation

contributing to the widespread grasslands in equatorial Africa and South America in the LGM. Glacial-Interglacial differences in $\delta^{13}\text{C}$ of vascular plant waxes from sediment cores off the East Atlantic coast close to the river mouths of the Congo and Angola basin, indicate 3-4 ‰ shifts towards higher $\delta^{13}\text{C}$ values and thus, relative increases of C4 abundance in the range of 20-40 %⁵⁹. Increased C4 contribution has also been inferred from another marine core retrieved at the Guinea Plateau margin recording Sahara/Sahel vegetation⁶⁰. It also indicates raised aridity, falling temperatures and exceptionally high C4 predominance for the period between 71 and 65 kyr BP, i.e. the MIS5/4 transition, which is also characterized by a strong increase (+4 ‰) in our $\delta^{13}\text{CH}_4$ record.

A comparable study from the Cariaco Basin in the tropical west Atlantic, reported a 4-5 ‰ $\delta^{13}\text{C}$ decrease in leaf waxes from the LGM to the Preboreal Holocene⁶². This probably documents a reoccupation of forest vegetation in the peripheral Amazonian lowlands, that potentially retracted under glacial conditions⁶⁵⁻⁶⁹. Moreover, huge land masses the size of Europe from South Thailand to Sumatra, Borneo and Java became exposed in South-East Asia when sea-level fell in glacial periods. This territory, known as Sundaland, was also vastly covered by savanna type vegetation with considerable C4 contribution^{70,71}.

A global shift of C3 to C4 plants may not be representative for the conditions encountered in permanent (tropical) wetlands. Intuitively, one may expect that the missing water limitation in such a wetland would reduce the adaptive pressure on plants in that ecosystem and hence level competitive advantages of one species against another. C3 plants, for example, are not forced into the natural trade-off between necessary stomatal opening for carbon sequestration and excessive water loss. In this light it is yet not fully understood, why large modern wetland ecosystems in tropical East Africa⁷², South Africa^{73,74} or areas of the Amazon floodplain⁷⁵ exhibit clear C4 plant predominance (mostly papyrus). Moreover, there is evidence that C4 dominance in east-equatorial Africa (at least near lake Challa) persisted during both wet and dry phases under glacial conditions⁷⁶. For the $\delta^{13}\text{CH}_4$ change observed in our record we speculate that seasonally inundated wetlands played an increasing role for CH_4 emissions during cold climate conditions. These tropical non-permanent wetlands should foster the shift to open grasslands with high C4 contribution, as the higher water use efficiency and productivity of the C4 plants under low CO_2 levels in glacial periods should prove advantageous in this environment of seasonally contrasting very dry to very wet conditions.

360 **2.3 Impact of location and habitat on the isotopic signature of C3 plants**

Environmental factors as humidity, light availability, CO₂ concentration and use of recycled CO₂ differ largely between C3 plant habitats like rainforest and savanna⁷⁷. Dense closed canopy rainforest habitats provide a higher degree of natural protection from wind movement and hence reduced water loss and air mass exchange, but on the other hand increase the competition for light intensity. The low photon flux caused by the light deficit for example diminishes carbon fixation rates, especially in the undergrowth vegetation. Lower vegetation layers furthermore assimilate more respired CO₂ that already underwent fractionation^{78,79}. Rainforest habitats have much higher water supply and air moisture levels compared to open vegetation types. Reduced evapo-transpirative water loss in closed canopies allows longer periods of opened leaf stomata and, thus, increased CO₂ levels in the leaf. Light deficit and high intracellular CO₂ levels enhance the discrimination of the heavier ¹³C isotope during photosynthesis⁸⁰. In contrast, open shrub, herb and grassy C3 vegetation is, especially in low latitudes, exposed to high levels of direct sunlight and high leaf temperatures. To avoid extensive water loss, the stomatal conductance of these plants is usually highly restricted³⁷, and carbon dioxide limitation in the leaf cells reduces the relative discrimination of the heavier isotope by the enzymes involved in photosynthesis. As a consequence of these effects, C3 rainforest plant material is found to be 3-4 ‰ more depleted than C3 plant material from open savanna⁷⁷.

2.4 Role of water table changes

380 Hydrological changes in the past have direct implications on water table heights in wetlands. The soil oxidative layer thickness directly affects the net/gross primary productivity and thus CH₄ emission strength of a given wetland system. But an increased/decreased oxidative layer thickness would also induce an enrichment/depletion in the mean δ¹³CH₄ signature of emitted methane as a higher/lower proportion of methane is oxidized on its way to the surface. This parameter is highly dependent on the local hydrology, topography and soil characteristics and poorly constrained spatially and over time. Our record suggests that it is of minor importance for the millennial scale variability of methane over the DO cycles as there is no remarkable imprint on δ¹³CH₄. A general contribution to the glacial-interglacial difference in δ¹³CH₄ due to enhanced global aridity in the course of the glaciation, however, cannot be ruled out.

390

References

1. Behrens, M.; Schmitt, J.; Richter, K.-U.; Bock, M.; Richter, U. C.; Levin, I. & Fischer, H. A gas chromatography/combustion/isotope ratio mass spectrometry system for high-precision $\delta^{13}\text{C}$ measurements of atmospheric methane extracted from ice core samples. *Rapid Commun Mass Spectrom*, **22**, 3261-3269 (2008).
2. Fischer, H.; Behrens, M.; Bock, M.; Richter, U.; Schmitt, J.; Loulergue, L.; Chappellaz, J.; Spahni, R.; Blunier, T.; Leuenberger, M. & Stocker, T. F. Changing boreal methane sources and constant biomass burning during the last termination. *Nature*, **452**, 864-867 (2008).
3. Poß, C. *Analysis of the variability of the atmospheric methane budget in high polar regions with a regional trajectory model and using measurements of stable isotopes*. PhD thesis, University of Heidelberg, Germany, (2003).
4. Calibration of the Heidelberg $\delta^{13}\text{CH}_4$ measurements was performed using pure CO_2 IAEA Standard Reference Materials (RM 8562: $\delta^{13}\text{C} = -3.72\text{‰}$, RM 8564: $\delta^{13}\text{C} = -10.45\text{‰}$, RM 8563: $\delta^{13}\text{C} = -41.59\text{‰}$ ⁵). The absolute agreement of the Heidelberg $\delta^{13}\text{CH}_4$ measurements on the VPDB CO_2 scale is estimated to be better than $\pm 0.1\text{‰}$. An intercomparison with three air samples from the southern hemisphere between Heidelberg and NIWA yielded a difference NIWA-Heidelberg $\delta^{13}\text{CH}_4 = 0.04 \pm 0.04\text{‰}$ ³.
5. Sowers, T. & Jubenville, J. A modified extraction technique for liberating occluded gases from ice cores. *J. Geophys. Res.*, **105**, 29155-29164 (2000).
6. Sowers, T.; Alley, R. B. & Jubenville, J. Ice Core Records of Atmospheric N_2O Covering the Last 106,000 Years. *Science*, **301**, 945-948 (2003).
7. Miteva, V.; Sowers, T. & Brenchley, J. Production of N_2O by Ammonia Oxidizing Bacteria at Subfreezing Temperatures as a Model for Assessing the N_2O Anomalies in the Vostok Ice Core. *Geomicrobiology Journal*, **24**, 451-459 (2007).
8. Sowers, T.; Rodebaugh, A.; Yoshida, N. & Toyoda, S. Extending records of the isotopic composition of atmospheric N_2O back to 1800 A.D. from air trapped in snow at the South Pole and the Greenland Ice Sheet Project II ice core. *Global Biogeochem. Cycles*, **16**, 1129-1129 (2002).
9. Sowers, T.; Bernard, S.; Aballain, O.; Chappellaz, J.; Barnola, J.-M. & Marik, T. Records of the $\delta^{13}\text{C}$ of atmospheric CH_4 over the last 2 centuries as recorded in Antarctic snow and ice. *Global Biogeochem. Cycles*, **19**, (2005).
10. Sowers, T. Atmospheric methane isotope records covering the Holocene period. *Quaternary Science Reviews*, **29**, 213-221 (2010).
11. Schmitt, J.; Seth, B.; Bock, M.; Fischer, H.; Möller, L.; Sapart, C.; Prokopiou, M.; Röckmann, T. & Sowers, T. On the interference of Kr during carbon isotope analysis of methane using continuous-flow combustion–isotope ratio mass spectrometry. *Atmos. Meas. Tech.*, **6**, 1425-1445 (2013).
12. Headly, M. A. & Severinghaus, J. P. A method to measure Kr/N_2 ratios in air bubbles trapped in ice cores and its application in reconstructing past mean ocean temperature. *J. Geophys. Res.*, **112**, D19105- (2007).
13. Petit, J. R.; Basile, I.; Leruyet, A.; Raynaud, D.; Lorius, C.; Jouzel, J.; Stievenard, M.; Lipenkov, V. Y.; Barkov, N. I.; Kudryashov, B. B.; Davis, M.; Saltzman, E. & Kotlyakov, V. Four climate cycles in Vostok ice core. *Nature*, **387**, 359-360 (1997).
14. Sowers, T.; Bender, M.; Raynaud, D. & Korotkevich, Y. S. $\delta^{15}\text{N}$ of N_2 in Air Trapped in Polar Ice: a Tracer of Gas Transport in the Firn and a Possible Constraint on Ice Age-Gas Age Differences. *J. Geophys. Res.*, **97**, 15683-15697 (1992).
15. Schwander, J.; Stauffer, B. & Sigg, A. Air mixing in firn and the age of the air at pore close-off. *Annals of Glaciology*, **10**, 141-145 (1988).
16. Trudinger, C. M.; Enting, L. G.; Etheridge, D. M.; Francey, R. J.; Levchenko, V. A.; Steele, L. P.; Raynaud, D. & Arnaud, L. Modeling air movement and bubble trapping in firn. *J. Geophys. Res.*, **102**, (1997).

17. Severinghaus, J. P.; Grachev, A. & Battle, M. Thermal fractionation of air in polar firn by seasonal temperature gradients. *Geochem. Geophys. Geosyst.*, **2**, (2001).
- 445 18. Schwander, J.; Sowers, T.; Barnola, J.-M.; Blunier, T.; Fuchs, A. & Malaize, B. Age scale of the air in the summit ice: Implication for glacial-interglacial temperature change. *J. Geophys. Res.*, **102**, 19483–19493 (1997).
- 450 19. Landais, A.; Barnola, J.; Kawamura, K.; Caillon, N.; Delmotte, M.; Van Ommen, T.; Dreyfus, G.; Jouzel, J.; Masson-Delmotte, V.; Minster, B.; Freitag, J.; Leuenberger, M.; Schwander, J.; Huber, C.; Etheridge, D. & Morgan, V. Firn-air $\delta^{15}\text{N}$ in modern polar sites and glacial-interglacial ice: a model-data mismatch during glacial periods in Antarctica?. *Quaternary Science Reviews*, **25**, 49-62 (2006).
- 455 20. Landais, A.; Dreyfus, G.; Capron, E.; Masson-Delmotte, V.; Sanchez-Goñi, M.; Desprat, S.; Hoffmann, G.; Jouzel, J.; Leuenberger, M. & Johnsen, S. What drives the millennial and orbital variations of $\delta^{18}\text{O}_{\text{atm}}$? *Quaternary Science Reviews*, **29**, 235-246 (2010).
21. EPICA community members, One-to-one coupling of glacial climate variability in Greenland and Antarctica. *Nature*, **444**, 195-198 (2006).
- 460 22. Bock, M.; Schmitt, J.; Behrens, M.; Möller, L.; Schneider, R.; Sapart, C. & Fischer, H. A gas chromatography/pyrolysis/isotope ratio mass spectrometry system for high-precision δD measurements of atmospheric methane extracted from ice cores. *Rapid Commun. Mass Spectrom.*, **24**, 621-633 (2010).
23. Lemieux-Dudon, B.; Blayo, E.; Petit, J.-R.; Waelbroeck, C.; Svensson, A.; Ritz, C.; Barnola, J.-M.; Narcisi, B. M. & Parrenin, F. Consistent dating for Antarctic and Greenland ice cores. *Quaternary Science Reviews*, **29**, 8-20 (2010).
- 465 24. Rohling, E. J.; Grant, K.; Bolshaw, M.; Roberts, A. P.; Siddall, M.; Hemleben, C. & Kucera, M. Antarctic temperature and global sea level closely coupled over the past five glacial cycles. *Nature Geosci*, **2**, 500-504 (2009).
- 470 25. Grant, K. M.; Rohling, E. J.; Bar-Matthews, M.; Ayalon, A.; Medina-Elizalde, M.; Ramsey, C. B.; Satow, C. & Roberts, A. P. Rapid coupling between ice volume and polar temperature over the past 150,000 years. *Nature*, **491**, 744-747 (2012).
26. Loulergue, L.; Schilt, A.; Spahni, R.; Masson-Delmotte, V.; Blunier, T.; Lemieux, B.; Barnola, J.-M.; Raynaud, D.; Stocker, T. F. & Chappellaz, J. Orbital and millennial-scale features of atmospheric CH_4 over the past 800,000 years.. *Nature*, **453**, 383-386 (2008).
- 475 27. Parrenin, F.; Barnola, J.-M.; Beer, J.; Blunier, T.; Castellano, E.; Chappellaz, J.; Dreyfus, G.; Fischer, H.; Fujita, S.; Jouzel, J.; Kawamura, K.; Lemieux-Dudon, B.; Loulergue, L.; Masson-Delmotte, V.; Narcisi, B.; Petit, J.-R.; Raisbeck, G.; Raynaud, D.; Ruth, U.; Schwander, J.; Severi, M.; Spahni, R.; Steffensen, J. P.; Svensson, A.; Udisti, R.; Waelbroeck, C. & Wolff, E. The EDC3 chronology for the EPICA Dome C ice core. *Clim. Past*, **3**, 485-497 (2007).
- 480 28. Lüthi, D.; Floch, M. L.; Bereiter, B.; Blunier, T.; Barnola, J.-M.; Siegenthaler, U.; Raynaud, D.; Jouzel, J.; Fischer, H.; Kawamura, K. & Stocker, T. F. High-resolution carbon dioxide concentration record 650,000-800,000 years before present.. *Nature*, **453**, 379-382 (2008).
29. Blunier, T. & Brook, E. J. Timing of Millennial-Scale Climate Change in Antarctica and Greenland During the Last Glacial Period. *Science*, **291**, 109-112 (2001).
- 485 30. Schilt, A.; Baumgartner, M.; Schwander, J.; Buiron, D.; Capron, E.; Chappellaz, J.; Loulergue, L.; Schüpbach, S.; Spahni, R.; Fischer, H. & Stocker, T. F. Atmospheric nitrous oxide during the last 140,000 years. *Earth and Planetary Science Letters*, **300**, 33-43 (2010).
31. Blunier, T.; Spahni, R.; Barnola, J.-M.; Chappellaz, J.; Loulergue, L. & Schwander, J. Synchronization of ice core records via atmospheric gases. *Clim. Past*, **3**, 325-330 (2007).
- 490 32. Ahn, J. & Brook, E. J. Atmospheric CO_2 and Climate on Millennial Time Scales During the Last Glacial Period. *Science*, **322**, 83-85 (2008).
33. Bereiter, B.; Lüthi, D.; Siegrist, M.; Schüpbach, S.; Stocker, T. F. & Fischer, H. Mode change of millennial CO_2 variability during the last glacial cycle associated with a bipolar marine carbon seesaw. *Proceedings of the National Academy of Sciences*, **109**, 9755-9760

- 495 (2012).
34. O'Leary, M. H. Carbon Isotope Fractionation In Plants. *Phytochemistry*, **20**, 553-567 (1981).
35. Farquhar, G. D.; Ehleringer, J. R. & Hubick, K. T. Carbon Isotope Discrimination and Photosynthesis Rid A-3722-2008. *Annual Review of Plant Physiology and Plant Molecular Biology*, **40**, 503-537 (1989).
- 500 36. Gerhart, L. M. & Ward, J. K. Plant responses to low [CO₂] of the past. *New Phytologist*, **188**, 674-695 (2010).
37. Farquhar, G. D.; O'Leary, M. H. & Berry, J. A. On the Relationship Between Carbon Isotope Discrimination and the Inter-cellular Carbon-dioxide Concentration In Leaves Rid A-3722-2008 Rid B-8211-2009. *Australian Journal of Plant Physiology*, **9**, 121-137 (1982).
- 505 38. Ehleringer, J. R. Implications of quantum yield differences on the distributions of C3 and C4 grasses. *Oecologia*, **31**, 255-267 (1978).
39. Cowling, S. A. & Sykes, M. T. Physiological Significance of Low Atmospheric CO₂ for Plant/Climate Interactions. *Quaternary Research*, **52**, 237-242 (1999).
- 510 40. Ehleringer, J. (2005). *The Influence of Atmospheric CO₂, Temperature, and Water on the Abundance of C3/C4 Taxa*. In: Baldwin, I.; Caldwell, M.; Heldmaier, G.; Jackson, R.; Lange, O.; Mooney, H.; Schulze, E.-D.; Sommer, U.; Ehleringer, J.; Denise Dearing, M. & Cerling, T. (Ed.), *Ecological Studies*, Springer New York.
41. Sankaran, M.; Hanan, N. P.; Scholes, R. J.; Ratnam, J.; Augustine, D. J.; Cade, B. S.; Gignoux, J.; Higgins, S. I.; Le Roux, X.; Ludwig, F.; Ardo, J.; Banyikwa, F.; Bronn, A.; Bucini, G.; Caylor, K. K.; Coughenour, M. B.; Diouf, A.; Ekaya, W.; Feral, C. J.; February, E. C.; Frost, P. G. H.; Hiernaux, P.; Hrabar, H.; Metzger, K. L.; Prins, H. H. T.; Ringrose, S.; Sea, W.; Tews, J.; Worden, J. & Zambatis, N. Determinants of woody cover in African savannas. *Nature*, **438**, 846-849 (2005).
- 515 42. Edwards, E. J.; Osborne, C. P.; Strömberg, C. A. E.; Smith, S. A. & Consortium, C. 4. G. The Origins of C4 Grasslands: Integrating Evolutionary and Ecosystem Science. *Science*, **328**, 587-591 (2010).
- 520 43. Prentice, I. C.; Harrison, S. P. & Bartlein, P. J. Global vegetation and terrestrial carbon cycle changes after the last ice age. *New Phytologist*, **189**, 988-998 (2011).
- 525 44. Bragg, F. J.; Prentice, I. C.; Harrison, S. P.; Eglinton, G.; Foster, P. N.; Rommerskirchen, F. & Rullkötter, J. Stable isotope and modelling evidence for CO₂ as a driver of glacial-interglacial vegetation shifts in southern Africa. *Biogeosciences*, **10**, 2001-2010 (2013).
45. Claussen, M.; Selent, K.; Brovkin, V.; Raddatz, T. & Gayler, V. Impact of CO₂ and climate on Last Glacial Maximum vegetation - a factor separation. *Biogeosciences Discuss.*, **9**, 15823-15852 (2012).
- 530 46. Huang, Y.; Street-Perrott, F. A.; Metcalfe, S. E.; Brenner, M.; Moreland, M. & Freeman, K. H. Climate Change as the Dominant Control on Glacial-Interglacial Variations in C3 and C4 Plant Abundance. *Science*, **293**, 1647-1651 (2001).
- 535 47. Zhang, Z.; Zhao, M.; Lu, H. & Faiia, A. M. Lower temperature as the main cause of C4 plant declines during the glacial periods on the Chinese Loess Plateau. *Earth and Planetary Science Letters*, **214**, 467-481 (2003).
48. Vidic, N. J. & Montañez, I. P. Climatically driven glacial-interglacial variations in C3 and C4 plant proportions on the Chinese Loess Plateau. *Geology*, **32**, 337-340 (2004).
- 540 49. Wang, G.; Feng, X.; Han, J.; Zhou, L.; Tan, W. & Su, F. Paleovegetation reconstruction using δ¹³C of Soil Organic Matter. *Biogeosciences*, **5**, 1325-1337 (2008).
50. Ehleringer, J. R.; Cerling, T. E. & Helliker, B. R. C4 photosynthesis, atmospheric CO₂, and climate. *Oecologia*, **112**, 285-299 (1997).
- 545 51. Street-Perrott, F. A.; Huang, Y.; Perrott, R. A.; Eglinton, G.; Barker, P.; Khelifa, L. B.; Harkness, D. D. & Olago, D. O. Impact of Lower Atmospheric Carbon Dioxide on Tropical Mountain Ecosystems. *Science*, **278**, 1422-1426 (1997).

52. Sage, R. F.; Wedin, D. A. & Li, M. (1999). 10 - *The Biogeography of C4 Photosynthesis: Patterns and Controlling Factors*. In: Sage, R. F. & Monson, R. K. (Ed.), *C4 Plant Biology*, Academic Press.
- 550 53. Sage, R. F. The evolution of C4 photosynthesis. *New Phytologist*, **161**, 341-370 (2004).
54. Harrison, S. P. & Prentice, C. I. Climate and CO₂ controls on global vegetation distribution at the last glacial maximum: analysis based on palaeovegetation data, biome modelling and palaeoclimate simulations. *Global Change Biology*, **9**, 983-1004 (2003).
- 555 55. Prentice, I. C. & Harrison, S. P. Ecosystem effects of CO₂ concentration: evidence from past climates. *Clim. Past*, **5**, 297-307 (2009).
56. Jolly, D. & Haxeltine, A. Effect of Low Glacial Atmospheric CO₂ on Tropical African Montane Vegetation. *Science*, **276**, 786-788 (1997).
57. Woillez, M.-N.; Kageyama, M.; Krinner, G.; de Noblet-Ducoudré, N.; Viovy, N. & Mancip, M. Impact of CO₂ and climate on the Last Glacial Maximum vegetation: results from the ORCHIDEE/IPSL models. *Clim. Past*, **7**, 557-577 (2011).
- 560 58. Wooller, M. J.; Swain, D. L.; Ficken, K. J.; Agnew, A. D. Q.; Street-Perrott, F. A. & Eglinton, G. Late Quaternary vegetation changes around Lake Rutundu, Mount Kenya, East Africa: evidence from grass cuticles, pollen and stable carbon isotopes. *J. Quaternary Sci.*, **18**, 3-15 (2003).
- 565 59. Rommerskirchen, F.; Eglinton, G.; Dupont, L. & Rullkötter, J. Glacial/interglacial changes in southern Africa: Compound-specific δ¹³C land plant biomarker and pollen records from southeast Atlantic continental margin sediments. *Geochem. Geophys. Geosyst.*, **7**, (2006).
60. Castañeda, I. S.; Mulitza, S.; Schefuß, E.; Lopes dos Santos, R. A.; Sinninghe Damsté, J. S. & Schouten, S. Wet phases in the Sahara/Sahel region and human migration patterns in North Africa. *Proceedings of the National Academy of Sciences*, **106**, 20159-20163 (2009).
- 570 61. Hessler, I.; Dupont, L.; Bonnefille, R.; Behling, H.; González, C.; Helmens, K. F.; Hooghiemstra, H.; Lebamba, J.; Ledru, M.-P.; Lézine, A.-M.; Maley, J.; Marret, F. & Vincens, A. Millennial-scale changes in vegetation records from tropical Africa and South America during the last glacial. *Quaternary Science Reviews*, **29**, 2882-2899 (2010).
- 575 62. Hughen, K. A.; Eglinton, T. I.; Xu, L. & Makou, M. Abrupt Tropical Vegetation Response to Rapid Climate Changes. *Science*, **304**, 1955-1959 (2004).
63. Punyasena, S. W.; Mayle, F. E. & McElwain, J. C. Quantitative estimates of glacial and Holocene temperature and precipitation change in lowland Amazonian Bolivia. *Geology*, **36**, 667-670 (2008).
- 580 64. Lane, C.; Horn, S.; Mora, C.; Orvis, K. & Finkelstein, D. Sedimentary stable carbon isotope evidence of late Quaternary vegetation and climate change in highland Costa Rica. *Journal of Paleolimnology*, **45**, 323-338 (2011).
65. Mayle, F. E.; Burbridge, R. & Killeen, T. J. Millennial-scale dynamics of southern Amazonian rain forests. *Science*, **290**, 2291-2294 (2000).
- 585 66. Turcq, B.; Cordeiro, R. C.; Sifeddine, A.; Simões Filho, F. F.; Albuquerque, A. L. S. & Abrão, J. J. Carbon storage in Amazonia during the Last Glacial Maximum: secondary data and uncertainties. *Chemosphere*, **49**, 821-835 (2002).
67. Mayle, F. E. & Beerling, D. J. Late Quaternary changes in Amazonian ecosystems and their implications for global carbon cycling. *Palaeogeography, Palaeoclimatology, Palaeoecology*, **214**, 11-25 (2004).
- 590 68. Mayle, F. E.; Beerling, D. J.; Gosling, W. D. & Bush, M. B. Responses of Amazonian ecosystems to climatic and atmospheric carbon dioxide changes since the last glacial maximum. *Philosophical Transactions of the Royal Society of London. Series B: Biological Sciences*, **359**, 499-514 (2004).
- 595 69. Anhuf, D.; Ledru, M.-P.; Behling, H.; Da Cruz Jr., F.; Cordeiro, R.; Van der Hammen, T.; Karmann, I.; Marengo, J.; De Oliveira, P.; Pessenda, L.; Siffeddine, A.; Albuquerque, A. & Da Silva Dias, P. Paleo-environmental change in Amazonian and African rainforest during the LGM. *Palaeogeography, Palaeoclimatology, Palaeoecology*, **239**, 510-527 (2006).

- 600 70. Bird, M. I.; Taylor, D. & Hunt, C. Palaeoenvironments of insular Southeast Asia during the Last Glacial Period: a savanna corridor in Sundaland? *Quaternary Science Reviews*, **24**, 2228-2242 (2005).
71. Wurster, C. M.; Bird, M. I.; Bull, I. D.; Creed, F.; Bryant, C.; Dungait, J. A. J. & Paz, V. Forest contraction in north equatorial Southeast Asia during the Last Glacial Period. *Proceedings of the National Academy of Sciences*, **107**, 15508-15511 (2010).
- 605 72. Jones, M. B. & Muthuri, F. M. Standing biomass and carbon distribution in a papyrus (*Cyperus papyrus* L.) swamp on Lake Naivasha, Kenya. *Journal of Tropical Ecology*, **13**, 347-356 (1997).
73. Kotze, D. C. & O'Connor, T. G. Vegetation variation within and among palustrine wetlands along an altitudinal gradient in KwaZulu-Natal, South Africa. *Plant Ecology*, **146**, 77-96
- 610 (2000).
74. Saunders, M.; Jones, M. & Kansiime, F. Carbon and water cycles in tropical papyrus wetlands. *Wetlands Ecology and Management*, **15**, 489-498 (2007).
75. Piedade, M. T. F.; Junk, W. J. & Long, S. P. The Productivity of the C₄ Grass *Echinochloa-polystachya* On the Amazon Floodplain Rid A-2488-2008. *Ecology*, **72**, 1456-1463 (1991).
- 615 76. Sinninghe Damsté, J. S.; Verschuren, D.; Ossebaar, J.; Blokker, J.; van Houten, R.; van der Meer, M. T.; Plessen, B. & Schouten, S. A 25,000-year record of climate-induced changes in lowland vegetation of eastern equatorial Africa revealed by the stable carbon-isotopic composition of fossil plant leaf waxes. *Earth and Planetary Science Letters*, **302**, 236-246
- 620 (2011).
77. Vogts, A.; Moossen, H.; Rommerskirchen, F. & Rullkötter, J. Distribution patterns and stable carbon isotopic composition of alkanes and alkan-1-ols from plant waxes of African rain forest and savanna C₃ species. *Organic Geochemistry*, **40**, 1037-1054 (2009).
78. Medina, E. & Minchin, P. Stratification of $\delta^{13}\text{C}$ values of leaves in Amazonian rain forests. *Oecologia*, **45**, 377-378 (1980).
- 625 79. Buchmann, N.; Guehl, J.-M.; Barigah, T. S. & Ehleringer, J. R. Interseasonal comparison of CO₂ concentrations, isotopic composition, and carbon dynamics in an Amazonian rainforest (French Guiana). *Oecologia*, **110**, 120-131 (1997).
80. Ehleringer, J. R.; Field, C. B.; Lin, Z.-F. & Kuo, C.-Y. Leaf carbon isotope and mineral composition in subtropical plants along an irradiance cline. *Oecologia*, **70**, 520-526 (1986).
- 630 81. Mitchell, L. E.; Brook, E. J.; Sowers, T.; McConnell, J. R. & Taylor, K. Multidecadal variability of atmospheric methane, 1000-1800 C.E.. *J. Geophys. Res.*, **116**, (2011).
82. Mischler, J. A.; Sowers, T. A.; Alley, R. B.; Battle, M.; McConnell, J. R.; Mitchell, L.; Popp, T.; Sofen, E. & Spencer, M. K. Carbon and hydrogen isotopic composition of methane over the last 1000 years. *Global Biogeochem. Cycles*, **23**, (2009).
- 635 83. Chappellaz, J.; Barnola, J. M.; Raynaud, D.; Korotkevich, Y. S. & Lorius, C. Ice-core record of atmospheric methane over the past 160,000 years. *Nature*, **345**, 127-131 (1990).

Figure legends

640 Figure S1 | Magnitude of the Kr effect $\Delta\delta^{13}\text{C}_{\text{Kr}}$ derived from two distinct methods for the AWI and PSU instrument

a) the new $\delta^{13}\text{CH}_4$ time series of Vostok (light blue) and EDML (red), the Holocene GISP II record¹¹ (dark blue, on its original time scale), and the published EDML record² over termination I, that was processed anew according to the procedures in this publication (purple). The corrected time series
645 are illustrated with thicker lines and large circle markers. The original records before the correction are shown as thin lines with small white markers.

b) The range of $\Delta\delta^{13}\text{C}_{\text{Kr}}$ values applied as individual correction to the respective datasets to account for the Kr-bias on $\delta^{13}\text{CH}_4$. The color coding is the same as in a). Note that $\Delta\delta^{13}\text{C}_{\text{Kr}}$ of both, Vostok and GISP II data measured at the PSU, were inferred indirectly from CH_4 mixing ratios, while for
650 the two EDML records the correction is based on the Kr-induced anomaly derived from the ion-current ratios (see section 1.3 for a detailed description of both approaches).

Figure S2 | Linear scaling of the size of interference on carbon isotope measurements caused by Kr ($\Delta\delta^{13}\text{C}_{\text{Kr}}$) relative to variations in CH_4 mixing ratios for the PSU instrument

655 Atmospheric krypton mixing ratios are considered constant over time¹³. The size of the interference (Kr effect or $\Delta\delta^{13}\text{C}_{\text{Kr}}$) thus scales with CH_4 concentrations. Measurements of three ambient air samples were used to infer a linear relationship between $\Delta\delta^{13}\text{C}_{\text{Kr}}$ and the inverted CH_4 mixing ratio for the PSU instrument, that is used to account for the Kr effect of ice core (Vostok, WDC05) and laboratory inter-calibration measurements (see section 1.3 for further details). Results for the IPY
660 cylinder with a mixing ratio representative for glacial conditions (“glacial”, 365 ppb) is shown as a light blue diamond, the one with “preindustrial” values (906 ppb) in orange, and the one representative for modern concentrations (“present-day”, 1852 ppb) in dark red, all illustrated with its corresponding 1σ error range. The linear relationship in red allowed a first order estimate of $\Delta\delta^{13}\text{C}_{\text{Kr}}$ for ice core samples measured at the PSU lab, based on interpolated CH_4 mixing ratios of
665 the respective samples.

Figure S3 | Model results to quantify fractionation processes in the firn column due to atmospheric CH_4 concentration changes

a) Artificial atmospheric methane pulse at the model firn “surface” (grey line), and its
670 corresponding concentration after the “bubble close-off” at the bottom of the firn column at three different accumulation rate and temperature regimens (“maximum” temperature: purple line;

“minimum” temperature: red line and “best guess” temperature: light blue line). b) Shifts of the carbon isotope signature of methane caused by the gravitational and diffusional fractionation in the firn column from the constant value at the “surface” (gray dashed line) to the signals enclosed in the model “bubbles” (colored lines) at the firn bottom, according to their respective scenario (color coding similar to a))

Figure S4 | Representation of major Dansgaard-Oeschger methane rises during the last glacial period, and the respective imprint on its carbon isotope signature

680 a) Six strong methane rises (color coding in the figure legends) coeval to major Dansgaard/Oeschger (DO) events (left and middle figure column) and the two ultimate terminations (right column) in a 6,000 year time window aligned and centered around the major methane rise (illustrated by the vertical gray line). All CH₄ data from the EDML ice core³⁰ b) Corresponding time windows of the respective $\delta^{13}\text{CH}_4$ data sections from Vostok and EDML (this study, color coding and alignment according to a)). The shaded bar represents the time window, in which data points might be biased by diffusional fractionation beyond our measurement uncertainty.

Tables

Supplementary Table 1 | Comparison of $\delta^{13}\text{CH}_4$ results for the measurements of air samples performed at the AWI and PSU laboratories, that were part of the „2007 - IPY International Ice Core Gas Intercalibration Exercise“.

Ambient air was diluted to resemble atmospheric methane mixing ratios typical for present day (1852 ppb), pre-industrial (906 ppb) and glacial (365 ppb) conditions. $\delta^{13}\text{CH}_4$ values are reported with respect to VPDB. The first two columns report original measurements, the following two columns the respective values after the correction for Kr interference. Deviations in the carbon isotopic signature caused by the ionized Kr ($\Delta\delta^{13}\text{C}_{\text{Kr}}$) and its dependency on CH_4 levels are summarized in the final column. The results are further used to infer the absolute standardization offset between both laboratories.

| Sample ID epoch | $\delta^{13}\text{CH}_4$ | 1σ | $\delta^{13}\text{CH}_4$ | 1σ | $\Delta\delta^{13}\text{C}_{\text{Kr}}$ |
|---------------------------------------|--------------------------|-----------|--------------------------|-----------|---|
| | (‰) | (‰) | (‰) | (‰) | |
| | Original | | Corrected for Kr | | |
| AWI analyses (5/2010) | | | | | |
| CA03560 present day | -47,14 | 0,05 | -47,33 | 0,06 | 0,19 |
| CC71560 preindustrial | -47,07 | 0,09 | -47,40 | 0,12 | 0,33 |
| CA01179 glacial | -46,25 | 0,11 | -46,97 | 0,13 | 0,72 |
| PSU analyses (7/2007) | | | | | |
| CA03560 present day | -47,08 | 0,16 | -47,20 | 0,16 | 0,12 |
| CC71560 preindustrial | -47,15 | 0,10 | -47,41 | 0,10 | 0,26 |
| CA01179 glacial | -46,86 | 0,06 | -47,52 | 0,06 | 0,66 |
| Difference (AWI - PSU) | | | | | |
| CA03560 present day | -0.06 | | -0,13 | | |
| CC71560 preindustrial | 0.08 | | 0,01 | | |
| CA01179 glacial | 0.61 | | 0,55 | | |
| Avg. lab offset | 0,21 | | 0,14 | | |
| St.dev. (1σ) | 0,35 | | 0,36 | | |

700 **Supplementary Table 2 | $\delta^{13}\text{CH}_4$ values of WDC05 A ice core material measured with the AWI
and PSU instruments to further test the alignment of both systems.**

No adjustments have been applied to correct for gravitational settling. Values denoted as “original” are inferred according to the standard routines in the respective laboratories, before the correction for Krypton interference. Acquisitions with the AWI instrument were treated similar to EDML ice and IPY air samples correcting the chromatograms for the Kr interference, PSU measurements using the CH_4 dependent $\Delta\delta^{13}\text{C}_{\text{Kr}}$ to account for Kr. WDC05A [CH_4] values and approximate age of the samples (black diamond) were interpolated from data of Mitchell et al.,2011⁸¹. Note, that the two PSU measurements (marked by asterisks) are not from the same depth as the AWI sample, but $\delta^{13}\text{CH}_4$ variability (1σ) is less than 0.3 ‰ over the depth interval 161.5 m (1593 AD) to 173.4 m (1540 AD) and thus in the the order of our analytical uncertainty⁸².

| Sample ID | Lab | Depth (m) | Age* (AD) | $\delta^{13}\text{CH}_4$ | 1σ | $\delta^{13}\text{CH}_4$ | 1σ | $\Delta\delta^{13}\text{C}_{\text{Kr}}$ | n |
|-----------|-----|-----------|-----------|--------------------------|------------------|--------------------------|-----------|---|---|
| | | | | (‰) | (‰) | (‰) | (‰) | | |
| | | | | Original | Corrected for Kr | | | | |
| WDC05A* | PSU | 164.96 | 1571 | -47,94 | - | -48,28 | - | 0,34 | - |
| WDC05A | AWI | 166.78 | 1564 | -47,53 | 0.03 | -47,81 | 0,04 | 0,28 | 2 |
| WDC05A* | PSU | 169.80 | 1551 | -47,53 | - | -47,87 | - | 0,34 | - |

715 **Supplementary Table 3 | Manual CH₄ tie-points used for the adjustment of the misaligned Vostok section in between 129-84 kyr BP²⁸.**

The synchronization was performed with EDC²⁶ and Vostok⁸³ atmospheric methane records. The EDC3 ages of the five listed Vostok sample depths were adjusted according to the corresponding EDC tie points. All Vostok records presented in this study are dated according to this adjustments.

| tie-point | EDC depth (m) | EDC3 age (years BP) | EDC CH₄ (ppb) | Vostok depth (m) | Vostok CH₄ (ppb) |
|------------------|----------------------|----------------------------|---------------------------------|-------------------------|------------------------------------|
| 1 | 1241.67 | 83627 | 500.7 | 1266.83 | 500.1 |
| 2 | 1367.89 | 95866 | 470.2 | 1440.34 | 470.0 |
| 3 | 1473.40 | 106781 | 510.1 | 1536.00 | 510.8 |
| 4 | 1543.59 | 115081 | 480.2 | 1635.97 | 480.4 |
| 5 | 1723.46 | 128871 | 559.9 | 1881.99 | 560.1 |

Supplementary Table 4 | Methane synchronization tie-points used for dating the Byrd ice core records shown in this work. The age conversion to the “Unified” age scale²³ is based on EDML³⁰ and Byrd²⁹ atmospheric methane records.

| tie-point | EDML depth (m) | “Unified” age (years BP) | EDML CH₄ (ppb) | Byrd depth (m) | Byrd CH₄ (ppb) |
|------------------|-----------------------|---------------------------------|----------------------------------|-----------------------|----------------------------------|
| 1 | 717.02 | 11599 | 609.35 | 1071.76 | 574.28 |
| 2 | 829.64 | 14543 | 529.66 | 1195.84 | 543.30 |
| 3 | 1070.95 | 23231 | 383.60 | 1446.29 | 361.95 |
| 4 | 1154.20 | 27748 | 392.50 | 1498.37 | 392.42 |
| 5 | 1173.61 | 28810 | 419.31 | 1526.10 | 417.05 |
| 6 | 1233.17 | 32339 | 435.59 | 1595.76 | 443.86 |
| 7 | 1260.48 | 33728 | 456.60 | 1617.35 | 417.67 |
| 8 | 1286.47 | 35417 | 467.63 | 1654.37 | 449.47 |
| 9 | 1337.80 | 38258 | 488.11 | 1716.45 | 490.03 |
| 10 | 1365.07 | 39433 | 423.15 | 1744.35 | 415.49 |
| 11 | 1403.97 | 41378 | 443.35 | 1780.49 | 422.27 |
| 12 | 1436.97 | 43074 | 452.35 | 1806.94 | 441.63 |
| 13 | 1489.88 | 46719 | 469.20 | 1863.57 | 461.97 |
| 14 | 1601.65 | 53264 | 491.10 | 1960.44 | 488.11 |
| 15 | 1627.36 | 54732 | 493.91 | 1973.59 | 491.04 |
| 16 | 1666.48 | 57333 | 532.10 | 2000.30 | 523.93 |
| 17 | 1680.64 | 58176 | 538.28 | 2011.48 | 533.62 |
| 18 | 1688.09 | 58586 | 497.84 | 2017.44 | 463.90 |
| 19 | 1760.37 | 63448 | 468.08 | 2062.90 | 476.49 |
| 20 | 1860.22 | 71706 | 470.32 | 2082.65 | 460.38 |
| 21 | 1914.24 | 75872 | 460.21 | 2100.52 | 455.18 |
| 22 | 1949.26 | 78706 | 480.43 | 2111.69 | 494.55 |
| 23 | 2023.03 | 85207 | 550.63 | 2133.58 | 546.72 |
| 24 | 2065.88 | 89241 | 493.35 | 2139.75 | 489.08 |

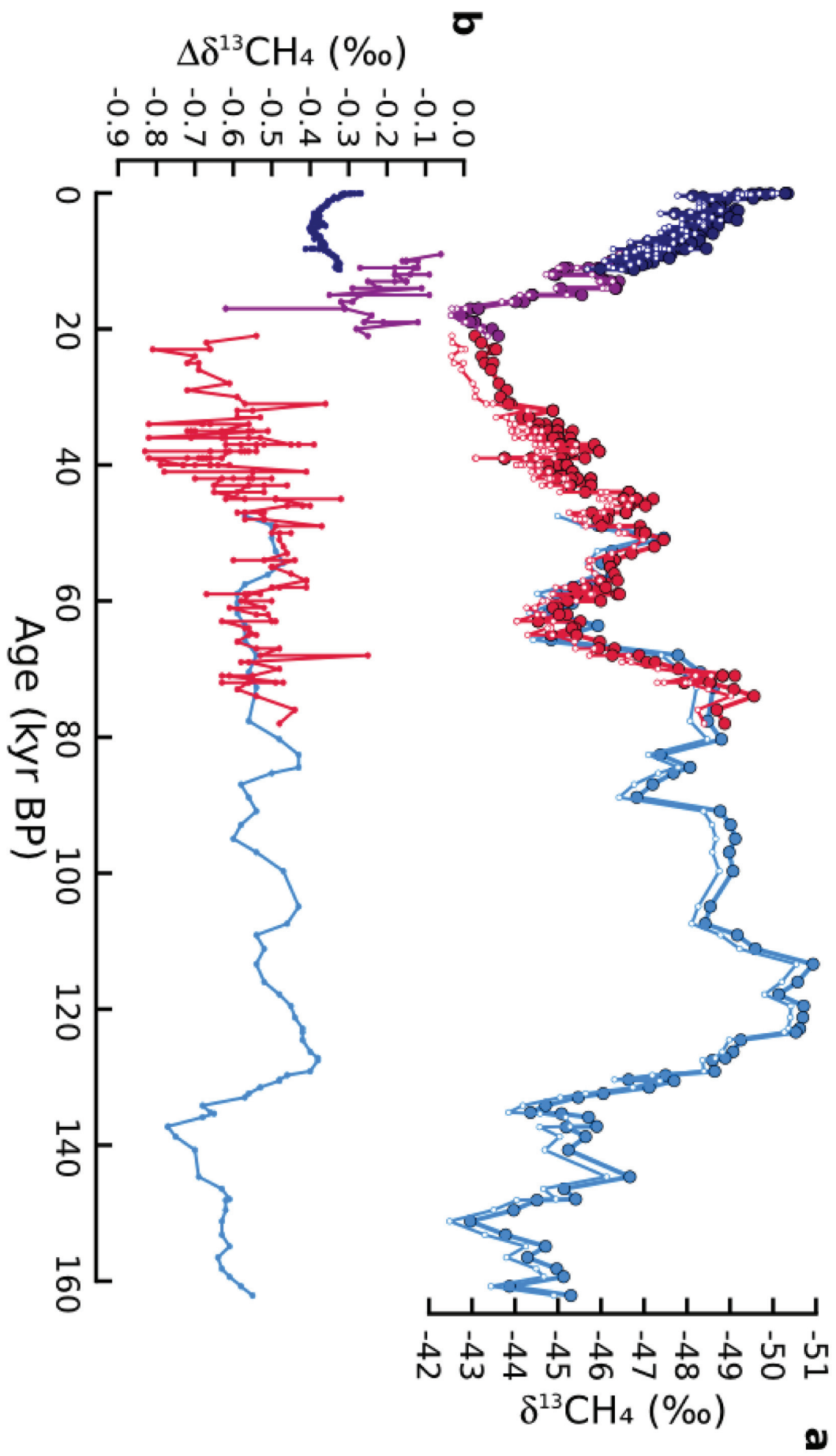


Figure S2

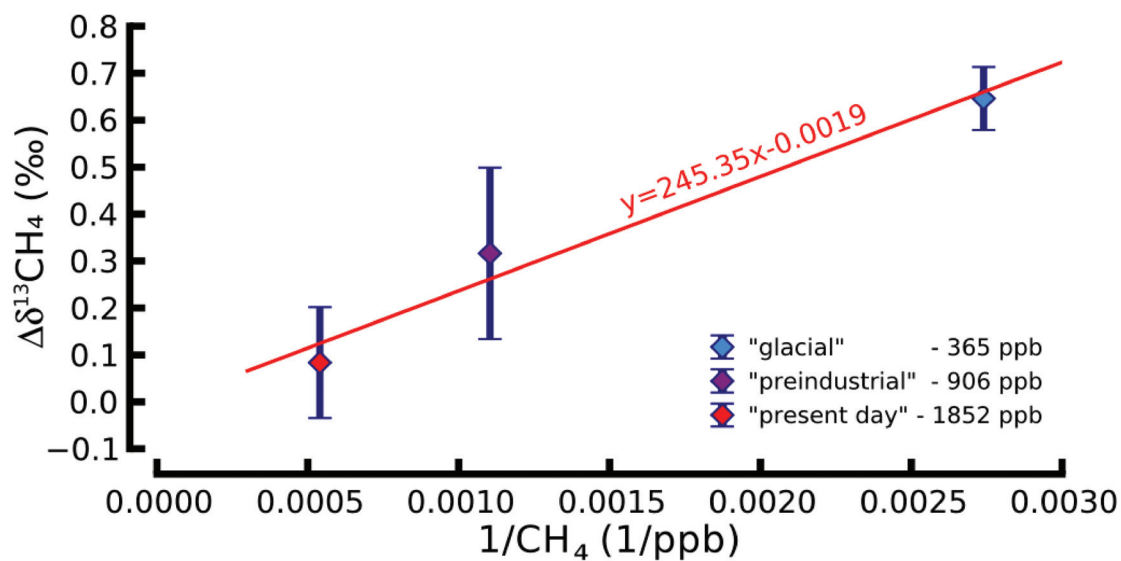


Figure S3

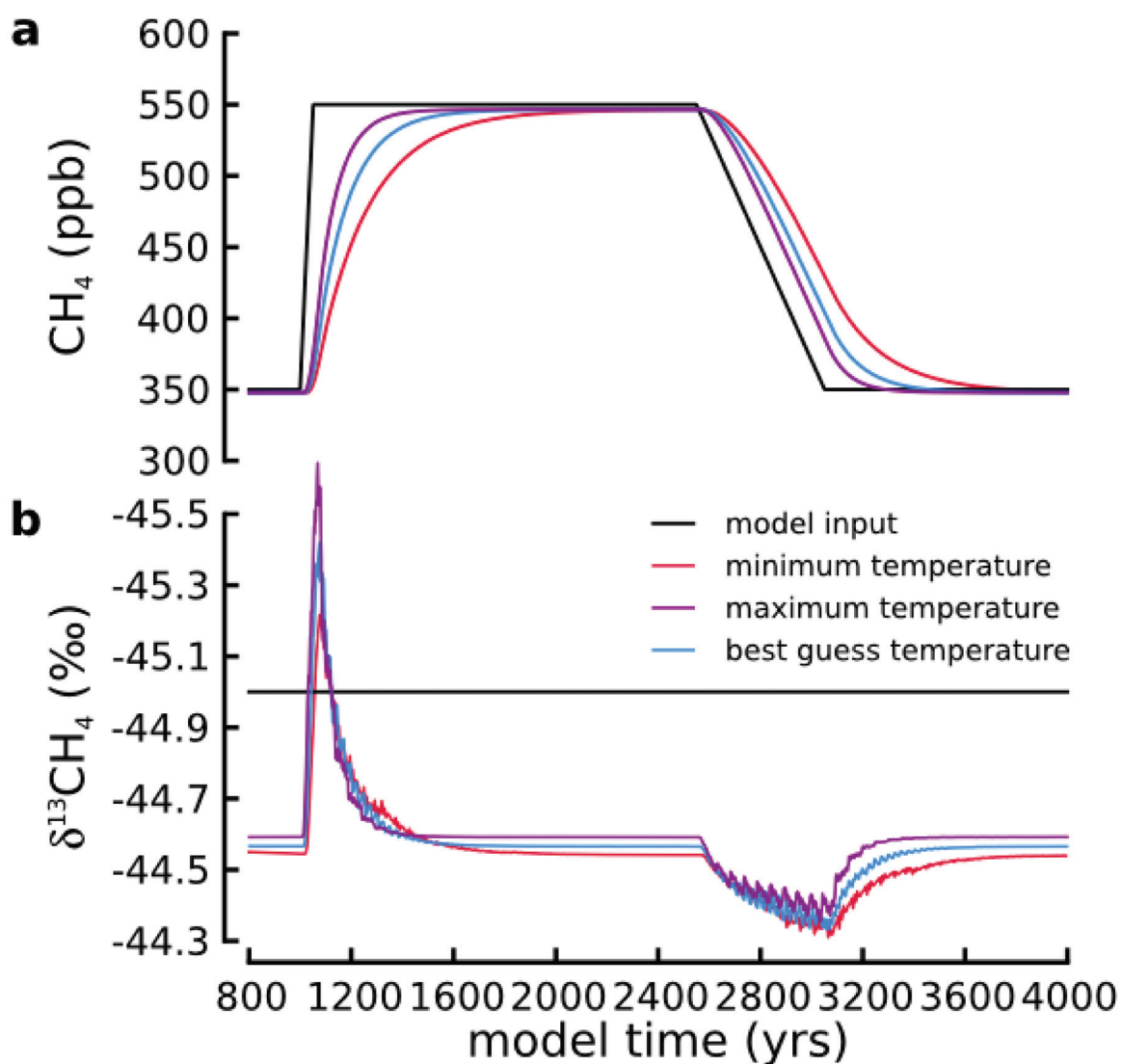
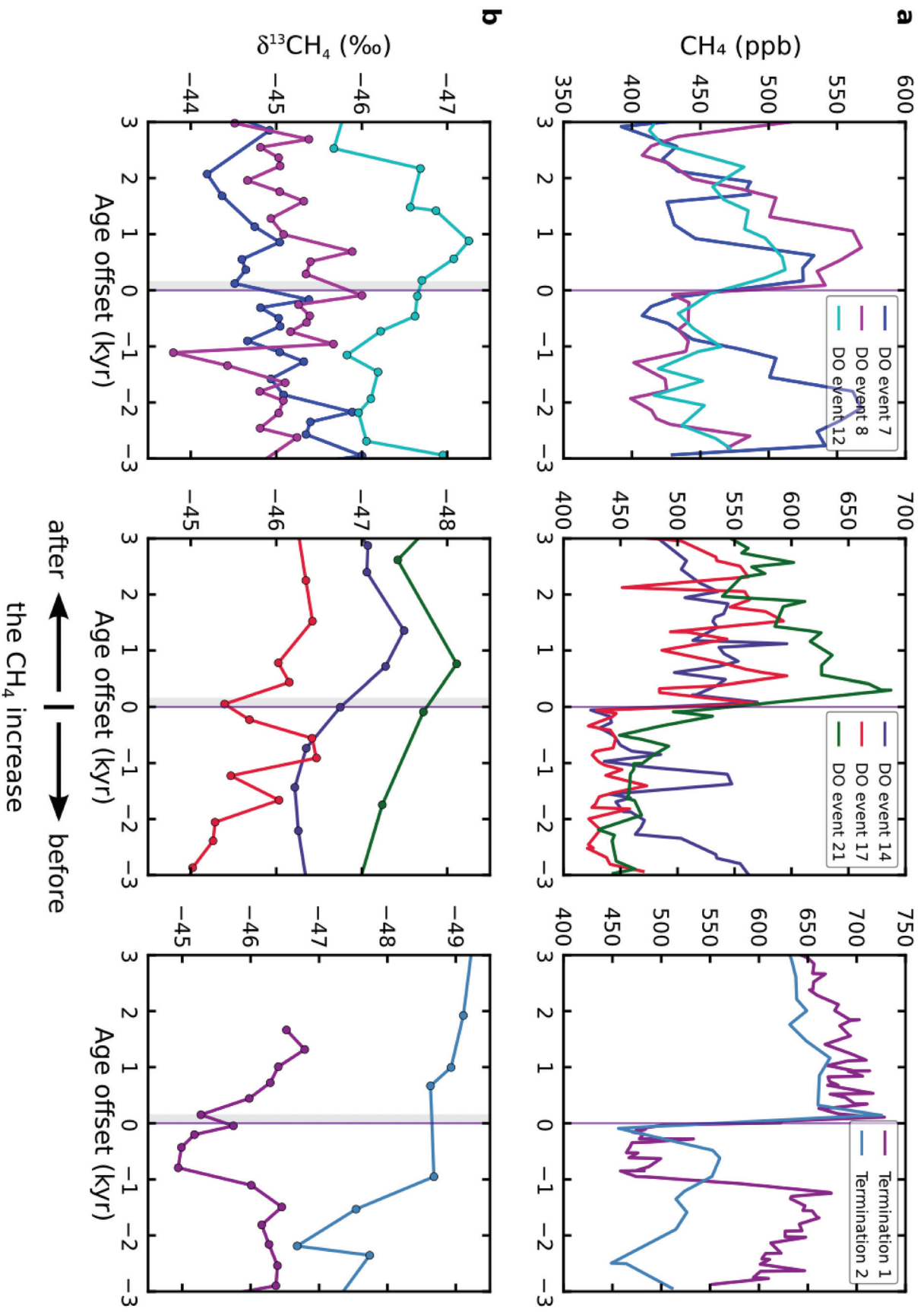


Figure S4



C. Carbon isotope data

EDML $\delta^{13}\text{CH}_4$ record for termination I

Note, this data was originally published by *Fischer et al.* (2008) and is only placed here for providing the krypton correction values ($\Delta\delta^{13}\text{C}_{\text{Kr}}$).

Columns:

- 1: EDML depth (m)
- 2: Gas Age, 'Unified' chronology, years before 1950 AD, see *Lemieux-Dudon et al.* (2010)
- 3: $\delta^{13}\text{CH}_4$ (‰) values corrected for machine specific drifts and referenced to VPDB
- 4: $\Delta\delta^{13}\text{C}_{\text{Kr}}$ (‰) shift caused by the MS interference with atmospheric krypton (see section 4.5)
- 5: $\delta^{13}\text{CH}_4$ (‰) values corrected for Kr interference
- 6: $\delta^{13}\text{CH}_4$ (‰) values (column 5) corrected for a constant glacial offset of 0.41‰ due to gravitational settling in the firn layer
- 7: replicate standard deviation (1σ , ‰)

| Depth (m) | Age (yr) | $\delta^{13}\text{C}_{\text{mc}}$ (‰) | Δ_{Kr} (‰) | $\delta^{13}\text{C}_{\text{Kr}}$ (‰) | $\delta^{13}\text{C}_{\text{gc}}$ (‰) | 1σ (‰) |
|-----------|----------|---------------------------------------|--------------------------|---------------------------------------|---------------------------------------|---------------|
| 647.00 | 9937 | -46.13 | 0.06 | -46.07 | -46.48 | |
| 660.00 | 10284 | -46.50 | 0.16 | -46.34 | -46.75 | |
| 672.00 | 10592 | -46.11 | 0.15 | -45.96 | -46.37 | |
| 684.00 | 10875 | -46.02 | 0.15 | -45.87 | -46.28 | 0.03 |
| 684.13 | 10878 | -45.93 | 0.12 | -45.81 | -46.22 | 0.03 |
| 696.00 | 11158 | -45.65 | 0.12 | -45.53 | -45.94 | |
| 709.00 | 11448 | -45.00 | 0.18 | -44.82 | -45.23 | |
| 720.13 | 11645 | -45.57 | 0.27 | -45.30 | -45.71 | |
| 731.00 | 11803 | -44.86 | 0.13 | -44.73 | -45.14 | |
| 743.00 | 12029 | -44.78 | 0.14 | -44.64 | -45.05 | 0.10 |
| 743.13 | 12032 | -44.53 | 0.09 | -44.44 | -44.85 | 0.10 |
| 757.00 | 12393 | -44.67 | 0.18 | -44.49 | -44.90 | |

continuation on next page

| Depth (m) | Age (yr) | $\delta^{13}\text{C}_{\text{mc}}(\text{‰})$ | $\Delta_{\text{Kr}}(\text{‰})$ | $\delta^{13}\text{C}_{\text{Kr}}(\text{‰})$ | $\delta^{13}\text{C}_{\text{gc}}(\text{‰})$ | 1σ (‰) |
|-----------|----------|---|--------------------------------|---|---|---------------|
| 768.00 | 12705 | -45.74 | 0.18 | -45.56 | -45.97 | |
| 781.00 | 13093 | -46.16 | 0.15 | -46.01 | -46.42 | |
| 792.00 | 13410 | -45.92 | 0.15 | -45.77 | -46.18 | 0.06 |
| 792.13 | 13413 | -45.83 | 0.18 | -45.65 | -46.06 | 0.06 |
| 804.00 | 13759 | -46.07 | 0.25 | -45.82 | -46.23 | |
| 816.00 | 14139 | -46.16 | 0.22 | -45.94 | -46.35 | |
| 828.13 | 14497 | -46.21 | 0.29 | -45.92 | -46.33 | |
| 839.00 | 14786 | -44.76 | 0.11 | -44.65 | -45.06 | |
| 852.13 | 15121 | -45.49 | 0.35 | -45.14 | -45.55 | |
| 864.00 | 15430 | -44.09 | 0.09 | -44.00 | -44.41 | |
| 877.00 | 15784 | -44.24 | 0.27 | -43.97 | -44.38 | |
| 888.13 | 16093 | -44.08 | 0.29 | -43.79 | -44.20 | |
| 913.13 | 16826 | -43.92 | 0.32 | -43.60 | -44.01 | |
| 924.13 | 17228 | -42.85 | 0.31 | -42.54 | -42.95 | |
| 934.00 | 17633 | -43.31 | 0.62 | -42.69 | -43.10 | 0.05 |
| 934.13 | 17638 | -43.10 | 0.31 | -42.79 | -43.20 | 0.05 |
| 961.00 | 18770 | -42.58 | 0.24 | -42.34 | -42.75 | |
| 973.00 | 19372 | -42.88 | 0.26 | -42.62 | -43.03 | 0.03 |
| 973.13 | 19378 | -42.90 | 0.21 | -42.69 | -43.10 | 0.03 |
| 984.00 | 19900 | -42.68 | 0.12 | -42.56 | -42.97 | |
| 996.00 | 20454 | -43.34 | 0.28 | -43.06 | -43.47 | |
| 1009.00 | 21010 | -43.45 | 0.25 | -43.20 | -43.61 | |

EDML $\delta^{13}\text{CH}_4$ record for the glacial

Columns:

- 1: EDML depth (m)
- 2: Gas Age, 'Unified' chronology, years before 1950 AD, see *Lemieux-Dudon et al. (2010)*
- 3: $\delta^{13}\text{CH}_4$ (‰) values corrected for machine specific drifts and referenced to VPDB
- 4: $\Delta\delta^{13}\text{C}_{\text{Kr}}$ (‰) shift caused by the MS interference with atmospheric krypton (see section 4.5)
- 5: $\delta^{13}\text{CH}_4$ (‰) values corrected for Kr interference
- 6: $\delta^{13}\text{CH}_4$ (‰) values (column 5) corrected for a constant glacial offset of 0.41‰ due to gravitational settling in the firn layer
- 7: replicate standard deviation (1σ , ‰)

| Depth (m) | Age (yr) | $\delta^{13}\text{C}_{\text{mc}}(\text{‰})$ | $\Delta_{\text{Kr}}(\text{‰})$ | $\delta^{13}\text{C}_{\text{Kr}}(\text{‰})$ | $\delta^{13}\text{C}_{\text{gc}}(\text{‰})$ | 1σ (‰) |
|-----------|----------|---|--------------------------------|---|---|---------------|
| 1019.00 | 21419 | -43.20 | 0.54 | -42.66 | -43.07 | |
| 1044.00 | 22393 | -43.47 | 0.67 | -42.80 | -43.21 | |
| 1068.00 | 23131 | -43.75 | 0.66 | -43.09 | -43.50 | |
| 1080.00 | 23772 | -43.96 | 0.81 | -43.15 | -43.56 | |
| 1092.00 | 24433 | -43.52 | 0.7 | -42.82 | -43.23 | |
| 1104.00 | 25119 | -43.61 | 0.72 | -42.89 | -43.30 | |
| 1116.00 | 25766 | -43.77 | 0.69 | -43.08 | -43.49 | |
| 1140.00 | 26991 | -43.72 | 0.69 | -43.03 | -43.44 | |
| 1163.00 | 28264 | -43.83 | 0.61 | -43.22 | -43.63 | |
| 1188.00 | 29595 | -44.12 | 0.72 | -43.40 | -43.81 | |
| 1200.00 | 30265 | -43.84 | 0.59 | -43.25 | -43.66 | |
| 1213.00 | 31147 | -44.06 | 0.57 | -43.49 | -43.90 | |
| 1224.00 | 31897 | -43.80 | 0.36 | -43.44 | -43.85 | |
| 1236.00 | 32545 | -45.05 | 0.55 | -44.50 | -44.91 | 0.03 |
| 1236.13 | 32554 | -45.03 | 0.59 | -44.44 | -44.85 | 0.03 |
| 1248.00 | 33330 | -44.33 | 0.59 | -43.74 | -44.15 | |
| 1260.00 | 33718 | -44.45 | 0.53 | -43.92 | -44.33 | |
| 1268.13 | 34268 | -45.12 | 0.82 | -44.30 | -44.71 | |
| 1272.00 | 34540 | -44.93 | 0.68 | -44.25 | -44.66 | 0.34 |
| 1272.13 | 34548 | -45.58 | 0.66 | -44.92 | -45.33 | 0.34 |
| 1277.13 | 34851 | -44.71 | 0.56 | -44.15 | -44.56 | |
| 1280.13 | 35035 | -44.82 | 0.63 | -44.19 | -44.60 | |
| 1284.00 | 35279 | -44.47 | 0.55 | -43.92 | -44.33 | 0.14 |
| 1284.13 | 35286 | -44.76 | 0.56 | -44.20 | -44.61 | 0.14 |
| 1289.13 | 35569 | -45.65 | 0.72 | -44.93 | -45.34 | |
| 1292.13 | 35712 | -45.08 | 0.71 | -44.37 | -44.78 | |
| 1296.00 | 35895 | -45.37 | 0.7 | -44.67 | -45.08 | 0.10 |
| 1296.13 | 35901 | -44.99 | 0.51 | -44.48 | -44.89 | 0.10 |
| 1299.13 | 36045 | -45.42 | 0.82 | -44.60 | -45.01 | |
| 1304.13 | 36304 | -44.84 | 0.63 | -44.21 | -44.62 | |
| 1308.00 | 36501 | -45.09 | 0.56 | -44.53 | -44.94 | 0.06 |
| 1308.13 | 36508 | -45.27 | 0.62 | -44.65 | -45.06 | 0.06 |
| 1311.13 | 36674 | -45.58 | 0.71 | -44.87 | -45.28 | |

continuation on next page

| Depth (m) | Age (yr) | $\delta^{13}\text{C}_{\text{mc}}(\text{‰})$ | $\Delta_{\text{Kr}}(\text{‰})$ | $\delta^{13}\text{C}_{\text{Kr}}(\text{‰})$ | $\delta^{13}\text{C}_{\text{gc}}(\text{‰})$ | 1σ (‰) |
|-----------|----------|---|--------------------------------|---|---|---------------|
| 1316.13 | 36982 | -45.02 | 0.53 | -44.49 | -44.90 | |
| 1320.00 | 37262 | -44.86 | 0.45 | -44.41 | -44.82 | 0.22 |
| 1320.13 | 37271 | -45.44 | 0.58 | -44.86 | -45.27 | 0.22 |
| 1325.13 | 37573 | -45.87 | 0.43 | -45.44 | -45.85 | |
| 1328.00 | 37747 | -45.40 | 0.39 | -45.01 | -45.42 | 0.06 |
| 1328.13 | 37754 | -45.51 | 0.62 | -44.89 | -45.30 | 0.06 |
| 1332.00 | 37969 | -45.16 | 0.52 | -44.64 | -45.05 | 0.26 |
| 1332.13 | 37976 | -45.70 | 0.54 | -45.16 | -45.57 | 0.26 |
| 1340.00 | 38351 | -45.90 | 0.54 | -45.36 | -45.77 | 0.19 |
| 1340.13 | 38357 | -46.37 | 0.62 | -45.75 | -46.16 | 0.19 |
| 1344.00 | 38516 | -45.25 | 0.57 | -44.68 | -45.09 | 0.13 |
| 1344.13 | 38521 | -45.50 | 0.56 | -44.94 | -45.35 | 0.13 |
| 1349.13 | 38718 | -45.77 | 0.83 | -44.94 | -45.35 | |
| 1352.00 | 38834 | -45.66 | 0.58 | -45.08 | -45.49 | 0.17 |
| 1352.13 | 38839 | -45.39 | 0.66 | -44.73 | -45.14 | 0.17 |
| 1356.00 | 38998 | -45.17 | 0.61 | -44.56 | -44.97 | 0.16 |
| 1356.13 | 39003 | -45.51 | 0.63 | -44.88 | -45.29 | 0.16 |
| 1361.13 | 39220 | -45.94 | 0.72 | -45.22 | -45.63 | |
| 1364.00 | 39370 | -44.23 | 0.68 | -43.55 | -43.96 | 0.20 |
| 1364.13 | 39378 | -43.80 | 0.66 | -43.14 | -43.55 | 0.20 |
| 1368.00 | 39600 | -44.30 | 0.67 | -43.63 | -44.04 | 0.35 |
| 1368.13 | 39608 | -45.01 | 0.69 | -44.32 | -44.73 | 0.35 |
| 1373.00 | 39910 | -45.47 | 0.82 | -44.65 | -45.06 | |
| 1376.00 | 40063 | -45.39 | 0.73 | -44.66 | -45.07 | 0.30 |
| 1376.13 | 40068 | -44.78 | 0.73 | -44.05 | -44.46 | 0.30 |
| 1380.00 | 40226 | -44.78 | 0.66 | -44.12 | -44.53 | 0.52 |
| 1380.13 | 40231 | -45.85 | 0.7 | -45.15 | -45.56 | 0.52 |
| 1385.13 | 40452 | -45.37 | 0.79 | -44.58 | -44.99 | |
| 1392.00 | 40721 | -45.00 | 0.64 | -44.36 | -44.77 | |
| 1395.41 | 40882 | -45.74 | 0.61 | -45.13 | -45.54 | 0.33 |
| 1395.54 | 40888 | -45.12 | 0.66 | -44.46 | -44.87 | 0.33 |
| 1403.00 | 41318 | -44.79 | 0.41 | -44.38 | -44.79 | |
| 1407.30 | 41558 | -45.83 | 0.78 | -45.05 | -45.46 | 0.13 |
| 1407.43 | 41564 | -45.35 | 0.55 | -44.80 | -45.21 | 0.13 |
| 1416.00 | 42018 | -45.12 | 0.55 | -44.57 | -44.98 | |

continuation on next page

| Depth (m) | Age (yr) | $\delta^{13}\text{C}_{\text{mc}}(\text{‰})$ | $\Delta_{\text{Kr}}(\text{‰})$ | $\delta^{13}\text{C}_{\text{Kr}}(\text{‰})$ | $\delta^{13}\text{C}_{\text{gc}}(\text{‰})$ | 1σ (‰) |
|-----------|----------|---|--------------------------------|---|---|---------------|
| 1418.99 | 42165 | -45.73 | 0.7 | -45.03 | -45.44 | 0.02 |
| 1419.12 | 42172 | -45.66 | 0.6 | -45.06 | -45.47 | 0.02 |
| 1427.00 | 42552 | -45.40 | 0.5 | -44.90 | -45.31 | |
| 1431.30 | 42765 | -45.70 | 0.56 | -45.14 | -45.55 | 0.21 |
| 1431.43 | 42772 | -46.19 | 0.63 | -45.56 | -45.97 | 0.21 |
| 1440.00 | 43239 | -45.63 | 0.65 | -44.98 | -45.39 | 0.11 |
| 1440.13 | 43246 | -45.22 | 0.46 | -44.76 | -45.17 | 0.11 |
| 1444.30 | 43548 | -45.72 | 0.52 | -45.20 | -45.61 | 0.15 |
| 1444.43 | 43560 | -46.06 | 0.56 | -45.50 | -45.91 | 0.15 |
| 1451.00 | 44202 | -45.81 | 0.59 | -45.22 | -45.63 | |
| 1455.30 | 44555 | -46.59 | 0.52 | -46.07 | -46.48 | 0.17 |
| 1455.43 | 44564 | -47.05 | 0.65 | -46.40 | -46.81 | 0.17 |
| 1465.00 | 45246 | -46.61 | 0.57 | -46.04 | -46.45 | 0.08 |
| 1465.13 | 45254 | -46.69 | 0.49 | -46.20 | -46.61 | 0.08 |
| 1466.00 | 45309 | -47.14 | 0.62 | -46.52 | -46.93 | 0.10 |
| 1466.13 | 45316 | -46.64 | 0.32 | -46.32 | -46.73 | 0.10 |
| 1475.00 | 45850 | -47.29 | 0.49 | -46.80 | -47.21 | |
| 1480.43 | 46169 | -47.02 | 0.4 | -46.62 | -47.03 | |
| 1487.00 | 46554 | -46.67 | 0.42 | -46.25 | -46.66 | |
| 1492.00 | 46834 | -46.66 | 0.46 | -46.20 | -46.61 | |
| 1499.00 | 47190 | -47.03 | 0.57 | -46.46 | -46.87 | 0.28 |
| 1499.13 | 47196 | -46.41 | 0.52 | -45.89 | -46.30 | 0.28 |
| 1504.00 | 47462 | -46.36 | 0.59 | -45.77 | -46.18 | |
| 1511.00 | 47885 | -45.91 | 0.53 | -45.38 | -45.79 | |
| 1516.00 | 48187 | -46.26 | 0.52 | -45.74 | -46.15 | |
| 1524.13 | 48664 | -46.23 | 0.57 | -45.66 | -46.07 | |
| 1528.00 | 48913 | -46.03 | 0.52 | -45.51 | -45.92 | |
| 1536.00 | 49422 | -45.97 | 0.37 | -45.60 | -46.01 | |
| 1540.00 | 49671 | -46.99 | 0.49 | -46.50 | -46.91 | |
| 1548.00 | 50169 | -47.00 | 0.5 | -46.50 | -46.91 | |
| 1552.00 | 50405 | -47.07 | 0.45 | -46.62 | -47.03 | |
| 1560.00 | 50879 | -47.09 | 0.48 | -46.61 | -47.02 | |
| 1578.00 | 51921 | -47.53 | 0.48 | -47.05 | -47.46 | |
| 1589.00 | 52558 | -47.30 | 0.47 | -46.83 | -47.24 | |
| 1602.00 | 53283 | -46.76 | 0.46 | -46.30 | -46.71 | |

continuation on next page

| Depth (m) | Age (yr) | $\delta^{13}\text{C}_{\text{mc}}(\text{‰})$ | $\Delta_{\text{Kr}}(\text{‰})$ | $\delta^{13}\text{C}_{\text{Kr}}(\text{‰})$ | $\delta^{13}\text{C}_{\text{gc}}(\text{‰})$ | 1σ (‰) |
|-----------|----------|---|--------------------------------|---|---|---------------|
| 1615.00 | 54011 | -46.47 | 0.52 | -45.95 | -46.36 | 0.05 |
| 1615.13 | 54018 | -46.45 | 0.6 | -45.85 | -46.26 | 0.05 |
| 1627.00 | 54711 | -46.21 | 0.44 | -45.77 | -46.18 | |
| 1639.00 | 55482 | -46.32 | 0.5 | -45.82 | -46.23 | 0.01 |
| 1639.13 | 55490 | -46.30 | 0.5 | -45.80 | -46.21 | 0.01 |
| 1651.00 | 56325 | -46.35 | 0.45 | -45.90 | -46.31 | |
| 1662.00 | 57051 | -46.38 | 0.41 | -45.97 | -46.38 | |
| 1674.00 | 57795 | -45.98 | 0.41 | -45.57 | -45.98 | |
| 1680.00 | 58139 | -46.20 | 0.5 | -45.70 | -46.11 | |
| 1687.00 | 58526 | -45.35 | 0.41 | -44.94 | -45.35 | |
| 1692.00 | 58804 | -45.72 | 0.48 | -45.24 | -45.65 | |
| 1698.00 | 59135 | -46.54 | 0.57 | -45.97 | -46.38 | |
| 1704.00 | 59487 | -46.69 | 0.67 | -46.02 | -46.43 | |
| 1709.00 | 59800 | -45.33 | 0.53 | -44.80 | -45.21 | 0.21 |
| 1709.13 | 59807 | -45.79 | 0.56 | -45.23 | -45.64 | 0.21 |
| 1716.00 | 60239 | -46.15 | 0.57 | -45.58 | -45.99 | |
| 1722.00 | 60632 | -45.33 | 0.5 | -44.83 | -45.24 | |
| 1727.00 | 60964 | -45.39 | 0.58 | -44.81 | -45.22 | |
| 1734.00 | 61443 | -45.09 | 0.52 | -44.57 | -44.98 | |
| 1740.00 | 61867 | -45.08 | 0.61 | -44.47 | -44.88 | |
| 1747.00 | 62395 | -45.34 | 0.54 | -44.80 | -45.21 | |
| 1751.00 | 62700 | -45.12 | 0.51 | -44.61 | -45.02 | |
| 1758.00 | 63253 | -44.48 | 0.5 | -43.98 | -44.39 | 0.15 |
| 1758.13 | 63263 | -44.76 | 0.49 | -44.27 | -44.68 | 0.15 |
| 1765.00 | 63812 | -45.74 | 0.63 | -45.11 | -45.52 | |
| 1770.00 | 64212 | -45.55 | 0.56 | -44.99 | -45.40 | |
| 1775.00 | 64619 | -45.48 | 0.57 | -44.91 | -45.32 | |
| 1782.00 | 65202 | -44.96 | 0.54 | -44.42 | -44.83 | |
| 1788.00 | 65728 | -45.58 | 0.56 | -45.02 | -45.43 | |
| 1800.00 | 66715 | -46.15 | 0.59 | -45.56 | -45.97 | |
| 1806.00 | 67216 | -46.08 | 0.54 | -45.54 | -45.95 | |
| 1812.00 | 67745 | -46.38 | 0.48 | -45.90 | -46.31 | |
| 1819.00 | 68344 | -46.38 | 0.53 | -45.85 | -46.26 | |
| 1824.00 | 68761 | -46.73 | 0.25 | -46.48 | -46.89 | |
| 1830.00 | 69245 | -47.24 | 0.58 | -46.66 | -47.07 | |

continuation on next page

| Depth (m) | Age (yr) | $\delta^{13}\text{C}_{\text{mc}}(\text{‰})$ | $\Delta_{\text{Kr}}(\text{‰})$ | $\delta^{13}\text{C}_{\text{Kr}}(\text{‰})$ | $\delta^{13}\text{C}_{\text{gc}}(\text{‰})$ | 1σ (‰) |
|-----------|----------|---|--------------------------------|---|---|---------------|
| 1837.00 | 69853 | -47.41 | 0.56 | -46.85 | -47.26 | |
| 1842.00 | 70286 | -47.87 | 0.48 | -47.39 | -47.80 | |
| 1854.00 | 71259 | -49.25 | 0.55 | -48.70 | -49.11 | |
| 1860.00 | 71690 | -49.07 | 0.61 | -48.46 | -48.87 | 0.05 |
| 1860.13 | 71699 | -49.00 | 0.63 | -48.37 | -48.78 | 0.05 |
| 1866.00 | 72110 | -47.54 | 0.47 | -47.07 | -47.48 | 0.45 |
| 1866.13 | 72118 | -48.61 | 0.63 | -47.98 | -48.39 | 0.45 |
| 1872.00 | 72519 | -48.63 | 0.49 | -48.14 | -48.55 | |
| 1878.00 | 72973 | -48.68 | 0.56 | -48.12 | -48.53 | |
| 1890.00 | 73989 | -49.27 | 0.59 | -48.68 | -49.09 | |
| 1902.00 | 74968 | -49.69 | 0.54 | -49.15 | -49.56 | |
| 1926.13 | 76769 | -48.72 | 0.44 | -48.28 | -48.69 | |
| 1950.00 | 78770 | -48.95 | 0.48 | -48.47 | -48.88 | |

Vostok $\delta^{13}\text{CH}_4$ record

Note, this dataset was measured at the Pennsylvania State University (PSU).

Columns:

- 1: Vostok depth (m)
- 2: Gas Age, 'Unified' gas age, years before 1950 AD, corrected for inconsistency in EDC3 dating (see section 5.2.4)
- 3: $\Delta\delta^{13}\text{C}_{\text{Kr}}$ (‰) deviations due to mass spectrometer interference with atmospheric krypton; see section 4.5), interpolated from Vostok CH_4 data (*Chappellaz et al.*, 1990)
- 4: $\delta^{13}\text{CH}_4$ (‰) values corrected for gravitational settling in the firn column
- 5: $\delta^{13}\text{CH}_4$ (‰) values (column 4) corrected for interpolated Kr deviation (column 3)
- 6: $\delta^{13}\text{CH}_4$ (‰) values (column 5) corrected for an inter-laboratory offset AWI-PSU of 0.14‰

| Depth (m) | Age (yr) | $\Delta_{\text{Kr}}(\text{‰})$ | $\delta^{13}\text{C}_{\text{gr}}(\text{‰})$ | $\delta^{13}\text{C}_{\text{Kr}}(\text{‰})$ | $\delta^{13}\text{C}_{\text{ac}}(\text{‰})$ |
|-----------|----------|--------------------------------|---|---|---|
| 800.0 | 48876.2 | 0.50 | -45.35 | -45.85 | -45.99 |
| 825.0 | 50718.6 | 0.50 | -46.88 | -47.38 | -47.52 |
| 851.0 | 52686.1 | 0.49 | -45.68 | -46.17 | -46.31 |

continuation on next page

| Depth (m) | Age (yr) | $\Delta_{\text{Kr}}(\text{‰})$ | $\delta^{13}\text{C}_{\text{gr}}(\text{‰})$ | $\delta^{13}\text{C}_{\text{Kr}}(\text{‰})$ | $\delta^{13}\text{C}_{\text{ac}}(\text{‰})$ |
|-----------|----------|--------------------------------|---|---|---|
| 877.0 | 54414.0 | 0.47 | -45.46 | -45.93 | -46.07 |
| 901.0 | 56118.2 | 0.51 | -45.67 | -46.18 | -46.32 |
| 923.0 | 57565.9 | 0.57 | -45.07 | -45.64 | -45.78 |
| 944.0 | 58928.6 | 0.59 | -44.29 | -44.88 | -45.02 |
| 965.0 | 60319.5 | 0.59 | -44.67 | -45.26 | -45.40 |
| 988.0 | 61801.5 | 0.59 | -44.11 | -44.70 | -44.84 |
| 1009.0 | 63629.8 | 0.57 | -45.28 | -45.85 | -45.99 |
| 1033.0 | 65728.2 | 0.57 | -44.19 | -44.76 | -44.90 |
| 1057.0 | 67978.6 | 0.54 | -47.17 | -47.71 | -47.85 |
| 1081.0 | 70483.8 | 0.56 | -47.67 | -48.23 | -48.37 |
| 1105.0 | 72721.6 | 0.54 | -47.99 | -48.53 | -48.67 |
| 1160.0 | 77618.5 | 0.56 | -47.84 | -48.40 | -48.54 |
| 1190.0 | 80323.9 | 0.48 | -48.24 | -48.72 | -48.86 |
| 1219.0 | 82588.3 | 0.43 | -46.87 | -47.30 | -47.44 |
| 1246.0 | 84440.1 | 0.43 | -47.56 | -47.99 | -48.13 |
| 1271.0 | 85293.8 | 0.50 | -47.10 | -47.60 | -47.74 |
| 1297.0 | 86949.3 | 0.58 | -46.54 | -47.12 | -47.26 |
| 1324.0 | 88850.3 | 0.56 | -46.19 | -46.75 | -46.89 |
| 1350.0 | 90882.3 | 0.54 | -48.15 | -48.69 | -48.83 |
| 1377.0 | 92886.8 | 0.58 | -48.35 | -48.93 | -49.07 |
| 1404.0 | 94931.9 | 0.60 | -48.44 | -49.04 | -49.18 |
| 1433.0 | 96925.5 | 0.54 | -48.36 | -48.90 | -49.04 |
| 1462.0 | 99697.0 | 0.47 | -48.52 | -48.99 | -49.13 |
| 1512.0 | 104908.4 | 0.43 | -48.03 | -48.46 | -48.60 |
| 1535.0 | 107432.9 | 0.46 | -47.88 | -48.34 | -48.48 |
| 1558.0 | 109107.0 | 0.54 | -48.55 | -49.09 | -49.23 |
| 1581.0 | 111132.7 | 0.52 | -48.99 | -49.51 | -49.65 |
| 1606.0 | 113387.9 | 0.54 | -50.31 | -50.85 | -50.99 |
| 1634.0 | 115996.2 | 0.52 | -49.97 | -50.49 | -50.63 |
| 1663.2 | 117841.0 | 0.48 | -49.57 | -50.05 | -50.19 |
| 1693.0 | 119541.8 | 0.45 | -50.18 | -50.63 | -50.77 |
| 1725.0 | 121223.5 | 0.44 | -50.17 | -50.61 | -50.75 |
| 1757.0 | 122852.4 | 0.42 | -50.12 | -50.54 | -50.68 |
| 1767.4 | 123391.4 | 0.42 | -50.03 | -50.45 | -50.59 |
| 1791.0 | 124527.3 | 0.42 | -48.75 | -49.17 | -49.31 |

continuation on next page

| Depth (m) | Age (yr) | $\Delta_{\text{Kr}}(\text{‰})$ | $\delta^{13}\text{C}_{\text{gr}}(\text{‰})$ | $\delta^{13}\text{C}_{\text{Kr}}(\text{‰})$ | $\delta^{13}\text{C}_{\text{ac}}(\text{‰})$ |
|-----------|----------|--------------------------------|---|---|---|
| 1826.5 | 126264.8 | 0.40 | -48.59 | -48.99 | -49.13 |
| 1843.2 | 127191.4 | 0.38 | -48.43 | -48.81 | -48.95 |
| 1849.1 | 127520.2 | 0.38 | -48.13 | -48.51 | -48.65 |
| 1879.4 | 129139.8 | 0.40 | -48.16 | -48.56 | -48.70 |
| 1895.2 | 129719.4 | 0.46 | -46.96 | -47.42 | -47.56 |
| 1909.2 | 130375.5 | 0.48 | -46.08 | -46.56 | -46.70 |
| 1912.2 | 130541.4 | 0.48 | -47.14 | -47.62 | -47.76 |
| 1930.2 | 131508.2 | 0.53 | -46.51 | -47.04 | -47.18 |
| 1945.2 | 132417.4 | 0.56 | -45.41 | -45.97 | -46.11 |
| 1954.9 | 132986.1 | 0.57 | -44.82 | -45.39 | -45.53 |
| 1978.2 | 134188.5 | 0.68 | -43.95 | -44.63 | -44.77 |
| 1993.9 | 135193.9 | 0.66 | -43.62 | -44.28 | -44.42 |
| 1996.2 | 135374.8 | 0.65 | -44.35 | -45.00 | -45.14 |
| 2002.7 | 135894.3 | 0.68 | -44.95 | -45.63 | -45.77 |
| 2017.8 | 137247.8 | 0.77 | -45.05 | -45.82 | -45.96 |
| 2018.8 | 137343.9 | 0.77 | -44.34 | -45.11 | -45.25 |
| 2033.8 | 138760.9 | 0.75 | -44.81 | -45.56 | -45.70 |
| 2051.0 | 140714.7 | 0.70 | -44.46 | -45.16 | -45.30 |
| 2084.0 | 144665.9 | 0.69 | -45.90 | -46.59 | -46.73 |
| 2099.3 | 146428.5 | 0.63 | -44.43 | -45.06 | -45.20 |
| 2113.3 | 147945.0 | 0.61 | -44.72 | -45.33 | -45.47 |
| 2114.9 | 148100.2 | 0.62 | -43.81 | -44.43 | -44.57 |
| 2129.2 | 149554.3 | 0.62 | -43.27 | -43.89 | -44.03 |
| 2145.0 | 151202.8 | 0.63 | -42.25 | -42.88 | -43.02 |
| 2162.3 | 153188.7 | 0.63 | -43.07 | -43.70 | -43.84 |
| 2177.0 | 154896.4 | 0.61 | -44.02 | -44.63 | -44.77 |
| 2191.0 | 156522.7 | 0.64 | -43.57 | -44.21 | -44.35 |
| 2206.0 | 158193.4 | 0.63 | -44.26 | -44.89 | -45.03 |
| 2220.0 | 159361.9 | 0.61 | -44.44 | -45.05 | -45.19 |
| 2235.0 | 160769.6 | 0.58 | -43.21 | -43.79 | -43.93 |
| 2250.0 | 162120.5 | 0.55 | -44.67 | -45.22 | -45.36 |

D. Python Code

D.1. Raw data processing

```
1 #!/usr/bin/python
# -*- coding: utf-8 -*-
# Last modified on Jul 20 20:28:21 2012
"""
6 Program to calculate the isotopy in CH4 concerning 13C and 18O.
The final values for the isotopies in 13C and 18O are given in permille
of the VPDBCO2 scale.
The condition between R17 and R18 (R17 = K*R18*a), as well as the Craig constants
values, can be modified in the paragraph 'Global constants'.
11 The properties of the working machine gas are listed there as well as the
Farraday cup resistors.
The following programs/definitions are called from the program:
    - peak
    - rectangular
16    - gaussian
    - background
    - calc_isotop
    - Craig
    - Santrock
21    - plotting
    - derivat
    - splinefit
    - read_data
    - write_library
26    - etc.

It can be chosen between the Craig-correction algorithm and the one developed
by Santrock et al.
The files that will be analyzed, are read in from the 'data'-folder and stored
31 to different archives according to the type of the analyzed file (Methan-Ref, Refloop, Airafter
or Sample).

Five libraries are generated:
36    - 'CH4_ref_Library.csv'
    - 'Refloop_Library.csv'
    - 'Loop_after_sample_Library.csv'
    - 'Sample_Library.csv'
    - 'RefAir_Library.csv'

41 Author information:
    Lars Moeller
    Alfred Wegener Institute for Polar and Marine Research
    P.O. Box 120161
    27515 Bremerhaven
46    Germany
    Lars.Moeller@awi.de
and
    Robert Schneider
    University of Bern
51    Climate and Environmental Physics
    schneider@climate.unibe.ch
"""

#####
56 # -----Used packages----- #
#####

import matplotlib
#matplotlib.rc("text", usetex=True)
61
from numpy import arange, linspace, sqrt, ones, max, argmax, argmin, nonzero
from numpy import concatenate, zeros, floor, exp, mean, std, array, sort, argsort
from numpy import append, delete, array_str, where, expand_dims, loadtxt
from scipy import stats
66 from time import localtime, sleep, strftime, strptime, mktime, asctime, ctime
#import scipy.io
from matplotlib import rcParams
import scipy.interpolate
import scipy.integrate
71 import scipy.optimize
import pylab
import os
#import os.path
```

```

import shutil
76 import sys
import csv
import locale
from Definitions_general import raw_plotter

81 --version-- = 1.3

# last modifications (last modified: 20.06.2008)
# - bug in the plotting procedure according to days_back removed
# - changed the background procedure according to 'shift'
86 # - moved the start (only 12 points left from the found) and end points (according to another
    end_slope)
#     for gauss peaks
# - switch in the header to avoid the plotting of the chromatogram
# - close file for the Header-file added by Melanie
# - check in the ref-library storage if the current ref type on the current date already exists
91 # - switch for the 'try'/except' condition to move folders to 'not working'

--version-- = 1.4

# modifications (last modified: see above )
96 # - added extended path and Datafolder structure support
# - introduced max amount of datasets in one script run to prevent crashes
# - no further need for preliminary lib files with fake data rows (2&3)
# - complete new data type determination algorithm with Ice-sample and Airoafter support
# - added appropriate supplementary information retrieval for Ice Samples and Airoafter types
101 # - this includes data columns storing the corresponding depth, ice origin, sample cut, sample weight,
    normalised sample weight, sample container, loop after number
# - Library Files (Refloops, Ice-sample and Airoafter) restructured and all changed to csv format
# - Script shows a warning, if Archive folder already exists so doubled lib entries might be present
# - Data is processed with its appropriate CO2 Reference gas
# - reorganized a bit for better usability and preconfiguration
106 # - corrected minor errors
# - Added much more feedback
# - Implemented "See no plot at all" feature to simply process existing data
# - and much more details i forgot to mention...

111 --version-- = 1.5

# modifications (last modified: see above )
# added 1.+2. rectangular peak isotopies and isot., Ampl., Area, Max Pos. and R.WMG_45/46 info for all
# 6 Reference Gauss peaks to the Ch4Ref Measurement library
# added support for Misc. RefAir Samples like Neumayer, Alert, Schauinsland etc. and built up its own
    library
116 # added support for B37 Ice samples
# added last modified and script version used info to all libs
# fixed bugs in the suppl. info retrieval
# fixed bug of not finding the peak limits after calling def gaussian through successive reduction of
    the the derivation detection limits
# completely new, more robust and sophisticated Ch4Ref Nr_the_day routine
121 # revised Symlink and better max_data per run routine
# all datasets have their creation time in utc secs added to the library (last column)
# Check for existing dataset with the same utc_sec time before writing the new
# removed the cut-off-bug of some large numbers after insufficient digits (e.g. Area)
# added library resorting algorithm after every script run (sort after utc creation time)
126 # plotting a raw data, a peak characteristic and a mean isotopy chromatogram has been revived ->
    variable plot_gauss_bounds = 'on'
# if demanded those plots can automatically be saved to disk -> variable save_chrom
# debugged the Gauss Peak finding algorithm
# Removed "See no plot at all" feature again
# Script may be started with arguments (run "scriptname --help" for further details)
131 # Chromatogram Plot Procedure edited for better data overview
# Added reference air sample and Intercomparison Ice recognition pattern
# Added peak detection ambiguity problem solution

--version-- = 1.6
136 # account for possible Krypton contamination of the CH4 sample peak by peak cut off x secs after peak
    maximum
# implemented Cut off Peak ends -> set p_cut_off variable
# log processing of individual measurements -> log_dir
# plot every individual measurement that is processed and save it -> plot_dir
141

#####
# -----Path and file parameter----- #
#####
146 ##### Path parameters #####

root_dir = '/home/lmoeller/Promotion/Messdaten/Processed_data/' # Data base folder
log_dir = root_dir+'Processing_Logs/Individual/'
151 plot_dir = root_dir+'Processing_Logs/Individual_plots/' #'/home/lmoeller/Dokumente/Abbildungen/PyPlots/
    Processed_by_script_v.'+str(--version--)+'/'
abs_path = '/home/lmoeller/Promotion/Messdaten/Raw_data/13C-Raw-Extracted/Pending/'

##### library and archive parameters #####
156 lib_path = root_dir+'Libraries'
lib_bck = root_dir+'Library_Backups' # Backup folder for Libs
arch_path = abs_path.rsplit("/",2)[0]+'Archive'

161 # variable to choose if data sets shall be moved to the archives and appended to the libraries
move_folders = 'off' # 'on' or 'off'

```

```

append_libraries = 'off' # 'on' or 'off'
#####
166 # -----Customization----- #
#####
##### Data File Categories #####

171 refl = 'Refloops'
    mref = 'CH4_Refs'
    ices = 'Ice_Samples'
    airt = 'Loops_after_Sample'
    refa = 'RefAir'
176
# Add search categories to identify Reference Air Samples
Ref_Airs = ['Neumayer', 'Gasmas', 'bar', 'Alert', 'CrystalAir', 'CAO']
Intercomp_ices = ['WDC05', 'B34', 'B37', 'ShGISP2']
181 ##### Define which csv Data folder to process #####

# Choose one or more of the File Categories above, or select "all" to process them all at once (Note
    that this will prevent you from plotting the chromatograms)
    dir_choice = [ices] #mref refl ices, airt, refa or 'all' -> in [] brackets !

# Determine the max amount of Measurements to be processed at once (number or "all")
186 max_data = 2 # "all"

# choose if the program shall allow errors or move error producing files to '/not working'
no_stop = 'off' # 'on'

191 ##
    Debug = False # True #
    peak_log = False # True #
    ##### print and plot parameters #####

196 # Determine General plot size
    f_w = 12 # figure width
    f_h = 8 # figure height
    rcParams['ytick.labelsize'] = "8"
    rcParams['xtick.labelsize'] = "8"
201
# variable to return the calculated isotopies of each peak after each run
print_peak_isotopies = 'on'

# variables to choose if chromatograms shall be generated/saved
206 plot_gauss_bounds = 'on' # 'on' or 'off'
    plot_raw_chrom = 'on' # 'on' or 'off'
    chrom_deriv = 'on' # 'on' or 'off' => Extra plot for the derivation
    chrom_peak_char = 'on' # 'on' or 'off'
    save_chrom = 'off' # 'on' or 'off' => if this is activated, the chromatograms won't be shown but
        saved to plot_dir
211
##### General Peak Properties #####

# variable to choose between two different choices to get the peak end
# change between 'slope', 'background' and 'cut_slope'
216 method_end = 'slope'
    if method_end == 'cut_slope':
        p_cut_off = 30 # time in 1/10 sec until the peak is cut off after the determined maximum
    else:
        p_cut_off = 0
221

# variable to choose the 17O correction algorithm (switch between 'Craig' and 'Santrock')
correction_method = 'Craig' # 'Santrock'

# variable to print optimized 18R values for each peak if corr. method ist Santrock (not Tested since
    v1.3)
226 print_optimized_results = 'off' # 'on'

# variable to apply a time shift
timeshift_application = 'off'

231 ## Background determination
    bg_shift = 30 # 30 Amount in x/10 Seconds that the Background det. precedes the Peak start
    bg_average = 50 # 50 Amount in x/10 Seconds that the constant Background is averaged over before
        bg_shift

##### peak start and peak end detection parameters #####
236
# define derivation method ('sum' or 'fit'); 'fit' is a lot more time consuming
derivat_method = 'sum'
# if 'fit' is applied, the gradient can be plotted in a raw-data plot
plot_derivation = 'on'
241

# slope-values to define peak_start and peak_end for gaussian and rectangular peaks
start_slope_gauss = 3500
end_slope_gauss = -100 # -100 -82426.8
start_slope_rec = 1e6
246 end_slope_rec = -1.7e4

# variable to choose if the whole rectangular peak is integrated or only a 'time_interval'
integrate_rec_small = 'on'
time_interval = 12
251

lib_exist = 'yes' # Do the paths and lib files for all data categories exist? (Better make sure they
    do!)

```

```

# I/O library filenames
library_refs = lib_path+'/%s.%ss.%s-CH4-ref-Library.csv'%(correction_method, p_cut_off/10.0, method_end
)
256 library_refloops = lib_path+'/%s.%ss.%s-Refloop-Library.csv'%(correction_method, p_cut_off/10.0,
method_end)
library_airafter = lib_path+'/%s.%ss.%s-Loop_after_sample-Library.csv'%(correction_method, p_cut_off
/10.0, method_end)
library_samples = lib_path+'/%s.%ss.%s-Sample-Library.csv'%(correction_method, p_cut_off/10.0,
method_end)
library_refair = lib_path+'/%s.%ss.%s-RefAir-Library.csv'%(correction_method, p_cut_off/10.0,
method_end)
libfiles = [library_refs, library_refloops, library_airafter, library_samples, library_refair]
261 ##### peak selections #####

# define the reference peak numbers for ref-files and non-ref-files
ref_peaks_ref = [1, 2] # peak number, all other peaks are referred to in ref-files
ref_peaks_non_ref = [1, 2, 3, 4] # peak number, all other peaks are referred to in non-ref-files
266

rcParams['text.usetex']=False
#####
# -----Global Constants----- #
#####
271

timestep = 0.1 # time interval in seconds between two measurements
enlargement = 100/timestep # enlargement of the points for the splinesfits
window = int(30.0/timestep) # time-interval of the floating window (peak detector)
276 fac = 1e-12 # scaling factor for the plot

# Faraday cup characteristics
resist44 = 5e8 # resistance of Faraday cup mass 44
resist45 = 5e10 # resistance of Faraday cup mass 45
281 resist46 = 1e11 # resistance of Faraday cup mass 46

# global parameters to scale the results to VPDBCO2 and to get the delta values
a = 0.528 # condition between R17 and R18: R17 = K*R18^a
R.13.VPDBCO2 = 0.0111241 # VPDBCO2 standard of 13C
R.17.VPDBCO2 = 0.00039108 # VPDBCO2 standard of 17O
286 R.18.VPDBCO2 = 0.00208837 # VPDBCO2 standard of 18O
K = R.17.VPDBCO2/R.18.VPDBCO2**a # calculated value for K

# CO2 - Working standard
291 # d13C isotope of CO2 ref gas to VPDB-CO2 reference material NBS-19
# d18O isotope of CO2 ref gas to VPDB-CO2 reference material NBS-19

Work_std=\
[{'Name': 'Std1', 'date': 'unknown', 'd13C': -49.35, 'd18O': -22.59},\
296 {'Name': 'Messer Btl-NR.:56216', 'intro.date': '080611', 'd13C': -25.3, 'd18O': -17.7},\
{'Name': 'AirLiquide Btl-NR.:11952', 'intro.date': '090317', 'd13C': -49.2, 'd18O': -19.4}]

# constants needed for Craig 17O correction algorithm
301 C1 = 1.0676
C2 = 0.0338
C3 = 1.0010
C4 = 0.0021

#####
306 ## Library Header Information ##
#####
hlines = 2 # Define how many headerlines are present in the lib files
ref_head = 'Date Ref.number dC.13.mean Stdev dC.13 1st.Rec dC.13 2nd.Rec dC.13 1st.Ref Ampl 1
st.Ref Area 1st.Ref pos_max.1st.Ref R.WMG.45 1st.Ref R.WMG.46 1st.Ref dC.13 2nd.Ref Ampl 2
nd.Ref Area 2nd.Ref pos_max.2nd.Ref R.WMG.45 2nd.Ref R.WMG.46 2nd.Ref dC.13 3rd.Ref Ampl 3
rd.Ref Area 3rd.Ref pos_max.3rd.Ref R.WMG.45 3rd.Ref R.WMG.46 3rd.Ref dC.13 4th.Ref Ampl 4
th.Ref Area 4th.Ref pos_max.4th.Ref R.WMG.45 4th.Ref R.WMG.46 4th.Ref dC.13 5th.Ref Ampl 5
th.Ref Area 5th.Ref pos_max.5th.Ref R.WMG.45 5th.Ref R.WMG.46 5th.Ref dC.13 6th.Ref Ampl 6
th.Ref Area 6th.Ref pos_max.6th.Ref R.WMG.45 6th.Ref R.WMG.46 6th.Ref Nr.the.day utc.sec'
refloop_head = 'Date refloop_number dC.13 1st.Ref dC.13 pre-peak dC.13 CH4.Peak dC.13 CO2.peak
dC.13 2nd.Ref Ampl 1st.Ref Ampl pre-peak Ampl CH4.Peak Ampl CO2.peak Ampl 2nd.Ref Area 1
st.Ref Area pre-peak Area44 CH4.Peak Area45 CH4.Peak Area46 CH4.Peak Area CO2.peak Area 2
nd.Ref pos_max.1st.Ref pos_max.pre-peak pos_max.CH4.Peak pos_max.CO2.peak pos_max.2nd.Ref
R.WMG.45 1st.Ref R.WMG.45 pre-peak R.WMG.45 CH4.Peak R.WMG.45 CO2.Peak R.WMG.45 2nd.Ref
R.WMG.46 1st.Ref R.WMG.46 pre-peak R.WMG.46 CH4.Peak R.WMG.46 CO2.Peak R.WMG.46 2nd.Ref
LoopVol[ml](STP) utc.sec'
311 refa_head = 'Date Air_origin dC.13 1st.Ref dC.13 pre-peak dC.13 CH4.Peak dC.13 CO2.peak dC.13 2
nd.Ref Ampl 1st.Ref Ampl pre-peak Ampl CH4.Peak Ampl CO2.peak Ampl 2nd.Ref Area 1st.Ref
Area pre-peak Area44 CH4.Peak Area CO2.peak Area 2nd.Ref pos_max.1st.Ref pos_max.pre-peak
pos_max.CH4.Peak pos_max.CO2.peak pos_max.2nd.Ref R.WMG.45 1st.Ref R.WMG.45 pre-peak
R.WMG.45 CH4.Peak R.WMG.45 CO2.Peak R.WMG.45 2nd.Ref R.WMG.46 1st.Ref R.WMG.46 pre-peak
R.WMG.46 CH4.Peak R.WMG.46 CO2.Peak R.WMG.46 2nd.Ref Ref.number LoopVol[ml](STP) utc.sec'
aira_head = 'Date Ice_origin Depth Cut dC.13 1st.Ref dC.13 pre-peak dC.13 CH4.Peak dC.13
CO2.peak dC.13 2nd.Ref Ampl 1st.Ref Ampl pre-peak Ampl CH4.Peak Ampl CO2.peak Ampl 2nd.Ref
Area 1st.Ref Area pre-peak Area44 CH4.Peak Area45 CH4.Peak Area46 CH4.Peak Area CO2.peak
Area 2nd.Ref pos_max.1st.Ref pos_max.pre-peak pos_max.CH4.Peak pos_max.CO2.peak
pos_max.2nd.Ref R.WMG.45 1st.Ref R.WMG.45 pre-peak R.WMG.45 CH4.Peak R.WMG.45 CO2.Peak
R.WMG.45 2nd.Ref R.WMG.46 1st.Ref R.WMG.46 pre-peak R.WMG.46 CH4.Peak R.WMG.46 CO2.Peak
R.WMG.46 2nd.Ref Loop-Nr Pot utc.sec'
sam_head = 'Date Ice_origin Depth Cut dC.13 1st.Ref dC.13 pre-peak dC.13 CH4.Peak dC.13 CO2.peak
dC.13 2nd.Ref Ampl 1st.Ref Ampl pre-peak Ampl CH4.Peak Ampl CO2.peak Ampl 2nd.Ref Area 1
st.Ref Area pre-peak Area44 CH4.Peak Area45 CH4.Peak Area46 CH4.Peak Area CO2.peak Area 2
nd.Ref pos_max.1st.Ref pos_max.pre-peak pos_max.CH4.Peak pos_max.CO2.peak pos_max.2nd.Ref
R.WMG.45 1st.Ref R.WMG.45 pre-peak R.WMG.45 CH4.Peak R.WMG.45 CO2.Peak R.WMG.45 2nd.Ref
R.WMG.46 1st.Ref R.WMG.46 pre-peak R.WMG.46 CH4.Peak R.WMG.46 CO2.Peak R.WMG.46 2nd.Ref
Weight Area.Norm Pot utc.sec'

```

```

'''
316 #####
# -----Definitions----- #
#####
'''
class Logger(object):
321     def __init__(self, fname="log.dat"):
        self.terminal = sys.stdout
        self.log = open(fname, "a")
        def write(self, message):
            self.terminal.write(message)
326         self.log.write(message)
        def flush():
            self.terminal.flush()
            self.log.flush()
        def __del__(self):
331         sys.stdout = self.terminal
            self.log.close()

#####
# write and read definitions
336 #####

def read_data(datafile):
    """
    Read the measurement datafile.
341     """
    print '-----'
    print 'Reading raw data file. This might take a while.'

    data = loadtxt(datafile, delimiter=',', usecols=(0,1,2), skiprows=1)
346     print 'Reading data finished. Processing ...'
    return data

#####

351 def Nonref_library(library_file, new_line, headline, type_file, datafile, supplementary_information,
    Maxima_position44, Amplitude44, Area44_array, dC_13_gauss, R_WMG_45, R_WMG_46):
    """
    Write the results of Nonref-Data to their corresponding libraries
    """
356     # read library data
    print '*****'
    print 'Adding new data to %s Library...' %(type_file)#,library_file
    #print os.path.exists(library_file)
361     libread = csv.reader(open(library_file, "rb"))
    csv_c = 1
    uselesline = 0
    for row in libread:
        #print 'Processing row: ',row
366         if csv_c == 2:
            lib_dummy = zeros((1,len(row)))
            if csv_c == hlines+1:
                print len(row), row, csv_c, hlines+1
                if len(row) <= 1:
371                     print 'Empty line in %s' %(library_file)
                        library_data=zeros((1,len(headline)))
                        uselesline = uselesline + 1
                elif row[0] == '0.0':
376                     print 'Detected dummy line in %s' %(library_file)
                        library_data = array(row,ndmin=2)
                        uselesline = uselesline + 1
                else:
                    library_data = array(row,ndmin=2)
381             elif csv_c > hlines+1:
                csv_row = array(row,ndmin=2)
                #print shape(row),len(headline),shape(library_data)
                library_data = append(library_data, csv_row, axis=0)
                csv_c = csv_c+1

386     ## Check if the actual dataset already exists in the library
    print 'Will try to append the following data line to array: \n', new_line[0,:]
    if len(where(library_data[:, -1].astype(float)==new_line[0][ -1].astype(float))[0]) == 1:
        print
        print '!!! The new dataset already exists in the library and will therefore be skipped !!!'
391     #break
    else:
        #print shape(library_data),shape(new_line)
        library_data = append(library_data, new_line, axis=0)
        print "\nDone!"
396     ## Remove dummy first line from library array if present
    if uselesline >= 1 and library_data[0,0] == '0.0':
        library_data= delete(library_data, 0,0)
        print 'Deleted dummy line in "%s"' %(library_file)
401     print '-----'

    ## Sort the whole array for oldest entries first (determined by utc time) before writing to disk
    library_data= library_data.take(argsort(library_data[:, -1].astype(float)), axis=-2)

    ## Write array to disk

```

```

406     csvlib = csv.writer(open(library_file, "w")) #, dialect='excel'
csvlib.writerow(('Last modified: '+strftime("%a %b %d %Y %H:%M:%S", localtime())+ ' with
    script version '+str(_version_)).split(' '))
csvlib.writerow(headline)
#csvlib.writerow('') # removed for better recarray handling
for writeline in range(len(library_data[:,0])):
411     csvlib.writerow(library_data[writeline,:])

#####
def peak_ambiguity(dC_13, Area44):
    global peak_amb
    peak_amb = True
    print " %s Attention!!! %s" % ('**'*5, '**'*5)
    print " There is ambiguity in the peak selection procedure - \n please select the 5 correct
        peaks manually!"
    print "\nThese are the detected peaks and their isotopies:\npeak nr ', ' dC_13 ', ' Area M44'
    for i in arange(len(dC_13)):
421     print '%(a0)4.0f %(a1)10.2f %(a2)12.0f' % {'a0': i+1, 'a1': dC_13[i], 'a2': Area44[i+4]}
    man_choice = []
    for e,typ in enumerate(["1st CH4 Ref","Pre","CH4 Sample","CO2","2nd CH4 Ref"]):
    print "\n%s. Please specify the correct number for the %s peak:"%(e+1,typ)
    satisfied_opt = 'nope'
426     while satisfied_opt != 'yep':
        sel_opt = raw_input()
        if sel_opt.isdigit()==False:
            print 'Selection is not even an integer, please try again...'
        elif int(sel_opt) not in range(15):
431     print 'Selection seems not correct, please try again...'
        else:
            print
            print ' Thank you very much - Your choice was number "%s" ...' %(sel_opt)
            satisfied_opt = 'yep'
436     man_choice.extend(sel_opt)
    return [int(n)-1 for n in man_choice]

#####
def write_library(result, sigma, type_file, datafile, supplementary_information, Maxima_position44,
    Amplitude44, Area44, Area45, Area46, dC_13_gauss, dC_13_rec, R_WMG45, R_WMG46):
441     """
    Determine the data type and write the results to their corresponding libraries (or call "def
    "" Nonref_library")

    ### append result to library
    # for the ref-library
    if type_file == 'Ref':
    print 'Adding new data to Methane Reference Library...'
    libread = csv.reader(open(library_refs, "rb"))
    csv_c = 1
451     uselessline = 0
    for row in libread:
        #print 'Processing row: ',row
        if csv_c == 1:
            lib_dummy = zeros((1,len(row)))
456     elif csv_c == hlines+1:
            if len(row) <= 1:
                library_refs_data=lib_dummy
                uselessline = uselessline + 1
            elif row[0] == '0.0':
461     print 'Detected zero filled dummy line in %s' %(library_refs)
                library_refs_data = array(row,ndmin=2)
                uselessline = uselessline + 1
        #
            library_refs_data= delete(library_refs_data, 0,0)
466     elif library_refs_data = array(row,ndmin=2)
        elif csv_c > hlines+1:
            csv_row = array(row,ndmin=2)
            library_refs_data = append(library_refs_data, csv_row, axis=0)
            csv_c = csv_c+1
471     #print 'Library Array contains the following lines: \n',library_refs_data

    ## Check which measurement number the actual dataset represents at the same day and actualize
    all entries with the same date
    if len(where(library_refs_data[:,0]==supplementary_information[0])[0]) >= 1 and not len(where(
        library_refs_data[:, -1].astype(float)==supplementary_information[2])[0]) >= 1: # find the
        same date occurrences (and check if the dataset already exists)
        occ_indices = where(library_refs_data[:,0]==supplementary_information[0])[0] # remember its
        indices
476     utc_list=[]
    for occ in occ_indices: # add utc time of all same day occurrences
        utc_list.append(library_refs_data[occ, -1].astype(float))
    utc_list.append(supplementary_information[2])# add utc time of new dataset
    utc_ar=array(utc_list).take(argsort(utc_list)) # convert list to array and sort it for
    oldest utc first
481     nr_day = where(utc_ar==supplementary_information[2])[0][0] +1 # get the position of the new
        dataset in the sorted sequence
    for occ in occ_indices:
        #print where(utc_ar==library_refs_data[occ, -1].astype(float))[0][0]
        #print library_refs_data[occ, (2, -2)]
        library_refs_data[occ, -2] = where(utc_ar==library_refs_data[occ, -1].astype(float))

```



```

[0][0] +1 # overwrite the existing entries in the lib with the new positions in
the sorted sequence
486     #print library_refs_data[occ,(2,-2)]
    #print supplementary_information[0:1], nr_day
else:
    nr_day = 1
# Create new array line (dummy entry necessary because of the not understood cut-off of entries
in newline) without utc information first
1.gauss Peak isotopy      amplitude      area      max_pos
Ratio 45                  Ratio46
isotopy      Amplitude      Area      Maxima_position44
R-WMG.45     Area44          Maxima_position44 R-WMG.45     Amplitude44
R-WMG.46     Maxima_position44 4.gauss Peak isotopy      Amplitude44 R-WMG.46     Area44
Maxima_position44 5.gauss Peak isotopy      Amplitude44 R-WMG.45     Area44
Peak isotopy  R-WMG.45          R-WMG.46     Maxima_position44
abs_num      utc_time
491 new_line = array(['longdummyentryforremoval', supplementary_information[0],
supplementary_information[1], round(result, 2), round(sigma, 2), round(dC_13_rec[0], 4),
round(dC_13_rec[1], 4), round(dC_13_gauss[0], 4), round(Amplitude44[2], 4), round(Area44[2],
4), round(Maxima_position44[2], 4), round(R-WMG.45[2]*1e3, 3), round(R-WMG.46[2]*1e3, 3),
round(dC_13_gauss[1], 4), round(Amplitude44[3], 4), round(Area44[3], 4), round(
Maxima_position44[3], 4), round(R-WMG.45[3]*1e3, 3), round(R-WMG.46[3]*1e3, 3), round(
dC_13_gauss[2], 4), round(Amplitude44[4], 4), round(Area44[4], 4), round(Maxima_position44
[4], 4), round(R-WMG.45[4]*1e3, 3), round(R-WMG.46[4]*1e3, 3), round(dC_13_gauss[3], 4), round(
Amplitude44[5], 4), round(Area44[5], 4), round(Maxima_position44[5], 4), round(R-WMG.45[5]*1
e3, 3), round(R-WMG.46[5]*1e3, 3), round(dC_13_gauss[4], 4), round(Amplitude44[6], 4), round(
Area44[6], 4), round(Maxima_position44[6], 4), round(R-WMG.45[6]*1e3, 3), round(R-WMG.46[6]*1
e3, 3), round(dC_13_gauss[5], 4), round(Amplitude44[7], 4), round(Area44[7], 4), round(
Maxima_position44[7], 4), round(R-WMG.45[7]*1e3, 3), round(R-WMG.46[7]*1e3, 3), nr_day,
supplementary_information[2]], ndmin=2)
new_line = expand_dims(delete(new_line,0), axis=0) # removes the dummy entry from array and
afterwards expands the dimension for appending procedure

## Check if the actual dataset already exists in the library
496 #print where(library_refs_data[:, -1].astype(float)==new_line[0][ -1].astype(float))[0], len(
where(library_refs_data[:, -1].astype(float)==new_line[0][ -1].astype(float))[0])
print 'Try to append the following data line to array: \n', new_line[0,: ]
if len(where(library_refs_data[:, -1].astype(float)==new_line[0][ -1].astype(float))[0]) == 1:
    print
    print '!!! The new dataset already exists in the library and will therefore be skipped !!!'
501 #break
else:
    library_refs_data = append(library_refs_data, new_line, axis=0)
    print '\nDone!'

506 #print uselesline, library_refs_data[0,0]
# Remove zero filled first line from library array
if uselesline >= 1 and library_refs_data[0,0] == '0.0':
    library_refs_data= delete(library_refs_data, 0,0)
511 print 'Deleted dummy line with zeroes in %s' %(library_refs)

## Sort the whole array for oldest entries first (determined by utc time) before writing to
disk
library_refs_data= library_refs_data.take(argsort(library_refs_data[:, -1].astype(float)), axis
=-2)

516 # Write array to disk
csvlib = csv.writer(open(library_refs, "w")) #, dialect='excel'
csvlib.writerow(('Last modified: '+strftime("%a %b %d %Y %H:%M:%S", localtime())+ ' with
script version '+str(__version__)).split(' '))
csvlib.writerow(ref_head.split(' '))
#csvlib.writerow('') # removed for better recarray handling
521 for writeline in range(len(library_refs_data[:,0])):
    csvlib.writerow(library_refs_data[writeline,:])

# for the non-ref-libraries
526 if type_file != 'Ref':
    # read library data
    if type_file == 'Reflump':
        library_file = library_refloops
        headerline = reflump_head.split(' ')
531 # Create new array line (dummy entry necessary because of the not understood cut-off of
entries in newline)
if len(dC_13_gauss) > 5:
    man_choice = peak_ambiguity(dC_13_gauss, Area44.array)
    ## Debugging
    for e, pos in enumerate(['longdummyentryforremoval', supplementary_information[0],
supplementary_information[1], round(dC_13_gauss[man_choice[0]], 4), round(
dC_13_gauss[man_choice[1]], 4), round(dC_13_gauss[man_choice[2]], 4), round(
dC_13_gauss[man_choice[3]], 4), round(dC_13_gauss[man_choice[4]], 4), round(
Amplitude44[4+man_choice[0]], 4), round(Amplitude44[4+man_choice[1]], 4), round(
Amplitude44[4+man_choice[2]], 4), round(Amplitude44[4+man_choice[3]], 4), round(
Amplitude44[4+man_choice[4]], 4), round(Area44[4+man_choice[0]], 4), round(Area44[4+
man_choice[1]], 4), round(Area44[4+man_choice[2]], 4), round(Area44[4+man_choice

```

536

```

[3], 4), round(Area44[4+man_choice[4]], 4), round(Maxima_position44[4+man_choice
[0]], 4), round(Maxima_position44[4+man_choice[1]], 4), round(Maxima_position44[4+
man_choice[2]], 4), round(Maxima_position44[4+man_choice[3]], 4), round(
Maxima_position44[4+man_choice[4]], 4), round(R.WMG.45[4+man_choice[0]]*1e3, 3),
round(R.WMG.45[4+man_choice[1]]*1e3, 3), round(R.WMG.45[4+man_choice[2]]*1e3, 3),
round(R.WMG.45[4+man_choice[3]]*1e3, 3), round(R.WMG.45[4+man_choice[4]]*1e3, 3),
round(R.WMG.46[4+man_choice[0]]*1e3, 3), round(R.WMG.46[4+man_choice[1]]*1e3, 3),
round(R.WMG.46[4+man_choice[2]]*1e3, 3), round(R.WMG.46[4+man_choice[3]]*1e3, 3),
round(R.WMG.46[4+man_choice[4]]*1e3, 3), supplementary_information[2],
supplementary_information[3])):
print e, pos

```

541

```

new_line = array(['longdummyentryforremoval', supplementary_information[0],
supplementary_information[1], round(dC.13-gauss[man_choice[0]], 4), round(
dC.13-gauss[man_choice[1]], 4), round(dC.13-gauss[man_choice[2]], 4), round(
dC.13-gauss[man_choice[3]], 4), round(dC.13-gauss[man_choice[4]], 4), round(
Amplitude44[4+man_choice[0]], 4), round(Amplitude44[4+man_choice[1]], 4), round(
Amplitude44[4+man_choice[2]], 4), round(Amplitude44[4+man_choice[3]], 4), round(
Amplitude44[4+man_choice[4]], 4), round(Area44[4+man_choice[0]], 4), round(Area44[4+
man_choice[1]], 4), round(Area44[4+man_choice[2]], 4), round(Area44[4+man_choice
[3]], 4), round(Area44[4+man_choice[4]], 4), round(Maxima_position44[4+man_choice
[0]], 4), round(Maxima_position44[4+man_choice[1]], 4), round(Maxima_position44[4+
man_choice[2]], 4), round(Maxima_position44[4+man_choice[3]], 4), round(
Maxima_position44[4+man_choice[4]], 4), round(R.WMG.45[4+man_choice[0]]*1e3, 3),
round(R.WMG.45[4+man_choice[1]]*1e3, 3), round(R.WMG.45[4+man_choice[2]]*1e3, 3),
round(R.WMG.45[4+man_choice[3]]*1e3, 3), round(R.WMG.45[4+man_choice[4]]*1e3, 3),
round(R.WMG.46[4+man_choice[0]]*1e3, 3), round(R.WMG.46[4+man_choice[1]]*1e3, 3),
round(R.WMG.46[4+man_choice[2]]*1e3, 3), round(R.WMG.46[4+man_choice[3]]*1e3, 3),
round(R.WMG.46[4+man_choice[4]]*1e3, 3), supplementary_information[2],
supplementary_information[3]))
else:
new_line = array(['longdummyentryforremoval', supplementary_information[0],
supplementary_information[1], round(dC.13-gauss[0], 4), round(dC.13-gauss[1], 4),
round(dC.13-gauss[2], 4), round(dC.13-gauss[3], 4), round(dC.13-gauss[4], 4), round(
Amplitude44[4], 4), round(Amplitude44[5], 4), round(Amplitude44[6], 4), round(
Amplitude44[7], 4), round(Amplitude44[8], 4), round(Area44[4], 4), round(Area44[5],
4), round(Area44[6], 4), round(Area44[7], 4), round(Area44[8], 4), round(
Maxima_position44[4], 4), round(Maxima_position44[5], 4), round(Maxima_position44
[6], 4), round(Maxima_position44[7], 4), round(Maxima_position44[8], 4), round(
R.WMG.45[4]*1e3, 3), round(R.WMG.45[5]*1e3, 3), round(R.WMG.45[6]*1e3, 3), round(
R.WMG.45[7]*1e3, 3), round(R.WMG.45[8]*1e3, 3), round(R.WMG.46[4]*1e3, 3), round(
R.WMG.46[5]*1e3, 3), round(R.WMG.46[6]*1e3, 3), round(R.WMG.46[7]*1e3, 3), round(
R.WMG.46[8]*1e3, 3), supplementary_information[2], supplementary_information[3]))
new_line = expand_dims(delete(new_line, 0), axis=0) # removes the dummy entry from array and
afterwards expands the dimension for appending procedure

```

546

```

elif type_file == 'Airafter':
library_file = library_airafter
headerline = aira_head.split(' ')
# Create new array line (dummy entry necessary because of the not understood cut-off of
entries in newline)
if len(dC.13-gauss) > 5:
man_choice = peak_ambiguity(dC.13-gauss, Area44_array)
new_line = array(['longdummyentryforremoval', supplementary_information[0],
supplementary_information[1], supplementary_information[2],
supplementary_information[3], round(dC.13-gauss[man_choice[0]], 4), round(
dC.13-gauss[man_choice[1]], 4), round(dC.13-gauss[man_choice[2]], 4), round(
dC.13-gauss[man_choice[3]], 4), round(dC.13-gauss[man_choice[4]], 4), round(
Amplitude44[4+man_choice[0]], 4), round(Amplitude44[4+man_choice[1]], 4), round(
Amplitude44[4+man_choice[2]], 4), round(Amplitude44[4+man_choice[3]], 4), round(
Amplitude44[4+man_choice[4]], 4), round(Area44[4+man_choice[0]], 4), round(Area44[4+
man_choice[1]], 4), round(Area44[4+man_choice[2]], 4), round(Area44[4+man_choice
[2]], 4), round(Area46[4+man_choice[2]], 4), round(Area44[4+man_choice[3]], 4), round(
Area44[4+man_choice[4]], 4), round(Maxima_position44[4+man_choice[0]], 4), round(
Maxima_position44[4+man_choice[1]], 4), round(Maxima_position44[4+man_choice[2]],
4), round(Maxima_position44[4+man_choice[3]], 4), round(Maxima_position44[4+
man_choice[4]], 4), round(R.WMG.45[4+man_choice[0]]*1e3, 3), round(R.WMG.45[4+
man_choice[1]]*1e3, 3), round(R.WMG.45[4+man_choice[2]]*1e3, 3), round(R.WMG.45[4+
man_choice[3]]*1e3, 3), round(R.WMG.45[4+man_choice[4]]*1e3, 3), round(R.WMG.46[4+
man_choice[0]]*1e3, 3), round(R.WMG.46[4+man_choice[1]]*1e3, 3), round(R.WMG.46[4+
man_choice[2]]*1e3, 3), round(R.WMG.46[4+man_choice[3]]*1e3, 3), round(R.WMG.46[4+
man_choice[4]]*1e3, 3), supplementary_information[4], supplementary_information[5],
supplementary_information[6]))
else:
new_line = array(['longdummyentryforremoval', supplementary_information[0],
supplementary_information[1], supplementary_information[2],
supplementary_information[3], round(dC.13-gauss[0], 4), round(dC.13-gauss[1], 4),
round(dC.13-gauss[2], 4), round(dC.13-gauss[3], 4), round(dC.13-gauss[4], 4), round(
Amplitude44[4], 4), round(Amplitude44[5], 4), round(Amplitude44[6], 4), round(
Amplitude44[7], 4), round(Amplitude44[8], 4), round(Area44[4], 4), round(Area44[5],
4), round(Area44[6], 4), round(Area45[6], 4), round(Area46[6], 4), round(Area44[7], 4),
round(Area44[8], 4), round(Maxima_position44[4], 4), round(Maxima_position44[5], 4),
round(Maxima_position44[6], 4), round(Maxima_position44[7], 4), round(
Maxima_position44[8], 4), round(R.WMG.45[4]*1e3, 3), round(R.WMG.45[5]*1e3, 3), round(
R.WMG.45[6]*1e3, 3), round(R.WMG.45[7]*1e3, 3), round(R.WMG.45[8]*1e3, 3), round(
R.WMG.46[4]*1e3, 3), round(R.WMG.46[5]*1e3, 3), round(R.WMG.46[6]*1e3, 3), round(

```

```

R_WMG_46[7]*1e3, 3),round(R_WMG_46[8]*1e3, 3),supplementary_information[4],
supplementary_information[5],supplementary_information[6]])
551 new_line = expand_dims(delete(new_line,0), axis=0) # removes the dummy entry from array and
    afterwards expands the dimension for appending procedure

elif type_file == 'Sample':
    library_file = library_samples
    headerline = sam_head.split(' ')
556 # Create new array line (dummy entry necessary because of the not understood cut-off of
    entries in newline)
    if len(dC_13-gauss) > 5:
        man_choice = peak_ambiguity(dC_13-gauss, Area44_array)
        new_line = array(['longdummyentryforremoval',supplementary_information[0],
            supplementary_information[1],supplementary_information[2],
            supplementary_information[3], round(dC_13-gauss[man_choice[0]], 4),round(
            dC_13-gauss[man_choice[1]], 4),round(dC_13-gauss[man_choice[2]], 4),round(
            dC_13-gauss[man_choice[3]], 4),round(dC_13-gauss[man_choice[4]], 4),round(
            Amplitude44[4+man_choice[0]], 4),round(Amplitude44[4+man_choice[1]], 4),round(
            Amplitude44[4+man_choice[2]], 4),round(Amplitude44[4+man_choice[3]], 4),round(
            Amplitude44[4+man_choice[4]], 4),round(Area44[4+man_choice[0]], 4),round(Area44[4+
            man_choice[1]], 4),round(Area44[4+man_choice[2]], 4),round(Area45[4+man_choice
            [2]], 4),round(Area46[4+man_choice[2]], 4),round(Area44[4+man_choice[3]], 4),round
            (Area44[4+man_choice[4]], 4),round(Maxima_position44[4+man_choice[0]], 4),round(
            Maxima_position44[4+man_choice[1]], 4),round(Maxima_position44[4+man_choice[2]],
            4),round(Maxima_position44[4+man_choice[3]], 4),round(Maxima_position44[4+
            man_choice[4]], 4),round(R_WMG_45[4+man_choice[0]]*1e3, 3),round(R_WMG_45[4+
            man_choice[1]]*1e3, 3),round(R_WMG_45[4+man_choice[2]]*1e3, 3),round(R_WMG_45[4+
            man_choice[3]]*1e3, 3),round(R_WMG_45[4+man_choice[4]]*1e3, 3),round(R_WMG_46[4+
            man_choice[0]]*1e3, 3),round(R_WMG_46[4+man_choice[1]]*1e3, 3),round(R_WMG_46[4+
            man_choice[2]]*1e3, 3),round(R_WMG_46[4+man_choice[3]]*1e3, 3),round(R_WMG_46[4+
            man_choice[4]]*1e3, 3),supplementary_information[4],round((Area44[6]*(200.0/float(
            supplementary_information[4]))), 4),supplementary_information[5],
            supplementary_information[6]])
        else:
561 new_line = array(['longdummyentryforremoval',supplementary_information[0],
            supplementary_information[1],supplementary_information[2],
            supplementary_information[3],round(dC_13-gauss[0], 4),round(dC_13-gauss[1], 4),
            round(dC_13-gauss[2], 4),round(dC_13-gauss[3], 4),round(dC_13-gauss[4], 4),round(
            Amplitude44[4], 4),round(Amplitude44[5], 4),round(Amplitude44[6], 4),round(
            Amplitude44[7], 4),round(Amplitude44[8], 4),round(Area44[4], 4),round(Area44[5],
            4),round(Area44[6], 4),round(Area45[6], 4),round(Area46[6], 4),round(Area44[7], 4),
            round(Area44[8], 4),round(Maxima_position44[4], 4),round(Maxima_position44[5], 4),
            round(Maxima_position44[6], 4),round(Maxima_position44[7], 4),round(
            Maxima_position44[8], 4),round(R_WMG_45[4]*1e3, 3),round(R_WMG_45[5]*1e3, 3),round
            (R_WMG_45[6]*1e3, 3),round(R_WMG_45[7]*1e3, 3),round(R_WMG_45[8]*1e3, 3),round(
            R_WMG_46[4]*1e3, 3),round(R_WMG_46[5]*1e3, 3),round(R_WMG_46[6]*1e3, 3),round(
            R_WMG_46[7]*1e3, 3),round(R_WMG_46[8]*1e3, 3),supplementary_information[4],round((
            Area44[6]*(200.0/float(supplementary_information[4]))), 4),
            supplementary_information[5],supplementary_information[6]])
        new_line = expand_dims(delete(new_line,0), axis=0) # removes the dummy entry from array and
            afterwards expands the dimension for appending procedure

elif type_file == 'RefAir':
    library_file = library_refair
566 headerline = refa_head.split(' ')
    # Create new array line (dummy entry necessary because of the not understood cut-off of
    entries in newline)
    if len(dC_13-gauss) > 5:
        man_choice = peak_ambiguity(dC_13-gauss, Area44_array)
        new_line = array(['longdummyentryforremoval',supplementary_information[0],
            supplementary_information[1], round(dC_13-gauss[man_choice[0]], 4),round(
            dC_13-gauss[man_choice[1]], 4),round(dC_13-gauss[man_choice[2]], 4),round(
            dC_13-gauss[man_choice[3]], 4),round(dC_13-gauss[man_choice[4]], 4),round(
            Amplitude44[4+man_choice[0]], 4),round(Amplitude44[4+man_choice[1]], 4),round(
            Amplitude44[4+man_choice[2]], 4),round(Amplitude44[4+man_choice[3]], 4),round(
            Amplitude44[4+man_choice[4]], 4),round(Area44[4+man_choice[0]], 4),round(Area44[4+
            man_choice[1]], 4),round(Area44[4+man_choice[2]], 4),round(Area44[4+man_choice
            [3]], 4),round(Area44[4+man_choice[4]], 4),round(Maxima_position44[4+man_choice
            [0]], 4),round(Maxima_position44[4+man_choice[1]], 4),round(Maxima_position44[4+
            man_choice[2]], 4),round(Maxima_position44[4+man_choice[3]], 4),round(
            Maxima_position44[4+man_choice[4]], 4),round(R_WMG_45[4+man_choice[0]]*1e3, 3),
            round(R_WMG_45[4+man_choice[1]]*1e3, 3),round(R_WMG_45[4+man_choice[2]]*1e3, 3),
            round(R_WMG_45[4+man_choice[3]]*1e3, 3),round(R_WMG_45[4+man_choice[4]]*1e3, 3),
            round(R_WMG_46[4+man_choice[0]]*1e3, 3),round(R_WMG_46[4+man_choice[1]]*1e3, 3),
            round(R_WMG_46[4+man_choice[2]]*1e3, 3),round(R_WMG_46[4+man_choice[3]]*1e3, 3),
            round(R_WMG_46[4+man_choice[4]]*1e3, 3),supplementary_information[2],
            supplementary_information[3],supplementary_information[4]])
571 else:
        new_line = array(['longdummyentryforremoval',supplementary_information[0],
            supplementary_information[1], round(dC_13-gauss[0], 4),round(dC_13-gauss[1], 4),
            round(dC_13-gauss[2], 4),round(dC_13-gauss[3], 4),round(dC_13-gauss[4], 4),round(
            Amplitude44[4], 4),round(Amplitude44[5], 4),round(Amplitude44[6], 4),round(
            Amplitude44[7], 4),round(Amplitude44[8], 4),round(Area44[4], 4),round(Area44[5],
            4),round(Area44[6], 4),round(Area44[7], 4),round(Area44[8], 4),round(
            Maxima_position44[4], 4),round(Maxima_position44[5], 4),round(Maxima_position44
            [6], 4),round(Maxima_position44[7], 4),round(Maxima_position44[8], 4),round(

```

```

R_WMG_45[4]*1e3, 3),round(R_WMG_45[5]*1e3, 3),round(R_WMG_45[6]*1e3, 3),round(
R_WMG_45[7]*1e3, 3),round(R_WMG_45[8]*1e3, 3),round(R_WMG_46[4]*1e3, 3),round(
R_WMG_46[5]*1e3, 3),round(R_WMG_46[6]*1e3, 3),round(R_WMG_46[7]*1e3, 3),round(
R_WMG_46[8]*1e3, 3),supplementary_information[2],supplementary_information[3],
supplementary_information[4]])
new_line = expand_dims(delete(new_line,0), axis=0) # removes the dummy entry from array and
afterwards expands the dimension for appending procedure
#print len(new_line)

576     else:
        print '*****'
        print 'Oh, oh - Data in "%s" has no corresponding Library file !!!' %(datafile)
        print '*****'
581     ## Call def Nonref_library to execute the writing
        #print 'Test:',run, file_type[run],supplementary_information, supplementary_information[run-1]
        Nonref_library(library_file, new_line, headerline, file_type[runs], datafile,
supplementary_information, Maxima_position44, Amplitude44, Area44, dC_13_gauss, R_WMG_45,
R_WMG_46)
586 #####
def not_working(datafile, file_type, folder):
archive_name = file_type+' archive'
if os.path.exists(abs_path+'not working/'+archive_name+'/'+folder) == True:
print
print '*****'
591     print 'Archive folder %s in "not working/" already exists!!!\n\n Skipping it...' %(folder)
print
print '*****'

else:
shutil.copytree(tmp_dir+folder, abs_path+'not working/'+archive_name+'/'+folder)
org_dir = os.readlink(tmp_dir+folder)
596     # shutil.rmtree(org_dir)
os.unlink(tmp_dir+folder)
print
print 'Errors ocured while processing dataset %s!!' %(datafile.split('/',10)[-1].rsplit('/',1)[0])
print '-> Data folder moved to "not working"!'
601     print '-----'

#####
# analysis definitions
#####
606 def Peak(time, mass44, mass45, mass46, runs):
"""
Subprogram to find the peaks, the peak type, their maxima, the Areas and the
backgound value.
611 The Peak-Maxima (value and position), peak start, peak end, the peak type and
peak number as well as its position, the background value and the average over
10 points of the simple derivation between two neighboured points are returned
for all three masses.
"""

616 # define global result arrays
mass_prime44 = [] # defines the derivation of the raw data
mass_prime45 = [] # defines the derivation of the raw data
mass_prime46 = [] # defines the derivation of the raw data
621 Maxima_time44 = [] # defines the position of the maxima
Maxima_value44 = [] # defines the value of the maxima
Maxima_time45 = [] # defines the position of the maxima
Maxima_value45 = [] # defines the value of the maxima
Maxima_time46 = [] # defines the position of the maxima
626 Maxima_value46 = [] # defines the value of the maxima
Area_all44 = [] # defines the value of the complete peak area
Area_all45 = [] # defines the value of the complete peak area
Area_all46 = [] # defines the value of the complete peak area
peak_start = [] # defines array for the peak start
631 peak_end = [] # defines array for the peak end
peak_number = [] # counts the peaks
background_const44 = [] # defines the constant background level
background_const45 = [] # defines the constant background level
background_const46 = [] # defines the constant background level
636 peak_type = [] # defines the peak type
bg_times = []
# starting conditions necessary to detect the peaks
iter = 0
peak_nr = 0
641 position0 = 0

# scan the time axis to find the peaks
for n in range(1, len(time)-window):

646     # get the derivation of mass over time
if derivat_method == 'sum':
mass_prime44.append(derivat(n, time, mass44, 20.0))
mass_prime45.append(derivat(n, time, mass45, 20.0))
mass_prime46.append(derivat(n, time, mass46, 20.0))
651

```

```

# calculate the center of gravity of a floating window to detect peaks
square_sum = sum(mass44[n: n+window+1]**2)
fourth_sum = sum(mass44[n: n+window+1]**4)
656 amplitude = sum(linspace(n, n+window, window+1)*mass44[n: n+window+1]**2)/square_sum
amplitude = sqrt(fourth_sum/square_sum)

# detect peak if certain conditions for position and amplitude
# are valid, detect peak only once (variable: iter)
if iter == 0 and abs(position-n-window/2.0) < 3.0:
661     width = (square_sum)**2/fourth_sum           # width of peak
        iter = 1                                   # condition to detect peak only once
#     ## bug search
#     if width < 300 and amplitude < 1e6 and time[position]-position0 > 30:
#         print max(time)-time[position]>100, 'because time %f minus %f is %f'%(max(time),time[
position],max(time)-time[position])
666     # condition for blank like peaks (width, ampl, distance to peak before and last to
        chromatogram end)
        if width < 300 and amplitude < 1e6 and time[position]-position0 > 30 and max(time)-time[
position]>100:

            # get peak number
            peak_nr = peak_nr + 1
671     # calculate Area(s), Maximum, Integrationlimits and backgrounds by calling def gaussian
        Area_blank_like, Max_t, Max_m, start, end, back_const,bg-time, timeshift = gaussian(
            position, width, time, mass44, mass45, mass46, peak_nr, runs)
        # print type of found peak before optimization starts
        print '-----'
        print 'Blank-like peak found at %(a1)1.2f; peak number %(a2)1.0f' % {'a1': Max_t[0], '
a2': peak_nr}
676     # save the peak position to detect peak only once
        position0 = Max_t[0]

        # append results to result-arrays
        Maxima_time44.append(Max_t[0])           # time of Maximum 44
681     Maxima_time45.append(Max_t[1])           # time of Maximum 45
        Maxima_time46.append(Max_t[2])           # time of Maximum 46
        Maxima_value44.append(Max_m[0])         # Maximum 44 in value
        Maxima_value45.append(Max_m[1])         # Maximum 45 in value
        Maxima_value46.append(Max_m[2])         # Maximum 46 in value
686     Area_all44.append(Area_blank_like[0])    # complete Area 44
        Area_all45.append(Area_blank_like[1])    # complete Area 45
        Area_all46.append(Area_blank_like[2])    # complete Area 46
        peak_start.append(start)                # peak start
        peak_end.append(end)                    # peak end
691     peak_number.append(peak_nr)             # peak number
        background_const44.append(back_const[0]) # constant background 44
        background_const45.append(back_const[1]) # constant background 45
        background_const46.append(back_const[2]) # constant background 46
696     peak_type.append('Gauss')               # type of the peak

# print results
if timeshift[1] != 0 or timeshift[2] != 0:
    print '%(a0)s %(a1)13.4f %(a2)7.4f %(a3)7.4f %(a4)s %(a5)9.2f %(a6)s %(a7)5.2f' %
        {'a0': 'Blank-like Areas (nAs):', 'a1': Area_blank_like[0]*1e-6, 'a2':
Area_blank_like[1]*1e-6, 'a3': Area_blank_like[2]*1e-6, 'a4': 'peak start (s)
:', 'a5': time[start], 'a6': 'timeshift 45:', 'a7': timeshift[2]}
    print '%(a0)s %(a1)10.4f %(a2)7.4f %(a3)7.4f %(a4)s %(a5)11.2f %(a6)s %(a7)5.2f' %
        {'a0': 'constant backgrounds (nA):', 'a1': back_const[0]*1e-6, 'a2':
back_const[1]*1e-6, 'a3': back_const[2]*1e-6, 'a4': 'peak end (s):', 'a5':
time[end], 'a6': 'timeshift 46:', 'a7': timeshift[2]}
701     else:
        print '%(a0)s %(a1)13.4f %(a2)7.4f %(a3)7.4f %(a4)s %(a5)9.2f' % {'a0': 'Blank-
like Areas (nAs):', 'a1': Area_blank_like[0]*1e-6, 'a2': Area_blank_like[1]*1e
-6, 'a3': Area_blank_like[2]*1e-6, 'a4': 'peak start (s):', 'a5': time[start]}
        print '%(a0)s %(a1)10.4f %(a2)7.4f %(a3)7.4f %(a4)s %(a5)11.2f' % {'a0': 'constant
backgrounds (nA):', 'a1': back_const[0]*1e-6, 'a2': back_const[1]*1e-6, 'a3':
back_const[2]*1e-6, 'a4': 'peak end (s):', 'a5': time[end]}

# condition for rectangular peak (in general widths of around 200)
706 if width > 160 and amplitude > 1e6:

    # get peak number
    peak_nr = peak_nr + 1

711     # calculate Area, Integrationlimits and backgrounds by calling def rectangular
        Area_rec, start, end, back_const = rectangular(position, width, time, mass44, mass45,
mass46, runs)

    # save the peak position to detect peak only once
    position0 = time[position]

716     # append results to result-arrays
        Area_all44.append(Area_rec[0])           # complete Area 44
        Area_all45.append(Area_rec[1])           # complete Area 45
        Area_all46.append(Area_rec[2])           # complete Area 46
721     Maxima_time44.append(0)                 # no Maximum 44 selected
        Maxima_time45.append(0)                 # no Maximum 45 selected
        Maxima_time46.append(0)                 # no Maximum 46 selected

```

```

726     Maxima_value44.append(0)           # no Maximum 44 selected
       Maxima_value45.append(0)         # no Maximum 45 selected
       Maxima_value46.append(0)         # no Maximum 46 selected
       peak_start.append(start)         # peak start
       peak_end.append(end)             # peak end
       peak_number.append(peak_nr)      # peak number
731     background_const44.append(back_const[0]) # constant background 44
       background_const45.append(back_const[1]) # constant background 45
       background_const46.append(back_const[2]) # constant background 46
       peak_type.append('Rec')          # type of the peak

736     # print results
       print '-----'
       print 'Rectangular peak found at %(a1)1.2f; peak number %(a2)1.0f' % {'a1': time[
         position], 'a2': peak_nr}
       print '%(a0)s %(a1)20.4f %(a2)7.4f %(a3)7.4f %(a4)s %(a5)8.2f' % {'a0': 'Rec Areas (
         nAs):', 'a1': Area_rec[0]*1e-6, 'a2': Area_rec[1]*1e-6, 'a3': Area_rec[2]*1e-6, '
         a4': 'peak start (s):', 'a5': time[start]}
       print '%(a0)s %(a1)10.4f %(a2)7.4f %(a3)7.4f %(a4)s %(a5)10.2f' % {'a0': 'constant
         backgrounds (nA):', 'a1': back_const[0]*1e-6, 'a2': back_const[1]*1e-6, 'a3':
         back_const[2]*1e-6, 'a4': 'peak end (s):', 'a5': time[end]}

741     # condition for gaussian peak
       if width <=160 and amplitude > 1e6:

746         # get peak number
           peak_nr = peak_nr + 1

           # calculate Area(s), Maximum, Integrationlimits and backgrounds
           Area_gauss, Max_t, Max_m, start, end, back_const, bg_time, timeshift = gaussian(position
             , width, time, mass44, mass45, mass46, peak_nr, runs)
           # print type of found peak before optimization starts
           print '-----'
751         print 'Gaussian peak found at %(a1)1.2f; peak number %(a2)1.0f' % {'a1': Max_t[0], 'a2
           ': peak_nr}

           # save the peak position to detect peak only once
           position0 = Max_t[0]

756         # append results to result-arrays
           Maxima_time44.append(Max_t[0]) # time of Maximum 44
           Maxima_time45.append(Max_t[1]) # time of Maximum 45
           Maxima_time46.append(Max_t[2]) # time of Maximum 46
           Maxima_value44.append(Max_m[0]) # Maximum 44 in value
           Maxima_value45.append(Max_m[1]) # Maximum 45 in value
           Maxima_value46.append(Max_m[2]) # Maximum 46 in value
761         Area_all44.append(Area_gauss[0]) # complete Area 44
           Area_all45.append(Area_gauss[1]) # complete Area 45
           Area_all46.append(Area_gauss[2]) # complete Area 46
766         peak_start.append(start) # peak start
           peak_end.append(end) # peak end
           peak_number.append(peak_nr) # peak number
           background_const44.append(back_const[0]) # constant background 44
           background_const45.append(back_const[1]) # constant background 45
771         background_const46.append(back_const[2]) # constant background 46
           peak_type.append('Gauss') # type of the peak
           bg_times.append(bg_time)

           # print results
           if timeshift[1] != 0 or timeshift[2] != 0:
776             print '%(a0)s %(a1)18.4f %(a2)7.4f %(a3)7.4f %(a4)s %(a5)8.2f %(a6)s %(a7)4.2f' %
               {'a0': 'Gauss Areas (nAs):', 'a1': Area_gauss[0]*1e-6, 'a2': Area_gauss[1]*1e
                 -6, 'a3': Area_gauss[2]*1e-6, 'a4': 'peak start (s):', 'a5': time[start], 'a6
                 ': 'timeshift 45:', 'a7': timeshift[1]}
             print '%(a0)s %(a1)10.4f %(a2)7.4f %(a3)7.4f %(a4)s %(a5)10.2f %(a6)s %(a7)4.2f'
               % {'a0': 'constant backgrounds (nA):', 'a1': back_const[0]*1e-6, 'a2':
                 back_const[1]*1e-6, 'a3': back_const[2]*1e-6, 'a4': 'peak end (s):', 'a5':
                 time[end], 'a6': 'timeshift 46:', 'a7': timeshift[2]}
           else:
             print '%(a0)s %(a1)18.4f %(a2)7.4f %(a3)7.4f %(a4)s %(a5)8.2f' % {'a0': 'Gauss
               Areas (nAs):', 'a1': Area_gauss[0]*1e-6, 'a2': Area_gauss[1]*1e-6, 'a3':
               Area_gauss[2]*1e-6, 'a4': 'peak start (s):', 'a5': time[start]}
             print '%(a0)s %(a1)10.4f %(a2)7.4f %(a3)7.4f %(a4)s %(a5)10.2f' % {'a0': 'constant
               backgrounds (nA):', 'a1': back_const[0]*1e-6, 'a2': back_const[1]*1e-6, 'a3':
               back_const[2]*1e-6, 'a4': 'peak end (s):', 'a5': time[end]}

781         # condition to detect each peak only once
           if iter != 0 and abs(position-n-window/2.0) > 4.0:
               iter = 0

786     # print the number of found peaks in the data
       print '-----'
       print 'Number of peaks found:', peak_number[-1]
       print
       #print bg_times
791     #figures[runs].get_axes()[0].set_ylim(100,150)#(min(background_const45)-(min(background_const45)
       /10)),(max(background_const46)+(max(background_const46)/10))
       #figures[runs].get_axes()[0].set_xlim(bg_times[1]-30,bg_times[1]+10)
       #figures[runs].get_axes()[0].set_xlim(bg_times[2]-30,bg_times[2]+10)

```

```

#figures[runs].get_axes()[0].set_view_interval(mean(bg_times[2])-30,mean(bg_times[2])+10,ignore=
    False)
return mass_prime44, Maxima_time44, Maxima_value44, Area_all44, background_const44, mass_prime45,
    Maxima_time45, Maxima_value45, Area_all45, background_const45, mass_prime46, Maxima_time46,
    Maxima_value46, Area_all46, background_const46, peak_start, peak_end, peak_type
796 #####

def rectangular(position, width, time, mass44, mass45, mass46,runs):
    """
801     Subprogram to find the area of a rectangular peak as identified before.
    A constant background is removed from the data.
    The Area, peak start, peak end and the constant background value is returned
    for all three masses.
    """
806     # define start parameters
    iter = 0
    Area = []
    peak_start = 0
    peak_end = 0
811     rec_bgrd = []
    resistances = [resist44, resist45, resist46]

    # # Debug
    # print 'Debug'
816 # print position, width, time, mass44, mass45, mass46

    # start scanning the peak for the limits
    for n in range(int(position)-int(width), int(position)+int(width)):
821         if n > len(time)-11:
            print 'Measurement stopped too early!'
            print
            sleep(60)
            Area = ones(3)
            bgrd_const = ones(3)
826         # get results of the complete detected peaks
        else:
            # get the derivation of the peak
            Derivation = derivat(n, time, mass44, 10.0)
831             # detect left peak limit using Derivation
            if iter == 0 and Derivation > start_slope_rec:
                # get peak start
                iter = 1
                peak_start = n
836             if iter != 0 and iter < 2 and Derivation <= -6e4:
                iter = 2
                # get peak end
                while Derivation < end_slope_rec:
                    n = n + 1
                    Derivation = derivat(n, time, mass44, 10.0)
                    peak_end = n
846             # integrate only in small range if intended according to time_interval
            if integrate_rec_small == 'on':
                peak_start_new = int((peak_end-peak_start)/2.)+peak_start-int(0.5*time_interval/
                    timestep)
                peak_end_new = int((peak_end-peak_start)/2.)+peak_start+int(0.5*time_interval/
                    timestep)
851             else:
                peak_start_new = peak_start
                peak_end_new = peak_end

            # get area under peak
            CG = 0
856             for mass in [mass44, mass45, mass46]:
                # get the constant peak background
                rec_bg, bg_time = background(time, mass, peak_start, resistances[CG],runs)
                rec_bgrd.append(rec_bg)
861             # calculate area
            rec_integrate = mass[peak_start_new:peak_end_new]-rec_bg*ones(len(mass[
                peak_start_new:peak_end_new]))
            Area.append(scipy.integrate.simps(rec_integrate, time[peak_start_new:peak_end_new]))
            CG = CG + 1
866     return Area, peak_start_new, peak_end_new, rec_bgrd

#####

def gaussian(position, width, time, mass44, mass45, mass46, peak_nr,runs):
871     """
    Subprogram to get the area under a gaussian peak as identified before.
    A constant background in front of the peak is.
    The Area, peak start, peak end, the Maxima in position and
    value as well as the background signal are returned for all three masses.
876     # define start parameters
    iter = 0
    Area = []
    peak_start = 0
881     peak_end = 0

```



```

Maxima_time = []
Maxima_value = []
bgrd_const = []
bgrd_times = []
886 timeshift_array = []
resist = [resist44, resist45, resist46]
slope_detect_start = start_slope_gauss
mass_pcuts=[]
Uncut_Area=[]
891 # Just if the peak limits are recognized successfully iter gets 3, so reduce the Derivation
      detection limit successively until it finds the peak start
while iter < 3 and slope_detect_start > 50:
    # start scanning the detected 44 peak for the limits using the given window position-width <-->
    position+width
    for n in range(int(position)-int(width), int(position)+int(width)):
        # define abort condition if measurement stopped during peak
896         if n > len(time)-11:
            print 'Measurement stopped too early!'
            print
            sleep(60)
            Area = ones(3)
901             bgrd_const = ones(3)
            Maxima_time = ones(3)
            Maxima_value = ones(3)

        # get the derivation of the peak
906         Derivation = derivat(n, time, mass44, 10.0)
         Derivation0 = derivat(n-1, time, mass44, 10.0)

        # detect left peak limit using Derivation
911         if iter == 0 and Derivation > slope_detect_start:
            # get peak start
            iter = 1
            peak_start = n-12
            if peak_nr > 4 and Debug:
                print '\nPstart: %1.2f,Pstart time: %1.2f,Derivation: %1.2f, slope_detect_start:
916                 %1.2f\n' %(peak_start, time[peak_start],Derivation, slope_detect_start)
            # get two different background signals for all three masses
            CG = 0
            for mass in [mass44, mass45, mass46]:
                bg_const, bg_time = background(time, mass, peak_start, resist[CG], runs)
921                 bgrd_const.append(bg_const)
                bgrd_times.append(bg_time)
                CG = CG + 1

        # get peak end
926         if iter != 0 and iter < 3 and Derivation <= -9e3:
            # continue peak scan
            if 'slope' in method.end:
                #print "Ding"
                #end_slope_gauss=-100 # tbr => just for a defined peak end cut
                while Derivation < end_slope_gauss:
931                     n = n+1
                     Derivation = derivat(n, time, mass44, 10.0)
                     ## Start DEBUG entry for a defined peak end cut
                     if n in range(21500,22500): #tbr => just for a defined peak end cut
936                         end_slope_gauss=-82426.8
                     else:
                         end_slope_gauss=-100
                         peak_end = n
                         ## End DEBUG Entries
                         peak_end = n+20 # default
941                         ## Start DEBUG entries for a defined peak end cut
                         if peak_end in range(22000,23000): #
                             peak_end = 22170
                             print derivat(peak_end, time, mass44, 10.0)
                             if peak_end > len(time):
946                                 print 'Peak End exceeds boundaries!'
                         if Debug:
                             print '\nPEnd time: %1.2f,Derivation: %1.2f, end_slope_gauss: %1.2f' %(time[
                                 peak_end],Derivation, end_slope_gauss)
                             ## End DEBUG Entries
                else:
951                     summe = 1000.0
                     while abs(summe/10.0-bgrd_const[0])>bgrd_const[0]+2e6:
                         n = n + 1
                         summe = sum(mass44[n:n+10])
956                         peak_end = n-10

                     ## Start DEBUG entry
                     if peak_nr == 7:
                         peak_end = peak_end -270

961 #         r_fig=pylab.figure(42,figsize = (6, 5))
#         figures[runs].get_axes()[2]=r_fig.add_subplot(111, autoscale_on=True)
#         #pylab.axis([-2, 22, -0.2, 0.2])
#         figures[runs].get_axes()[2].plot(time[peak_start-(bg_shift+bg_average):peak_end], (
mass45[peak_start-(bg_shift+bg_average):peak_end]-bgrd_const[1])/(mass44[peak_start-(bg_shift+
bg_average):peak_end]-bgrd_const[0]), 'bo-')
#         figures[runs].get_axes()[2].plot(time[peak_start-(bg_shift+bg_average):peak_end], (
mass46[peak_start-(bg_shift+bg_average):peak_end]-bgrd_const[2])/(mass44[peak_start-(bg_shift+
bg_average):peak_end]-bgrd_const[0]), 'go-')

```

```

966     # definition of chromatogram number
    CG = 0

971     # get results for all three masses
    for n,mass in enumerate([mass44, mass45, mass46]):
        # get peak maximum in time and position
        position_new = peak_start+argmax(mass[peak_start:peak_end])
        # make a spline fit around the center of gravity position
        # of the peak to find the real maxima => def splinefit
976         raster = 7
        left_lim = int(position_new)-raster
        right_lim = int(position_new)+raster
        peak_time_enlarged, peak_value_enlarged = splinefit(time[left_lim:right_lim], mass[
            left_lim:right_lim], enlargement)
        # save the splinefit Maxima and their position
981         Maxima_time.append(peak_time_enlarged[argmax(peak_value_enlarged)])
        Maxima_value.append(max(peak_value_enlarged))

    # define the peak arrays in time and mass
    if "cut" in method_end:
986         #print "Pre-Cut indices P.Start/Max/End: %s/%s/%s"%(peak_start, position_new,
            peak_end)
            peak_cut=position_new+p_cut_off
            if Debug:# n == 0 and
                print "\nMass %s Pre-/Post-Cut Indices P.Start/End: %s/%s - %s/%s\n"
                    "%([44,45,46][n], peak_start, peak_end, peak_start, peak_cut)
                print "Difference in Indices/ Time: %s / %s"%(peak_end-peak_cut, time[
                    peak_end]-time[peak_cut])
991                 print "Background Time: %s"%(bgrd_times[CG])
                peak_time = time[peak_start:peak_cut]
                peak_value = mass[peak_start:peak_cut]
            else:
996                 peak_time = time[peak_start:peak_end]
                peak_value = mass[peak_start:peak_end]

    # get complete peak area (including second peak, background already removed)
    area_all_int = peak_value-bgrd_const[CG]*ones(len(peak_value))

1001

    # apply timeshift if intended
    if timeshift_application == 'on':
        timeshift = Maxima_time[CG]-Maxima_time[0]

1006

        # plot the timeshift
        ts_fig=pylab.figure(8,figsize = (6, 5))
        ts_sbplt=ts_fig.add_subplot(111, autoscale_on=False)
        #pylab.axis([-2, 22, -0.2, 0.2])
        ts_sbplt.set_title('Timeshift to mass44 of each peak')
1011        ts_sbplt.set_xlim(-2, 22)
        ts_sbplt.set_ylim(-0.2, 0.2)
        ts_sbplt.set_xticks(10*arange(3),('Mass44', 'Mass45', 'Mass46'))
        ts_sbplt.set_ylabel('timeshift to mass44 (s)')
        ts_sbplt.plot([10*CG], [timeshift], 'bo')

1016

        # get the timeshift correction
        timeshift_correction = (peak_value[-1]-peak_value[0])*timeshift
        timeshift_array.append(timeshift)

1021

    else:
        timeshift_correction = 0
        timeshift_array.append(0)

    # append Area to array
1026    Area.append(scipy.integrate.simps(area_all_int, peak_time)+timeshift_correction)

    # plot the fit curve and peak sections to the raw-data if intended
    if plot_gauss_bounds == 'on':
1031        chrom_sfl_plots.append(('Uncut Peak as line',time[peak_start:peak_end], mass[
            peak_start:peak_end]*resist[CG]*fac, 'g-'))
        chrom_sfl_plots.append(('Peak Max. Splines',peak_time_enlarged,
            peak_value_enlarged*resist[CG]*fac, 'r-'))
        #figures[runs].get_axes()[0].plot(peak_time, peak_value*resist[CG]*fac, 'g-')
        #figures[runs].get_axes()[0].plot(peak_time_enlarged, peak_value_enlarged*
            resist[CG]*fac, 'r-', lw=2)
        if "cut" in method_end:
1036            mass_pcuts.append(mass[peak_cut]*resist[CG]*fac) # retrieve the scaled y-value
                for determination of plot y-limits
            Uncut_Area.append(scipy.integrate.simps(mass[peak_start:peak_end]-bgrd_const[CG]*
                ones(len(mass[peak_start:peak_end])), time[peak_start:peak_end])+
                timeshift_correction) #calculate the Area with normal slope end
        # prepare for next chromatogram
        CG = CG + 1
        iter = 3
1041    if "cut" in method_end:
        peak_cuts.append(mass_pcuts)
        Peak_Area_cut.append(Area)
        Peak_Area_Uncut.append(Uncut_Area)
    if plot_gauss_bounds == 'on':
1046        if iter != 0:

```

```

chrom_r45_plots.append((time[peak_start-(bg_shift+bg_average):peak_end], (mass45[
    peak_start-(bg_shift+bg_average):peak_end]-bgrd_const[1])/(mass44[peak_start-(
    bg_shift+bg_average):peak_end]-bgrd_const[0]), 'b.-'))
chrom_r46_plots.append((time[peak_start-(bg_shift+bg_average):peak_end], (mass46[
    peak_start-(bg_shift+bg_average):peak_end]-bgrd_const[2])/(mass44[peak_start-(
    bg_shift+bg_average):peak_end]-bgrd_const[0]), 'm.-'))
chrom_r45_plots.append((time[peak_start], [(mass45[peak_start]-bgrd_const[1])/(mass44
    [peak_start]-bgrd_const[0]), 'r|'))
chrom_r46_plots.append((time[peak_start], [(mass46[peak_start]-bgrd_const[2])/(mass44
    [peak_start]-bgrd_const[0]), 'r|'))
1051 chrom_r45_plots.append((time[peak_end], [(mass45[peak_end]-bgrd_const[1])/(mass44[
    peak_end]-bgrd_const[0]), 'r|'))
chrom_r46_plots.append((time[peak_end], [(mass46[peak_end]-bgrd_const[2])/(mass44[
    peak_end]-bgrd_const[0]), 'r|'))
chrom_r45_plots.append((Maxima.time[1], [(mass45[argmax(mass44[left_lim:right_lim])]-
    bgrd_const[1])/(mass44[argmax(mass44[left_lim:right_lim])]-bgrd_const[0]), 'rv'))
chrom_r46_plots.append((Maxima.time[2], [(mass46[argmax(mass44[left_lim:right_lim])]-
    bgrd_const[2])/(mass44[argmax(mass44[left_lim:right_lim])]-bgrd_const[0]), 'rv'))
    # time[argmax(mass44[left_lim:right_lim])]
1056 slope_detect_start = slope_detect_start-5
if slope_detect_start < start_slope_gauss-5:
    print "!!! Attention !!!\nThe peak start slope threshold had to be reduced\nfrom %s
        (header value) to %s in order\nto find the peak start."%(start_slope_gauss,
        slope_detect_start)
## If no Peak is detectable at all, fill everything with dummy values
if iter== 0 and peak_start== 0 and peak_end== 0 :
1061     print 'Could not characterize the detected peak, so i fill it with dummy values'
    Area = ones(3)
    bgrd_const = ones(3)
    Maxima.time = ones(3)
    Maxima.value = ones(3)
    peak_start = int(position)-int(width)
1066     peak_end = int(position)+int(width)

    return Area, Maxima.time, Maxima.value, peak_start, peak_end, bgrd_const, bg_time, timeshift_array

#####
1071 # final calculation definitions
#####

def calc_isotop(Area44_array, Area45_array, Area46_array):
    """
1076 Subprogram to calculate the isotopic ratios d13C and d18O from the
    obtained peak areas.
    First of all, the scale is changed to VPDBCO2 using global constants.
    Afterwards, a system of equation is solved for each peaks leading to
    the Ratios for 13R, 17R and 18R in VPDBCO2. This is used to get the
1081 isotopy of oxygen and carbon in per mill.
    """
    # define arrays, the different WMG ratios will get stored to
    R_samp_WMG_45_array = []
1086 R_samp_WMG_46_array = []

    # change the scale from working-measurement-gas (WMG) to VPDBCO2
    for i in arange(len(Area44_array)):
        ## get the ratios 46 and 45 in WMG scale
1091 Area44 = Area44_array[i]
        Area45 = Area45_array[i]
        Area46 = Area46_array[i]

        R_samp_WMG_45 = (Area45)/(Area44)
1096 R_samp_WMG_46 = (Area46)/(Area44)
        R_samp_WMG_45_array.append(R_samp_WMG_45)
        R_samp_WMG_46_array.append(R_samp_WMG_46)

    ## define the characteristic ratios for the WMG by calculating a mean over all rectangular peaks
1101 R_WMG_45_running = 0
    R_WMG_46_running = 0
    for ref_peak_nr in ref_peaks: # sum up all peak WMG ratios
        R_WMG_45_running = R_WMG_45_running + R_samp_WMG_45_array[ref_peak_nr-1]
        R_WMG_46_running = R_WMG_46_running + R_samp_WMG_46_array[ref_peak_nr-1]
1106 R_WMG_45 = R_WMG_45_running/len(ref_peaks) # calculate the mean for Mass45
    R_WMG_46 = R_WMG_46_running/len(ref_peaks) # calculate the mean for Mass46

    # calculate the delta values using Craig correction
    if correction_method == 'Craig':
1111 d_18_samp_VPDBCO2_array, d_13_samp_VPDBCO2_array = Craig(R_samp_WMG_45_array,
        R_samp_WMG_46_array, R_WMG_45, R_WMG_46)
        R_samp_45_array = R_samp_WMG_45_array # left unchanged
        R_samp_46_array = R_samp_WMG_46_array

    # calculate the delta values using Santrock correction
1116 if correction_method == 'Santrock':
        R_samp_46_array, R_samp_45_array, d_18_samp_VPDBCO2_array, d_13_samp_VPDBCO2_array = Santrock(
            R_samp_WMG_45_array, R_samp_WMG_46_array, R_WMG_45, R_WMG_46)

    return R_samp_46_array, R_samp_45_array, d_18_samp_VPDBCO2_array, d_13_samp_VPDBCO2_array,
        R_samp_WMG_45_array, R_samp_WMG_46_array
1121 #####

```

```

#####
def Santrock(R_samp_WMG_45_array, R_samp_WMG_46_array, R_WMG_45, R_WMG_46):
    """
    1126     calculate the delta values using Santrock correction
    """
    d_18_samp_VPDBCO2_array = []
    d_13_samp_VPDBCO2_array = []
    R_samp_VPDBCO2_45_array = []
    1131     R_samp_VPDBCO2_46_array = []

    # get the characteristic ratios for the reference material (RM) (NBS-19-CO2)
    R_RM_45 = R_13_VPDBCO2*(dC_13_RM_VPDBCO2+1.0)+2*R_17_VPDBCO2*(dO_18_RM_VPDBCO2+1.0)**a
    R_RM_46 = 2*R_17_VPDBCO2*(dO_18_RM_VPDBCO2+1.0)**a*R_13_VPDBCO2*(dC_13_RM_VPDBCO2+1.0) + (
    1136         R_17_VPDBCO2*(dO_18_RM_VPDBCO2+1.0)**a)**2 + 2*R_18_VPDBCO2*(dO_18_RM_VPDBCO2+1.0)

    # start the calculation of the deltas d13C, d18O for each peak
    for i in arange(len(R_samp_WMG_45_array)):
        # get peak number
        peak_number = i + 1
    1141

        # get isotopy of result
        d_45_samp_WMG = R_samp_WMG_45_array[i]/R_WMG_45 - 1.0
        d_46_samp_WMG = R_samp_WMG_46_array[i]/R_WMG_46 - 1.0

    1146         # change the 45R and 46R ratios to VPDBCO2 scale
        R_samp_VPDBCO2_45 = R_RM_45*(d_45_samp_WMG+1.0)
        R_samp_VPDBCO2_46 = R_RM_46*(d_46_samp_WMG+1.0)
        R_samp_VPDBCO2_45_array.append(R_samp_VPDBCO2_45)
        R_samp_VPDBCO2_46_array.append(R_samp_VPDBCO2_46)
    1151

        # start values for the iteration to get 18R
        R_samp_VPDBCO2_18 = R_samp_VPDBCO2_46/2.0
        R_samp_VPDBCO2_18_new = R_samp_VPDBCO2_46/3.0

    1156         # start while loop to solve equation
        while abs(R_samp_VPDBCO2_18_new-R_samp_VPDBCO2_18)>10**(-12):
            R_samp_VPDBCO2_18 = R_samp_VPDBCO2_18_new
            A = 2*K*R_samp_VPDBCO2_45*R_samp_VPDBCO2_18**(a-2)
            B = 2-3*K**2*R_samp_VPDBCO2_18**(2.0*a-1.0)
    1161             C = -R_samp_VPDBCO2_46
            R_samp_VPDBCO2_18_new = (-B+(B**2-4*A*C)**(0.5))/(2.0*A)
            R_samp_VPDBCO2_18 = R_samp_VPDBCO2_18_new

        # print optimized results
        if print_optimized_results == 'on':
            print '-----',
            print '%(a0)s %(a1)13.0f' % {'a0': 'peak number:', 'a1': peak_number}
            print '%(a0)s %(a1)13.2f' % {'a0': 'd45_samp_WMG:', 'a1': d_45_samp_WMG*1000.0}
            print '%(a0)s %(a1)13.2f' % {'a0': 'd46_samp_WMG:', 'a1': d_46_samp_WMG*1000.0}
    1171             print '%(a0)s %(a1)13.2g' % {'a0': 'Optimized value:', 'a1': -R_samp_VPDBCO2_46 + 2*
                R_samp_VPDBCO2_18+2*R_samp_VPDBCO2_18**a*K*R_samp_VPDBCO2_45-3*R_samp_VPDBCO2_18**(2*a
                )*K**2}
            print

        # calculate the ratios 17R (oxygen) and 13R (carbon)
        R_samp_VPDBCO2_17 = R_samp_VPDBCO2_18**a*K
    1176         R_samp_VPDBCO2_13 = R_samp_VPDBCO2_45 - 2*R_samp_VPDBCO2_17

        # calculate the isotopies d18O and d13C in VPDBCO2 (in per mill)
        d_18_samp_VPDBCO2_array.append((R_samp_VPDBCO2_18/R_18_VPDBCO2-1.0)*1000.0)
        d_13_samp_VPDBCO2_array.append((R_samp_VPDBCO2_13/R_13_VPDBCO2-1.0)*1000.0)
    1181

    return R_samp_VPDBCO2_46_array, R_samp_VPDBCO2_45_array, d_18_samp_VPDBCO2_array,
        d_13_samp_VPDBCO2_array

#####
def Craig(R_samp_WMG_45_array, R_samp_WMG_46_array, R_WMG_45, R_WMG_46):
    """
    calculate the delta values using Craig correction
    1191
    """
    d_18_samp_VPDBCO2_array = []
    d_13_samp_VPDBCO2_array = []

    for i in arange(len(R_samp_WMG_45_array)):
        # get peak number
        peak_number = i + 1
    1196

        # get isotopy of result referred to reference peak
        d_45_samp_WMG = R_samp_WMG_45_array[i]/R_WMG_45 - 1.0
        d_46_samp_WMG = R_samp_WMG_46_array[i]/R_WMG_46 - 1.0
    1201

        # get isotopies d13C, d18O referred to reference peak
        d_13_samp_WMG = (C1*d_45_samp_WMG-C2*C3*d_46_samp_WMG)/(1.0-C2*C4)
        d_18_samp_WMG = (C3*d_46_samp_WMG-C1*C4*d_45_samp_WMG)/(1.0-C2*C4)

    1206         # change to VPDB standard scale
        d_13_samp_VPDBCO2 = 1000.0*(d_13_samp_WMG + dC_13_RM_VPDBCO2 + (dC_13_RM_VPDBCO2*d_13_samp_WMG)
        )

```

```

d_18_samp_VPDBCO2 = 1000.0*(d_18_samp_WMG + dO_18_RM_VPDBCO2 + (dO_18_RM_VPDBCO2*d_18_samp_WMG)
)
# calculate the isotopies d18O and d13C in VPDBCO2 (in per mill)
1211 d_13_samp_VPDBCO2_array.append(d_13_samp_VPDBCO2)
d_18_samp_VPDBCO2_array.append(d_18_samp_VPDBCO2)
return d_18_samp_VPDBCO2_array, d_13_samp_VPDBCO2_array
1216 #####
# tools used in other definitions
#####
if derivat_method == 'sum':
1221 def derivat(i, x_data, y_data, length):
    """
    Calculates the gradient between two neighbored data-points and averages
    the gradients over 'length' calculated gradients.
    """
    1226 d_average = 0
    for k in range(int(length)):
        d_average = d_average + (y_data[i+k+1]-y_data[i+k])/(x_data[i+k+1]-x_data[i+k])
    return d_average/length
1231 else:
    def derivat(i, x_data, y_data, length):
        """
        Calculates the linear regression of 'length' data-points.
        """
    1236 # define subprogram
    def derivation_fit(x0, x_data_to_fit, y_data_to_fit):
        """
        Subprogram, that finds the linear fit to the data.
        """
    1241 fit_func = x_data_to_fit*x0[0]+x0[1]
        # err is the deviation which is to be optimized
        err = sum((fit_func-y_data_to_fit)**2)
    1246 return err
        # get linear fit of the data
        x0 = x_fit_array[-1]
        x_fit = scipy.optimize.fmin(derivation_fit, x0, args=(x_data[i:i+length+1], y_data[i:i+length
        +1]), disp=0)
    1251 # append results to array for plotting and limit detection
        x_fit_array.append(x_fit)
        x_fit_position.append(x_data[i+int(length/2.0)])
    1256 # plot the linear graph if intended
        if plot_derivation == 'on':
            pylab.figure(30)
            pylab.plot(x_data[i:i+length+1], x_data[i:i+length+1]*x_fit[0]+x_fit[1], 'k-')
    1261 return x_fit[0]
#####
def splinefit(input_x, input_y, enlargement):
1266 """
    Subprogram to find the splinefit of 3rd order of the 1D array input_y
    in the range input_x and extend the data to output_x. output_y is returned.
    Args: input data for x and y and the factor, the x-axis shall be enlarged/
    depend.
    """
    1271 splinefit = scipy.interpolate.splrep(input_x, input_y, s=0)
        output_x = arange(min(input_x), max(input_x)+1.0/enlargement, 1.0/enlargement)
        output_y = scipy.interpolate.splev(output_x, splinefit)
    1276 return output_x, output_y
#####
def background(data_x, data_y, end_point, resist, runs):
    """
    1281 Get the background data, that has to be subtracted from the raw data.
        # set the plot length
        plot_length = 0.0
    1286 # get the x- and y-data the spline will be made to
        bg_time = data_x[end_point-plot_length-bg_shift-bg_average: end_point+1-bg_shift]
        bg_value = data_y[end_point-plot_length-bg_shift-bg_average: end_point+1-bg_shift]
    1291 background_const = sum(data_y[end_point-bg_average-1-bg_shift: end_point-1-bg_shift])/bg_average
        # plot the background values to the raw-data if intended
        if plot_gauss_bounds == 'on':
            chrom_sfl_plots.append(('Bckgr.', bg_time, background_const*ones(len(bg_value))*resist*fac, 'm
            -'))
            #figures[runs].get_axes()[0].plot(bg_time, background_const*ones(len(bg_value))*resist*fac, 'm
            -', lw=3)
1296

```

```

    return background_const, mean(bg_time)

#####
1301 def creation_time_array(act_dir):
    '''
    Sort data folder names in the given directory according to its creation time and return sorted
    folder and utc info
    '''
    creation_time_utc = []
1306 # list the folders placed in specified data folder directory
    folders = os.listdir(act_dir)
    # get the creation time of each datafolder
    # locale.setlocale(locale.LC_ALL, 'en_US.UTF-8') # set the locale info to english to understand the
    date format
1311 for name in folders:
    # Read header information for time & date of the measurement converted to utc seconds
    file=open(act_dir+'/'+name+'/HEADER.TXT')
    for i in range(4):
        line = file.readline()
        if i == 2: # Read in the Masslynx generated "Acquired Date:" information in the format
            e.g. "31-Oct-2008"
1316         date = line[18:-2] # the 'readline' command also reads line-terminations (in unix
            case \r\n => last 2 chars)
        if i == 3: # Read in the Masslynx generated "Acquired Time:" information in the format
            e.g. "11:07:18"
            date_time = line[18:-2] # the 'readline' command also reads line-terminations (in
            unix case \r\n => last 2 chars)
            # Calculate the exact measurement time
            # print date+date_time
1321         utc_time = mktime(strptime(date+date_time, "%d-%b-%Y%H:%M:%S")) # translate the
            date and date_time info to utc
            creation_time_utc.append(utc_time)
        # close file
        file.close()

1326 # sort the data folders for the oldest first
    sorted_indices = argsort(creation_time_utc)
    # print len(sorted_indices), sorted_indices, len(folders), folders, len(array(folders)), array(folders)
    , len(creation_time_utc), creation_time_utc
    folders_sort = array(folders).take(sorted_indices)
    creation_time_utc = array(creation_time_utc).take(sorted_indices, axis=-1)
1331 return folders_sort, creation_time_utc

#####
1336 # plotting procedures
#####
def plotting(datafile, mass, time, Maxima_position, Amplitude, start, end, mass_prime, Area, resistance
    , dC_13_rec, dC_13_gauss, already_peaks_rec, already_peaks_gauss, type_file, runs):
    """
    Subprogram, that plots the raw-data and the results for an immediate analysis of the current data-
    set.
1341 """
    ## define the plotted labels and text
    # labels = ['mass 44', 'mass 45', 'mass 46']
    Amplitude_scaled = [1]
    if type_file == 'Ref':
1346         label = datafile.rsplit('/',2)[1][7:-4]
        elif type_file == 'Refloop':
            # label = datafile.rsplit('/',2)[1][7:14]+datafile.rsplit('/',2)[1][-8:-4]

            label = datafile.rsplit('/',2)[1][7:-4]
1351
        elif file_type[runs] == 'RefAir':
            label = datafiles[runs].rsplit('/',2)[1][7:-4]
        else:
            label = datafile.rsplit('/',2)[1][datafile.rsplit('/',2)[1].find('ED'):datafile.rsplit('/',2)
            [1].find('G0')+3]+'-'+type_file
1356
    ## plot the raw-data and the maxima of the peaks
    chrom_sf1_plots.append(('raw data', time, mass*resistance*fac, '.'))
    # figures[runs].get_axes()[0].plot(time, mass*resistance*fac, '.')
    for i in Amplitude:
1361         Amplitude_scaled.append(i*resistance*fac)
    chrom_sf1_plots.append(('Pos. Maxima Marker', Maxima_position, Amplitude_scaled, 'cv'))
    # figures[runs].get_axes()[0].plot(Maxima_position, Amplitude_scaled, 'cv', ms=5)
    # plot the integration limits to the raw-data
    for begin in start:
1366         chrom_sf1_plots.append(('Peak Start Marker', [time[begin]], [mass[begin]*resistance*fac], 'r|'))
        # figures[runs].get_axes()[0].plot([time[begin]], [mass[begin]*resistance*fac], 'r|', ms=10)
    for finish in end:
        chrom_sf1_plots.append(('Peak End Marker', [time[finish-1]], [mass[finish-1]*resistance*fac], 'r
        |'))
        # figures[runs].get_axes()[0].plot([time[finish-1]], [mass[finish-1]*resistance*fac], 'r|', ms
        =10)
1371 # figures[runs].get_axes()[0].autoscale_view(tight=True, scalex=True, scaley=True)
    # plot the derivation of the raw-data in a subplot
    if chrom_deriv is 'on':
        if derivat_method == 'fit':
            if resistance == resist44:

```

```

1376         x_fit_plot = []
            for x_fit in x_fit_array:
                x_fit_plot.append(x_fit[0])
            drv_sbplt1.plot(x_fit_position, x_fit_plot[1:], 'r.')
        else:
1381         drv_sbplt1.plot(time[1:-window]+10*timestep*ones(len(time[1:-window])), mass_prime, 'r-')
#         if resistance == resist44:
#             ## add a label to the actual chromatogram
#             figures[runs].get_axes()[0].text((min(time)+max(time))/2-len(label)*25,2000, label, fontsize
#             =6) #, bbox=dict(facecolor='grey', alpha=0.1) Enter text in subplot object
1386         if chrom_peak_char is 'on':
#             ## plot the d13C isotopies of all ref peaks for intermediate control of the system
#             functionality
            chr_sub3.plot(arange(already_peaks_rec+1, already_peaks_rec+1+len(dC_13_rec)), dC_13_rec, 'bo
            -')
#rcParams['text.usetex']=False
            if type_file == 'Ref' or type_file == 'Refloop' and int(label.split('-')[2]) %2 == 0:
                chr_sub3.annotate(label, xy=(already_peaks_rec+(len(dC_13_rec)/2) +0.5,mean(dC_13_rec)),
                xytext=((already_peaks_rec+2 -0.6),(min(dC_13_rec)+(mean(dC_13_rec)*0.0002))),
                xycoords='data',textcoords='data', arrowprops=dict(edgecolor='red', facecolor='red',
                width= 1,headwidth=4, shrink=0.05),fontsize=8)
1391         else:
            chr_sub3.annotate(label, xy=(already_peaks_rec+(len(dC_13_rec)/2) +0.5,mean(dC_13_rec)),
            xytext=((already_peaks_rec+2 -0.6),(max(dC_13_rec)-(mean(dC_13_rec)*0.0002))),
            xycoords='data',textcoords='data', arrowprops=dict(edgecolor='red', facecolor='red',
            width= 1,headwidth=4, shrink=0.05),fontsize=8)
#rcParams['text.usetex']=True
#             ## plot the d13C isotopies of all gauss peaks for intermediate control of the system
#             functionality
            chr_sub4.plot(arange(already_peaks_gauss+1, already_peaks_gauss+1+len(dC_13_gauss)),
            dC_13_gauss, 'ko-')
1396         if not len(dC_13_gauss) == 0:
            if type_file == 'Ref' or type_file == 'Refloop' and int(label.split('-')[2]) %2 == 0:
                chr_sub4.annotate(label, xy=(already_peaks_gauss+(len(dC_13_gauss)/2) +0.5,mean(
                dC_13_gauss)), xytext=(already_peaks_gauss+(len(dC_13_gauss)/2),min(dC_13_gauss)+(
                mean(dC_13_gauss)*0.001))), xycoords='data',textcoords='data', arrowprops=dict(
                edgecolor='cyan', facecolor='cyan',width= 1,headwidth=4, shrink=0.05), fontsize=8)
            else:
                chr_sub4.annotate(label, xy=(already_peaks_gauss+(len(dC_13_gauss)/2) +0.5,mean(
                dC_13_gauss)), xytext=(already_peaks_gauss+(len(dC_13_gauss)/2),(max(dC_13_gauss)-(
                mean(dC_13_gauss)*0.001))), xycoords='data',textcoords='data', arrowprops=dict(
                edgecolor='cyan', facecolor='cyan',width= 1,headwidth=4, shrink=0.05), fontsize=8)
1401         #chr_sub4.text(chr_sub4.get_xlim()[1]-len(dC_13_gauss)/2,sum(dC_13_gauss)/len(dC_13_gauss)
            +0.15, label, fontsize=10) # Enter text in subplot object chr_sub4.get_xlim()[1]-len(
            dC_13_gauss)/2

#print len([already_peaks_gauss+3]),len(dC_13_gauss)
            if type_file != 'Ref' and len(dC_13_gauss)>=3:
#             highlight the sample peaks in green color (simulations and samples)
1406             chr_sub4.plot([already_peaks_gauss+3], [dC_13_gauss[2]], 'go')

1411 #####
#             -Main Calculation Routine-
#####
# define main program to get the isotopic results for the current datafile
1416 def main(datafile, time_start, already_peaks_rec, already_peaks_gauss, type_file, runs):
#         read raw-data
            data = read_data(datafile)
1421         # store raw-data in columns
            time = arange(len(data[:, 0])*timestep+timestep*ones(len(data[:, 0]))+time_start*ones(len(data[:,
            0])))
            mass44 = data[:, 0]
            mass45 = data[:, 1]
            mass46 = data[:, 2]
1426         # plot the derivation of the raw data
            if plot_derivation == 'on' and derivat.method != 'sum':
                pylab.figure(30)
                pylab.title('Raw data and the gradient of the data points')
1431                 pylab.ylabel('Intensity/fA')
                pylab.xlabel('time/s')
                pylab.plot(time, mass44, 'bo')

#####
1436         ## Call def Peak() to detect all peaks and calculate its derivation, Maxima (position and value),
            complete area under the curve,
            ## the background values and the integration limits as well as the peak type (rectangular or
            gaussian)
            mass_prime44, Maxima_position44, Amplitude44, Area44, background_const44, mass_prime45,
            Maxima_position45, Amplitude45, Area45, background_const45, mass_prime46, Maxima_position46,
            Amplitude46, Area46, background_const46, start, end, peaks = Peak(time, mass44, mass45, mass46
            , runs)

#####

```



```

1441  ## For all detected Peaks get the isotopic ratios by calling def calc_isotop()
1442  ## using the calculated peak areas and print results (if intended)
1443  R_46, R_45, dO_18, dC_13, R_WMG_45, R_WMG_46 = calc_isotop(Area44, Area45, Area46)
1444
1445  if print_peak_isotopies == 'on':
1446      print '-----'
1447      print 'peak nr ', ' dC_13 ', ' dO_18 '
1448      for i in arange(len(dC_13)):
1449          print '%(a0)4.0f %(a1)10.2f %(a2)7.2f' % {'a0': i+1, 'a1': dC_13[i], 'a2': dO_18[i]}
1450      print
1451
1452  ## separete the delta values of the rectangular peaks from the one of the gauss peaks
1453  dC_13_rec = []
1454  dC_13_gauss = []
1455  peaks_rec = []
1456  peaks_gauss = []
1457
1458  for i in arange(len(peaks)):
1459      if peaks[i] == 'Rec':
1460          peaks_rec.append(i)
1461          dC_13_rec.append(dC_13[i])
1462      if peaks[i] == 'Gauss':
1463          peaks_gauss.append(i)
1464          dC_13_gauss.append(dC_13[i])
1465
1466  ## get mean value and standard deviation of all peaks detected in the chromatogram
1467  # for rectangular peaks
1468  Mean_rec = mean(dC_13_rec)
1469  sigma_rec = std(dC_13_rec, ddof=1) # stats.std(dC_13_rec)
1470  #print '\n !!! Debug line 1367:\n stats std: %s - numpy std %s of values in dC_13_rec: %s'%(
1471      sigma_rec, std(dC_13_rec, ddof=1), dC_13_rec )
1472
1473  # for gaussian peaks
1474  if type.file == 'Ref':
1475      Mean_gauss = mean(dC_13_gauss) # mean over all methane gauss peaks
1476      sigma_gauss = std(dC_13_gauss, ddof=1)#stats.std(dC_13_gauss)
1477  else:
1478      Mean_gauss = mean(array([dC_13_gauss[0], dC_13_gauss[-1]])) # mean over the two enframing
1479      reference methane gauss peaks
1480      sigma_gauss = std(array([dC_13_gauss[0], dC_13_gauss[-1]]), ddof=1)#stats.std(array([dC_13_gauss
1481      [0], dC_13_gauss[-1]]))
1482
1483  # plot the results and the raw-data if intended
1484  if plot_gauss_bounds == 'on':
1485      plotting(datafile, mass45, time, Maxima_position45, Amplitude45, start, end, mass_prime45,
1486          Area45, resist45, dC_13_rec, dC_13_gauss, already-peaks_rec, already-peaks_gauss,
1487          type.file, runs)
1488      plotting(datafile, mass46, time, Maxima_position46, Amplitude46, start, end, mass_prime46,
1489          Area46, resist46, dC_13_rec, dC_13_gauss, already-peaks_rec, already-peaks_gauss,
1490          type.file, runs)
1491      plotting(datafile, mass44, time, Maxima_position44, Amplitude44, start, end, mass_prime44,
1492          Area44, resist44, dC_13_rec, dC_13_gauss, already-peaks_rec, already-peaks_gauss,
1493          type.file, runs)
1494
1495  # plot the integration limits to the ratio subplots
1496  for begin in start:
1497      chrom_sf2_plots.append(([time[begin], [mass45[begin]*resist45/(mass44[begin]*resist44)], 'r
1498      |'))
1499      chrom_sf2_plots.append(([time[begin], [mass46[begin]*resist46/(mass44[begin]*resist44)], 'r
1500      |'))
1501  for finish in end:
1502      chrom_sf2_plots.append(([time[finish-1], [mass45[finish-1]*resist45/(mass44[finish-1]*
1503      resist44)], 'r|'))
1504      chrom_sf2_plots.append(([time[finish-1], [mass46[finish-1]*resist46/(mass44[finish-1]*
1505      resist44)], 'r|'))
1506  chrom_sf2_plots.append((time, (mass45*resist45/(mass44*resist44)), '-'))
1507  chrom_sf2_plots.append((time, (mass46*resist46/(mass44*resist44)), '-'))
1508  # get value for already calculated peaks in former script runs to get a daily results plot
1509  already-peaks_rec = already-peaks_rec + len(peaks_rec)
1510  already-peaks_gauss = already-peaks_gauss + len(peaks_gauss)
1511
1512  # redefine the Maxima_position-values because one Chromatogram is plotted after the other
1513  Maxima_position44_true = Maxima_position44 - time_start*ones(len(Maxima_position44))
1514
1515  return Mean_rec, sigma_rec, Mean_gauss, sigma_gauss, time[-1], already-peaks_rec,
1516      already-peaks_gauss, Maxima_position44_true, Amplitude44, Area44, Area45, Area46, dC_13_gauss,
1517      dC_13_rec, R_WMG_45, R_WMG_46
1518  ,,,
1519  #####
1520  # -----Main Program----- #
1521  #####
1522  ## Set the locale to US english
1523  locale.setlocale(locale.LC_ALL, 'en.US.UTF-8') # set the locale info to english to understand the date
1524  formats etc.
1525
1526  #####
1527  ### Overriding options by start arguments
1528  type_dict={'refl': refl, 'mref': mref, 'aira': aira, 'ices': ices, 'refa': refa}

```

```

1516 if 'all' in dir_choice:
    dir_choice = [mref, refl, ices, aira, refa]
    ## Check if the script has been started with arguments
    if len(sys.argv) > 1:
        if sys.argv[1].startswith('--'):
1521             opt = sys.argv[1][2:] # hole sys.argv[1], aber ohne die ersten beiden Zeichen
                if opt == '?' or opt == 'hilfe' or opt == 'help':
                    print '\n\
Dieses Programm prozessiert Masslynx Roh Daten Files im csv Format.
Werden keine Optionen übergeben, startet das Skript mit den Standard-Einstellungen.
1526 Als Optionen koennen angegeben werden:
--hilfe,--?,--help : Gibt diese Hilfe aus

Synopsis: %s [- option [Anzahl]]

1531     -type      Prozessiere Files des angegebenen Typs aus [mref,refl,aira,ices,refa]
    [Anzahl]    hintereinander abzuarbeitenden Rohdaten (des selben Typs!)

    '''%(sys.argv[0])
        sys.exit()
1536 elif sys.argv[1].startswith('-'):
    #print sys.argv[1][1:], type_dict[sys.argv[1][1:]],[mref, refl, ices, aira, refa]
    if sys.argv[1][1:].strip() in type_dict.keys():
        dir_choice = [type_dict[sys.argv[1][1:]]]
    else:
1541         print "%s" ist eine falsche Eingabe - Abbruch!"%(sys.argv[1:])
                sys.exit()
        if len(sys.argv) > 2 and sys.argv[2].strip().isdigit() is True:
            max_data = int(sys.argv[2].strip())
        else:
1546         print "%s" ist eine falsche Eingabe - Abbruch!"%(sys.argv[1:])
                sys.exit()
    else:
        print 'Unbekannte Option - Nichts zu tun!'
        sys.exit()
1551 #####
    ## Check for the existence of necessary paths
    print '*****'
    print
    print 'Checking path information...'
    for pex in [root_dir, log_dir, abs_path]:
        if os.path.exists(pex) != False:
            print 'Path "%s" => confirmed' %(pex)
1561         else:
                print 'Path "%s" could not be found. Aborting...'%(lib_f)
                    sys.exit()
    if os.path.exists(lib_path) != True:
        print 'Library directory could not be found!!!'
        print 'Please check whether the specified path information "%s" is correct! Aborting the script now
1566         !!!' %(lib_path)
                sys.exit()
    else:
        print 'Library directory "%s" found.' %(lib_path)
    if save_chrom == 'on' and len(dir_choice) == 1:
        if os.path.exists(plot_dir+dir_choice[0]+'/') != True:
1571             os.makedirs(plot_dir+dir_choice[0]+'/')
                print 'Plot folder "%s" created' %(plot_dir+dir_choice[0]+'/')
        else:
            print 'Plot directory "%s" found.' %(plot_dir+dir_choice[0]+'/')
1576 #####
    ## Find the raw data folders, symlink them to a temp folder and sort them

    ## define start arrays
1581 #creation_time = []
        file_type = []
        datafiles = []
        supplementary_information = []
        dates = []
1586

        print '*****'
        tmp_dir=abs_path+'temp/'

1591 ## create temporary data folder and enter it
        if os.path.exists(tmp_dir) == True:
            print 'Cleaning remainders of prior script runs...'
            shutil.rmtree(tmp_dir)
        start_dir=os.getcwd() # remember where the script was started
1596 os.makedirs(tmp_dir)
        os.chdir(tmp_dir)

    ## Determine the total amount of files to be processed following the option dir_choice in the header
    totdat_c = 0
1601 for cat_sel in dir_choice:
    if os.path.exists(abs_path+cat_sel) == False:
        print 'Selected datatype folder "%s" does not exist and will be skipped' %(cat_sel)
        continue

```

```

    totdat_c = totdat_c + len(os.listdir(abs_path+cat_sel))
1606 print 'Found the total amount of %i raw data folders.' %(totdat_c)
if totdat_c == 0:
    print 'Nothing to do then - i will stop the script now !'
    sys.exit()
if max_data == 'all':
1611 max_data = totdat_c
    print 'No max. amount of raw data folders specified - ALL will be analyzed!'
elif max_data > totdat_c:
    print 'The specified "max. amount" of %i exceeds the available datafolders in the directory tree,\n
        so i will just use the %i available ones.' %(max_data,totdat_c)
    max_data = totdat_c
1616 print '-----'
    ## create Symlinks in joint data folder for each leaf folder (*.raw)
    for cat_sel in dir_choice:
        ## Start of the Symlink creation cycles
1621 print 'Processing %s files...' %(cat_sel)
        if os.path.exists(abs_path+cat_sel) == False:
            print 'Selected datatype folder "%s" does not exist and will be skipped' %(cat_sel)
            continue
        work_dir=abs_path+cat_sel
1626 ## Determine the amount of runs as specified in the header (option max_data)
        dat_c = len(os.listdir(work_dir))
        if max_data >= dat_c:
            print 'All "%i" folders will be used!' %(dat_c)
            print '-----'
1631 else:
            print 'Found %i datafolders - due to the specified restriction i will just analyze %i of them.'
                %(dat_c, max_data)
            print '-----'

    ## Following Procedure is for large amounts of datasets that exceed the specified amount in the
    header(max_data)
1636 ## To assure that the oldest dataset in the tree is always written first into the library
    if dat_c > max_data:
        print 'Folders get sorted for oldest first...'
        # Sort actual folder by creation time
1641 folders_sort, creation_time_utc = creation_time_array(work_dir)
        # Create Symlinks for the specified amount of measurements
        for max_c in folders_sort[0:max_data]:
            if os.path.exists(tmp_dir+max_c) == False:
                os.symlink(work_dir+'/' +max_c,max_c)
                print 'Created Symbolic Link of %s in temporary working directory!' %(max_c)
1646 else:
                print 'Symbolic Link of %s already exists in the directory! Proceeding...' %(max_c)
            print '*****'
            print 'The script reached the specified max. amount of datafolders to be analyzed!'
            print 'No further symlinks will be created...'
            print '*****'
1651 break
        else:
            for full_path, dir_w, file_w in os.walk(work_dir):
                dat_dir = full_path.rsplit('/',1)[1]
1656 if (full_path[-3:] != 'raw'):
                    continue
                elif os.path.exists(tmp_dir+dat_dir) == True:
                    print 'Symbolic Link of %s already exists in the directory! Proceeding...' %(dat_dir)
1661 else:
                    print 'Created Symbolic Link of %s temporary working directory!' %(dat_dir)
                    if os.path.exists(tmp_dir+dat_dir) == False:
                        os.symlink(full_path, dat_dir)
            print '-----'
1666 max_data = max_data-dat_c
    ## let the symlinks in the temp. dir get analyzed for creation time (in utc) and sorted accordingly
    folders_sort, creation_time_utc = creation_time_array(tmp_dir[:-1])
    ## determine its containing data type by folder name analysis
    ## -> provides data type relevant supplementary information and stores it in its array
1671 for c_dir in range(len(folders_sort)):
    current_folder = folders_sort[c_dir]
    date_str = strftime("%y%m%d",localtime(creation_time_utc[c_dir]))
    if 'CH4Ref' in current_folder:
        file_type.append('Ref')
1676 dates.append(date_str)
        abs_num = current_folder[:-4].rsplit('-',1)[1]
        supplementary_information.append([date_str, abs_num,creation_time_utc[c_dir]])
        del(abs_num)
    elif 'RefLoop' in current_folder:
1681 file_type.append('Refloop')
        dates.append(date_str)
        abs_num = current_folder[:-4].rsplit('-',1)[1]
        inj_loops = int(current_folder.split('mal')[1].strip()[2:])*int(current_folder.split('mal')[0].
            strip()[:-1]) # delivers loop vol and how often it was injected in float type
        supplementary_information.append([date_str, abs_num, inj_loops,creation_time_utc[c_dir]])
1686 del(abs_num, inj_loops) # clear up vars
    elif 'Schleife' in current_folder and current_folder.find('bar') <= 0:
        file_type.append('Airafter')
        dates.append(date_str)
        airt_split = current_folder[:-4].split('-')

```

```

1691 loop_num =aira_split [len(aira_split)-1].strip()
cut = aira_split [len(aira_split)-3].strip() # provides cut type
if 'B37' in current_folder:
    if len(aira_split) == 7: # pot info present
        tag = 3
1696     pot = aira_split [2]
    if len(aira_split) == 5: # pot info absent
        tag = 1
        pot = 'unspec.'
1701     origin = aira_split [tag].split('-')[0]
    depth = str(float(aira_split [tag].split('-')[1])-1+((int(aira_split [tag].split('-')[2])-1)
        *0.11)).replace(",",".") # as sample numbering consists of the x-th meter and cuts of
        y-1 * 11cm
    else:
        depth = aira_split [len(aira_split)-4].strip().replace(",",".")
        origin = aira_split [len(aira_split)-5].strip() # provides sample origin
        if aira_split [len(aira_split)-6].strip() != date_str:
1706             pot = aira_split [len(aira_split)-6].strip()
        else:
            pot = 'unspec.' # No information about sample container available
            tag = 'unused'
        supplementary_information.append([date_str, origin, depth, cut, loop_num, pot,creation_time_utc
        [c_dir]])
1711 del(origin,aira_split,depth,cut,loop_num,pot,tag)
elif ('EDML' in current_folder) or (current_folder[-5:-4] == 'g'):
    file_type.append('Sample')
    dates.append(date_str)
    sam_split = current_folder[:-4].split('-')
1716 weight = sam_split [len(sam_split)-1][:-1].strip().replace(',','.') # get the proper sample
    weight
    cut = sam_split [len(sam_split)-2].strip() # provides cut type
    if 'B37' in current_folder:
        if len(sam_split) == 6: # pot info present
1721             tag = 3
            pot = sam_split [2]
        if len(sam_split) == 4: # pot info absent
            tag = 1
            pot = 'unspec.'
1726             origin = sam_split [tag].split('-')[0]
        depth = str(float(sam_split [tag].split('-')[1])-1+((int(sam_split [tag].split('-')[2])-1)
            *0.11)).replace(",",".") # as sample numbering consists of the x-th meter and cuts of
            y-1 * 11cm
        else:
            depth = sam_split [len(sam_split)-3].strip().replace(",",".")
            origin = sam_split [len(sam_split)-4].strip() # provides sample origin
            if sam_split [len(sam_split)-5].strip() != date_str:
1731                 pot = sam_split [len(sam_split)-5].strip()
            else:
                pot = 'unspec.' # No information about sample container available
                tag = 'unused'
            supplementary_information.append([date_str, origin, depth, cut, weight, pot,creation_time_utc [
            c_dir]])
1736 del(origin,sam_split,depth,cut,weight,pot,tag) # clear up vars
#elif ('Neumayer' in current_folder) or ('Gasmas' in current_folder) or ('bar' in current_folder)
# or ('Alert' in current_folder):
elif True in [air in current_folder for air in Ref_Airs]:
    file_type.append('RefAir')
    dates.append(date_str)
1741     refa_split = current_folder[:-4].split('-')
    origin=refa_split [1].strip()
    abs_num =refa_split [-1].strip()
    if 'mal' in current_folder:
        for n in refa_split:
1746             if 'mal' in n:
                STP = int(n.split('mal')[1].strip()[:2])*int(n.split('mal')[0].strip()[:-1:])
    elif 'bar' in current_folder:
        for n in refa_split:
            if 'ml' in n:
1751                 V = int(n[: -2])
                if 'bar' in n:
                    p = float(n[: -3].replace(',','.'))
                STP = p*V
            del(V,p)
1756 supplementary_information.append([date_str, origin, abs_num, STP, creation_time_utc [c_dir]])
del(abs_num,origin,STP,refa_split) # clear up vars
else:
    print
    print 'WARNING!!! Data folder "%s" could not get recognized !!!' %(current_folder)
1761     print
    print 'I will stop the operation now to prevent erroneous database entries!'
    sys.exit()
for datafile in os.listdir(tmp_dir+current_folder):
    if datafile[-4:] == '.csv' and datafile != 'AWI Test.csv':
1766         datafiles.append(tmp_dir+current_folder+'/' +datafile)
#     print 'Test supplementary_information array:'
#     for i in range(len(supplementary_information)):
#         print supplementary_information [i]
1771 del(totdat_c,dat_c,date_str,max_data) # clear up vars ,cat_sel

```

```

#####
### Create lib files with header info and with dummy zeros as first data line if they do not exist
print '*****'
1776 print
print 'Checking library path information...'

if lib_exist != 'yes':
    if os.path.exists(lib_bck) == False:
1781         os.makedirs(lib_bck)
        print 'Library Backup folder "%s" created' %(lib_bck)
    if (os.path.exists(lib_path) == False):
        os.makedirs(lib_path)
1786     else:
        print 'Library Folders found...'

    for lib_f in libfiles:
        if os.path.exists(lib_f) == False:
1791             lib_miss = lib_f
            lib_z=array('',ndmin=2)
            if lib_miss == library_refs:
                csvlib = csv.writer(open(lib_miss, "w")) #, dialect='excel'
                csvlib.writerow(['Created: '+ctime()])
1796             csvlib.writerow(ref_head.split(' '))
                csvlib.writerow('')
                lib_z=zeros((1,len(ref_head.split(' '))))
                csvlib.writerow(lib_z[0,:])
                print 'Library file %s created' %(lib_miss)
1801             elif lib_miss == library_refloops:
                csvlib = csv.writer(open(lib_miss, "w")) #, dialect='excel'
                csvlib.writerow(['Created: '+ctime()])
                csvlib.writerow(refloop_head.split(' '))
                csvlib.writerow('')
1806             lib_z=zeros((1,len(refloop_head.split(' '))))
                csvlib.writerow(lib_z[0,:])
                print 'Library file %s created' %(lib_miss)
            elif lib_miss == library_airaafter:
                csvlib = csv.writer(open(lib_miss, "w")) #, dialect='excel'
1811             csvlib.writerow(['Created: '+ctime()])
                csvlib.writerow(air_head.split(' '))
                csvlib.writerow('')
                lib_z=zeros((1,len(air_head.split(' '))))
                csvlib.writerow(lib_z[0,:])
1816             print 'Library file %s created' %(lib_miss)
            elif lib_miss == library_samples:
                csvlib = csv.writer(open(lib_miss, "w")) #, dialect='excel'
                csvlib.writerow(['Created: '+ctime()])
                csvlib.writerow(sam_head.split(' '))
                csvlib.writerow('')
1821             lib_z=zeros((1,len(sam_head.split(' '))))
                csvlib.writerow(lib_z[0,:])
                print 'Library file %s created' %(lib_miss)
            elif lib_miss == library_refair:
1826             csvlib = csv.writer(open(lib_miss, "w")) #, dialect='excel'
                csvlib.writerow(['Created: '+ctime()])
                csvlib.writerow(refa_head.split(' '))
                csvlib.writerow('')
                lib_z=zeros((1,len(refa_head.split(' '))))
1831             csvlib.writerow(lib_z[0,:])
                print 'Library file %s created' %(lib_miss)
            else:
                print 'Was not able to assign %s to a library file' %(lib_miss)
1836         print 'Please restart the script now...'
        sys.exit()
    else:
        print
        print 'All %i library files were set to be existing ...' %(len(libfiles))
        print
1841     for lib_f in libfiles:
        if os.path.exists(lib_f) != False or append_libraries == 'off':
            print 'File "%s" => confirmed' %(lib_f.rsplit('/')[1])
        else:
            print 'File "%s" does not exist!'%(lib_f)
1846         sys.exit()
print '*****'

## make safety copy of all libraries
if append_libraries == 'on':
1851     for types, library in zip([mref, refl, aira, ices, refa], libfiles):
        if types in dir_choice:
            shutil.copy(library, lib_bck+'/'+'Backup_'+strftime("%y%m%d-%H%M.", localtime())+library.
            rsplit('/',1)[1])
        ,,,
#####
### Start the Calculation Main Routine ###
#####
, , ,
# define start arrays
Mean.rec_array = []

```

```

1861 sigma_rec_array = []
Mean_gauss_array = []
sigma_gauss_array = []
R_WMG_45_array = []
R_WMG_46_array = []
1866 dC_13_gauss_array = []
Maxima_position44_array = []
Amplitude44_array = []
Area44_array = []
plot_index = []
1871 labels=[]
figures=[]
peak_amb = False # Set the Peak ambiguity flag to False - if there is one, it will be switched if its
def is called

if derivat_method != 'sum':
1876 x_fit_array = [[1.0, 1.0]]
x_fit_position = []

# define start parameters
time_end = 0
1881 already_peaks_rec = 0
already_peaks_gauss = 0

'''
1886 #####
# try the main program for the datafile
'''

# count index
1891 index_worked = 0
for runs in arange(len(datafiles)):
    chrom_sf1_plots=[]
    peak_cuts=[]
    chrom_r45_plots=[]
1896 chrom_r46_plots=[]
    Peak_Area_Uncut = []
    Peak_Area_cut = []
    ## Determine the measurement label to use in Figures etc.
    if file_type[runs] == 'Ref':
1901 label = datafiles[runs].rsplit('/',2)[1][7:-4]
    elif file_type[runs] == 'Refloop':
        label = datafiles[runs].rsplit('/',2)[1][7:-4]
    elif file_type[runs] == 'RefAir':
1906 label = datafiles[runs].rsplit('/',2)[1][7:-4]
    else:
        if 'EDML' in datafiles[runs]:
            label = datafiles[runs].rsplit('/',2)[1][datafiles[runs].rsplit('/',2)[1].find('ED') :
            datafiles[runs].rsplit('/',2)[1].find('GO')+3]
        elif 'B37' in datafiles[runs]:
1911 label = datafiles[runs].rsplit('/',2)[1][datafiles[runs].rsplit('/',2)[1].find('B37') :
            datafiles[runs].rsplit('/',2)[1].find('g')-7]
        else:
            label = datafiles[runs].rsplit('/',2)[1].rsplit("-",1)[0].split("-",3)[-1] #'
            Unknown.Sample.name'
    labels.append(label)
    ## set the stdout to be logged in a file as well as the console
    log_fn=method_end+"%ss_%s_%s.log"%(p_cut_off/10.0,correction_method,label)
1916 log_f=log_dir+file_type[runs]+" "+log_fn
    if os.path.exists(log_f):
        os.remove(log_f) # delete old log file if existings
    sys.stdout = Logger(log_f)
    ## Message for the log file
1921 print "\nProcessing performed at %s:\n\nPeak end cut off: %s secs\n"%(asctime(),p_cut_off/10.)

    ## Build figure instances for later use in def main, rectangular, gaussian and background
    if plot_gauss_bounds == 'on':
        chrom_plot=pylab.figure(runs,figsize=[f_wh,f_ht])
1926 pylab.figtext(0.8, 0.02,'created: '+asctime(),size=9)
        chrom_plot.suptitle(label)
        ##### Column with 1.ref Peak plots
        ## Subplot 1 of raw data get_axes()[runs]
        cp_sp1=chrom_plot.add_subplot(331)
1931 cp_sp1.set_title('1. CH4 Ref Peak', fontsize=10)
        cp_sp1.set_ylabel('Intensity/GV', fontsize=10)
        pylab.setp(pylab.getp(pylab.gca(), 'yticklabels'), fontsize=8)

        ## Subplot 2 - Ratio 45 and 46
1936 cp_sp2=chrom_plot.add_subplot(334, sharex=cp_sp1)
        cp_sp2.set_ylabel('45/44', fontsize=10)
        pylab.setp(pylab.getp(pylab.gca(), 'yticklabels'), fontsize=8)

        ## Subplot 3 - Ratio 45 and 46 without BG
1941 cp_sp3=chrom_plot.add_subplot(337, sharex=cp_sp1)
        cp_sp3.set_ylim(-0.01,0.03)
        cp_sp3.set_ylabel('46/44', fontsize=10)
        cp_sp3.set_xlabel('time/s')
        pylab.setp(pylab.getp(pylab.gca(), 'yticklabels'), fontsize=8)

```

```

1946 ##### Column with Sample Peak plots
cp_sp4=chrom_plot.add_subplot(332)
cp_sp4.set_title('Sample Peak', fontsize=10)
cp_sp5=chrom_plot.add_subplot(335, sharex=cp_sp4)
1951 cp_sp6=chrom_plot.add_subplot(338, sharex=cp_sp4)
cp_sp6.set_xlabel('time/s')
##### Column with 2nd Ref. Peak plots
cp_sp7=chrom_plot.add_subplot(333)
cp_sp7.set_title('2. CH4 Ref Peak', fontsize=10)
1956 cp_sp7.yaxis.set_label_position("right")
cp_sp8=chrom_plot.add_subplot(336, sharex=cp_sp7)
cp_sp8.yaxis.set_label_position("right")
cp_sp9=chrom_plot.add_subplot(339, sharex=cp_sp7)
cp_sp9.yaxis.set_label_position("right")
1961 cp_sp9.set_xlabel('time/s')
for ax in [0,1,3,4,6,7]:
    pylab.setp(chrom_plot.get_axes()[ax].get_xticklabels(), visible=False)
for ax in [3,4,5]:
    pylab.setp(chrom_plot.get_axes()[ax].get_yticklabels(), visible=False)
1966 for ax in [6,7,8]:
    chrom_plot.get_axes()[ax].yaxis.set_ticks_position("right")
if chrom_peak_char is 'on':
    ## Subplot 3/4 of peak characteristics
    #plot_list[1]=pylab.figure(1,figsize=[f_wh,f_ht])
    peak_char=pylab.figure(200,figsize=[f_wh,f_ht])
1971 chr_sub3 = peak_char.add_subplot(221)
chr_sub3.set_xlabel('peak number in all rec peaks', fontsize=8)
chr_sub3.set_title('Todays characteristics of methane reference peak isotopies', fontsize
=10)
chr_sub3.set_ylabel(r'$\delta\;^{13}C\;(\%_0)\;rec$', fontsize=8)
1976 pylab.setp(pylab.getp(chr_sub3, 'yticklabels'), fontsize=6)
chr_sub4 = peak_char.add_subplot(223)
chr_sub4.set_xlabel('peak number in all gauss peaks', fontsize=8)
chr_sub4.set_ylabel(r'$\delta\;^{13}C\;(\%_0)\;gauss$', fontsize=8)
1981 pylab.setp(pylab.getp(chr_sub4, 'yticklabels'), fontsize=6)

if chrom_deriv is 'on':
    plot_deriv=pylab.figure(300,figsize=[f_wh,f_ht])
    drv_sbplt1=plot_deriv.add_subplot(111)
1986 drv_sbplt1.set_ylabel('Derivation of the Intensity/(fA/s)', fontsize=12)

1986 ## Check if
if pylab.strptime2num("%y%m%d")(supplementary_information[runs][0]) >= pylab.strptime2num("%y%m%d")
(Work_std[1]['intro_date']) \
and pylab.strptime2num("%y%m%d")(supplementary_information[runs][0]) <= pylab.strptime2num("%y%m%d
")(Work_std[2]['intro_date']):
    print
    '*****'

1991 print 'This measurement was conducted in the period of CO2 working standard gas bottle "%s"%(
Work_std[1]['Name'])
print 'I will adjust the isotopies for the calculation according to the header information ...'
dC_13_RM_VPDBCO2 = Work_std[1]['d13C']/1000.0
dO_18_RM_VPDBCO2 = Work_std[1]['d18O']/1000.0
elif pylab.strptime2num("%y%m%d")(supplementary_information[runs][0]) >= pylab.strptime2num("%y%m%d
")(Work_std[2]['intro_date']):
1996 print
    '*****'

print 'This measurement was conducted in the period of CO2 working standard gas bottle "%s"%(
Work_std[2]['Name'])
print 'I will adjust the isotopies for the calculation according to the header information ...'
dC_13_RM_VPDBCO2 = Work_std[2]['d13C']/1000.0
dO_18_RM_VPDBCO2 = Work_std[2]['d18O']/1000.0
2001 else:
    print
    '*****'

print 'The following measurement was conducted in the period BEFORE the new CO2 Reference gas
bottles'
print 'I will adjust the isotopies for the calculation according to the header information ...'
2006 dC_13_RM_VPDBCO2 = Work_std[0]['d13C']/1000.0
dO_18_RM_VPDBCO2 = Work_std[0]['d18O']/1000.0
print 'and use "%s" for delta13C and "%s" for delta18O (both in permille).'%(dC_13_RM_VPDBCO2*1000,
dO_18_RM_VPDBCO2*1000)
print
    '*****'

if no_stop == 'on':
    # do the program and do not allow errors (move error producing files to 'not working')
2011 try:
    # define the reference peak for the chosen datafile to chart
    if file_type[runs] == 'Ref':
        ref_peaks = ref_peaks_ref
    if file_type[runs] != 'Ref':
2016 ref_peaks = ref_peaks_non_ref

```



```

# get the results in 13_C for the gauss and rectangular peaks, that are not sample peaks
# for the daily analysis and for new library entries
print '-----'
print 'Current dataset: ', folders_sort[runs], ' Script run: ', runs+1
2021 print 'Measured: ', ctime(supplementary_information[runs][-1])
## Call def 'main'
Mean_rec, sigma_rec, Mean_gauss, sigma_gauss, time_end, already_peaks_rec,
already_peaks_gauss, Maxima_position44, Amplitude44, Area44, Area45, Area46,
dC_13_gauss, dC_13_rec, R_WMG_45, R_WMG_46 = main(datafiles[runs], time_end,
already_peaks_rec, already_peaks_gauss, file_type[runs])

2026 ### write results to libraries
if append_libraries == 'on':
## Call def 'write_library'
write_library(Mean_gauss, sigma_gauss, file_type[runs], datafile,
supplementary_information[runs], Maxima_position44, Amplitude44, Area44, Area45,
Area46, dC_13_gauss, dC_13_rec, R_WMG_45, R_WMG_46)

# append results to arrays
2031 Mean_rec_array.append(Mean_rec)
sigma_rec_array.append(sigma_rec)
Mean_gauss_array.append(Mean_gauss)
sigma_gauss_array.append(sigma_gauss)
2036 dC_13_gauss_array.append(dC_13_gauss)
Maxima_position44_array.append(Maxima_position44)
Amplitude44_array.append(Amplitude44)
Area44_array.append(Area44)
R_WMG_45_array.append(R_WMG_45)
2041 R_WMG_46_array.append(R_WMG_46)

### move current datafolder to archive
# get archive name
archive_name = file_type[runs]+' archive'
if file_type[runs] == 'Refloop':
2046 archive_name = file_type[runs]+' archive'+ '/' + str(supplementary_information[runs][2])
[-1]+'mal'+str(supplementary_information[runs][2])[:-2]+'ml'
elif (file_type[runs] == 'Sample') or (file_type[runs] == 'Airafter'):
if 'AWI' in folders_sort[runs]:
archive_name = file_type[runs]+' archive'+ '/' + 'EDML-AWI'
2051 elif 'Bern' in folders_sort[runs] or 'BERN' in folders_sort[runs]:
archive_name = file_type[runs]+' archive'+ '/' + 'EDML-Bern'
elif 'Gr' in folders_sort[runs]:
archive_name = file_type[runs]+' archive'+ '/' + 'EDML-Grble'
elif True in [ice in dat_folder for ice in Intercomp_ice]:
if 'B37' in folders_sort[runs]:
2056 if len(folders_sort[runs].split('-')) == 6 or len(folders_sort[runs].split('-')
) == 7:
archive_name = file_type[runs]+' archive/B37/'+folders_sort[runs].split('-')
[3].rsplit('-',1)[0]
if len(folders_sort[runs].split('-')) == 4 or len(folders_sort[runs].split('-')
) == 7:
archive_name = file_type[runs]+' archive/B37/'+folders_sort[runs].split('-')
[1].rsplit('-',1)[0]
else:
2061 archive_name = file_type[runs]+' archive'+ '/' + 'Intercomparison'
if move_folders == 'on':
arch_dir=arch_path+'/' + archive_name+'/' + folders_sort[runs]
if os.path.exists(arch_dir) == True:
print
'*****'
2066 print 'Archive folder %s already exists!!!\n\n !!! Better check for double entries
in its library file !!!' %(folders_sort[runs])
print
'*****'
else:
shutil.copytree(tmp_dir+folders_sort[runs], arch_dir)
2071 org_dir = os.readlink(tmp_dir+folders_sort[runs])
shutil.rmtree(org_dir)
os.unlink(tmp_dir+folders_sort[runs])
# get new index
index_worked = index_worked + 1
2076 plot_index.append(runs+1)
print
print 'Data folder moved to Archive!'
print '-----'
# do exception if error occurred
except:
2081 not_working(datafiles[runs], file_type[runs], folders_sort[runs])

#####
### do the program and allow errors
else:
2086 ## define the reference peak for the choosen datafile to chart
#print file_type[runs]
if file_type[runs] == 'Ref':
ref_peaks = ref_peaks_ref
if file_type[runs] != 'Ref':
2091 ref_peaks = ref_peaks_non_ref

```

```

## get the results in 13_C for the gauss and rectangular peaks, that are not sample peaks
## for the daily analysis and for new library entries
print '-----'
2096 print 'Current dataset: ', folders_sort[runs], ' Script run: ', runs+1
print 'Measured: ', ctime(supplementary_information[runs][-1])

## Call def 'main'
Mean_rec, sigma_rec, Mean-gauss, sigma-gauss, time_end, already-peaks_rec, already-peaks-gauss,
Maxima_position44, Amplitude44, Area44, Area45, Area46, dC_13-gauss, dC_13-rec, R.WMG_45,
R.WMG_46 = main(datafiles[runs], time_end, already-peaks_rec, already-peaks-gauss,
2101 file_type[runs], runs)

## Abort if chromatogram seems abnormal -> copy dataset to 'not working' and unlink it (def
not_working)
if file_type[runs] == 'Ref':
    if len(dC_13-gauss) != 6 or len(dC_13-rec) != 2:
        print
        '*****',
2106 print '!!! Unusual peak pattern for %s measurement detected !!! \nFound %i rectangular
and %i gauss-like ones.' %(file_type[runs], len(dC_13-rec), len(dC_13-gauss))
print
print 'Will skip this dataset and not write it to the library!'
not_working(datafiles[runs], file_type[runs], folders_sort[runs])
continue
2111 elif file_type[runs] != 'Ref':
    if len(dC_13-gauss) < 3 or len(dC_13-rec) != 4:
        print
        '*****',
        print '!!! Unusual peak pattern for %s measurement detected !!! \nFound %i rectangular
and %i gauss-like ones.' %(file_type[runs], len(dC_13-rec), len(dC_13-gauss))
2116 print
print 'Will skip this dataset and not write it to the library!'
not_working(datafiles[runs], file_type[runs], folders_sort[runs])
continue
### write results to libraries
if append-libraries == 'on':
    # Call def 'write-library'
    write_library(Mean-gauss, sigma-gauss, file_type[runs], datafile, supplementary_information
[runs], Maxima_position44, Amplitude44, Area44, Area45, Area46, dC_13-gauss, dC_13-rec
, R.WMG_45, R.WMG_46)
    print
    print 'Data written to library!'
    print '-----',
#
#
#
2126 # append results to arrays
Mean_rec_array.append(Mean_rec)
sigma_rec_array.append(sigma_rec)
2131 Mean-gauss_array.append(Mean-gauss)
sigma-gauss_array.append(sigma-gauss)
dC_13-gauss_array.append(dC_13-gauss)
Maxima_position44_array.append(Maxima_position44)
Amplitude44_array.append(Amplitude44)
Area44_array.append(Area44)
2136 R.WMG_45_array.append(R.WMG_45)
R.WMG_46_array.append(R.WMG_46)

### move current datafolder to archive
# get archive name
2141 archive_name = file_type[runs]+' archive'
if file_type[runs] == 'Refloop':
    archive_name = file_type[runs]+' archive'+'/'+str(supplementary_information[runs][2]/10)+'
mal'+10ml'
elif (file_type[runs] == 'Sample') or (file_type[runs] == 'Airafter'):
2146 if 'AWI' in folders_sort[runs]:
    archive_name = file_type[runs]+' archive'+'/'+ 'EDML-AWI'
elif 'Bern' in folders_sort[runs] or 'BERN' in folders_sort[runs]:
    archive_name = file_type[runs]+' archive'+'/'+ 'EDML-Bern'
elif 'Gr' in folders_sort[runs]:
    archive_name = file_type[runs]+' archive'+'/'+ 'EDML-Grble'
2151 elif True in [ice in folders_sort[runs] for ice in Intercomp-ice]:
    if 'B37' in folders_sort[runs]:
        if len(folders_sort[runs].split('-')) == 6 or len(folders_sort[runs].split('-')) ==
7:
            archive_name = file_type[runs]+' archive/B37'+folders_sort[runs].split('-')
[3].rsplit('-',1)[0]
        if len(folders_sort[runs].split('-')) == 4 or len(folders_sort[runs].split('-')) ==
5:
2156 archive_name = file_type[runs]+' archive/B37'+folders_sort[runs].split('-')
[1].rsplit('-',1)[0]
    else:
        archive_name = file_type[runs]+' archive'+'/'+ 'Intercomparison'
if move_folders == 'on':
    arch_dir=arch_path+'/' +archive_name+'/' +folders_sort[runs]
2161 if os.path.exists(arch_dir) == True:
    print
    '*****',

```

```

print 'Archive folder %s already exists!!!\n\n Better check for double entries in its
      library file!' %(folders_sort[runs])
print
'*****'
else:
2166     shutil.copytree(tmp_dir+folders_sort[runs], arch_dir)
        org_dir = os.readlink(tmp_dir+folders_sort[runs])
        shutil.rmtree(org_dir)
        os.unlink(tmp_dir+folders_sort[runs])
        print
2171     print 'Data folder moved to Archive!'
        print '-----',
        # get new index
        index_worked = index_worked + 1
        plot_index.append(runs+1)
2176     #####
        ## Plot results
        if plot_gauss_bounds == 'on':
            for art in chrom_sf1_plots:
                #print tuple(art)
2181                 if "Marker" in art[0]:
                    cp_sp1.plot(art[1], art[2], art[3], mew=3, ms=20)
                    cp_sp4.plot(art[1], art[2], art[3], mew=3, ms=20)
                    cp_sp7.plot(art[1], art[2], art[3], mew=3, ms=20)
2186                 else:
                    cp_sp1.plot(art[1], art[2], art[3])
                    cp_sp4.plot(art[1], art[2], art[3])
                    cp_sp7.plot(art[1], art[2], art[3])
                [(cp_sp1.get_lines()[1].set_markeredgewidth(3), cp_sp4.get_lines()[1].set_markeredgewidth(3),
                  cp_sp7.get_lines()[1].set_markeredgewidth(3)) for l in [e for e, art in enumerate(
                    chrom_sf1_plots) if "r" in art[3]]] ## adjust the markersize of all Markers
2191     ## Ratios 45/44
            for art in chrom_r45_plots:
                cp_sp2.plot(art[0], art[1], art[2])
                cp_sp5.plot(art[0], art[1], art[2])
                cp_sp8.plot(art[0], art[1], art[2])
                [(cp_sp2.get_lines()[1].set_markeredgewidth(3), cp_sp5.get_lines()[1].set_markeredgewidth(3),
                  cp_sp8.get_lines()[1].set_markeredgewidth(3)) for l in [e for e, art in enumerate(
                    chrom_r45_plots) if "r" in art[2]]] ## adjust the markersize of all Markers
2196     ## Ratios 46/44
            for art in chrom_r46_plots:
                cp_sp3.plot(art[0], art[1], art[2])
                cp_sp6.plot(art[0], art[1], art[2])
                cp_sp9.plot(art[0], art[1], art[2])
2201                [(cp_sp3.get_lines()[1].set_markeredgewidth(3), cp_sp6.get_lines()[1].set_markeredgewidth(3),
                  cp_sp9.get_lines()[1].set_markeredgewidth(3)) for l in [e for e, art in enumerate(
                    chrom_r46_plots) if "r" in art[2]]] ## adjust the markersize of all Markers

if not peak_amb: # if this is a non-standard chromatogram (too many peaks), the following
doesnt make sense
#####
2206     ## Plot Peak Maximum Lines in
        ## raw data subfigures
        cp_sp1.axvline(x=chrom_sf1_plots[98][1][4], linewidth=1, color='r') # vline at Mass 44 (
            Index 98) peak x position (Index 1)
        cp_sp4.axvline(x=chrom_sf1_plots[98][1][6], linewidth=1, color='r')
        cp_sp7.axvline(x=chrom_sf1_plots[98][1][8], linewidth=1, color='r')
        ##Ratio subfigures
2211     cp_sp2.axvline(x=chrom_r45_plots[3][0], linewidth=1, color='r')
        cp_sp5.axvline(x=chrom_r45_plots[11][0], linewidth=1, color='r')
        cp_sp8.axvline(x=chrom_r45_plots[19][0], linewidth=1, color='r')
        cp_sp3.axvline(x=chrom_r46_plots[3][0], linewidth=1, color='r')
        cp_sp6.axvline(x=chrom_r46_plots[11][0], linewidth=1, color='r')
2216     cp_sp9.axvline(x=chrom_r46_plots[19][0], linewidth=1, color='r')
        #####
        ## Plot Peak Cut off Lines in
        if "cut" in method_end:
            ## raw data subfigures
2221     cp_sp1.axvline(x=chrom_sf1_plots[98][1][4]+p_cut_off/10.0, linewidth=1, color='k') #
                vline at Mass 44 (Index 98) peak x position (Index 1)
            cp_sp4.axvline(x=chrom_sf1_plots[98][1][6]+p_cut_off/10.0, linewidth=1, color='k')
            cp_sp7.axvline(x=chrom_sf1_plots[98][1][8]+p_cut_off/10.0, linewidth=1, color='k')
            ## ratio subfigures
            cp_sp2.axvline(x=chrom_r45_plots[3][0]+p_cut_off/10.0, linewidth=1, color='k')
2226     cp_sp5.axvline(x=chrom_r45_plots[11][0]+p_cut_off/10.0, linewidth=1, color='k')
            cp_sp8.axvline(x=chrom_r45_plots[19][0]+p_cut_off/10.0, linewidth=1, color='k')
            cp_sp3.axvline(x=chrom_r45_plots[3][0]+p_cut_off/10.0, linewidth=1, color='k')
            cp_sp6.axvline(x=chrom_r45_plots[11][0]+p_cut_off/10.0, linewidth=1, color='k')
            cp_sp9.axvline(x=chrom_r45_plots[19][0]+p_cut_off/10.0, linewidth=1, color='k')
2231     #####
            ## Adjust y-limits for ...
            ## 1st row of plots
            sp1_end_m=max(peak_cuts[0])+10.
            sp4_end_m=max(peak_cuts[2])+10.
2236     sp7_end_m=max(peak_cuts[4])+10.
        else:
            sp1_end_m=chrom_sf1_plots[92][2][0]+3.
            sp4_end_m=chrom_sf1_plots[94][2][0]+3.

```

```

    sp7_end_m=chrom_sf1_plots [96][2][0]+3.
2241 cp-sp1.set_ylim(chrom_sf1_plots [63][2][0]-1.,sp1_end_m) # Set ylims for 1.Ref Fig Column -
    lower: Mass 46 Peak Start Marker, upper: Mass 44 Peak End Marker; both plusminus
    offset
    cp-sp4.set_ylim(chrom_sf1_plots [65][2][0]-1.,sp4_end_m)
    cp-sp7.set_ylim(chrom_sf1_plots [67][2][0]-1.,sp7_end_m)
    ## x-limits
    cp-sp1.set_xlim(chrom_sf1_plots [63][1][0]-0.5,chrom_sf1_plots [72][1][0]+5.) #-30. Set xlims
    for 1.Ref Figure Column
2246 cp-sp4.set_xlim(chrom_sf1_plots [65][1][0]-0.5,chrom_sf1_plots [74][1][0]+5.) #-20. Set xlims
    for Sample Figure Column
    cp-sp7.set_xlim(chrom_sf1_plots [67][1][0]-0.5,chrom_sf1_plots [76][1][0]+5.) #-30. Set xlims
    for 2.Ref Figure Column
    ## y-limits 2nd row of plots
    sp2_max_y=pylab.interp(chrom_r45_plots [3][0],chrom_r45_plots [0][0],chrom_r45_plots [0][1]) #
    determine the y-position at its x-pos. of the peak maximum on the interpolated ratio
2251 sp5_max_y=pylab.interp(chrom_r45_plots [11][0],chrom_r45_plots [8][0],chrom_r45_plots [8][1])
    sp8_max_y=pylab.interp(chrom_r45_plots [19][0],chrom_r45_plots [16][0],chrom_r45_plots
    [16][1])

    cp-sp2.set_ylim(sp2_max_y-0.0005,sp2_max_y+0.0005)
    cp-sp5.set_ylim(sp5_max_y-0.0005,sp5_max_y+0.0005)
    cp-sp8.set_ylim(sp8_max_y-0.0005,sp8_max_y+0.0005)
2256 ## y-limits 3rd row of plots
    sp3_max_y=pylab.interp(chrom_r46_plots [3][0],chrom_r46_plots [0][0],chrom_r46_plots [0][1]) #
    determine the y-position at its x-pos. of the peak maximum on the interpolated ratio
    sp6_max_y=pylab.interp(chrom_r46_plots [11][0],chrom_r46_plots [8][0],chrom_r46_plots [8][1])
    sp9_max_y=pylab.interp(chrom_r46_plots [19][0],chrom_r46_plots [16][0],chrom_r46_plots
    [16][1])

2261 cp-sp3.set_ylim(sp3_max_y-0.0005,sp3_max_y+0.0005)
    cp-sp6.set_ylim(sp6_max_y-0.0005,sp6_max_y+0.0005)
    cp-sp9.set_ylim(sp9_max_y-0.0005,sp9_max_y+0.0005)
    else:
2266 cp-sp1.set_xlim(740, 780)
    cp-sp4.set_xlim(2060, 2140)
    cp-sp7.set_xlim(2400, 2500)
    ## Final plot adjustmensts
    chrom_plot.subplots_adjust(left=0.06, bottom=0.07, right=0.94, top=0.92,hspace=0.1, wspace=0.1)
    #, wspace=0.5
2271 figures.append(chrom_plot)
    if "cut" in method_end:
        rel_area=[[100.-(Peak_Area_cut [p][m]/Peak_Area_Uncut [p][m]*100.) for m in range(3)] for p in
        [0,2,4]]
        print "\n+++++\nMethane peak area loss:\n
        _____\nPeak      Mass44      Mass45      Mass46\n
        for e, n in enumerate(rel_area):
2276 print "%s%8.2f, %8.2f, %8.2f"%(["1.Ref ", "Sample", "2.Ref "][e],n[0],n[1],n[2])

    ## show/save the figures
    if plot_gauss_bounds == 'on' and save_chrom != 'on':
        if rcParams['backend']== 'Qt4Agg':
            pylab.show() #chrom_plot.show()
2281 elif plot_gauss_bounds == 'on' and save_chrom == 'on':
    # if dir_choice [0] == 'CH4_Refs' or dir_choice [0] == 'Refloops ':
    # plot_names=[plot_dir+dir_choice [0]+'/' + dir_choice [0]+str(min(array(
    supplementary_information, ndmin=2)[: ,1].astype(int)))+to'+str(max(array(supplementary_information
    , ndmin=2)[: ,1].astype(int)))+'-'+n+'.png' for n in plot_list]
    # ##for combined plot
    # plot_name=dir_choice [0]+'/' + dir_choice [0]+str(min(array(supplementary_information ,
    ndmin=2)[: ,1].astype(int)))+to'+str(max(array(supplementary_information , ndmin=2)[: ,1].astype(int)
    ))+'.png'
2286 # else:
    plot_name=dir_choice [0]+'/' + label+'_%s_%ss.png'%(method_end, p_cut_off/10.0) #strftime("%y%
    n%d.%H.%M", localtime())
    chrom_plot.set_size_inches( (f_wh, f_ht) )
    chrom_plot.savefig(plot_dir+plot_name, format='png') #,papertype='a4'
    #print os.path.exists(arch_dir+'/' + plot_name.rsplit("/",1)[1]),arch_dir+'/' + plot_name.
    rsplit("/",1)[1]
2291 if move_folders is "on" and os.path.exists(arch_dir+'/' + plot_name.rsplit("/",1)[1])==False:
    #
    shutil.move(plot_dir+plot_name, arch_dir+'/')
    print 'Peak boundary figure "%s" got saved!' %(plot_name.rsplit('/',1)[1])
    else:
    print 'Peak boundary figure "%s" got saved to directory "%s"! ' %(plot_name.rsplit
    ('/',1)[1],plot_dir.split('/',7)[-1]+dir_choice [0])
2296 pylab.close(chrom_plot)
    #print
    if not peak_amb and file_type [runs]!="Ref":# and "cut" in method_end:
    #####
    ## Calc. Peak Width for all 3 Masses at 10% Height
2301 idc=[97,57,77] # Base indices for M44/45/46 artists in chrom_sf1_plots list - check [(art [0],n)
    for n,art in enumerate(chrom_sf1_plots)] for details

    p_heights=[(chrom_sf1_plots [n+1][2][6]-chrom_sf1_plots [n+8][2][0]) for n in idc]
    p_heights_10p=[n/10. for n in p_heights]

```



```

2371  shutil.move(log_f, arch_dir+'/')
      ## reset variables
      time_end=0
      #del(chrom_sf1.plots)

2376  ### plot and print today mean-value results if intended
      if (plot_gauss_bounds == 'on') and len(Mean_rec_array) > 0:
          if chrom_peak_char is 'on':
              # plot the rectangular peaks
              chr_sub5 = peak_char.add_subplot(222)
2381      #pylab.axis([0, index_worked+1, min(Mean_rec_array)-max(sigma_rec_array)-0.05, max(
              Mean_rec_array)+max(sigma_rec_array)+0.05])
              chr_sub5.set_title('Todays results of Methane peak isotopies', fontsize=10)
              chr_sub5.set_ylabel(r'Mean  $\delta^{13}C$   $(\%_0)$  of rectangular peaks', fontsize=8)
              chr_sub5.set_xlabel('Measurement run', fontsize=8)
              chr_sub5.set_xlim(0, index_worked+1)
              chr_sub5.set_ylim(min(Mean_rec_array)-max(sigma_rec_array)-0.05, max(Mean_rec_array)+max(
              sigma_rec_array)+0.05)
2386      pylab.setp(pylab.getp(chr_sub5, 'yticklabels'), fontsize=6)
              #pylab.xticks(arange(1, index_worked+1), plot_index)
              chr_sub5.set_xticks(arange(1, index_worked+1), plot_index)
              chr_sub5.errorbar(arange(1, index_worked+1), Mean_rec_array, sigma_rec_array, fmt='bo-', ecolor
              ='k', capsize=3)

2391      # plot the gauss peaks
              chr_sub6 = peak_char.add_subplot(224)
              #pylab.axis([0, index_worked+1, min(Mean_gauss_array)-max(sigma_gauss_array)-0.05, max(
              Mean_gauss_array)+max(sigma_gauss_array)+0.05])
              chr_sub6.set_ylabel(r'Mean  $\delta^{13}C$   $(\%_0)$  of gaussian peaks', fontsize=10)
              chr_sub6.set_xlabel('Measurement run', fontsize=8)
2396      chr_sub6.set_xlim(0, index_worked+1)
              chr_sub6.set_ylim(min(Mean_gauss_array)-max(sigma_gauss_array)-0.05, max(Mean_gauss_array)+max(
              sigma_gauss_array)+0.05)
              pylab.setp(pylab.getp(chr_sub6, 'yticklabels'), fontsize=6)
              chr_sub6.set_xticks(arange(1, index_worked+1), plot_index)
              #pylab.xticks(arange(1, index_worked+1), plot_index)
2401      chr_sub6.errorbar(arange(1, index_worked+1), Mean_gauss_array, sigma_gauss_array, fmt='go-',
              ecolor='k', capsize=3)

      ## Last Changes to Figure plot_chrom
2406      #cp_sp2.autoscale_view(tight=True, scalex=False, scaley=True)

      ## Last Changes to derivation plot Figure
      if chrom_deriv is 'on':
          drv_sbplt1.autoscale_view(tight=True, scalex=True, scaley=True)

2411

      # print today mean-value results
      print '-----'
2416      print 'Summary of reference peaks -'
      print 'Mean isotopie and standard deviation:'
      print
      print '%(a0)s   %(a1)s   %(a2)s   %(a3)s' % {'a0': 'Measurement', 'a1': 'Meas. type', 'a2': '
      gaussian peaks', 'a3': 'rectangular peaks'}
      for cmlp in arange(index_worked):
          print '%(a0)11s %(a1)8s %(a2)13.2f (%(a3)1.2f) %(a4)9.2f (%(a5)1.2f)' % {'a0': labels[cmlp], '
          a1': file_type[cmlp], 'a2': Mean_gauss_array[cmlp], 'a3': sigma_gauss_array[cmlp], 'a4':
          Mean_rec_array[cmlp], 'a5': sigma_rec_array[cmlp]}
2421      #print '%(a0)9.0f %(a1)22s %(a2)14.2f (%(a3)1.2f) %(a4)9.2f (%(a5)1.2f)' % {'a0': cmlp+1, 'a1':
          file_type[cmlp], 'a2': Mean_gauss_array[cmlp], 'a3': sigma_gauss_array[cmlp], 'a4':
          Mean_rec_array[cmlp], 'a5': sigma_rec_array[cmlp]}
      print

2426  locale.setlocale(locale.LC_ALL, '') # reset the locale info to default system locale

      #pylab.show()
2431  ## Clean up
      os.chdir(root_dir)
      print '*****
      print '*****          Clean Up Procedure          *****'
      print '***          ***'

2436  if (os.path.exists(tmp_dir) == True) and (len(os.listdir(tmp_dir))==0):
          os.rmdir(tmp_dir)
          print '* No remainders found in temp folder, so its being removed! *'
      else:
          print '* The temporary folder is not empty - skipping removal *'
2441  print '*****'
      os.chdir(start_dir)

```

D.2. Post processing

```

2  # -*- coding: utf-8 -*-
  """
  Created on Tue Nov  9 18:21:46 2010

  @author: lmoeller
  """
7  '''
  *****
  *Apply Splinefit Correction*
  *****
12  Last modifications: Mon 09 Dec 2012 19:01:11 PM CET
  '''

17  __version__ = 1.0
  # Checks if the path info is correct
  # Reads all libraries into arrays
  # Removes outliers in CH4 ref und Refloop data according to the information specified in the header
  # and unusable isotopy data entries
  # Corrects numbering errors (duplicates) in CH4 ref data
22  # Calculates Splinefits in CH4 ref ranges specified in the header and plots them
  # Calculates the Differences of the individual data points in the CH4 ref data and its corresponding
  # fitted value and creates dayly mean differences
  # Corrects the individual Refloop isotopies with the corresponding dayly mean difference

  __version__ = 1.1
27  # Introduced Neymayer Offset Calculation and Correction
  # Exports spline corrected dataset to file for better accessibility

32  __version__ = 1.2
  # gravitational correction included
  # faster external dataset reading via loadtxt included
  # included different reflow volumina support

37  __version__ = 1.3
  # New Reference Loop Bottle (former CrystalAir) incorporated

42  __version__ = 1.4
  # Added new age scale choice options
  # Heinrich event bars included

47  __version__ = 1.5
  # Data validation option in form of milestone exports and plots included

  __version__ = 1.6 # Fri Jan 21 17:15:54 2011
52  # Correction for depth error caused by changes in the procedure of the 30cm sampling (bio) of gas cuts
  # before 2004 (bags below 1572) samples taken from bottom, after 2004 from top

  '''
  #####
57  # - Module selection - #
  #####
  from time import localtime, strftime, strptime, mktime, asctime
  from datetime import datetime
62  from matplotlib.mlab import find
  import matplotlib
  import pylab
  #matplotlib.rcParams["text", usetex=True)
  from numpy import array, take, argsort, sort, append, delete, arange, unique, where, diff, array_split,
  # mean, std, \
67  var, shape, clip, sqrt, unique, loadtxt, savetxt, copy, concatenate, ones
  import scipy.interpolate
  import csv
  from matplotlib.mlab import csv2rec, rec_append_fields
  from os.path import exists
72  from os import makedirs, listdir, remove
  import sys
  import locale
  import numpy.core.records as rec

77  '''
  #####
  # - Parameters - #
  #####
82  ##### General path parameters #####

  root_dir = '/home/lmoeller/Promotion/Messdaten/Processed-data/'
  log_dir = root_dir+'Processing_Logs/'
  ext_dir = '/home/lmoeller/Promotion/Messdaten/External_datasets/'
87  eval_dir='/home/lmoeller/Dokumente/Abbildungen/PyPlots/Evaluation/'
  dbg_stage=1
  ##### External data file parameters #####

```



```

#ext_list = [ext_dir+n for n in ['EDML_Dep_Age_Mix_d15N.csv', 'EDML_d18O.tab',
CO2_AhnBrook_and_Blunier_2008.csv', 'Luethi_unofficial_dml_co2_260608.csv']] #EDML_Age_d18O.csv
ext_data=[
92 {' name': 'CH4.EDML', 'file': 'EDML_Dep_Age_Mix_d15N.csv', 'header': 2, 'delimiter': ',', 'columns': None, 'scale
': 'Gicc05', 'label': '$\mathrm{[CH_4]}$ (ppbv)', 'color': 'g', 'dth-idx': 0, 'age-idx': 1, 'dat-idx': 2,
comment': 'taken from Epica 2006'}, \
{' name': 'CH4.DML.EDML1', 'file': 'edml_ch4_0-140KYrBP_EPSL.csv', 'header': 10, 'delimiter': ',', 'columns':
None, 'scale': 'EDML1', 'label': '$\mathrm{[CH_4]}$ (ppbv)', 'color': 'g', 'dth-idx': 0, 'age-idx': 1, 'dat-
idx': 2, 'comment': 'extended dataset 0-140kyBP excerpt from EPSL. Schilt, Capron 2010'}, \
{' name': 'CO2.EDML', 'file': 'Luethi_unofficial_dml_co2_260608.csv', 'header': 3, 'delimiter': ',', 'columns':
None, 'scale': 'EDML1', 'label': '$\mathrm{[CO_2]}$ (ppmv)', 'color': '#4169E1', 'dth-idx': 1, 'age-idx
': 2, 'dat-idx': 3, 'comment': ''}, \
{' name': 'CH4.EDC', 'file': 'edc-ch4-2008.tab', 'header': 155, 'delimiter': '\t', 'columns': (0, 1, 2), 'scale':
EDC3', 'label': '$\mathrm{[CH_4]}$ (ppbv)', 'color': 'dodgerblue', 'dth-idx': 1, 'age-idx': 2, 'dat-idx': 3,
comment': ''}, \
{' name': 'CO2.EDC', 'file': 'edc-co2-2008_composite.txt', 'header': 7, 'delimiter': ' ', 'columns': None, 'scale
': 'EDC3', 'label': '$\mathrm{[CO_2]}$ (ppmv)', 'color': 'purple', 'dth-idx': 0, 'age-idx': 1, 'dat-idx': 3,
comment': 'composite dataset from Monnin, Petit, Siegenthaler, Luethi'}, \
97 {' name': 'CO2.Byrd', 'file': 'CO2_AhnBrook_and_Blunier_2008.csv', 'header': 4, 'delimiter': ',', 'columns':
None, 'scale': 'GISP2', 'label': 'r"$\mathrm{[CO_2]}$ (ppbv)"', 'color': '#2F4F4F', 'dth-idx': 1, 'age-idx
': 3, 'dat-idx': 3, 'comment': ''}, \
]

##### library parameters #####
102 lib_path = root_dir+'Libraries/'

# library filenames
library_refs = lib_path+'Craig_slope_CH4_ref_Library.csv'
library_refloops = lib_path+'Craig_slope_Refloop_Library.csv'
107 library_airafter = lib_path+'Craig_slope_Loop_after_sample_Library.csv'
library_samples = lib_path+'Craig_slope_Sample_Library.csv'
library_refair = lib_path+'Craig_slope_RefAir_Library.csv'
lib_list = [library_refs, library_refloops, library_samples, library_airafter, library_refair]

112 ## Load corrected data - removed peak contribution from Krypton
#Kryp_cor=csv2rec("/home/lmoeller/Dropbox/Freigabe/Methan_Paper_Lars/TeufelimHeuhaufen/Script Jochen/
Kr_correction_EDML_samples.csv", convertedr={0:str}) # raw values from an older version of Jochens
Kr correction procedure
#Kryp_cor=csv2rec("/home/lmoeller/Dropbox/Freigabe/Methan_Paper_Lars/TeufelimHeuhaufen/Script Jochen/
Kr_correction_EDML_samples_extd.csv", convertedr={0:str}) # values from an older version of Jochens
Kr correction procedure, extended by add. info
Kryp_cor=csv2rec(root_dir+"Krypton_corrected/Sept2012/Kr_correction_EDML_samples_extd_upd070912.csv",
convertedr={0:str})
IPY_cor=csv2rec(root_dir+"Krypton_corrected/Okt2012/IPY_cyl_Krcorr_AWI_LM.csv", convertedr={0:str})
117 IPY_names=['CAO3560', 'CC71560', 'CAO1179']; IPY_era=['present day', 'preindustrial', 'glacial']
NMLKr=csv2rec(root_dir+"Krypton_corrected/Dez2012/Neumayer_Kr.corrected_Dec2012.csv", convertedr={1:str
})
#lib_list = [lib_path+n for n in ['CH4_ref_Library.csv', 'Refloop_Library.csv',
Loop_after_sample_Library.csv', 'Sample_Library.csv', 'RefAir_Library.csv']]
data_cat = ['CH4-Ref', 'Refloop', 'Sample', 'Airafter', 'RefAir']

122 ##### splinefitting procedure #####

enlargement = 10,100,1000 # enlargement of the points for the splinefit (num plots 1000, date
plots 10)
## mrefs
spl_ord = 3 # define splinefit order
127 spl_smth = 4 # define splinefit smoothness

## reflows
rspl_ord = 3 # Spline order an smth that suits reflows better, best known value: 3
rspl_smth_a = 4.0 # 4 has been finally chosen to be the best fitting candidate
132 rspl_smth_b = 1.3 # 1.3 has been finally chosen to be the best fitting candidate
# variables to set the start & end point for the splinefit ranges by absolute measurement number
spl_start_list = 699,802, 967, 1061, 1314, 1514, 1637, 1761, 2063 # ohne Korrektur 699, 1060, 1511,
1631, 1755,2064
spl_end_list = 801, 908,1060, 1313, 1513, 1636, 1760, 2033,"max" # ohne Korrektur 1059, 1510, 1630,
1754, 1766,2063

137 ##### print and plot parameters #####

## Main options

## Plot Sample data?
142 smpl_plot = 'on' # 'on'/'off'
#... in a presentation plot?
pres_plot = 'off' # 'on' or else
## Shall the EDML ice origin be plotted?
plot_origin = 'on' # 'on' or else
147 ## Plot Airafter data?#
aira_plot = 'off'
## Plot Reference Air data?
air_plot = 'off' # 'on' or else
# which one?
152 air_list = ['CAO8463', 'SynthAir', 'CAO1179', 'CAO3560', 'CAO1760', 'CC71560', 'Alert', 'CrystalAir',
Dome13', 'Dome6', 'Neumayer', 'Schauninsland', 'CAO8289'] # []
# determine if the methane refs and the reflows shall be plotted
mref_plt = 'off' # 'on' 'off'
refl_plt = 'off' # 'on' 'off'

157 # Plot Refloop data with Sample Measurement dates?

```

```

plot_sampltrend = 'off' #'on'/'off'
mday_start = '080422' # which date should be the start for this plot?

# Plot a Spline Comparison of Mref, Refl and Airafter
162 spl_compare = 'off' #'on' 'off'
export = 'off' # State 'on' to have the corrected d13C record being exported to file root_dir+export_fn
      (see export section below)

### Additional options
167 eval_run = "off" #'on" # if "on"/"off" remember to set header values for NM_offset und Niveau Correction
      factor to Nil/its values!!
debug_refl = 'off' # create a LoopSplineplot
debug_refl_num = 'off' #plot refl numbers in the LoopSplineplot
debug_corr = 'off' # remember to set header values for NM_offset und Niveau Correction factor to 0 if
      set to on!! Create a previous and after Correction scenario plot.
dbgrafa_plot = 'off' # show all refAir measurements as vertical bars in the LoopSplineplot or as
      scatter in the Correction plot
172 dbgice_plot = "off" # show all Ice measurements measurements as vertical bars in the LoopSplineplot
dbgice_replicates = "off" # show all Replicates as vertical bars in the LoopSplineplot
dbg_firstMref_plot = "off"

# determine if the splinefit data of the methane refs shall be plotted together with the Refloops
177 plot_mrefspl = 'off' # 'off' 'on'

# determine if splinefit data of Refloops shall be plotted
plot_lspl = 'on' # 'on' 'off'

182 # determine if only data of regular 20ml Refloops shall be plotted
regloop_only = 'yes' # 'yes' or else

# Determine General plot size
f_wh = 16 # figure width
187 f_ht = 10 # figure height

### Column assignment
iso_col = 2,4,6,6,4,6 # Isotopy column position of data category (see data_cat for the order)
ord_col = [44,34,38,37,35,38] # Column number where the ordinal date information is stored for
      plotting (same sequence as data_cat list)
192 ##### sample outlier removal options #####

# What kind of Ice and Airafter samples shall be plotted and which datasets shall be excluded?
ice_origin = 'EDML' #, 'EDML' or 'all'
197 Intercomp_ice = ['WDC05', 'B34', 'ShGISP2', 'B37']
EDML_Startdate='080301' # dates before this will be ignored completely!!
#remove_dates = ['080624','080606','080804','080731'] # 1. obvious outlier (Peakareas malicious),
      2.-4. difference pre-After loop >= 0.30 ['080729' EDML-Grbl 1328 => 0.21; '080604' EDML-Grbl',
      '1340'=> 0.25; '080625', 'EDML-Bern', '1349' => 0.24; '080605', 'EDML-Grbl', '1352' => 0.23] ;
      Grnbl1328 800603 kl.Topfflansch undicht
remove_dates = ['080624','090407', '100323', '100713'] # # remove specific datasets in the list
      identified by the date string in EDML library
remove_dates.extend(["070112","070329","070426","070411"]) # measurements obviously outlying in pre-Phd
      period
202 remove_dates.extend(["070321", "070410", "070328", "070424"]) # measurements no included in Fischer08 (
      depth 899,827,912,887 all G01)
B37_Startdate='080301' # dates before this will be ignored completely
B37_ol=["080520","090115"] # Messung abgebrochen >0.3 Sample to Airafter diff; Metallfritte vergessen->
      Wasser in der Leitung?!
# Select the ice range to be used
dml_range = "both" # "glacial", "T1", "both"
207 # Select the age scale to be used
age_choice = 'EDML' # 'Gicc05' 'EDML'
## Should sample data meeting the "max.diff" constraint be removed from the sample dataset?
rem_max = 'yes' #'yes' 'nope'
## Include Heinrich events in plots?
212 plot_hein = 'no' # 'yes'/'no'
heinrich_dates = [12,16.8,24,31,38,45,60] # Hemming(2004) Gisp2 Age scale

##### reference data outlier removal options #####
##### GENERAL
217 ## state "yes" to remove obvious outliers from the reference data libs ('CH4-Ref', 'Refl loop')
rem_ol = 'yes' #'yes' 'nope'
## state "yes" if all outlier removal feedback shall be written to a file (see def read_data for
      filename etc.)
ol_log = 'yes' #'yes'
## how much feedback do you want to get
222 verb_lvl = 'dontcare' # 'tonsof' or close to nothing
# Ignore_list entries, overrides the following thresholds completely !!
thres_ign = ['080624', '080711', '080819']
ol_manual=["033","071", "09"]
ol_manual.extend([str(num) for num in
      [20,21,24,25,26,27,32,43,53,54,73,75,88,112,131,159,161,188,207,221,222,223,244,268,269,320,323,325,359,382,411,426
      #,426(090513 wirklich Outlier?)
227
##### REFERENCE LOOPS AND METHANE
## How many days should have max. passed between the compared measurements (means x days before and
      after the indiv. measurement)
d_past = 1.5
## threshold to identify and remove isotopy outliers (deviation from preceding and following values in
      permille)
232 iso_thr = 0.2 # permille for methane refs
iso_thr_refl = 0.3 # permille for refl loops

```

```

## threshold to identify and remove peak characteristics (Height or Area) outliers (deviation from
    preceding and following values in percent)
peak_thr = 20.0 # percent
## max. allowed Stdev to trigger removal of the dataset from CH4 Reference data array
237 stdv_thr = 0.20 # permille

##### DIFFERENCE LOOP BEFORE AND AFTER ICE MEASUREMENT
## max. allowed Difference between an Airafter measurement isotopy and its preceding Refloop
242 max.diff = 0.3 # permille

##### REFERENCE AIR CONSTRAINTS
## Neumayer measurements (measurement number) that should be ignored for calculations
nm_ol = ["02", "15"] #, "12" added sample "01" in Dec 2012, because no Kr correction was performed on
    it
## Neumayer Isotopy (measured at Heidelberg on an dual inlet irmMS MAT252 with lsigma=0.04,n=7)
247 NM_iso = -46.97 #, (permille), most recent Reference Value by Ingeborg Levin, updated 2008 from old
    value -47.07 (used in Behrens2008 drafts)
NM_offset = -0.02 #0.12 für finalen ord.3 smth.4&1.3 Spline (Dez 2010), 0.02 (March2011), -0.02 after
    Kr Correction Decl2
Btl_niveau_cor = 0.2166 # vor Outlier Review 0.4087, danach 0.3566 für final ord.3 smth.4&1.3 Spline (
    Dez 2010), 0.2566 (March2011); 0.2040 für Corr. über Crystalair (Mai2011), 0.2166 after Kr
    Correction Decl2

## Gravitational correction
252 #grav_slope = 0.0108219340094 # d15N/d18O Gradient/slope on EDML
#grav_incpt = 0.949463023128 # d15N/d18O intercept on EDML
grav_corfac = 0.41 #on EDML
'''
257 #####
# - Definitions
#####
'''
locale.setlocale(locale.LC_ALL, 'en_US.UTF-8')
262 #####
## data read and manipulation definitions
#####
'''
267 ## Find outliers and remove them according to the given threshold in the script header
'''
def outliers(library_file, library_data):
    #print library_data.shape
    if library_file == library_refloops:
        rem_list = list(where(library_data[:, 4]=='nan')[0])
    elif library_file == library_refs:
        rem_list = list(where(library_data[:, 2]=='nan')[0])
    del_nan = len(rem_list) # determines the amount of nan entries in the list for later use
277 print 'Screening Array for Outliers according to the specified thresholds in the script header...'
    print
    if ol_log == 'yes':
        log_file = strftime("%y%m%d.%H.%M.", localtime()) + library_file.rsplit('/', 1)[1][:-4] + '_outliers.
            log'
        file = open(log_dir + 'Corr.Outliers/' + log_file, 'w')
282 file.writelines('### Last script run: ' + asctime(localtime()) +
            '###\n')
        file.writelines('### This file contains the datasets in the ' + library_file.rsplit('/', 1)
            [1][:-4] + ' that met the\n### following specified thresholds and constraints:\n')
        file.writelines('\n')
    if library_file == library_refs:
        if ol_log == 'yes':
287 file.writelines(' Isotopy deviation: ' + str(iso_thr) + ' permille in
            delta13C from the preceding and following measurement. \n')
        file.writelines(' Standard deviation constraint: ' + str(stdv_thr) + ' permille
            deviation from the mean\n')
        file.writelines('\n')
        file.writelines(
            '*****'+
            '\n')
    for nan in rem_list:
292 if ol_log == 'yes':
        file.writelines(' array line ' + str(nan) + ' (number: ' + library_data[nan, 1] + ', date: ' +
            library_data[nan, 0] + ') ' + ' has no isotopy value (nan!) ' + '\n')
        else:
            if verb_lvl == 'tonsof':
                print 'Removing array line %s (number: %s, date: %s) because isotopy value is not a
                    number!...'%(nan, library_data[nan, 1], library_data[nan, 0] )
297 #print len(library_data)
    library_data = delete(library_data, rem_list, 0)
    #print len(library_data)
    for thres in range(1, len(library_data[:, 2]) - 2):
        # find outliers according to specified isotopy deviation
302 if abs(library_data[thres, 2].astype(None) - library_data[thres - 1, 2].astype(None)) > iso_thr
            and abs(library_data[thres, 2].astype(None) - library_data[thres + 1, 2].astype(None)) >
            iso_thr:
            text = 'Isotopy dev. => [' + library_data[thres - 1, 2] + '< ' + library_data[thres, 2] + '>[' +
                library_data[thres + 1, 2] + ']' in line: ' + str(thres) + ', date: ' + library_data[thres
                    , 0] + ', number: ' + library_data[thres, 1]
            rem_list.append(thres)
            if ol_log == 'yes':

```

```

307         file.writelines(text+'\n')
        else:
            if verb_lvl == 'tonsof':
                print text
            # find outliers according to specified max. allowed Stdev value
            elif library_data[thres,3].astype(None) > stdv_thr:
312         text='Stdev thres. => '+library_data[thres,3]+' standard deviation, line '+str(thres
            )+' (number: '+library_data[thres,1]+' , date: '+library_data[thres,0]+' )'
            rem_list.append(thres)
            if ol_log == 'yes':
                file.writelines(text+'\n')
317         else:
            if verb_lvl == 'tonsof':
                print text
            rem_data = "dummy"
        if library_file == library_refloops:
322         ## Add all irregular (!='20' ml Volume) Refloops datasets to the ignore list
            thres_ign.extend(unique(library_data[find(library_data[:, -2]!='20'),0]))

            if ol_log == 'yes':
                file.writelines('    Peak Height/Area leaps: '+str(int(peak_thr))+ ' percent
                deviation from preceding and following values\n')
                file.writelines('    Isotopy deviation: '+str(iso_thr_refl)+ ' permille
                in delta13C from the preceding and following measurement. \n')
327         file.writelines('!!! Ignored datasets:'+str(thres_ign)+' !!!\n')
                file.writelines('\n')
                file.writelines('*****'+'\n')
            for nan in rem_list:
                if ol_log == 'yes':
332         file.writelines('    array line '+str(nan)+' (number: '+library_data[nan,1]+' , date: '+
                library_data[nan,0]+' )'+' has no isotopy value (nan!)+'\n')
                else:
                    if verb_lvl == 'tonsof':
                        print 'Removing array line %s (number: %s,date: %s) because isotopy value is not a
                        number!...'%(nan,library_data[nan,1],library_data[nan,0] )
                    library_data= delete(library_data,rem_list,0)
337         for thres in range(1, len(library_data[:,0])-2):
            # Skip dataset directly if date is in the Ignore list
            if library_data[thres,0] in thres_ign:
                continue
            daydiff_mins= abs(pylib.date2num(datetime(*localtime(float(library_data[thres,-1]))[:6]))-
            pylib.date2num(datetime(*localtime(float(library_data[thres-1,-1]))[:6])))
342         daydiff_plus= abs(pylib.date2num(datetime(*localtime(float(library_data[thres+1,-1]))[:6]))
            -pylib.date2num(datetime(*localtime(float(library_data[thres,-1]))[:6])))
            day_text= '\n    !!! More than the specified %s days have passed between this \n and its
            preceding (No. "%s" on "%s" -> -%1.f days)\n or following (No. "%s" on "%s"-> +%1.
            f days) measurement!!!'%(d_past,library_data[thres-1,1],library_data[thres-1,0],
            daydiff_mins,library_data[thres+1,1],library_data[thres+1,0],daydiff_plus)
            # find outliers according to specified isotopy deviation
            if abs(library_data[thres,4].astype(None)-library_data[thres-1,4].astype(None)) >
            iso_thr_refl and abs(library_data[thres,4].astype(None)-library_data[thres+1,4].astype
            (None)) > iso_thr_refl:
            # In order to rule out false positives check if too much time has passed between the
            # measurements and that the deviation is not exceeded too far
347         if (daydiff_mins + daydiff_plus)/2 < d_past*3 and (abs(library_data[thres,4].astype(
            None)-library_data[thres-1,4].astype(None))+abs(library_data[thres,4].astype(None)-library_data[
            thres+1,4].astype(None))/2 >= (iso_thr_refl+0.1) :
                rem_list.append(thres)
            #
            #
            #
            # the combination of passed time and deviation values points to a false positive
            day_text= day_text + "\n    !!! There is indication that this was a false positive
            , so it has NOT been removed !!!\n    mean days difference: %s (%s) mean deviation: %s (%s-%s)
            "%(((daydiff_mins + daydiff_plus)/2),d_past*3,(abs(library_data[thres,4].astype(None)-library_data
            [thres-1,4].astype(None))+abs(library_data[thres,4].astype(None)-library_data[thres+1,4].astype(
            None)))/2,iso_thr_refl+0.1,(abs(library_data[thres,4].astype(None)-library_data[thres-1,4].astype(
            None))+abs(library_data[thres,4].astype(None)-library_data[thres+1,4].astype(None))/2 >= (
            iso_thr_refl+0.1))
352         text='Isotopy dev => ['+library_data[thres-1,4]+'< '+library_data[thres,4]+' >['+
            library_data[thres+1,4]+' ] in line: '+str(thres)+' , date: '+library_data[thres
            ,0]+' , number: '+library_data[thres,1]
            line = text if daydiff_mins < d_past and daydiff_plus < d_past else text+day_text
            if ol_log == 'yes':
                file.writelines(line+'\n')
357         else:
            if verb_lvl == 'tonsof':
                print line
            # find outliers according to specified Peak characteristics threshold ... in Peak Area
            Column
            elif abs(library_data[thres,14].astype(None)-library_data[thres-1,14].astype(None)) >
            library_data[thres,14].astype(None)*(peak_thr/100) and abs(library_data[thres,14].
            astype(None)-library_data[thres+1,14].astype(None)) > library_data[thres,14].astype(
            None)*(peak_thr/100):
                rem_list.append(thres)
362         text='Peak Area => ['+str("%.6e" % (library_data[thres-1,14].astype(None)/1e+15))
            +']< '+str("%.6e" % (library_data[thres,14].astype(None)/1e+15))+ '>['+str("%.6e
            " % (library_data[thres+1,14].astype(None)/1e+15)) +'] As, line '+str(thres)+' (
            number: '+library_data[thres,1]+' , date: '+library_data[thres,0]+' )'

```

```

line = text if daydiff_mins < d_past and daydiff_plus < d_past else text+day_text
if ol_log == 'yes':
    file.writelines(line+'\n')
else:
367     if verb_lvl == 'tonsof':
        print line
    # ... in Peak Height Column
    elif abs(library_data[thres,9].astype(None)-library_data[thres-1,9].astype(None)) >
        library_data[thres,9].astype(None)*(peak_thr/100) and abs(library_data[thres,9].astype
        (None)-library_data[thres+1,9].astype(None)) > library_data[thres,9].astype(None)*(
        peak_thr/100):
372     rem_list.append(thres)
    text='Peak Height => ['+str("%.6f" % (library_data[thres-1,9].astype(None)/1e+06))
        +']< '+str("%.6f" % (library_data[thres,9].astype(None)/1e+06))+'] >['+str("%.6f"
        % (library_data[thres+1,9].astype(None)/1e+06)) +'] nA, line '+str(thres)+' ('
        number: '+library_data[thres,1]+' , date: '+library_data[thres,0]'+')'
    line = text if daydiff_mins < d_past and daydiff_plus < d_past else text+day_text
    if ol_log == 'yes':
        file.writelines(line+'\n')
        #file.writelines(' array line '+str(thres)+' (number: '+library_data[thres,1]'+',
        date: '+library_data[thres,0]'+')'+') met the Peak characteristics directive (
        Height)'+'\n')
377     else:
        if verb_lvl == 'tonsof':
            print line
    #print len(rem_list),rem_list[del_nan:], library_data[rem_list, 1],len(library_data)
    rem_data = library_data[array(rem_list[del_nan:]),:]
382     library_data= delete(library_data,rem_list[del_nan:],0)
    #print len(library_data)
    if ol_log == 'yes':
        file.writelines('\n')
        file.writelines(##### Summary #####'\n')
387     file.writelines('\n')
        file.writelines('A total of '+str(len(rem_list))+') datasets have been identified as outliers
        under the given constraints!'+'\n')
        file.close()
        print '%s array data sets have been identified as outliers and were therefore being removed
        from it!\n See the logfile "%s" for further details!' %(len(rem_list),log_file) #str(
        rem_list).strip('[').strip(']')
    print
392     else:
        if ol_log != 'yes':
            print ##### Summary #####'\n'
            print 'A total of '+str(len(rem_list))+') datasets have been identified as outliers under
            the given constraints \nand have been removed from the array!'+'\n'

397     print '-----\n'
    ## sort all files in logdir by date and delete all except the newest 8
    for oldest in take(listdir(log_dir+'Corr-Outliers/'), argsort([(mktime(strptime(name[:12],"%y%m%d.%H
        .%M")) for name in listdir(log_dir+'Corr-Outliers/') if len(name.split('.') == 3)])[: -8]):
402     print 'Removing old Log-files "%s"'%(oldest)
        remove(log_dir+'Corr-Outliers/'+oldest)
    ,, return library_data, rem_list, rem_data

#####
407     ### Check for duplicates in abs. measurement number column and fix those errors

def rem_dupl_num(libarray):
    num_col=libarray[:, 1].astype(int)
    doubles_indices = []
    for num in num_col: # find those duplicate entries in the whole number column
412     if len(where(num_col==num)[0]) > 1 and where(num_col==num)[0][1:] not in doubles_indices: #
        positive finding criteria met and number not already in the list
            doubles_indices= append(doubles_indices, where(num_col==num)[0][1:])
    print #
    print '!!! ----- ATTENTION ----- !!!\n'
    print '!!! Found %s duplicate entries in the abs. measurement number column!!!' %(len(
417     doubles_indices))
        print ' This will cause problems during the splinefit calculation!\n'
        print 'I'll renumber the whole column according to these following duplicates:\n'
        print ' Indices %s were found to be double entries...\n' %(str(list(doubles_indices.astype(int)))
        )
    print '!! Please note that the x-axis number range has therefore changed as follows: !!\n'
    ### Correct the abs. numbering column of the libdata
422     leaps = append(doubles_indices[where(diff(doubles_indices) >1)], max(doubles_indices).astype(int)
        # indexes of following leaps (diff > 1) in doubles_indices
    dupl_groups = array_split(doubles_indices,tuple([where(diff(doubles_indices) >1)[0][0]+1])) #
        splitted duplicate groups found by leaps (diff > 1) in doubles_indices
        # raise the nums in org data following a duplicate entry group according to its amount of
        members
    new_ncol = num_col[:doubles_indices[0]] # copy column section of the org. data till the first
        duplicate occurrence to new_col
    raiser = 0 # amount that the sections following duplicates need to be raised
427     for i in range(len(dupl_groups)):
        raiser = raiser+len(dupl_groups[i])
        if i == len(leaps)-1:
            add_section = num_col[leaps[i]+1:len(num_col)]+raiser # final section
        else:

```

```

432         add_section = num_col[leaps[i]+1:leaps[i+1]+1-len(dupl_groups[i+1])+raiser # intermediate
            sections
            # give the duplicates an appropriate number and add it also to the new num_col
            add_cor_dup = num_col[min(dupl_groups[i]):max(dupl_groups[i])+1]+raiser
            new_ncol = append(new_ncol, add_cor_dup)
            new_ncol = append(new_ncol, add_section)
437     print '    Range section %i to %i was adjusted by +%i' %(min(add_section),max(add_section),
            raiser)
    print '-----\n'
    # sort new_ncol and the data array
    sorted_indices=argsort(new_ncol)
    libarray= libarray.take(sorted_indices, axis=-2) # sort the data array
442     new_ncol= new_ncol.take(sorted_indices, axis=-1)# sort new_ncol
    libarray[:,1] = new_ncol # insert the sorted number column
    return libarray

447 '''
#####
### Read the library data # and call outlier routine if demanded
'''

452 def read_data(library_file):
    """
    Read the specified library and return its array'ed dataset.
    """
    print '*****'
457     print 'Reading library file "%s". \nThis might take a while...' %(library_file.rsplit('/',1)[1])

    # Read in String-array
    libread = csv.reader(open(library_file, "rb"))
462     row_c = 1
    for row in libread:
        if row_c == 3:
            library_data = array(row, ndmin=2)
            #print library_data
467     elif row_c > 3:
            library_data = append(library_data, array(row, ndmin=2), axis=0)

        row_c = row_c+1

472     print 'Reading of %s lines finished. Data array returned ...' %(len(library_data))
    print '*****\n'
    ## Remove all irregular Refloop datasets (Volume != 20 ml) if chosen in header
    if regloop_only == 'yes' and library_file == library_refloops:
477     library_data=library_data[find(library_data[:, -2]=='20'),:]
    ## Call def outliers if intended
    if rem_ol == 'yes' and library_file == library_refs:
        library_data, rem_list, rem_data= outliers(library_file, library_data)
    elif rem_ol == 'yes' and library_file == library_refloops:
        rem_list = find([ol_man in ol_manual for ol_man in library_data[:, 1]])
482     rem_data = library_data[rem_list, :]
        library_data=delete(library_data, rem_list, 0)
    else:
        rem_list, rem_data = ['dummy']*2
    return library_data, rem_list, rem_data
487 '''
#####
### Read the external datasets
'''

492 def read_extdata(datafile, headerlines, delimiter, col=None):
    """
    Read external datafile -Not suitable for string type!
    """
497     print '*****'
    print 'Reading external dataset "%s". \nThis might take a while...' %(datafile.rsplit('/',1)[1])
    #print datafile, headerlines, delimiter, col
    #data = read_array(datafile, separator=delimiter, lines=(headerlines, -1))
    data = loadtxt(datafile, delimiter=delimiter, skiprows=headerlines, usecols=col)
502     print 'Reading of %s lines finished. Data array returned ...' %(len(data))
    print '*****\n'
    return data

507 '''
Find those Airref datasets that meet the constraint to have a difference to its corresponding refloop
,, bigger than 0.3 permille (var.. max_diff)
,,

512 def loop_diff (refl, aira, iso_refl, iso_aira):
    print
    '*****'

    print 'Comparing "%s" and "%s" libraries for isotopy differences...\n' %(data_cat[aira], data_cat[
        refl])
    find_refl = list(); negatives = list(); find_aira = list(); counter = 0; diff_list = list()
    for search in range(len(libarray_nlst[aira][:, 0])):
        #print len(where(libarray_nlst[aira][:, 0]==libarray_nlst[aira][search, 0])[0])
517     ## search for occur. of indiv. Airafter date in the Refloop date column

```

```

if len(where(libarray_nlst[refl][:, 0]==libarray_nlst[aira][search, 0])[0]) == 1: #Airafter
    date does exist in Refloop array?
    w = where(libarray_nlst[refl][:, 0]==libarray_nlst[aira][search, 0])[0][0]
    diff = (libarray_nlst[aira][search, iso_aira].astype(None)-libarray_nlst[refl][w, iso_refl
    ].astype(None)).round(3)
    aira_nam = libarray_nlst[aira][search, 0]+'-'+libarray_nlst[aira][search, 1]+'-'+
    libarray_nlst[aira][search, 2]+'-'+libarray_nlst[aira][search, 3]
522 refl_nam = data_cat[refl]+'-'+libarray_nlst[refl][w, 0]+'-'+libarray_nlst[refl][w, 1]
    diff_list.append([aira_nam, refl_nam, diff])
    if abs(diff) >= max_diff:
        if verb_lvl == 'tonsof':

527         if counter is 0:
            print '\
Airafter dataset <== Max.%s permille allowed ==> Refloop dataset
            isotopy Abs. diff isotopy
"%s" %3f <== %3f ==> %3f "%s" '\%(max_diff,aira_nam.replace('Grenoble', 'Grbl'),
    libarray_nlst[aira][search, iso_aira].astype(float),diff, libarray_nlst[refl][w, iso_refl].astype(
float), refl_nam)
532         else:
            print "%s" %3f <== %3f ==> %3f "%s"'\%(aira_nam.replace('Grenoble
', 'Grbl'), libarray_nlst[aira][search, iso_aira].astype(float),diff,
    libarray_nlst[refl][w, iso_refl].astype(float), refl_nam)
            find_refl.append(w)
            find_aira.append(search)
            counter = counter+1
537         elif len(where(libarray_nlst[refl][:, 0]==libarray_nlst[aira][search, 0])[0]) > 1:
            print 'The dataset index %i has more reloop counterparts than expected (%i)' % (search,
    len(where(libarray_nlst[refl][:, 0]==libarray_nlst[aira][search, 0])[0]))
        else:
            negatives.append(libarray_nlst[aira][search, 0])
542 #         if verb_lvl == 'tonsof':

            print
            print 'Found %i Airafter datasets exceeding the given constraint of max. %s permille in the
            max_diff variable' %(len(find_refl),max_diff)
            print
            print 'The following %i Airafter date(s) couldn't be found in the Refloop database:' %(len(unique(
            negatives)))
547         print unique(negatives)
            print
            print
            print
            print '*****'

    return find_refl,find_aira,diff_list

552 ...
#####
### Convert a time information sequence from 'Secs since utc start' to a day ordinal (days since utc
... start)
557 def sec_to_ord(seq):
    #print 'Converting time information from float sec since utc start to date ordinal...\n'
    o_col = []
    for utc_sec in seq.astype(None):
        o_col.append(pylab.date2num(datetime(*localtime(utc_sec)[:6])))# convert each float sec to
        struct.time tuple(localtime()), translate to datetime object (datetime()), transform to
        day ordinal for plotting (pylab.date2num())
562 return o_col

    # Alternative conversion
    #dateconv = strptime2num("%y%m%d%H%M%S") # convert from str to ordinal function by given fmt
    #dateconv(strftime("%y%m%d%H%M%S",localtime(utc_sec))) # convert the newly generated (by strftime
    out of localtime-tuple) string to
567 # or short:
    # pylab.strptime2num("%y%m%d%H%M%S")(strftime("%y%m%d%H%M%S",localtime(utc_sec)))
    # for a whole sequence
    # map(lambda utc: pylab.strptime2num("%y%m%d%H%M%S")(strftime("%y%m%d%H%M%S",localtime(utc))),
    libarray_nlst[2][:,-4].astype(float))
...
572 #####
### Find and return the Indices in External datasets
### that correspond to given data ranges (depth or age in the range val_min to val_max)
### Make sure that val_min, val_max are assigned with the same val_round value when calling this def!

577 #def ext_idc(val_col, val_min, val_max, val_round):
    ## print val_min, val_max, val_round
    # while len(where(val_col.astype(float).round(decimals=val_round)==val_min)[0]) < 1 and val_min >
    min(val_col.astype(float)):
    # val_min = val_min-1
    # else:
582 # min_idx=where(val_col.astype(float).round(decimals=val_round)==val_min)[0][0]
    # if min_idx < 5:
    # min_idx = 5
    # while len(where(val_col.astype(float).round(decimals=val_round)==val_max)[0]) < 1 and val_max <
    max(val_col.astype(float)):
    # val_max = val_max+1
587 # else:
    ## print find(val_col.astype(float).round(decimals=val_round+1)==val_max.round(decimals=

```



```

val_round+1)), val_col[find(val_col.astype(float).round(decimals=val_round+1)==val_max.round(
decimals=val_round+1)).round(decimals=val_round+1)
##      print val_max, where(val_col.astype(float).round(decimals=val_round)==val_max)[0], find(
val_col.astype(float).round(decimals=val_round)==val_max.round(decimals=val_round)), val_col[where(
val_col.astype(float).round(decimals=val_round)==val_max)[0]] , max(val_col.astype(float), val_max
.round(decimals=val_round+1)
##      max_idx=where(val_col.astype(float).round(decimals=val_round)==val_max)[0][0]
#      while len(find(val_col.astype(float).round(decimals=val_round+1)==val_max.round(decimals=
val_round+1))) == 0:
592 #          val_round= val_round-1
#          else:
#              max_idx = max(find(val_col.astype(float).round(decimals=val_round+1)==val_max.round(
decimals=val_round+1)))
##              print min_idx, max_idx
#              return min_idx, max_idx
597 def ext_idc(val_col, val_min, val_max, val_round):
#print val_min, min(val_col.astype(float)),
try:
    while len(where(val_col.astype(float).round(decimals=val_round)==val_min)[0]) < 1 and val_min >
min(val_col.astype(float)):
val_min = val_min-1
602     else:
min_idx=where(val_col.astype(float).round(decimals=val_round)==val_min)[0][0]
if min_idx < 5:
min_idx = 5
except:
607 #     print '\n\nThe datasets minimal age (%s kyBP) exceeds the specified lower age range limit (%s
kyBP)! \nI will use %s as lower limit now...'%(min(val_col.astype(float)), x_limits[0], min(val_col
.astype(float)))
min_idx= 0
try:
    while len(where(val_col.astype(float).round(decimals=val_round)==val_max)[0]) < 1 and val_max <
max(val_col.astype(float)):
val_max = val_max+1
612     else:
max_idx=where(val_col.astype(float).round(decimals=val_round)==val_max)[0][0]
except:
#     print '\n\nThe datasets maximal age (%s kyBP) is inferior to the specified upper age range
limit (%s kyBP)! \n
#     I will use %s as upper limit now...'%(max(val_col.astype(float)), x_limits[1], max(val_col.
.astype(float)))
617     max_idx= -1
,, return min_idx, max_idx
,,
#####
622 ## Calculate the mean Neumayer RefAir Mean and Stdev for Neumayer Correction
def Neumayer_correction(data_array, iso_col, idc=None):
remove_idc=[where(data_array[:, -5].astype(int) ==n)[0][0] for n in nm_ol]
if idc != None:
627     remove_idc.extend(idc)
remove_idc = list(unique(remove_idc))
cropped_data_array=delete(data_array, remove_idc, axis=0)
return mean(cropped_data_array[:, iso_col].astype(float)), std(cropped_data_array[:, iso_col].astype(
float)), var(cropped_data_array[:, iso_col].astype(float)), len(cropped_data_array), remove_idc
632 '''
#####
# Find replicates in sample data, calculate a mean and std.dev of them,
# append columns with its data to array and del the 2nd repl
# This is needed to make use of errorbar plots etc.
637 '''
def sample_replicates(smpl_dsrt, i_col, o_col):
corr_idc = tuple(where(smpl_dsrt[:, o_col+1].astype(None)!=0.0)[0]) # Return those indices, where
age information is present and make a tuple of it
slib_dpsrt_red = smpl_dsrt.take(array(corr_idc), axis=-2) # get the library entries of those
indices
# find duplicate entries in the whole depth column
G02_indices = []; std_col = []; mn_uncor_col = []; std_uncor_col = []
for dupl in range(len(slib_dpsrt_red[:, 2])):
# print [where(slib_dpsrt_red[:, 2]==slib_dpsrt_red[dupl, 2])[0][dp] for dp in range(2, len(where(
slib_dpsrt_red[:, 2]==slib_dpsrt_red[dupl, 2])[0]))]
# print slib_dpsrt_red[dupl, 2].astype(float).round(decimals=1)//1
idc = where(slib_dpsrt_red[:, 2].astype(float).round(decimals=1)//1==slib_dpsrt_red[dupl, 2].
astype(float).round(decimals=1)//1)[0]
647     if len(idc) > 1 and ([idc[dp] for dp in range(1, len(idc))][0] not in G02_indices): #
positive finding criteria met and number not already in the list
# print [where(slib_dpsrt_red[:, 2]==slib_dpsrt_red[dupl, 2])[0][dp] for dp in range(1, len(
where(slib_dpsrt_red[:, 2]==slib_dpsrt_red[dupl, 2])[0]))][0]
w = tuple(idc)
mn_uncor_col.append(mean(slib_dpsrt_red[w, i_col].astype(None)).round(decimals=3))
std_uncor_col.append(std(slib_dpsrt_red[w, i_col].astype(None)).round(decimals=3))
652     mn_col.append(mean(slib_dpsrt_red[w, o_col+1].astype(None)).round(decimals=3))
std_col.append(std(slib_dpsrt_red[w, o_col+1].astype(None)).round(decimals=3))
G02_indices= append(G02_indices, int(idc[1:]))
# notdpthsort_idc = append(notdpthsort_idc, find([date in smpl_dsrt[idc, 0] for date in
libarray_nlst[2][:, 0]))

```

```

657     slib_dpsrt_red[w[0],3]=slib_dpsrt_red[w[0],3]+'+'+slib_dpsrt_red[w[1],3] # correct the cut
        name to a merged version
        #print w,smpl_dsrt[indc,0],libarray_nlst[2][indc,0]#notdpthsort_idc #len(mn_col),len(
            std_col)
    else:
        #print dupl, tuple(idc),mean(slib_dpsrt_red[dupl,i_col].astype(None)).round(decimals=3),
            mean(slib_dpsrt_red[tuple(idc),i_col].astype(None)).round(decimals=3)
        mn_uncor_col.append(mean(slib_dpsrt_red[tuple(idc),i_col].astype(None)).round(decimals=3))
662     std_uncor_col.append(std(slib_dpsrt_red[tuple(idc),i_col].astype(None)).round(decimals=3))
        mn_col.append(mean(slib_dpsrt_red[tuple(idc),o_col+1].astype(None)).round(decimals=3))
        std_col.append(std(slib_dpsrt_red[tuple(idc),o_col+1].astype(None)).round(decimals=3))
    #print G02_indices.astype(int),mn_col, std_col,
    #array(mn_col,ndmin=2).transpose()
667     #print slib_dpsrt_red.shape, smpl_dsrt.shape, mn_uncor_col

    ## Append the mean and std. of the corrected isotopy values from both cuts to the arrays
    slib_dpsrt_red = append(slib_dpsrt_red,array(mn_col,ndmin=2).transpose(),axis=1)
672     slib_dpsrt_red = append(slib_dpsrt_red,array(std_col,ndmin=2).transpose(),axis=1)

    smpl_dsrt= append(smpl_dsrt,array(mn_uncor_col,ndmin=2).transpose(),axis=1)
    smpl_dsrt= append(smpl_dsrt,array(std_uncor_col,ndmin=2).transpose(),axis=1)
    smpl_dsrt= append(smpl_dsrt,array(mn_col,ndmin=2).transpose(),axis=1)
    smpl_dsrt= append(smpl_dsrt,array(std_col,ndmin=2).transpose(),axis=1)
677     #print slib_dpsrt_red.shape, smpl_dsrt.shape

    ## Delete replicate depth entries

    slib_dpsrt_red = delete(slib_dpsrt_red,G02_indices,axis=0) # delete double depth entries recorded
682     in G02_indices list
    run_c = 0
    ## ... also from the uncorrected mean and std. list
    for l in G02_indices.astype(int):
        #print mn_uncor_col[l-run_c]
        del mn_uncor_col[l-run_c]
687     del std_uncor_col[l-run_c]
        run_c = run_c + 1
    return slib_dpsrt_red, smpl_dsrt, mn_uncor_col, std_uncor_col, G02_indices.astype(int)

692 def ref_plot(lib,data_array,typus,o_col,i_col):
    fig = pylab.figure(figsize=[f_wh,f_ht])
    pylab.figtext(0.8,0.02,'created: '+asctime(localtime()),size=9)
    #####
    ## Subplot 1
    #####
697     fig.suptitle('Library entries and Corrected values of '+typus+' data',fontsize=16)
    old_bottle = find(data_array[:,o_col].astype(None)<733773.0) # select all datasets before
        01.01.2010
    new_bottle = find(data_array[:,o_col].astype(None)>733773.0) # select all datasets after
        01.01.2010
    #tmcorr_idc = tuple(where(data_array[:, -1].astype(None)!=0.0)[0]) # select the indices of the tm
        corr. col where data != 0
702

    slabel = 'Splinefit ord. '+str(spl_ord)+' smth. '+str(spl_smth)
    rlable = 'Splinefit ord. %s smth. %s/%s'%(rspl_ord,rspl_smth_a,rspl_smth_b)

    if lib == 1 and '20ml' in typus:
707     spla = fig.add_subplot(321)
        splb = fig.add_subplot(322)
        spla.set_title("Old Reference bottle range",fontsize=12)
        splb.set_title("New Reference bottle range",fontsize=12)
        org_label=typus+' library data (uncorrected)'
712     tmcorr_label=typus+' (spline corrected)'
        spla.set_ylabel(r'$\delta\;^{13}\text{C}\;(\text{‰})$')
        spla.plot_date(data_array[old_bottle,o_col].astype(None),data_array[old_bottle,i_col].astype(
            None),fmt='bo-',tz=None,xdate=True,ydate=False,label='$\delta\;^{13}\text{C}\;(\text{‰})$'+
            org_label)
        splb.plot_date(data_array[new_bottle,o_col].astype(None),data_array[new_bottle,i_col].astype(
            None),fmt='bo-',tz=None,xdate=True,ydate=False,label='$\delta\;^{13}\text{C}\;(\text{‰})$'+
            org_label)
717     if plot_mrefspl == 'on':
        ## Add the methane ref data
        ## Calculate the spline fit of Methane Ref data (x=date ordinal y= raw isotopy)
        if shape(libarray_nlst[0])[1] is not 45:
            libarray_nlst[0] = append(libarray_nlst[0],array(map(lambda utc: pylab.strptime2num("%m%
                %d%H%M%S"%(strftime("%m%d%H%M%S",localtime(utc))),libarray_nlst[0][:,-1].
                astype(None)),ndmin=2).transpose(),axis=1)
            spl_mref = scipy.interpolate.splprep(libarray_nlst[0][:,-1].astype(None),libarray_nlst
                [0][:,2].astype(None),k=spl_ord,s=spl_smth)
722     spl_mref_x = arange(min(libarray_nlst[0][:,-1].astype(None)),max(libarray_nlst[0][:,-1].
                astype(None))+1.0/enlargement[0],1.0/enlargement[0]) # reduce stepping between x-
                datapoints
            spl_mref_y = scipy.interpolate.splev(spl_mref_x,spl_mref)

            spl.plot_date(libarray_nlst[0][:,-1].astype(None),libarray_nlst[0][:,2].astype(None),
                color='0.85',fmt='o-',tz=None,xdate=True,ydate=False,label='$\delta\;^{13}\text{C}\;(\text{‰})$'+
                ' of methane refs.')
            spl.plot_date(spl_mref_x,spl_mref_y,color='mediumorchid',fmt='-',lw=2,tz=None,xdate=
                True,ydate=False,label=slabel+' methane refs total range')

```

```

727     #pylab.plot_date(mref_rsplars[:,0], mref_rsplars[:,1], color= 'dodgerblue',fmt= '- ',lw=2, tz=
        None, xdate=True, ydate=False, label=slabel+' methane refs indiv. ranges')
    if plot_lspl == 'on':

        # old bottle
        spla.plot_date(splrefl_old_x, splrefl_old_y, color= 'purple', fmt= '- ',lw=2, tz=None, xdate
732         =True, ydate=False, label=rlabel+' reflows ')
        spla.text(0.75,0.8, 'Splinefit to data difference:\n mean: %0.3f permille\n std.:
            %0.3f'%(mean(abs(spldif_old)),sqrt(sum(spldif_old**2)/len(spldif_old))), bbox=dict(
            facecolor='0.5', alpha=0.5), fontsize=8, transform = spla.transAxes) # Enter text in
            subplot object at relative position (0-1)
        spla.add_line(pylab.Line2D([min(splrefl_old_x).round(),max(splrefl_old_x).round()],[
            loopspl_old_mean,loopspl_old_mean], linewidth=1, linestyle='-', color='k'))
        spla.text(max(splrefl_old_x).round()-140,loopspl_old_mean, 'Spline Mean: %0.3f'%(
            loopspl_old_mean), fontsize=8) # Enter text in subplot object at ax pos. , bbox=dict(
            facecolor='0.5', alpha=0.5)
        # new bottle
        splb.plot_date(splrefl_new_x, splrefl_new_y, color= 'purple', fmt= '- ',lw=2, tz=None, xdate
737         =True, ydate=False, label=rlabel+' reflows ')
        splb.text(0.75,0.8, 'Splinefit to data difference:\n mean: %0.3f permille\n std.:
            %0.3f'%(mean(abs(spldif_new)),sqrt(sum(spldif_new**2)/len(spldif_new))), bbox=dict(
            facecolor='0.5', alpha=0.5), fontsize=8, transform = splb.transAxes) # Enter text in
            subplot object at relative position (0-1)
        splb.add_line(pylab.Line2D([min(splrefl_new_x).round(),max(splrefl_new_x).round()],[
            loopspl_new_mean,loopspl_new_mean], linewidth=1, linestyle='-', color='k'))
        splb.text(max(splrefl_new_x).round()-10,loopspl_new_mean, 'Spline Mean: %0.3f'%(
            loopspl_new_mean), fontsize=8) # Enter text in subplot object at ax pos. , bbox=dict(
            facecolor='0.5', alpha=0.5)
        spla.legend(loc='lower left', numpoints = 3, prop = matplotlib.font_manager.FontProperties(size
            =8)) # 0, ur1, ul2, uc9, lr4, ll3,
        #splb.legend(loc='lower left', numpoints = 3, prop = matplotlib.font_manager.FontProperties(
            size=8)) # 0, ur1, ul2, uc9, lr4, ll3,
742     mn_correfa= spltiff_mean;std_correfa =spltiff_err;var_correfa=spltiff_err**2;rep=len(
        spltiff_overall)
    else:
        spl = fig.add_subplot(311, autoscale_on=True)
        org_label=typus+' library data (uncorrected)'
        tmcorg_label=typus+' (spline corrected)'
747     spl.set_ylabel(r'$\delta\text{ }^{13}\text{C } \text{ }(\text{‰})$')
        import matplotlib.ticker as ticker
        N = len(data_array)
        ind = arange(N)
        ## Remove outliers for Data refrence calculations(mean, stdev, var)
        if typus =='Neumayer':
752     mn_correfa, std_correfa, var_correfa, rep, rem_idc = Neumayer_correction(data_array, o_col+1)
            box_str = typus+' data preferences (corrected) *:\n mean: %0.3f permille\n std.:
                %0.3f permille\n var.: %0.3f permille\n * outliers removed No. %s'%(mn_correfa,
                std_correfa, var_correfa, nm_ol)
        else:
757     mn_correfa=mean(data_array[:, o_col+1].astype(float))
            std_correfa=std(data_array[:, o_col+1].astype(float))
            var_correfa=var(data_array[:, o_col+1].astype(float))
            rep = len(data_array)
            box_str = typus+' data preferences (corrected):\n mean (n=%i): %0.3f permille\n std
                .: %0.3f permille\n var.: %0.3f permille'%(rep, mn_correfa, std_correfa, var_correfa)
762     # Convert from ordinals to str "%d-%m-%Y"
        def format_date(x, pos=None):
            thisind = clip(int(x+0.5), 0, N-1)
            return datetime(*localtime(data_array[:, o_col - 1][thisind].astype(None))[ :6] ).strftime('%d-%
                m-%Y')
        spl.plot(ind, data_array[:, o_col+1].astype(None), 'o-', label='$\delta\text{ }^{13}\text{C } \text{ }(\text{‰})$ '+
767         tmcorg_label)
        if typus =='Neumayer':
            spl.plot(ind[tuple(rem_idc)], data_array[tuple(rem_idc), o_col+1].astype(None), 'o',ms=4,
                mfc = 'red')
        spl.text(0.01,0.74, box_str, bbox=dict(facecolor='0.5', alpha=0.2), fontsize=8, transform =
            spl.transAxes) # Enter text in subplot object at relative position (0-1)
        spl.xaxis.set_major_formatter(ticker.FuncFormatter(format_date))
772     #fig.autofmt_xdate()
        yfmt = spl.yaxis.get_major_formatter()
        yfmt.set_powerlimits((-2, 10))
        spl.yaxis.get_major_formatter().set_scientific(False)
        yfmt.set_scientific(False)
777     #spl.draw()
        spl.invert_yaxis
        spl.legend(loc='lower left', numpoints = 3, prop = matplotlib.font_manager.FontProperties(size
            =8)) # 0, ur1, ul2, uc9, lr4, ll3,
        spl.autoscale_view(tight=False)

        #####
782     ### Subplot 2
        #####

        #pylab.xlabel('Measurement date range')
        if lib == 1:
787     sp2a = fig.add_subplot(323)

```

```

sp2a.set_ylabel(r'$\delta\;^{\{13\}}\text{C}\;(\%_{\text{0}})$')
sp2b = fig.add_subplot(324)
## Plot uncorrected dataset
sp2a.plot_date(data_array[old_bottle, o_col].astype(None), data_array[old_bottle, i_col].astype(
None), color='0.75', fmt='o-', tz=None, xdate=True, ydate=False, label='$\delta\;^{\{13\}}\text{C}\;(\%_{\text{0}})$ '+org_label)
792 sp2b.plot_date(data_array[new_bottle, o_col].astype(None), data_array[new_bottle, i_col].astype(
None), color='0.75', fmt='o-', tz=None, xdate=True, ydate=False, label='$\delta\;^{\{13\}}\text{C}\;(\%_{\text{0}})$ '+org_label)

## Plot tm corrected dataset
sp2a.plot_date(data_array[old_bottle, o_col].astype(None), data_array[old_bottle, o_col+1].astype(
None), color='darkblue', fmt='o-', tz=None, xdate=True, ydate=False, label='$\delta\;^{\{13\}}\text{C}\;(\%_{\text{0}})$ '+tmc_or_label)
sp2b.plot_date(data_array[new_bottle, o_col].astype(None), data_array[new_bottle, o_col+1].astype(
None), color='darkblue', fmt='o-', tz=None, xdate=True, ydate=False, label='$\delta\;^{\{13\}}\text{C}\;(\%_{\text{0}})$ '+tmc_or_label)
797 sp2a.legend(loc='lower left', numpoints = 3, prop = matplotlib.font_manager.FontProperties(size
=8)) # 'best' 0, url, ul2, uc9, lr4, ll3,
#sp2b.legend(loc='lower left', numpoints = 3, prop = matplotlib.font_manager.FontProperties(
size=8)) # 'best' 0, url, ul2, uc9, lr4, ll3,
else:
sp2 = fig.add_subplot(312, sharex=sp1)
sp2.set_ylabel(r'$\delta\;^{\{13\}}\text{C}\;(\%_{\text{0}})$')
802 if typus == 'Neumayer':
remove_idx=[where(data_array[:, -5].astype(int) == n)[0][0] for n in nm_ol]
cropped_data_array=delete(data_array, remove_idx, axis=0)
mn_refa=mean(cropped_data_array[:, i_col].astype(float))
std_refa=std(cropped_data_array[:, i_col].astype(float))
807 var_refa=var(cropped_data_array[:, i_col].astype(float))
box_str = typus+' data preferences (uncorrected) *:\n mean: %0.3f permille\n std.:
%0.3f permille\n var.: %0.3f permille\n * outliers removed No. %s'%(mn_refa,
std_refa, var_refa, nm_ol)
else:
mn_refa=mean(data_array[:, i_col].astype(float))
std_refa=std(data_array[:, i_col].astype(float))
812 var_refa=var(data_array[:, i_col].astype(float))
box_str = typus+' data preferences (uncorrected):\n mean: %0.3f permille\n std.:
%0.3f permille\n var.: %0.3f permille'%(mn_refa, std_refa, var_refa)

sp2.text(0.01,0.74 ,box_str , bbox=dict(facecolor='0.5', alpha=0.2), fontsize=8, transform =
sp2.transAxes) # Enter text in subplot object at relative position (0-1)

817 sp2.plot(ind, data_array[:, i_col].astype(None) , 'o-', color= '0.75', label='$\delta\;^{\{13\}}\text{C}\;(\%_{\text{0}})$ '+org_label)
sp2.plot(ind, data_array[:, o_col+1].astype(None) , 'o-', color= 'darkblue', label='$\delta\;^{\{13\}}\text{C}\;(\%_{\text{0}})$ '+tmc_or_label)
sp2.xaxis.set_major_formatter(ticker.FuncFormatter(format_date))
sp2.yaxis.get_major_formatter().set_scientific(False)
#fig.autofmt_xdate()
822 sp2.invert_yaxis
sp2.legend(loc='lower left', numpoints = 3, prop = matplotlib.font_manager.FontProperties(size
=8)) # 'best' 0, url, ul2, uc9, lr4, ll3,
sp2.autoscale_view(tight=False)

#####
827 ## Subplot 3 - Plot the two methane ref peaks
#####

if lib == 1:
sp3a = fig.add_subplot(325)
sp3a.set_ylabel(r'$\delta\;^{\{13\}}\text{C}\;(\%_{\text{0}})$ Ref Peaks')
sp3a.set_xlabel('Measurement date range')
sp3b = fig.add_subplot(326)
sp3b.set_xlabel('Measurement date range')
# old bottle
837 mean_mrefs = map(lambda x: mean(x), zip(data_array[old_bottle, i_col-2].astype(float), data_array[
old_bottle, i_col+2].astype(float)))
std_mrefs = map(lambda x: std(x), zip(data_array[old_bottle, i_col-2].astype(float), data_array[
old_bottle, i_col+2].astype(float)))
sp3a.plot_date(data_array[old_bottle, o_col].astype(None), mean_mrefs, color='blue', fmt='o-',
tz=None, xdate=True, ydate=False, label='$\delta\;^{\{13\}}\text{C}\;(\%_{\text{0}})$ Ref Peaks')
pylab.setp(pylab.getp(pylab.gca(), 'xticklabels'), visible=False)
sp3a.errorbar(data_array[old_bottle, o_col].astype(None), mean_mrefs, std_mrefs, color='blue',
fmt='o-', ecolor='r', capsize=3) #, label='$\delta\;^{\{13\}}\text{C}\;(\%_{\text{0}})$ Ref Peaks'
842 pylab.setp(pylab.getp(pylab.gca(), 'xticklabels'), visible=True)
sp3a.legend(loc='lower left', numpoints = 3, prop = matplotlib.font_manager.FontProperties(size
=8)) # 'best' 0, url, ul2, uc9, lr4, ll3,
# new bottle
mean_mrefs = map(lambda x: mean(x), zip(data_array[new_bottle, i_col-2].astype(float), data_array[
new_bottle, i_col+2].astype(float)))
std_mrefs = map(lambda x: std(x), zip(data_array[new_bottle, i_col-2].astype(float), data_array[
new_bottle, i_col+2].astype(float)))
847 sp3b.plot_date(data_array[new_bottle, o_col].astype(None), mean_mrefs, color='blue', fmt='o-',
tz=None, xdate=True, ydate=False, label='$\delta\;^{\{13\}}\text{C}\;(\%_{\text{0}})$ Ref Peaks')
pylab.setp(pylab.getp(pylab.gca(), 'xticklabels'), visible=False)

```

```

sp3b.errorbar(data_array[new_bottle,o_col].astype(None),mean_mrefs ,std_mrefs , color= 'blue',
              fmt='o-', ecolor='r', capsize=3) #, label='$\delta\;^{13}\$C \$(\%_0)\$ Ref Peaks'
pylab.setp(pylab.getp(pylab.gca(), 'xticklabels'), visible=True)
#sp3b.legend(loc='lower left', numpoints = 3, prop = matplotlib.font_manager.FontProperties(
size=8)) #'best' 0, url, ul2, uc9, lr4, ll3,
852
### Add the methan ref data
if plot_mrefspl == 'on' and lib == 1:
#   ## Calculate the spline fit of Methane Ref data (x=date ordinal y= raw isotopy)
#   spl_mref = scipy.interpolate.splrep(libarray_nlst[0][:, -1].astype(None),libarray_nlst
857 #   [0][:, 2].astype(None),k=spl_ord, s=spl_smth)
#   splmref_x = arange(min(libarray_nlst[0][:, -1].astype(None)), max(libarray_nlst[0][:, -1].
astype(None))+1.0/enlargement[0], 1.0/enlargement[0]) # reduce stepping between x-datapoints
#   splmref_y = scipy.interpolate.splev(splmref_x, spl_mref)
#
pylab.plot_date(libarray_nlst[0][:, -1].astype(None),libarray_nlst[0][:, 2].astype(None),
               color= '0.85',fmt='o-', tz=None, xdate=True, ydate=False, label='$\delta\;^{13}\$C \$(\%_0)\$'+
' of methane refs.')
pylab.plot_date(splmref_x, splmref_y, color= 'mediumorchid', fmt= '-',lw=2, tz=None, xdate=
True, ydate=False,label=slabel+' methane refs total range')
862 #pylab.plot_date(mrefsrsplar[:,0], mrefsrsplar[:,1], color= 'dodgerblue',fmt= '-',lw=2, tz=
None, xdate=True, ydate=False, label=slabel+' methane refs indiv. ranges')

else:
mean_mrefs = map(lambda x: mean(x),zip(data_array[:,i_col-2].astype(float),data_array[:,i_col
+2].astype(float)))
std_mrefs = map(lambda x: std(x),zip(data_array[:,i_col-2].astype(float),data_array[:,i_col+2].
astype(float)))
867 sp3 = fig.add_subplot(313, sharex=sp1)
sp3.set_ylabel(r'\delta\;^{13}\$C \$(\%_0)\$ Ref Peaks')
sp3.set_xlabel('Measurement date range')
sp3.plot(ind,mean_mrefs, 'o-', color= 'blue', label='$\delta\;^{13}\$C \$(\%_0)\$ Ref Peaks')
pylab.setp(pylab.getp(sp3, 'xticklabels'), visible=False)
872 sp3.errorbar(ind,mean_mrefs ,std_mrefs , color= 'blue', fmt='o-', ecolor='r', capsize=3) #,
label='$\delta\;^{13}\$C \$(\%_0)\$ Ref Peaks'
pylab.setp(pylab.getp(sp3, 'xticklabels'), visible=True)
sp3.xaxis.set_major_formatter(ticker.FuncFormatter(format_date))
yfmt = sp3.yaxis.get_major_formatter()
yfmt.set_scientific(False)
877 sp3.invert_yaxis
fig.autofmt_xdate()
sp3.legend(loc='lower left', numpoints = 3, prop = matplotlib.font_manager.FontProperties(size
=8)) #'best' 0, url, ul2, uc9, lr4, ll3,
sp3.autoscale_view(tight=False)
882 ## Adjustments etc.
if '20ml' in typus:
fig.subplots_adjust(left=0.06, bottom=0.06, right=0.96, top=0.94, hspace=0.12, wspace = 0.10)
elif lib == 1:
fig.subplots_adjust(left=0.06, bottom=0.06, right=0.96, top=0.96, hspace=0.12)
else:
887 fig.subplots_adjust(left=0.06, right=0.96, top=0.96, bottom=0.1, hspace=0.12)

## append figure to the plotlist
892 #refa_dic.append({'cat':data_cat[lib], 'type':typus, 'data':data_array, 'fig':fig, 'iso_mean(n=%s)'\%(
rep):mn_correfa, 'iso_stddev(n=%s)'\%(rep):std_correfa})

def sample_plot(smpl_dsrt, o_col, i_col, splrefl_old_x, splrefl_old_y):
897 org_label=data_cat[2]+' library data (uncorrected)'
tmc_or_label=data_cat[2]+' (spline corrected)'
#tmc_or_idc = tuple(where(data_array[:, -1].astype(None)!=0.0)[0]) # select the indices of the tm
corr_col where data != 0
902 #####
### Sample Figure 1
### Plot Sample data by depth and Age and the Methane Concentration
#####
smpl_fig1=pylab.figure(figsize=[f_wh, f_ht])
pylab.figtext(0.8, 0.02, 'created: '+asctime(localtime()), size=9)
907 ## PLOT the tm corr dataset alone with [CH4] axis
pylab.subplot(211)
pylab.title('Spline Corrected values of '+data_cat[2]+' data')
pylab.ylabel(r'\delta\;^{13}\$C \$(\%_0)\$')
#print smpl_dsrt[:,(0,1,2,i_col,-4,-3,-2,-1)]
912 corr_idc = tuple(where(smpl_dsrt[:,o_col+1].astype(None)!=0.0)[0]) # Return those indices, where
age information is present and make a tuple of it
slib_dpsrt_red = smpl_dsrt.take(array(corr_idc), axis=-2) # get the library entries of those
indices
#print slib_dpsrt_red[:,(0,1,2,i_col,-4,-3,-2,-1)], corr_idc
917 # plot uncorr dataset by depth
pylab.plot(slib_dpsrt_red[:,2].astype(None),slib_dpsrt_red[:, i_col].astype(None), 'o-', color=
'red', label='$\delta\;^{13}\$C \$(\%_0)\$ '+org_label)
## Inverse y-axis
pylab.gca().set_ylim(pylab.gca().get_ylim()[: -1])

```

```

922 # plot tm corr dataset
pylab.plot(slib_dpsrt_red[:,2].astype(None),slib_dpsrt_red[:, o_col+1].astype(None) , 'o-', color=
'darkblue', label='$\delta\;^{\{13\}}\text{C}\; \text{\%0}\$'+tmcor_label)

if plot_origin == 'on' and ice_origin is 'EDML':
927     def ice_orig(name_col):
        '''Find the name strings of the individual ice origins in the spec. Column and return their
            index tuples'''
        orig_awi = list(where(name_col=='EDML-AWI')[0])
        orig_bern = list(where(name_col=='EDML-Bern')[0])
        orig_bern.extend(list(where(name_col=='EDML-BERN')[0]))
        orig_grbl = list(where(name_col=='EDML-Grbl')[0])
932     orig_grbl.extend(list(where(name_col=='EDML-Grenoble')[0]))
        return tuple(sort(orig_awi)), tuple(sort(orig_bern)), tuple(sort(orig_grbl))
    # get the indices of the ice origin
    orig_awi,orig_bern,orig_grbl=ice_orig(slib_dpsrt_red[:,1])
    # plot tm corr dataset ice origin
937     pylab.plot(slib_dpsrt_red[orig_grbl,2].astype(None),slib_dpsrt_red[orig_grbl, o_col+1].astype(
        None) , 'o', color='darkblue',ms=4,mfc='yellow', label='Grenoble samples')
    pylab.plot(slib_dpsrt_red[orig_awi,2].astype(None),slib_dpsrt_red[orig_awi, o_col+1].astype(
        None) , 'o', color='darkblue',ms=4,mfc='white', label='AWI samples')
    pylab.plot(slib_dpsrt_red[orig_bern,2].astype(None),slib_dpsrt_red[orig_bern, o_col+1].astype(
        None) , 'o', color='darkblue',ms=4,mfc='red', label='Bern Samples')
    pylab.legend(loc=2, numpoints=3, prop=matplotlib.font_manager.FontProperties(size=10)) #'best'
        0, url, ul2, uc9, lr4, ll3,

942 if ice_origin is 'EDML':
    ## Add the second y-axis with [CH4] data
    ax2 = pylab.twinx()
    pylab.ylabel('$[CH4]$ in ppbv', color='g')
    # determine the CH4 depth range for plotting
947     min_idx,max_idx=ext_idc(ch4_data['data'][:,ch4_data['dth-idx']],min(slib_dpsrt_red[:,2].astype(
        float).round(decimals=0)),max(slib_dpsrt_red[:,2].astype(float).round(decimals=0)),0)
    if min_idx>=3 and max_idx<=(len(ch4_data['data'])-3):
        pylab.plot(ch4_data['data'][min_idx-3:max_idx,ch4_data['dth-idx']],ch4_data['data'][min_idx
            -3:max_idx,ch4_data['dat-idx']], 'g-', label='$CH4$')
    else:
        pylab.plot(ch4_data['data'][min_idx-3:,ch4_data['dth-idx']],ch4_data['data'][min_idx-3:,
            ch4_data['dat-idx']], 'g-', label='$CH4$')
952     pylab.yticklabels = pylab.getp(pylab.gca(), 'yticklabels')
    pylab.setp(pylab.yticklabels, 'color', 'g', fontsize='medium')
    pylab.gca().autoscale_view(tight=True, scalex=True, scaley=False)

#pylab.xlim(comp[min_idx-3,0].astype(float).round(decimals=0),comp[max_idx,0].astype(float).round(
    decimals=0))
957 #print pylab.Axis.get_view_interval()

#####
## Plot the tm corr dataset with mean values of the same depth
#####
962     sfig1.sp12=smpl_fig1.add_subplot(212)#, sharex=sfig1.sp11
    sfig1.sp12.set_ylabel(r'$\delta\;^{\{13\}}\text{C}\; \text{\%0}\$')
    sfig1.sp12.set_xlabel('Depth range')

if ice_origin is 'EDML':
967     ## Call def sample_replicates to find replicates in sample data, calculate a mean and std_dev
    of those repl, append columns with its data to array and del the 2nd repl
    ## This is used for the errorbar plots
    slib_dpsrt_red, smpl_dsrt,mn_uncor_col, std_uncor_col, repl_idc = sample_replicates(smpl_dsrt,
        i_col,o_col)
    ## Plot the tm corrected dataset in a new figure with errorbars
    # uncorr
972     sfig1.sp12.errorbar(slib_dpsrt_red[:,2].astype(None), mn_uncor_col, std_uncor_col, color='red'
        , fmt='o-', ecolor='b', capsize=3, label='$\delta\;^{\{13\}}\text{C}\; \text{\%0}\$'+org_label)
    # tm corr
    sfig1.sp12.errorbar(slib_dpsrt_red[:,2].astype(None), slib_dpsrt_red[:, -2].astype(None),
        slib_dpsrt_red[:, -1].astype(None), color='darkblue', fmt='o-', ecolor='k', capsize=3,
        label='$\delta\;^{\{13\}}\text{C}\; \text{\%0}\$'+tmcor_label) #, visible=False,label='Standard deviation
        in $\delta\;^{\{13\}}\text{C}\; \text{\%0}\$')
    sfig1.sp12.autoscale_view(tight=True, scalex=True, scaley=False)

977     ## Add the second y-axis with [CH4] data
    sfig1b.sp11 = pylab.twinx()
    sfig1b.sp11.set_ylabel('$[CH4]$ in ppbv', color='g')
    if min_idx>=3 and max_idx <=(len(ch4_data['data'])-3):
        sfig1b.sp11.plot(ch4_data['data'][min_idx-3:max_idx,ch4_data['dth-idx']],ch4_data['data'][:
            min_idx-3:max_idx,ch4_data['dat-idx']], 'g-', label='$CH4$')
982     else:
        sfig1b.sp11.plot(ch4_data['data'][min_idx-3:,ch4_data['dth-idx']],ch4_data['data'][min_idx
            -3:,ch4_data['dat-idx']], 'g-', label='$CH4$')
    pylab.setp(pylab.yticklabels(sfig1b.sp11, 'yticklabels'), 'color', 'g', fontsize='medium')

if plot_origin == 'on':
987     # get the indices of the ice origin
    orig_awi,orig_bern,orig_grbl=ice_orig(slib_dpsrt_red[:,1])
    # plot them
    sfig1.sp12.plot(slib_dpsrt_red[orig_grbl,2].astype(None),slib_dpsrt_red[orig_grbl, -2].
        astype(None) , 'o', color='darkblue',ms=4,mfc='yellow', label='Grenoble samples')

```

```

sfig1_sp12.plot(slib_dpsrt_red[orig_awi,2].astype(None),slib_dpsrt_red[orig_awi,-2].astype
992 (None), 'o', color='darkblue',ms=4,mfc='white', label='AWI samples')
sfig1_sp12.plot(slib_dpsrt_red[orig_bern,2].astype(None),slib_dpsrt_red[orig_bern,-2].
    astype(None), 'o', color='darkblue',ms=4,mfc='red', label='Bern Samples')
sfig1_sp12.invert_yaxis()
else:
    sfig1_sp12.plot(slib_dpsrt_red[:,2].astype(None),slib_dpsrt_red[:, i_col].astype(None), 'o-',
        color='red', label='\delta\;^{13}C $(\%_0)$ '+org_label)
    sfig1_sp12.plot(slib_dpsrt_red[:,2].astype(None),slib_dpsrt_red[:, o_col+1].astype(None), 'o
997 -, color='darkblue', label='\delta\;^{13}C $(\%_0)$ '+tmcor_label)
    #xfmt = sfig1_sp12.xaxis.get_major_formatter()
    #xfmt.set_powerlimits((-2, 10))
    #sfig1_sp12.xaxis.get_major_formatter().set_scientific(False)
    #xfmt.set_scientific(False)
sfig1_sp12.legend(loc=2, numpoints = 3, prop = matplotlib.font_manager.FontProperties(size=10))#
1002 best' 0, url1, ul2, uc9, lr4, ll3,

smpl_fig1.subplots_adjust(left=0.06, bottom=0.06, right=0.94, top=0.96, hspace=0.12)

#pylab.close(smpl_fig1)

1007 #####
### Sample Figure 2
### Plot Neumayer corrected data by depth and age with mean errors
#####
tmcor_label=data_cat[2]+' (Neumayer+spline corrected)'
1012 smpl_fig2=pylab.figure(figsize=[f_w,h_t])
pylab.figtext(0.8, 0.02,'created: '+asctime(localtime()),size=9)
## PLOT the tm corr dataset alone with [CH4] axis
sfig2_sp11=smpl_fig2.add_subplot(211)
1017 sfig2_sp11.set_title('Neumayer Corrected values of '+data_cat[2]+' data')
sfig2_sp11.set_ylabel(r'\delta\;^{13}C $(\%_0)$')
sfig2_sp11.set_xlabel('Depth range [m]')

if ice_origin is 'EDML':
1022 ## Plot the tm corrected dataset in a new figure with errorbars
# uncorr
sfig2_sp11.errorbar(slib_dpsrt_red[:,2].astype(None), mn_uncor_col, std_uncor_col, color='red
    ', fmt='o-', ecolor='b', capsize=3, label='\delta\;^{13}C $(\%_0)$ '+org_label)
#tm corrected
sfig2_sp11.errorbar(slib_dpsrt_red[:,2].astype(None), slib_dpsrt_red[:, -2].astype(None),
1027 slib_dpsrt_red[:, -1].astype(None), color='darkblue', fmt='o-', ecolor='k', capsize=3,
    label='\delta\;^{13}C $(\%_0)$ '+tmcor_label) #, visible=False, label='Standard deviation
    in \delta\;^{13}C $(\%_0)$'

if plot_origin == 'on':
    sfig2_sp11.plot(slib_dpsrt_red[orig_grbl,2].astype(None),slib_dpsrt_red[orig_grbl,-2].
        astype(None), 'o', color='darkblue',ms=4,mfc='yellow', label='Grenoble samples')
    sfig2_sp11.plot(slib_dpsrt_red[orig_awi,2].astype(None),slib_dpsrt_red[orig_awi,-2].astype
1032 (None), 'o', color='darkblue',ms=4,mfc='white', label='AWI samples')
    sfig2_sp11.plot(slib_dpsrt_red[orig_bern,2].astype(None),slib_dpsrt_red[orig_bern,-2].
        astype(None), 'o', color='darkblue',ms=4,mfc='red', label='Bern Samples')

## Add the second y-axis with [CH4] data
sfig2_sp11b = sfig2_sp11.twinx()
sfig2_sp11b.set_ylabel('[CH4] in ppbv', color='g')
if min_idx>=3 and max_idx <=(len(ch4_data['data'])-3):
1037 sfig2_sp11b.plot(ch4_data['data'][min_idx-3:max_idx, ch4_data['dth-idx']], ch4_data['data']
    min_idx-3:max_idx, ch4_data['dat-idx'], 'g-', label='$CH_4$')
else:
    sfig2_sp11b.plot(ch4_data['data'][min_idx-3, ch4_data['dth-idx']], ch4_data['data'][min_idx
    -3, ch4_data['dat-idx']], 'g-', label='$CH_4$')
pylab.setp(pylab.getp(sfig2_sp11b, 'yticklabels'), 'color', 'g', fontsize='medium')
1042 sfig2_sp11b.autoscale_view(tight=True, scalex=True, scaley=False)

else:
    sfig2_sp11.plot(slib_dpsrt_red[:,2].astype(None),slib_dpsrt_red[:, i_col].astype(None), 'o-',
        color='red', label='\delta\;^{13}C $(\%_0)$ '+org_label)
    sfig2_sp11.plot(slib_dpsrt_red[:,2].astype(None),slib_dpsrt_red[:, o_col+1].astype(None), 'o
1047 -, color='darkblue', label='\delta\;^{13}C $(\%_0)$ '+tmcor_label)
## Inverse y-axis etc.
sfig2_sp11.legend(loc=2, numpoints = 3, prop = matplotlib.font_manager.FontProperties(size=10)) #
    best' 0, url1, ul2, uc9, lr4, ll3,
sfig2_sp11.invert_yaxis()

# Re-sort the dataset for plotting by age
1052 #slib_dpsrt_red = slib_dpsrt_red.take(argsort(slib_dpsrt_red[:, -3].astype(None)), axis=-2) # Sort
    by age column
#mn_uncor_age = array(mn_uncor_col, ndmin=2).transpose().take(argsort(slib_dpsrt_red[:, -3].astype(
    None)), axis=-2)
#print slib_dpsrt_red.shape, len(mn_uncor_age),mn_uncor_age.shape
## Plot the tm corr dataset alone with mean values of the same depth
sfig2_sp12=smpl_fig2.add_subplot(212)
1057 sfig2_sp12.set_ylabel(r'\delta\;^{13}C $(\%_0)$')
sfig2_sp12.set_xlabel('%s Age range'%(age_choice))

if ice_origin is 'EDML':

```



```

1062     ## Plot the tm corrected dataset in a new subplot with errorbars
    # uncorr
    sfig2_spl2.errorbar(slib_dpsrt_red[:, -3].astype(None), mn_uncor_col, std_uncor_col, color= 'red',
        ffmt='o-', ecolor='b', capsize=3, label='$\delta\;^{\{13\}}C\; \$(\%_0)\$ '+org_label)
    # tmcorr
    sfig2_spl2.errorbar(slib_dpsrt_red[:, -3].astype(None), slib_dpsrt_red[:, -2].astype(None),
        slib_dpsrt_red[:, -1].astype(None), color= 'darkblue', ffmt='o-', ecolor='k', capsize=3,
        label='$\delta\;^{\{13\}}C\; \$(\%_0)\$ '+tmcor_label) #, visible=False, label='Standard deviation
        in $\delta\;^{\{13\}}C\; \$(\%_0)\$'
1067     if plot_origin == 'on' and ice_origin is 'EDML':

        #orig_awi, orig_bern, orig_grbl=ice_orig(slib_dpsrt_red[:, 1])
        sfig2_spl2.plot(slib_dpsrt_red[orig_grbl, -3].astype(None), slib_dpsrt_red[orig_grbl, -2].
            astype(None), 'o', color= 'darkblue', ms=4, mfc= 'yellow', label='Grenoble samples')
        sfig2_spl2.plot(slib_dpsrt_red[orig_awi, -3].astype(None), slib_dpsrt_red[orig_awi, -2].
            astype(None), 'o', color= 'darkblue', ms=4, mfc= 'white', label='AWI samples')
        sfig2_spl2.plot(slib_dpsrt_red[orig_bern, -3].astype(None), slib_dpsrt_red[orig_bern, -2].
            astype(None), 'o', color= 'darkblue', ms=4, mfc= 'red', label='Bern Samples')
1072

    ## Add the second y-axis with [CH4] data
    sfig2_spl2b = sfig2_spl2.twinx()
    sfig2_spl2b.set_ylabel('$[CH_4]$ in ppbv', color='g')
    # determine the CH4 age range for plotting
1077     min_idx, max_idx=ext_idc(ch4_data['data'][:, ch4_data['age-idx']], min(slib_dpsrt_red[:, -3].astype
        (float)).round(decimals=-1), max(slib_dpsrt_red[:, -3].astype(float)).round(decimals=-1), -1)
    #min_idx, max_idx=ext_idc(comp[:, 1], min(), max(), -2)
    if min_idx >= 3 and max_idx <= (len(ch4_data['data']) - 3):
        sfig2_spl2b.plot(ch4_data['data'][min_idx-3:max_idx, ch4_data['age-idx']], ch4_data['data'][
            min_idx-3:max_idx, ch4_data['dat-idx']], 'g-', label='$CH_4$', )
1082     else:
        sfig2_spl2b.plot(ch4_data['data'][min_idx-3:, ch4_data['age-idx']], ch4_data['data'][min_idx
            -3:, ch4_data['dat-idx']], 'g-', label='$CH_4$', )
        pylab.setp(pylab.getp(sfig2_spl2b, 'yticklabels'), 'color', 'g', fontsize='medium')
        sfig2_spl2b.autoscale_view(tight=True, scalex=True, scaley=False)
    else:
1087     sfig2_spl2.plot(slib_dpsrt_red[:, -3].astype(None), slib_dpsrt_red[:, i_col].astype(None), 'o-',
        color= 'red', label='$\delta\;^{\{13\}}C\; \$(\%_0)\$ '+org_label)
        sfig2_spl2.plot(slib_dpsrt_red[:, -3].astype(None), slib_dpsrt_red[:, o_col+1].astype(None), 'o
            -', color= 'darkblue', label='$\delta\;^{\{13\}}C\; \$(\%_0)\$ '+tmcor_label)

    ## Inverse y-axis etc.
    sfig2_spl2.legend(loc=2, numpoints = 3, prop = matplotlib.font_manager.FontProperties(size=10)) #'
1092     best' 0, url1, ul2, uc9, lr4, ll3,
    sfig2_spl2.invert_yaxis()

    # ## Plot the two methane ref peaks
    # pylab.subplot(313)
    # pylab.ylabel(r'$\delta\;^{\{13\}}C\; \$(\%_0)\$ Ref Peaks')
1097 # pylab.xlabel('Gicc05 Age range')
    # pylab.errorbar(slib_dpsrt_red[:, -3].astype(None), map(lambda x: mean(x), zip(slib_dpsrt_red[:, 4].
        astype(float), slib_dpsrt_red[:, 8].astype(float))), map(lambda x: std(x), zip(slib_dpsrt_red[:, 4].
        astype(float), slib_dpsrt_red[:, 8].astype(float))), color= 'red', ffmt='o-', ecolor='b', capsize=3,
        label='$\delta\;^{\{13\}}C\; \$(\%_0)\$ Ref Peaks')

    pylab.subplots_adjust(left=0.06, bottom=0.06, right=0.94, top=0.96, hspace=0.12)
    #pylab.close(smpl_fig2)
1102

#####
### Sample Figure 3
### Plot data for corrected / uncorrected comparison by age
### Subplot 1 - Plot the corr. dataset against CH4 Konz. with depth
1107 #####
    if ice_origin is 'EDML':
        smpl_fig3=pylab.figure(figsize=[f_wh, f_ht])
        pylab.figtext(0.8, 0.02, 'created: '+asctime(localtime()), size=9)
        ## PLOT the uncorr dataset alone with [CH4] axis
1112     sfig3_spl1=smpl_fig3.add_subplot(211)
        sfig3_spl1.set_title('Corrected '+data_cat[2]+' data vs. [CH$_4$] and [CO$_2$]')
        sfig3_spl1.set_ylabel(r'$\delta\;^{\{13\}}C\; \$(\%_0)\$')
        sfig3_spl1.set_xlabel('Sample Depth')

1117     # Plot the uncorr dataset with errorbars
    #sfig3_spl1.set_errorbar(slib_dpsrt_red[:, -3].astype(None), mn_uncor_col, std_uncor_col, color=
        'red', ffmt='o-', ecolor='b', capsize=3, label='$\delta\;^{\{13\}}C\; \$(\%_0)\$ '+org_label)
    ## Plot the tm corrected dataset with errorbars
    sfig3_spl1.errorbar(slib_dpsrt_red[:, 2].astype(None), slib_dpsrt_red[:, -2].astype(None),
        slib_dpsrt_red[:, -1].astype(None), color= 'darkblue', ffmt='o-', ecolor='k', capsize=3,
        label='$\delta\;^{\{13\}}C\; \$(\%_0)\$ '+tmcor_label) #, visible=False, label='Standard deviation
        in $\delta\;^{\{13\}}C\; \$(\%_0)\$'
1122     repl=find(slib_dpsrt_red[:, 3]=='G01+G02')
    from matplotlib.transforms import offset_copy
    transOffset = offset_copy(sfig3_spl1.transData, fig=smpl_fig3, x=-0.1, y=0.20, units='inches')
    for x, y, stdev in zip(slib_dpsrt_red[repl, 2].astype(None), slib_dpsrt_red[repl, -2].astype(None)
        ), slib_dpsrt_red[repl, -1].astype(None)):
        pylab.text(x, y, '%.3f' % (stdev), fontsize=8, transform=transOffset)
1127     if plot_origin == 'on':

```

```

# # uncorr values
# sfig3_spl1.set_plot(slib_dpsrt_red[orig_grbl,-3].astype(None),mn_uncor_age[orig_grbl,0].
astype(None), 'o', color='darkblue',ms=4,mfc='yellow', label='Grenoble samples')
# sfig3_spl1.set_plot(slib_dpsrt_red[orig_awi,-3].astype(None),mn_uncor_age[orig_awi,0].
astype(None), 'o', color='darkblue',ms=4,mfc='white', label='AWI samples')
# sfig3_spl1.set_plot(slib_dpsrt_red[orig_bern,-3].astype(None),mn_uncor_age[orig_bern,0].
astype(None), 'o', color='darkblue',ms=4,mfc='red', label='Bern Samples')
1132 # corr dataset
sfig3_spl1.plot(slib_dpsrt_red[orig_grbl,2].astype(None),slib_dpsrt_red[orig_grbl,-2].
astype(None), 'o', color='darkblue',ms=4,mfc='yellow', label='Grenoble samples')
sfig3_spl1.plot(slib_dpsrt_red[orig_awi,2].astype(None),slib_dpsrt_red[orig_awi,-2].astype
(None), 'o', color='darkblue',ms=4,mfc='white', label='AWI samples')
sfig3_spl1.plot(slib_dpsrt_red[orig_bern,2].astype(None),slib_dpsrt_red[orig_bern,-2].
astype(None), 'o', color='darkblue',ms=4,mfc='red', label='Bern Samples')
if plot_hein == 'yes':
1137 min_idx,max_idx=ext_idc(ch4_data['data'][:,ch4_data['dth-idx']],min(smpl_dsrt[:,2]).astype(
float).round()-1,max(smpl_dsrt[:,2]).astype(float).round()-1,0)
if min_idx>=5 and max_idx<=(len(ch4_data['data'])-5):
spl_agedep = scipy.interpolate.splrep(ch4_data['data'][min_idx-5:max_idx,ch4_data['age-
idx']].astype(float),ch4_data['data'][min_idx-5:max_idx,ch4_data['dth-idx']].
astype(float),k=spl_ord, s=spl_smth)
else:
spl_agedep = scipy.interpolate.splrep(ch4_data['data'][min_idx:,ch4_data['age-idx']].
astype(float),ch4_data['data'][min_idx:,ch4_data['dth-idx']].astype(float),k=
spl_ord, s=spl_smth)
1142 hein_dep = scipy.interpolate.splev([h*1000.0 for h in heinrich_dates], spl_agedep)
[(sfig3_spl1.axvspan(xmin=(hevent-15), xmax=(hevent+15), facecolor='g', edgecolor='g',
alpha=0.05)) for hevent in hein_dep[2:]]
from matplotlib.transforms import offset_copy
transOffset = offset_copy(sfig3_spl1.transData, fig=smpl_fig3,x=-0.1,y=0.20,units='inches
')
for n, d in enumerate(hein_dep):
1147 pylab.text(d, -49.0, '%s' % ('H'+str(n)), fontsize=18, transform=transOffset)
## Add the second y-axis with [CH4] data
sfig3_spl1b = sfig3_spl1.twinx()
sfig3_spl1b.set_ylabel('%[CH4]$ in ppbv', color='g')
if min_idx>=3 and max_idx <=(len(ch4_data['data'])-3):
1152 sfig3_spl1b.plot(ch4_data['data'][min_idx-3:max_idx,ch4_data['dth-idx']],ch4_data['data'][
min_idx-3:max_idx,ch4_data['dat-idx']], 'g-', label='$CH_4$', )
else:
sfig3_spl1b.plot(ch4_data['data'][min_idx-3:,ch4_data['dth-idx']],ch4_data['data'][min_idx
-3:,ch4_data['dat-idx']], 'g-', label='$CH_4$', )
pylab.setp(pylab.getp(sfig3_spl1b, 'yticklabels'), 'color', 'g', fontsize='medium')
smpl_fig3.subplots_adjust(left=0.06, bottom=0.06, right=0.94, top=0.96, hspace=0.12)
1157 sfig3_spl1b.autoscale_view(tight=True, scalex=True, scaley=False)
## Inverse y-axis etc.len()
l1=sfig3_spl1.legend(loc=2, numpoints = 3, prop = matplotlib.font_manager.FontProperties(size
=10)) # 'best' 0, url1, ul2, uc9, lr4, ll3,
l1.legendPatch.set_alpha(0.5)
sfig3_spl1.invert_yaxis()
1162 sfig3_spl1.minorticks_on()
## Add suppl. info to subplot
#print len(smpl_dsrt), len(find(slib_dpsrt_red[:,3]== 'G01+G02')),mean(slib_dpsrt_red[find(
slib_dpsrt_red[:,3]== 'G01+G02'),-1].astype(float).round(3))
sfig3_spl1b.text(0.85,0.1,'Summary:\nDatasets: %i\nReplicates: %i\nRepl.Mean Stdev: %0.3
f permille %\n(len(smpl_dsrt), len(find(slib_dpsrt_red[:,3]== 'G01+G02')),mean(
slib_dpsrt_red[find(slib_dpsrt_red[:,3]== 'G01+G02'),-1].astype(float).round(3))), bbox=
dict(facecolor="0.5", alpha=0.2), fontsize=10, transform = sfig3_spl1b.transAxes)
1167 #####
## Subplot 2 - Plot the corr. dataset against CO2 Konz. and Age
#####
ax1= pylab.subplot(212)
1172 pylab.ylabel(r'$\delta^{13}C$ $(\%_0)$')
pylab.xlabel('%s Age range'%(age.choice))
## Plot the tm corrected dataset in a new subplot with errorbars
leg=[]; art=[]
1177 art1=pylab.errorbar(slib_dpsrt_red[:, -3].astype(None), slib_dpsrt_red[:, -2].astype(None),
slib_dpsrt_red[:, -1].astype(None), color='darkblue', fmt='o-', ecolor='k', capsize=3) #,
label='$\delta^{13}C$ $(\%_0)$' +tmcor.label, visible=False,label='Standard deviation in
$\delta^{13}C$ $(\%_0)$'
art.append(art1[0])
leg.append('$\delta^{13}C$ $(\%_0)$' +tmcor.label)
if plot_origin == 'on' and ice_origin is 'EDML':
1182 #orig_awi,orig_bern,orig_grbl=ice_orig(slib_dpsrt_red[:,1])
art2=pylab.plot(slib_dpsrt_red[orig_grbl,-3].astype(None),slib_dpsrt_red[orig_grbl,-2].
astype(None), 'o', color='darkblue',ms=4,mfc='yellow', label='Grenoble samples')
art.append(art2)
art3=pylab.plot(slib_dpsrt_red[orig_awi,-3].astype(None),slib_dpsrt_red[orig_awi,-2].
astype(None), 'o', color='darkblue',ms=4,mfc='white', label='AWI samples')
art.append(art3)
1187 art4=pylab.plot(slib_dpsrt_red[orig_bern,-3].astype(None),slib_dpsrt_red[orig_bern,-2].
astype(None), 'o', color='darkblue',ms=4,mfc='red', label='Bern Samples')

```

```

    art.append(art4)
    #print leg
    leg.extend([n.get_label() for n in ax1.get_lines()[3:]])
    #print leg
1192    ## Inverse y-axis etc.
    #pylab.legend(loc=2, numpoints = 3, prop = matplotlib.font_manager.FontProperties(size=10)) #'
        best, 0, url, ul2, uc9, lr4, ll3,
#    pylab.gca().set_ylim(pylab.gca().get_ylim()[::-1])
#    from matplotlib.transforms import offset_copy
1197    transOffset = offset_copy(ax1.transData, fig=smpl_fig3, x=-0.1, y=0.20, units='inches')
    if ice_origin is 'EDML':
        #repl=find(slib_dpsrt_red[:,3]== 'G01+G02')
        for x, y, dpth in zip(slib_dpsrt_red[:, -3].astype(None), slib_dpsrt_red[:, -2].astype(None),
            slib_dpsrt_red[:, 2]):
            pylab.text(x, y, '%s' % (dpth), fontsize=6, transform=transOffset)
1202    if plot_hein == 'yes':
        [(ax1.axvspan(xmin=(hevent-0.75)*1000.0, xmax=(hevent+0.75)*1000.0, facecolor='g',
            edgecolor='g', alpha=0.05)) for hevent in heinrich_dates[2:]]

    ## Add the second y-axis with [CO2] data
    ax2 = pylab.twinx()
    # Ahn dataset
1207    #mi_idx, ma_idx=ext_idc(CO2_ahn['data'][:, 2], min(slib_dpsrt_red[:, -3].astype(float).round(
        decimals=-1)), max(slib_dpsrt_red[:, -3].astype(float).round(decimals=-1)), -1)
    pylab.ylabel('%[CO2] in ppmv', color='dodgerblue')
    #pylab.errorbar(CO2_ahn['data'][mi_idx-3:ma_idx+3, 2].astype(float), CO2_ahn['data'][mi_idx-
        3:ma_idx+3, 3].astype(float), CO2_ahn['data'][mi_idx-3:ma_idx+3, 4].astype(float), color
        = 'green', fmt='-', ecolor='y', capsized=3, label='%[CO2]', )
    #art5=pylab.plot(CO2_ahn['data'][mi_idx-3:ma_idx+3, 2].astype(float), CO2_ahn['data'][mi_idx-
        3:ma_idx+3, 3].astype(float), '-', color='dodgerblue', label='%[CO2] GISP2 dated (Ahn
        , Brook 2008)')
#    DML dataset
1212    mi_idx, ma_idx=ext_idc(CO2_dml['data'][:, 1], min(slib_dpsrt_red[:, -3].astype(float).round(
        decimals=-1)), max(slib_dpsrt_red[:, -3].astype(float).round(decimals=-1)), -1)
    art6=pylab.plot(scipy.interpolate.splev(CO2_dml['data'][mi_idx:ma_idx, 0].astype(float),
        spl_depage), CO2_dml['data'][mi_idx:ma_idx, 2].astype(float), '-', color='royalblue',
        label='%[CO2] EDML1 dated (unoff. DML record)')
    print shape(CO2_dml['data'][:, 0].astype(float)), shape(scipy.interpolate.splev(CO2_dml['data']
        )[:, 0].astype(float), spl_depage))
    savetxt("/home/lmoeller/Promotion/Messdaten/External/datasets/CO2_EDML1_age.csv", append(
        array(CO2_dml['data'][:, 0].astype(float), ndmin=2).transpose(), array(scipy.interpolate.
        splev(CO2_dml['data'][:, 0].astype(float), spl_depage), ndmin=2).transpose(), axis=1),
        fmt="%0.1f")
    leg.extend([n.get_label() for n in ax2.get_lines()])
1217    pylab.yticklabels = pylab.getp(pylab.gca(), 'yticklabels')
    pylab.setp(pylab.yticklabels, 'color', 'dodgerblue', fontsize='medium')
    #print leg
    l=ax2.legend((art1[0], art2, art3, art4, art6), leg, loc=2, numpoints = 3, prop = matplotlib.
        font_manager.FontProperties(size=10))
1222    l.legendPatch.set_alpha(0.5)

#    pylab.ylabel('%[CH4] in ppbv', color='g')
#    pylab.plot(comp[mi_idx-3:max_idx, 1], comp[mi_idx-3:max_idx, 2], 'g-', label='%CH4', )
#    pylab.yticklabels = pylab.getp(pylab.gca(), 'yticklabels')
#    pylab.setp(pylab.yticklabels, 'color', 'g', fontsize='medium')
1227

pylab.subplots_adjust(left=0.06, bottom=0.06, right=0.94, top=0.96, hspace=0.12)
pylab.gca().autoscale_view(tight=True, scalex=True, scaley=False)

if pres_plot is 'on':
1232    #####
    ### Plot data ONLY by age as presentation plot
    pylab.figure(figsize=[f_wh, f_ht])
    pylab.figtext(0.8, 0.02, 'created: '+asctime(localtime()), size=11)
    pylab.subplot(111)
1237    pylab.title('Preliminary  $\delta^{13}C_{CH_4}$  record over Dansgaard Oeschger events 7
        and 8', fontsize=24)
    pylab.ylabel('  $\delta^{13}C$   $(\%_0)$ ', color='b', fontsize=24) #, x= -0.01

    xticklabels = pylab.getp(pylab.gca(), 'xticklabels')
    pylab.setp(xticklabels, fontsize=36, visible=False)
1242    pylab.gca().set_ylim(-42.0, -46.0)
    yticklabels = pylab.getp(pylab.gca(), 'yticklabels')

    #print pylab.getp(pylab.gca(), 'yticklabels')[0].get_position()
1247    pylab.setp(yticklabels, color='blue', x=-0.01, fontsize=18) # org entry 'color', 'b',
        cornflowerblue, va='baseline'
    #print pylab.getp(pylab.gca(), 'yticklabels')[0].get_position()

    ## Plot the uncorrected dataset in a new figure with errorbars
    pylab.errorbar(slib_dpsrt_red[:, -3].astype(None), mn_uncor_col, std_uncor_col, color='blue', lw
        =2, fmt='o-', ecolor='k', capsized=3, label='  $\delta^{13}C$   $(\%_0)$  '+org_label)
1252

    ## Plot the tm corrected dataset in a new figure with errorbars
    #pylab.plot(slib_dpsrt_red[:, -3].astype(None), slib_dpsrt_red[:, -2].astype(None), 'bo-', lw=3,

```

```

        label='\delta\;^{13}C $(\%_0)$ '+tmcor_label) #, visible=False,label='Standard deviation
        in '\delta\;^{13}C $(\%_0)$'

1257     ## Add the second y-axis with [CH4] data
        ax2 = pylab.twinx()
        pylab.xlabel('%s Age range [years BP]%(age_choice), fontsize=24)
        xticklabels = pylab.getp(pylab.gca(), 'xticklabels')
        pylab.setp(xticklabels, y= -0.015, fontsize=20)
1262     pylab.ylabel('$[CH4]$ in ppbv', color='r', fontsize=24)
        pylab.plot(ch4_data['data'][min_idx-3:max_idx, ch4_data['age-idx']], ch4_data['data'][min_idx-3:
            max_idx, ch4_data['dat-idx']], 'r-',lw=2, label='%CH4$')
        yticklabels = pylab.getp(pylab.gca(), 'yticklabels')
        pylab.setp(yticklabels, 'color', 'r', x= 1.01, fontsize=20) # ,linespacing = 2.0,ha= 'right',
            x= 1.0,va='baseline'
        #print pylab.get_position('yticklabels')
1267     pylab.gca().autoscale_view(tight=True, scalex=True, scaley=False)
        #pylab.subplots_adjust(left=0.06, bottom=0.06, right=0.94, top=0.96, hspace=0.12)

    return smpl_dsrt, slib_dpsrt_red

1272 def debugplot(data_array,case,comment,line="dashed",msize=6):
    print "Adding %s stage to milestone plot..."%(case)
    # fig = pylab.figure(figsize=[f_wh,f_ht])
    # pylab.figtext(0.8, 0.02,'Comment: '+comment,size=9)
    # splt = fig.add_subplot()
1277     #global figclr #,color= str(figclr)
    evfg.plot(data_array[:,2].astype(float),data_array[:, -1].astype(float), linestyle=line, marker='o',
        ms=msize, label=case)
    #figclr += 0.1

1282 def milestone(data_array,case,comment,dbg_plot= None): #,line=None
    global dbg_stage
    ext_fn=str(dbg_stage)+'_'+case+'IceSampleData'+'.csv'
    print '-----'
1287     print 'Exporting milestone to file "%s" in the log folder\n "%s"...'%(ext_fn,eval_dir)
    csvfile = csv.writer(open(eval_dir+ext_fn, "wb"),'excel')
    csvfile.writerow('# This file contains EDML ice sample delta13C %s data \n\
        # Created: %s\n\
        # Comment: %s\
1292     %(case,strftime("%a %b %d %Y at %H:%M:%S",localtime()),comment))
    headerline = 'Date Ice_origin Depth Cut utc ord d13C'
    csvfile.writerow(headerline.split(' '))
    [csvfile.writerow(line) for line in append(array(map(lambda utc: strftime("%d-%b-%Y", localtime(utc)
        )),data_array[:, -3].astype(float)), ndmin=2).transpose(),data_array[:,1:],axis=1)]
    dbg_stage += 1
1297     if dbg_plot != None:
        debugplot(data_array,case,comment)

    ,,,
#####
1302     #-----Main Program-----#
    ,,,
#####
1307     ### Check for the existence of all necessary paths

    if exists(lib_path) != True:
        print 'Library directory could not be found!!!'
        print 'Please check whether the specified path information "%s" is correct! Aborting the script now
            !!!' %(lib_path)
        sys.exit()
1312     else:
        print 'Library directory "%s" found.' %(lib_path)
    if ol_log == 'yes':
        if exists(log_dir) != True:
            makedirs(log_dir)
1317         print 'Log file folder "%s" created' %(log_dir)
        else:
            print 'Log directory "%s" found.' %(log_dir)
    print '*****'

1322     ,,,
#####
    Data reading and Index correction procedures ...
    ,,,

1327     libarray_nlst = ['library_'+ n.replace('-', '_') for n in data_cat]
    lib_sortlst = ['lib_sort_'+ n.replace('-', '_') for n in data_cat]
    remlist=['remlist_'+ n.replace('-', '_') for n in data_cat]
    rem_data=['rem_data_'+ n.replace('-', '_') for n in data_cat]
    #print libarray_nlst, remlist

1332     ## Read in all libraries to corresponding array by calling def read_data
    for n in range(len(libarray_nlst)):
        libarray_nlst[n], remlist[n],rem_data[n] = read_data(lib_list[n])

1337     ## Check for double entries in utc_float column and correct that by calling def rem_dupl_utc
    utc_col = libarray_nlst[n][:, -1]

```

```

#print len(utc_col), len(unique(utc_col))
if len(utc_col) > len(unique(utc_col)):
    libarray_nlst[n] = rem_dupl_utc(libarray_nlst[n], n)
1342 #print len(utc_col), len(unique(utc_col))
if len(utc_col) > len(unique(utc_col)): # If the call of the rem_dupl_utc routine didn't work for
any reason
    print 'There were unsolvable problems in the %s library' %(data_cat[n])

### Check for duplicates in abs. measurement number column of Methane ref library and call def to
fix
1347 if n ==0:
    #num_col = libarray_nlst[n][:, 1].astype(int)
    if len(libarray_nlst[n][:, 1]) > len(unique(libarray_nlst[n][:, 1].astype(int))): # check if
duplicate entries of an abs. measurement number is present (pos. if duplicate free array (
unique func.) is smaller than the org. data array)
        print 'Checking for duplicates in Number column of the "%s" library...\n' %(data_cat[n])
        libarray_nlst[n] = rem_dupl_num(libarray_nlst[n])
1352

## Read external data files
#comp =read_extdata(ext_list[0],2,',')

1357 #CO2_ahn = read_extdata(ext_list[2],4,',')
#CO2_dml = read_extdata(ext_list[3],4,',')

## Correct CO2_ahn dataset for age 1000s seperator in raw data
#CO2_ahn['data'][: ,1:3]=CO2_ahn['data'][: ,1:3].astype(float)*1000
1362 ### Create the dl5N dataset
#dl5N = comp.take(where(comp[:,-1].astype(None)!=0.0)[0], axis=-2)

# find(array([dset['scale'] for dset in ext_data])==age_choice)
for n, dset in enumerate(ext_data):
1367 ## Read external data files
dset['data']=read_extdata(ext_dir+dset['file'],dset['header'],dset['delimiter'],dset['columns'])
# make Corrections
if dset['name'] == 'CO2.Byrd':
    ## Correct CO2_Ahn dataset for age 1000s seperator in raw data
1372 dset['data'][: ,1:3]=dset['data'][: ,1:3].astype(float)*1000 # valid only for Ahn, Brook
CO2_ahn = ext_data[n]
if dset['name'] == 'CO2.EDML':
    CO2_dml = ext_data[n]
1377 if dset['name'] == 'CH4.EDML':
    ## Remove two double entries in dataset "CH4.DML"
dset['data'] = delete(dset['data'],(94,215), axis=0)
ch4_data = dset
#print dset['name'],dset['scale']
if 'CH4.DML' in dset['name'] and dset['scale']==age_choice:
1382 ch4_data = ext_data[n]

'''
#####
1387 #Reflow, Ice Sample and Airafter Library Data spline Correction...
'''

## Generate Ordinal Column for Refloop dataset

libarray_nlst[1] = append(libarray_nlst[1],array(sec_to_ord(libarray_nlst[1][:,-1],ndmin=2).transpose
(), axis=1)#Append the ordinal info to the Refloop array in a new column
1392 ## Find the indices of all reflows for the old and new (since 2010) synth Air bottle
rl_old_idc = find(libarray_nlst[1][:,-1].astype(None)<733773.0) # select all datasets before 01.01.2010
rl_new_idc = find(libarray_nlst[1][:,-1].astype(None)>733773.0) # select all datasets after 01.01.2010
## Find the indices of the regular 20 ml loops for the old and new (since 2010) synth Air bottle
#Normloop_idx_old=find(libarray_nlst[1][find(libarray_nlst[1][:,-3]=='20'),-1].astype(None)<733773.0)
# old bottle <733773.0 = 1.1.2010
1397 Normloop_idx_old=filter(lambda x:x in rl_old_idc,find(libarray_nlst[1][:,-3]=='20')) # find all
indices of reflows that are older than 2010 and are reg. 20 ml ones
Normloop_idx_new=filter(lambda x:x in rl_new_idc,find(libarray_nlst[1][:,-3]=='20')) # new bottle >
733773.0

## Calculate the spline fit of OLD Bottle uncorrected reflow data (x=date ordinal y= raw isotopy)
spl_refl_old = scipy.interpolate.splrep(libarray_nlst[1][Normloop_idx_old, 34].astype(None),
libarray_nlst[1][Normloop_idx_old, 4].astype(None),k=rspl_ord, s=rspl_smth_a)
1402 spl_refl_old_x = arange(min(libarray_nlst[1][Normloop_idx_old, -1].astype(None)), max(libarray_nlst[1][
Normloop_idx_old, -1].astype(None))+1.0/enlargement[0], 1.0/enlargement[0]) # reduce stepping
between x-datapoints
spl_refl_old_y = scipy.interpolate.splev(spl_refl_old_x, spl_refl_old)

## Calculate the spline fit of NEW Bottle uncorrected reflow data (x=date ordinal y= raw isotopy)
spl_refl_new = scipy.interpolate.splrep(libarray_nlst[1][Normloop_idx_new, 34].astype(None),
libarray_nlst[1][Normloop_idx_new, 4].astype(None),k=rspl_ord, s=rspl_smth_b)# rspl_ord
1407 spl_refl_new_x = arange(min(libarray_nlst[1][Normloop_idx_new, -1].astype(None)), max(libarray_nlst[1][
Normloop_idx_new, -1].astype(None))+1.0/enlargement[0], 1.0/enlargement[0]) # reduce stepping
between x-datapoints
spl_refl_new_y = scipy.interpolate.splev(spl_refl_new_x, spl_refl_new)

## calculate the mean over the two reflow data ranges
loopspl_old_mean = mean(spl_refl_old_y)#-40.93(1sigma plusminus0.46) for spl-sm 4
1412 loopspl_new_mean = mean(spl_refl_new_y)#-49.43(1sigma plusminus0.06) for spl-sm 1.3

## calculate the mean of the data to spline difference for the old and new bottle range and its error

```

```

spldif_old=libarray_nlst[1][Normloop_idx_old, 4].astype(None)-scipy.interpolate.splev(libarray_nlst[1][
    Normloop_idx_old, -1].astype(None), spl_refl_old) #old bottle range
spldif_new=libarray_nlst[1][Normloop_idx_new, 4].astype(None)-scipy.interpolate.splev(libarray_nlst[1][
    Normloop_idx_new, -1].astype(None), spl_refl_new)
1417 spldif_overall=append(spldif_old, spldif_new)
spldiff_mean = mean(abs(spldif_overall)) # 0.08 (1sigma plusminus0.05) for spl-sm 4&1.3
spldiff_err=sqrt(sum(spldif_overall**2)/len(spldif_overall)) # 0.1 for spl-sm 4&1.3
#del spl_dif
print '-----',
1422 print 'Calculating Refloop splines...'
print ' spline settings of order %s and smoothness %s/%s led to a \n mean spline to data
    difference of %3f per mille (error %4f)'%(rspl_ord, rspl_smth_a, rspl_smth_b, spldiff_mean,
    spldiff_err)

if debug_refl == 'on':
    Spl_Fig = pylab.figure(figsize=[f_wh, f_ht])
1427 plfg=Spl_Fig.add_subplot(111)
    plfg.plot_date(splrefl_old_x, splrefl_old_y, 'm-', label="Spline k%s s%s"%(rspl_ord, rspl_smth_a))
    plfg.plot_date(splrefl_new_x, splrefl_new_y, 'k-', label="Spline k%s s%s"%(rspl_ord, rspl_smth_b))
    #plfg.plot_date(libarray_nlst[1][Normloop_idx_new, 34].astype(None), scipy.interpolate.splev(
        libarray_nlst[1][Normloop_idx_new, 34].astype(None), spl_refl_new), 'bo', label="new Refl x-
        value represented on Spline")
    #plfg.plot_date(libarray_nlst[1][Normloop_idx_old, 34].astype(None), scipy.interpolate.splev(
        libarray_nlst[1][Normloop_idx_old, 34].astype(None), spl_refl_old), 'ro', label="old Refl x-
        value represented on Spline")
1432 plfg.plot_date(libarray_nlst[1][Normloop_idx_old, 34].astype(None), libarray_nlst[1][
    Normloop_idx_old, 4].astype(None), 'bo', label="Old bottle Refl values")
    plfg.plot_date(libarray_nlst[1][Normloop_idx_new, 34].astype(None), libarray_nlst[1][
    Normloop_idx_new, 4].astype(None), 'go', label="New bottle Refl values")

rem_data[1] = append(rem_data[1], array(sec_to_ord(rem_data[1][:, -1], ndmin=2).transpose(), axis=1)
1437 plfg.plot_date(rem_data[1][:, 34].astype(None), rem_data[1][:, 4].astype(None), 'ro', label="Removed
    Refl values")
    if debug_refl_num == 'on':
        from matplotlib.transforms import offset_copy
        transOffset = offset_copy(plfg.transData, fig=Spl_Fig, x=0.0, y=0.10, units='inches')
        #for x, y, dpth in zip(libarray_nlst[1][Normloop_idx_old, 34].astype(None), libarray_nlst[1][
            Normloop_idx_old, 4].astype(None), libarray_nlst[1][Normloop_idx_old, 0]):
            # pylab.text(x, y, '%s' % (dpth), fontsize=6, transform=transOffset)
1442 #for x, y, dpth in zip(libarray_nlst[1][Normloop_idx_new, 34].astype(None), libarray_nlst[1][
            Normloop_idx_new, 4].astype(None), libarray_nlst[1][Normloop_idx_old, 0]):
            # pylab.text(x, y, '%s' % (dpth), fontsize=6, transform=transOffset)
            for x, y, num in zip(rem_data[1][:, 34].astype(None), rem_data[1][:, 4].astype(None), rem_data
                [1][:, 1]):
                pylab.text(x, y, '%s' % (num), fontsize=6, transform=transOffset)
            for x, y, num in zip(libarray_nlst[1][:, 34].astype(None), libarray_nlst[1][:, 4].astype(None),
                libarray_nlst[1][:, 1]):
1447 pylab.text(x, y, '%s' % (num), fontsize=6, transform=transOffset)

    plfg.add_line(pylab.Line2D([min(splrefl_old_x).round(), max(splrefl_old_x).round()], [
        loopspl_old_mean, loopspl_old_mean], linewidth=1, linestyle='-', color='k'))

    plfg.text(max(splrefl_old_x).round()-140, loopspl_old_mean, 'SynthAir-bottle: %0.3f'%(
        loopspl_old_mean), fontsize=8) # Enter text in subplot object at ax pos. , bbox=dict(facecolor
        ='0.5', alpha=0.5)
1452 plfg.add_line(pylab.Line2D([min(splrefl_new_x).round(), max(splrefl_new_x).round()], [
        loopspl_new_mean, loopspl_new_mean], linewidth=1, linestyle='-', color='k'))
    plfg.text(max(splrefl_new_x).round()-10, loopspl_new_mean, 'CrystalAir: %0.3f'%(loopspl_new_mean),
        fontsize=8) # Enter text in subplot object at ax pos. , bbox=dict(facecolor='0.5', alpha=0.5)
    plfg.fill_between(splrefl_old_x, loopspl_old_mean, splrefl_old_y, where=splrefl_old_y >=
        loopspl_old_mean, facecolor='0.5', alpha=0.5)
    plfg.fill_between(splrefl_old_x, loopspl_old_mean, splrefl_old_y, where=splrefl_old_y <=
        loopspl_old_mean, facecolor='0.8', alpha=0.5)
    plfg.fill_between(splrefl_new_x, loopspl_new_mean, splrefl_new_y, where=splrefl_new_y >=
        loopspl_new_mean, facecolor='0.5', alpha=0.5)
1457 plfg.fill_between(splrefl_new_x, loopspl_new_mean, splrefl_new_y, where=splrefl_new_y <=
        loopspl_new_mean, facecolor='0.8', alpha=0.5)

#savetxt(eval_dir+'ReflSpl_to_data_diff'+'_k%s%s_spldiff_mean_%.3f_spldiff_err_%.4f'%(rspl_ord,
1462 ',, rspl_smth, spldiff_mean, spldiff_err)'+'.tab', spldif_overall, fmt="%s", delimiter='\t')
## Append the reloop mean corrected Isotopies to reloop data array in a new column

merged_cor_col = append(\
1467 ((libarray_nlst[1][rl_old_idc, iso_col[1]].astype(None)-(scipy.interpolate.splev(libarray_nlst[1][
    rl_old_idc, ord_col[1]].astype(None), spl_refl_old)-loopspl_old_mean)-NM_offset).round(decimals
    =4), # calculate the deviation of the raw isotopy data from the spline and the mean of the spline
    for the old... \
    ((libarray_nlst[1][rl_new_idc, iso_col[1]].astype(None)-(scipy.interpolate.splev(libarray_nlst[1][
    rl_new_idc, ord_col[1]].astype(None), spl_refl_new)-loopspl_new_mean)-Btl_niveau_cor)).round(
    decimals=4)) # and for the new reloop air bottle range and merge them into one dataset
    libarray_nlst[1] = append(libarray_nlst[1], array(merged_cor_col, ndmin=2).transpose(), axis=1) # add the
    merged dataset to the whole dataarray

```

```

#spl_rec=rec.array(" loops", merged_cor_col)
1472 first_mref = [n for n in data_cat]
first_mref[0]=append((scipy.interpolate.splev(libarray_nlst[1][rl_old_idc, ord_col[1]].astype(None),
spl_refl_old)-loopspl_old_mean),(scipy.interpolate.splev(libarray_nlst[1][rl_new_idc, ord_col[1]].
astype(None), spl_refl_new)-loopspl_new_mean))
first_mref[1] = append(\
((libarray_nlst[1][rl_old_idc, 2].astype(None)-(scipy.interpolate.splev(libarray_nlst[1][rl_old_idc,
ord_col[1] ].astype(None), spl_refl_old)-loopspl_old_mean)-NM_offset)).round(decimals=4), #
calculate the deviation of the raw isotopy data from the spline and the mean of the spline for the
old... \
((libarray_nlst[1][rl_new_idc, 2].astype(None)-(scipy.interpolate.splev(libarray_nlst[1][rl_new_idc,
ord_col[1]].astype(None), spl_refl_new)-loopspl_new_mean)-Btl_niveau_cor)).round(decimals=4))
1477 ',,
### Krypton Correction Section
',,
#####
1482 ##### EDML ICE

### Date/Time conversions
#
# Kryp_cor.date=[datetime(*strptime(date,'%Y%m%d')[:6]).strftime('%Y%m%d') for date in Kryp_cor.date]
1487 # Kryp_cor=rec_append_fields(Kryp_cor," utc_sec",[mktime(strptime(date,'%Y%m%d'))for date in Kryp_cor.
date])
# #Kryp_cor=delete(Kryp_cor,filter(lambda x:x in find([d<mktime(strptime(EDML_Startdate, "%Y%m%d")) for
d in Kryp_cor.utc_sec]),find([d>mktime(strptime("070610", "%Y%m%d"))for d in Kryp_cor.utc_sec])))
#
### Identify datasets
kryp_ix=[find(libarray_nlst[2][:,0]==d)[0] for d in Kryp_cor.date]
1492 # #lib_k= copy(libarray_nlst[2][kryp_ix,:])
# Kryp_cor=rec_append_fields(Kryp_cor," depth",libarray_nlst[2][kryp_ix,2].astype(None))
# Kryp_cor=rec_append_fields(Kryp_cor," cut",libarray_nlst[2][kryp_ix,3])
# Kryp_cor=rec_append_fields(Kryp_cor," d13C_LM_raw",libarray_nlst[2][kryp_ix,iso_col[2]].astype(None))
#
1497 # #rec2csv(Kryp_cor," /home/lmoeller/Dropbox/Freigabe/Methan_Paper_Lars/TeufelimHeuhaufen/Script Jochen/
Kr_correction_raw_EDML_samples_extd.csv")
#
### Replace the sample data isotopic values with the ones corrected for krypton contribution
libarray_nlst[2][kryp_ix,iso_col[2]] = Kryp_cor.d13c_corr
1502
#ix=[find(Kryp_cor.date == d)[0] for d in smpl_dsrt[:,0]]

#Kryp_cor_VPDB=rec_append_fields(Kryp_cor.take(ix)," d13C_JScor_VPDB",smpl_dsrt[:,39].astype(float))
#Kryp_cor_VPDB=rec_append_fields(Kryp_cor.VPDB," mgd_d13C_JScor_VPDB",smpl_dsrt[:, -2].astype(float))
1507 #Kryp_cor_VPDB=rec_append_fields(Kryp_cor.VPDB," JScor_VPDB_std",smpl_dsrt[:, -1].astype(float))
#Kryp_cor_VPDB=rec_append_fields(Kryp_cor.VPDB," depth",smpl_dsrt[:,2].astype(float))
#Kryp_cor_VPDB=Kryp_cor.VPDB.take(argsort(Kryp_cor.VPDB.running_nr))
#Kryp_cor_VPDB=rec_append_fields(Kryp_cor.VPDB," intp_ch4",interp(Kryp_cor.VPDB.depth,CH4_E.depth, CH4_E
.ch4, left=0, right=0).round(2))
1512 #rec2csv(Kryp_cor.VPDB,root_dir+"Krypton_corrected/Dez2012/Kr_correction_raw&VPDB_EDML_samples.csv")
##### Add original Kr uncorrected values for comparison - comment out the replacement line before
applying this
#Kryp_cor_VPDB2=csv2rec(root_dir+"Krypton_corrected//Okt2012/Kr_correction_raw&VPDB_EDML_samples.csv",
converterd={0:str})
#ix=[find(Kryp_cor.VPDB2.date == d)[0] for d in smpl_dsrt[:,0]]
#Kryp_cor_VPDB2=Kryp_cor.VPDB2.take(ix)
1517 #Kryp_cor_VPDB2=rec_append_fields(Kryp_cor.VPDB2," d13C_LM_VPDB",smpl_dsrt[:,39].astype(float))
#Kryp_cor_VPDB2=rec_append_fields(Kryp_cor.VPDB2," mgd_d13C_LM_VPDB",smpl_dsrt[:, -2].astype(float))
#Kryp_cor_VPDB2=rec_append_fields(Kryp_cor.VPDB2," LM_VPDB_std",smpl_dsrt[:, -1].astype(float))
##Kryp_cor_VPDB2=Kryp_cor.VPDB2.take(argsort(Kryp_cor.VPDB2.running_nr))
#rec2csv(Kryp_cor.VPDB2,root_dir+"Krypton_corrected/Dez2012/Kr_correction_raw&VPDB_EDML_samples.csv")
1522 #####
##### Neumayer Samples #####
#kryp_nm=[find(libarray_nlst[4][:,0]==d) for d in NM_Kr.date]
lib_kr_ix=[]
1527 NM_Kr_ix=[]
for n,dt in enumerate(libarray_nlst[4][:,0]):
if libarray_nlst[4][n,1]=="Neumayer":
if dt in NM_Kr.date:
if dt not in ['080619', '070531']:
1532 print n,libarray_nlst[4][n,0],libarray_nlst[4][n,32],libarray_nlst[4][n,iso_col[4]],
NM_Kr.nr.take(find(NM_Kr.nr==libarray_nlst[4][n,32].astype(int))),NM_Kr.d13c_raw.
take(find(NM_Kr.nr==libarray_nlst[4][n,32].astype(int))),NM_Kr.d13c.take(find(
NM_Kr.nr==libarray_nlst[4][n,32].astype(int))),NM_Kr.d13c_origcorrected.take(find(
NM_Kr.nr==libarray_nlst[4][n,32].astype(int)))
lib_kr_ix.append(n)
NM_Kr_ix.append(find(NM_Kr.nr==libarray_nlst[4][n,32].astype(int))[0])
elif dt == '070531' and libarray_nlst[4][n,32] == '01':
print "boop"
1537 lib_kr_ix.append(n)
NM_Kr_ix.append(find(NM_Kr.nr==libarray_nlst[4][n,32].astype(int))[0])
elif dt == '080619' and libarray_nlst[4][n,32] == '16':
print "beep"
lib_kr_ix.append(n)
1542 NM_Kr_ix.append(find(NM_Kr.nr==libarray_nlst[4][n,32].astype(int))[0])

```



```

else:
    libarray_nlst[4][n,32]
libarray_nlst[4][lib.kr.ix, iso_col[4]] = NM.Kr.d13c.take(NM.Kr.ix)
1547 #####
##### IPY Intercal Cylinders
# in dieser Variante nach einem erfolgreichen Lauf durchführen!

##Refair_orig=copy(libarray_nlst[4])
1552 #IPY_ix=find([nm in IPY_names for nm in libarray_nlst[4][:,1]])
#IPY_orig=libarray_nlst[4][IPY_ix,:]
#IPY_intcal_offset=IPY_orig[:, iso_col[4]].astype(None)-IPY_orig[:, -1].astype(None)
#IPY_cor=rec.append_fields(IPY_cor, 'intcal.orgvscal', IPY_intcal_offset)
#IPY_cor=rec.append_fields(IPY_cor, 'd13c-corr-VPDB', IPY_cor.d13c-corr-IPY_intcal_offset)
1557 #rec2csv(IPY_cor, "/home/lmoeller/Dropbox/Freigabe/Methan-Paper-Lars/TeufelimHeuhaufen/Script Jochen/
Okt2012/IPY.cyl.Krcorr-AWI.raw&VPDB.LM.csv")
'''
## Internal Calibration - Detrend data from oven shifts
1562 # Append a column with internally corrected values
for i in range(2, len(libarray_nlst)):
    libarray_nlst[i] = append(libarray_nlst[i], array(sec_to_ord(libarray_nlst[i][:, -1], ndmin=2).
        transpose(), axis=1) # Append the ordinal info to the array in a new column
        old_idc = find(libarray_nlst[i][:, -1].astype(None) < 733773.0) # select all datasets before
        01.01.2010
        new_idc = find(libarray_nlst[i][:, -1].astype(None) > 733773.0) # select all datasets after 01.01.2010
1567 merged_cor_col = append(
((libarray_nlst[i][old_idc, iso_col[i]].astype(None) - (scipy.interpolate.splev(libarray_nlst[i][old_idc,
ord_col[i]].astype(None), spl_refl_old) - loopspl_old_mean) - NM_offset).round(decimals=4), \
((libarray_nlst[i][new_idc, iso_col[i]].astype(None) - (scipy.interpolate.splev(libarray_nlst[i][new_idc,
ord_col[i]].astype(None), spl_refl_new) - loopspl_new_mean) - Btl_niveau_cor).round(decimals=4))
libarray_nlst[i] = append(libarray_nlst[i], array(merged_cor_col, ndmin=2).transpose(), axis=1) #
Append the refloop mean corrected Isotopies to the array in a new column

1572
# Sort the array according to depth, first replacing possible ',' in string, round to 3 digits after
the comma
libarray_nlst[2][:, 2] = array(map(lambda x: float(x.replace(',', '.')), libarray_nlst[2][:, 2])).round(3)
libarray_nlst[2] = libarray_nlst[2].take(argsort(libarray_nlst[2][:, 2].astype(float)), axis=-2)
1577 if eval_run=="on":
## Export Data stage 1 "Raw"
Eval_Fig = pylab.figure(figsize=[f_wh, f_ht])
evfg=Eval_Fig.add_subplot(111)
1582 evfg.set_title("Evaluation Milestone plot", fontsize=12)
evfg.set_ylabel(r'$\delta\text{ }^{13}\text{C } (\text{‰})$')
milestone(libarray_nlst[2].take([0, 1, 2, 3, 37, 38, 6], axis=-1), "Raw", "No alterations made", 'plot it!') #
## Export Data stage 2 "Refloop Corrected"
milestone(libarray_nlst[2].take([0, 1, 2, 3, 37, 38, 39], axis=-1), "VPDB-Linked", "Corrected for Machine
trends, for NM and Bottle Niveau offsets")
1587
'''
#####
Remove data of a certain period or origin out of the sample dataset
1592 '''
## Select certain ice origin following the header option "ice_origin" from sample and Airafter database
## Remove all EDML/B37 entries prior to e.g. 733102.0 (ordinal for '080301') => calc. by using date2num
(datetime(*strptime(date, "%y%mt%d")[ :6]) or better e.g. pylab.strptime2num('%y%mt%d')(
EDML_Startdate)
## See Parameter section for selected date ranges
1597 if ice_origin != 'all':
if ice_origin == 'B37':
libarray_nlst[2] = libarray_nlst[2].take(where(libarray_nlst[2][:, 1] == ice_origin)[0], axis=-2)
# samples
libarray_nlst[3] = libarray_nlst[3].take(where(libarray_nlst[3][:, 1] == ice_origin)[0], axis=-2)
# airafter
export_fn = 'B37_splcorr_data'
1602 libarray_nlst[2] = libarray_nlst[2].take(where(libarray_nlst[2][:, 38].astype(None) > pylab.
date2num(datetime(*strptime(B37_Startdate, "%y%mt%d")[ :6]))) [0], axis=-2)
elif ice_origin == 'EDML':
nlist=['date', 'ice_origin', 'depth', 'cut', 'dc_13 1st_ref', 'dc_13 pre_peak', 'dc_13 ch4_peak',
'dc_13 co2_peak', 'dc_13 2nd_ref', 'ampl 1st_ref', 'ampl pre_peak', 'ampl ch4_peak',
'ampl co2_peak', 'area 2nd_ref', 'area 1st_ref', 'area pre_peak', 'area ch4_peak', 'area
co2_peak', 'area 2nd_ref', 'pos_max_1st_ref', 'pos_max_pre_peak', 'pos_max_ch4_peak',
'pos_max_co2_peak', 'pos_max_2nd_ref', 'r_wmg_45 1st_ref', 'r_wmg_45 pre_peak', 'r_wmg_45
ch4_peak', 'r_wmg_45 co2_peak', 'r_wmg_45 2nd_ref', 'r_wmg_46 1st_ref', 'r_wmg_46
pre_peak', 'r_wmg_46 ch4_peak', 'r_wmg_46 co2_peak', 'r_wmg_46 2nd_ref', 'weight',
'area_norm', 'pot', 'utc_sec', 'ordinals', 'corr_iso', 'dml1_age']
dlist=[('date', '|S6'), ('ice_origin', '|S13'), ('depth', '|S7'), ('cut', '|S3'), ('dc_13 1
st_ref', '<f8'), ('dc_13 pre_peak', '<f8'), ('dc_13 ch4_peak', '<f8'), ('dc_13 co2_peak',
'<f8'), ('dc_13 2nd_ref', '<f8'), ('ampl 1st_ref', '<f8'), ('ampl pre_peak', '<f8'), ('
ampl ch4_peak', '<f8'), ('ampl co2_peak', '<f8'), ('area 1st_ref', '<f8'), ('area 2nd_ref', '<f8'), ('area pre_peak', '<f8'), ('area ch4_peak', '<f8'), ('area co2_peak', '<f8'),
('area 2nd_ref', '<f8'), ('pos_max_1st_ref', '<f8'), ('pos_max_pre_peak', '<f8'), ('
pos_max_ch4_peak', '<f8'), ('pos_max_co2_peak', '<f8'), ('pos_max_2nd_ref', '<f8'), ('
r_wmg_45 1st_ref', '<f8'), ('r_wmg_45 pre_peak', '<f8'), ('r_wmg_45 ch4_peak', '<f8'), ('
r_wmg_45 co2_peak', '<f8'), ('r_wmg_45 2nd_ref', '<f8'), ('r_wmg_46 1st_ref', '<f8'), ('

```

```

    r_wmg_46_pre_preak', '<f8'), ('r_wmg_46_ch4_peak', '<f8'), ('r_wmg_46_co2_peak', '<f8'),
    ('r_wmg_46_2nd_ref', '<f8'), ('weight', '<f8'), ('area_norm', '<f8'), ('pot', '|S1'), ('
    utc_sec', '<f8'), ('ordinals', '<f8'), ('corr_iso', '<f8'), ('dml_lage', '<f8')
No_dml = rec.array([libarray_nlst[2][find([Ice in Intercomp_ice for Ice in libarray_nlst
    [2][:,1]])],x] for x in range(shape(libarray_nlst[2])[1]), names=nlst[-1], dtype=dlist
    [-1]) # alle cols
1607 No_dml = rec.append_fields(No_dml, nlst[-1], sec_to_ord(No_dml. utc_sec))
non_dml= copy(libarray_nlst[2].take(find([Ice in Intercomp_ice for Ice in libarray_nlst
    [2][:,1]), axis=-2))
libarray_nlst.append(non_dml)
libarray_nlst[2] = libarray_nlst[2].take(find([Ice not in Intercomp_ice for Ice in
    libarray_nlst[2][:,1]), axis=-2)
libarray_nlst[3] = libarray_nlst[3].take(find([Ice not in Intercomp_ice for Ice in
    libarray_nlst[3][:,1]), axis=-2)
1612
    #removed_date = libarray_nlst[2].take(where(libarray_nlst[2][:,38].astype(None)<pylab.
    date2num(datetime(*strptime(EDML_Startdate, "%y%a%d")[:6]))[0], axis=-2)
del_dml = find(libarray_nlst[2][:,38].astype(None)<pylab.date2num(datetime(*strptime(
    EDML_Startdate, "%y%a%d")[:6])))
del_dml = filter(lambda x:x in del_dml, find(libarray_nlst[2][:,38].astype(None)>pylab.date2num(
    datetime(*strptime("070610", "%y%a%d")[:6])))
1617 ## Remove data following the given date list
del_dml =append(del_dml, find([rm.date in remove_dates for rm.date in libarray_nlst[2][:,0]))
removed_dml = libarray_nlst[2].take(del_dml, axis=-2)
#print shape(libarray_nlst[2])
libarray_nlst[2] = delete(libarray_nlst[2], del_dml, 0)
#print shape(libarray_nlst[2])
1622
    if dml_range == "glacial":
        export_fn = 'Dekryptonized_EDML_Glacial_Internalcorr_data'
        range_dml = find(libarray_nlst[2][:,2].astype(None)>1015)
        libarray_nlst[2]= libarray_nlst[2].take(range_dml, axis=-2)
1627
    elif dml_range == "T1":
        export_fn = 'Dekryptonized_EDML_Termination_Internalcorr_data'
        range_dml = find(libarray_nlst[2][:,2].astype(None)<1015)
        libarray_nlst[2]= libarray_nlst[2].take(range_dml, axis=-2)
1632
    else:
        export_fn = 'Dekryptonized_EDML_Glacial&Termination_Internalcorr_data'
        # for rem in remove_dates:
        #     #removed_sel = append(removed_date, array(libarray_nlst[2].take(where(libarray_nlst
        # [2][:,0]==rem)[0], axis=-2), ndmin=2), axis=0)
        #     libarray_nlst[2] = libarray_nlst[2].take(where(libarray_nlst[2][:,0]!=rem)[0], axis=-2)
1637
    else:
        export_fn = 'All_Ice_splcorr_data.csv'
        del_ice=find([rm_ice not in Intercomp_ice for rm_ice in libarray_nlst[2][:,1]])
        libarray_nlst[2] = delete(libarray_nlst[2], del_ice, 0)
1642
    if eval_run=="on":
        ## Export Data stage 3 "EDML.only"
        milestone(libarray_nlst[2].take([0,1,2,3,37,38,39], axis=-1), "VPDB-Linked&EDMLOnly", "Removed B37 and
            other ice origins", 'yes!')

        ## Export Data stage 4 "EDML.Selected"
        milestone(libarray_nlst[2].take([0,1,2,3,37,38,39], axis=-1), "SplCorr&EDMLSelected", "Removed obvious
            outliers")
1647
        debugplot(removed_dml.take([0,1,2,3,37,39], axis=-1), "Specifically removed datapoints", "Removed by
            specified dates and date range", "None", 6)
        #plfg.plot_date(removed_sel[-len(remove_dates):,38], removed.date[-len(remove_dates):,39], 'o', label
            ="Removed selected datasets")

        from matplotlib.transforms import offset_copy
        transOffset = offset_copy(evfg.transData, fig=Eval_Fig, x=-0.1, y=0.20, units='inches')
1652
        for x, y, dpth in zip(removed_dml.take([0,1,2,3,37,39], axis=-1)[: , 2].astype(None), removed_dml.take
            ([0,1,2,3,37,39], axis=-1)[: , -1].astype(None), removed_dml.take([0,1,2,3,37,39], axis=-1)[: , 0])
            :
            pylab.text(x, y, '%s' % (dpth), fontsize=8, transform=transOffset)

        # Should sample data meeting the "max_diff" constraint be removed from the sample dataset?
        if rem_max is 'yes':
1657
            refl_diff, aira_diff, diff_list = loop_diff(1,3, iso_col[1], iso_col[3])
            diff_dates=[diff[0].split('-')[0] for diff in diff_list if abs(diff[-1]) > max_diff]
            if eval_run=="on":
                debugplot(libarray_nlst[2][find([dates in diff_dates for dates in libarray_nlst[2][:,0]])], :).take
                    ([0,1,2,3,37,39], axis=-1), r"Looppdiff-exceeds( \textgreater %s)%(max_diff)", "datapoints that
                    exceed the given threshold", "None", 8)
1662
        #
        #
        #for i in range(len(libarray_nlst[2])):
        #     ## add a vertical line at every sample measurement date and a text box to it
1667
        #     plfg.add_line(pylab.Line2D([libarray_nlst[2][i, 38].astype(None), libarray_nlst[2][i,38].astype(
            None)], [-48.6, -49.8], linewidth=1, linestyle='-', color='0.5'))
        #     plfg.text(libarray_nlst[2][i, 38].astype(None), -48.55, libarray_nlst[2][i,2]+"-"+libarray_nlst
            [2][i,3]+"-"+str((libarray_nlst[2][i,6].astype(None)-libarray_nlst[2][i,39].astype(None))),
            rotation=45, fontsize=8)

        if debug_refl == 'on' and debug_corr == 'on':
            color=['#4169E1', 'crimson', '#2F4F4F', 'r', 'dodgerblue', 'purple', 'teal', 'm', 'g', 'k', 'c', 'b', 'g', 'y']

```

```

1672 if dbgrefa_plot == "on":
    for i, (typus) in enumerate(unique(libarray_nlst [4][:,1])):
        if typus in air_list:
            for n, (dset) in enumerate(libarray_nlst [4][find(libarray_nlst [4][:,1] == typus), :]):
                if dset [35].astype(None) < 733773.0:
1677     plfg.add_line(pylab.Line2D([dset [35].astype(None), dset [35].astype(None)
                                ],[-41.1,-40.1], linewidth=1, linestyle='-',color=color[i])) #
                plfg.text(dset [ 35].astype(None), -40, typus+"-"+dset[0]+"-"+dset[32]+"-"+dset
                        [4]+"-"+dset [36],rotation=45, fontsize=8)
                else:
                plfg.add_line(pylab.Line2D([dset [35].astype(None), dset [35].astype(None)
                                ],[-50,-49], linewidth=1, linestyle='-',color=color[i])) #
                plfg.text(dset [35].astype(None), -49.02, typus+"-"+dset[0]+"-"+dset[32]+"-"+
                        dset[4]+"-"+dset [36],rotation=45, fontsize=8)
1682
    Btl_Fig = pylab.figure(figsize=[f_wh, f_ht])
    btfg=Btl_Fig.add_subplot(111)
    Btl_Fig.suptitle(" Reference Gases after Spline Correction (sm. %s,%s)"%(rspl.smth_a,rspl.smth_b))
    btfg.add_ylabel(ur'$\delta\backslash; \{13\}C ( \u2030 )')
1687 btfg.set_xlabel(r'Date')
    btfg.invert_yaxis
    btfg.plot_date(libarray_nlst [1][Normloop_idx_old, 34].astype(None),libarray_nlst [1][
        Normloop_idx_old, 35].astype(None), 'bo',label="SynthAir bottle Refl values")
    btfg.plot_date(libarray_nlst [1][Normloop_idx_new, 34].astype(None),libarray_nlst [1][
        Normloop_idx_new, 35].astype(None), 'ro',label="CrystalAir Refl values")
1692 #btfg.add_line(pylab.Line2D([min(splrefl_old_x).round(),max(splrefl_old_x).round()),[
        loopspl_old_mean,loopspl_old_mean], linewidth=1, linestyle='-', color='k'))
    btfg.add_line(pylab.Line2D([min(splrefl_old_x).round(),max(splrefl_old_x).round()),[mean(
        libarray_nlst [1][Normloop_idx_old, 35].astype(None)),mean(libarray_nlst [1][Normloop_idx_old,
        35].astype(None))], linewidth=1, linestyle='-', color='k'))
    btfg.text(max(splrefl_old_x).round()-10,mean(libarray_nlst [1][Normloop_idx_old, 35].astype(None)),
        ur'SynthAir spline mean: %0.2f\u00b1%0.2f'%(mean(libarray_nlst [1][Normloop_idx_old, 35].
        astype(None)),std(libarray_nlst [1][Normloop_idx_old, 35].astype(None))), fontsize=8) # Enter text in
        subplot object at ax pos. , bbox=dict(facecolor='0.5', alpha=0.5)
    btfg.add_line(pylab.Line2D([min(splrefl_new_x).round(),max(splrefl_new_x).round()),[mean(
        libarray_nlst [1][Normloop_idx_new, 35].astype(None)),mean(libarray_nlst [1][Normloop_idx_new,
        35].astype(None))], linewidth=1, linestyle='-', color='k'))
    btfg.text(max(splrefl_new_x).round()-10,mean(libarray_nlst [1][Normloop_idx_new, 35].astype(None)),
        ur'CrystalAir spline mean: %0.2f\u00b1%0.2f'%(mean(libarray_nlst [1][Normloop_idx_new, 35].
        astype(None)),std(libarray_nlst [1][Normloop_idx_new, 35].astype(None))), fontsize=8) # Enter
        text in subplot object at ax pos. , bbox=dict(facecolor='0.5', alpha=0.5)
1697
    syn_ix=find(libarray_nlst [4][:,1] == "SynthAir")
    syn_ix=filter(lambda x:x in syn_ix,find([date not in ["100520","101008"] for date in libarray_nlst
        [4][:,0]]))
1702
    cry_ix=find(libarray_nlst [4][:,1] == "CrystalAir")
    cry_ix=filter(lambda x:x in cry_ix,find(libarray_nlst [4][:,35].astype(None)>733295.0)) #733467.0->
        pylab.strptime2num("%y%mf%d")("090301")
    cry_ix=filter(lambda x:x in cry_ix,find([date not in
        ['081216','081217','081218','081218','081219','090109','090112','090513','091001'] for date in
        libarray_nlst [4][:,0]])) # org ["090513", "090526","091001"]
    cry_ix=delete(cry_ix,[list(cry_ix).index(s) for s in find([date[0] in ['090316','090319'] and date
        [1] == "2.0" for date in libarray_nlst [4][:,(0,33) ]])]) # delete specific measurements with 1
        x10ml of days in the given list
    cao_ix=find(libarray_nlst [4][:,1] == "CAO8463")
    cao_ix=filter(lambda x:x in cao_ix,find(libarray_nlst [4][:,35].astype(None)>733832.0)) #pylab.
       .strptime2num("%y%mf%d")("100301")
1707
    nm_ix=find(libarray_nlst [4][:,1] == "Neumayer")
    nm_ix=filter(lambda x:x in nm_ix,find([NR not in nm.ol for NR in libarray_nlst [4][:,32]]) # [NR in
        ["16", "17"] for NR in libarray_nlst [4][:,32]])
    btfg.plot_date(libarray_nlst [4][syn_ix,35].astype(None),libarray_nlst [4][syn_ix, 36].astype(None),
        'bo',label="SynthAir")
    btfg.plot_date(libarray_nlst [4][cry_ix,35].astype(None),libarray_nlst [4][cry_ix, 36].astype(None),
        'ro',label="CrystalAir")
1712
    btfg.plot_date(libarray_nlst [4][cao_ix,35].astype(None),libarray_nlst [4][cao_ix, 36].astype(None),
        'co',label="Boulder")
    btfg.plot_date(libarray_nlst [4][nm_ix,35].astype(None),libarray_nlst [4][nm_ix, 36].astype(None),
        'mo',label="Neumayer")
    btfg.add_line(pylab.Line2D([min(libarray_nlst [4][syn_ix,35].astype(None)).round(),max(libarray_nlst
        [4][syn_ix,35].astype(None)).round()),[mean(libarray_nlst [4][syn_ix, 36].astype(None)),mean(
        libarray_nlst [4][syn_ix, 36].astype(None))], linewidth=1, linestyle='-', color='k'))
    btfg.text(max(libarray_nlst [4][syn_ix,35].astype(None)).round()+5,mean(libarray_nlst [4][syn_ix,
        36].astype(None)), ur'SynthAir: %0.2f\u00b1%0.2f'%(mean(libarray_nlst [4][syn_ix, 36].astype(
        None)),std(libarray_nlst [4][syn_ix, 36].astype(None))), fontsize=8) # Enter text in subplot
        object at ax pos. , bbox=dict(facecolor='0.5', alpha=0.5)
1717
    btfg.add_line(pylab.Line2D([min(libarray_nlst [4][cry_ix,35].astype(None)).round(),max(libarray_nlst
        [4][cry_ix,35].astype(None)).round()),[mean(libarray_nlst [4][cry_ix, 36].astype(None)),mean(
        libarray_nlst [4][cry_ix, 36].astype(None))], linewidth=1, linestyle='-', color='k'))
    btfg.text(max(libarray_nlst [4][cry_ix,35].astype(None)).round()+5,mean(libarray_nlst [4][cry_ix,
        36].astype(None)), ur'CrystalAir: %0.2f\u00b1%0.2f'%(mean(libarray_nlst [4][cry_ix, 36].astype(
        None)),std(libarray_nlst [4][cry_ix, 36].astype(None))), fontsize=8) # Enter text in subplot
        object at ax pos. , bbox=dict(facecolor='0.5', alpha=0.5)

```

```

btfg.add_line(pylab.Line2D([min(libarray_nlst[4][cao_ix,35].astype(None)).round(),max(libarray_nlst
[4][cao_ix,35].astype(None)).round()],[mean(libarray_nlst[4][cao_ix,36].astype(None)),mean(
libarray_nlst[4][cao_ix,36].astype(None))],linewidth=1,linestyle='-',color='k'))
btfg.text(max(libarray_nlst[4][cao_ix,35].astype(None)).round()+5,mean(libarray_nlst[4][cao_ix,
36].astype(None)),ur'Boulder: %0.2f\u00b1%0.2f'%(mean(libarray_nlst[4][cao_ix,36].astype(
None)),std(libarray_nlst[4][cao_ix,36].astype(None))),fontsize=8)# Enter text in subplot
object at ax pos. , bbox=dict(facecolor='0.5',alpha=0.5)
btfg.add_line(pylab.Line2D([min(libarray_nlst[4][nm_ix,35].astype(None)).round(),max(libarray_nlst
[4][nm_ix,35].astype(None)).round()],[mean(libarray_nlst[4][nm_ix,36].astype(None)),mean(
libarray_nlst[4][nm_ix,36].astype(None))],linewidth=1,linestyle='-',color='k'))
1722 btfg.text(max(libarray_nlst[4][nm_ix,35].astype(None)).round()+5,mean(libarray_nlst[4][nm_ix,36].
astype(None)),ur'Neumayer: %0.2f\u00b1%0.2f'%(mean(libarray_nlst[4][nm_ix,36].astype(None)),
std(libarray_nlst[4][nm_ix,36].astype(None))),fontsize=8)# Enter text in subplot object at
ax pos. , bbox=dict(facecolor='0.5',alpha=0.5)

# Was ist die Isotopie der Refloops an den Tagen der Bestimmung von Neumayer?
nm_dates = libarray_nlst[4][nm_ix,0]#[ '070531', '070601', '070601', '070604', '070604',
'071101', '071102', '080211', '080212', '080213', '080613', '080618', '080619', '080623',
'080825', '080826']
nm_loops=filter(lambda x:x in Normloop_idx_old,find([date in nm_dates for date in libarray_nlst
[1][:,0]]))#
1727 btl_nmcor=mean(libarray_nlst[1][nm_loops,35].astype(None)).round(2)-(mean(libarray_nlst[4][nm_ix,
36].astype(None)-NM_iso).round(2))# calculate the isotopy value of the Refloop bottle"
SynthAir" linked to V-PDB
### ...und was der Offset des "SynthAir" und "CrystalAir" Regiments?
### Niveau-Ausgleich über SynthAir...
nv_cor=mean(libarray_nlst[4][syn_ix,36].astype(None)).round(2)-(loopspl_old_mean-mean(
libarray_nlst[4][nm_ix,36].astype(None)-NM_iso).round(2))
### Niveau-Ausgleich über CrystalAir
1732 #nv_cor=(loopspl_new_mean-mean(libarray_nlst[4][cry_ix,36].astype(None)).round(2)+mean(
libarray_nlst[4][nm_ix,36].astype(None)-NM_iso).round(2))

### Angewendet auf die Daten
### Refloops
merged_nm_col = append(\
1737 ((libarray_nlst[1][rl_old_idc, iso_col[1]].astype(None)-(scipy.interpolate.splev(libarray_nlst[1][
rl_old_idc, -2].astype(None), spl_refl_old)-loopspl_old_mean)-mean(libarray_nlst[4][nm_ix,
36].astype(None)-NM_iso).round(2))).round(decimals=4),# calculate the deviation of the raw
isotopy data from the spline and the NM offset for the old... \
((libarray_nlst[1][rl_new_idc, iso_col[1]].astype(None)-(scipy.interpolate.splev(libarray_nlst[1][
rl_new_idc, -2].astype(None), spl_refl_new)-loopspl_new_mean)-nv_cor)).round(decimals=4))#
and for the new reflow air bottle range and merge them into one dataset
libarray_nlst[1] = append(libarray_nlst[1],array(merged_nm_col,ndmin=2).transpose(),axis=1)# add
the merged dataset to the whole dataarray
## alle anderen
for i in range(2,len(libarray_nlst)):
1742 old_idc = find(libarray_nlst[i][:,ord_col[i]].astype(None)<733773.0)# select all datasets
before 01.01.2010
new_idc = find(libarray_nlst[i][:,ord_col[i]].astype(None)>733773.0)# select all datasets
after 01.01.2010
merged_cor_col = append(\
((libarray_nlst[i][old_idc, iso_col[i]].astype(None)-(scipy.interpolate.splev(libarray_nlst[i][
old_idc, ord_col[i]].astype(None), spl_refl_old)-loopspl_old_mean)-mean(libarray_nlst[4][nm_ix,
36].astype(None)-NM_iso).round(2))).round(decimals=4),# calculate the deviation of the raw
isotopy data from the spline and the mean of the spline for the old... \
((libarray_nlst[i][new_idc, iso_col[i]].astype(None)-(scipy.interpolate.splev(libarray_nlst[i][
new_idc, ord_col[i]].astype(None), spl_refl_new)-loopspl_new_mean)-nv_cor)).round(decimals=4))
# and for the new reflow air bottle range and merge them into one dataset
1747 libarray_nlst[i] = append(libarray_nlst[i],array(merged_cor_col,ndmin=2).transpose(),axis=1)#
Append the reflow mean corrected Isotopies to the array in a new column

Cor_Fig = pylab.figure(figsize=[f_wh,f_ht])
1752 corfg=Cor_Fig.add_subplot(111)
Cor_Fig.suptitle(" Reference Gases after Spline+NM Correction (sm. %s,%s)%(rspl-smth_a,rspl-smth_b)
)
corfg.set_ylabel(ur'$\delta\text{ }^{13}\text{C}$ ( \u2030 )$')
corfg.set_xlabel(r'Date')
#corfg.invert_yaxis()
1757 corfg.plot_date(libarray_nlst[1][Normloop_idx_old,34].astype(None),libarray_nlst[1][
Normloop_idx_old,36].astype(None),'bo',label="SynthAir bottle Refl values")
corfg.plot_date(libarray_nlst[1][Normloop_idx_new,34].astype(None),libarray_nlst[1][
Normloop_idx_new,36].astype(None),'ro',label="CrystalAir Refl values")

#corfg.add_line(pylab.Line2D([min(spl_refl_old_x).round(),max(spl_refl_old_x).round()],[
loopspl_old_mean,loopspl_old_mean],linewidth=1,linestyle='-',color='k'))
corfg.add_line(pylab.Line2D([min(spl_refl_old_x).round(),max(spl_refl_old_x).round()],[mean(
libarray_nlst[1][Normloop_idx_old,36].astype(None)),mean(libarray_nlst[1][Normloop_idx_old,
36].astype(None))],linewidth=1,linestyle='-',color='k'))
1762 corfg.text(max(spl_refl_old_x).round()-10,mean(libarray_nlst[1][Normloop_idx_old,36].astype(None)),
ur'SynthAir Spline Mean: %0.2f\u00b1%0.2f'%(mean(libarray_nlst[1][Normloop_idx_old,36].
astype(None)),std(libarray_nlst[1][Normloop_idx_old,36].astype(None))),fontsize=8)# Enter
text in subplot object at ax pos. , bbox=dict(facecolor='0.5',alpha=0.5)
corfg.add_line(pylab.Line2D([min(spl_refl_new_x).round(),max(spl_refl_new_x).round()],[mean(
libarray_nlst[1][Normloop_idx_new,36].astype(None)),mean(libarray_nlst[1][Normloop_idx_new,
36].astype(None))],linewidth=1,linestyle='-',color='k'))

```

```

corfg.text(max(splrefl_new_x).round()-10,mean(libarray_nlst[1][Normloop_idx_new, 36].astype(None)),
ur'CrystalAir-bottle: %0.2f\u00b1%0.2f'%(mean(libarray_nlst[1][Normloop_idx_new, 36].astype(
None)),std(libarray_nlst[1][Normloop_idx_new, 36].astype(None))), fontsize=8) # Enter text in
subplot object at ax pos. , bbox=dict(facecolor='0.5', alpha=0.5)

1767 corfg.plot_date(libarray_nlst[4][syn_ix, 35].astype(None), libarray_nlst[4][syn_ix, 37].astype(None),
'bo', label="SynthAir")
corfg.plot_date(libarray_nlst[4][cry_ix, 35].astype(None), libarray_nlst[4][cry_ix, 37].astype(None),
'ro', label="CrystalAir")
corfg.plot_date(libarray_nlst[4][cao_ix, 35].astype(None), libarray_nlst[4][cao_ix, 37].astype(None),
'co', label="Boulder")
corfg.plot_date(libarray_nlst[4][nm_ix, 35].astype(None), libarray_nlst[4][nm_ix, 37].astype(None),
'mo', label="Neumayer")

1772 corfg.add_line(pylab.Line2D([min(libarray_nlst[4][syn_ix, 35].astype(None)).round(), max(
libarray_nlst[4][syn_ix, 35].astype(None)).round()], [mean(libarray_nlst[4][syn_ix, 37].astype(
None)), mean(libarray_nlst[4][syn_ix, 37].astype(None))], linewidth=1, linestyle='-', color='k
'))
corfg.text(max(libarray_nlst[4][syn_ix, 35].astype(None)).round()+5, mean(libarray_nlst[4][syn_ix,
37].astype(None)), ur'SynthAir: %0.2f\u00b1%0.2f'%(mean(libarray_nlst[4][syn_ix, 37].astype(
None)), std(libarray_nlst[4][syn_ix, 37].astype(None))), fontsize=8) # Enter text in subplot
object at ax pos. , bbox=dict(facecolor='0.5', alpha=0.5)
corfg.add_line(pylab.Line2D([min(libarray_nlst[4][cry_ix, 35].astype(None)).round(), max(
libarray_nlst[4][cry_ix, 35].astype(None)).round()], [mean(libarray_nlst[4][cry_ix, 37].astype(
None)), mean(libarray_nlst[4][cry_ix, 37].astype(None))], linewidth=1, linestyle='-', color='k
'))
corfg.text(max(libarray_nlst[4][cry_ix, 35].astype(None)).round()+5, mean(libarray_nlst[4][cry_ix,
37].astype(None)), ur'CrystalAir: %0.2f\u00b1%0.2f'%(mean(libarray_nlst[4][cry_ix, 37].astype(
None)), std(libarray_nlst[4][cry_ix, 37].astype(None))), fontsize=8) # Enter text in subplot
object at ax pos. , bbox=dict(facecolor='0.5', alpha=0.5)
corfg.add_line(pylab.Line2D([min(libarray_nlst[4][cao_ix, 35].astype(None)).round(), max(
libarray_nlst[4][cao_ix, 35].astype(None)).round()], [mean(libarray_nlst[4][cao_ix, 37].astype(
None)), mean(libarray_nlst[4][cao_ix, 37].astype(None))], linewidth=1, linestyle='-', color='k
'))

1777 corfg.text(max(libarray_nlst[4][cao_ix, 35].astype(None)).round()+5, mean(libarray_nlst[4][cao_ix,
37].astype(None)), ur'Boulder: %0.2f\u00b1%0.2f'%(mean(libarray_nlst[4][cao_ix, 37].astype(
None)), std(libarray_nlst[4][cao_ix, 37].astype(None))), fontsize=8) # Enter text in subplot
object at ax pos. , bbox=dict(facecolor='0.5', alpha=0.5)
corfg.add_line(pylab.Line2D([min(libarray_nlst[4][nm_ix, 35].astype(None)).round(), max(libarray_nlst
[4][nm_ix, 35].astype(None)).round()], [mean(libarray_nlst[4][nm_ix, 37].astype(None)), mean(
libarray_nlst[4][nm_ix, 37].astype(None))], linewidth=1, linestyle='-', color='k'))
corfg.text(max(libarray_nlst[4][nm_ix, 35].astype(None)).round()+5, mean(libarray_nlst[4][nm_ix, 37].
astype(None)), ur'Neumayer: %0.2f\u00b1%0.2f'%(mean(libarray_nlst[4][nm_ix, 37].astype(None)),
std(libarray_nlst[4][nm_ix, 37].astype(None))), fontsize=8) # Enter text in subplot object at
ax pos. , bbox=dict(facecolor='0.5', alpha=0.5)

colr=['#4169E1', '#2F4F4F', 'crimson', 'teal', 'dodgerblue', 'purple', 'yellow', 'g', 'm', 'slategrey',
'darkgrey', 'lightgreen']
1782 if dbgrefa_plot == "on":
print '-----',
print "Reference Air Sample Overview:\n\nSample type: Mean: Std:"
for i, (typus) in enumerate(unique(libarray_nlst[4][:, 1])):
dset = libarray_nlst[4][find(libarray_nlst[4][:, 1] == typus)]
1787 if typus in ['CAO8289', 'CAO1179']:
dset = delete(dset, (0), axis=0) # remove outliers
if typus == 'CC71560':
dset = delete(dset, (2), axis=0) # remove outliers
if typus == 'CAO8463':
1792 dset = dset.take(find(dset[:, 35].astype(None) > 733832.0), axis=0) #pylab.strptime2num
("%y%a%d")("100301")
print "%s(n=%i) %4.2f %4.2f"%(typus, len(dset), mean(dset[:, ord_col[4]+1].astype(None)), std(
dset[:, ord_col[4]+1].astype(None)))
if typus in air_list and typus not in ["CAO8463", "CrystalAir", "SynthAir", "Neumayer"]:
corfg.plot_date(dset[:, 35].astype(None), dset[:, 37].astype(None), "o", color=colr[i])
#corfg.text(dset[:, 35].astype(None), -40, typus+"-"+dset[0]+"-"+dset[32]+"-"+dset
[4]+"-"+dset[36], rotation=45, fontsize=8)
1797 corfg.annotate("%i-%s-%0.2f%0.2f"%(i, typus, mean(dset[:, 37].astype(None)), std(dset[:,
37].astype(None))), xy=(mean(dset[:, 35].astype(None)), mean(dset[:, 37].astype(
None))), xytext=(mean(dset[:, 35].astype(None))-30, mean(dset[:, 37].astype(None))
-1.0), xycoords='data', textcoords='data', arrowprops=dict(edgecolor='black',
facecolor='0.5', width=1, headwidth=4, shrink=0.05), fontsize=8)

### Add Intercal Ice to the plot
for i, (typus) in enumerate(unique(libarray_nlst[5][:, 1])):
dset = libarray_nlst[5][find(libarray_nlst[5][:, 1] == typus)]
if "B37" in typus:
1802 #B37= Smp_misc.ucor.take(find(Smp_misc.ucor.ice_origin=="B37"))
#B37.sort(order=['depth',])
#s1=find(dset[:, 38].astype(None)<pylab.date2num(datetime(*strptime("070610", "%y%a%d")
[:6])))
#s2=find(dset[:, 38].astype(None)<pylab.date2num(datetime(*strptime('080301', "%y%a%d")
[:6])))
#s1=filter(lambda x:x not in s1, s2)
1807 #s3=find(dset[:, 38].astype(None)>pylab.date2num(datetime(*strptime('090701', "%y%a%d")
[:6])))

```

```

#           s4=find(dset[:,38].astype(None)<pylab.date2num(datetime(*strptime("100301", "%y%m%d")
#           [:6])))
#           sel2=filter(lambda x:x in s3,s4)
#           dels=list(s2);dels.extend(find([rm_date in B37_ol for rm_date in dset[:, 0]]))
#           dset = delete(dset,(dels),axis=0) # remove outliers
1812 #           #print dset[:,39].astype(None)
#           old_idc = find(dset[:,38].astype(None)<733773.0) # select all datasets before 01.01.2010
#           new_idc = find(dset[:,38].astype(None)>733773.0) # select all datasets after 01.01.2010
#           dset[old_idc,39]=dset[old_idc,39].astype(None)-0.02
#           dset[new_idc,39]=dset[new_idc,39].astype(None)-nv_cor
1817 #           print typus, dset[:,39].astype(None)
#           corfg.plot_date(dset[:, 38],dset[:, 39],"o", color=color[:, -1][i])
#           corfg.annotate("%i-%s-%0.2f,%0.2f"%(i+1,typus,mean(dset[:, 39].astype(None)),std(dset[:,
39].astype(None))), xy=(mean(dset[:, 38].astype(None)),mean(dset[:, 39].astype(None))), xytext=(
mean(dset[:, 38].astype(None)-30,mean(dset[:, 39].astype(None))-1.0), xycoords='data', textcoords
='data', arrowprops=dict(edgecolor='black', facecolor='0.5',width=1,headwidth=4, shrink=0.05),
fontsize=8)
#
#           old_idc = find(non_dml[:,38].astype(None)<733773.0) # select all datasets before 01.01.2010
1822 #           new_idc = find(non_dml[:,38].astype(None)>733773.0)
#           non_dml[old_idc,39]=non_dml[old_idc,39].astype(None)-0.02
#           non_dml[new_idc,39]=non_dml[new_idc,39].astype(None)-nv_cor
#           no_dml=non_dml.take(find(non_dml[:,1] == "B37"),axis=0)
#           no_dml= delete(no_dml,(dels),axis=0) # find(no_dml[:,38].astype(None)>pylab.date2num(datetime
(*strptime("100101", "%y%m%d")[:6])))
1827 #           print no_dml[:,39].astype(None)
#           corfg.plot_date(no_dml[:, 38].astype(None),no_dml[:,39].astype(None),"o", color="white", ms
=3)
'''
#####
1832 Add chosen age column to Ice Sample array...(see header)
'''
#####
## Find the depth of sample dataset in the chosen Depth Age relationship dataset
print '-----'
1837 print 'Adding %s age column to data...'%(age.choice)
print
### Remove two double entries in dataset "comp" first
#comp =delete(comp,(95,216), axis=0)
1842 #####
## Set the different Cuts to their corresponding top depth (Cut "G01" 12,5cm above Cut "G02") ...
# by first replacing possible ',' in string, round to 3 digits after the comma
libarray_nlst[2][:,2]=array(map(lambda x: float(x.replace(',','.')),libarray_nlst[2][:,2])).round(3)
# and second add 12,5cm where the Cut is "G02"
1847 libarray_nlst[2][tuple(where(libarray_nlst[2][:,3]== 'G02')[0]),2]=libarray_nlst[2][tuple(where(
libarray_nlst[2][:,3]== 'G02')[0]),2].astype(float)+.125
## sort sample array by depth/age
smpl_dsrt = libarray_nlst[2].take(argsort(libarray_nlst[2][:,2].astype(float)), axis=-2)
if eval_run == "on":
1852 ## Export Data stage 5 "Sorted by depth"
milestone(smpl_dsrt.take([0,1,2,3,37,38,39],axis=-1),"Data_depthsorted","All trend corrections
applied and outlier removed")
if ice_origin == 'EDML':
1857 # Call def to find corresponding Indices for the given depth range
min_idx,max_idx=ext_idc(ch4_data['data'][: ,ch4_data['dth-idx']],min(smpl_dsrt[:,2].astype(float).
round()-1),max(smpl_dsrt[:,2].astype(float).round()-1),0)
## Calculate a spline over the depth range
if min_idx>=5 and max_idx<=(len(ch4_data['data'])-5):
spl_dep_age = scipy.interpolate.splrep(ch4_data['data'][min_idx-5:max_idx,ch4_data['dth-idx']].
astype(float),ch4_data['data'][min_idx-5:max_idx,ch4_data['age-idx']].astype(float),k=
spl_ord, s=spl_smth)
1862 else:
spl_dep_age = scipy.interpolate.splrep(ch4_data['data'][min_idx:,ch4_data['dth-idx']].astype(
float),ch4_data['data'][min_idx:,ch4_data['age-idx']].astype(float),k=spl_ord, s=spl_smth)
## Calculate the spline representation for The Ice depth
splda_y = scipy.interpolate.splev(smpl_dsrt[:, 2].astype(None), spl_dep_age)
1867 ## Append the new age colum to the ice sample array
smpl_dsrt = append(smpl_dsrt,array(splda_y,ndmin=2).transpose(), axis=1)
else:
from scipy import stats
gradient, intercept, r_value, p_value, std_err = stats.linregress(ch4_data['data'][:10,ch4_data['
dth-idx']],ch4_data['data'][:10,ch4_data['age-idx']]) # calculate a depth/age relationship
from EDML CH4 dataset
1872 smpl_dsrt = append(smpl_dsrt,array(((smpl_dsrt[:, 2].astype(None))*gradient+intercept).round(1),
ndmin=2).transpose(), axis=1)
print '-----'
print "Intercomparison Ice Overview:\n\nSample type:      Mean:      Std:"
for n, typus in enumerate(unique(smpl_dsrt[:,1])):
dset = smpl_dsrt.take(find(smpl_dsrt[:,1]==typus),axis=0)
1877 print "%s (n=%i) %4.2f %4.2f"%(typus,len(dset),mean(dset[:, ord_col[2]+1].astype(None)),std(dset
[:, ord_col[2]+1].astype(None)))
'''

```



```

#####
Apply Gravitational Correction
1882 if ice_origin == 'EDML':
    # Subtract the Gravi Factor
    smpl_dsrt[:, -2] = smpl_dsrt[:, -2].astype(None)-grav_corfac
1887 print '-----'
    print 'Calculating Gravitational Correction with constant offset of %s\n for glacial conditions
        calculated through Landais/Capron data...\n'%(grav_corfac)
if eval_run == "on":
    ## Export Data stage 6 "Gravitational Correction"
    milestone(smpl_dsrt.take([0,1,2,3,37,38,39], axis=-1),"Data_dsrted&Gravicorr","Applied Graviational
1892 Correction (constant offset), all trend corrections applied and outlier removed")
    ...
#####
Plotting Routines...
1897

## plot sample types
if smpl_plot == 'on':
1902 if ice_origin == 'EDML':
    smpl_dsrt, smpl_dcor=sample_plot(smpl_dsrt, ord_col[2], iso_col[2], splrefl_old_x, splrefl_old_y)
    # call def for plotting and return the depth sorted dataset and a replicate merged
    version of it
    ## Apply the Neymayer Offset Correction Factor
    #smpl_dsrt[:, -2] = (smpl_dsrt[:, -2].astype(None)-NM_offset).round(3)
    ## Calculate the Mean Stddev of the Ice Samples from replicated datasets
1907 print '-----'
    print 'Mean Stddev of the Ice Samples with replicate datasets: %s permille (n=%i)\n'%(mean(
        smpl_dcor[tuple(where(smpl_dcor[:,3]== 'G01+G02')[0]), -1].astype(float)).round(3), len(
        tuple(where(smpl_dcor[:,3]== 'G01+G02')[0])))
    # elif ice_origin == 'B37':
    # smpl_dsrt, smpl_dcor=sample_plot(smpl_dsrt, ord_col[2], iso_col[2], splrefl_old_x, splrefl_old_y)
    # call def for plotting and return the depth sorted dataset and a replicate merged version of it
    ref_plot(3, libarray_nlst[2], 'B37ice', ord_col[2], iso_col[2])
1912 else:
    cat_idx = data_cat.index('Sample')
    for i, (typus) in enumerate(Intercomp_ice):
        ref_plot(3, libarray_nlst[cat_idx][find(libarray_nlst[cat_idx][:,1] == typus),:], typus,
            ord_col[2], iso_col[2])
1917 #smpl_dcor, smpl_dsrt, mn_uncor_col, std_uncor_col, repl_idc = sample_replicates(smpl_dsrt, iso_col[2],
    ord_col[2])
if eval_run == "on":
    ## Export Data stage 7 "Replicates concatenated"
    milestone(smpl_dsrt.take([0,1,2,3,37,38,39], axis=-1),"Replicates","All corrections applied, outlier
    removed, sorted by depth and concatenated Replicate measurements")
1922

## Add a bar a and a caption of every ice measurement done troughout the reflow dataset
if debug_refl == 'on':
    std_wo_ob, std_wo_nb, std_w_ob, std_w_nb=std(libarray_nlst[1][Normloop_idx_old, 4].astype(None)),std(
        libarray_nlst[1][Normloop_idx_new, 4].astype(None)),std(libarray_nlst[1][Normloop_idx_old,
        35].astype(None)),std(libarray_nlst[1][Normloop_idx_new, 35].astype(None))
    var_ar=(ones(4)*[std_wo_ob, std_wo_nb, std_w_ob, std_w_nb])**2
1927 box_txt="Precision for Refloos without Trend correction...\n old bottle: %s\t new bottle: %s
    \n and with spline correction...\n old bottle: \t%s new bottle:\t%s"%(std(libarray_nlst[1][
    Normloop_idx_old, 4].astype(None)).round(2), std(libarray_nlst[1][Normloop_idx_new, 4].astype(
    None)).round(2), std(libarray_nlst[1][Normloop_idx_old, 35].astype(None)).round(2), std(
    libarray_nlst[1][Normloop_idx_new, 35].astype(None)).round(2))
    plfg.text(0.03,0.04 ,box_txt , bbox=dict(facecolor='0.5', alpha=0.2), fontsize=12, transform = plfg
    .transAxes)
#for i in range(len(removed_sel)):
# ## add a vertical line at every sample measurement date and a text box to it
# plfg.add_line(pylab.Line2D([removed_sel[i, 38].astype(None), removed_sel[i,38].astype(None)
],[-41.1,-40.1], linewidth=1, linestyle='-', color='red'))
1932 # plfg.text(removed_sel[i, 38].astype(None), -40, removed_sel[i,2]+"-"+removed_sel[i,3]+"-"+str((
    removed_sel[i,6].astype(None)-removed_sel[i,39].astype(None)), rotation=45, fontsize=8)

if dbgice_plot == "on":
    for i, (typus) in enumerate(unique(libarray_nlst[2][:,1])):
        #if typus in Intercomp_ice:
1937 for n, (dset) in enumerate(libarray_nlst[2][find(libarray_nlst[2][:,1] == typus), :]):
            if dset[38].astype(None)<733773.0:
                plfg.add_line(pylab.Line2D([dset[38].astype(None), dset[38].astype(None)],[-41.1,-40.1],
                    linewidth=1, linestyle='-',color=color[i])) #
                plfg.text(dset[38].astype(None), -40, "%s %s-%s%-uncor %s-cor."%(typus, dset[0], dset
                    [2], dset[6], dset[39]), rotation=45, fontsize=8)
            else:
1942 plfg.add_line(pylab.Line2D([dset[38].astype(None), dset[38].astype(None)],[-50,-49],
                    linewidth=1, linestyle='-',color=color[i])) #
                plfg.text(dset[38].astype(None), -49.02,"%s %s-%s%-uncor %s-cor."%(typus, dset[0], dset
                    [2], dset[6], dset[39]), rotation=45, fontsize=8)
if dbgice_replicates == "on":
    for i, (typus) in enumerate(unique(libarray_nlst[2][:,3])):

```



```

constraint = find([std(libarray_nlst [2][idx,39].astype(None))>0.2 for idx in zip(repl_idc
-1,repl_idc)])
1947 pick=filter(lambda x:x in find(libarray_nlst [2][:,3] == typus),append(repl_idc [constraint] ,
repl_idc [constraint]-1))
for n, (dset) in enumerate(libarray_nlst [2][pick, :]):
if dset [38].astype(None)<733773.0:
plfg.add_line(pylab.Line2D([dset [38].astype(None),dset [38].astype(None)
],[ -41.1, -40.1], linewidth=1, linestyle='-',color=color [i])) #
plfg.text(dset [38].astype(None), -40, " %s-%s-%s-uncor %s-cor."%(dset [2],dset [0],
dset [6],dset [39]),rotation=45, fontsize=8)
1952 else:
plfg.add_line(pylab.Line2D([dset [38].astype(None),dset [38].astype(None)],[ -50, -49],
linewidth=1, linestyle='-',color=color [i])) #
plfg.text(dset [38].astype(None), -49.02, " %s-%s-%s-uncor %s-cor."%(dset [2],dset [0],
dset [6],dset [39]),rotation=45, fontsize=8)
# for n,smoothey in enumerate(arange(rspl_smth_a -.6,rspl_smth_a +1.0,0.4)):#range(1,4)
# #splold_numrange=range(1,len(libarray_nlst [1][find(libarray_nlst [1][:,ord_col [1]].astype(None)
<733773.0),ord_col [1]])+1)
1957 # spl_reflvar_old = scipy.interpolate.splev(libarray_nlst [1][find(libarray_nlst [1][:,ord_col
[1]].astype(None)<733773.0),ord_col [1]].astype(None),libarray_nlst [1][find(libarray_nlst [1][:,
ord_col [1]].astype(None)<733773.0),4].astype(None),k=rspl_ord, s=smoothey)
# splrefl_oldvar_x = arange(min(libarray_nlst [1][find(libarray_nlst [1][:,ord_col [1]].astype(None)
)<733773.0),ord_col [1]].astype(None)),max(libarray_nlst [1][find(libarray_nlst [1][:,ord_col [1]].
astype(None)<733773.0),ord_col [1]].astype(None))+1.0/enlargement [0],1.0/enlargement [0]) # reduce
stepping between x-datapoints
# splrefl_oldvar_y = scipy.interpolate.splev(splrefl_oldvar_x, spl_reflvar_old)
# spldifold_overall=libarray_nlst [1][find(libarray_nlst [1][:,ord_col [1]].astype(None)<733773.0),
4].astype(None)-scipy.interpolate.splev(libarray_nlst [1][find(libarray_nlst [1][:,ord_col [1]].
astype(None)<733773.0),ord_col [1]].astype(None),spl_reflvar_old)
# spldifold_mean = mean(abs(spldifold_overall))
1962 # spldifold_err=sqrt(sum(spldifold_overall**2)/len(spldifold_overall))
# plfg.plot(splrefl_oldvar_x,splrefl_oldvar_y,"-",color=color [n+2],label="Old Bottle Spline
smooth.%s - difference %0.2f, err. %0.2f"%(smoothey,spldifold_mean,spldifold_err))
# for n,smoothey in enumerate([rspl_smth_b -.01,rspl_smth_b +0.1]):
# #splnew_numrange=range(splold_numrange[-1]+1,splold_numrange[-1]+1+len(libarray_nlst [1][find(
libarray_nlst [1][:,ord_col [1]].astype(None)>733773.0),ord_col [1]])
# spl_reflvar_new = scipy.interpolate.splev(libarray_nlst [1][find(libarray_nlst [1][:,ord_col
[1]].astype(None)>733773.0),ord_col [1]].astype(None),libarray_nlst [1][find(libarray_nlst [1][:,
ord_col [1]].astype(None)>733773.0),4].astype(None),k=rspl_ord, s=smoothey)
1967 # splrefl_newvar_x = arange(min(libarray_nlst [1][find(libarray_nlst [1][:,ord_col [1]].astype(None)
)>733773.0),ord_col [1]].astype(None)),max(libarray_nlst [1][find(libarray_nlst [1][:,ord_col [1]].
astype(None)>733773.0),ord_col [1]].astype(None))+1.0/enlargement [0],1.0/enlargement [0]) # reduce
stepping between x-datapoints
# splrefl_newvar_y = scipy.interpolate.splev(splrefl_newvar_x, spl_reflvar_new)
# spldifnew_overall=libarray_nlst [1][find(libarray_nlst [1][:,ord_col [1]].astype(None)>733773.0),
4].astype(None)-scipy.interpolate.splev(libarray_nlst [1][find(libarray_nlst [1][:,ord_col [1]].
astype(None)>733773.0),ord_col [1]].astype(None),spl_reflvar_new)
# spldifnew_mean = mean(abs(spldifnew_overall))
1972 # spldifnew_err=sqrt(sum(spldifnew_overall**2)/len(spldifnew_overall))
# plfg.plot(splrefl_newvar_x,splrefl_newvar_y,"-",color=color [n+2],label="New Bottle Spline
smooth.%s - difference %0.2f, err. %0.2f"%(smoothey,spldifnew_mean,spldifnew_err))
'''
Are the first Mref Peaks a good qualitative measure for a spline
'''
1977 if dbg_firstMref_plot == "on" :
ice_loops=concatenate(array([find(libarray_nlst [1][:,0]==date) for date in libarray_nlst [2][:,0] if
find(libarray_nlst [1][:,0]==date)!=0],ndmin=1),axis=1)
fstmref_fig = pylab.figure(figsize=[f_wh,f_ht])

1982 for i in range(1,len(libarray_nlst)-2):
old_idc = find(libarray_nlst [i][:,ord_col [i]].astype(None)<733773.0) # select all datasets
before 01.01.2010
new_idc = find(libarray_nlst [i][:,ord_col [i]].astype(None)>733773.0) # select all datasets
after 01.01.2010
first_mref [i] =append(\
((libarray_nlst [i][old_idc, iso_col [i]-2].astype(None)-(scipy.interpolate.splev(libarray_nlst [i][
old_idc, ord_col [i]].astype(None), spl_refl_old)-loopspl_old_mean)-NM_offset)).round(decimals
=4),
1987 ((libarray_nlst [i][new_idc, iso_col [i]-2].astype(None)-(scipy.interpolate.splev(libarray_nlst [i][
new_idc, ord_col [i]].astype(None), spl_refl_new)-loopspl_new_mean)-Btl_niveau_cor)).round(
decimals=4))
if i == 1:
fstmref_fig.add_subplot(3,1,i)
pylab.title("1st-Mref Peak, corrected by smth. %s/%s spline"%(rspl_smth_a,rspl_smth_b))
plot_date(libarray_nlst [i][filter(lambda x:x in old_idc,ice_loops),ord_col [i]].astype(None)
),first_mref [i][filter(lambda x:x in old_idc,ice_loops)],"wo",ms=10)
1992 plot_date(libarray_nlst [i][filter(lambda x:x in new_idc,ice_loops),ord_col [i]].astype(None)
),first_mref [i][filter(lambda x:x in new_idc,ice_loops)],"wo",ms=10)
print mean(first_mref [i][filter(lambda x:x in old_idc,ice_loops)]),std(first_mref [i][
filter(lambda x:x in old_idc,ice_loops)])
print mean(first_mref [i][filter(lambda x:x in new_idc,ice_loops)]),std(first_mref [i][
filter(lambda x:x in new_idc,ice_loops)])
else:
fstmref_fig.add_subplot(3,1,i, sharex=ax)

```

```

1997     plot_date(libarray_nlst[i][old_idc, ord_col[i]].astype(None), first_mref[i][old_idc], "bo")
        plot_date(libarray_nlst[i][new_idc, ord_col[i]].astype(None), first_mref[i][new_idc], "ro")
        pylab.ylabel(data_cat[i])
        ax = pylab.gca()
2002     ax.add_line(pylab.Line2D([min(libarray_nlst[i][old_idc, ord_col[i]].astype(None)).round(), max(
        libarray_nlst[i][old_idc, ord_col[i]].astype(None)).round()], [mean(first_mref[i][old_idc])
        , mean(first_mref[i][old_idc])], linewidth=1, linestyle='-', color='k'))
        ax.text(max(libarray_nlst[i][old_idc, ord_col[i]].astype(None)).round()-10, mean(first_mref[i][
        old_idc]), ur'%0.2f', 1 sigma %0.2f'%(mean(first_mref[i][old_idc]), std(first_mref[i][
        old_idc])), fontsize=8) # Enter text in subplot object at ax pos. , bbox=dict(facecolor
        ='0.5', alpha=0.5)
        ax.add_line(pylab.Line2D([min(libarray_nlst[i][new_idc, ord_col[i]].astype(None)).round(), max(
        libarray_nlst[i][new_idc, ord_col[i]].astype(None)).round()], [mean(first_mref[i][new_idc])
        , mean(first_mref[i][new_idc])], linewidth=1, linestyle='-', color='k'))
        ax.text(max(libarray_nlst[i][new_idc, ord_col[i]].astype(None)).round()-10, mean(first_mref[i][
        new_idc]), ur'%0.2f', 1 sigma %0.2f'%(mean(first_mref[i][new_idc]), std(first_mref[i][
        new_idc])), fontsize=8) # Enter text in subplot object at ax pos. , bbox=dict(facecolor
        ='0.5', alpha=0.5)

2007     ### Spline Comparison #####
        ## Show Splines of MRef, Refloops and Airafter datasets

        if spl_compare is 'on':
2012     color=['#4169E1', 'crimson', '#2F4F4F', 'purple', 'teal', 'dodgerblue', 'r', 'm', 'g', 'k', 'c', 'b', 'g', 'y']
        Splcor_fig = pylab.figure(figsize=[f_wh, f_ht])
        pylab.figtext(0.8, 0.02, created: '+asctime(localtime()), size=9)
        splcor_spl = Splcor_fig.add_subplot(211)
        pylab.title('Spline Comparison of MRef, Refloops and Airafter datasets')
2017     #org_label=data_cat[lib]+' library data (uncorrected)'
        slabel = 'Splinefit'
        rlabel = 'Splinefit'
        pylab.xlabel('Measurement date range')
        pylab.ylabel(r'$\delta^{13}C$ $(\%0)$')
2022     plot_mrefspl = 'on'
        for lib in (1.):
            org_label=data_cat[lib]+' library data (uncorrected)'
            if plot_mrefspl == 'on' and lib == 1:
                ### Add the methan ref data
                ## Calculate the spline fit of Methane Ref data (x=date ordinal y= raw isotopy)
                if shape(libarray_nlst[0])[1] is not 45:
                    # Append ordinal column if not present
                    libarray_nlst[0] = append(libarray_nlst[0], array(map(lambda utc: pylab.strptime2num("%y
                    %m%d%H%M%S")(strtime("%y%m%d%H%M%S", localtime(utc))), libarray_nlst[0][:, -1].
                    astype(None)), ndmin=2).transpose(), axis=1)
                    mr_old_idc = find(libarray_nlst[0][:, -1].astype(None) < 733773.0) # select all datasets
                    before 01.01.2010
2032     mr_new_idc = find(libarray_nlst[0][:, -1].astype(None) > 733773.0) # select all datasets after
                    01.01.2010

                    spl_mref_old = scipy.interpolate.splrep(libarray_nlst[0][mr_old_idc, -1].astype(None),
                    libarray_nlst[0][mr_old_idc, 2].astype(None), k=spl_ord, s=spl_smth)
                    splmref_x_old = arange(min(libarray_nlst[0][mr_old_idc, -1].astype(None)), max(
                    libarray_nlst[0][mr_old_idc, -1].astype(None))+1.0/enlargement[0], 1.0/enlargement[0])
                    # reduce stepping between x-datapoints
2037     splmref_y_old = scipy.interpolate.splev(splmref_x_old, spl_mref_old)
                    spl_mref_new = scipy.interpolate.splrep(libarray_nlst[0][mr_new_idc, -1].astype(None),
                    libarray_nlst[0][mr_new_idc, 2].astype(None), k=spl_ord, s=1)
                    splmref_x_new = arange(min(libarray_nlst[0][mr_new_idc, -1].astype(None)), max(
                    libarray_nlst[0][mr_new_idc, -1].astype(None))+1.0/enlargement[0], 1.0/enlargement[0])
                    # reduce stepping between x-datapoints
                    splmref_y_new = scipy.interpolate.splev(splmref_x_new, spl_mref_new)

2042     pylab.plot_date(libarray_nlst[0][mr_old_idc, -1].astype(None), libarray_nlst[0][mr_old_idc,
                    2].astype(None), color='0.85', fmt='o-', ms=4, tz=None, xdate=True, ydate=False,
                    label='Methane refs library data')
                    pylab.plot_date(splmref_x_old, splmref_y_old, color='mediumorchid', fmt='-', lw=2, ms=4,
                    tz=None, xdate=True, ydate=False, label=slabel+' methane refs, smth.: '+str(spl_smth))
                    pylab.plot_date(libarray_nlst[0][mr_new_idc, -1].astype(None), libarray_nlst[0][mr_new_idc,
                    2].astype(None), color='0.85', fmt='o-', ms=4, tz=None, xdate=True, ydate=False)
                    pylab.plot_date(splmref_x_new, splmref_y_new, color='mediumorchid', fmt='-', lw=2, ms=4,
                    tz=None, xdate=True, ydate=False)

2047     #pylab.plot_date(mref_rsplarr[:,0], mref_rsplarr[:,1], color='dodgerblue', fmt='-', lw=2, tz=
                    None, xdate=True, ydate=False, label=slabel+' methane refs indiv. ranges')
        if lib == 1:
            line_fmt = 'bo'
            ### Add the data of the two methane ref peaks in reflow measurements
2052     # mean_mrefs = map(lambda x: mean(x), zip(libarray_nlst[lib][:, iso_col[lib]-2].astype(float),
                    libarray_nlst[lib][:, iso_col[lib]+2].astype(float))
            # std_mrefs = map(lambda x: std(x), zip(libarray_nlst[lib][:, iso_col[lib]-2].astype(float),
                    libarray_nlst[lib][:, iso_col[lib]+2].astype(float))
            # pylab.plot_date(libarray_nlst[lib][:, ord_col[lib]].astype(None), mean_mrefs, color='black
            ', fmt='o', ms=4, tz=None, xdate=True, ydate=False, label='Reflow MRef peaks mean')
            # pylab.setp(pylab.getp(pylab.gca(), 'xticklabels'), visible=False)

```

```

#         pylab.errorbar(libarray_nlst[lib][:, ord_col[lib]].astype(None), mean_mrefs, std_mrefs,
color= '0.35', fmt='o', ecolor='r', mfc='k', ms = 4, capsize=3) #, label='$\delta\;^{\{13\}}C\;$(\%-0)
$ Ref Peaks'
2057 #         pylab.setp(pylab.getp(pylab.gca(), 'xticklabels'), visible=True)
#         else:
#             line_fmt= 'ro'
#             pylab.gca().set_ylim(pylab.gca().get_ylim()[::-1])
#             ## Remove outliers in the two datasets and those meeting the max-diff constraint
2062 #             libarray_nlst[lib] = libarray_nlst[lib].take(where(libarray_nlst[3][:, iso_col[lib]].astype
(None)>-42)[0], axis=-2)
#             libarray_nlst[lib] = libarray_nlst[lib].take(where(libarray_nlst[3][:, iso_col[lib]].astype
(None)<-40)[0], axis=-2)
#             refl_diff, aira_diff, diff_list = loop_diff(1, lib, iso_col[1], iso_col[lib])
#             air_outies = find([dates in diff_dates for dates in libarray_nlst[3][:, 0]])
2067 #         if plot_lspl == 'on' and lib == 1:
#             ## Calculate the spline fit of uncorrected reloop data (x=date ordinal y= raw isotopy)
#             spl_refl_old = scipy.interpolate.splprep(libarray_nlst[lib][:, ord_col[lib]].astype(None),
#             libarray_nlst[lib][:, iso_col[lib]].astype(None), k=rspl_ord, s=rspl_smth)
#             spl_refl_old_x = arange(min(libarray_nlst[lib][:, ord_col[lib]].astype(None)), max(
#             libarray_nlst[lib][:, ord_col[lib]].astype(None))+1.0/enlargement[0], 1.0/enlargement
#             [0]) # reduce stepping between x-datapoints
#             spl_refl_old_y = scipy.interpolate.splev(spl_refl_old_x, spl_refl_old)
2072 #         pylab.plot_date(libarray_nlst[lib][:, ord_col[lib]].astype(None), libarray_nlst[lib][:,
iso_col[lib]].astype(None), fmt= line_fmt, ms = 4, tz=None, xdate=True, ydate=False,
label=org_label)
#         pylab.plot_date(spl_refl_old_x, spl_refl_old_y, color= 'cyan', fmt= '-', lw=2, tz=None, xdate
=True, ydate=False, label=rlabel+' reloops', order %i smoothey %s/%s '%(rspl_ord,
rspl_smth_a, rspl_smth_b))
#         pylab.plot_date(spl_refl_new_x, spl_refl_new_y, color= 'cyan', fmt= '-', lw=2, tz=None, xdate
=True, ydate=False)
#         else:
2077 #         pylab.plot_date(libarray_nlst[lib][:, ord_col[lib]].astype(None), libarray_nlst[lib][:,
iso_col[lib]].astype(None), fmt= line_fmt, tz=None, xdate=True, ydate=False, label=
org_label)
#         pylab.plot_date(libarray_nlst[lib][air_outies, ord_col[lib]].astype(None), libarray_nlst[lib
][air_outies, iso_col[lib]].astype(None), fmt= "wo", tz=None, xdate=True, ydate=False
, label="RefltoAirref Outlier")
#         pylab.legend(loc='lower left', numpoints = 3, prop = matplotlib.font_manager.FontProperties(
size=10)) # 0, url, ul2, uc9, lr4, ll3,
2082 ##### See if any splinefit props. of the Airafter could be appropriate
#         splcor_sp2=Splcor_fig.add_subplot(212, sharex=splcor_spl, sharey=splcor_spl)
#         pylab.xlabel('Measurement date range')
#         pylab.ylabel(r'$\delta\;^{\{13\}}C\;$(\%-0)$')
#         ## Mref splines
2087 #         pylab.plot_date(splmref_x, splmref_y, color= 'mediumorchid', fmt= '-', lw=2, tz=None, xdate=True,
ydate=False, label=slabel+' methane refs total range')
#         pylab.plot_date(mref_rsplars[:, 0], mref_rsplars[:, 1], color= 'dodgerblue', fmt= '-', lw=2, tz=None,
xdate=True, ydate=False, label=slabel+' methane refs indiv. ranges')
#         pylab.plot_date(libarray_nlst[0][mr_old_idc, -1].astype(None), libarray_nlst[0][mr_old_idc, 2].
astype(None), color= '0.85', fmt='o-', ms = 4, tz=None, xdate=True, ydate=False, label='Methane
refs library data')
#         pylab.plot_date(libarray_nlst[0][mr_old_idc, -1].astype(None), libarray_nlst[0][mr_old_idc, 2].
astype(None), color= '0.85', fmt='o-', ms = 4, tz=None, xdate=True, ydate=False, label='Methane
refs library data')
#         pylab.plot_date(libarray_nlst[0][mr_new_idc, -1].astype(None), libarray_nlst[0][mr_new_idc, 2].
astype(None), color= '0.85', fmt='o-', ms = 4, tz=None, xdate=True, ydate=False)
2092 #         pylab.plot_date(splmref_x_old, splmref_y_old, color= 'mediumorchid', fmt= '-', lw=2, ms = 4, tz=None
, xdate=True, ydate=False, label=slabel+'Methane refs')
#         pylab.plot_date(libarray_nlst[0][mr_new_idc, -1].astype(None), libarray_nlst[0][mr_new_idc, 2].
astype(None), color= '0.85', fmt='o-', ms = 4, tz=None, xdate=True, ydate=False)
#         spline_mrefdiff = mean(splmref_y_new)-loopspl_new.mean
#         pylab.plot_date(splmref_x_new, splmref_y_new-spline_mrefdiff, color= 'mediumorchid', fmt= '-', lw=2,
ms = 4, tz=None, xdate=True, ydate=False)
2097 ##### Loop splines
#         uncorrected reloop data
#         pylab.plot_date(spl_refl_old_x, spl_refl_old_y, color= 'cyan', fmt= '-', lw=2, tz=None, xdate=True,
ydate=False, label=rlabel+' reloops', order %i smoothey %s/%s '%(rspl_ord, rspl_smth_a,
rspl_smth_b))
#         pylab.plot_date(spl_refl_new_x, spl_refl_new_y, color= 'cyan', fmt= '-', lw=2, tz=None, xdate=True,
ydate=False)
2102 #         Mref peak spline data in Refloop measurement
#         spl_mrefl_old = scipy.interpolate.splprep(libarray_nlst[1][Normloop_idx_old, ord_col[1]].astype(None)
, map(lambda x: mean(x), zip(libarray_nlst[1][Normloop_idx_old, iso_col[1]-2].astype(float),
libarray_nlst[1][Normloop_idx_old, iso_col[1]+2].astype(float))), k=rspl_ord, s=rspl_smth_a)
#         spl_mrefl_y_old = scipy.interpolate.splev(spl_refl_old_x, spl_mrefl_old)
#         pylab.plot_date(spl_refl_old_x, spl_mrefl_y_old, color= 'dodgerblue', fmt= '-', lw=2, tz=None, xdate=
True, ydate=False, label=rlabel+'Refl methane peaks mean (s=%s/%s) '%(rspl_smth_a, rspl_smth_b))
2107 #         spl_mrefl_new = scipy.interpolate.splprep(libarray_nlst[1][Normloop_idx_new, ord_col[1]].astype(None)
, map(lambda x: mean(x), zip(libarray_nlst[1][Normloop_idx_new, iso_col[1]-2].astype(float),
libarray_nlst[1][Normloop_idx_new, iso_col[1]+2].astype(float))), k=rspl_ord, s=rspl_smth_b)

```

```

splmrefl_y_new = scipy.interpolate.splev(splrefl_new_x, splmrefl_new)
spline_mrefmdiff = mean(splmrefl_y_new)-loopspl_new_mean
pylab.plot_date(splrefl_new_x, splmrefl_y_new-spline_mrefmdiff, color= 'dodgerblue',fmt= '-',lw=2,
                tz=None, xdate=True, ydate=False)

2112 ## Sample data
ice_loops=concatenate(array([find(libarray_nlst[1][:,0]==date) for date in libarray_nlst[2][:,0] if
                             find(libarray_nlst[1][:,0]==date)!=0],ndmin=1), axis=1)
pylab.plot_date(libarray_nlst[1][ice_loops, ord_col[1]].astype(None),libarray_nlst[1][ice_loops,
                iso_col[1]-2].astype(None),"wo", ms= 10, label="1st Mref peak in Loops on Sample days")
pylab.plot_date(libarray_nlst[1][:, ord_col[1]].astype(None),libarray_nlst[1][:, iso_col[1]-2].
                astype(None),"bo", label="1st Mref peak in Loops")
pylab.plot_date(libarray_nlst[2][:, ord_col[2]].astype(None),libarray_nlst[2][:, iso_col[2]-2].astype
                (None),"ro", label="1st Mref peak in Samples")

2117 ##Airafter data
#pylab.plot_date(libarray_nlst[3][:, ord_col[3]].astype(None),libarray_nlst[3][:, iso_col[3]].
                astype(None), fmt= 'ro', tz=None, xdate=True, ydate=False, label='$\delta\;^{\{13\}}C\;^{\{0\}}$ '+
                org_label)
# mean_maira = map(lambda x: mean(x),zip(libarray_nlst[3][:, iso_col[3]-2].astype(float),
                libarray_nlst[3][:, iso_col[3]+2].astype(float))
# std_maira = map(lambda x: std(x),zip(libarray_nlst[3][:, iso_col[3]-2].astype(float),libarray_nlst
                [3][:, iso_col[3]+2].astype(float))
2122 # pylab.plot_date(libarray_nlst[3][:, ord_col[3]].astype(None),mean_maira, color= 'green', fmt='o',
ms= 4, tz=None, xdate=True, ydate=False, label='Airafter MRef peaks mean')
# pylab.setp(pylab.getp(pylab.gca(), 'xticklabels'), visible=False)
# pylab.errorbar(libarray_nlst[3][:, ord_col[3]].astype(None),mean_maira, std_maira, color='b', fmt
                ='o', ecolor='r', mfc='b', ms= 4, capsize=3, label='Airafter MRef peaks mean') #, label='$\delta
                \;^{\{13\}}C\;^{\{0\}}$ Ref Peaks'
# pylab.setp(pylab.getp(pylab.gca(), 'xticklabels'), visible=True)

2127 ## Airafter outliers
#pylab.plot_date(libarray_nlst[3].take(aira_diff, axis=-2)[:, ord_col[3]].astype(None),
                libarray_nlst[3].take(aira_diff, axis=-2)[:, iso_col[3]].astype(None), fmt= 'o', color= 'green'
                , tz=None, xdate=True, ydate=False, label='Airafter datasets with loop-diff. $\geq\;0.3$
                permille ')
pylab.legend(loc='lower left', numpoints = 3, prop = matplotlib.font_manager.FontProperties(size
                =10)) # 0, url, ul2, uc9, lr4, ll3,
pylab.subplots_adjust(left=0.06, bottom=0.06, right=0.96, top=0.96, hspace=0.12)

2132 # ''
# Plot Refloops Splines as Numbers
# ''
#
#
# Splcor2_fig = pylab.figure(figsize=[f_wh,f_ht])
2137 # pylab.figtext(0.8, 0.02, 'created: '+asctime(localtime()),size=9)
# splcor2_spl=Splcor2_fig.add_subplot(211, autoscale_on=False)
# pylab.title('Spline Quality Plot')
# pylab.xlabel('Measurement num range')
# pylab.ylabel(r'$\delta\;^{\{13\}}C\;^{\{0\}}$')
2142 # splcor2_spl.set_xlim(300, 445)
# splcor2_spl.set_ylim(-42.3, -40)
#### pylab.plot_date(libarray_nlst[0][mr_old_idc, -1].astype(None),libarray_nlst[0][mr_old_idc, 2].
                astype(None), color= '0.85',fmt='o-', ms= 4, tz=None, xdate=True, ydate=False, label='Methane
                refs library data')
#### pylab.plot_date(libarray_nlst[0][mr_new_idc, -1].astype(None),libarray_nlst[0][mr_new_idc, 2].
                astype(None), color= '0.85',fmt='o-', ms= 4, tz=None, xdate=True, ydate=False)
##
2147 ## pylab.plot_date(splmref_x_old, splmref_y_old, color= 'mediumorchid', fmt= '-',lw=2, ms= 4, tz=
None, xdate=True, ydate=False,label=slabel+' methane refs ')
#### pylab.plot_date(libarray_nlst[0][mr_new_idc, -1].astype(None),libarray_nlst[0][mr_new_idc, 2].
                astype(None), color= '0.85',fmt='o-', ms= 4, tz=None, xdate=True, ydate=False)
## spline_mrefdiff = mean(splmref_y_new)-loopspl_new_mean
## pylab.plot_date(splmref_x_new, splmref_y_new-spline_mrefdiff, color= 'mediumorchid', fmt= '-',lw
                =2, ms= 4, tz=None, xdate=True, ydate=False)
##
2152 ## Loop splines
## #uncorrected reloop data
## pylab.plot_date(splrefl_old_x, splrefl_old_y, color= 'cyan', fmt= '-',lw=2, tz=None, xdate=True,
                ydate=False,label=rlabel+' reloops old, order %i smoothey %s'%(rspl_ord,rspl_smth_a))
## pylab.plot_date(splrefl_new_x, splrefl_new_y, color= 'cyan', fmt= '-',lw=2, tz=None, xdate=True,
                ydate=False,label=rlabel+' reloops new, order %i smoothey %s'%(rspl_ord,rspl_smth_b))
## pylab.plot_date(libarray_nlst[1][:, ord_col[1]].astype(None),libarray_nlst[1][:, iso_col[1]].
                astype(None), fmt= "bo", tz=None, xdate=True, ydate=False, label="Reflow data")
2157 ## # Mref peak spline data in Refloop measurement
#### spl_mrefl_old = scipy.interpolate.splev(libarray_nlst[1][Normloop_idx_old, ord_col[1]].astype(
                None),map(lambda x: mean(x),zip(libarray_nlst[1][Normloop_idx_old, iso_col[1]-2].astype(float),
                libarray_nlst[1][Normloop_idx_old, iso_col[1]+2].astype(float))),k=rspl_ord, s=3)
#### splmrefl_y_old = scipy.interpolate.splev(splrefl_old_x, spl_mrefl_old)
#### pylab.plot_date(splrefl_old_x, splmrefl_y_old, color= 'dodgerblue',fmt= '-',lw=2, tz=None, xdate
                =True, ydate=False, label=rlabel+' methane peaks mean')
#### spl_mrefl_new = scipy.interpolate.splev(libarray_nlst[1][Normloop_idx_new, ord_col[1]].astype(
                None),map(lambda x: mean(x),zip(libarray_nlst[1][Normloop_idx_new, iso_col[1]-2].astype(float),
                libarray_nlst[1][Normloop_idx_new, iso_col[1]+2].astype(float))),k=rspl_ord, s=1)
2162 #### splmrefl_y_new = scipy.interpolate.splev(splrefl_new_x, spl_mrefl_new)
#### spline_mrefmdiff = mean(splmrefl_y_new)-loopspl_new_mean

```

```

### pylab.plot_date(splrefl_new_x, splmrefl_y_new-spline_mrefmdiff, color='dodgerblue',fmt='-',lw
=2, tz=None, xdate=True, ydate=False)
## ##Airafter data
## #pylab.plot_date(libarray_nlst[3][:, ord_col[3]].astype(None),libarray_nlst[3][:, iso_col[3]].
astype(None), fmt='ro', tz=None, xdate=True, ydate=False, label='\$\\delta\;^{\{13\}}\$C \$(\%_0)\$ '+
org_label)
2167 ### mean_maira = map(lambda x: mean(x),zip(libarray_nlst[3][:, iso_col[3]-2].astype(float),
libarray_nlst[3][:, iso_col[3]+2].astype(float)))
### std_maira = map(lambda x: std(x),zip(libarray_nlst[3][:, iso_col[3]-2].astype(float),
libarray_nlst[3][:, iso_col[3]+2].astype(float)))
##### pylab.plot_date(libarray_nlst[3][:, ord_col[3]].astype(None),mean_maira, color='green', fmt='o'
, ms=4, tz=None, xdate=True, ydate=False, label='Airafter MRef peaks mean')
##### pylab.setp(pylab.getp(pylab.gca(), 'xticklabels'), visible=False)
### pylab.errorbar(libarray_nlst[3][:, ord_col[3]].astype(None),mean_maira, std_maira, color='b',
fmt='o', ecolor='r', mfc='b', ms=4, capsize=3, label='Airafter MRef peaks mean') #, label='\$\\
delta\;^{\{13\}}\$C \$(\%_0)\$ Ref Peaks'
2172 ### pylab.setp(pylab.getp(pylab.gca(), 'xticklabels'), visible=True)
##
## ## Airafter outliers
## #pylab.plot_date(libarray_nlst[3].take(aira_diff, axis=-2)[:, ord_col[3]].astype(None),
libarray_nlst[3].take(aira_diff, axis=-2)[:, iso_col[3]].astype(None), fmt='o', color='green',
tz=None, xdate=True, ydate=False, label='Airafter datasets with loop-diff. \$\\geq\$ 0.3 permille ')
# 0, url1, ul2, uc9, lr4, ll3,
2177 #
# ice_loops=concatenate(array([find(libarray_nlst[1][:,0]==date) for date in libarray_nlst[2][:,0]
if find(libarray_nlst[1][:,0]==date)!=0],ndmin=1), axis=1)
# for n,smoothey in enumerate(arange(rspl_smth_a-.5,rspl_smth_a+1.0,0.5)):#range(1,4)
# splold_numrange=range(1,len(libarray_nlst[1][find(libarray_nlst[1][:,ord_col[1]].astype(None)
<733773.0), ord_col[1]))+1)
# spl_reflnum_old = scipy.interpolate.splep(splold_numrange,libarray_nlst[1][find(libarray_nlst
[1][:,ord_col[1]].astype(None)<733773.0), 4].astype(None),k=rspl_ord, s=smoothey)
2182 # splrefl_oldnum_x = arange(min(splold_numrange), max(splold_numrange)+1.0/enlargement[0], 1.0/
enlargement[0]) # reduce stepping between x-datapoints
# splrefl_oldnum_y = scipy.interpolate.splev(splrefl_oldnum_x, spl_reflnum_old)
# spldifnum_overold=libarray_nlst[1][find(libarray_nlst[1][:,ord_col[1]].astype(None)<733773.0),
4].astype(None)-scipy.interpolate.splev(splold_numrange, spl_reflnum_old)
# spldifnumold_mean = mean(abs(spldifnum_overold))
# spldifnumold_err=sqrt(sum(spldifnum_overold**2)/len(spldifnum_overold))
2187 # pylab.plot(splrefl_oldnum_x,splrefl_oldnum_y, "-", color= color[:: -1][n+2], label= "Old Bottle
Spline smooth. %s - difference %0.2f, err. %0.2f"%(smoothey,spldifnumold_mean,spldifnumold_err)
)
#
#
# splcor2_sp2=Splcor2_fig.add_subplot(212, autoscale_on=False)
# pylab.xlabel('Measurement num range')
# pylab.ylabel(r'\$\\delta\;^{\{13\}}\$C \$(\%_0)\$')
2192 # splcor2_sp2.set_xlim(440,560)
# splcor2_sp2.set_ylim(-50, -49)
# ## spline over reloop number
# for n,smoothey in enumerate([rspl_smth_b-0.1,rspl_smth_b,rspl_smth_b+0.1]): #arange(1.2,1.4,0.1)
2197 # splnew_numrange=range(splold_numrange[-1]+1,splold_numrange[-1]+1+len(libarray_nlst[1][find(
libarray_nlst[1][:,ord_col[1]].astype(None)>733773.0), ord_col[1]))
# spl_reflnum_new = scipy.interpolate.splep(splnew_numrange,libarray_nlst[1][find(libarray_nlst
[1][:,ord_col[1]].astype(None)>733773.0), 4].astype(None),k=rspl_ord, s=smoothey)
# splrefl_newnum_x = arange(min(splnew_numrange), max(splnew_numrange)+1.0/enlargement[0], 1.0/
enlargement[0]) # reduce stepping between x-datapoints
# splrefl_newnum_y = scipy.interpolate.splev(splrefl_newnum_x, spl_reflnum_new)
# spldifnum_overnew=libarray_nlst[1][find(libarray_nlst[1][:,ord_col[1]].astype(None)>733773.0),
4].astype(None)-scipy.interpolate.splev(splnew_numrange, spl_reflnum_new)
2202 # spldifnumnew_mean = mean(abs(spldifnum_overnew))
# spldifnumnew_err=sqrt(sum(spldifnum_overnew**2)/len(spldifnum_overnew))
# pylab.plot(splrefl_newnum_x,splrefl_newnum_y, "-", color= color[:: -1][n+2], label= "New Bottle
Spline smooth. %s - difference %0.2f, err. %0.2f"%(smoothey,spldifnumnew_mean,spldifnumnew_err)
)
#
#
# splcor2_sp1.plot(splold_numrange,libarray_nlst[1][find(libarray_nlst[1][:,ord_col[1]].astype(None)
<733773.0), 4].astype(None),"wo")
2207 # splcor2_sp1.plot(append(splold_numrange,splnew_numrange)[ice_loops],libarray_nlst[1][ice_loops,
4].astype(None),"o",color="0.7")
#
#
## #
# spldif_old=libarray_nlst[1][Normloop_idx_old, 4].astype(None)-scipy.interpolate.splev(
libarray_nlst[1][Normloop_idx_old, -1].astype(None), spl_refl_old) #old bottle range
##spldif_new=libarray_nlst[1][Normloop_idx_new, 4].astype(None)-scipy.interpolate.splev(libarray_nlst
[1][Normloop_idx_new, -1].astype(None), spl_refl_new)
2212 #
##
## print '-----'
## print 'Calculating Refloop splines by reloop number ...'
## print ' spline settings of order %s and smoothness %s/%s led to a \n mean spline to data
difference of %3f per mille (error %4f)'%(rspl_ord,rspl_smth_a,rspl_smth_b,spldifnum_mean,
spldifnum_err)
## box_str = 'date mean spline to data difference: %0.3f permille, err.: %0.3f permille\nnumber
mean spline to data difference: %0.3f permille, err.: %0.3f permille'%(spldiff_mean,spldiff_err,
spldifnum_mean,spldifnum_err)
2217 ## splcor2_sp1.text(0.2,0.04,box_str, bbox=dict(facecolor='0.5', alpha=0.2), fontsize=12,
transform = splcor2_sp1.transAxes)

```

```

#
#
#
# pylab.plot(splnew_numrange, libarray_nlst[1][find(libarray_nlst[1][:, ord_col[1]].astype(None)
2222 # >733773.0), 4].astype(None), "wo")
#
# pylab.plot(append(splold_numrange, splnew_numrange)[ice_loops], libarray_nlst[1][ice_loops, 4].
# astype(None), "o", color="0.7")
# splcor2_sp1.legend(loc='lower left', numpoints = 3, prop = matplotlib.font_manager.FontProperties(
# size=10))
# splcor2_sp2.legend(loc='lower left', numpoints = 3, prop = matplotlib.font_manager.FontProperties(
# size=10))
2227 # pylab.subplots_adjust(left=0.06, bottom=0.06, right=0.96, top=0.96, hspace=0.12)
',,
#####
### Export spline-corrected sample dataset to file
2232
if export is 'on':
    if splm_plot is not 'on':
        ## Call def sample_replicates to find replicates in sample data, calculate a mean and std_dev
        ## of those repl, append columns with its data to array and del the 2nd repl
        ## This is used for the errorbar plots
2237     smpl_dcor, smpl_dsrt, mn_uncor_col, std_uncor_col, repl_idc = sample_replicates(smpl_dsrt,
        iso_col[2], ord_col[2])
        ## Apply the Neumayer Correction Factor
        #smpl_dsrt[:, -2] = ((smpl_dsrt[:, -2].astype(None)-NM_offset)).round(3)
        ## Convert Bag Number/Depth to real sample depth
        if dml_range != "T1":
2242         exc_sets=range(0, len(smpl_dsrt))
         exc_nr=find(smpl_dsrt[:, 1]=='EDML-Bern')
         exc_nr=filter(lambda x:x in exc_nr, find(smpl_dsrt[:, 2].astype(float)>1390))# find alle Bern
         samples above 1390m as their depth is not given in bag number but depth already
         ## Correction for 30cm from Top/Bottom Mixup -> see version information in the header
         err_30=find(smpl_dsrt[:, 2].astype(float)>=1571)
2247         exc_sets= delete(exc_sets, exc_nr)
        else:
         exc_sets=range(0, len(smpl_dsrt))
         err_30=exc_sets
2252     smpl_dsrt[exc_sets, 2]=smpl_dsrt[exc_sets, 2].astype(float)-1 # apply correction
     smpl_dsrt[err_30, 2]=smpl_dsrt[err_30, 2].astype(float)+0.3
     del exc_sets, err_30

     export_fn=export_fn.rsplit('-', 1)[0]+'-'+age_choice+'.csv'
     print '-----'
2257     print 'Exporting %s dataset to file "%s" to the library folder\n "%s"...'%(ice_origin, export_fn,
        lib_path)
     csvfile = csv.writer(open(lib_path+export_fn, "wb"), 'excel')
     csvfile.writerow(('# This file contains EDML ice sample delta13C data corrected for dayly trends,\n
        \
        # for the calculated Neumayer offset of %0.3f permille (pos. means values are to heavy)\n\
        # and for gravitational separation calc. with a constant EDML value of %s, typical for glacial
        conditions (Landais, Capron)\n\
2262 # Created: %s\n\
        # Age scale: %s\n\
        # Excluded Data:\n\
        # datasets prior to %s\n\
        # selected datasets: %s\n\
2267 # Data sorted by Depth/Age!\
        '%(NM_offset, grav_corfac, strftime("%a %b %d %Y at %H:%M:%S", localtime()), age_choice, strftime("%a %b %d
        %Y", strftime(EDML_Startdate, "%y/%m/%d")), map(lambda l: strftime("%a %b %d %Y", strftime(l, "%y/%m/%d
        ")), remove_dates))).split('dummy'))
     csvfile.writerow(('Date Ice_origin Depth Cut dC_13 1st_Ref dC_13 pre_peak dC_13 CH4.Peak
        dC_13 CO2.peak dC_13 2nd_Ref Ampl 1st_Ref Ampl pre_peak Ampl CH4.Peak Ampl CO2.peak Ampl
        2nd_Ref Area 1st_Ref Area pre_peak Area CH4.Peak Area CO2.peak Area 2nd_Ref
        pos_max.1st_Ref pos_max.pre_peak pos_max.CH4.Peak pos_max.CO2.peak pos_max.2nd_Ref
        R.WMG.45 1st_Ref R.WMG.45 pre_peak R.WMG.45 CH4.Peak R.WMG.45 CO2.Peak R.WMG.45 2nd_Ref
        R.WMG.46 1st_Ref R.WMG.46 pre_peak R.WMG.46 CH4.Peak R.WMG.46 CO2.Peak R.WMG.46 2nd_Ref
        Weight Area.Norm Pot utc ord corr d13.CH4 Age ucor mn d13.CH4 ucor std.dev corr mn
        d13.CH4 corr std.dev').split(' '))
     #csvfile.writerow('')
     #map(lambda line: csvfile.writerow(line), append(array(map(lambda utc: strftime("%d-%b-%Y",
        localtime(utc)), smpl_dsrt[:, -8].astype(None)), ndmin=2).transpose(), smpl_dsrt[:, 1:], axis=1)) #
        write string array lines to file
2272 [ csvfile.writerow(line) for line in append(array(map(lambda utc: strftime("%d-%b-%Y", localtime(utc)
        )), smpl_dsrt[:, -8].astype(None)), ndmin=2).transpose(), smpl_dsrt[:, 1:], axis=1)]

    ## Do the export for the EDML replicate merged version (smpl_dcor) of the data
    if ice_origin == 'EDML':
2277     export_fn=export_fn.rsplit('-', 1)[0]+'-'+age_choice+'-plotset.csv'
        ## Convert Bag Number/Depth to real sample depth
        if dml_range != "T1":
            exc_sets=range(0, len(smpl_dcor))
            exc_nr=find(smpl_dcor[:, 1]=='EDML-Bern')
2282     exc_nr=filter(lambda x:x in exc_nr, find(smpl_dcor[:, 2].astype(float)>1390))# find alle Bern
            samples above 1390m as their depth is not given in bag number but depth already
            ## Correction for 30cm from Top/Bottom Mixup -> see version information in the header

```



```

err_30=find(smpl_dcor[:,2].astype(float)>=1571)
exc_sets= delete(exc_sets,exc_nr)
del exc_nr
2287 else:
exc_sets=range(0,len(smpl_dcor))
err_30=exc_sets
smpl_dcor[exc_sets,2]=smpl_dcor[exc_sets,2].astype(float)-1 # apply bag/depth correction
smpl_dcor[err_30,2]=smpl_dcor[err_30,2].astype(float)+0.3
2292 del exc_sets,err_30
## have the mean sample depth computed for replicates an non-repl
smpl_dcor[find(smpl_dcor[:,3]=='G01+G02'),2]=smpl_dcor[find(smpl_dcor[:,3]=='G01+G02'),2].
astype(None)+0.125 # set the depth of the repl. to sample top depth + 12,5cm
smpl_dcor[find(smpl_dcor[:,3]!='G01+G02'),2]=smpl_dcor[find(smpl_dcor[:,3]!='G01+G02'),2].
astype(None)+0.0625 # set the depth of the non-repl. to sample top top depth + 6,25cm (
half of the specific cut)

2297 ## Calculate the resulting mean sample age and replace the old values
smpl_dcor[:, -3]=scipy.interpolate.splev(smpl_dcor[:, 2].astype(None), spl_depage).round()
## Replace the date column values with interpretable date format values
smpl_dcor[:,0]=map(lambda utc: strftime("%d-%b-%Y", localtime(utc)),smpl_dcor[:, -6].astype(None
))
## Select essential data columns for the plotting dataset
2302 smpl_dcor=smpl_dcor.take([0,1,2,3,-3,-2,-1], axis=1)
## Apply the Neumayer Correction
##smpl_dcor[:, -2] = (smpl_dcor[:, -2].astype(None)-NM_offset).round(3)
## Write the data to file
print 'Exporting %s dataset (replicate merged version) to file "%s" too...'%(ice_origin ,
export_fn)
2307 csvfile = csv.writer(open(lib_path+export_fn, "wb"),'excel')
csvfile.writerow(('# This file contains EDML ice sample delta13C data corrected for dayly
trends,\n\
# for the calculated Neumayer offset of %0.3f permille (pos. means values are to heavy)\n\
# and for gravitational separation calc. with a constant EDML value of %s, typical for glacial
conditions (Landais, Capron)\n\
# Created: %s\n\
2312 # Age scale: %s\n\
# Excluded Data:\n\
# datasets prior to %s\n\
# selected datasets: %s\n\
# Data sorted by Depth/Age!\
2317 '%(NM_offset,grav_corfac, strftime("%a %b %d %Y at %H:%M:%S",localtime()),age_choice, strftime("%a %b %d
%Y",strptime(EDML.Startdate, "%y/%m/%d")),map(lambda l: strftime("%a %b %d %Y",strptime(1, "%y/%m/%d")
), remove_dates))).split('dummy'))
csvfile.writerow(('Date Ice_origin Mean Depth Cut Mean Age corr mn dl3-CH4 corr std_dev')
.split(' '))
#csvfile.writerow('')
#map(lambda line: csvfile.writerow(line),append(array(map(lambda utc: strftime("%d-%b-%Y",
localtime(utc)),smpl_dsrt[:, -8].astype(None)), ndmin=2).transpose(),smpl_dsrt[:,1:], axis
=1)) # write string array lines to file
[ csvfile.writerow(line) for line in smpl_dcor]
2322 # savetxt(log_dir+"Measured_samples.tab", libarray_nlst[2].take(argsort(libarray_nlst[2][:,2].astype
(float)), axis=-2)[:,(0,1,2,3,-6)], fmt="%s" ,delimiter='t')

if eval_run=="on":
2327 ##evfg.invert_yaxis
Eval_Fig.subplots_adjust(left=0.05, bottom=0.05, right=0.99, top=0.95)
evfg.legend(loc='lower left', numpoints = 3, prop = matplotlib.font_manager.FontProperties(size=8))

if debug_refl == 'on':
2332 plfg.legend(loc='upper right', numpoints = 3, prop = matplotlib.font_manager.FontProperties(size=8)
)
Spl_Fig.subplots_adjust(left=0.03, bottom=0.03, right=0.99, top=0.98)

if debug_refl == 'on' and debug_Corr == 'on':
2337 btfg.legend(loc='lower left', numpoints = 3, prop = matplotlib.font_manager.FontProperties(size=8))
corfg.legend(loc='lower left', numpoints = 3, prop = matplotlib.font_manager.FontProperties(size=8)
)
Btl_Fig.subplots_adjust(left=0.05, bottom=0.08, right=0.99, top=0.95)
Cor_Fig.subplots_adjust(left=0.05, bottom=0.08, right=0.99, top=0.95)

pylab.show()

```


E. Acknowledgements

I thank Prof. Heinrich Miller for accepting me as his PhD student, for the support during my thesis and for providing almost perfect conditions for scientific research in the Glaciology Department of the AWI. I am further very grateful that I had the chance to participate in the 2009 field campaign of the NEEM ice core drilling project. Certainly an experience I will never forget.

Special thanks go out to Hubertus Fischer for an excellent supervision and invaluable support in every aspect of this thesis. I am especially grateful for the great interest in my work, the always positive and constructive feedback, for the guidance towards the finalization of this project, for maintaining such an excellent team spirit, for the patience to answer also the 999'th email promptly and target-orientated and so much more. That all helped to make the distance between Bern and Bremerhaven (and Hamburg) somehow bridgeable and emotionally far less distant. And last but not not least, I am very grateful for the chance to live in the wonderful city of Bern and to be a part of the KUP family for some time. I cannot imagine how you may have done better - thank you very much, Hubertus!

I am also very much indebted to Jochen Schmitt for your so much appreciated support during the frustrating phases in the lab, the patience to read my contemporary epic mails, the will to comprehend them and to find solutions to the problems. I am further very grateful for sharing so much of your laboratory experience and vast knowledge about technical and scientific questions - and some of your exceptional, philosophical views on the world. I have learned a lot. Thank you also for the interest in the interpretation of the data and your invaluable input to our think-tank, for the many comments and refinements on the way.

Now it may seem as if there would be nothing left to be said about my great colleague Michael Bock. However, most of the above also fully applies to you, Michl. Thank you for all your input, your curiosity, the many things I could learn from you, and for being an inspiration of how to tackle or overcome obstacles along the path with a positive attitude. I am glad that we have met and shared paths for some time, during and especially beyond office times. I am grateful for your immense support, and that you became a good friend over the years.

I thank Melanie Behrens for letting me put hands on 'her baby', for teaching me to love it and how to treat it right. Thank you for sharing your lab experience and your support.

Many thanks go out to ...

... Robert "Rob" Schneider for the great time we had in Bremerhaven and in Bern. Thank you for introducing me to Python (be also cursed for it!) and for all the help with the processing scripts. You and your funny attitude helped to put things in perspective sometimes. Thanks also for your great hospitality during the visits in Bern.

... the entire Glaciology department at the AWI for the great spirit and the chance to get insights into all the diverse aspects of polar science that are united in this group.

... my room-mates Ilka Weikusat and Kerstin Mertens for the fun and diversions in the office. Without you I wouldn't have made it to join the mensa caravan on time. Thank you for the many great and inspiring conversations, Ilka.

... Birthe Twarloh for your expertise in ice-cream, your value for the team spirit and for the organization of social events outside the AWI

... my many (former) fellow PhD colleagues Maria Hörhold, Anna Wegner, Christine Wesche, Reinhardt Drews, Veit Helm, Kathrin Wolf and Katrin Haasemann for making work, mensa walks, coffee breaks and live in Bremerhaven always worthwhile.

... the AWI 'seniors' Olaf Eisen, Johannes Freitag, Hans Oerter, Frank Wilhelms, Coen Hofstede, Daniel Steinhage for the scientific input and for welcoming me in your circle and sharing your knowledge.

... Sepp Kipfstuhl for his creative and odd thinking, for holding the flags up for fundamental research and the good time at NEEM.

... Peter Köhler for having an open ear for my problems, his assistance to understand the carbon cycle and the many things I could learn from you.

... Fernando Valero-Delgado for taking care of the ice, his share in acquiring the 'Vibiemme' and his proficiency to organize that much cake in these three years.

... Andreas Frenzel for his assistance in IT issues.

... York Schlomann for his sense of humor and the good conversations.

... the AWI for the chance get in touch with young scientists from all over the world and the multiple training courses.

... the "homies" for hundreds of coffees and evening beers on the roof and all the things that made evening life in Bremerhaven more than just bearable. Thank you for the great time!

... the whole KUP members in Bern for welcoming me in their midst. You helped a lot to make my time in your city a wonderful experience and memory.

... Sarah Eggleston for the great effort to improve this manuscript, and for reminding me of English punctuation. Thank you big time!

... Doris Rätz for the great assistance in the administrative tasks to make that happen.

... the NEEM 2009 field campaign team for sharing a wonderful experience.

... anyone that I might have forgotten. I am sorry!

Special thanks go out to Nina Wittenberg for... ah well, I think I show how grateful I am rather than writing about it.

But most of all I thank my parents for the invaluable support during every step of my life, for the great love and unlimited trust in me and my abilities. This one is dedicated to you.

N a m e : Lars Möller Datum 18.10.2013

Anschrift : Armbruststrasse 18, 20257 Hamburg

E r k l ä r u n g

Hiermit versichere ich, dass ich

1. die Arbeit ohne unerlaubte fremde Hilfe angefertigt habe,
2. keine anderen als die von mir angegebenen Quellen und Hilfsmittel benutzt habe und
3. die den benutzten Werken wörtlich oder inhaltlich entnommenen Stellen als solche kenntlich gemacht habe.

Hamburg _____, den 18.10.2013

(Unterschrift)